






Universitat Autònoma de Barcelona

ADVERTIMENT. L'accés als continguts d'aquesta tesi queda condicionat a l'acceptació de les condicions d'ús establertes per la següent llicència Creative Commons:  http://cat.creativecommons.org/?page_id=184

ADVERTENCIA. El acceso a los contenidos de esta tesis queda condicionado a la aceptación de las condiciones de uso establecidas por la siguiente licencia Creative Commons:  <http://es.creativecommons.org/blog/licencias/>

WARNING. The access to the contents of this doctoral thesis it is limited to the acceptance of the use conditions set by the following Creative Commons license:  <https://creativecommons.org/licenses/?lang=en>



Universitat Autònoma de
Barcelona Facultat de Ciències
Departament de Química

SULPHIDE-SULPHIDE BOND AS A TOOLKIT FOR THE MODULAR SYNTHESIS OF (MULTI)FUNCTIONAL MUSSEL-INSPIRED COATINGS

PhD Thesis

PhD in Chemistry

Chemistry Department
Science Faculty

Carolina Casagualda Clapés

2021

Supervisors:

Dr. Félix Busqué Sánchez

Dr. Daniel Ruiz Molina

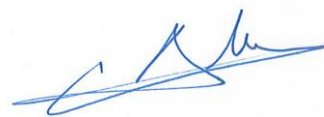
Dr. Ramon Alibés Arqués

Memòria presentada per aspirar
al grau de Doctor per Carolina Casagualda Clapés



Carolina Casagualda Clapés

Amb el vist-i-plau de,



Dr. Félix Busqué Sánchez Dr. Daniel Ruiz Molina Dr. Ramon Alibés Arqués

*Escriurem que tot no va ser fàcil, cantarem la nostra vida en un paper.
Marxarem amb els dies regalats, i amb els somriures dels que ja no hi puguin ser.*

Escriurem, Miki Núñez

A tots els que han format part d'aquesta història
Als meus quatre avis

ACKNOWLEDGMENTS

Quiero empezar por agradecer a mis tres directores de tesis, los doctores Félix, Ramon y Daniel. Félix, gracias por creer en mí desde tercero de carrera, por la confianza que depositaste y por darme la oportunidad de trabajar con vosotros y ser una *Font* más. Ramon gràcies per aquests 5 anys, per tot el que m'has ensenyat i pel teu sentit de l'humor. Y Dani, gracias por acogerme en tu grupo de investigación y siempre estar dispuesto a echarme una mano. ¡Al final os voy a echar de menos a los tres! También agradecer a los demás doctores de los grupos de investigación y, en general, de la planta de orgánica que han estado allí durante todos estos años y que también forman parte de toda esta experiencia: Marta, Pau, Jordi H., Rosi, Ona, Roser, Adelina, Claudio, Fernando y Josep.

Pero si estoy escribiendo estas líneas, es porque he terminado mi tesis, y esto no hubiera sido posible sin esas personas que, como ya dijo en su día el ahora Dr. Jurado, componen la familia *Font*; Sílvia, Gisela, Rubén, Sergio, Kevin y Adri.

Sílvia, la meva *big labmate*! Però no hi hauria unes *big i little labmates* sense una *middle*! Sílvia i Laia, amb vosaltres vaig començar aquesta aventura al 2014 (encara no sabia el que m'esperava). Sense dubte, l'etapa més feliç d'aquests 6 anys va ser amb vosaltres. Recordo amb nostàlgia aquelles tardes de *performances*, de concerts d'OT, els nostres Montpellers, els menús que ens preparàvem i totes les nostres converses. Gràcies per haver-me ensenyat, mimat i fotrem alguna que altra bronca ben merescuda... veu exercir a la perfecció el vostre paper de *big i middle labmates*. Sempre sereu el meu *LabTeam453*!

Y qué decir de mi dúo masculino favorito... Sergio y Kevin. Me habéis dado la vida en los peores momentos de esta tesis, no sé que hubiera hecho sin vosotros... tirarme por la ventana! Ahora te tendría que llamar Dr. Jurado, pero para mí siempre serás mi Sergio, el que sabe de todo de síntesis y que siempre está dispuesto a echarme un cable (con algo a cambio claro está), el que da los mejores abrazos por la mañana, el que sabe escuchar y entender, y el que siempre tiene las palabras correctas para levantarte el ánimo. Te quiero mucho y recuerda que tenemos un viaje pendiente en *Saint Andrews*. Y qué decir de mi *partner in crime* (espero que sepas ya lo que significa), Kevin, tú sí eres quien más ha aguantado mis locuras, mis dramas y mi malhumor... ¡Y todo eso sin volverte tú más loco! Gracias, gracias por ser mi vecino de vitrina, por llevar ese lab 453 a lo más alto, por ser el mejor organizador de eventos de la planta, por todos esos momentos vividos entre esas 4 paredes, por ser mi mayor apoyo y por ser un gran amigo. Os quiero mucho a los dos.

Al resto de la familia *Font*, cada uno aportando su toque que ha hecho que este grupo sea único; la nostra pija, la nostra Gisela, una crack tant a nivell professional com personal; el bohemio del grupo, l'Adri, el que el seu punt de vista no et deixa indiferent; y el que podríamos decir que es el más introvertido del grupo, Rubén, pero que te suelta cada una en el momento justo que te descoloca y te ríes. ¡Gracias a todos por haber formado parte de esta importante historia, sin duda, lo mejor que me llevo de este doctorado!

También agradecer a nuestros predecesores del grupo *Font* y a los que han ido incorporándose; Bea, Benaiges, Cristina Simó, Ruth, Andrea F., Alba y Marc. ¡Un placer haber coincidido con vosotros en algún momento! Y Batten, no me olvido de ti, ahora si serás amo y señor del Lab453... ¡Mantenlo a flote!

Y qué decir de nuestros vecinos, los *Moreno* que sin ellos las barbacoas, los Ports de Comte, y los Paddles no habrían sido lo mismo! Al meu *Farinho*, gràcies per regalar-me tants bons moments. Al Reyes, por más partidos como ése 6-1 que vivimos. Al Salabert y a la Carol, ¡Cómo me he llegado a reír con vosotros! Al Dr. Granados, fue un placer tenerte como profesor y aún más como compañero; las risas contigo están aseguradas. A la Laura i al Marc V., us desitjo el millor.

A los demás compañeros de otras plantas; al Rodri, a la Gloria i en especial al meu company de *bodycombat*, en Quim! Un plaer haver coincidit amb tu en aquesta etapa i veure que encara hi ha joves amb una gran il·lusió cap a la investigació!

Y si tuve mucha suerte con los compañeros en orgánica, también la tuve con los del grupo *Nanosfun*. En especial agradecer a Miguel, mi compañero de tesis, con el que empecé a trabajar mano a mano en este proyecto. Te deseo lo mejor. A Roger, gràcies per donar-me els millors moments en el ICN2. Tu, l'Alexis i el Payam... quina època! Però sobretot gràcies per fer-me veure la vida d'una altra manera. Y como no a mi amigo Salvi, o mejor dicho mi salvador. Si tuviera que agradecerte todo lo que has llegado a hacer por mí, este párrafo sería más largo que toda la tesis en si. Gracias por ser el mejor compañero, el mejor profesor y el mejor amigo. Por ayudarme siempre que tenía un problema, por entenderme sin volverte loco (esto es un logro) y por aguantar todas mis locuras. Simplemente gracias por cruzarte en mi camino. Sólo volvería a repetir todo esto con tal de volver a coincidir contigo. ¡Vaya viaje nos espera en 2022! Y al resto del grupo, gracias por acogerme, por enseñarme y por formar parte de esta etapa importante: Àlex J., Bea, Héctor, Christian, Xiao, Junda, Noe e Ivana.

Agrair també als diferents serveis que han fet possible la majoria de les caracteritzacions de la tesi: al Servei d'Anàlisi Química (SAQ) de la UAB per fer-nos els ICP-MS i els anàlisis elementals, al Servei de Ressonància Magnètica Nuclear (sermn) de la UAB, en especial a la Eva, i al servei de microscòpia electrònica del ICN2, en especial al Marcos. També agrair al Javi Saiz, del ICN2, per l'ajuda rebuda en el Zetasizer o en la microscòpia òptica, i a l'Alejandro Gómez, del grup de *Magnetic Nanostructures Group* (MNG), per l'ajuda en la preparació de les nanopartícules de magnetita.

Y para terminar en el ámbito académico, agradecer a Paula Alfonso y a la Dr. Julia Lorenzo, del IBB, el interés mostrado por nuestros sistemas y por el trabajo tan riguroso que han realizado con tan poco tiempo para obtener algunos resultados preliminares.

Però tot allò que comporta una tesi no solament es queda a la universitat, sinó que també afecte a la teva vida personal. Per tant, aquesta tesi també va per a elles, les meves amigues de tota la vida; Núria, Desi i Alba. Les que pot passar el temps, mesos sense veure'ns, però que sempre estan allà, amigues de veritat i per sempre. Gràcies per tot! Us estimo.

Però si m'hi poso a pensar, tot això comença ara farà 15 anys amb la primera professora de Química que vaig tenir, la que em va descobrir aquesta ciència, la Fina Miras. Sense ella de ben segur que a dia d'avui no seria química. Gràcies per ensenyar-me-la d'una manera que fes que m'encantés i no l'odiés.

Dedicar-la també a les persones més importants de la meva vida, tota la meva família; tiets, tietes, cosins i cosines, però sobretot als meus pares, Francesc i Carolina, i al meu germà, Marc. Gràcies simplement per estar allà, donar suport i animar, i per mostrar-vos sempre tant orgullosos. Al final sí hi haurà una Dra. Casagualda de veritat a casa, *alias* Dra. Pix!

I als que ja no hi son, els meus quatre avis, que de ben segur haguessin estat ben orgullosos que la seva neta es convertís en doctora. Qui ho hauria de dir, la que de petita volia ser peixatera... però al final també he acabat treballant amb guants, balances i potinejant una mica.

Un especial agraïment simbòlic als meus petits "Beatles", Lennon i McCartney, gossa i gat, el meu duet preferit.

Y ahora sí, para acabar, al que sin buscarlo ni esperarlo apareció así, sin más, a 3 meses de acabar la tesis. No te puedo agradecer que me hayas ayudado, que me hayas animado ni que hayas aguantado mi malhumor durante estos 4 años... ¡De la que te has librado! Aunque ya

vivirás tu propia experiencia en el doctorado y yo encantada de volverla a vivir esta vez de mera espectadora. Pero sí quiero darte las gracias por entrar en mi vida en el momento adecuado, por haber hecho que estos meses haya sido más feliz y por ser un gran compañero de viaje, que espero que sea muy largo. Y Dani, al final sí será cierto que el *Friends will be friends* dejará de sonar para dejar paso al *Somebody to love*.

Funding Sources

This work was supported by projects MAT2015-70615-R from the Spanish Government and by FEDER funds. ICN2 acknowledges support from the Severo Ochoa Program (MINECO, Grant SEV-2013-0295) and the CERCA Programme/Generalitat de Catalunya. I thank the *Ministerio de Educación, Cultura y Deporte* for the predoctoral grant FPU15/03245.

TABLE OF CONTENTS

ABBREVIATIONS	1
FORMULA INDEX	5
CHAPTER 1. <i>General Introduction</i>	9
1.1. Catechols in nature.....	11
1.2. Chemistry of catechols.....	12
1.3. Polymerisation of catechols.....	14
1.3.1. Approach I. Polymerisation through the catechol moiety.....	15
1.3.2. Approach II. Catechols grafted to polymeric backbones.....	18
1.3.3. Approach III. Building blocks.....	20
1.4. A novel polymerisation strategy based on sulphur chemistry.....	22
1.4.1. Synthetic methodologies.....	25
1.4.2. Synthetic advantages.....	26
1.5. References.....	27
CHAPTER 2. <i>Objectives</i>	33
CHAPTER 3. <i>PEGylation as a Strategy for Improving Nanoparticle Biocompatibility</i>	39
3.1. Introduction.....	41
3.1.1. Coatings based on cat-PEG derivatives.....	41
3.1.1.1. Polymerisation of cat-PEG based molecules.....	42
3.1.1.2. Post-functionalisation of primer coatings.....	43
3.1.1.3. Copolymerisation.....	45
3.1.2. Work programme.....	47
3.2. Synthesis of the building blocks and a targeting molecule.....	49
3.2.1. Synthesis of monosubstituted S-catechol tris-thiol intermediate 4	50
3.2.2. Synthesis of mPEG-functionalised building block 5	51
3.2.3. Synthesis of mPEG-functionalised building block 6	55
3.2.4. Synthesis of peg-functionalised building block 7	57
3.2.4.1. Synthesis of heterobifunctional PEG derivative 26	58
3.2.4.2. Synthesis of building block 7	62
3.2.5. Synthesis of fluorescein-functionalised building block 8	64
3.2.6. Synthesis of fluorescein-functionalised styrenic derivative 36	67
3.2.7. Synthesis of amino-glucofuranose derivative 41	68
3.3. Sulphur-based polymerisation reaction.....	71
3.3.1. Characterisation methodology.....	71
3.3.2. Polymerisation reaction.....	72

3.4.	Nanoparticle coatings.....	79
3.4.1.	Coatings onto mesoporous silica nanoparticles.....	79
3.4.2.	Coatings onto magnetite nanoparticles.....	82
3.4.2.1.	Preparation of MNPs.....	82
3.4.2.2.	Coating of mnps with P7	83
3.4.2.3.	Functionalisation of coated MNPs.....	85
3.4.3.	Multifunctional coatings.....	93
3.5.	Summary.....	96
3.6.	References.....	99
CHAPTER 4.	<i>Hydrophobic and Hydrophilic Coatings</i>	107
4.1.	Introduction.....	109
4.1.1.	Oleo-/hydrophobic coatings.....	110
4.1.1.1.	Post-functionalisation of catechol-based primer coatings.....	110
4.1.1.2.	Polymerisation of functionalised catechol-based molecules.....	114
4.1.1.3.	Polysaccharide-based coatings and copolymerisation.....	116
4.1.2.	Hydrophilic coatings.....	118
4.1.3.	Work programme.....	120
4.2.	Synthesis of the building blocks.....	121
4.2.1.	Synthesis of C ₁₈ -functionalised buildingblock 9	122
4.2.2.	Synthesis of C ₁₈ -functionalised styrenic derivative 46	124
4.2.3.	Synthesis of fluorine-functionalised building block 10	124
4.3.	Sulphur-based polymerisation reaction.....	126
4.4.	Macroscopic surface coatings.....	127
4.4.1.	Coatings with C ₁₈ -functionalised building blocks 9 and 46 , and their corresponding products P9 and P46 from the polymerisation.....	127
4.4.1.1.	Hydrophobic surfaces.....	127
4.4.1.2.	Hydrophobic textiles.....	134
4.4.2.	Coatings with fluorine-functionalised building block 10 and its corresponding product P10 from the polymerisation.....	139
4.4.2.1.	Oleo-/hydrophobic surfaces.....	139
4.4.2.2.	Oleo-/Hydrophobic textiles.....	141
4.4.3.	Coatings with mPEG-functionalised building block 6 and its corresponding product P6 from the polymerisation.....	143
4.4.4.	Multifunctional coatings.....	145
4.5.	Summary.....	149

4.6. References	151
CHAPTER 5. Summary and Conclusions	155
CHAPTER 6. Experimental Section	163
6.1. General procedures	165
6.1.1. Spectroscopy.....	165
6.1.2. Mass spectrometry.....	165
6.1.3. Chromatography.....	166
6.1.4. Microscopy.....	166
6.1.5. Other techniques.....	167
6.2. Experimental description	167
6.2.1. Synthesis of functional building blocks.....	168
6.2.2. Synthesis of glucose derivatives.....	186
6.3. Methodologies	190
6.4. References	195
ANNEX. Spectra of Selected Compounds	197
A1. NMR and IR spectra	199
A1.1. Building blocks.....	199
A1.2. Products from polymerisation reactions.....	224
A1.3. Copolymers.....	232
A1.4. Glucose derivatives.....	237
A2. GPC spectra	245
A2.1. GPC spectra with both IR (top) and UV (bottom) detectors of building block 6	245
A2.2. GPC spectra with both IR (top) and UV (bottom) detectors of P6	245
A2.3. GPC spectra with both IR (top) and UV (bottom) detectors of building block 9	245
A2.4. GPC spectrum with IR detector of P9	246
A2.5. GPC spectra with both IR (top) and UV (bottom) detectors of building block 46	246
A2.6. GPC spectra with both IR (top) and UV (bottom) detectors of P46	247
A3. EDX spectra	247
A3.1. Images from EDX experiments of pristine and coated surfaces with P9 <i>via ex situ</i> polymerisation in solution	247
A3.2. Images from EDX experiments of coated surfaces with P9 <i>via</i> <i>in situ</i> polymerisation.....	249

A3.3. Images from EDX experiments of coated surfaces with P6 <i>via ex situ</i> polymerisation in solution.....	250
A3.4. Images from EDX experiments of coated surfaces with P6 <i>via in situ</i> polymerisation.....	251

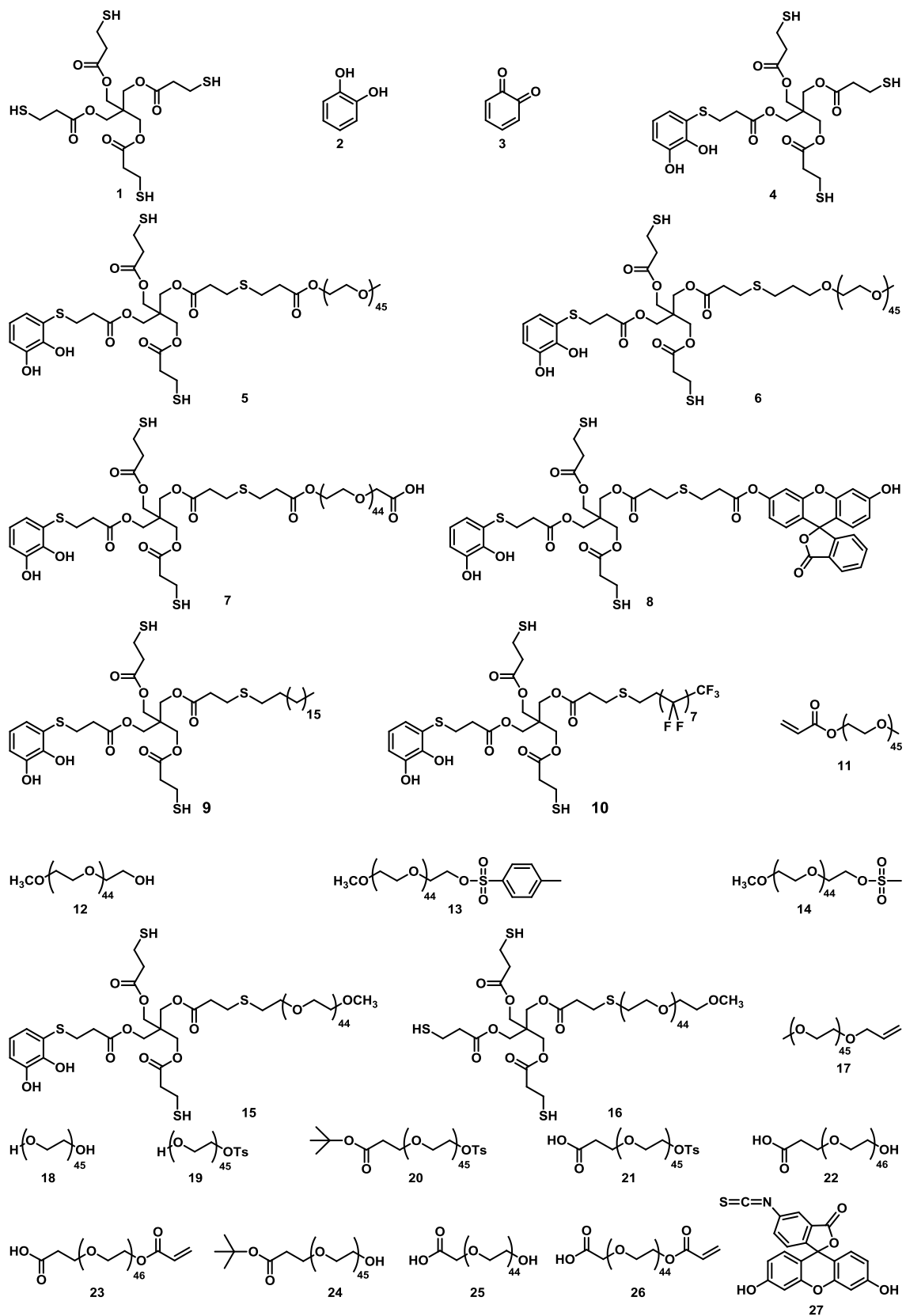
ABBREVIATIONS

Abs.	absolute	DMAP	4-(dimethylaminopropyl) pyridine
AcOH	acetic acid	DMF	dimethylformamide
AFM/SPM	atomic force microscopy/scanning probe microscopy	DMPP	dimethylphenylphosphine
AIBN	azobisisobutyronitrile	DOSY	diffusion ordered NMR spectroscopy
Ala	alanine	DOX	doxorubicin
Anh.	anhydrous	DPPA	diphenylphosphoryl azide
Atm.	atmosphere	EDCI	1-ethyl-3-(3-dimethylaminopropyl)carbodiimide
BBB	blood-brain barrier	EDX	energy-dispersive x-ray spectroscopy
BGNPs	bioactive glass NPs	e.g.	<i>exempli gratia</i> (for example)
BHT	butylated hydroxytoluene	EGTA	ethylene glycol-bis(β -aminoethyl ether)- <i>n,n,n',n'</i> -tetraacetic acid
Bs	broad signal	Equiv.	equivalent
BSA	bovine serum albumin	et al.	<i>et alia</i> (and others)
CA	contact angle	EtOAc	ethyl acetate
ca.	circa	EtOH	ethanol
Cat	catechol	GPC	gel permeation chromatography
CCDP	2-chloro-3',4'-dihydroxyacetophenone	h	hour
CHT	chitosan	HA	hyaluronic acid
CNT	carbon nanotube	HNT	halloysite nanotube
COS	chitooligosaccharides	HRMS	high resolution mass spectroscopy
Cys	cysteine	i.e.	<i>id est</i> (that is)
DA	dopamine	IONP	<i>iron oxide np</i>
DAPI	4',6-diamidino-2-phenylindole	IR (ATR)	infrared spectroscopy in attenuated total reflection
DBAD	di- <i>tert</i> -butyl azodicarboxylate	LBL	layer-by-layer
DBU	1,8-diazabicyclo [5.4.0]undec-7-ene	L-DOPA	3,4-dihydroxyphenyl-L-alanine
DIPEA	<i>N,N</i> -diisopropylethylamine	Me-	methyl
DLS	dynamic light scattering	mfps	mussel foot proteins
DMA	dopamine methacrylamide	Min	minute

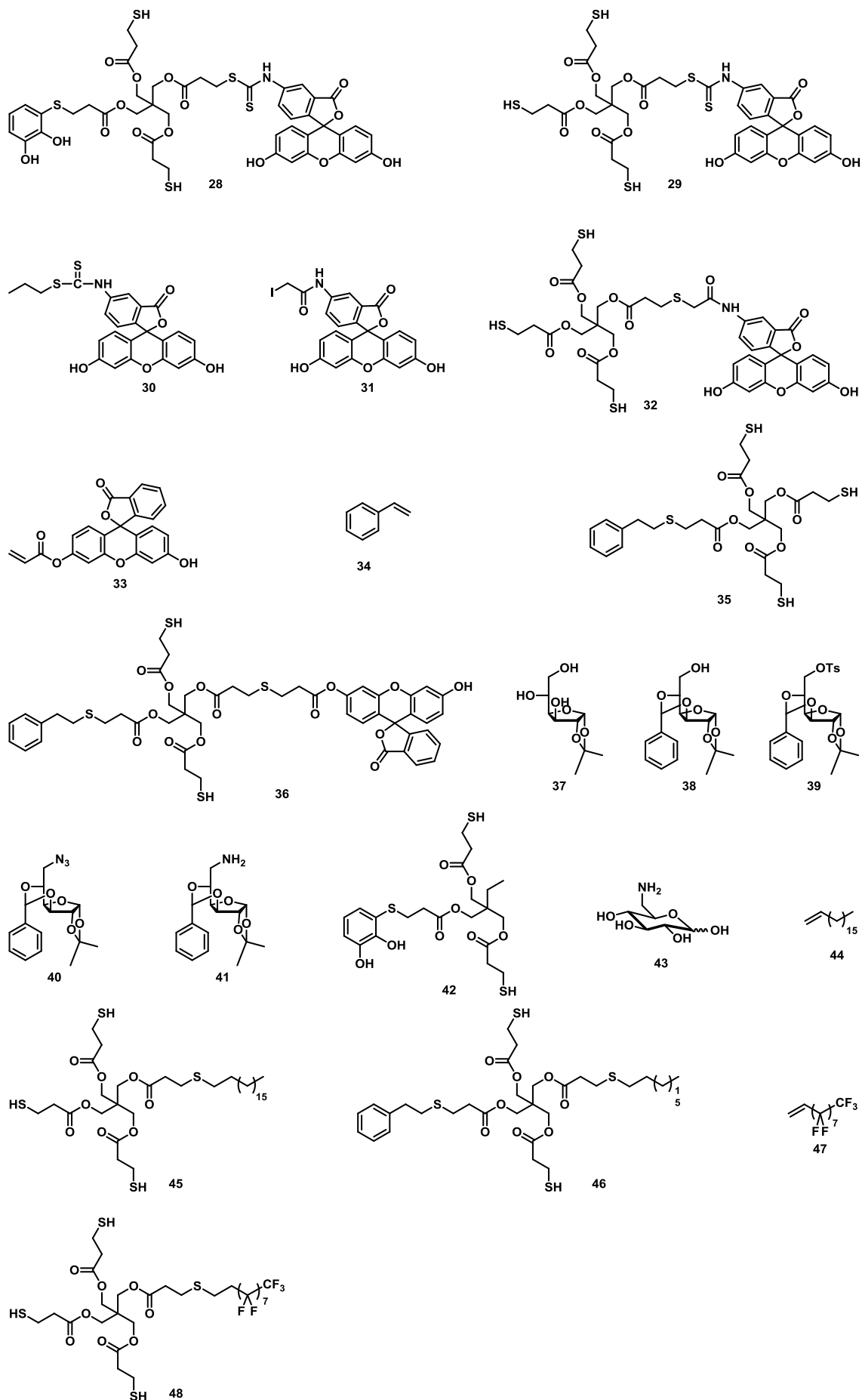
Abbreviations

ML	multidentate ligand	PPEGMA	poly((polyethylene glycol) methyl ether methacrylate)
MNP	magnetite NP	PTT	photothermal therapy
MRI	magnetic resonance imaging	PU	polyurethane
MSNP	mesoporous silica NP	Py	pyridine
MW	microwave	QDs	quantum dots
Mw	molecular weight	Quant.	quantitative
MWCNTs	multi-walled carbon nanotubes	RAFT	reversible addition fragmentation chain-transfer
NMR	nuclear magnetic resonance	rt	room temperature
NP	nanoparticle	SAMs	self-assembled monolayers
OA	oleic acid	SDS	dodecyl sulphate
OCA	oil contact angle	SEM	scanning electron microscopy
-OMs	mesylate	SGNPs	spiky gold NPs
-OTs	tosylate	S_N2	bimolecular nucleophilic substitution
o/w	oil in water	SS	stainless steel
PA	polyamine	STEM	scanning transmission electron microscopy
PBS	phosphate buffer saline	<i>t</i>-BuO	<i>tert</i> -butoxyde
PCL	poly(ϵ -caprolactone)	TDC	tetradecane
PD	Parkinson's disease	TEA	triethylamine
PDA	polydopamine	TEM	transmission electron microscopy
PDI	polydispersity index	Temp.	temperature
PDMA	poly(dimethylaminoethyl methacrylate)	TFA	trifluoroacetic acid
PDMS	poly(dimethylsiloxane)	THF	tetrahydrofuran
PEG	polyethylene glycol chain	TLC	thin layer chromatography
PEO	polyethylene oxide	TRIS	tris(hydroxymethyl)aminomethane
PES	polyethersulphone	Tyr	tyrosine
PFA	paraformaldehyde	UV	ultraviolet
PI	polyimide	vs.	<i>versus</i>
PLGA	poly(lactic- <i>co</i> -glycolic acid)	WCA	water contact angle
PMMA	poly(methyl methacrylate)		

FORMULA INDEX



Formula Index



CHAPTER 1

GENERAL INTRODUCTION

“I think Nature’s imagination is so much greater than man’s, she’s never gonna let us relax!” – Richard Phillips Feynman

1.1. CATECHOLS IN NATURE¹

Catechols (cat) (*o*-dihydroxybenzene) are aromatic derivatives bearing two neighbouring (*ortho*-) hydroxyl groups that can be found in a wide variety of environments in nature because of their physicochemical versatility. Although the catechol is an apparently simple moiety, its chemistry is more complex and challenging than one could expect. The presence of two hydroxyl groups in adjacent positions makes this moiety ideal for bidentate coordination and hydrogen bonding either to metal ions, surfaces or other organic functional groups. In accordance with these range of functionalities, naturally occurring catechols perform a variety of functions and can exist either as simple molecular systems, forming part of supramolecular structures, coordinated to different metal ions, or, as macromolecules.² For example, catecholamine neurotransmitters, such as dopamine (DA), noradrenaline and adrenaline, occupy key positions in the regulation of physiological processes and the development of neurological, cardiovascular, psychiatric and endocrine diseases (Figure 1.1a).³ The health benefits of dietary polyphenolics present in wines, chocolate, tea, fruits and vegetables are related to their antioxidant properties, which reduce the risk of degenerative and chronic diseases.^{4,5} Siderophores are ones of the strongest soluble Fe³⁺ binding agents known compounds secreted by microorganisms (Figure 1.1b).² But among all of them, particularly relevant is the presence of the catecholic amino acid 3,4-dihydroxyphenyl-L-alanine (L-DOPA) in adhesive proteins of mussels (Figure 1.1c).

The strong underwater adhesion shown by some catechol-containing natural materials has attracted increasing attention during the last years and has become a source of inspiration for novel synthetic materials. Several marine organisms like mussels and sandcastle worms^{6,7} secrete proteinaceous substances that contain a high concentration of the catecholic amino acid L-DOPA, which has been directly associated to their strong adhesion to virtually any substrate.^{8,9} The role of the L-DOPA moiety in natural adhesives is two-fold: on one hand, it serves as anchor as it can adsorb onto surfaces by different mechanisms, such as metal bidentate coordination,^{10,11} π - π stacking, π -cation, or, electrostatic and hydrogen bonding.^{9,12} Besides, the oxidised DOPA-quinone form is formed readily at pH \sim 8.5 and enables chemical reaction with nucleophiles (*e.g.* thiols and amines). In addition, the presence of these multiple intermolecular interactions and the quinone can act as covalent cross-linkers providing cohesion to the adhesive.^{13,14,15}

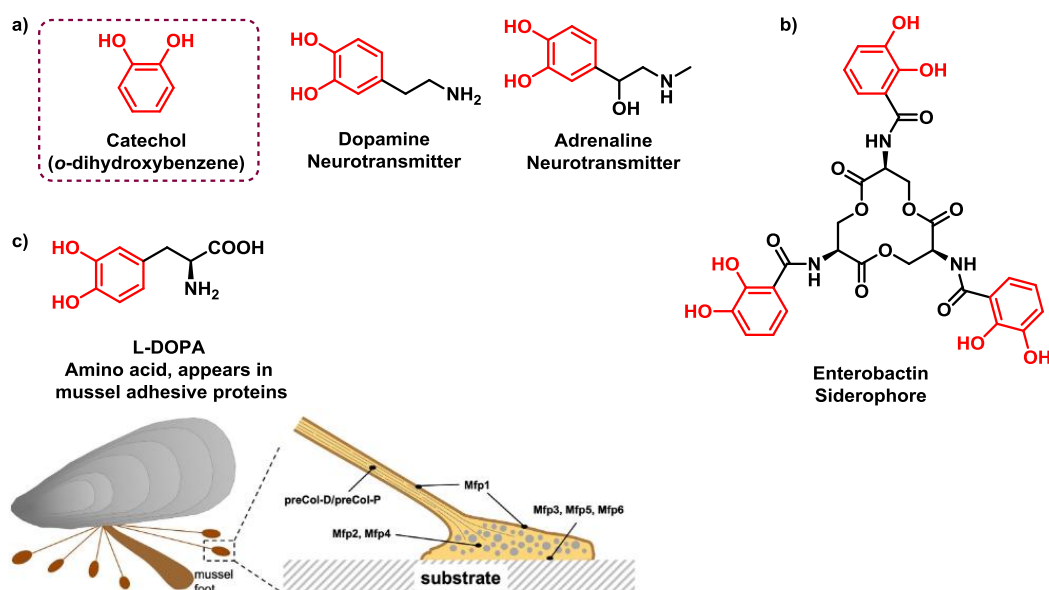


Figure 1.1. Chemical structures of a variety of natural catechol derivatives with different activities and functions. a) Catechol moiety, and DA and adrenaline neurotransmitters. b) Enterobactin, an Fe^{3+} chelating agent siderophore. c) L-DOPA amino acid present in mussel foot proteins (top). The mussel byssus. The core of the adhesive plaque consists of a porous complex coacervate with mussel foot proteins (mfps) with low L-DOPA concentrations (mpf 2, 4). Mfps at the adhesive interface (mpf 3, 5, 6) have high L-DOPA content.¹⁶

1.2. CHEMISTRY OF CATECHOLS

Most of the amazing properties of catechols previously described are attributed to their rich chemistry. However, fully understanding of it is still the subject of active study. Catechol moieties might exist in three possible oxidation states: the fully reduced catechol form, the semi-oxidised free-radical state called semiquinone and the completely oxidised form quinone. In the presence of an oxidant, the oxidation of catechol can occur spontaneously under mild basic conditions to give the corresponding semiquinone through a one-electron transfer and the quinone by a two electron process. Quinones are strong electrophiles and can react with nucleophilic moieties, such as amines, through Michael-type reactions or giving Schiff-base-type adducts (Figure 1.2),¹⁷ resulting in adhesion to wet surfaces.

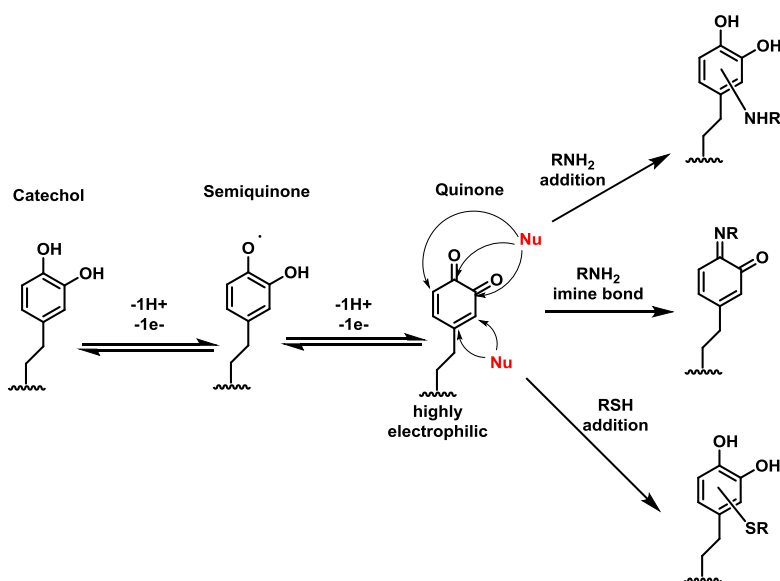


Figure 1.2. Redox activity and reactivity of the catechol group.

Moreover, the catechol group can physically interact with various organic/inorganic materials through metal coordination, π - π stacking, cation- π interaction, and hydrogen bonding, all of which are responsible for the mussel adhesion (Figure 1.3).¹⁸

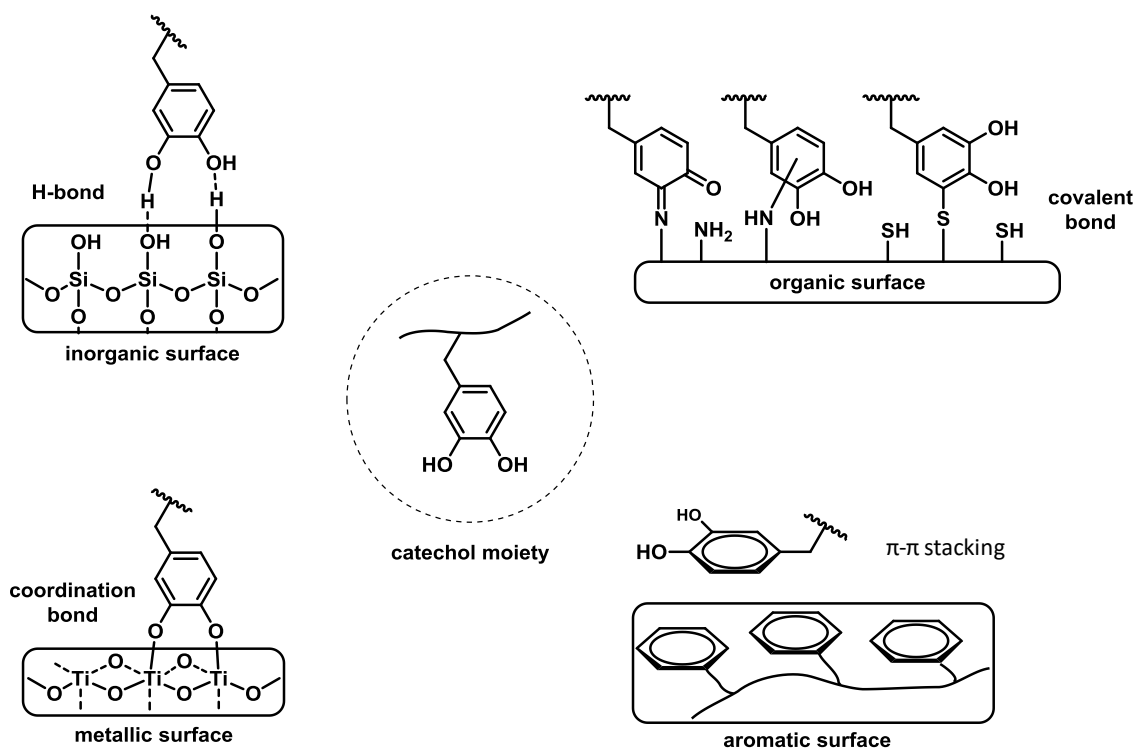


Figure 1.3. Typical interactions of catechols with different surfaces.¹⁹

Interestingly, there are a lot of studies about the role of the catechol moiety in the absorption processes, but none of them related with the amino group in the case of catechol materials that contain amines in their structures (e.g. DA, or, L-DOPA). It is suggested that amines can interact *via* ionic interactions with negatively charged surfaces,^{20,21} and through Michael-type

addition and Schiff-base formation can intermolecular cross-link with *o*-quinones.²² Therefore, having both catechol moiety and amino group would create a synergistic effect to reproduce the mussel's adhesive properties.²³

Nonetheless, the final adhesive properties of these materials also depend on whereas these catechol units are organised (i) as individual units, (ii) as self-assembled monolayers (SAMs), or (iii) as polymers. It is well known that catechol-based polymeric materials offer more robustness and effectiveness due to the synergic effect that exists between the catechol moieties. In fact, catechol-based polymers are the most extended studied and are explained below.

1.3. POLYMERISATION OF CATECHOLS

Synthetic catecholic polymers have been prepared through different routes and the three main approaches used are the following ones (Figure 1.4):

- **Approach I. Polymerisation through the catechol moiety.** It consists in polymerising catechol-based molecules through the aromatic ring, taking advantage on its ability to be oxidised under mild basic conditions and consequently to be attacked by nucleophiles. To date, this approach is the most followed one and it includes polydopamine (PDA) which is the most used catechol-based coating by excellence.
- **Approach II. Catechols grafted to polymeric backbones.** In this approach, catechol units are grafted into an already formed polymer, such it can be polysaccharides. Though less followed than the previous approach, several examples have been reported bringing novel features and a multidisciplinary character.
- **Approach III. Building blocks.** The polymerisation takes place through a functionality presents on the catechol (*e.g.* acrylate group). Although it is not a very exploited approach, it offers multiple advantages, such as higher functionalisation degree and synthetic control on the final structure.

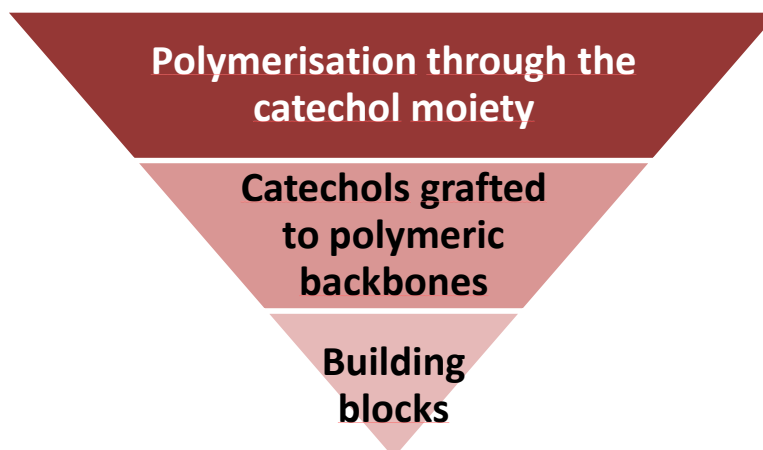


Figure 1.4. The three main approaches used to polymerise catechol-based molecules grouped in decreasing number of publications.

1.3.1. APPROACH I. POLYMERISATION THROUGH THE CATECHOL MOIETY

In this approach, the polymerisation of catechol-based compounds takes place through the aromatic ring of the catechol moiety. Among all the examples, the most prominent ones are (i) the self-polymerisation of DA²⁴ and (ii) the polymerisation between catechols and amines.²⁵

I. The self-polymerisation of dopamine

It always implies oxidation of the catechol moiety, and PDA is mainly obtained by 3 methods:

- Electropolymerisation.
- Enzymatic oxidation.
- Auto-oxidation of DA by air in a basic aqueous buffer, which is the most widely used strategy due to its simplicity (one-pot preparation).²⁶

Finally, depending on the preparation mode and the post-functionalisation, a wide range of PDAs can be obtained with different compositions, chain lengths and connectivity and all this allows tailoring the properties of the resultant products.²⁴

With regard to the structure of PDA and although there is a controversial issue, tentatively it can be said that it is made of 5,6-dihydroxyindole oligomers (Figure 1.5).

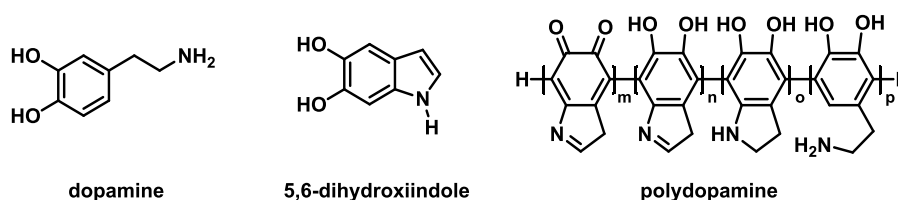


Figure 1.5. Chemical structure of DA, 5,6-dihydroxyindole and representative model for PDA structural components.²⁷

Actually, PDA may also bear DA units and indole moieties covalently linked, wherein catechol moieties can exist in different oxidation states. In 2012 Hong *et al.* reported that covalent polymerisation and non-covalent self-assembly occur during PDA formation.²⁸

PDA possesses many properties such as good biocompatibility, strong and robust cohesion properties, simple preparation processes, and easy functionalisation due to the presence of many reactive groups that allows obtaining several multifunctional materials. In fact, it is the most widely reported catecholamine coating and came into the focus of organic chemistry and material science in 2007 when Lee *et al.* reported that under mildly alkaline conditions, aqueous dopamine was able to form polymeric coatings on virtually all tested substrates.²⁴ Due to these interesting characteristics, the interest for PDA has significantly increased in recent years, mainly in biology, environmental (water purification, oil-water separation...), material science, surface engineering, catalysis (chemo- and photocatalysis), energy (batteries and supercapacitors),²⁹ and biomedicine. Specially, relevant examples in biomedicine are biosensing, bioimaging,³⁰ antibiosis, and cancer theranostics.^{31,32} For instance, Han *et al.* prepared a core-shell nanocomposite consisting of PDA nanoparticle (NP) cores and cancer-specific photosensitisers (PS)-conjugated hyaluronan shells (PHPD-NPs) to overcome the low selectivity for tumour sites and undesirable photo-activation for photothermal therapy (PTT).³³ The tumour specificities of the PHPD-NPs were continuously monitored by *in vivo* image station. The fluorescence signals from the tumour site were steadily increased over time (till 5 h post-injection), whereas in the normal tissue, a slight fluorescence signal increase was observed during the experimental period (Figure 1.6).

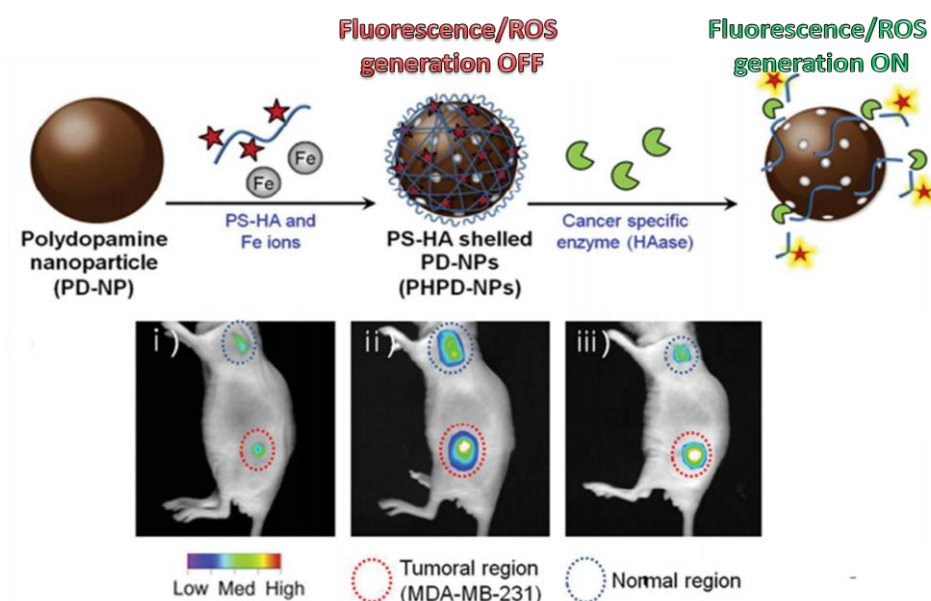


Figure 1.6. Preparation process of photosensitizer-hyaluronic acid conjugates shielded PDA NPs (PHPD-NPs) and their photo-activity on-off control and *in vivo* tumour target specificity studies (bottom) in tumour-bearing mice: (i) 10 min post-injection, (ii) 2 h post-injection, (iii) 5 h post-injection images.³³

Furthermore, Nam *et al.* demonstrated that PTT combined with chemotherapy can trigger potent anti-tumor immunity against disseminated tumors.³⁴ Specifically, they developed PDA-coated spiky gold NPs (SGNPs) as a new photothermal agent with extensive photothermal stability and efficiency (Figure 1.7).

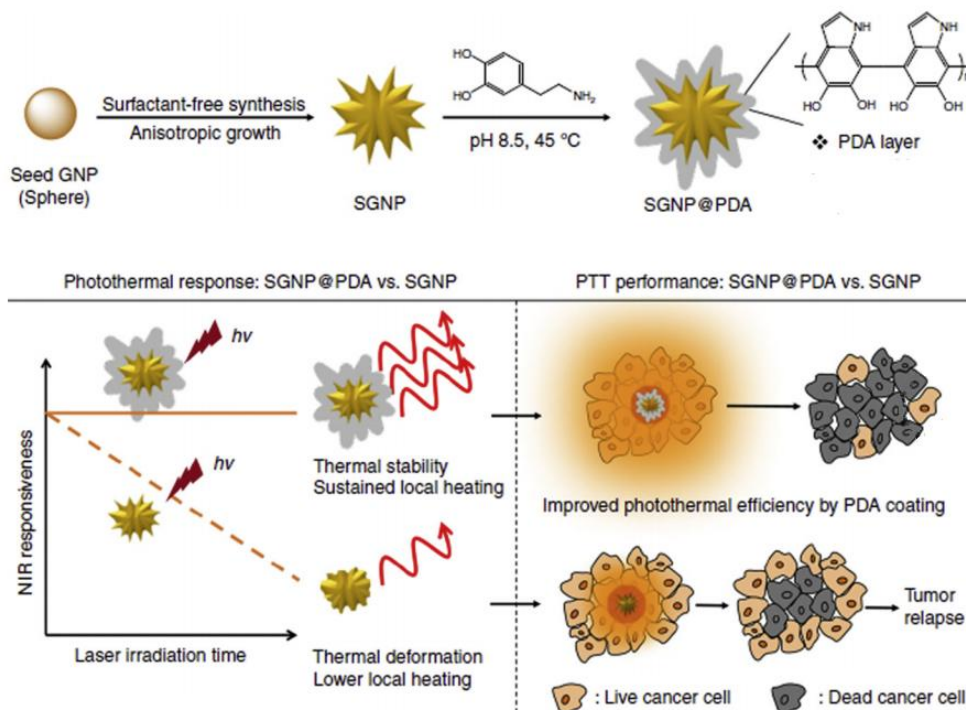


Figure 1.7. Schematic illustration of the development of SGNPs coated with PDA as a new photothermal agent with extensive photothermal stability and efficiency (top). The combination chemo-photothermal therapy triggered potent anti-tumor immunity in vivo and exerted strong anti-tumor efficacy against local primary tumors.³⁴

II. Polymerisation between catechols and amines

Our research groups followed a new approach, mimicking PDA, based on the use of ammonia to act as a nucleophile on the reactive *o*-quinones thus formed under basic aqueous media (Figure 1.8a)²⁵ in the presence of oxygen. In this way already functionalised monomers can be used to avoid the post-functionalisation (like happens with PDA). Nanomaterials for water treatment,³⁵ or, coatings that confer oleo-/hydrophobic character²⁵ and drug release alternatives³⁶ have been obtained. More recently, it has also been demonstrated that bis-amino groups would represent a milder alternative to ammonia (Figure 1.8b).³⁷ This design ensured both a robust *-i.e.* non-hydrolysable- attachment of the functional moiety to the catechol ring, and an accurate control of the degree of functionalisation of the final material.

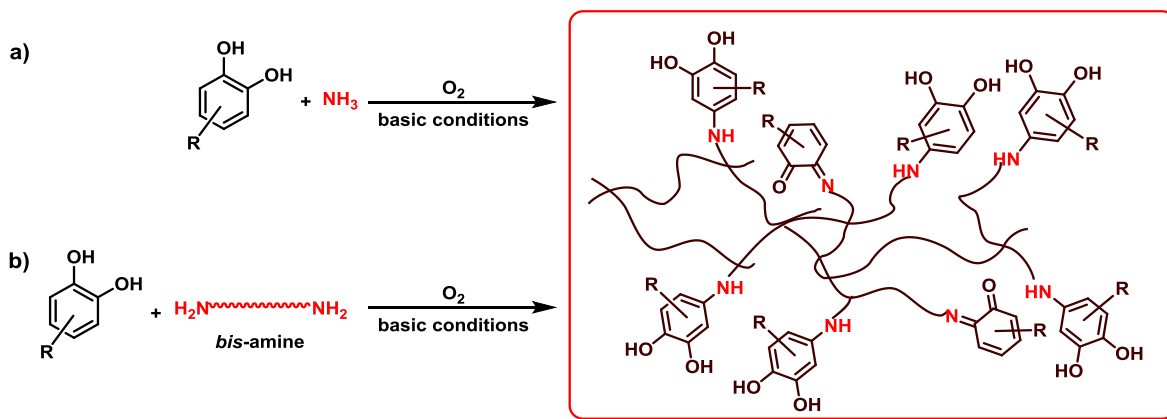


Figure 1.8. Polymerisation of catechol-based compounds with nitrogen-based molecules *via* Michael-type reaction, or, Schiff-base formation.

Nevertheless, despite the successful results reported, this approach exhibits some drawbacks. First, the dark-brown/black colour associated to PDA or its analogues is not suitable for certain applications.²³ Second, the high waste of the precursor material when polymerisation takes place in solution, leading with poor practical applications.³² Third, the difficult control of post-functionalisation, which relies on the existence of a sufficient amount of reactive groups in the primer coating that cannot be controlled, or, the long synthetic route to afford the respective catecholic derivatives, comprising protection/deprotection of the catechol ring. And finally, the impossibility to elucidate the final structure of PDA and its analogues because complicated redox reactions are involved and a series of intermediates are produced. All this has evoked the need to find other methodologies with better synthetic control.

1.3.2. APPROACH II. CATECHOLS GRAFTED TO POLYMERIC BACKBONES

This approach is very common to prepare adhesives and it consists in functionalising polymers, such as polysaccharides or peptides, with catechol units that bear reactive groups (Figure 1.9).^{38,39} Thus, the catechol moiety does not undergo any structural change as experienced in PDA.

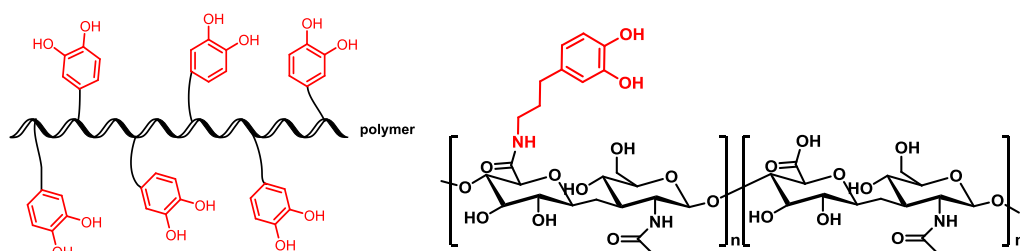


Figure 1.9. Schematic illustration of a polymeric backbone functionalised with catechols (left) and real dopamine-hyaluronic acid (DA-HA) conjugate (right).⁴⁰

This approach is of special relevance in medical science, since biomaterials need to present biocompatibility, stability, and non-toxicity.^{41,42,43,44} During the last years, a variety of mussel-inspired polymer adhesives have drawn much attention because of their unique wet-resistant adhesion properties in addition to the biological requirements previously described.^{2,45,46} For instance, catechol-modified chitosans (CHTs) have been used to fabricate antifouling coatings with excellent biocompatibility onto polyethersulphone (PES) ultrafiltration membranes.⁴⁷ Furthermore, using layer-by-layer (LBL) technique a lot of freestanding multilayer films have been formed based on (i) CHT and DA-modified hyaluronic acid (HA), which present an enhanced cell adhesion, proliferation and viability,⁴⁰ and (ii) CHT, DA-modified HA and bioactive glass nanoparticles (BGNPs) with high potential to be used in guided tissue regeneration applications, due to their bioactive behaviour necessary for the formation of new bone, enhanced adhesion and tuneable properties.^{48,49,50} Moreover, chitooligosaccharides (COS) based on catechol and PEG moieties were used as multidentate ligand (ML) for preparing robust biocompatible magnetic iron oxide nanoparticles (IONPs) useful for magnetic resonance imaging under physiological conditions (Figure 1.10a).^{51,52} Besides, taking advantage on the ability for self-organising complexes with HA and PDA, some protein drug carriers have been developed and investigated.⁵³ Finally, beyond working with CHTs, dextrans have been also modified with catechols for antifouling surface coatings,⁵⁴ and DA-HA conjugates have been used to coat commonly used implantable substrates making them resistant to both non-specific protein adsorption and cell adhesion on the surfaces (Figure 1.10b).⁵⁵ Therefore, as already demonstrated, this approach turns out really successfully to obtain bio-adhesives using different phenolic moieties into commercially available synthetic polymers.^{56,57,58,59} However, when specific functionalities need to be incorporated into the material, the catecholic polymers often have to be synthesised from simple building blocks.

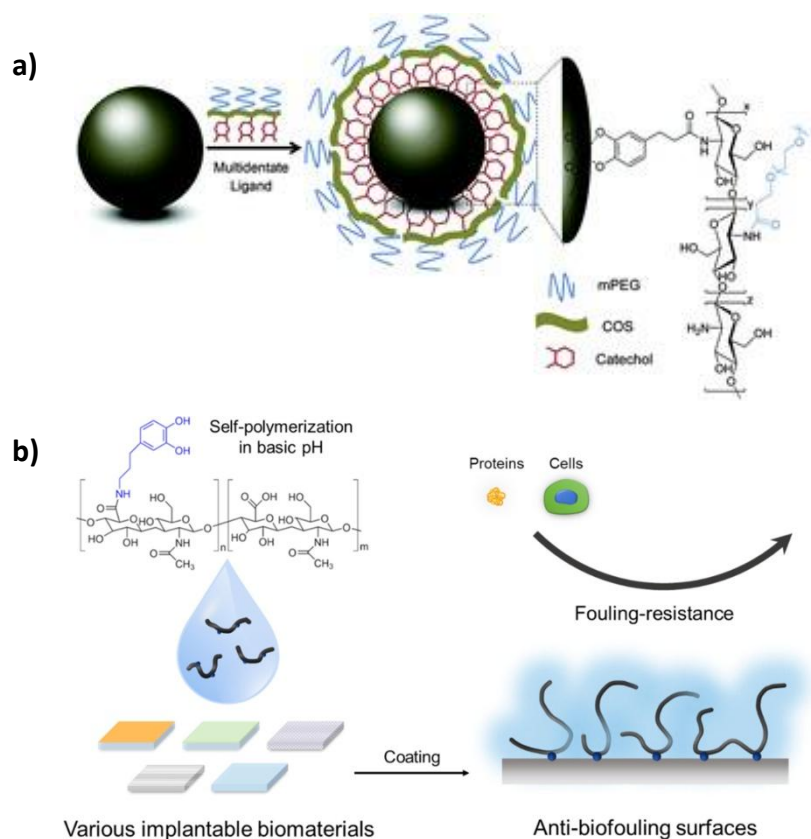


Figure 1.10. a) Stabilisation and functionalisation of hydrophobic IONPs with a COS based ML.⁵¹ b) Schematic of DA-HA-coating for anti-biofouling. Commonly used biomaterials (polyimide (PI), Au, poly(methyl methacrylate) (PMMA), polytetrafluoroethylene (PTFE), and polyurethane (PU)) for implantation were tested for DA-HA coating and evaluation of the coating effects on biofouling-resistant properties.⁵⁵

1.3.3. APPROACH III. BUILDING BLOCKS

This approach consists in polymerising catechol-based molecules through a reactive pendent group (*e.g.* styrenic, acrylate, *N*-carboxyanhydride...), thus the catechol ring does not suffer any kind of oxidation reaction and remains unaffected. Although significant research has focused on using natural building blocks to form functional materials (Figure 1.11),^{60,61,62,63} the synthesis of synthetic phenols allows for a limitless variety of possibilities.

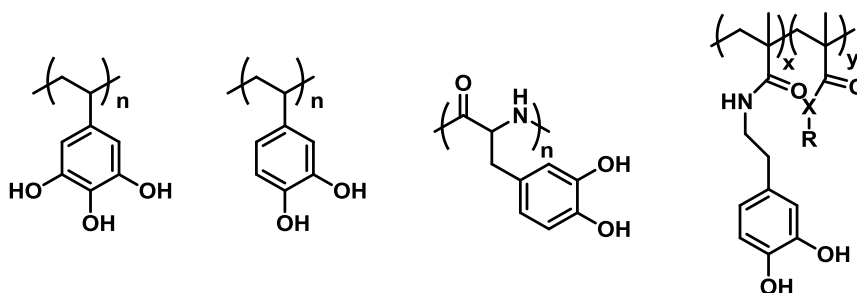


Figure 1.11. Examples of synthetic building blocks: polygallol and polycatechols.

A prototype example is dopamine methacrylamide (DMA) (Figure 1.12). DMA has been copolymerised with various co-monomers such as 2-methoxyethyl acrylate⁶⁴ and aminoethyl methacrylamide⁶⁵ to allow adhesion under wet conditions and for DNA immobilisation, respectively.

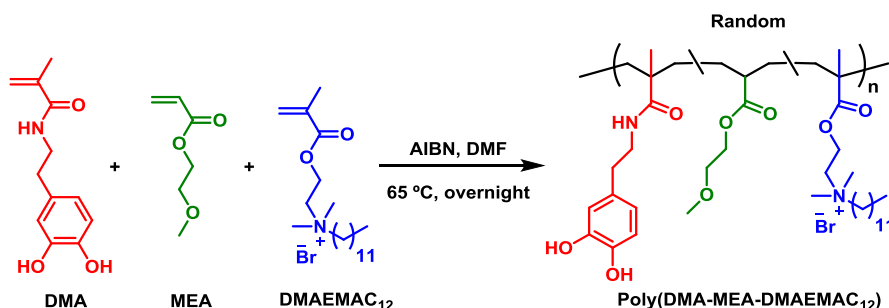


Figure 1.12. Synthesis of antimicrobial random copolymers including catechol and ammonium units, obtained from polymerisation of acrylamide and acrylate derivatives.⁶⁶

Other examples include grafted brushes for antifouling applications with fluorine-containing polymers, such as poly(2,2,3,3,3-pentafluoropropyl acrylate),⁶⁷ and the incorporation of glycopolymer-based monomers to mimic the immunogenic properties of natural pathogens.⁶⁸ Moreover, host-guest chemistry can be incorporated into DMA systems with an adamantyl co-monomer, thereby allowing for reversible adhesion.⁶⁹ Beyond using methacrylamide groups, catechol-containing acrylamides have been copolymerised with fluoropolymers to create superamphiphobic fabrics and halloysite nanotubes (HNT),^{70,71} and with polyethylene glycol (PEG) derivatives to obtain antifouling coatings.⁷² Furthermore, catechol-based methacrylates have been used to generate micelles for drug delivery,⁷³ and have been copolymerised with PEG-methacrylates affording favourable coatings on various surfaces with excellent antifouling behaviour.⁷⁴

Another well-studied monomer is the commercially available 3,4-dimethoxystyrene. The use of this monomer led to poly[(3,4-dihydroxystyrene)-*co*-styrene] being synthesised, and its adhesive properties have been studied under various conditions.^{75,76} A homopolymer of 3,4-dimethoxystyrene⁷⁷ was accessed through reversible addition fragmentation chain-transfer (RAFT) polymerisation, and upon demethylation, the free catechol moieties were investigated for their metal-binding capacity, which was independent of molecular weight. *N*-carboxyanhydride ring opening polymerisation has been used to obtain ultra-low fouling mussel-inspired charged polypeptides⁷⁸ with exceptional infection-resistant coating on medical catheters.⁷⁹ In addition, through carbodiimide mediated polyesterification several hydrophobic polyester adhesives containing catechol moieties have been synthesised with excellent lap-shear strength and resistance to water penetration,⁸⁰ and *via* anionic ring opening

polymerisation using catechol-functionalised epoxides, PEG-based block copolyethers have been obtained with superior antifouling properties (Figure 1.13),⁸¹ and have been used to coat CdSe quantum dots (QDs) and TiO₂ nanoparticles individually as well as both materials together in a complex hybrid structure.⁸²

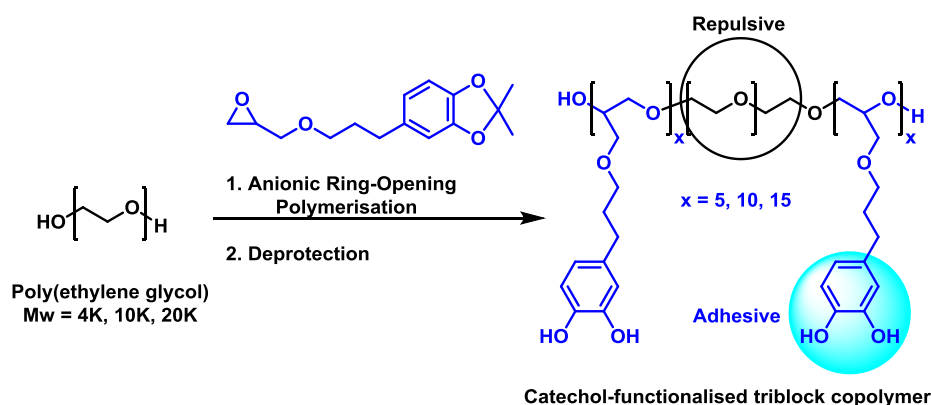


Figure 1.13. Synthetic scheme of catechol-functionalised triblock copolymers.⁸¹

This approach has also been helpful to explore the structure-function relationships between the components of synthetic phenolic polymers. For example, a fundamental study on the polarity of the backbone has shown additional complexity in underwater adhesion.⁸³ Other investigations into redox-active catechol-based polymers have shown performance effects for electrochemical energy storage.⁸⁴ Furthermore, switching from catechol to gallol moieties changes the properties, for example, the underwater adhesion of a polymer can be increased seven-fold.⁸⁵

To conclude, this approach is very promising. It allows incorporating several functionalities into phenolic materials, and it is gained a higher control on the structure of the resulting polymers, but with few examples so far reported. Therefore, the syntheses of novel approaches that fully exploit the advantages of this approach are strongly required.

1.4. A NOVEL POLYMERISATION STRATEGY BASED ON SULPHUR CHEMISTRY

In order to achieve that, in this Doctoral Thesis a new building block that includes (i) a catechol moiety (in green), (ii) a polymerisation unit based on pentaerythritol tetrakis(3-mercaptopropionate) (in red), (iii) and a functional group with a property to be conferred (in blue) has been designed (Figure 1.14).

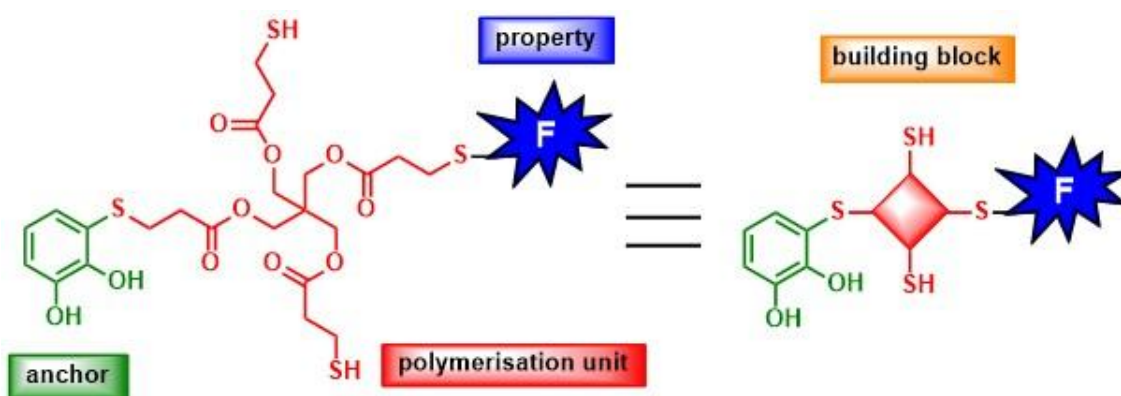


Figure 1.14. Schematic representation of the designed building block containing the catechol unit (in green), the polymerisation unit (in red) and the functional group (F) (in blue) used in this Thesis.

The basic scaffold for the modular design of all monomers reported in this Thesis is pentaerythritol tetrakis(3-mercaptopropionate) **1**, a cross-linking agent widely used in commercial coatings, adhesives, and sealants. The presence of four thiol end-groups in this compound allows for the simultaneous incorporation of a catechol ring and a functional group, and two free thiols remain for further polymerisation. The overall synthetic strategy would rely on the use of three different coupling reactions:

1. Adsorption

The nucleophilic addition of thiol groups to *o*-benzoquinone (as prepared *in situ* from cheap, commercial pyrocatechol) would be used to conjugate the catechol moiety to the thiol-functionalised scaffold **1**, following a reported procedure of our research group for the functionalisation of *o*-benzoquinone with functional mono-thiols, with slight modifications (Figure 1.15).⁸⁶

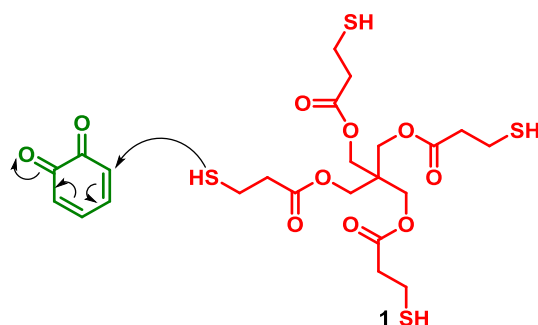


Figure 1.15. 1,6-conjugated addition of a thiol group to quinone.

For this, inspiration was drawn from the alleged role of free thiol groups of cysteine (Cys) residues in mfps, which are thought to bind to *o*-quinone moieties arising from the spontaneous oxidation of catecholic moieties in tyrosine (Tyr) residues. This conjugation effectively cross-links the protein, while at the same time restore the catecholic/adhesive function.⁸⁷ Although thiol-catechol conjugation had previously been used for synthetic

purposes to cross-link polymers,⁸⁸ the formation of catechol-based polymers through the formation of -S-S- bonds is completely new.

2. Functionality

Thiol-ene reactions would be used to bind functional moieties bearing terminal vinyl groups. The number of functional groups that can be used here is countless, but for the present Doctoral Thesis it was decided to use, as a proof-of-concept, those shown in Figure 1.16. Three PEG chains to provide stability in aqueous environments, biocompatibility and targeting onto NPs for bioapplication purposes; long aliphatic and partially fluorinated chains to change the wettability of macroscopic surfaces; and a fluorescent tag to demonstrate the modular chemistry of the new strategy proposed.

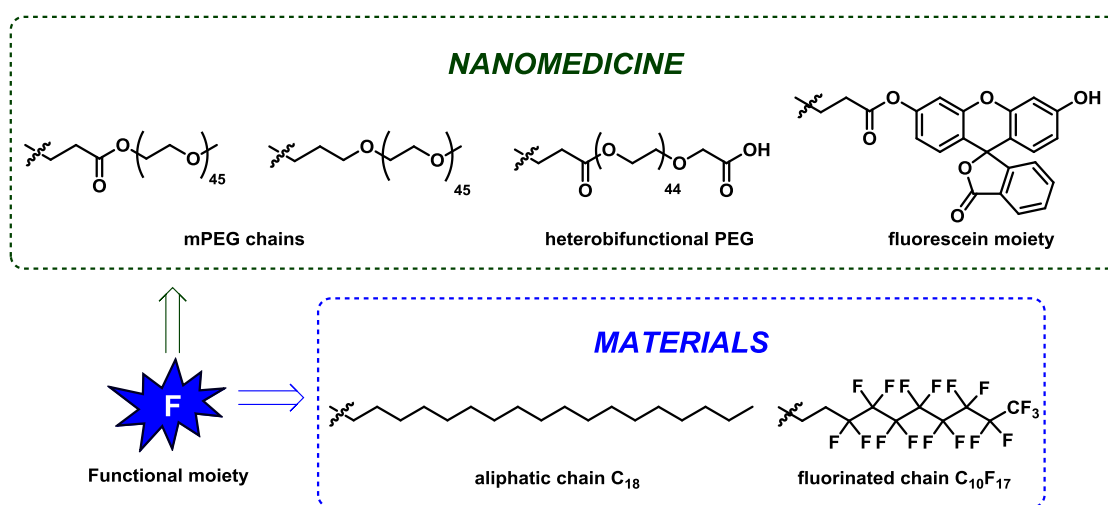


Figure 1.16. Molecular structures of the six functional groups (F) used in this toolkit. PEG chains and a fluorescein derivative would be used for some bioapplications in the nanomedicine field, whereas aliphatic and fluorinated chains would be used in materials field as oleo-/hydrophobic coatings.

3. Polymerisation

It is expected to be effected by coupling of the remaining, un-substituted thiol groups into disulphide bridges (Figure 1.17). Advantage is taken of the key fact that the oxidative coupling may be carried out in very mild and selective conditions -particularly, without need to protect the catechol moieties-, by using iodine.

This polymerisation reaction will be always carried out with a 3-5% of a doping catechol-functionalised tris-thiol molecule **4**. These doping agents could trigger the reticulation of the resulting polymers making them insoluble in the reaction medium and facilitate their isolation.

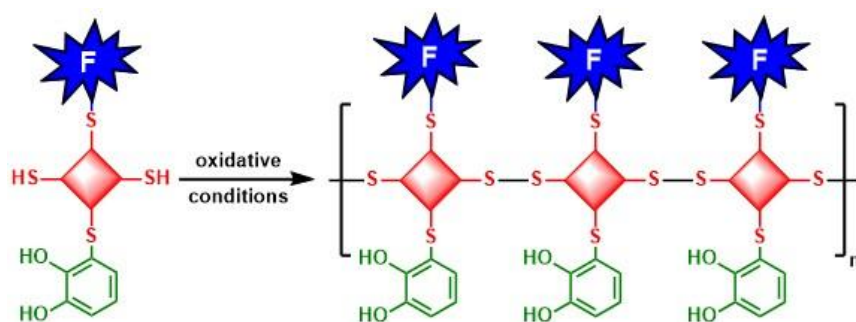


Figure 1.17. Schematic representation of how the polymerisation could take place by forming disulphide bonds through the core of the building block (in red), maintaining the catechol unit unchanged.

1.4.1. SYNTHETIC METHODOLOGIES

Regarding the synthesis of the building blocks, specifically, two different strategies would be tested (Figure 1.18). In the first one (route A), the conjugate addition of the tetrakis-thiol **1** to freshly prepared *o*-benzoquinone **3** could afford the monosubstituted S-catechol tris-thiol **4**, which after purification would react with a vinyl-terminated functional moiety *via* a radical-catalysed thiol-ene reaction to yield the desired S-catechol-functionalised bis-thiol **I**. By following the second strategy (route B), the reversal of the two aforementioned synthetic steps would provide first a functionalised tris-thiol scaffold **II**, which would be subsequently conjugated to *o*-benzoquinone **3** to yield the corresponding functional catechol monomer **I**. Although both strategies offer the same optimal atom efficiency on paper, route A was initially preferred on a general basis because it requires the optimisation of a single conjugate addition, yielding a common catechol tris-thiol intermediate which may be then used as a common gateway to any functional monomer. Route B, however, involves the optimisation of both synthetic steps for each functional derivative, so it would be only used for specific cases when it afforded a higher overall yield.

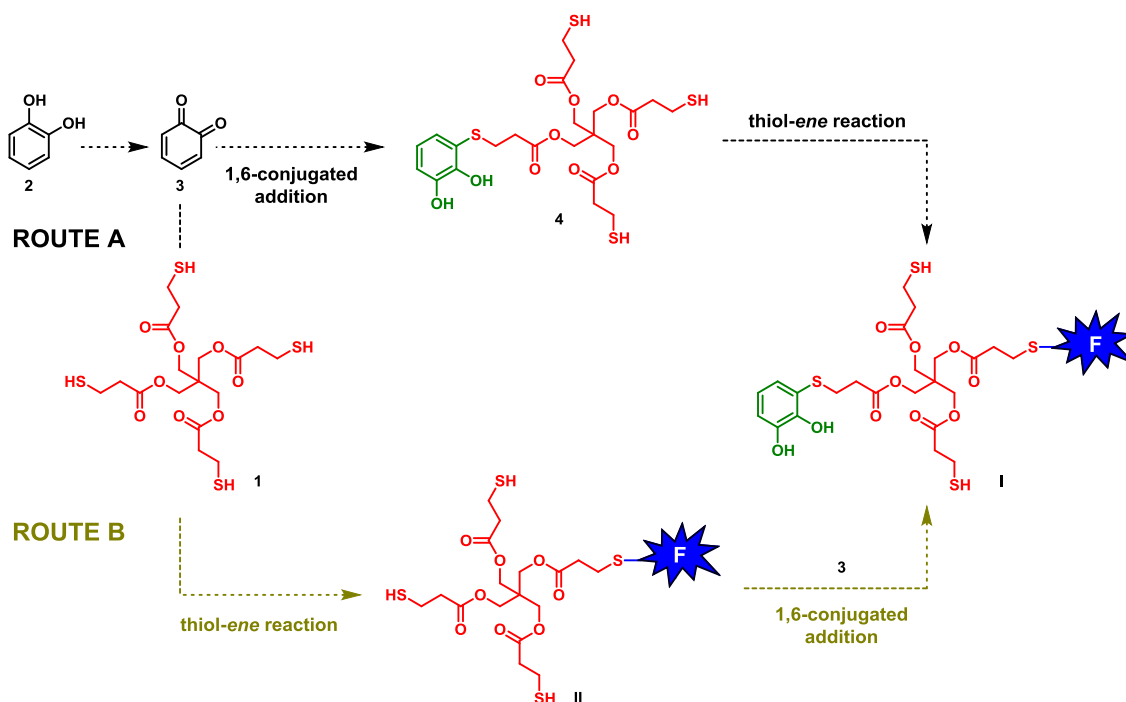


Figure 1.18. Schematic synthetic routes A and B to obtain S-catechol functionalised bis-thiols I.

1.4.2. SYNTHETIC ADVANTAGES

The advantages provided by this synthetic strategy are potentially manifold:

- I. It provides a robust aryl-thioether bond between the functional moiety and the catechol ring.
- II. The catechol moiety is spontaneously regenerated by tautomerism right after the thiol-quinone conjugation.
- III. This modular strategy could allow incorporating different functionalities depending on the final purpose using a unified methodology.
- IV. The synthesis is cost-efficient and its atom efficiency is optimal, thanks to the fact that there are no protection/deprotection steps, as well as to the use of readily available pyrocatechol as starting material.
- V. Because of the negligible mesomeric effect of the sulphur atom directly attached to the aromatic ring, the charge density on the ring of the catechol-thioether conjugate should be comparable to that of the parent pyrocatechol, making both roughly equally stable to oxidation.
- VI. The structure of the monomers, with both a catechol moiety and (at least) two thiol groups in their structure, opens up the possibility to effect polymerisation through a reversible mechanism by forming disulphide bonds. In particular, disulphide bridging of the main polymeric backbone should make such polymers biodegradable.

As far as the polymerisation strategy is concerned, it has been designed for:

- I. Obtaining non-coloured polymers with known linear structures. This polymerisation strategy was designed to get a better synthetic control on the structure of the resulting polymers, and to obtain them colourless, what would be a very important feature for some applications, mainly in materials' field, since the coated surfaces would not change their appearance.
- II. Being versatile and chemically modular to get control of the functionality or a combination of them.
- III. Obtaining biocoatings thanks to the presence of PEG chains.

To sum up, in this Doctoral Thesis a novel catechol-based toolkit is proposed for coating and changing the wettability of surfaces.

1.5. REFERENCES

- ¹ Guardingo, M. Doctoral Thesis, Universitat Autònoma de Barcelona, **2015**.
- ² Sedó, J.; Saiz-Poseu, J.; Busqué, F.; Ruiz-Molina, D. *Adv. Mater.* **2013**, *25*, 653-701.
- ³ Eisenhofer, G.; Kopin, I. J.; Goldstein, D. S. *Pharmacol. Rev.* **2004**, *56*, 331-349.
- ⁴ Quideau, S.; Deffieux, D.; Douat-Casassus, C.; Pouységu, L. *Angew. Chem. Int. Ed.* **2011**, *50*, 586-621.
- ⁵ Pandey, K. B.; Rizvi, S. I. *Oxid. Med. Cell. Longev.* **2009**, *2*, 270-278.
- ⁶ Stewart, R. J.; Weaver, J. C.; Morse, D. E.; Waite, J. H. *J. Exp. Biol.* **2004**, *207*, 4727-4737.
- ⁷ Waite, J. H.; Jensen, R. A.; Morse, D. E. *Biochemistry* **1992**, *31*, 5733-5738.
- ⁸ Papov, V. V.; Diamond, T. V.; Biemann, K.; Waite, J. H. *J. Bio. Chem.* **1995**, *270*, 20183-20192.
- ⁹ Anderson, T. H.; Yu, J.; Estrada, A.; Hammer, M. U.; Waite, J. H.; Israelachvili, J. N. *Adv. Func. Mater.* **2010**, *20*, 4196-4205.
- ¹⁰ Li, S. C.; Chu, I. N.; Gong, X. Q.; Diebold, U. *Science* **2010**, *328*, 882-884.
- ¹¹ Mcbrlde, M. B.; Wessellnk, L. G. *Environ. Sci. Technol.* **1988**, *22*, 703-708.
- ¹² Waite, J. H.; Housley, T. J.; Tanzer, M. L. *Biochemistry* **1985**, *24*, 5010-5014.
- ¹³ Burzio, L. A.; Waite, J. H. *Biochemistry* **2000**, *39*, 11147-11153.
- ¹⁴ Yu, M.; Hwang, J.; Deming, T. J. *J. Am. Chem. Soc.* **1999**, *121*, 5825-5826.
- ¹⁵ Yu, J.; Wei, W.; Menyo, M. S.; Masic, A.; Waite, J. H.; Israelachvili, J. N. *Biomacromolecules* **2013**, *14*, 1072-1077.
- ¹⁶ Balkenende, D. W. R.; Winkler, S. M.; Messersmith, P. B. *Eur. Polym. J.* **2019**, *116*, 134-143.

-
- ¹⁷ Abul-Hajj, Y. J.; Tabakovic, K.; Gleason, W. B.; Ojala, W. H. *Chem. Res. Toxicol.* **1996**, *9*, 434-438.
- ¹⁸ Chen, T.; Yang, M.; Yang, H.; Wang, R.; Wang, S.; Zhang, H.; Zhang, X.; Zhao, Z.; Wang, J. *J. Ind. Eng. Chem.* **2019**, *69*, 179-186.
- ¹⁹ Lyu, Q.; Hsueh, N.; Chai, C. L. *ACS Biomater. Sci. Eng.* **2019**, *5*, 2708-2724.
- ²⁰ Suci, P. A.; Geesey, G. G. *J. Colloid Interface Sci.* **2000**, *230*, 340-348.
- ²¹ Olivieri, M. P.; Wollman, R. M.; Hurley, M. I.; Swartz, M. F. *Biofouling* **2002**, *18*, 149-159.
- ²² Lee, H.; Scherer, N. F.; Messersmith, P. B. *Proc. Natl. Acad. Sci. U.S.A.* **2006**, *103*, 12999-13003.
- ²³ Hu, H.; Dyke, J. C.; Bowman, B. A.; Ko, C.-C.; You, W. *Langmuir* **2016**, *32*, 9873-9882.
- ²⁴ Lee, H.; Dellatore, S. M.; Miller, W. M.; Messersmith, P. B. *Science*, **2007**, *318*, 426-430.
- ²⁵ Saiz-Poseu, J.; Sedó, J.; García, B.; Benaiges, C.; Parella, T.; Alibés, R.; Hernando, J.; Busqué, F.; Ruiz-Molina, D. *Adv. Mater.* **2013**, *25*, 2066-2070.
- ²⁶ Liu, Y.; Ai, K.; Lu, L. *Chem. Rev.* **2014**, *114*, 5057-5115.
- ²⁷ Liebscher, J.; Mrowczynski, R.; Scheidt, H. A.; Filip, C.; Hadade, N. D.; Turcu, R.; Bende, A.; Beck, S. *Langmuir* **2013**, *29*, 10539-10548.
- ²⁸ Hong, S.; Na, Y. S.; Choi, S.; Song, I. T.; Kim, W. Y.; Lee, H. *Adv. Funct. Mater.* **2012**, *22*, 4711-4717.
- ²⁹ Huang, Q.; Chen, J.; Liu, M.; Huang, H.; Zhang, X.; Wei, Y. *Chem. Engin. J.* **2020**, *387*, 124019-124034.
- ³⁰ Wu, L.; Zhang, F.; Wei, Z.; Li, X.; Zhao, H.; Lv, H.; Ge, R.; Ma, H.; Zhang, H.; Yang, B.; Li, J.; Jiang, J. *Biomater. Sci.* **2018**, *6*, 2714-2725.
- ³¹ Farokhi, M.; Mottaghitalab, F.; Saeb, M. R.; Thomas, S. *J. Control. Release* **2019**, *309*, 203-219.
- ³² Xiao, Y.; Chen, L.; Chen, X.; Xiao, B. *J. drug target.* **2020**, *28*, 142-153.
- ³³ Han, J.; Wooram, P.; Sin-jung, P.; Na, K. *ACS Appl. Mater. Inter.* **2016**, *12*, 7739-7747.
- ³⁴ Nam, J.; Son, S.; Ochyl, L. J.; Kuai, R.; Schwendeman, A.; Moon, J. *Nat. Commun.* **2018**, *9* (1), 1074-1086.
- ³⁵ García, B.; Saiz-Poseu, J.; Gras-Charles, R.; Hernando, J.; Alibés, R.; Novio, F.; Sedó, J.; Busqué, F.; Ruiz-Molina, D. *ACS Appl. Mater. Inter.* **2014**, *6*, 17616-17625.
- ³⁶ Nador, F.; Guisasola, E.; Baeza, A.; Moreno-Villaécija, M. A.; Vallet-Regí, M.; Ruiz-Molina, D. *Chem-Eur. J.* **2017**, *23*, 2753-2758.
- ³⁷ Suárez-García, S.; Sedó, J.; Saiz-Poseu, J.; Ruiz-Molina, D. *Biomimetics* **2017**, *2* (4), 22.
- ³⁸ Hong, S. H.; Ryu, J. H.; Lee, H. *J. Ind. Eng. Chem.* **2019**, *79*, 425-430.

- ³⁹ Campelo, C. S.; Chevallier, P.; Loy, C.; Vieira, R. S.; Mantovani, D. *Macromol. Biosci.* **2020**, *20*, 1900253-1900263.
- ⁴⁰ Neto, A. I.; Cibrão, A. C.; Correia, C. R.; Carvalho, R. R.; Luz, G. M.; Ferrer, G. G.; Botelho, G.; Picart, C.; Alves, N. M.; Mano, J. F. *Small* **2014**, *10*, 2459-2469.
- ⁴¹ Jayakumar, R.; Nwe, N.; Tokura, S.; Tamura, H. *Int. J. Biol. Macromol.* **2007**, *40*, 175-181.
- ⁴² Kim, S. E. Song S.-H.; Yun Y. P.; Choi B.-J.; Kwon I. K.; Bae M. S.; Moon H.-J.; Kwon Y.-D. *Biomaterials* **2011**, *32*, 366-373.
- ⁴³ Junter, G.-A.; Thebault, P.; Lebrun, L. *Acta Biomater.* **2016**, *30*, 13-25.
- ⁴⁴ Campelo, C. S. Chevallier, P.; Vaz, J. M.; Vieira, R. S.; Mantovani, D. *Mater. Sci. Eng. C* **2017**, *72*, 682-691.
- ⁴⁵ Lee, B. P; Messersmith, P. B.; Israelachvili, J. N.; Waite, J. H. *Annu. Rev. Mater. Res.* **2011**, *41*, 99-132.
- ⁴⁶ Phuong, P. T. M.; Won, H. J.; Oh, Y. J.; Lee, H. S.; Lee, K. D.; Park, S. Y. *J. Ind. Eng. Chem.* **2019**, *80*, 749-756.
- ⁴⁷ Wang, R.; Xie, Y.; Xiang, T.; Sun, S.; Zhao, C. *J. Mater. Chem. B*, **2017**, *5*, 3035-3046.
- ⁴⁸ Rodrigues, J. R.; Alves, N. M.; Mano, J. F. *RSC Adv.* **2016**, *6*, 75988-75999.
- ⁴⁹ Moreira, J.; Vale, A. C.; Pires, R. A.; Botelho, G.; Reis, R. L.; Alves, N. M. *Molecules* **2020**, *25*, 840-870.
- ⁵⁰ Almeida, A. C.; Vale, A. C.; Pires, R. A.; Reis, R. L.; Alves, N. M. *J. Biomed. Mater. Res. Part B Appl. Biomater.* **2020**, *108*, 1412-1427.
- ⁵¹ Lu, C.; Park, M. K.; Lu, C.; Lee, Y. H.; Chai, K. Y. *J. Mater. Chem. B* **2015**, *3*, 3730-3737.
- ⁵² Stephen, Z. R.; Dayringer, C. J.; Lim, J. J.; Revia, R. A.; Halbert, M. V.; Jeon, M.; Bakthavatsalam, A.; Ellenbogen, R. G.; Zhang, M. *ACS Appl. Mater. Inter.* **2016**, *8*, 6320-6328.
- ⁵³ Lim, D. G.; Prim, R. E.; Kang, E.; Jeong, S. H. *Int. J. Pharm.* **2018**, *542*, 288-296.
- ⁵⁴ Jeong, Y.; Kim, K.-A.; Kang, S. M. *Polymers* **2017**, *9*, 376-383.
- ⁵⁵ Lee, S.; Kim, S.; Park, J.; Lee, J. Y. *Int. J. Biol. Macromol.* **2020**, *151*, 1314-1321.
- ⁵⁶ Lee, B. P.; Dalsin, J. L.; Messersmith, P. B. *Biomacromolecules* **2002**, *3*, 1038-1047.
- ⁵⁷ Su, J.; Chen, F.; Cryns, V. L.; Messersmith, P.B. *J. Am. Chem. Soc.* **2011**, *133*, 11850-11853.
- ⁵⁸ Lee, H.; Lee, K.D.; Pyo, K. B.; Park, Y.; Lee, H. *Langmuir* **2010**, *26*, 3790-3793.
- ⁵⁹ Lee, Y.; Lee, S. H.; Kim, J. S.; Maruyama, A.; Chen, X.; Park, T.G. *J. Controlled Release* **2011**, *155*, 3-10.
- ⁶⁰ Ejima, H.; Richardson, J. J.; Liang, K.; Best, J. P.; van Koeverden, M. P.; Such, G. K.; Cui, J.; Caruso, F. *Science* **2013**, *341*, 154-157.

-
- ⁶¹ Maier, G. P.; Rapp, M. V.; Waite, J. H.; Israelachvili, J. N.; Butler, A. *Science* **2015**, *349*, 628-632.
- ⁶² Lee, H.; Lee, B. P.; Messersmith, P. B. *Nature* **2007**, *448*, 338-341.
- ⁶³ Filippidi, E.; Cristiani, T.R.; Eisenbach, C. D.; Waite, J. H.; Israelachvili, J. N.; Ahn, B. K.; Valentine, M. T. *Science* **2017**, *358*, 502-505.
- ⁶⁴ Glass, P.; Chung, H.; Washburn, N. R.; Sitti, M. *Langmuir* **2009**, *25*, 6607-6612.
- ⁶⁵ Ham, H. O.; Liu, Z.; Lau, K. H.; Lee, H.; Messersmith, P. B. *Angew. Chem. Int. Ed.* **2011**, *50*, 732-736.
- ⁶⁶ Han, H.; Wu, J.; Avery, C. W.; Mizutani, M.; Jiang, X.; Kamigaito, M.; Chen, Z.; Xi, C.; Kuroda, K. *Langmuir* **2011**, *27*, 4010-4019.
- ⁶⁷ Xu, B.; Sun, X.; Wu, C.; Hu, J.; Huang, X. *Polym. Chem.* **2017**, *8*, 7499-7506.
- ⁶⁸ Wen, M.; Liu, M.; Xue, W.; Yang, K.; Chen, G.; Zhang, W. *ACS Macro Lett.* **2018**, *7*, 70-74.
- ⁶⁹ Zhao, Y.; Wu, Y.; Wang, L.; Zhang, M.; Chen, X.; Liu, M.; Fan, J.; Liu, J.; Zhou, F.; Wang, Z. *Nat. Commun.* **2017**, *8*, 2218-2225.
- ⁷⁰ Ma, W.; Ameduri, B.; Takahara, A. *ACS Omega* **2020**, *5*, 8169-8180.
- ⁷¹ Ma, W.; Higaki, Y.; Takahara, A. *Adv. Mater. Inter.* **2017**, *4*, 1700907-1700915.
- ⁷² Li, L.; Yan, B.; Zhang, L.; Tian, Y.; Zeng, H. *Chem. Commun.* **2015**, *51*, 15780-15783.
- ⁷³ Wu, S.; Kuang, H.; Meng, F.; Wu, Y.; Li, X.; Jinga, X.; Huang, Y. *J. Mater. Chem.* **2012**, *22*, 15348-15356.
- ⁷⁴ Duan, J.; Wu, W.; Wei, Z.; Zhu, D.; Tu, H.; Zhang, A. *Green Chem.* **2018**, *20*, 912-920.
- ⁷⁵ Matos-Pérez, C. R.; White, J. D.; Wilker, J. J. *J. Am. Chem. Soc.* **2012**, *134*, 9498-9505.
- ⁷⁶ North, M. A.; Del Grosso, C. A.; Wilker, J. J. *ACS Appl. Mater. Inter.* **2017**, *9*, 7866-7872.
- ⁷⁷ Isakova, A.; Topham, P. D.; Sutherland, A. J. *Macromolecules* **2014**, *47*, 2561-2568.
- ⁷⁸ Miaoer Yu; M; Deming, T. J. *Macromolecules* **1998**, *31*, 4739-4745.
- ⁷⁹ Gao, Q.; Li, X.; Yu, W.; Jia, F.; Yao, T.; Jin, Q.; Ji, J. *ACS Appl. Mater. Inter.* **2020**, *12*, 2999-3010.
- ⁸⁰ Xu, Y.; Liu, Q.; Narayanan, A.; Jain, D.; Dhinojwala, A.; Joy, A. *Adv. Mater. Inter.* **2017**, *4*, 1700506-1700511.
- ⁸¹ Shin, E.; Lim, C.; Kang, U. J.; Kim, M.; Park, J.; Kim, D.; Choi, W.; Hong, J.; Baig, C.; Lee, D. W.; Kim, B.-S. *Macromolecules* **2020**, *53*, 3551-3562.
- ⁸² Klöckner, B.; Niederer, K.; Fokina, A.; Frey, H.; Zentel, R. *Macromolecules* **2017**, *50*, 3779-3788.
- ⁸³ Mu, Y.; Wu, X.; Pei, D.; Wu, Z.; Zhang, C.; Zhou, D.; Wan, X. *ACS Biomater. Sci. Eng.* **2017**, *3*, 3133-3140.

-
- ⁸⁴ Patil, N.; Aqil, A.; Ouhib, E.; Admassie, S.; Inganas, O.; Jerome, C.; Detrembleur, C. *Adv. Mater.* **2017**, *29*, 1703373-1703381.
- ⁸⁵ Zhan, K.; Kim, C.; Sung, K.; Ejima, H.; Yoshie, N.; *Biomacromolecules* **2017**, *18*, 2959-2966.
- ⁸⁶ Mancebo-Aracil, J.; Casagualda, C.; Moreno-Villaécija, M. A.; Nador, F.; García-Pardo, J.; Franconetti-García, A.; Busqué, F.; Alibés, R.; Esplandiu, M. J.; Ruiz-Molina, D.; Sedó-Vegara, *Chem. Eur. J.* **2019**, *25*, 12367-12379.
- ⁸⁷ Yu, J.; Wei, W.; Danner, E.; Ashley, R. K.; Israelachvili, J. N.; Waite, J. H. *Nat. Chem. Biol.* **2011**, *7*, 588- 590.
- ⁸⁸ a) Varun, B. V.; Prabhu, K. R. *J. Org. Chem.* **2014**, *79*, 9655-9668; b) Abdel-Mohsen, H. T.; Conrad, J.; Beifuss, U. *Green Chem.* **2014**, *16*, 90-95; c) Bandyopadhyay, P.; Bhattacharya, B.; Majhi, K.; Majee, P.; Sarkar, U.; Seikh, M. M. *Chem. Phys. Lett.* **2017**, *686*, 88-96.

CHAPTER 2

OBJECTIVES

The main objective of this Doctoral Thesis is to validate the designed strategy for the modular fabrication of (multi)functional coatings based on catechol compounds. To achieve this ambitious objective, the following sub-objectives should be followed:

OBJECTIVE I. Synthesis of the functionalised building blocks

Synthesise six new prepolymeric functional catecholic building blocks (Figure 2.1). PEGylated and fluorescein-functionalised building blocks (**5**, **6**, **7** and **8**) would be used for biomedical applications (Objective II), whereas building blocks **9** and **10** would be used for controlling the wettability of flat surfaces (Objective III).

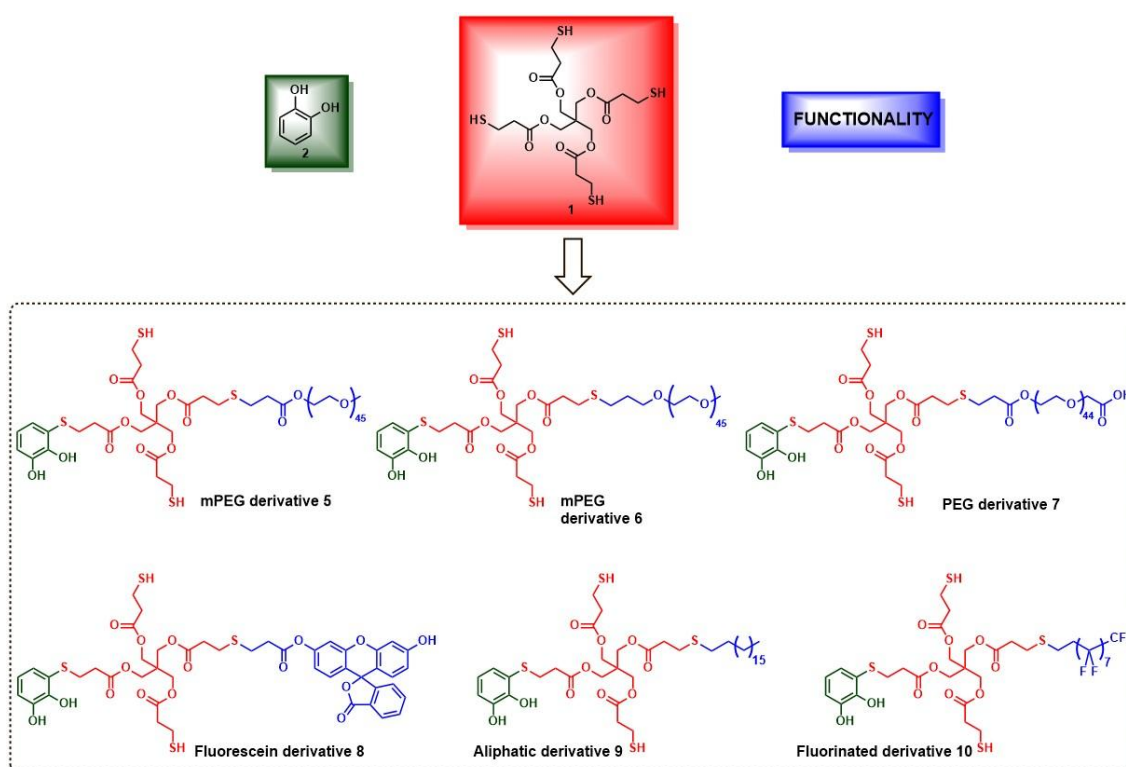


Figure 2.1. On the top, the three main parts of the building block consisting in (i) a catechol moiety (green); (ii) the polymerisation unit (red); and (iii) the group with the property to be conferred (blue). Below, the main six building blocks synthesised in this Thesis: three PEG derivatives (**5**, **6** and **7**), a fluorescein derivative **8**, an aliphatic derivative **9**, and a fluorinated derivative **10**.

OBJECTIVE II. Development of a novel polymerisation strategy

Design a new controlled strategy to polymerise catechol derivatives following approach III based on the coupling of the remaining, un-substituted thiol groups of the building blocks into disulphide bridges (Figure 2.2).

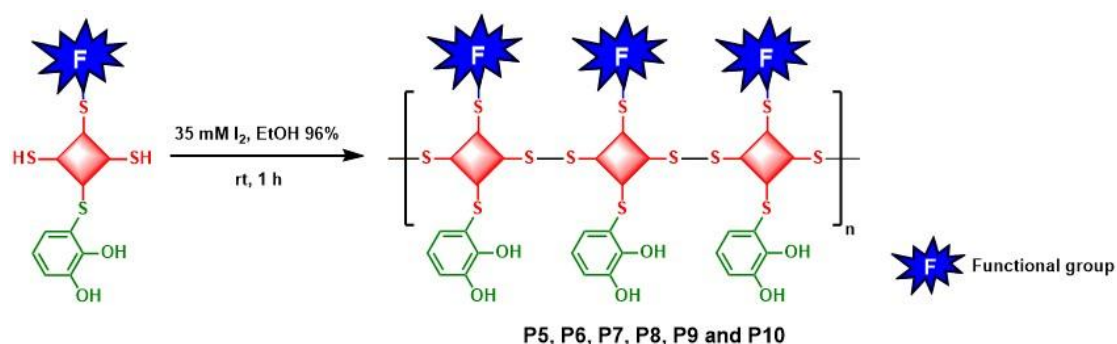


Figure 2.2. Representation of the polymerisation reaction of these building blocks under mild oxidative conditions through the core of the molecule.

OBJECTIVE III. The use of the catechol-based toolkit for nanoparticle coating

Demonstrate the synthetic feasibility of the designed approach to obtain PEG-based coatings made of **P5**, **P6**, and **P7** over different families of NPs (Figure 2.3). More in detail, it is wanted to achieve the next two goals:

- As a proof-of-concept, coat MSNPs with mPEG-/fluorescein-functionalised materials **P5**, **P6**, and **P8** to study their stability in aqueous media, cytotoxicity, and cell penetration ability.
- Specifically, coat Fe_3O_4 NPs with the HOOC-terminated PEG derivative **P7**, and post-functionalise them with a molecular fragment (*e.g.* sugar derivative) that would act as a targeting molecule.

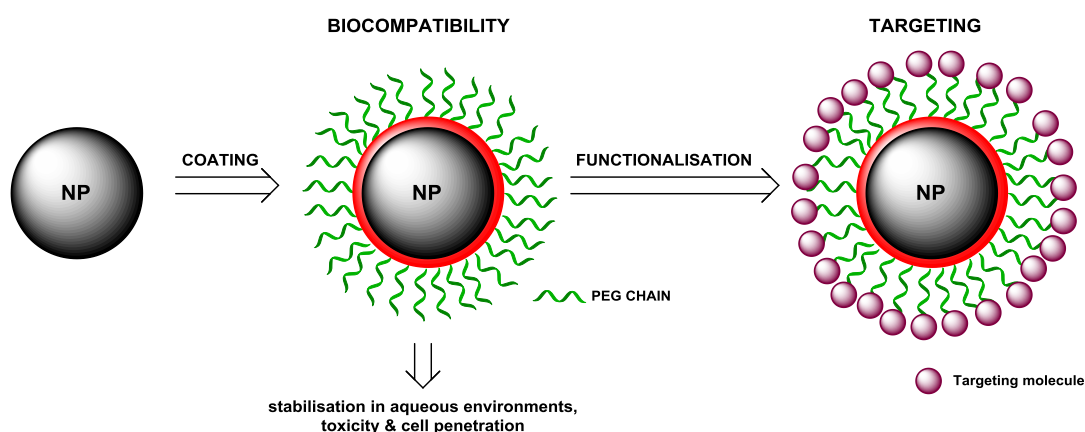


Figure 2.3. Scheme of the two steps to follow in order to reach the final aim. Firstly, the coatings made of the mPEG-functionalised materials **P5** and **P6** onto MSNPs to study their stability, toxicity, and cell penetration ability. Secondly, the functionalisation of the cat-PEG **P7** coating onto MNPs with targeting molecules.

OBJECTIVE IV. Obtaining of oleo-/hydrophobic and hydrophilic coatings

Formation of functional coatings made from the functionalised products **P6**, **P9**, and **P10** to control the wettability of different macrostructures, conferring them hydrophilicity, or, oleo-/hydrophobicity (Figure 2.4).

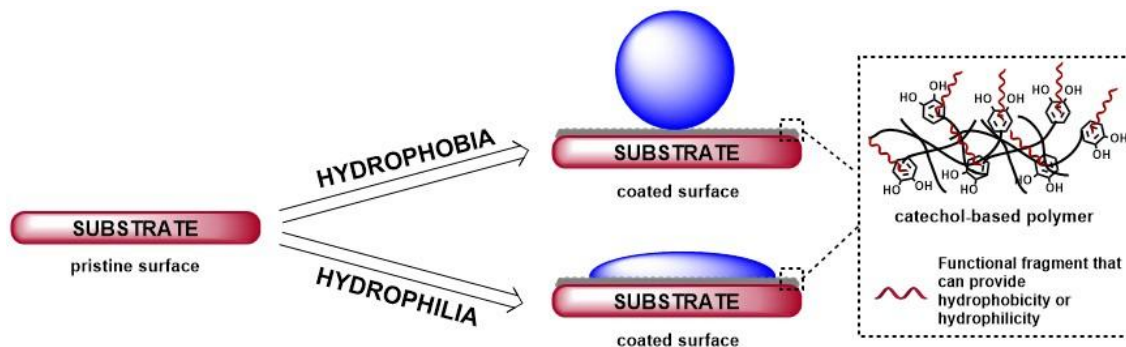


Figure 2.4. Schematic representation of a water droplet onto a substrate coated with a colourless functionalised catecholic polymeric material that change the wettability of the surface by increasing the water contact angle (WCA) for the hydrophobic surface and decreasing the WCA for the hydrophilic one.

To go deeper into it, it is wanted to achieve the next three points:

- As a proof-of-concept, coat glass and metals surfaces with products **P6**, **P9** and **P10** in order to modify their wettability making them hydrophilic, or, oleo-/hydrophobic.
- For a real application, coat textile fibres with the product **P9** obtained from the polymerisation reaction of the C₁₈-functionalised building block in order to obtain hydrophobic textiles useful for water treatments.

OBJECTIVE V. Demonstration of the flexibility and the modular chemistry of this approach

Demonstrate the versatility of the designed approach by polymerising different building blocks to systematically fine-tune the wettability of surfaces at will over a broad range of water contact angle (WCA). For this, fluorescein-functionalised derivative **8** will be combined with a second building block, molecule **9**.

CHAPTER 3

PEGYLATION AS A STRATEGY FOR IMPROVING NANOPARTICLE BIOCOMPATIBILITY

This chapter includes the synthesis and polymerisation of several catecholic building blocks containing PEG chains. As a proof-of-concept, the corresponding products from the polymerisation reactions will be used as coatings onto MSNPs, and their stability, toxicity, and cell penetration ability of the resulting functional NPs will be tested. For a real application, coatings onto MNPs will be performed with cat-PEG materials ending with carboxylic acid groups onto their surfaces to further couple a targeting molecule.

3.1. INTRODUCTION

3.1.1. COATINGS BASED ON CAT-PEG DERIVATIVES

Several examples can be found in which many different macroscopic substrates have been coated with cat-PEG-based polymers, showing hydrophilic surfaces, and antifouling and antimicrobial character.^{1,2} These coatings have been also used to stabilise and functionalise nanostructures, such as NPs, nanosheets, and carbon nanotubes (CNTs), making them biocompatible and biodegradable into physiological media; very suitable strategy in the biomedical field (*e.g.* diagnostic and therapy) (Figure 3.1a). And finally, another application would be the formation of tissue adhesives.

Now, the main results so far described up to now for the synthesis of cat-PEG coatings towards biomedical applications will be summarised and grouped as described next (Figure 3.1b):

- **Approach I. Polymerisation through the catechol moiety**
 - Polymerisation of cat-PEG-based molecules
 - Post-functionalisation of primer coatings
- **Approach II. Catechol grafted to polymeric backbones**
 - No examples had been reported using this approach for the formation of cat-PEG-based coatings when this doctoral thesis was started in 2016.
- **Approach III. Building blocks**
 - Copolymerisation

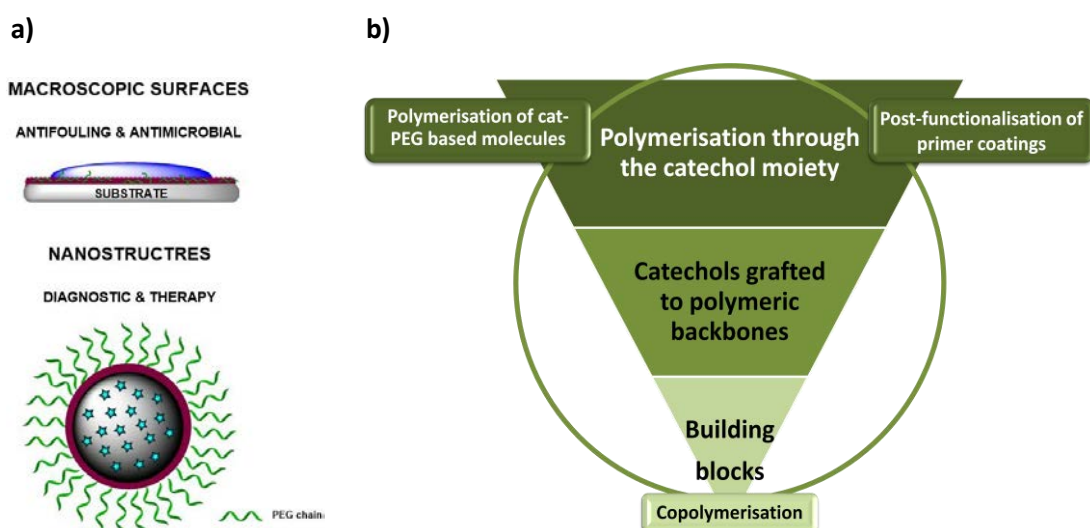


Figure 3.1. a) Schematic representation of a water droplet onto a cat-PEGylated macroscopic surface (top) and a nanostructure coated with a cat-PEGylated material (bottom). b) Scheme that shows the main general three strategies that can be followed to obtain cat-PEGylated coatings.

Regardless of which strategy is used, the majority of these coatings have been done with linear PEG chains, although some examples in which the coatings have been performed with branched PEGylated molecules can be found too.

3.1.1.1. Polymerisation of cat-PEG based molecules

The most frequently used strategy for coating substrates is the polymerisation of cat-PEG-based molecules in which catechols and PEG chains are bound together through a covalent bond directly, or, with a short spacer in between. The polymerisation takes place under oxidative conditions in basic pH and the surfaces are coated *via ex situ* treatments (Figure 3.2).

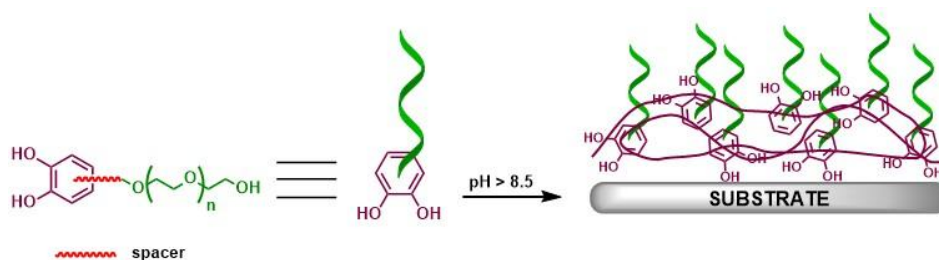


Figure 3.2. Schematic representation of *ex situ* coatings from cat-PEG-based polymers.

For example, pancreatic islets have been coated with 6-arm-PEG-based polymeric materials after transplantations to prevent the dissociation and reducing immune cell invasion.^{3,4,5} Furthermore, these cat-PEG polymers have been also cross-linked to obtain adhesive tissues (Figure 3.3), that have been tested on porcine,^{6,7,8,9} bovine¹⁰ and mice^{11,12} skins, and on fetal membranes too.¹³ Besides, this kind of adhesives not only has been tested with animal's tissues, but also onto substrates, such as glass¹⁴ or silicon.¹⁵

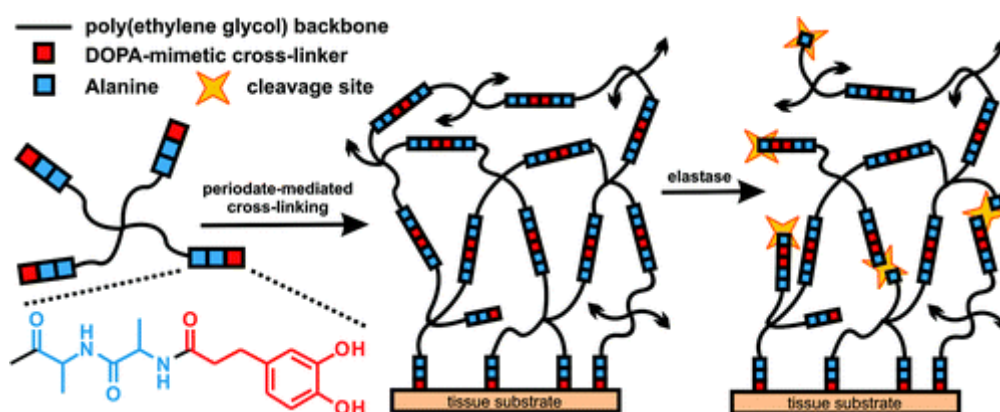


Figure 3.3. a) Oxidative cross-linking of enzymatically degradable macromonomer formed by DOPA linked to the PEG backbone through an Ala-Ala dipeptide (cAAPEG) yields rapid and simultaneous gelation and tissue adhesion. In the presence of neutrophil elastase, the Ala-Ala dipeptide linker (blue) is cleaved to provide cell-mediated structural degradation. Black arrowheads indicate continuation of the cross-linked hydrogel matrix.¹¹

As far as coating onto nanostructures is concerned, Fe_3O_4 , MnO and Au NPs have been dispersed in both aqueous and organic environments after being coated.¹⁶ Furthermore, coated metal NPs, such as Au and Ag , with plasmon resonance behaviour have been seen to be suitable for diagnostic and therapy,¹⁷ and reduced graphene oxide (rGO) coated with cat-PEG polymer (QC-PEG) with Pluronic and quantum dots have been used for drug release of Doxorubicin (DOX).¹⁸ Finally, poly(L-DOPA)-based self-assembly nanodrug have been used to improve treatment in Parkinson's disease (PD) model mice and suppress DA-induced dyskinesia.¹⁹

Furthermore, following this polymerisation strategy polymers,^{20,21,22} metals (Figure 3.4),^{23,24,25} metal oxides,^{1,26,27,28,29} and electrospun nanofibres meshes³⁰ have been coated successfully with cat-PEG polymeric materials showing antifouling character. And to obtain antimicrobial surfaces, reduced graphene oxide,³¹ glass² and polystyrene beads³² have been coated.

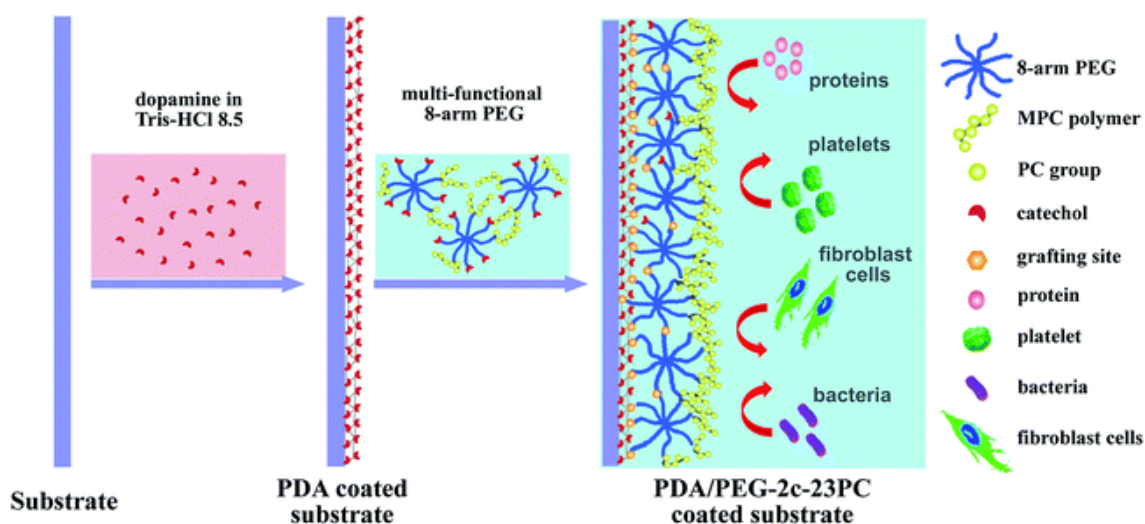


Figure 3.4. The schematic illustration of coating construction and fouling resistance of the PDA-mediated phosphorylcholine and catechol end-capped 8-arm PEG coating.²⁵

3.1.1.2. Post-functionalisation of primer coatings

Another strategy is the post-functionalisation of primer coatings, and in these cases two strategies can be found: (i) a primer coating based on PEGylated materials is formed onto the surface and then the polymerisation of a catechol derivative takes place onto it (e.g. self-polymerisation of DA) (Figure 3.5a), or, (ii) the surface is first coated with catechol-based polymers, commonly PDA, and then it is functionalised with PEG chain derivatives through covalent bonds (Figure 3.5b).

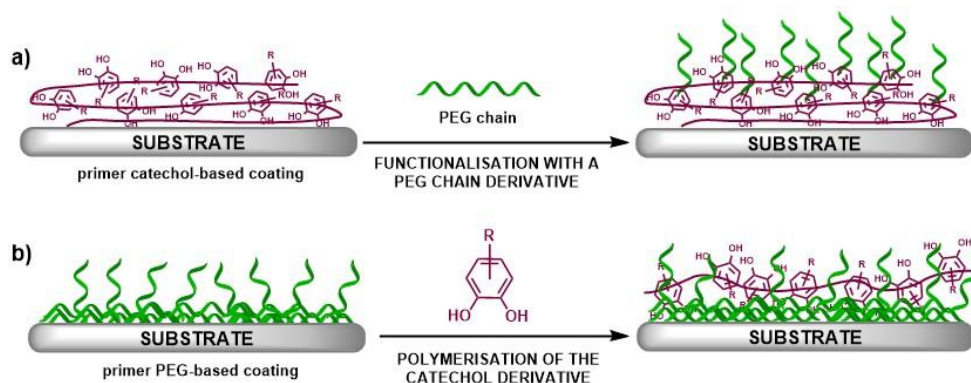


Figure 3.5. a) A substrate is coated with a catechol-based polymer, followed by the functionalisation with PEG chain derivatives. b) The catechol-based polymer is functionalised within a PEGylated surface.

Cheng *et al.* post-functionalised poly(lactic-co-glycolic acid) (PLGA) fibrous scaffolds with various molecules (*i.e.* PEG polymer, arginylglycylaspartic acid (RGD) peptide and bFGF growth factor for cell repellent, adhesion and proliferation, respectively) *via* mussel-inspired PDA coating in aqueous solutions.³³ This method for bio-modification provided a facile and effective strategy to combine drug and bio-function in one system, thus facilitating a synergistic effect of drug-therapy and bio-signal when such biomaterial was used for regenerative medicine. Furthermore, there are some studies on cell adhesion and migration onto substrates that have been previously PEGylated and post-functionalised with a catechol derivative, such as stainless steel surfaces³⁴ and poly(ϵ -caprolactone) (PCL)-PEG micro-³⁵/nanofibres.³⁶ With regard to nanostructures, MoS₂ nanosheets have been used for drug delivery and photothermal cancer treatment (Figure 3.6),³⁷ and PEGylated CNTs *via* a mussel-inspired chemistry have been evaluated for intracellular delivery of Doxorubicin.³⁸ Finally, multi-walled carbon nanotubes (MWCNT),³⁹ and Fe₃O₄ NPs⁴⁰ have been coated with polymeric cat-PEG materials and stabilised in aqueous and organic media.

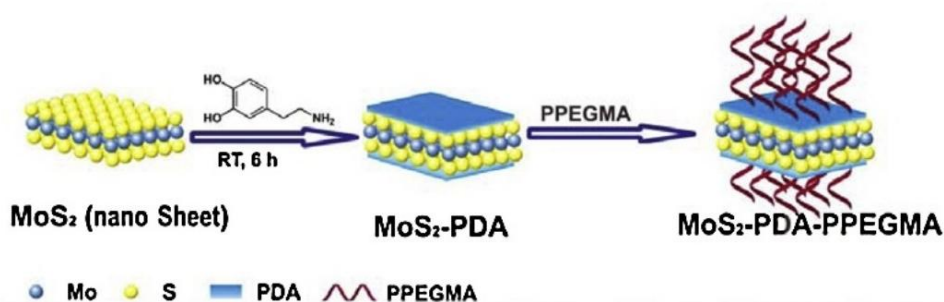


Figure 3.6. Preparation of MoS₂ nanosheets-based nanocomposites (MoS₂-PDA-PPEGMA) through Michael addition reaction between amino-terminated PEG methyl ether methacrylate (PPEGMA) and MoS₂-PDA.³⁷

Finally, several surfaces have been coated with different cat-PEG-based polymers showing antimicrobial and antifouling properties. For example, in 2012 Xu *et al.* coated titanium surfaces with poly(dopamine acrylamide)-*co*-poly(propargyl acrylamide) copolymer and post-functionalised them with PEG chains,⁴¹ and one year later they coated microfiltration membranes with poly(dopamine acrylamide)-grafted poly(vinylidene fluoride) which could be further functionalised *via* spontaneous reduction and chelating of Ag and Au NPs on the surface, and *via* grafting of thiol-terminated PEG (PEG-SH).⁴² Finally, Cheng *et al.* functionalised PES membranes coated with PDA with different PEG chains to control the water flux of those membranes.⁴³

3.1.1.3. Copolymerisation

Using approach III, the copolymerisation through reactive pendant groups between molecules that contain catechol moieties and PEG chains is another alternative to form coatings based on cat-PEG derivatives (Figure 3.7). Sometimes, other molecules that bear other functionalities (fluorescent tags, cyclodextrins...) can also be copolymerised with these PEG- and catechol-based molecules to introduce other features to the coating. Nowadays, there are not many examples following this strategy and they deserve to be studied further.



Figure 3.7. Polymerisation of molecules containing catechol moieties and PEG chains through reactive pendant groups. Coatings *via ex situ* treatments.

To start with, in 2015 Mattson *et al.* developed a facile synthetic strategy for the functionalisation of well-defined polyether copolymers with control over the number and location of catechol groups.⁴⁴ That strategy could allow studying the effects of polymer architecture, molecular weight, and catechol incorporation in the adhesive properties of surface-anchored polyethylene oxide (PEO). Besides, cat-PEGylated copolymers have also been used as hydrogel adhesives for bovine heart tissues.⁴⁵ Furthermore, Yuan *et al.* showed that a supramolecular approach, combining both catechol-metal ion coordination and polymer self-assembly together, could organise polymers into hybrid nanoassemblies ranging from solid particles, homogeneous vesicles to Janus vesicles (Figure 3.8),⁴⁶ which could totally disassemble in response to proteins. Moreover, this kind of copolymeric adhesives have been also tested on metals, such as aluminium.^{47,48}

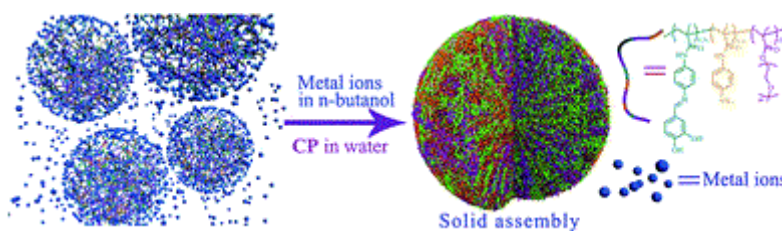


Figure 3.8. Schematic illustration of the formation of solid-like assemblies.⁴⁶

To coat Fe_3O_4 NPs with a glycomonomer-based on cat-PEG derivate and rhodamine B has been useful for bioimaging.⁴⁹ Moreover, this type of magnetic NPs has been coated with polysaccharides grafted with catechol moieties and PEG chains for gene therapy⁵⁰ and as contrast agents.⁵¹ Coated SiO_2 NPs has displayed high water dispersibility and has showed controlled release kinetics of cisplatin.⁵² And coated AuNPs with a copolymer containing β -cyclodextrin has been designed as a smart carrier and traceable delivery probe of the chemotherapeutic Doxorubicin drug (Figure 3.9).⁵³ On top of that, polymeric micelles^{54,55} and nanocarriers⁵⁶ based on cat-PEG copolymers have been used as drug delivery systems. Besides, it has also published the self-assembly of amphiphilic block copolymers into spherical micelles, which displayed improved resistance against bovine serum albumin (BSA) adsorption, when compared to an unmodified surface.⁵⁷

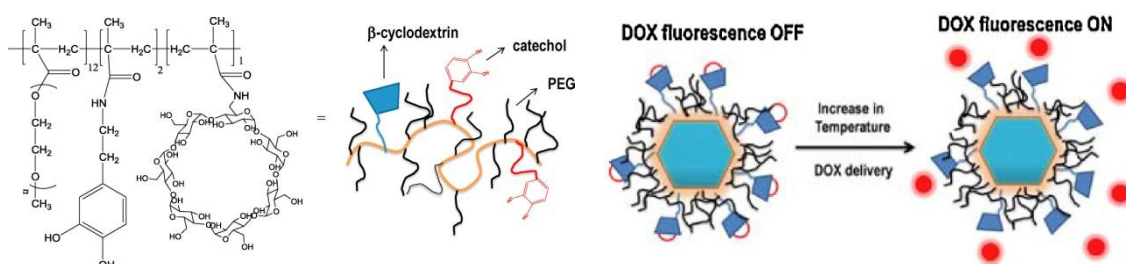


Figure 3.9. Chemical structure of PEG-catechol-cyclodextrin copolymer and its schematic representation (left). Illustration of the influence of the temperature in both the Doxorubicin delivery and trigger ON of its fluorescence (right).⁵³

Finally, multidentate cat-/PEG-derivatised oligomers have exhibited strong affinity to magnetic nanocrystals,⁵⁸ or, NPs⁵⁹ presenting long-term colloidal stability in aqueous media. And Wan *et al.* developed a surface modification of CNTs with a biocompatible polymer PEG *via* a mussel-inspired strategy. The dispersibility as well as biocompatibility of these PEGylated CNTs has been subsequently investigated showing remarkable enhancement in both aqueous and organic solvents.⁶⁰

With regard to the fabrication of antifouling surfaces, metals,^{61,62,63,64} metal oxides,⁶⁵ and mica surfaces^{66,67} have been coated with cat-PEG-based copolymers. Sometimes, to enhance the antifouling activity, fluorine brushes are incorporated within the copolymers. Furthermore, we can also obtain surfaces that combine both antimicrobial and antifouling properties. For

example, Cheng *et al.* immersed contact lenses into an aqueous solution of cat-PEG-functionalised copolymers resulting in robust and stable coating on the lens surfaces, which survived the harsh condition of autoclaving and remained on the surface for a typical device application lifetime.⁶⁸

3.1.2. WORK PROGRAMME

As already described in this introduction, there are several examples of cat-PEG systems already reported in the literature of application in biomedicine. Most of the examples were obtained following approach I, in less degree approach II, and only few examples were found following approach III, where coatings were mainly made of copolymers of PEG- and catechol-based molecules.

In this chapter, it is aimed to demonstrate the validity of our approach with PEGylated coatings of NPs. Due to their large surface area, when exposed in a physiology environment, NPs tend to interact with plasma proteins, causing size increase that often results in serious agglomeration. These particles are also considered as an intruder by the innate immunity system and can be readily recognised and engulfed by the macrophage cells. In both cases, the particles will be removed from the blood circulation system and lose their function quickly, leading to dramatic reduction in efficiency in NP-based diagnostics and therapeutics. In order to overcome such problems, these NPs are usually coated with a layer of hydrophilic and biocompatible polymer such as dextran,⁶⁹ dendrimers,⁷⁰ or, PEG chains.⁷¹

Especially, the cat-PEG systems used here are the ones represented in the next Figure.

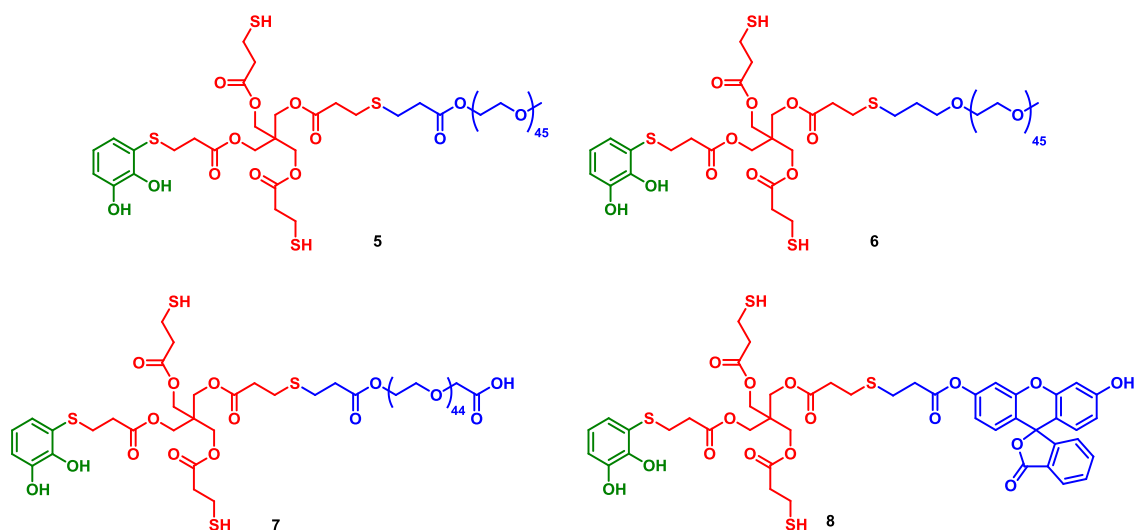


Figure 3.10. Molecular structures of four target molecules functionalised with Me-terminated PEG chains (**5** and **6**), a HOOC-terminated PEG chain (**7**) and a fluorescein derivative (**8**).

The two Me-terminated PEG-functionalised building blocks **5** and **6** were synthesised following route A (see *Chapter 1*, Figure 1.18) from S-catechol tris-thiol **4**. The unique difference between these two mPEGylated intermediates is the moiety allowing the linkage between the PEG chain and the rest of the compound (ester **5** vs. ether **6**). For comparison purposes, compounds **7** and **8** were also obtained following route A. The PEGylated derivative **7** ending with a carboxylic acid group would be post-functionalised with a targeting molecule, whereas fluorescein derivative **8** would allow the identification of coatings in a straightforward way due to its fluorescent properties.

Once these monomers have been obtained, the next step is the controlled polymerisation (Figure 3.11).

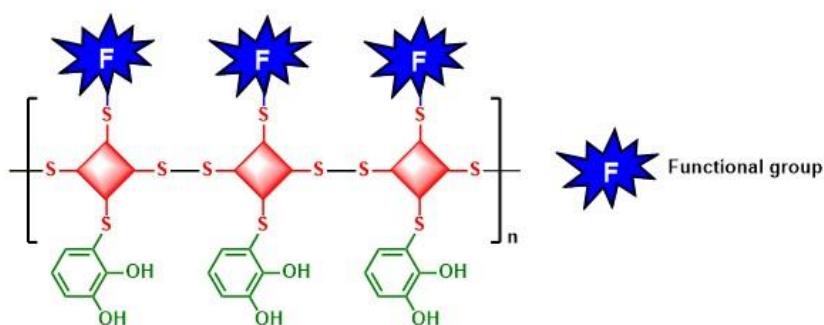


Figure 3.11. Illustration of a linear polymer polymerised through disulphide bonds.

Under mild oxidative conditions, it will be pretended to polymerise building blocks **5**, **6**, **7** and **8** through the tetrakis moiety by forming disulphide bonds as represented in Figure 3.11. Furthermore, by combining mPEG- and fluorescein-functionalised building blocks **6** and **8** would allow obtaining polymers, named **C6-8**, bearing properties with quite interest in the biomedical field.

Afterwards, and once the polymers have been prepared, the next step is the coating of NPs. For this, two families have been selected. First one is that of mesoporous silica NPs (MSNPs) because of their stability and because it is known that catechol moieties can form hydrogen-bonding, or even covalent bonds with hydroxyls groups exposed onto their surface. The second ones magnetite NPs (MNPs, Fe₃O₄ NPs) have been chosen due to their properties, small (< 10 nm) and magnetic, and because over the last years, MNPs have merged as promising candidates for biomedical imaging, as contrast agents for magnetic resonance imaging (MRI),⁷² drug and gene delivery,⁷³ magnetothermal therapy,⁷⁴ biosensors and bioseparation⁷⁵ because of their high magnetic moment, low toxicity, low coercivity, ultra-fine sizes, biocompatibility and superparamagnetic properties.

The last synthetic step of the approach to demonstrate the success of the project is the functionalisation of the PEG layer made of derivative **7** with a glucopyranose derivative (Figure 3.12). The reason for this is because this molecule has been used for targeting the blood-brain barrier (BBB) in humans due to the presence of glucose transporters on it. As far as MNPs targeting the brain is concerned,^{76,77} some examples can be found in the literature where functionalised MNPs have been used brain-targeted theranostics,⁷⁸ as therapy delivery systems^{79,80} and as contrast agents to detect BBB damages.⁸¹

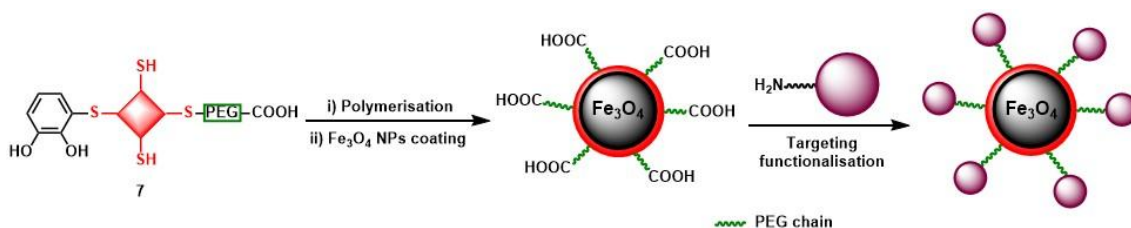


Figure 3.12. First, building block **7** will be polymerised using our disulphide bond-based approach. Afterwards, model NPs, such as magnetite ones, are expected to be coated with this polymer. Finally, this coating would be functionalised with a BBB-shuttle through residual carboxylic acids exposed onto the surface.

This strategy consists in (i) using building block **7** to obtain a polymeric cat-PEG material **P7**, (ii) using that **P7** to coat MNPs, and (iii) post-functionalising that coating with the BBB-shuttle, which should facilitate the crossing across the BBB, through the residual carboxylic acids exposed onto the surface.

Finally, once the viability of these polymers to coat NPs have been demonstrated, and as a proof-of-concept, the *in vitro* toxicity and cell internalisation of MSNPs as example coated with the copolymer bearing fluorescein moieties and PEG chains **C6-8** will be studied.

On top of that, and for comparison reasons, a fluorescein-functionalised building block containing a styrene moiety instead of a catechol one will be synthesised and tested as coating to demonstrate the role of catechol in the adhesion properties. This one was chosen as model blank molecule because of their fast and easy coating's identification.

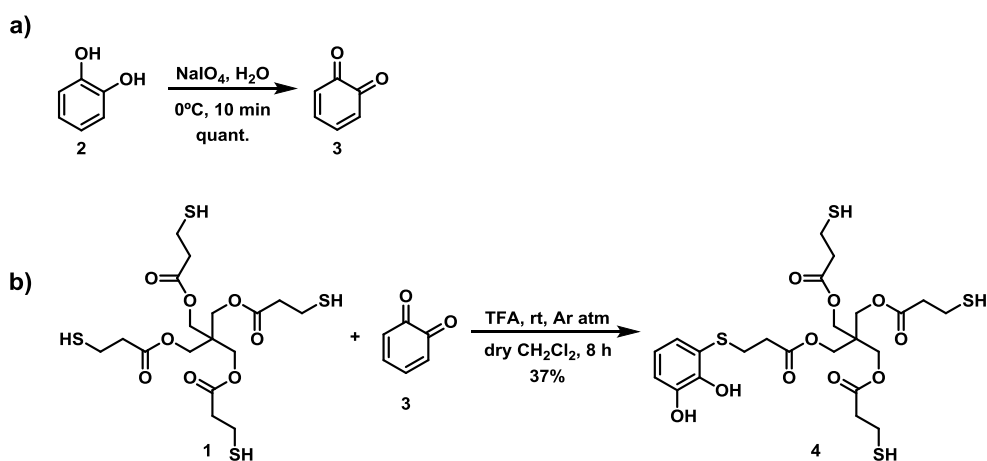
3.2. SYNTHESIS OF THE BUILDING BLOCKS AND A TARGETING MOLECULE

It must be remarked that long PEG functionalised derivatives cannot be purified by column chromatography through silica gel, since different PEG functionalised derivatives show very similar physicochemical properties. In the literature it is found that PEG molecules are usually isolated from reaction media by means of precipitation with Et₂O.⁸² Therefore, all long PEGylated derivatives can precipitate under these conditions and, despite being impossible to separate mixtures of them, mainly pure derivatives can be obtained through several recrystallisations. Hence, the conversions of reactions involved were carefully optimised (>

95%) in order to avoid some purifying issues. All the final PEGs derivatives and the corresponding PEGylated intermediates were characterised by ^1H - and ^{13}C NMR.

3.2.1. SYNTHESIS OF MONOSUBSTITUTED S-CATECHOL TRIS-THIOL INTERMEDIATE 4

The synthesis of the different building blocks started with the formation of the monosubstituted S-catechol tris-thiol **4** by two tandem reactions, already studied in our research groups.⁸³ The oxidation of the commercial pyrocatechol **2** to the *o*-quinone **3** (Scheme 3.1a) was achieved in 10 min, through a two-electron transfer process, using an aqueous solution of (meta)sodiumperiodate at 0 °C. The quinone was extracted from the reaction mixture with CH_2Cl_2 , and it was added into a freshly prepared solution of pentaerythritol tetrakis(3-mercaptopropionate) **1** under inert atmosphere. The reaction mixture was stirred for 8 h at rt in the dark (Scheme 3.1b). The crude was purified by a flash column chromatography performed using silica gel affording the intermediate **4** in 37% yield.



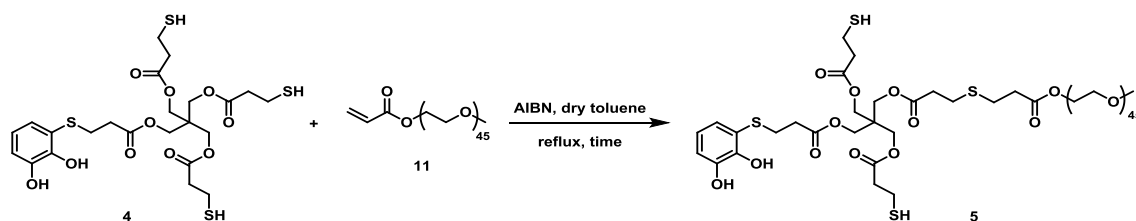
Scheme 3.1. a) Oxidation of pyrocatechol to obtain quinone **3**. b) Formation of intermediate **4** through a 1,6-conjugated addition.

As this reaction progressed, it was observed that the solution turned from dark red to pale yellow indicating that the amount of quinone **3** was diminishing due to its conjugation with the pentaerythritol tetrakis(3-mercaptopropionate) **1** and subsequent, recovering of the aromaticity. In this nucleophilic attack different by-products can be formed since quinone has several electrophilic positions. However, only the product resulting of the 1,6-conjugated addition was observed, in accordance with our previous work.⁸³

3.2.2. SYNTHESIS OF mPEG-FUNCTIONALISED BUILDING BLOCK 5

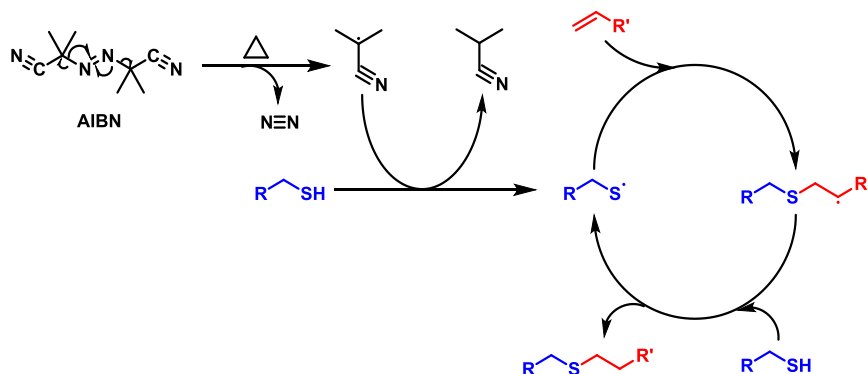
The *S,S'*-cat-mPEG bis-thiol **5** was obtained from the commercial PEG methyl ether acrylate **11**, allowing its preparation through two synthetic strategies: (i) *via* a radical-catalysed thiol-ene reaction,⁸⁴ and (ii) *via* a thia-Michael reaction.⁸⁵

I. *Radical-catalysed thiol-ene reaction*



Scheme 3.2. Radical thiol-ene reaction to obtain mPEG **5**.

This reaction was carried out between intermediate **4** and the commercial PEG methyl ether acrylate **11** using AIBN as catalyst initiator (Scheme 3.2). It consists in the formation of sulphur-carbon bond through a radical mechanism, in which a catalytic AIBN amount is activated on temperature higher than 70 °C, decomposing in nitrogen and radical species that eventually generate radicals onto sulphurs, which can react with olefins to form the final sulphur-carbon bonds through a catalytic cycle (Scheme 3.3).



Scheme 3.3. Mechanism of a thiol-ene reaction using AIBN as radical initiator.

As already mentioned previously, it was necessary to obtain good conversions to the desired product in order to avoid future purifying issues. Hence, different reaction conditions were tested to get values of conversion nearest to 100% (Table 3.1).

Table 3.1. Reaction conditions tested for obtaining mPEG derivative **5**.

Entry	AIBN	Intermediate 4	Time	(Yield)/Conversion*
1	0.2 equiv.	1.0 equiv.	6 h	33%*
2	0.5 equiv.	1.7 equiv.	overnight	complex mixture
3	0.2 equiv.	1.1 equiv.	overnight	50%*
4	0.2 equiv.	2.0 equiv.	24 h	(67%)

* Conversions were calculated by integrating the remaining protons of the double bond from the acrylate group in the ^1H NMR spectra of the products.

All the reactions were carried out at reflux temperature and both AIBN and intermediate **4** were added in 3 portions. Using 0.2 equiv. of AIBN and 1 equiv. of catecholic molecule **4** (Table 3.1, entry 1), it was achieved a conversion value of 33%. In order to improve this result, longer reaction times and more equivalents of both AIBN and intermediate **4** were used (entry 2). However, it was seen that those conditions disfavoured the reaction, yielding a complex mixture. Therefore, the catalytic amount of AIBN was reduced to 0.2 equiv. and it was worked with a few excess of **4** in order to favour the monosubstitution in front of possible multi-additions of mPEG chains in the core (entry 3). Using those conditions, only a conversion of 50% of the expected mPEG **5** was obtained. Finally, it was achieved almost a total conversion to the desired mPEG **5** (entry 4) working with 0.2 equiv. of AIBN, and 2 equiv. of catecholic molecule **4** for 1 day. This reaction was monitored by ^1H NMR observing the total disappearance of protons coming from the acrylate group of **11** (Figure 3.13). The reaction was stopped after a total conversion to the desired product was observed, and the solid was purified by means of precipitation with CH_2Cl_2 and Et_2O to afford the final mPEGylated compound **5** as a white solid in 67% yield.

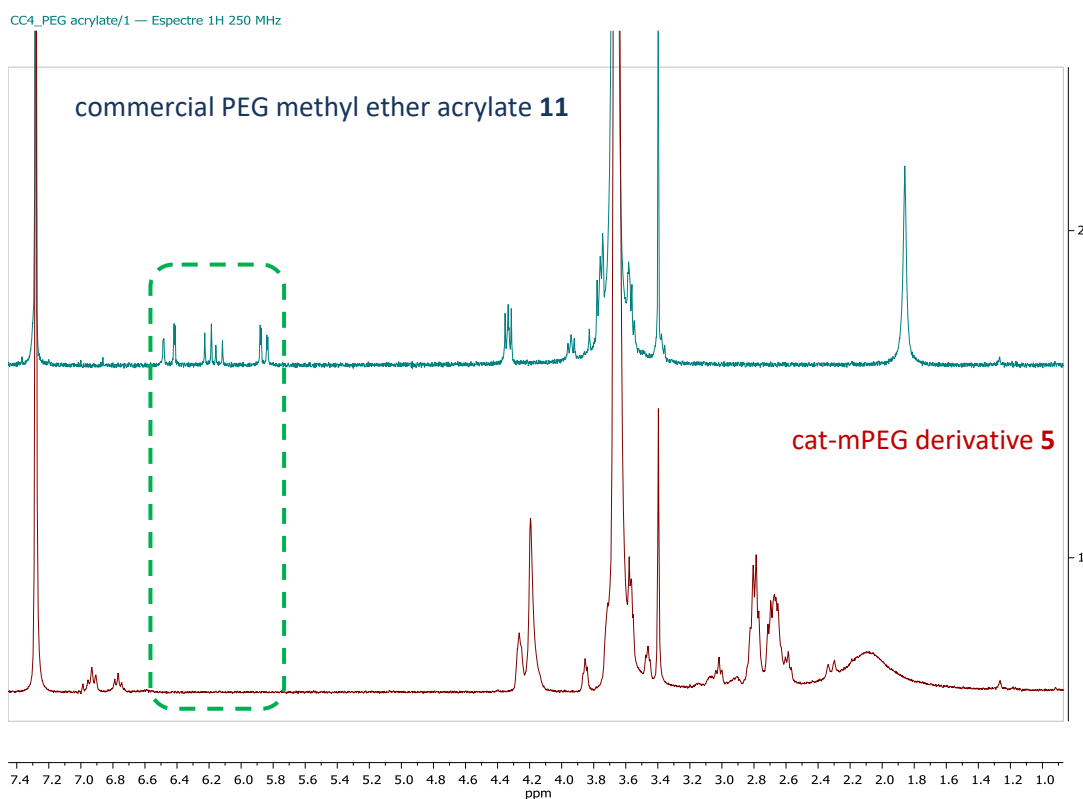
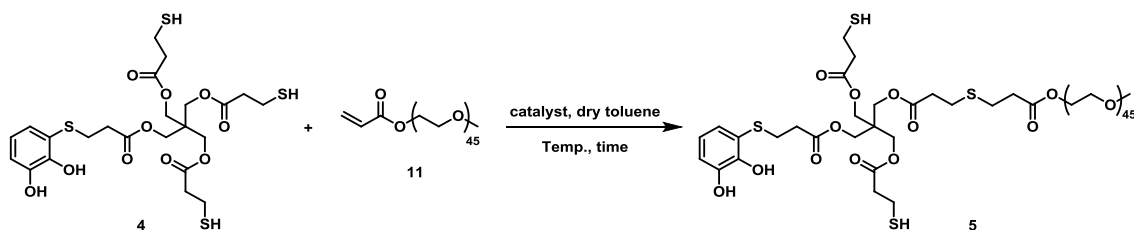


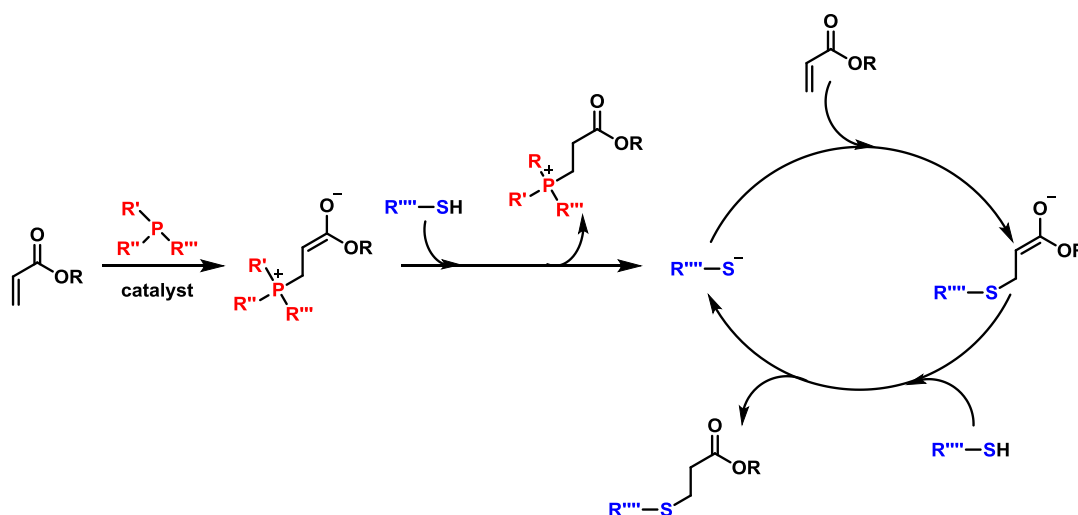
Figure 3.13. Comparison of ^1H NMR spectra (250 MHz, CDCl_3) between commercial PEG methyl ether acrylate **11** (top) and cat-mPEG derivative **5** (bottom). The total disappearance of acrylate proton signals (highlighted in green) from 5.8 to 6.5 ppm means the successful conjugation of the fluorescent tag to the intermediate **4**.

II. Thia-Michael reaction



Scheme 3.4. Synthesis of mPEG **5** via thia-Michael reaction.

To carry out this reaction, some catalysts are used to generate thiolates and make feasible the reaction as shown in the next Scheme, taking a phosphine as example.



Scheme 3.5. Proposed anionic chain mechanism *via* nucleophilic initiation for the phosphine-mediated thia-Michael reaction with an acrylic substrate.

Different reaction conditions were tested, including two kind of catalyst, an amine (1,8-diazabicyclo [5.4.0]undec-7-ene, DBU) and a phosphine (dimethylphenylphosphine, DMPP) (Table 3.2).

Table 3.2. Different trials for the preparation of molecule **5** *via* thia-Michael reaction.

Entry	Solvent	Catalyst	Temperature	Intermediate 4	Time	(yield)/Conversion*
1	THF	0.6 equiv. DBU	rt	1.1 equiv.	3 h	65%*
2	toluene	0.05 equiv. DMPP	30 °C	4.7 equiv.	4 h	< 20%*
3	toluene	0.1 equiv. DMPP	30 °C	1.1 equiv.	3 h	80%*
4	toluene	0.1 equiv. DMPP	30 °C	2.3 equiv.	4 h	(78%)

* Conversions were calculated by integrating the remaining protons of the double bond from the acrylate group in the ^1H NMR spectra of the products.

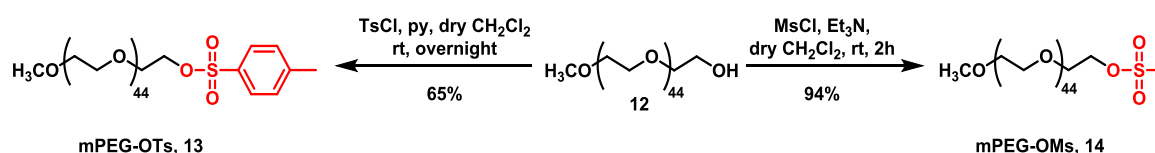
All reactions were carried out under inert atmosphere with dry solvents. It was found that the best catalyst to use in that reaction was DMPP, since with a higher amount of DBU, worse conversion values were obtained (Table 3.2, entry 1 vs. entries 3 and 4). Working with DMPP, it was observed that at least 0.1 equiv. of the catalyst were needed (entries 3 and 4) to obtain moderate/high conversion values, since working with only 0.05 equiv. of this phosphine (entry 2) a conversion lower than 20% was obtained. Finally, it was seen that 0.1 equiv. of DMPP and 2.3 equiv. of intermediate **4** at 30 °C for 4 h (entry 4) were the best reaction conditions to obtain a good conversion to the desired product **5**, which was isolated by means of precipitation with CH_2Cl_2 and Et_2O as a white powder in 78% yield.

Advantages of this second synthetic pathway *via* thia-Michael reaction vs. radical-catalysed thiol-ene reaction are that the reaction conditions used are milder, and lower temperatures and shorter reaction times are required. Furthermore, the purity of the final mPEG derivative **5**

via thia-Michael reaction was higher than the one obtained via the radical reaction, in which more by-products were formed coming from the decomposition of AIBN.

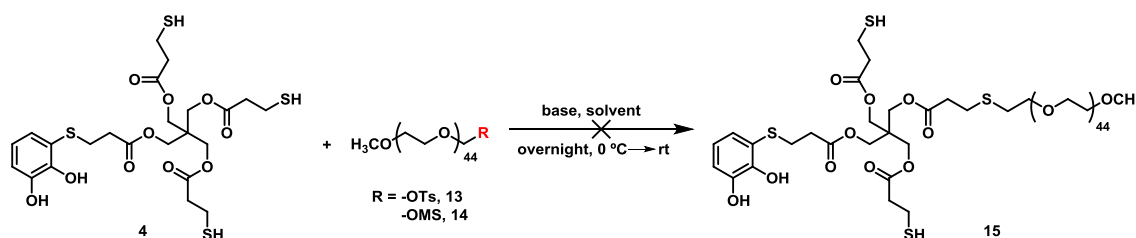
3.2.3. SYNTHESIS OF mPEG-FUNCTIONALISED BUILDING BLOCK 6

Previous to obtain the second mPEG derivative **6**, which would be linked to the rest of the compound (molecule **4**) through an ether, the syntheses of other analogues compounds were attempted by following another synthetic pathway showed below. Firstly, it was tried to convert the hydroxyl of commercial mPEG **12** in two good leaving groups (e.g. tosylate (-OTs),⁸⁶ and mesylate (-OMs)⁸⁷) (Scheme 3.6) in order to allow the reaction with the catecholic molecule **4** through a simple nucleophilic substitution reaction (S_N2).



Scheme 3.6. Synthesis of the two different mPEG derivatives **13** and **14** from commercial PEG monomethyl ether **12**.

With these two mPEG chains (**13** and **14**) in hands, the nucleophilic substitution reaction with intermediate **4** was attempted (Scheme 3.7).



Scheme 3.7. S_N2 reaction between catecholic intermediate **4** and mPEGylated derivatives in order to obtain S,S' -cat-PEG bis-thiol **15**.

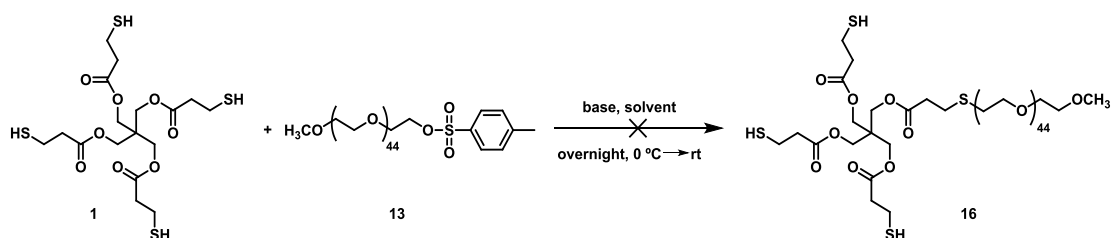
Different reaction conditions (different solvents and bases) were used to try to obtain the S,S' -cat-PEG bis-thiol **15** (Table 3.3).

Table 3.3. Unsuccessfully reaction conditions tested to obtain **15**.

Entry	mPEG	Base	Solvent	Yield
1	-OTs, 13	1 equiv. potassium <i>tert</i> -butoxide	THF	-
2	-OTs, 13	3 equiv. potassium <i>tert</i> -butoxide	THF	-
3	-OTs, 13	3 equiv. potassium <i>tert</i> -butoxide	THF + DMF	-
4	-OTs, 13	8 equiv. pyridine	CH ₂ Cl ₂	-
5	-OTs, 13	3 equiv. butyl lithium	THF	-
6	-OMs, 14	3 equiv. butyl lithium	CH ₂ Cl ₂	-

In all cases, the reactions were carried out under anhydrous conditions and with 1 equiv. of the mPEGylated derivative. It was worked with the two leaving groups, using 3 different bases (potassium *tert*-butoxide, pyridine (py) and butyl lithium) in different quantities (ranging from 3 to 8 equiv.), and with different solvents. Unexpectedly, none of the 8 reactions attempted furnished the mPEG **15**. Both starting materials, mPEG derivatives and intermediate **4**, were recovered; starting mPEGs precipitated into the Et₂O media, whereas intermediate **4** was found in the soluble medium.

Before discarding this synthetic approach, the order of the synthetic steps was changed, trying first the functionalisation with the mPEG-OTs chain **13** of the commercial starting material pentaerythritol tetrakis(3-mercaptopropionate) **1** and second the coupling of the catechol moiety (Scheme 3.8).

**Scheme 3.8.** Attempt to functionalise molecule **1** with the mPEG-OTs chain **13** via S_N2.

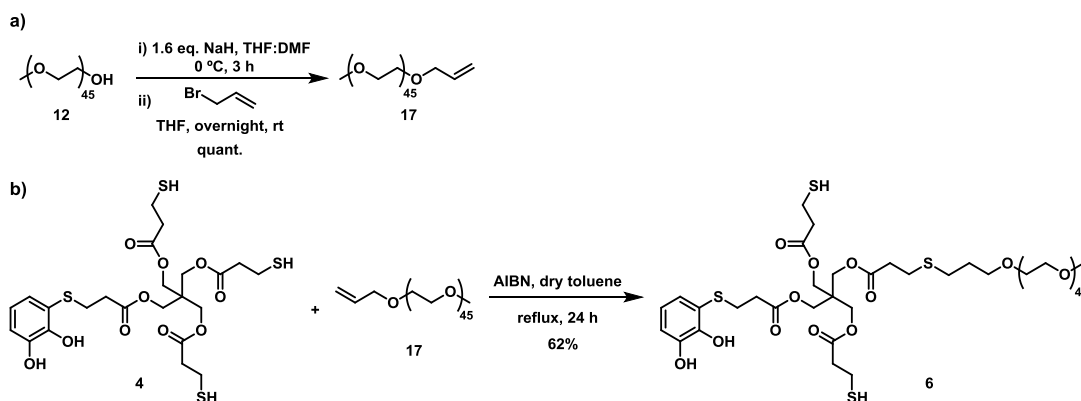
In order to favour the functionalisation of **1** with one mPEG chain, an excess of this core was used. In this case, it was worked with the strongest base butyl lithium and different solvents (Table 3.4).

Table 3.4. Four different reaction conditions tested for the preparation of mPEG derivative **16**.

Entry	mPEG-OTs 13	Base	Solvent	Yield
1	0.8 equiv.	1.3 equiv. butyl lithium	THF	-
2	1.0 equiv.	1.3 equiv. butyl lithium	THF	-
3	0.6 equiv.	1.2 equiv. butyl lithium	CH ₂ Cl ₂	-
4	0.5 equiv.	1.1 equiv. butyl lithium	DMF	-

Unfortunately, the same unsuccessful results were obtained; both starting reagents **1** and **13** were recovered separately. It was hypothesised that the sulphide was not nucleophilic enough to attack the electrophilic position of molecules **13** and **14**.

Consequently, it was decided to target compound **6** using the radical-catalysed thiol-ene reaction, as it worked for synthesising mPEG **5**. Therefore, first the commercial mPEG **12** had to be derivatised to the corresponding allyl ether,⁸⁸ followed by the radical reaction to obtain **6** (Scheme 3.9).



Scheme 3.9. Synthetic route for the preparation of mPEG **6**. a) Functionalisation of commercial PEG methyl ether **12** with an allyl group. b) Radical-catalysed thiol-ene reaction between intermediates **4** and **17** to afford S,S'-cat-PEG bis-thiol **6**.

The corresponding alkoxyde of **12** was formed using NaH as base to attack onto the allylic position of the allyl bromide (Scheme 3.9a).⁸⁸ Thus, the allylic ether mPEG **17** was obtained as a white powder in a quantitative manner after being purified by precipitation with Et₂O.

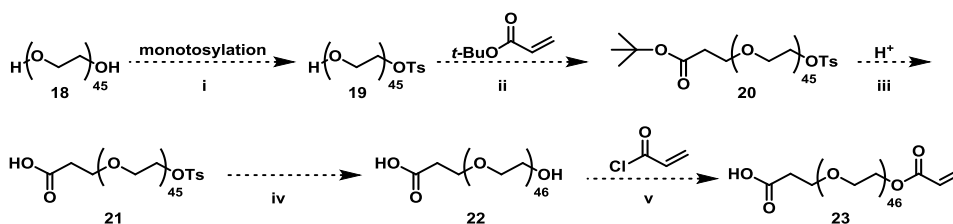
Afterwards, once intermediate **17** was obtained, the radical-catalysed thiol-ene reaction (Scheme 3.9b) was carried out using the same reaction conditions already optimised for the synthesis of mPEG derivative **5** (0.2 equiv. of AIBN and 2 equiv. of intermediate **4**) (Table 3.1, entry 4, see pag. 49) in dry toluene. The reaction was monitored by ¹H NMR until the total disappearance of the protons coming from the allyl group of **17** occurred. The final mPEGylated compound **6** was obtained in 62% yield after precipitation with CH₂Cl₂ and Et₂O.

3.2.4. SYNTHESIS OF PEG-FUNCTIONALISED BUILDING BLOCK **7**

To obtain PEG-functionalised derivative **7**, first the heterobifunctional PEG **26** having an acrylate and carboxylic acid groups in each ends had to be synthesised.

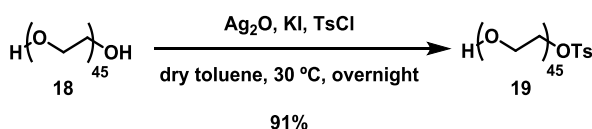
3.2.4.1. Synthesis of heterobifunctional PEG derivative 26

Firstly and considering the bibliographic precedents, the following synthetic pathway was proposed to obtain a very similar analogue compound **23** (Scheme 3.10). The synthesis would start with the known monoderivatisation of one of the terminal alcohols in the corresponding tosylate group. Secondly, the addition of the remaining alcohol to the *tert*-butyl ester of acrylic acid through a 1,4-conjugated addition, followed by the hydrolysis of such ester would render the carboxylic acid-based molecule. Finally, the two last steps would consist in the transformation of the tosylate group in the corresponding acrylate.



Scheme 3.10. Synthetic route to obtain heterobifunctional PEG **23** that includes a (i) monotosylation; (ii) a functionalisation with an acrylic ester followed by its (iii) acidic hydrolysis; (iv) the removal of tosylate group; (v) and the final functionalisation to the acrylate **23**.

Therefore, the synthesis started with the monotosylation of one of the ending alcohols as an unusual protective step (Scheme 3.11). That reaction was quite well studied and already reported in the literature.^{82,89} In this case, the yield obtained was very good (91%) and the purification of the monosubstituted product was quite straightforward.



Scheme 3.11. Monotosylation of commercial diol PEG **18**.

The good yield of this reaction could be due to the coordination of the silver cation with the oxygen atoms in the PEG backbone (Figure 3.14).⁹⁰ Hsu *et al.*⁹¹ as well as Mahou *et al.*⁸² attributed the selectivity toward monofunctionalised PEG with intramolecular hydrogen bonding, which was favoured by the chelate formation. They proposed that intramolecular hydrogen bonding was responsible for deprotonation of one hydroxyl group by silver oxide, suggesting that the other hydroxyl group became less acidic. Furthermore, the role of KI was also investigated by Bouzide *et al.*⁹² reporting that KI enhance the tosylation reaction rates, as it converted the tosyl chloride to the much more reactive tosyl iodide *in situ*.

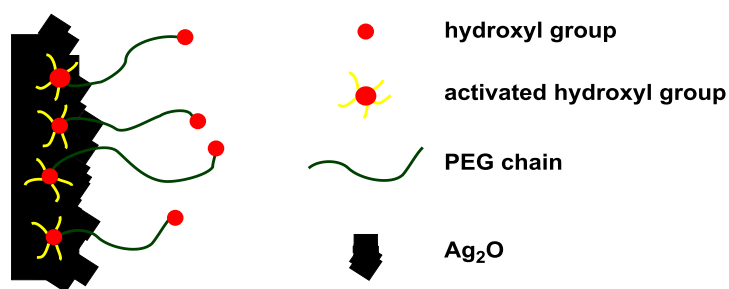
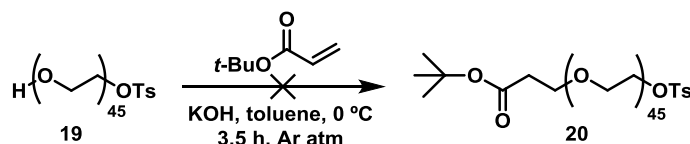


Figure 3.14. Surface controlled non-symmetric activation of PEG at the heterogeneous silver oxide catalyst particles.⁹⁰

Afterwards, in order to obtain the carboxylic acid group on the other end, the first methodology tested was to functionalise intermediate **19** with the *tert*-butyl ester of acrylic acid through an oxa-Michael addition so as to obtain derivative **20** (Scheme 3.12), following similar conditions used in literature.⁹³



Scheme 3.12. The incorporation of an ester group *via* an oxa-Michael addition between the alcohol of **19** and commercial *tert*-butyl acrylate resulted unsuccessfully.

Unfortunately, this reaction did not take place, since starting PEG **19** was recovered totally (Table 3.5, entry 1). A possible explanation could be the low solubility of tosylate PEG **19** in toluene. Therefore, the stronger base NaH and dry THF were used to overcome solubility issues, and longer reaction times were attempted.

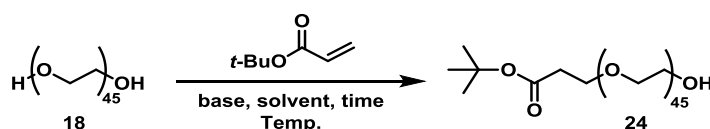
Table 3.5. Reaction conditions used to obtain *tert*-butyl ester-based PEG **20** and their corresponding conversions.

Entry	Base	Solvent	Time	Temperature	<i>tert</i> -butyl acrylate	Conversion
1	0.2 equiv. KOH	toluene	3.5 h	0 °C	1.7 equiv.	0%
2	1.0 equiv. NaH	THF	overnight	rt	1.4 equiv.	45%
3	0.4 equiv. NaH	THF	overnight	rt	3 equiv.	52%
4	0.4 equiv. NaH	THF	24 h	0 °C → rt	9 equiv.*	78%

* Those 9 equiv. of *tert*-butyl acrylate were added in 3 portions.

Eventually, working with 1 equiv. of NaH and an excess of *tert*-butyl acrylate (entry 2), we obtained a 45% conversion to the PEG derivative **20**. Being not a good enough conversion, it was tested the use of a catalytic amount of NaH and more equivalents of *tert*-butyl acrylate (3 and 9 equiv., entries 3 and 4). Finally, by adding 9 equiv. of the commercial ester in 3 portions

over 1 day, a conversion of 78% to the expected derivative **20** was obtained. Remarkably, the best results were obtained when the base was used under stoichiometric amounts (entries 3 and 4).^{94,95,96} Despite these improvements, compound **20** could not be isolated with a high purity degree. Before discarding this synthetic route, the order of the synthetic steps was changed, trying first the functionalisation with *tert*-butyl acrylate of the commercial starting material PEG **18** (Scheme 3.13) in similar reaction conditions than in the best previous case, using NaH or DBU as bases under stoichiometric amounts (Table 3.6).⁸⁵ Both reactions were carried out in dry THF.



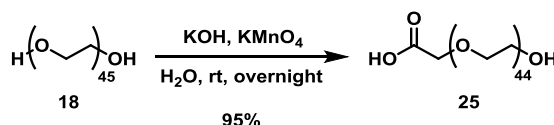
Scheme 3.13. Functionalisation of commercial PEG chain **18** with the *tert*-butyl acrylate.

Table 3.6. Reaction conditions used to obtain PEG derivative **24** and their corresponding conversions.

Entry	Base	Time	Temperature	<i>tert</i> -butyl acrylate	Conversion
1	0.5 equiv. NaH	overnight	0 °C → rt	0.9 equiv.	50%
2	0.01 equiv. DBU	4 h	rt	0.9 equiv.	0%

Unfortunately, working with the initial diol PEG **18** under these conditions did not allow obtaining ester **24** with good conversions values. On one hand, when NaH was used (Table 3.6, entry 1), it was concluded that only the 50% of commercial PEG diol **18** was converted to the ester-PEG **24** by integrating the protons signals of *tert*-butyl group and comparing them with the number of protons of the PEG chain in its ¹H NMR spectrum. On the other hand, using DBU the initial commercial PEG **18** was obtained unaltered (entry 2).

Hence, as this approach did not work, another one was attempted by trying to oxidise directly one of the two terminal alcohols of starting PEG diol **18** using a solution of KMnO₄ and KOH in water (Scheme 3.14) following a described procedure.^{97,98}



Scheme 3.14. Oxidation of one alcohol of PEG **18** to carboxylic acid using KMnO₄.

After several trials and working with different equivalents of KOH and KMnO_4 (Table 3.7), it was found out that by using 15.8 equiv. of the base KOH and 1.9 equiv. of oxidant KMnO_4 (entry 3) the monooxidised product **25** was obtained in excellent yield (95%). By adding more equivalents of both KOH and KMnO_4 reagents (entry 1), the dioxidised product was isolated. The ^1H NMR spectrum of **25** showed a new singlet signal integrating 2 protons at 4.17 ppm, coming from the methylene group between the oxygen and the carboxylic moiety ($-\text{CH}_2\text{COOH}$), thus confirming the oxidation of one alcohol.

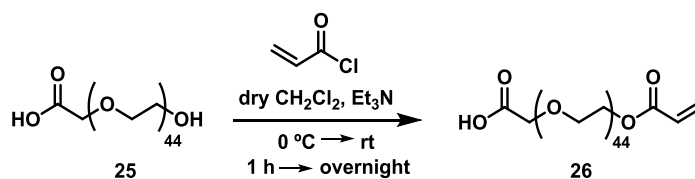
Table 3.7. Oxidative conditions to obtain one carboxylic acid-based PEG **25**.

Entry	KOH	KMnO_4	-OH oxidation*	Yield
1	28 equiv.	2.5 equiv.	2	-
2	9 equiv.	1 equiv.	< 0.9	-
3	15.8 equiv.	1.4 equiv.	1	95%

* From ^1H NMR spectra and integrating the singlet that appears at 4.17 ppm, which corresponds to the methylene next to the formed carboxylic acid, it can be determined the oxidation degree of the alcohols; 2 means that the two alcohols has been oxidised to carboxylic acid; < 0.9 means that less than one alcohol has been oxidised; and 1 means the mono-oxidation of the starting PEG **18**.

Afterwards, the second step was the functionalisation of the remaining alcohol as the corresponding acrylate derivative, necessary to bind the PEG chain to thiol-catechol unit **4** through a thia-Michael reaction, as already explained in the introduction of this chapter.

Therefore, PEG derivative **25** was functionalised with commercial acryloyl chloride (Scheme 3.15). This reaction was attempted using, first, 1 equiv. of acryloyl chloride and 1.3 equiv. of triethylamine (TEA) as a base to neutralise the HCl formed in the reaction, in dry CH_2Cl_2 , for 1 h at 0°C and letting the reaction mixture stirring overnight at rt.^{99,100}



Scheme 3.15. Functionalisation of the second alcohol with an acrylate group to obtain the final heterobifunctional PEG **26**.

In this first attempt, after purifying the resulting PEG by precipitation with Et_2O , in the ^1H NMR spectrum the signals of protons of the double bond from the acrylate group could be distinguished, and their integration allowed to determine that acrylate functionality was successfully introduced to the PEG chain **25** with an 80% of conversion (Table 3.8, entry 1). As in other cases, the conversion had to be improved to values nearest the 100%, so as to avoid

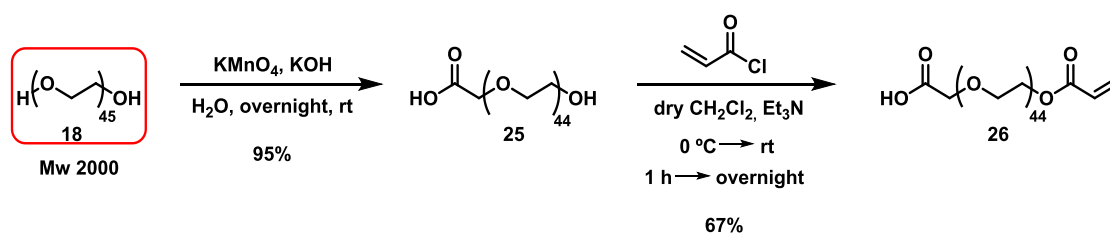
future purification issues. In consequence, other trials were attempted using more equivalents of acryloyl chloride and TEA (entries 2-4).

Table 3.8. Reaction conditions tested to obtain the final heterobifunctional PEG **26**.

Entry	Et ₃ N	Acryloyl chloride	Molecular sieves	(yield)/conversion*
1	1.3 equiv.	1.0 equiv.	No	80%*
2	2.0 equiv.	2.7 equiv.	No	(54%)
3	1.9 equiv.	2.8 equiv.	Yes	(58%)
4	1.4 equiv.	2.0 equiv.	Yes	(67%)

By increasing the equivalents of acryloyl chloride and TEA (entry 2) the heterobifunctional PEG **26** was obtained with a conversion > 95% in 54% yield. On the attempt to optimise this reaction, molecular sieves were added in order to remove residual water that PEG could contain and avoid possible hydrolysis of the acryloyl chloride. Consequently, the yield increased a little bit up to 58% (entry 3). Finally, in order to avoid the formation of the acid anhydride, the equivalents of both acryloyl chloride and TEA were reduced to 2 and 1.4 equiv., respectively, and the conversion was enough improved (> 95%) to allow the isolation of pure **26** in 67% yield (entry 4).

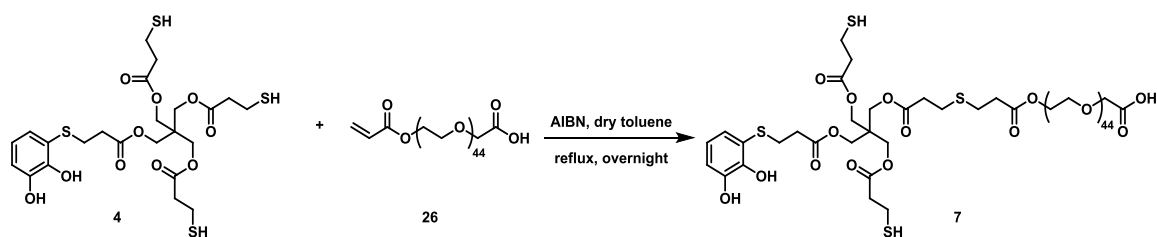
To sum up, the heterobifunctional PEG **26** was obtained from a linear synthesis of 2 steps in 64% overall yield (Scheme 3.16). This short synthesis comprised firstly the monooxidation of one of the terminal alcohols to carboxylic acid and secondly the addition of an acrylate group on the other end.



Scheme 3.16. Synthetic route to afford the desired heterobifunctional PEG **26** in 64% overall yield.

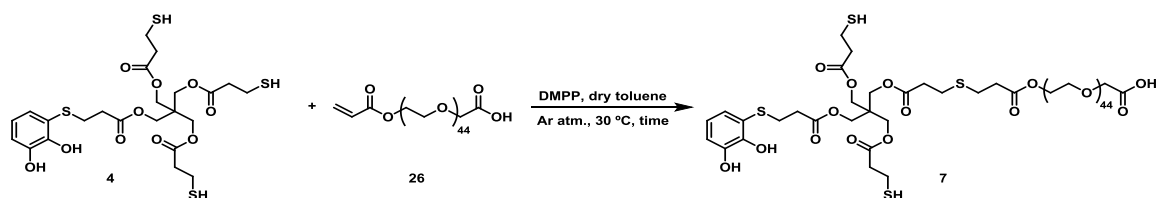
3.2.4.2. Synthesis of building block 7

S-catechol tris-thiol **4** was conjugated with the heterobifunctional PEG **26** *via* the both thiol-ene reactions previously studied, either through a radical or a thia-Michael mechanism.

I. Radical-catalysed thiol-ene reaction

Scheme 3.17. Radical-catalysed thiol-ene reaction to bind together the catechol intermediate **4** with the heterobifunctional PEG **26**.

To carry out this reaction, 0.4 equiv. of AIBN and 4 equiv. of catecholic derivative **4** were used in reflux temperature of dry toluene, overnight. In this case, only 50% conversion of the desired product **7** was achieved.

II. Thia-Michael reaction

Scheme 3.18. Thia-Michael reaction between acrylate group from PEG **26** and one of the free thiols from catecholic intermediate **4**.

The first attempt took place for 4 h, under inert atmosphere, at 30 °C, with an excess of catechol derivative **4**, so as to favour the monosubstitution, and using a catalytic DMPP amount (0.14 equiv.) (Scheme 3.18).

By ^1H NMR it was checked that under these conditions there was roughly a 50% of conversion to the desired product **7** (Table 3.9, entry 1). Thus, longer reaction times and more equivalents of DMPP were used to improve the conversion value (entries 2-4).

Table 3.9. Reaction conditions tested to afford cat-PEG derivative **7**.

Entry	Activator	Catechol 4	Time	(Yield)/conversion*
1	0.14 equiv. DMPP	4.7 equiv.	4 h	50%*
2	0.25 equiv. DMPP	6.9 equiv.	5.5 h	(55%)
3	0.40 equiv. DMPP	9.9 equiv.	5.5 h	(63%)
4	0.40 equiv. DMPP	5.7 equiv.	5 h	(67%)

By using longer reaction times and more equivalents of DMPP, but still being in a catalytic amount, the final product **7** was obtained with a conversion near to 100% in 55% yield after

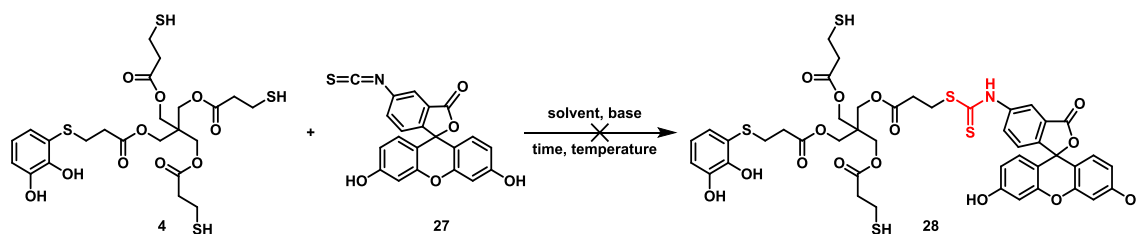
being purified by precipitation with Et₂O several times (entry 2). In order to improve the yield, more equivalents of DMPP and catechol derivative **4** were used, increasing the yield up to 63% (entry 3). However, using a large amount of catechol-based molecule **4** made difficult the purification of the resulting PEG **7**, requiring many recrystallisations with Et₂O. Therefore, another attempt was performed using the same equivalents of DMPP, but decreasing the amount of catecholic derivative **4** to 5.7 equiv. (entry 4). Under those conditions, the cat-PEG molecule **7** was obtained in 67% yield.

To conclude, thia-Michael reaction was a more suitable reaction for this kind of conjugation, since the expected product **7** could be obtained in almost a 100% of conversion with a moderate yield (67%), and the final purity was greater than the one obtained when the radical thiol-ene reaction was used, since less by-products were formed and all they were removed in the purification process.

3.2.5. SYNTHESIS OF FLUORESCEIN-FUNCTIONALISED BUILDING BLOCK **8**

In order to obtain fluorescein derivative **8** from the monosubstituted S-catechol tris-thiol **4**, firstly two approaches were attempted using different kind of commercial fluorescein derivatives to synthesise analogues compounds.

First, the reaction was attempted with the isothionate derivative **27** in order to obtain the final thiourea **28** (Scheme 3.19).¹⁰¹



Scheme 3.19. Unsuccessfully trial of obtaining derivative **28**.

Although different reaction conditions were used, in any case successful results were obtained (Table 3.10).

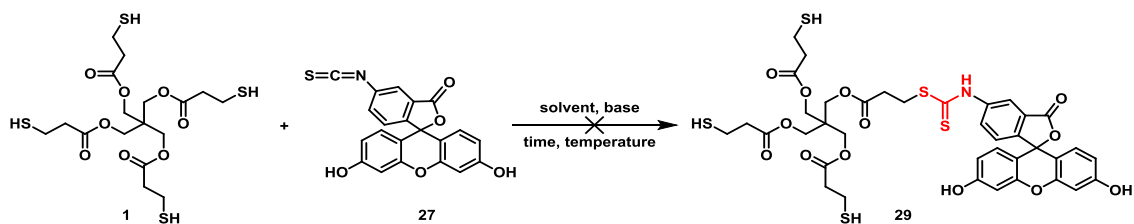
Table 3.10. Two reaction conditions for the synthesis of molecule **28**.

Entry	Base	Solvent	Time	Temperature (°C)	Yield
1	-	dry acetone	20 h	reflux	-
2	3.4 equiv. NaH	dry THF	overnight	reflux	-

Firstly, the reaction was attempted in dry acetone at reflux temperature (Table 3.10, entry 1) following an already described procedure for this kind of reaction.⁸³ Nevertheless, this reaction

did not work, since both starting materials **4** and **27** were recovered. Therefore, the same reaction was attempted in dry THF and using NaH as a base to obtain the corresponding thiolate (entry 2). Unfortunately, a complex reaction mixture was obtained.

Before discarding this synthetic approach, the order of the synthetic steps was changed, trying first the functionalisation with fluorescein derivative of the core **1** (Scheme 3.20) in order to ensure that the catechol moiety did not influence on the reaction (Route B, see Chapter 1, Figure 1.18).

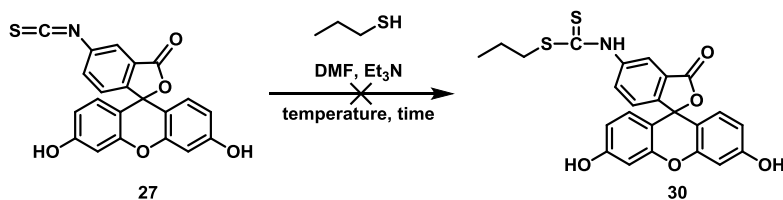


Scheme 3.20. Functionalisation of tetrakis-thiol **1** with the fluorescein derivative **27**.

Table 3.11. Several reaction conditions to obtain S-fluorescein-functionalised tris-thiol **29**.

Entry	Base	Solvent	Time	Temperature (°C)	Yield
1	1.4 equiv. Et ₃ N	dry THF	48 h	rt	-
2	1.4 equiv. Et ₃ N	dry CH ₃ CN	24 h	50 °C	-
3	1.5 equiv. Et ₃ N	dry DMF	24 h	140 °C	-
4	2.5 equiv. EGTA	borate buffer pH 9.2	overnight	rt	-

This reaction was attempted using TEA in three different dry solvents (THF, CH₃CN and DMF), and at different temperatures (from rt to 140 °C) (Table 3.11, entries 1-3). In any cases the final product S-fluorescein tris-thiol **29** was identified. As last try, that reaction was carried out in a basic borate buffer using an excess of ethylene glycol-bis(β-aminoethyl ether)-*N,N,N',N'*-tetraacetic acid (EGTA)¹⁰² (entry 4). However, the expected product was not obtained either. Since with molecule **1**, without previous functionalisation, it was not able to obtain the intermediate **29**, the reaction using as simple model thiol 3-propanthiol was tested (Scheme 3.21).



Scheme 3.21. Trial of constructing reaction with 3-propanthiol.

The reaction was attempted twice, and conditions and results are summarised in the next Table.

Table 3.12. Reaction conditions used in order to form the thiourea moiety.

Entry	Base	Molecule 27	Time	Temperature (°C)	Yield
1	1.4 equiv. Et ₃ N	1.5 equiv.	24 h	40 °C	-
2*	1.5 equiv. Et ₃ N	0.7 equiv.	1 h	100 °C	-

* Entry 2 was carried out under microwave (MW) irradiation into a microwave reactor.

Both reactions were carried out in dry DMF and ~ 1.4 equiv. of TEA were used. It was worked with an excess (Table 3.12, entry 1) and under stoichiometric amount (entry 2) of fluorescein 5(6)-isothiocyanate **27**, and with different reaction times and temperatures. Even, the second reaction was carried out using a microwave reactor. Unfortunately, the thiourea intermediate **30** was not obtained. It seemed that sulphur was not a good enough nucleophile to attack the isothiocyanate group in the chemical context of fluorescein structure. For this reason, another strategy was attempted to obtain the fluorescein-based derivative.

This second synthetic strategy consisted in using 5-(iodoacetamido)fluorescein **31**, an usual reactive in the biological field,¹⁰³ but not in preparative organic synthesis. Nonetheless, it was tried to carry out the corresponding S_N2 reaction (Scheme 3.22) between pentaerythritol tetrakis(3-mercaptopropionate) **1** and 5-(iodoacetamido)fluorescein **31** in two different media; the first one consisted of dry DMF using DIPEA as a base (Table 3.13, entry 1),¹⁰⁴ and the second one of a phosphate buffer at pH 7.4 (entry 2).¹⁰³

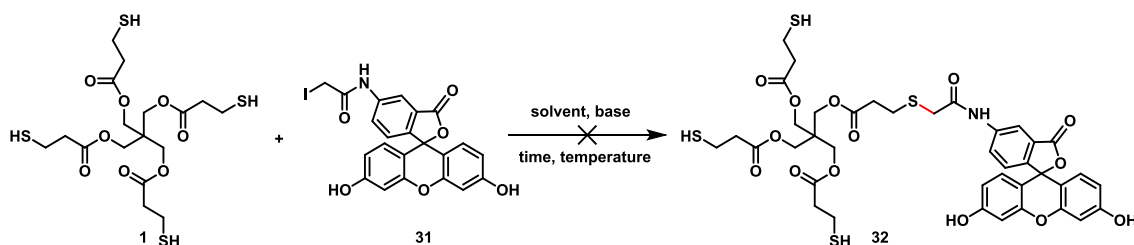
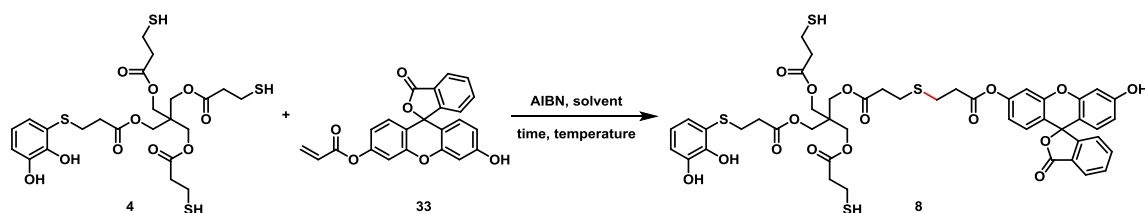
**Scheme 3.22.** Trial of synthesis of fluorescein-functionalised molecule **32** via S_N2 reaction.

Table 3.13. Reaction conditions into an organic (entry 1), and an aqueous (entry 2) media in order to obtain intermediate **32**.

Entry	Base	Solvent	Time	Temperature	Yield
1	1.1 equiv. DIPEA	dry DMF	overnight	rt	-
2	-	phosphate buffer pH 7.4	overnight	rt	-

Unfortunately, none of these two reactions allowed isolating compound **32**. In all cases, both starting materials **1** and **31** were recovered separately after being purified by flash column chromatography.

Finally, a third approach was attempted, using the commercial fluorescein *O*-acrylate **33** (Scheme 3.23) and catecholic intermediate **4**, based on the radical-catalysed thiol-ene reaction.⁸⁴



Scheme 3.23. Synthesis of fluorescent compound **8** through the radical thiol-ene reaction.

In the next Table are summarised the two reactions conditions attempted and the results obtained.

Table 3.14. The thiol-ene trials between tris-thiol **4** and fluorescein *O*-acrylate derivative **33**.

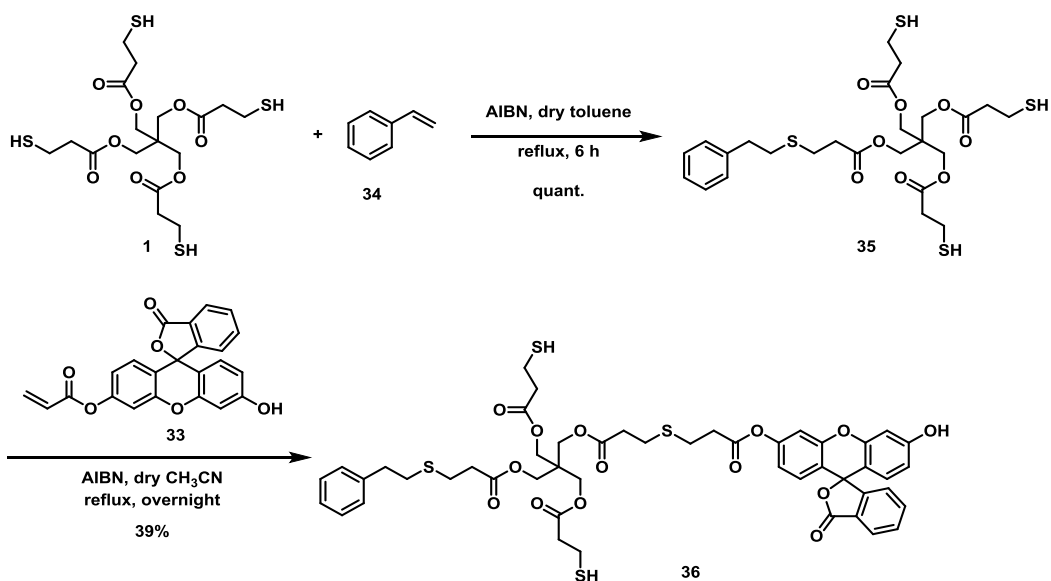
Entry	AIBN	Solvent	Time	Temperature (°C)	Yield
1	0.2 equiv.	dry toluene	overnight	reflux	-
2	0.2 equiv.	dry CH ₃ CN	overnight	reflux	50%

To carry out this radical reaction, a catalytic amount of AIBN (0.2 equiv.) was used. The first trial was in refluxing dry toluene (Table 3.14, entry 1). Nevertheless, since fluorescein **33** was not soluble in it, that reaction did not work. Therefore, the same reaction conditions were used in dry CH₃CN (entry 2) to solve solubility issues. This reaction was monitored by ¹H NMR observing the disappearance of olefinic protons of the acryloyl group of **33**. The reaction was stopped after total conversion to the desired product and the crude was purified by a flash column chromatography to afford target compound **8** as an orange powder in 50% yield.

3.2.6. SYNTHESIS OF FLUORESCHEIN-FUNCTIONALISED STYRENIC DERIVATIVE **36**

As already mentioned in the introduction of this chapter, a fluorescein-functionalised building block containing a styrene moiety was synthesised to demonstrate the role of catechol in the adhesion properties.

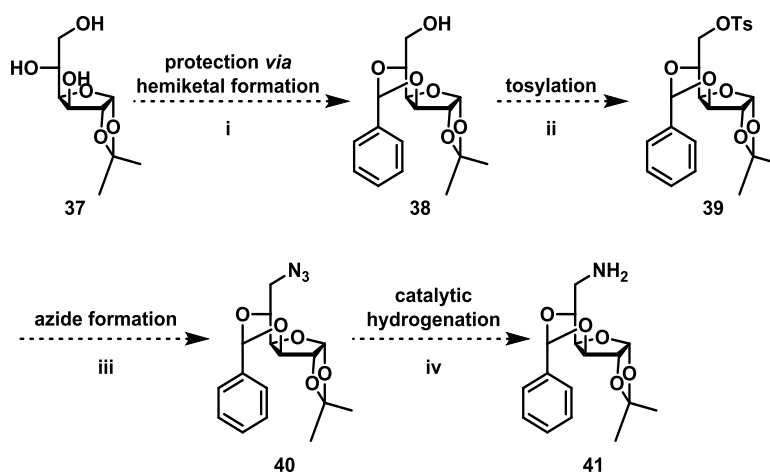
This styrenic derivative was synthesised by means of two consecutive radical-catalysed thiol-ene reactions (Scheme 3.24) with the conditions already studied for the catecholic compound **8**. As in previous cases, the functionalisation of molecule **1** with styrene **34** to obtain intermediate **35** was followed by ¹H NMR, observing the disappearance of protons' signals from the double bond of styrene. In that case, no purification methods were required since oil **35** was obtained quite pure in a quantitative manner. From this molecule, the target compound **36** was prepared in 39%, after purification by column chromatography.



Scheme 3.24. Synthesis of the fluorescein-functionalised styrenic derivative **36**.

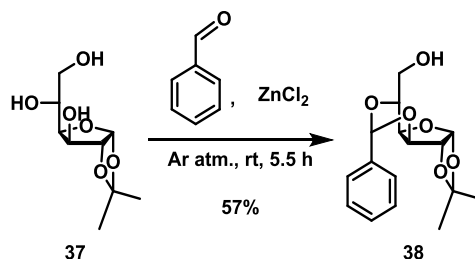
3.2.7. SYNTHESIS OF AMINO-GLUCOFURANOSE DERIVATIVE **41**

To obtain this sugar derivative, the following synthetic route (Scheme 3.25) was proposed. The synthesis would start with the protection of the two vicinal alcohols of the commercial 1,2-*O*-isopropylidene- α -D-glucopyranoside **37** by forming an hemiketal using benzaldehyde. Then, the remaining primary alcohol would be tosylated in order to allow the introduction of an azido group. Finally, a catalytic hydrogenation would deliver the amino-glucopyranoside derivative **41**.



Scheme 3.25. Synthetic pathway to obtain amino-glucopyranoside derivative **41** that includes (i) protection of the two vicinal alcohols forming an hemiketal using benzaldehyde; (ii) tosylation of the remaining primary alcohol; (iii) introduction of the azido; and followed by (iv) catalytic reduction of the azido to obtain a primary amine.

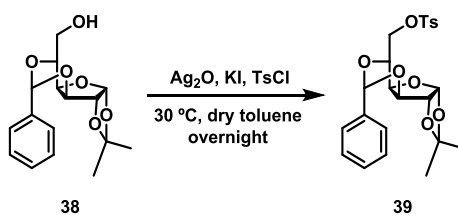
As already mentioned, the synthesis started from the commercial triol **37**. In the first reaction, the two secondary vicinal alcohols were protected using benzaldehyde, which was distilled previously, in order to form the hemiketal **38** (Scheme 3.26). This reaction was carried out using zinc chloride as Lewis Acid.¹⁰⁵



Scheme 3.26. Protection of the two vicinal secondary alcohols through a hemiketal.

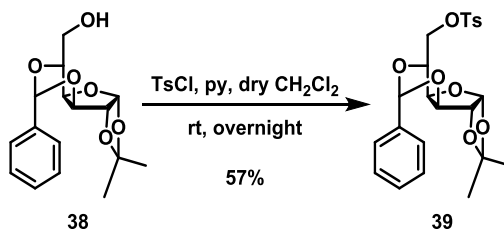
The protected sugar **38** was purified by crystallisations with hexane and at the end it was obtained in 57% yield.

Then, the remaining primary alcohol was tosylated following the same reaction conditions used to prepare PEGylated compound **19** (Scheme 3.27).^{82,89}



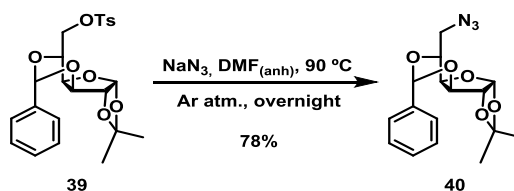
Scheme 3.27. Tosylation of the primary alcohol of sugar **38**.

Under those conditions, a conversion higher than 90% towards tosylated derivative **39** was achieved. Nonetheless, in order to achieve almost a 100% conversion this reaction was also attempted under usual basic conditions using anhydrous pyridine, 3 equiv. of *p*-toluenesulfonyl chloride and dry CH₂Cl₂ (Scheme 3.28). Under those conditions a total conversion towards tosylate intermediate was almost achieved obtaining **39** in 57% yield after being recrystallised with hexane several times.



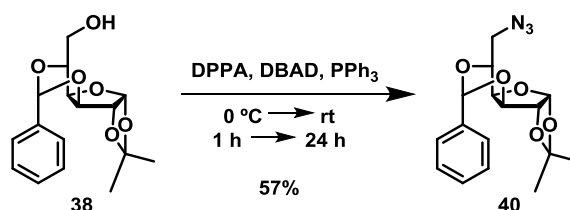
Scheme 3.28. Tosylation of the primary alcohol of sugar **38** using pyridine and *p*-toluenesulfonyl chloride.

The next step consisted in substituting the tosylate group by an azide. This reaction was carried out using 7 equiv. of NaN_3 , in dry DMF, at 90 °C, and was left to progress overnight (Scheme 3.29).⁸² The final azide intermediate **40** was obtained in 78% yield and was used in the next step without further purification.



Scheme 3.29. Formation of the azido group **40** from tosylate **39**.

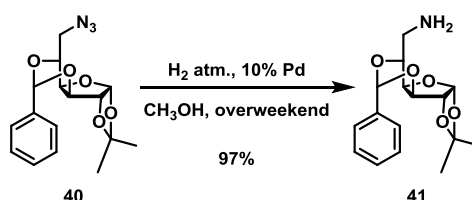
Furthermore, from protected glucofuranose derivative **38**, the azide-based glucose **40** was obtained directly through a Mitsunobu reaction,¹⁰⁶ avoiding the formation of tosylate intermediate **39** (Scheme 3.30).



Scheme 3.30. Mitsunobu reaction to obtain azide **40** from alcohol **38**.

To obtain this derivative **40**, first it was prepared a phosphonium salt with PPh₃ and di-*tert*-butyl azodicarboxylate (DBAD) at 0 °C. Afterwards, alcohol **38** and diphenylphosphoryl azide (DPPA) as the azide source were added and the reaction was left stirring for 1 day to reach rt. The crude was purified by a column chromatography to afford the product **40** as a white solid in 57% yield, thus improving the previous synthesis of this molecule **40** through tosylate intermediate **39** from common alcohol precursor (44% overall yield).

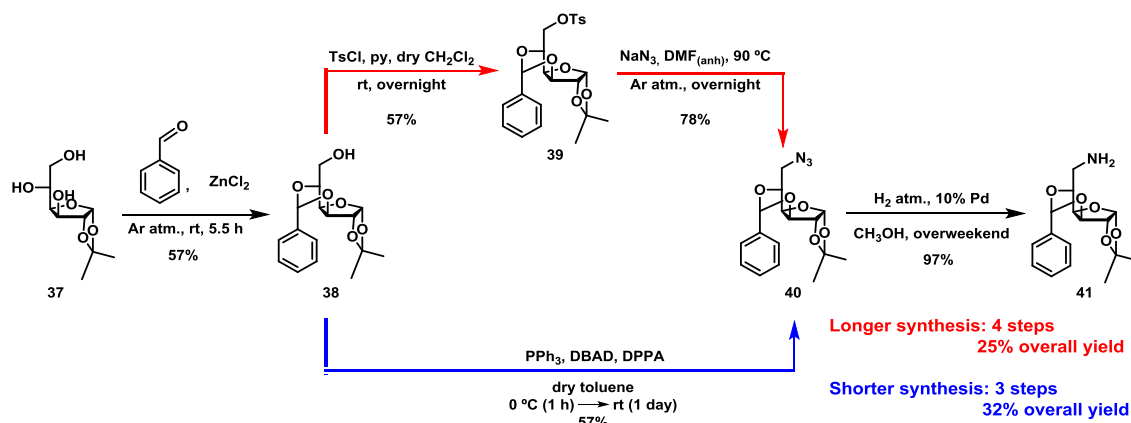
Finally, in order to obtain the final amino-glucofuranose derivative **41**, azide **40** was reduced under H₂ atmosphere with 10% w/w of Pd on activated charcoal.^{96,107}



Scheme 3.31. Hydrogenation of the azide group to afford the amine **41**.

Afterwards, the reaction mixture was filtered over Celite® in order to remove Pd and concentrated under vacuum, affording crude material **41**, which was recrystallised with hexane, finally affording amino sugar **41** in 97% yield.

In summary, the amino-glucofuranose derivative **41** could be obtained through a linear synthesis either (i) by forming a tosylate-glucofuranose derivative **38** in 4 steps in 25% overall yield (Scheme 3.32, red line), or, (ii) *via* three synthetic steps that included a Mitsunobu reaction in 32% overall yield (Scheme 3.32, blue line).



Scheme 3.32. Two different ways to obtain the amino-glucofuranose derivative **41**; *via* the formation of a tosylate intermediate (red line) and through a Mitsunobu reaction (blue line).

3.3. SULPHUR-BASED POLYMERISATION REACTION

3.3.1. CHARACTERISATION METHODOLOGIES

The products obtained from polymerisation reactions were characterised by different techniques, such as ^1H NMR, DOSY NMR experiments and gel permeation chromatography (GPC). ^1H NMR and DOSY experiments were performed in THF- d_8 , whereas GPC analyses were performed in THF. A first rough value of the polymerisation degree in the material was determined by ^1H NMR, calculating the ratio of thiol's peak between the starting monomer and the resulting product from the polymerisation reaction. For some of the materials, their polymerisation degrees were also determined calculating the corresponding molecular weights by means of GPC and DOSY NMR techniques. To prepare GPC samples, the derivatives obtained after polymerisation were dissolved in THF (1 or 2 mg/mL) and filtered through 0.22 μm nylon filters. To determine the polymerisation degree by DOSY NMR experiments, firstly a calibration curve was needed. Hence, four patterns with known molecular weights were used: 1-decene, 1-octadecene, PEG methyl ether 2000 and PEG methyl ether 5000. Their diffusion coefficients were measured, and the diffusion coefficients of the products obtained from the

polymerisation reactions were interpolated into the calibrate curve to know approximate values of their molecular weights.

3.3.2. POLYMERISATION REACTION

Once the different building blocks (**5**, **6**, **7**, **8**, and **36**) were synthesised and characterised, they were polymerised using the strategy based on the formation of disulphide bonds under mild oxidative conditions using a solution of resublimed iodine in EtOH 96% (Figure 3.15).¹⁰⁸ These mild conditions are compatible with the different functional fragments present in the building blocks.

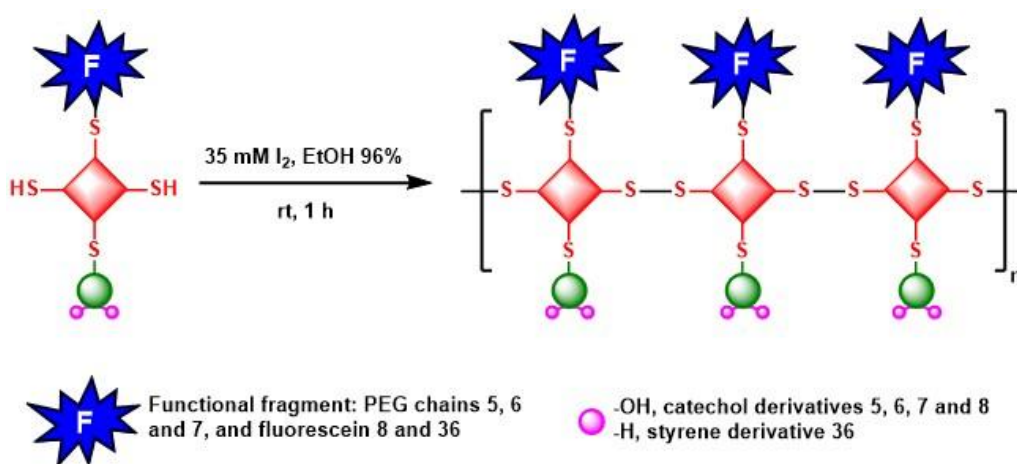


Figure 3.15. Mild oxidative polymerisation of synthesised building blocks using a solution of iodine in EtOH 96%.

In the general procedure of this polymerisation strategy, the monomers were dissolved in EtOH 96% and a 35 mM solution of resublimed iodine (1 equiv.) in the same solvent was added dropwise. Whereas monomers were soluble in the media, the corresponding products resulting from the polymerisation reaction were not, being easy to isolate and washed them with fresh solvent (Table 3.15). It was observed that small percentages (3-5%) of the doping tris-thiol molecule **4** favoured the intermolecular S-S bond formation, thus the polymerisation. On the contrary, whether the polymerisation reaction was not doped by this tris-thiol, the resultant products did not precipitate in the media, being impossible to isolate them. (*Note:* From now on, *P* is referred to the product obtained from the polymerisation reaction).

Table 3.15. Yields of the polymerisation reactions based on the amount of the solid precipitate vs. the initial amount of each monomer **5**, **6**, **7**, **8** and **36**.

Products from the polymerisation reaction	Yield (%)
P5 (mPEG-functionalised catecholic derivative, (-acryl))	45%
P6 (mPEG-functionalised catecholic derivative, (-allyl))	28%
P7 (HOOC-PEG-functionalised catecholic derivative, (-acryl))	41%
P8 (fluorescein-functionalised catecholic derivative)	34%
P36 (fluorescein-functionalised styrenic derivative)	29%

This step-growth type polymerisation was followed by ^1H NMR and it was seen that catechol moiety did not suffer any kind of oxidation process. Furthermore, it was also observed that the intensity of thiol proton signal decreased, as expected if the polymerisation takes place through thiols by forming disulphide bonds and not through the catechol moiety (see *Annex A2* for GPC spectra).

Product **P7** was studied in detail as a standard to optimise the reaction conditions of this polymerisation strategy. Firstly, building block **7** was polymerised without using any kind of doping molecule. In this case, different solvents, concentrations, and order of addition were evaluated in order to optimise such reaction (Table 3.16).

Table 3.16. Different polymerisation conditions tested to polymerise building block **7**.

Entry	Solvent	Concentration	Equiv. I_2	Time	Order of addition*	Yield
1	THF	20 mg/mL	1.1	1 h	Into PEG	52%
2	CHCl_3	18 mg/mL	1.3	1 h	Into PEG	34%
3	abs. EtOH	20 mg/mL	1.1	1 h	Into PEG	70%
4	EtOH 96%	20 mg/mL	1.1	1 h	Into PEG	43%
5	abs. EtOH	41 mg/mL	1.1	1 h	Into PEG	69%
6	EtOH 96%	42 mg/mL	1.2	2 h	Into I_2	54%
7	EtOH 96%	54 mg/mL	1.1	1 h	Into PEG	55%

All the reactions were carried out at rt. The yields obtained were based on the final amount obtained after polymerisation vs. the initial amount used of starting monomer **7**. Abs.: absolute. * Into PEG means that the solution of I_2 is added dropwise into the monomer's solution, and into I_2 the opposite way.

In all the cases it was used an excess of iodine in order to favour the formation of longer oligomers. However, in none of those cases precipitated materials were obtained. As a general procedure to treat those soluble samples, a saturated aqueous solution of $\text{Na}_2\text{S}_2\text{O}_3$ was added into reaction mixtures to quench the excess of iodine. The soluble materials were extracted with CH_2Cl_2 and the combine organic extracts were dried with anhydrous Na_2SO_4 , filtered and concentrated under vacuum. The residues were dissolved in the minimal volume of CH_2Cl_2 and

Et₂O was added until cloudiness appeared. The mixtures were stored in the fridge overnight. Afterwards, the white precipitates were filtered, washed with fresh solvent and dried under vacuum. After doing this first screening, it was observed that after 1 h of reaction the polymerisation had finished, since no improvements were observed after 2 h (Table 3.16, entry 6). The polymerisation reaction was carried out in THF and CHCl₃ achieving yields of 52% and 34%, respectively (entries 1 and 2), and when it was carried out with both absolute EtOH (entries 3 and 5) and EtOH 96% (entries 4, 6, 7), it was observed that with the first one the highest yield (70%) was obtained (entry 3). Furthermore, it was studied whether the order of addition could influence on the formation of the oligomers. Commonly, a solution of iodine was added dropwise into a solution of the cat-PEG derivative **7** while stirring, but the addition of a cat-PEG **7** solution into an iodine one was also attempted (entry 6). However, no significant differences were observed.

Once the cat-PEG derivatives were isolated, they were analysed by GPC and ¹H NMR techniques. GPC analyses revealed only one peak at around ~ 2500-2800 in all the cases. That number corresponded to the molecular weight of the monomer **7** and no more peaks corresponding to oligo-/polymeric forms appeared. Nevertheless, by ¹H NMR it was observed the disappearance of the thiol proton's signal at 1.64 ppm, indicating that disulphide bonds had been formed (Figure 3.16).

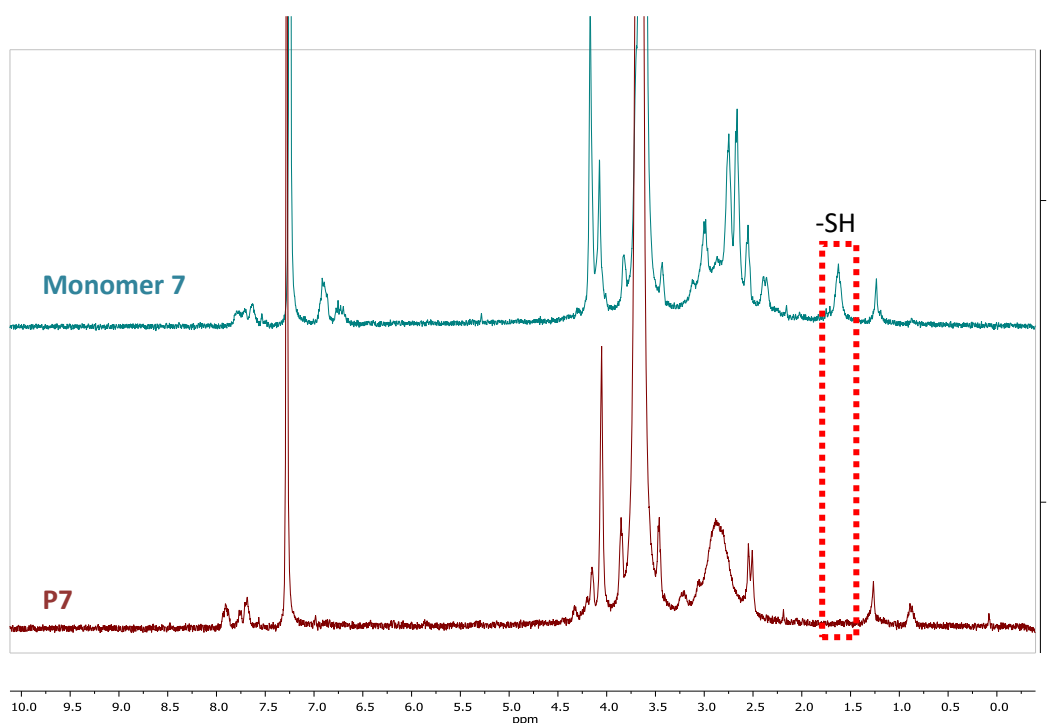


Figure 3.16. ¹H NMR spectra of the starting monomer **7** (blue) and the product resultant from the polymerisation reaction **P7** (red). It is observed the disappearance of the thiols' proton signal at 1.64 ppm in the ¹H NMR spectrum of the **P7**.

After these first results, it was concluded that monomer **7**, working under those conditions, tended to cycle itself as shown in Figure 3.17. This cyclation is favoured since the pentaerythritol tetrakis(3-mercaptopropionate) (in red) is a tetrahedron with four identical branches in 109° and contains a long PEG chain in a mushroom conformation surrounding it, which makes the polymerisation difficult.

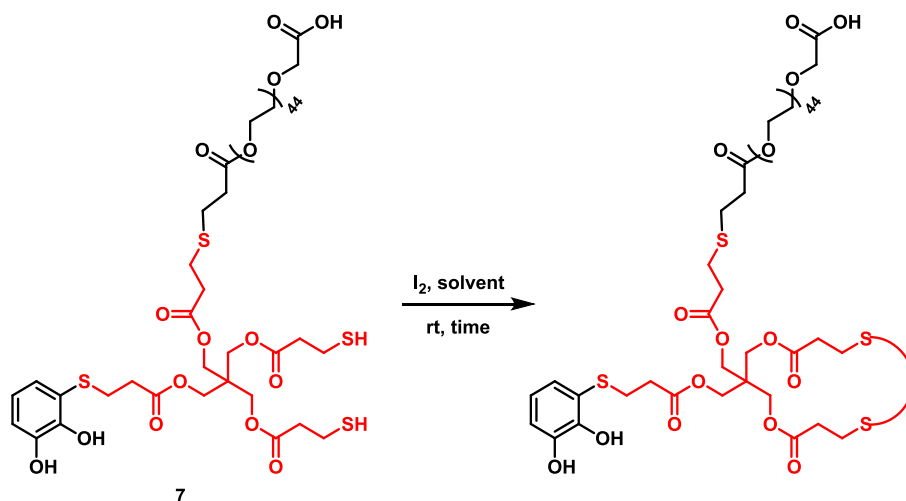


Figure 3.17. Possible cyclation of cat-PEG monomer **7** between the two free thiols.

As already mentioned, in order to favour the formation of intermolecular S-S bond and to avoid the cyclation of the monomer **7**, the polymerisation reaction was carried out by doping it with different amounts of S-catechol tris-thiol **4** as shown in Figure 3.18 and Table 3.17.

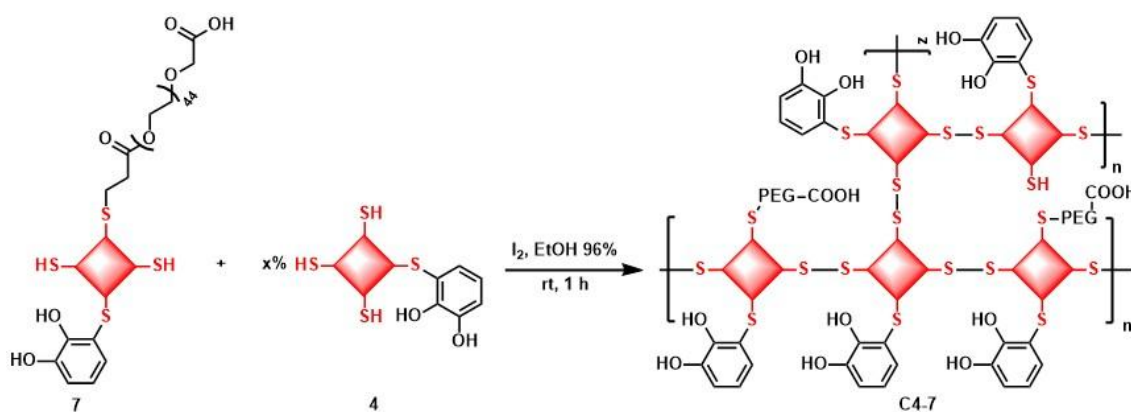


Figure 3.18. Copolymerisation of cat-PEG **7** with intermediate **4**. Since molecule **4** has three thiols, the product obtained could present a cross-linked structure.

Table 3.17. Different polymerisation conditions tested to copolymerise intermediate **7** with catecholic molecule **4**.

Entry	Doping (4)	Equiv. I ₂	Yield
1	18% cat-(SH) ₃	1.1	54%
2	6% cat-(SH) ₃	1.1	40%
3	3% cat-(SH) ₃	1.1	16%
4	3% cat-(SH) ₃	1.4	8%

In all the cases the solution of I₂ was added dropwise into the mixture of **4** and **7**, and the reactions were carried out at rt. The yields obtained were based on the final amount obtained of PEGylated derivatives vs. the initial amount of starting monomer **7** used.

By doping with derivative **4**, a precipitate was formed, and then isolated, washed with fresh EtOH 96%, and dried under vacuum. By adding more cross-linker **4**, a higher amount of precipitated material was obtained (Table 3.18, entry 1). However, the most doped ones (entries 1 and 2) were very sticky and less soluble in common organic solvents. Therefore, less amount of molecule **4** was used in order to trigger the polymerisation of cat-PEG **7**, but without a lot of cross-linking (entries 3 and 4). Trying these conditions, it was observed that an increase of the equivalents of iodine disfavoured the formation of the precipitate (entry 4) getting lower yields, may be due to the acidic medium formed because of the presence of HI. None of the four doped cross-linked materials were soluble in THF, so GPC analyses could not be performed. Nonetheless, by ¹H NMR it was observed the disappearance of thiols' peak at 1.64 ppm (Figure 3.19).

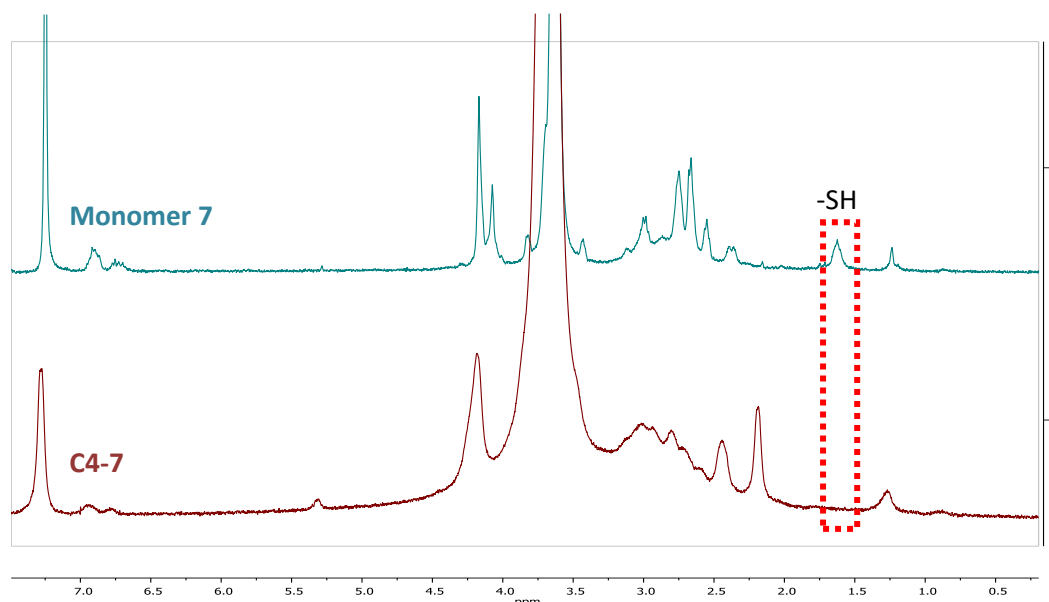


Figure 3.19. ¹H NMR spectra of the starting monomer **50** (blue) and the resulting cross-linked **C4-7** (red). It is observed the disappearance of the thiols' proton signal at 1.64 ppm in the ¹H NMR spectrum of the derivative **C4-7**.

In summary, using compound **4** as doping agent, the resulting product of polymerisation was obtained in low yield (16%) as a sticky solid and insoluble in THF, probably because its possible cross-linked structure. Therefore, the polymerisation was also tried by doping it with a new molecule similar to **4**, but with only two thiols. In that way, it was ensured that monomer **7** was polymerised without cross-linking (Figure 3.20).

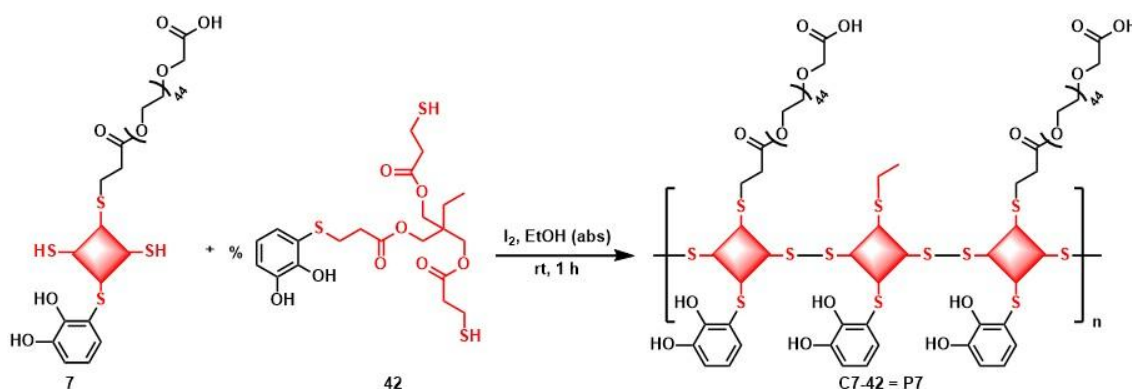


Figure 3.20. Copolymerisation between cat-PEG **7** and S-catechol-bis-thiol **42**.

This polymerisation reaction was tested using different conditions summarised in the next Table.

Table 3.18. Different polymerisation conditions tested to polymerise building block **7** with catecholic molecule **42**.

Entry	Solvent	Doping (42)	Temperature	Equiv. I ₂	Time	Yield
1	abs. EtOH	10% cat-(SH) ₂	rt	0.74	1 h	39%
2	abs. EtOH	3% cat-(SH) ₂	rt	0.75	1 h	34%
3	abs. EtOH	2.2% cat-(SH) ₂	rt	0.79	1 h	41%
4	abs. EtOH	0.5% cat-(SH) ₂	rt	0.71	1 h	36%
5	abs. EtOH	3.5% cat-(SH) ₂	rt	1.1	2.5 h	55%
6	abs. EtOH + DMF	2.4% cat-(SH) ₂	40 °C	0.74	1 h	26%

In all the cases the solution of iodine was added dropwise into the mixtures of **7** and **42**.

In all the cases a precipitate was obtained, and then isolated, washed with fresh absolute EtOH, and dried under vacuum. Preferably, the polymerisation reactions were carried out using under stoichiometric amounts of iodine in order to avoid the formation of long polymers, which would be less soluble in common organic solvents, and to prevent the formation of a very acidic medium. Doped cat-PEG **7** with bis-thiol **42** in a range of 0.5% to 10% provided yields between 30-40% (Table 3.18, entries 1-5), except when it was used an excess of iodine (entry 5), getting the highest yield (55%), and when the reaction was attempted in a mixture of absolute EtOH and DMF at 40 °C (entry 6), where the lowest yield (26%) was obtained. Apart from those two cases, it seemed that the amount of doping molecule **42** in that range did not

influence on the formation of the resulting product **P7**. Finally, GPC analyses of those precipitates were performed and it was found that no relevant peaks appeared in their spectra. Furthermore, in that case it was not possible to check the presence of some free thiol groups after polymerisation by ^1H NMR due to the presence of a broad signal at 1.70 ppm in the spectra of the products obtained from the polymerisation reactions.

In other experiments, when the cat-PEGylated starting monomer **7** was run in the GPC, a peak at $M_n \sim 2600$ was identified. Therefore, if nothing was detected by GPC when those products obtained from the polymerisation reaction of **7** doped with **42** were ran, that meant that those samples were at least short oligomers which were not soluble in THF as already seen in the first experiments performed. Hence, in an indirect way, it could be assumed that by doping the cat-PEG derivative **7** with molecule **42** a mixture of oligomers can be obtained.

Once it was studied in detail the polymerisation of PEGylated derivative **7** and observing the importance of having doping molecules to favour the polymerisation against the cyclation, the next derivatives **5**, **6** and **8**, were directly polymerised with the presence of the impurity dragged from their synthesis (intermediate **4**). Due to solubility issues, only the PEGylated derivative **P6** could be characterised by the three ^1H NMR, DOSY experiments and GPC techniques since fluorescein-functionalised materials **P8** and **P36** were only soluble in acetone, and the mixtures of the other PEGylated derivative **P5** resulting from the polymerisations were not soluble in THF. In the case of **P6**, it was observed that the three methods were comparable because the values obtained from all of them were in the same order of magnitude (Table 3.19).

Table 3.19. Polymerisation's degree of cat-PEG-functionalised **P6** determined by ^1H NMR, DOSY experiments and GPC.

Derivative	^1H NMR	DOSY	GPC ^a			
			IR		UV	
			Mn	Mw	Mn	Mw
P6	dimer/trimer	dimer				
			5415 Da	7899 Da	7922 Da	12340 Da
			dimer	trimer	trimer	4/5 units

All three techniques suggested that the mPEGylated building block **6** polymerised up to 2-5 units (see *Annex A2.1-2* for GPC spectra). The small degree of polymerisation could be attributed to the fact that the building block **6** had a long PEGylated chain that it would not be stretched, but in a mushroom conformation, providing high steric hindrance, thus preventing

^a GPC analyses were performed in collaboration of Dr. Haritz Sardon from the Innovative Polymers Group led by Dr. David Mecerreyes at POLYMAT (Basque Center for Macromolecular Design and Engineering).

further polymerisation through the thiol groups. With regard to **P5**, it could be only characterised by ^1H NMR in CDCl_3 due to solubility issues in THF. By integrating the protons of $-\text{SH}$ at 1.64 ppm, it was estimated that its degree of polymerisation was around 2/3 units. As far as fluorescent derivatives **P8** and **P36** were concerned, since their ^1H NMR spectra recorded in $(\text{CD}_3)_2\text{CO}$ were messy and only broad signal bands were observed, it was difficult to determine their degree of polymerisation (see *Annex A1.2* for ^1H NMR spectra).

3.4. NANOPARTICLE COATINGS

3.4.1. COATINGS ONTO MESOPOROUS SILICA NANOPARTICLES

With mPEGylated derivatives **5**, **6**, **P5** and **P6**, coatings onto mesoporous SiO_2 NPs (MSNPs, $\varnothing \sim 200 \text{ nm}$)^b were performed. As a general procedure (Figure 3.21a), 10 mg of NPs were dispersed in 1 mL HPLC grade CH_2Cl_2 and a solution of $\sim 7 \text{ mM}$ of the corresponding mPEGylated derivative was added into it, and the mixture was left to stir at 500 rpm overnight at rt. The final dispersion was centrifuged at 14000 rpm for 2 min and the resulting MSNPs were washed with fresh CH_2Cl_2 three times in order to remove the excess of mPEG derivatives.

Those MSNPs were characterised by different techniques; scanning transmission electron microscopy (STEM), energy-dispersive X-ray spectroscopy (EDX), dynamic light scattering (DLS) and ζ -potential measurements.

From STEM images (Figure 3.21b) PEGylated coatings onto the MSNPs were identified; they were observed as thin lighter layers (*ca.* 20 nm) surrounding the NPs, whereas the non-treated MSNPs did not show any organic shell surrounding them. In the case of MSNPs@**P6**, the coating was evinced in the EDX line scan (Figure 3.21c) by the presence of carbon (red line) across the whole diameter of coated particles, in contradistinction to the oxygen signal (blue line), which appeared circumscribed to their inner sections, *i.e.* to the mineral cores.

^b These MSNPs were provided by Dr. Christian Bellacanzone from *Nanostructured Functional Materials* research group at *Institut Català de Nanociència i Nanotecnologia* (ICN2).

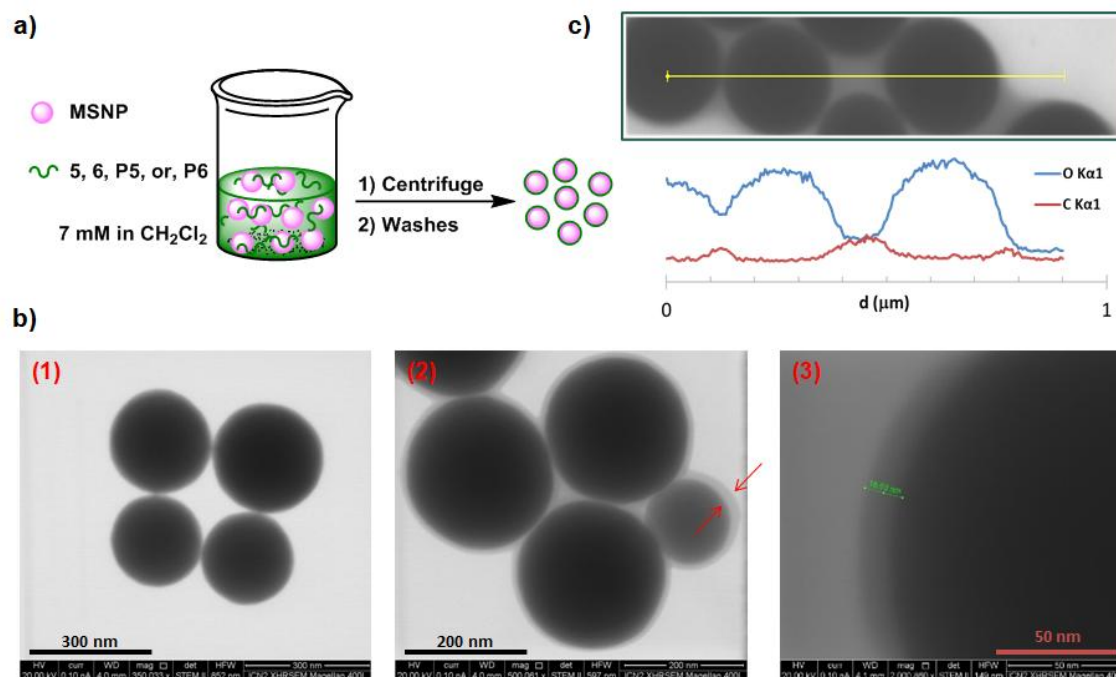


Figure 3.21. a) Schematic representation of the coating procedure onto MSNPs. b) STEM images of untreated MSNPs (1), P5-coated MSNPs (2) and P6-coated ones (3). c) EDX line scan profile along the line drawn across the diameter of P6-coated MSNPs.

Beyond an electronic microscopy characterisation, coated MSNPs with **5** and **P5** were also characterised by DLS and ζ -potential measurements in different pH. In order to carry out those experiments, untreated and treated MSNPs (0.5-1 mg) were dispersed in 1 mL of different aqueous solutions in a pH range from 2 to 12. DLS results (Figure 3.22) revealed that the treated and the untreated MNPs were stabilised between pH 4 and 12 with sizes around 200-250 nm. At pH 2, aggregates were formed with sizes higher than 1 μm due to the worse electrostatic stabilisation and the progressive coating disaggregation from the NPs.

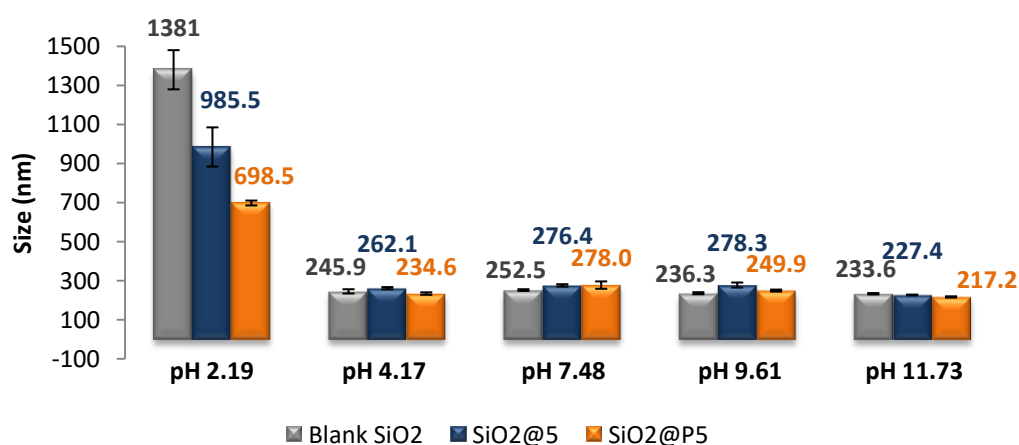


Figure 3.22. a) DLS analyses of untreated (grey) and treated (blue and orange) MSNPs at different pH. DLS values are the average of three measurements.

Furthermore, changes on the ζ -potential values (Figure 3.23) of treated MSNPs vs. pristine ones revealed that the surface of these NPs had changed, thus they had been coated with both mPEGylated derivatives **5** and **P5** (blue and orange, respectively). **P5**-coated MSNPs showed ζ -potential values closer to 0 mV, meaning that more organic chains and less hydroxyls were exposed onto their surface, whereas **5**-coated MSNPs presented ζ -potential values nearer to the pristine MSNPs ones, meaning that more hydroxyl groups and less methyl ones were exposed onto their surface. A possible explanation for those significant differences between MSNPs@**5** and MSNPs@**P5**, mainly between pH 4 and 10, could be that with **P5** a more efficient coating and more robust against washes was obtained vs. with derivative **5**.

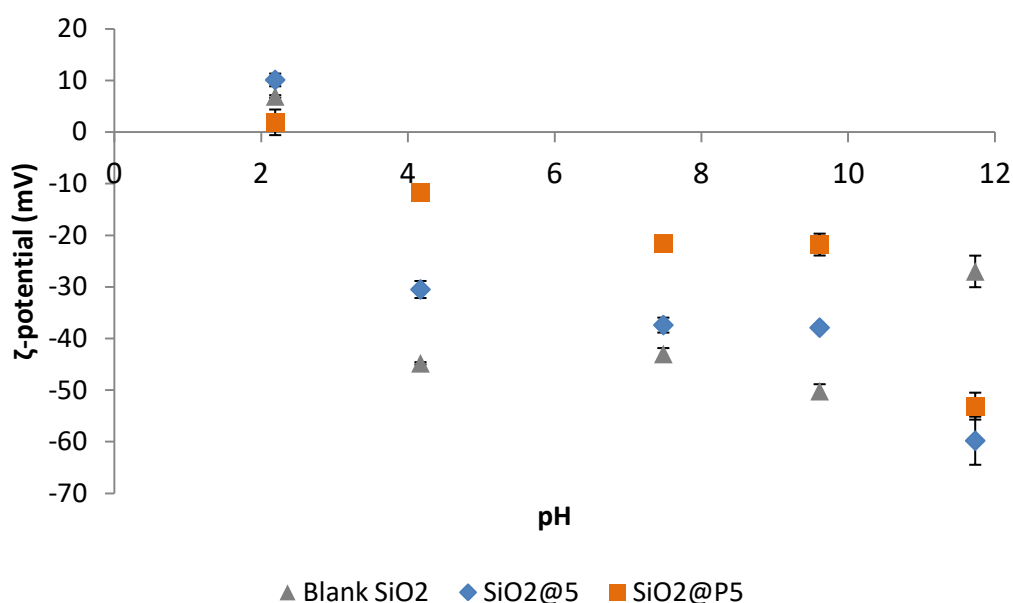


Figure 3.23. ζ -potential values of untreated (grey) and treated (blue and orange) MSNPs at different pH. ζ -potential values are the average of three measurements.

Further experiments to confirm that the coating described was coming from the catechol-based polymers, the experiments were repeated now with **8** and **P8** to confer fluorescence to MSNPs. Following the same general procedure described before (see Figure 3.21a) using HPLC grade acetone, MSNPs were coated with both fluorescent derivatives **8** and **P8**. It was observed that NPs treated with catecholic fluorescein-functionalised derivatives (**8** and **P8**) were coated successfully, since they showed fluorescence under UV light (Figure 3.24a, left), and also when they were observed with an optical microscope in a fluorescence mode with an Alexa Fluor 488 filter. Furthermore, these catechol-based fluorescent coatings were also characterised by STEM. They were observed as thin lighter layers surrounding the NPs (Figure 3.24b).

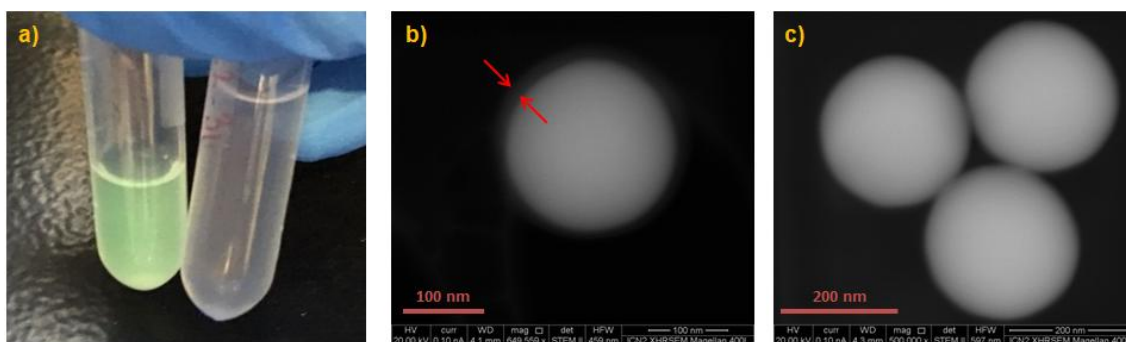


Figure 3.24. a) **P8**-coated MSNPs (left) and **P36**-coated MSNPs (right) under UV lamp at 254 nm. STEM image of b) MSNP@**P8** and c) MSNP@**P36**.

As already explained at the beginning of this chapter, for comparison reasons, the fluorescein-functionalised derivatives containing styrene moieties **36** and **P36** were also used to attempt to coat MSNPs to check the role of catechol in the adhesion properties. It was observed that the NPs treated with these derivatives did not show any fluorescence by any tested method (Figure 3.24a, right) and from STEM images it was seen that MSNPs@**P36** looked like pristine MSNPs, without non-organic material surrounding them (Figure 3.24c). Thus, this simple example showed the important role of the catechol moiety as an anchor in this kind of absorption processes; in this case mainly forming hydrogen bonding with hydroxyl groups exposed onto the surface of MSNPs.

3.4.2. COATINGS ONTO MAGNETITE NANOPARTICLES

As already explained at the beginning of this chapter, PEGylated derivative **P7** was directed to coat MNPs.

3.4.2.1. Preparation of MNPs

MNPs stabilised with oleic acid (Fe_3O_4 @OA NPs) were synthesised by thermal decomposition of $\text{Fe}(\text{acac})_3$ in a mixture of organic solvents following a similar approach to the one developed by Muro-Cruces *et al.*¹⁰⁹ Thus, $\text{Fe}(\text{acac})_3$, sodium oleate, and oleic acid in a mixture of solvents were heated up to 110 °C and kept at this temperature during 1.5 h under vacuum. During this time, reactive intermediates were formed. The reaction mixture was then heated up to 290 °C, kept at this temperature during 1 h under argon flow. In this step, the nucleation and the subsequent growing of the NPs took place. Finally, the reaction mixture was cooled down to 50 °C (Figure 3.25). The resulting MNPs were purified by washing with isopropanol and acetone. Finally, the MNPs were redispersed in CHCl_3 (~ 6.5 mg/mL).

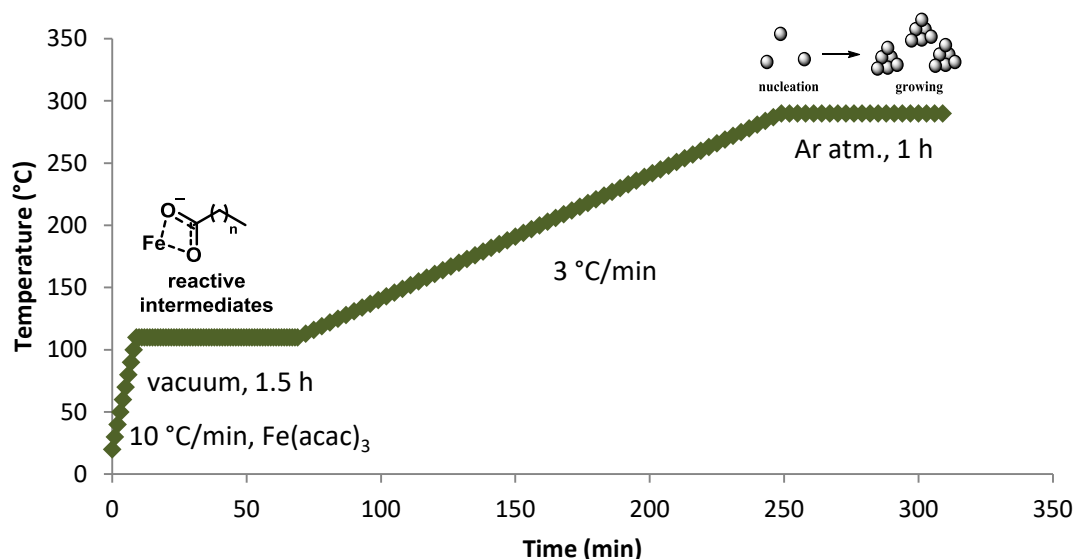


Figure 3.25. Steps for the synthesis of $\text{Fe}_3\text{O}_4@OA$ NPs. With a heating rate of $10\text{ }^\circ\text{C}/\text{min}$, the reaction mixture was heated to $110\text{ }^\circ\text{C}$ for 1.5 h in order to start forming coordination bonds between Fe(III) and carboxylate groups from oleic acid. Afterwards, the temperature was heated up to $290\text{ }^\circ\text{C}$ with a heating rate of $3\text{ }^\circ\text{C}/\text{min}$ and let for 1 h in order to generate $\text{Fe}_3\text{O}_4@OA$ NPs.

The resulting NPs were characterised by transmission electron microscopy (TEM) (Figure 3.26). They had hexagonal morphology with a diameter of 8 nm, and they were well dispersed.

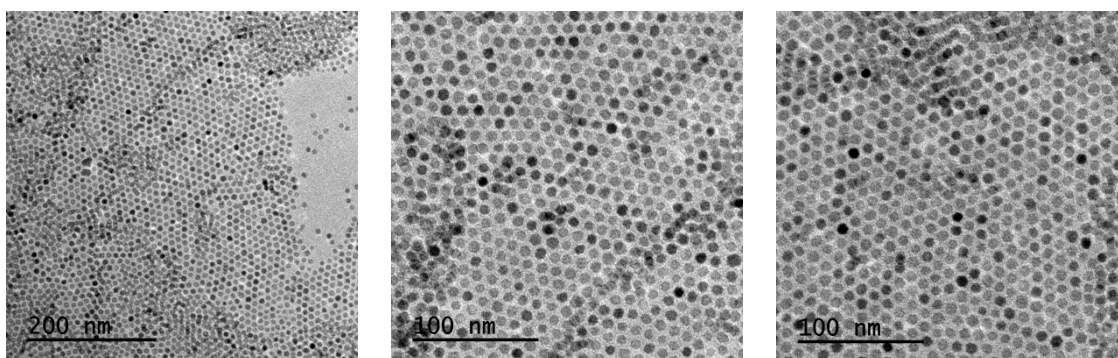


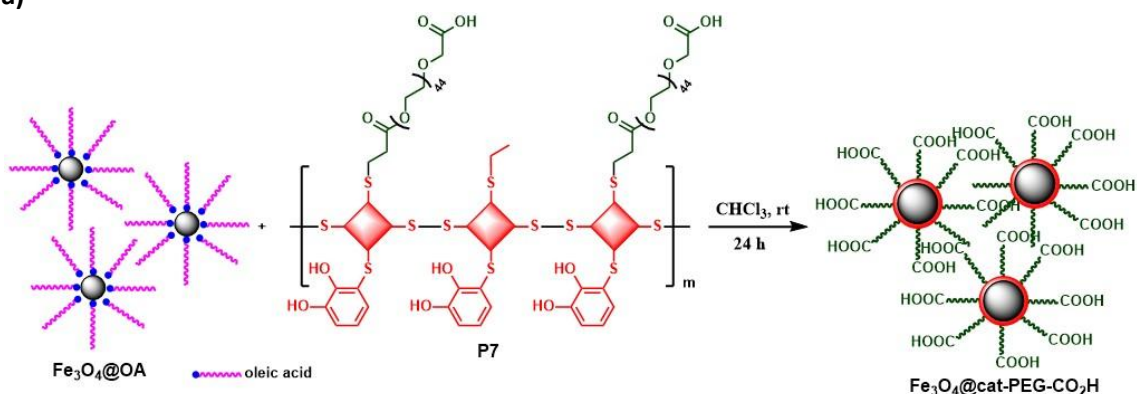
Figure 3.26. TEM images of $\text{Fe}_3\text{O}_4@OA$ NPs with hexagonal morphology and good monodispersity that favour an excellent packing of the NPs.

3.4.2.2. Coating of MNPs with P7

Once the MNPs were stabilised with oleic acid ($\text{MNP}@OA$) and suspended in CHCl_3 , they were coated with the cat-PEG derivative **P7** by a ligand exchange procedure.⁷² Firstly, precipitate **P7** was solubilised in CHCl_3 , and the non-soluble fraction was filtered off. Secondly, the soluble **P7** fraction ($\sim 8\text{ mg}/\text{mL}$) was added dropwise into a suspension of $\text{MNP}@OA$. The mixture was left stirring at rt for 24 h (Figure 3.27a). After this time, it was tried to isolate the treated MNPs by centrifuging at 13300 rpm for 15 min at $4\text{ }^\circ\text{C}$, however they did not precipitate. Therefore, the same volume of water was added into the suspension of MNPs in CHCl_3 and by hand-shaking the MNPs were transferred into the aqueous phase (Figure 3.27b), and washed with CHCl_3

once to eliminate the residual non-attached **P7** derivative. Following the same experimental procedure with uncoated MNPs, they remained in the organic phase.

a)



b)

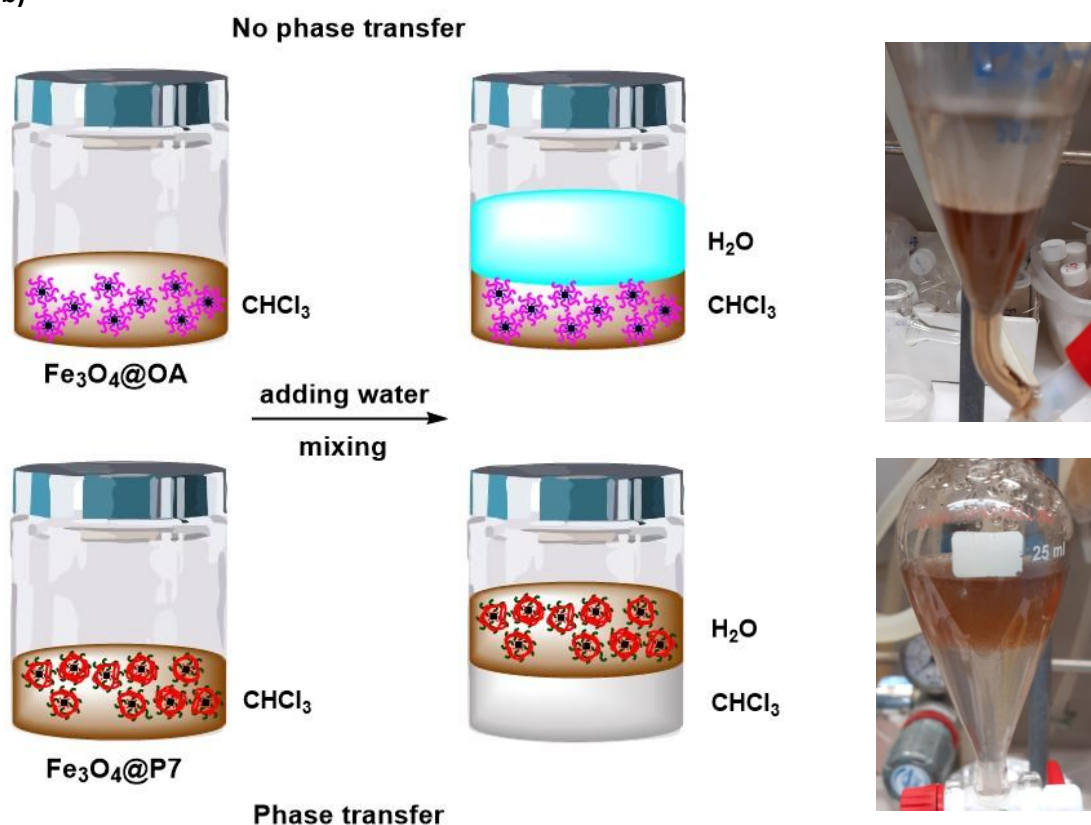


Figure 3.27. a) Schematic representation of coating of Fe₃O₄ NPs with cat-PEG copolymer **P7** via ligand exchange methodology. b) Illustration of phase transfer procedure (left), and Fe₃O₄ NPs making good colloidal suspension in CHCl₃ when they are stabilised by OA (right, top), and Fe₃O₄ NPs suspended in water when they are stabilised by cat-PEG **P7** (right, bottom).

To conclude, it was observed that those PEGylated coated NPs formed a good colloidal suspension in the aqueous phase. Thus, it was proved that synthesised cat-PEG **P7** derivative could be used to coat these kind of small NPs and make them stable in an aqueous environment due to the hydrophilicity of PEG chains.

3.4.2.3. Functionalisation of coated MNPs

Once **P7**-coated MNPs were obtained, they were functionalised with a targeting molecule. In this case, it was chosen an amino-glucose derivative which could act as a BBB-shuttle, for instance. But before functionalising them with the synthesised amino-glucufuranose derivative **41**, some trials with a simple model amine, such as the commercial allylamine, were performed in order to simplify the first studies, since this amine presents characteristic allylic protons easy to identify by ^1H NMR.

1. Functionalisation of coated MNPs with a model amine

Using the coupling agent 1-ethyl-3-(3-dimethylaminopropyl)carbodiimide (EDCI) and 4-(dimethylaminopropyl)pyridine (DMAP),¹¹⁰ the amide bond between allylamine and the residual carboxylic acid groups exposed onto the surface of the coated NPs would be formed (Figure 3.28).

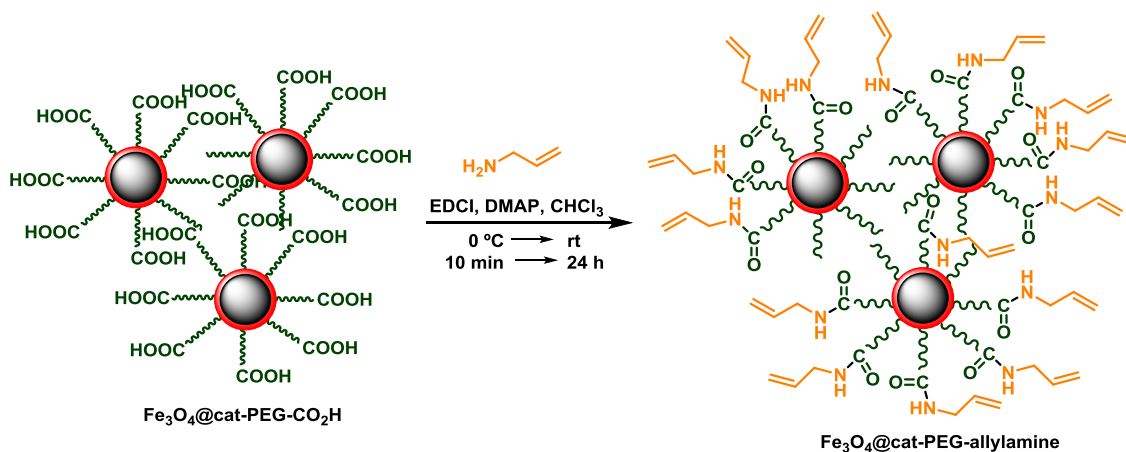


Figure 3.28. Schematic representation of the functionalisation of MNPs' coating with allylamine *via* amide bond construction.

In order to simplify the experimental procedure and to obtain higher overall yield at the end, once the MNPs were coated with **P7**, they were not transferred into an aqueous phase, but in the same reaction mixture, within a nitrogen atmosphere, it was added an excess of allylamine and DMAP at $0\text{ }^\circ\text{C}$. After 10 min, EDCI was added, and the resulting reaction mixture was left stirring for 24 h at rt. Afterwards, the $\text{MNPs@cat-PEG-allylamine}$ were transferred into an aqueous phase, washed with CHCl_3 to remove the excess of reagents, and isolated in 56% yield.

To study the chemical composition of the resulting coating, the MNPs were degraded in an acidic medium and analysed by ^1H NMR. Hence, once the NPs had been transferred into the aqueous phase, the water was removed under vacuum and the MNPs were redispersed in

deuterium methanol (CD_3OD). Five drops of DCl (35% wt in D_2O) were added and the NPs were let into that acidic medium overnight before recording a ^1H NMR (Figure 3.29).

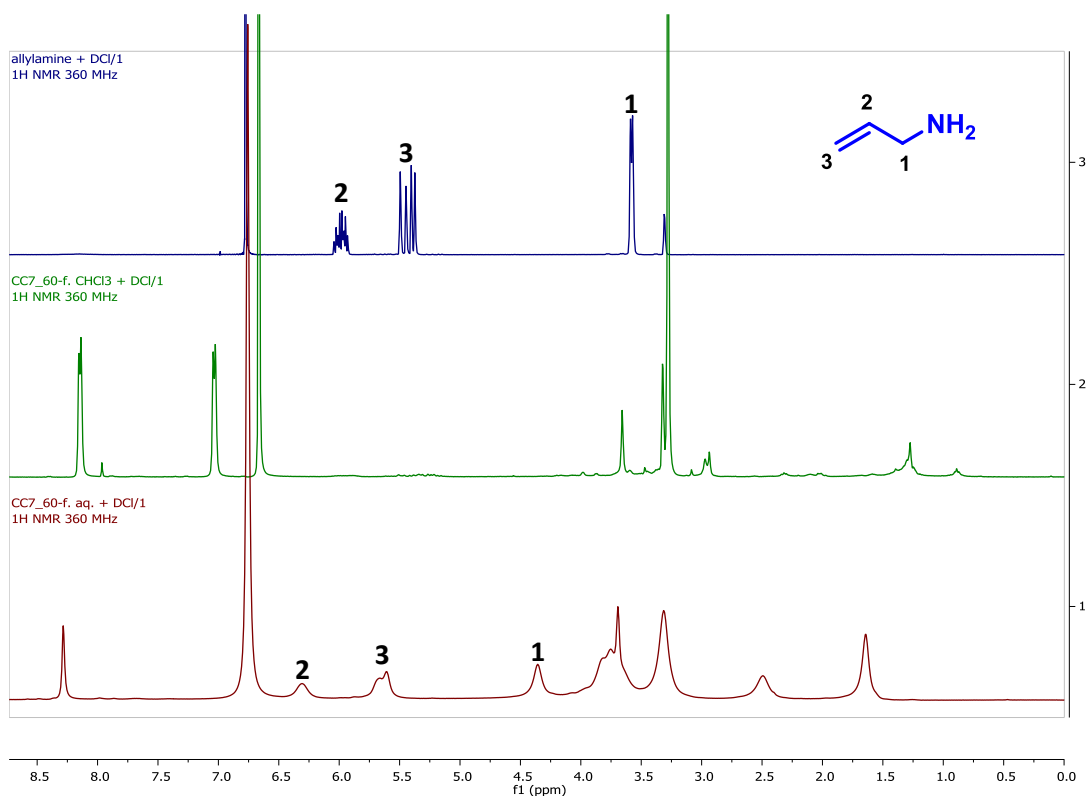


Figure 3.29. ^1H NMR spectra from the commercial allylamine (in blue), the residue obtained in the CHCl_3 phase once the MNPs have been transferred in the aqueous one (in green), and the MNPs@cat-PEG-allylamine transferred into the aqueous phase (in red). All the ^1H NMRs were performed in CD_3OD and all the samples were treated with 5 drops of DCl and let overnight.

In the ^1H NMR spectrum it was observed that MNPs were coated successfully with the cat-PEG derivative **P7** and transferred into the aqueous phase in 56% yield, since in the resting CHCl_3 phase (^1H NMR spectrum in green) it was not observed the presence of the organic compounds constituents of the coating, only the presence of DMAP. Furthermore, in the ^1H NMR spectrum from the aqueous phase (in red), it could be distinguished the characteristic protons from the allyl group of the allylamine, probe that the functionalisation took place successfully, and those protons were a little bit shifted to lower fields, suggesting the formation of the amide bond (H-1, 3.58 ppm for allylamine vs. 4.36 ppm for the amide bond).

II. Functionalisation of coated MNPs with the amino-glucofuranose derivative 41

Once it was proved that this strategy worked to functionalise those MNPs with the model allylamine, the same coupling with the synthesised amino-glucofuranose derivative **41** was also attempted (Figure 3.30). After the coupling, the MNPs@cat-PEG-sugar were transferred into the aqueous phase, washed with CHCl_3 , and isolated in 72% yield.

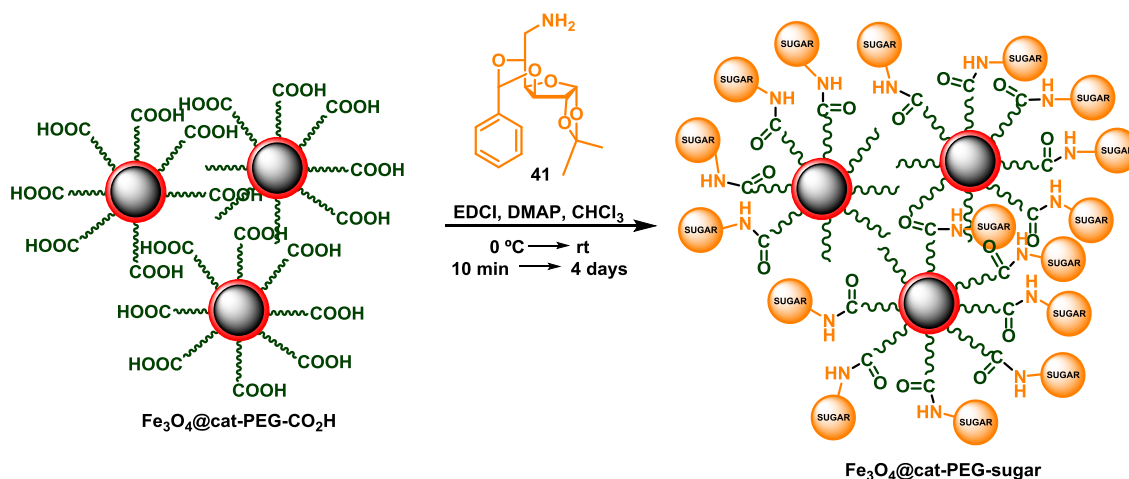


Figure 3.30. Schematic representation of the functionalisation of MNPs' coating with amino-glucufuranose derivative **41** via amide bond construction.

To characterise those coated NPs the same procedure was followed; they were degraded in an acidic medium and analysed by ^1H NMR as already described before. From the ^1H NMR spectra, it was concluded that the initial MNPs had been coated with the copolymer **P7**, and the amino-glucufuranose derivative **41** was successfully incorporated onto the coating, since in the ^1H NMR spectrum from the degraded NPs, the proton's signals coming from the sugar derivative **41** in the regions between 1.0-1.5 ppm; 3.0-5.5 ppm; and 7.2-8.0 ppm, and the peak corresponding to the PEG chain at 2.9 ppm were identified (Figure 3.31).

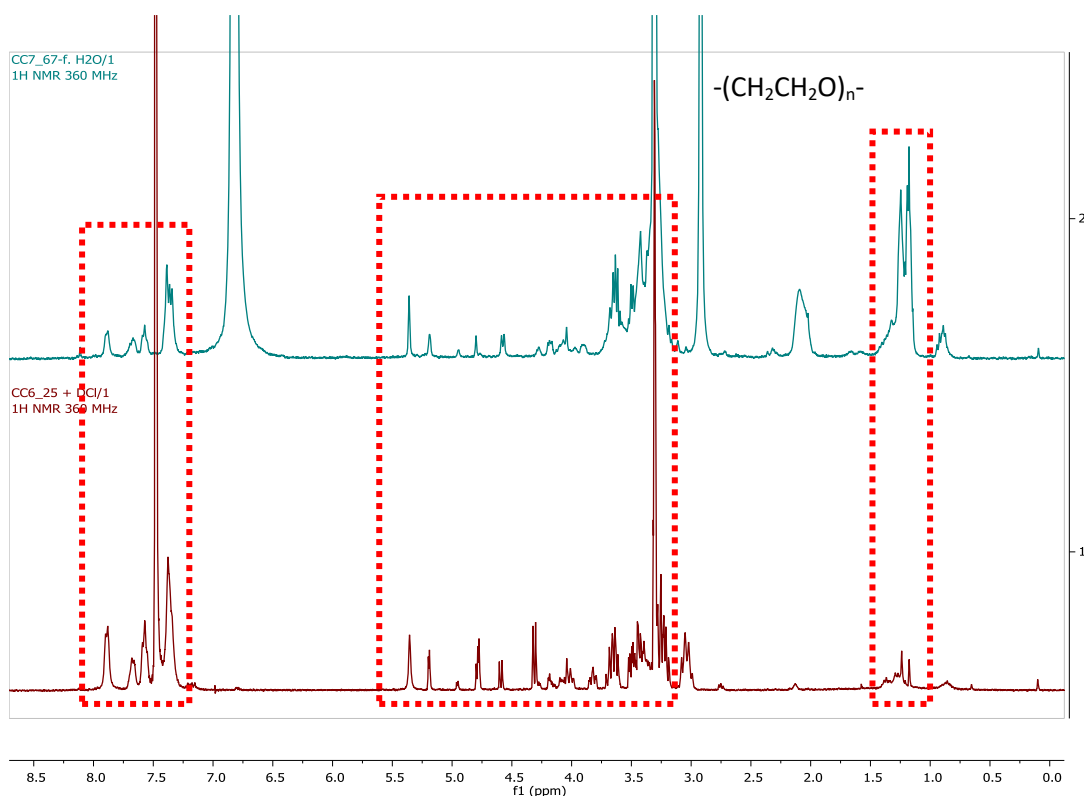


Figure 3.31. ^1H NMR spectra from the MNPs@cat-PEG-sugar transferred into the aqueous phase (in blue), and the starting amino-glucufuranose derivative **41** (in red). Both ^1H NMRs were performed in CD_3OD and the two samples were previously treated with 5 drops of DCl overweekend. Peaks corresponding to the amino sugar are dashed framed in red, and the peak at 2.92 ppm in the above spectrum corresponds to the PEG chain.

The next step was the deprotection and the formation of the 6-membered ring of amino-glucufuranose derivatives exposed onto the surface of the MNPs. Usually, ketal protecting groups are cleavage under acidic conditions, commonly using trifluoroacetic acid (TFA), or, HCl .^{105,111,112} Firstly, an strong acidic mixture of TFA/ H_2O 1:2 was used on the attempt to achieve the total deprotection of **41** (Table 3.20, entry 1).¹⁰⁵ Even though both protecting groups, benzaldehyde and acetone, were removed, under those deprotection conditions the NPs were degraded. This fact was confirmed by NMR because the good resolution of the spectrum. Indeed, with the NPs the spectrum is not well resolved and only very broad peaks are seen due to (i) the lack of mobility of the ligands in solution, as they are immobilised onto the surface of the NPs, and because (ii) of having a superparamagnetic material, it creates field interferences. In our case, and as expected, it was obtained a ^1H NMR spectrum with good resolution. Hence, these harsh conditions were not seemed to be suitable for our systems because, first, the strong acidic medium disintegrated the MNPs, and second, as the pH decreases, the coordination bonds between Fe(III) and catechol units were lost (Figure 3.32),^{113,114} consequently removing the PEGylated coating.

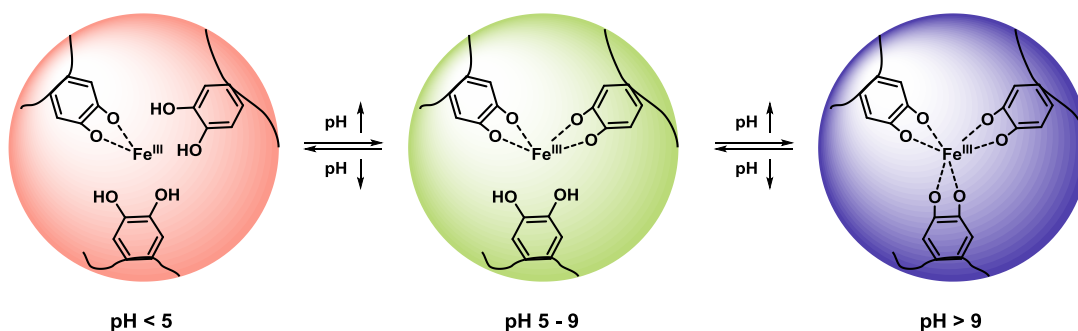


Figure 3.32. Schematic representation of catechol-Fe³⁺ ion complexes at different pH levels.¹¹³

Therefore, in order to deprotect the amino-glucufuranose derivatives and keep the NPs unchanged, an equilibrium between catechol-Fe³⁺ coordination and ketal's deprotection must be found. First, mild acidic conditions using a mixture of acetic acid/water 3:1 for 15.5 h¹¹⁵ (entry 2) were used. Under these conditions the benzaldehyde was deprotected in 11%. Therefore, stronger acidic conditions were used (entry 3); AcOH/H₂O 5:1 for 24 h.¹¹⁶ In this case, a 25% of the benzaldehyde was deprotected. Finally, the temperature was increased up to 50 °C achieving a removal of 54% of the benzaldehyde protecting group (entry 4).^{115,117}

Table 3.20. Results obtained from deprotection conditions used.

Entry	Solvents	ratio	Concentration (mg/mL)	Time	Temperature	Benzaldehyde deprotection (%)
1	TFA:H ₂ O	1:2	1.6 mg/mL	1.5 h	rt	100%
2	AcOH:H ₂ O	3:1	1.6 mg/mL	15.5 h	rt	11%
3	AcOH:H ₂ O	5:1	1.35 mg/mL	24 h	rt	25%
4	AcOH:H ₂ O	3:1	1.5 mg/mL	overnight	50 °C	54%

These results were determined from ¹H NMR, integrating the protons coming from the sugar and the aromatic ring. In all the cases, the acetone group was totally removed. Furthermore, it was checked that working under those mild acidic conditions the coating was kept onto the surface of the NPs, since after degrading them with DCl and recording ¹H NMR spectra, the peak coming from the PEG chain at 2.9 ppm was still being observed (Figure 3.33).

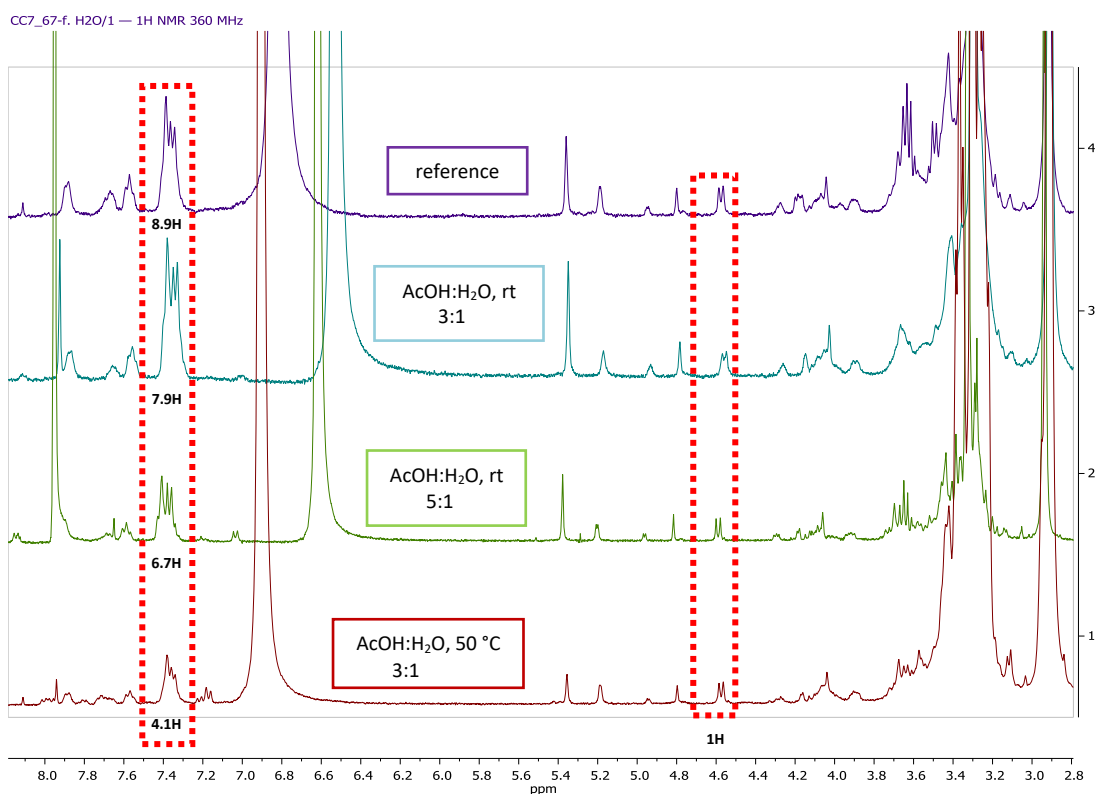
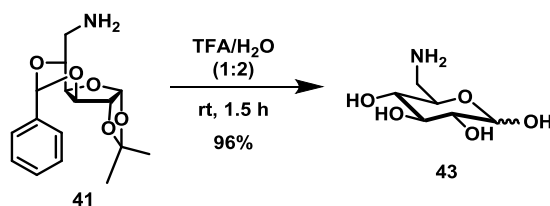


Figure 3.33. ^1H NMR spectra recorded in CD_3OD with five drops of DCl, except for the fifth spectrum (garnet) where DCl was not added. On the top, ^1H NMR spectrum of the $\text{MNPs@cat-PEG-sugar}$ as reference, previously to the deprotection. Below, ^1H NMR spectra of the final $\text{MNPs@cat-PEG-sugar}$ using different deprotection conditions.

Since this strategy did not work as desired, the deprotection of the amino-glucufuranose **41** was attempted before the coupling reaction with the PEG chain using strong acidic conditions with TFA (Scheme 3.33).¹⁰⁵



Scheme 3.33. Deprotection of both ketal groups, and 6-membered ring formation.

Once the amino-glucopyranose derivative **43** totally deprotected was obtained, the coupling reaction with carboxylic acids exposed onto the surface of $\text{Fe}_3\text{O}_4@\text{P7}$ was carried out (Figure 3.34). It was hypothesised that since the primary amine is a stronger nucleophile vs. secondary alcohols, the amide bond formation would prevail over the ester bond formation. In that case, the same previous coupling reaction conditions (EDCI and DMAP) were used, adding an organic base, such as *N,N'*-Diisopropylethylamine (DIPEA), in order to deprotonate the amine of derivative **43**.

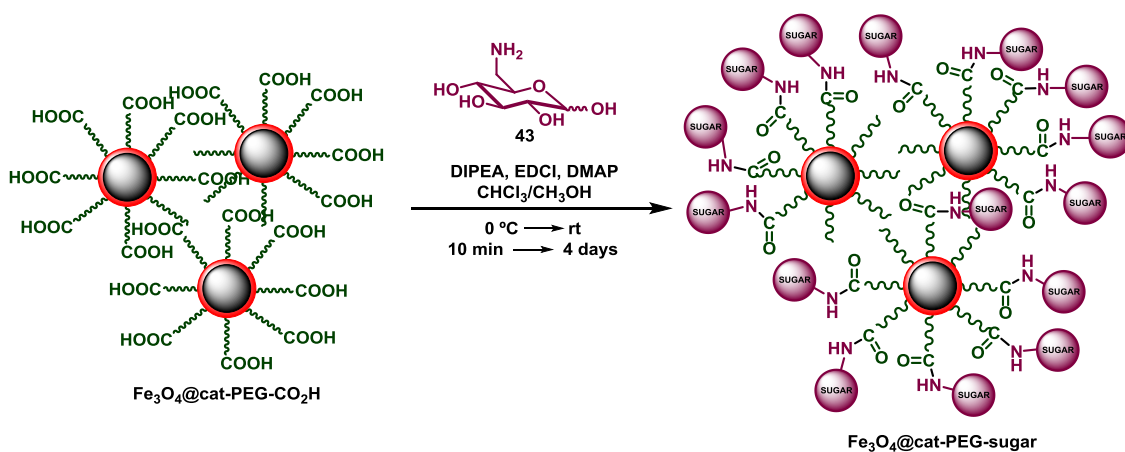


Figure 3.34. Schematic representation of the functionalisation of MNPs' coating with amino-glucopyranose derivative **43** via amide bond construction.

To determine if the coupling reaction had occurred, the degraded MNPs@cat-PEG-sugar by adding DCI were analysed by ^1H - and ^{13}C NMR experiments (Figure 3.35). In the ^{13}C NMR spectrum, the signals corresponding to the sugar (between 100 - 120 ppm, and at 40 ppm), to the pentaerythritol tetrakis(3-mercaptopropionate) (between 15 - 56 ppm, and at 159 ppm (C-3)), to the catechol moiety (between 140-130 ppm), and to the PEG chain (at 39, 44 and 71 ppm), were identified. Moreover, a new peak at 160 ppm was observed which could match with the new amide bond formed (C-14).

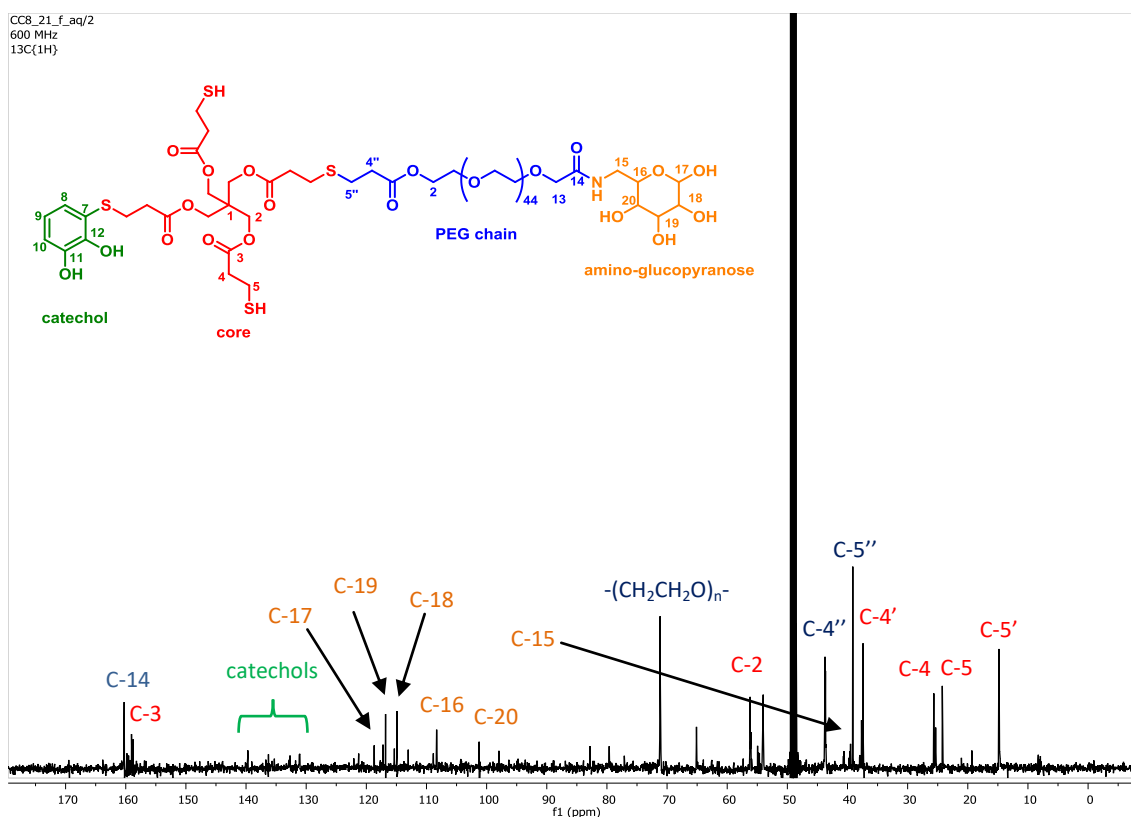


Figure 3.35. ^{13}C NMR spectrum in CD_3OD of MNP@cat-PEG-amino-glucopyranose treated with 5 drops of DCl (35% wt in D_2O). In green signals corresponding to the catechol moiety; in red signals corresponding to the pentaerythritol tetrakis(3-mercaptopropionate); in blue signals corresponding to the PEG chain; and in orange signals corresponding to the amino-glucopyranose derivative.

As a complementary technique, DLS was used in order to corroborate the functionalisation with amino-glucopyranose derivative **43**. Hence, some DLS and ζ -potential measurements were performed at different pH (acidic, neutral and basic) with NPs only coated with the cat-PEG **P7**, and with NPs functionalised with the amino-glucopyranose derivative MNPs@cat-PEG-sugar (Table 3.21).

Table 3.21. ζ -potential and size values of **P7**-coated MNPs and already functionalised MNPs with amino-glucopyranose derivative **43** at different pH; acidic, neutral and basic.

pH	4.93	7.00	11.16	PBS + 10% BSA
ζ-potential (mV)				
MNP@cat-PEG-COOH	-14.7 ± 0.208	-13.9 ± 0.85	-38.8 ± 3.45	0.563 ± 0.0312
MNP@cat-PEG-sugar	6.95 ± 0.258	3.27 ± 1.25	9.51 ± 0.85	-0.468 ± 0.0348
Size (nm)				
MNP@cat-PEG-COOH	238.0 ± 8.96	358.8 ± 36.92	340.1 ± 22.74	271.5 ± 39.97
MNP@cat-PEG-sugar	597.1 ± 55.49	932.0 ± 194.6	565.5 ± 69.84	105.8 ± 2.051

It was observed significant changes on the surface charge when the oligomeric coating had been functionalised with amino-glucopyranose derivative **43**. For MNP@cat-PEG-COOH the ζ -potential values were negative, whereas once they were functionalised, the ζ -potentials became positive and closer to 0 mV. That made sense, since there were not functional groups susceptible to gain or lose protons easily contrary to remaining carboxylic acids groups exposed onto the surface. These significant changes on the ζ -potential values might be further evidence that the coating had been functionalised properly with the sugar derivative. Moreover, when the sizes were measured, bigger aggregates for MNP@cat-PEG-sugar were observed than MNP@cat-PEG-COOH. Since these last ones had more negatively surface charge, the electrostatic stabilisation was higher, the stabilisation better, and the size of the NPs smaller. On the contrary, when carboxylic acid groups were reacted with amino groups of glucopyranose derivatives to form amide bonds, these charges were lost (ζ -potential values closer to 0 mV), and in consequence, the electrostatic stabilisation was worse and MNP@cat-PEG-sugar tended to collapse and form aggregates with bigger sizes. The stability of these MNPs was further studied in phosphate buffer saline (PBS) (pH 7.4) with 10% bovine serum albumin (BSA) in order to simulate physiological environments, since they are the most similar conditions that will be used for carrying out *in vitro* and *in vivo* experiments. It was observed that MNPs@cat-PEG-sugar formed aggregates of *ca.* 100 nm with ζ -potential values slightly negatives closer to 0 mV.

The objectives set at the beginning of this chapter have been successfully achieved and now these MNPs@cat-PEG-sugar are being used by Dr. Julia Lorenzo and Paula Alfonso in some *in vitro* and *in vivo* experiments. However, due to the current pandemic situation, the experiments have been delayed and preliminary results are not obtained yet.

3.4.3. MULTIFUNCTIONAL COATINGS

So far, it has been demonstrated the synthetic feasibility of our approach to obtain PEG-based coatings over different families of NPs. But as already mentioned, one of the main advantages is the flexible and modular chemistry of this approach. To go deeper into it, in the last section of this chapter it is aimed to demonstrate that multifunctional coating can be also obtained in a controlled manner. First, the copolymerisation between cat-mPEG building block **6** with fluorescein-functionalised building block **8** was tested. The resulting product, named copolymer **C6-8**, was obtained by mixing 80% of derivative **6** and 20% of derivative **8** in 48% yield using the same experimental procedure for the polymerisation reaction; dissolving both monomers in EtOH 96% and adding dropwise a 35 mM solution of iodine (1 equiv.) in EtOH

96%. After 1 h of stirring at rt, the precipitated derivatives were isolated, washed several times with fresh EtOH 96% and dried with a gentle flux of nitrogen (Figure 3.36).

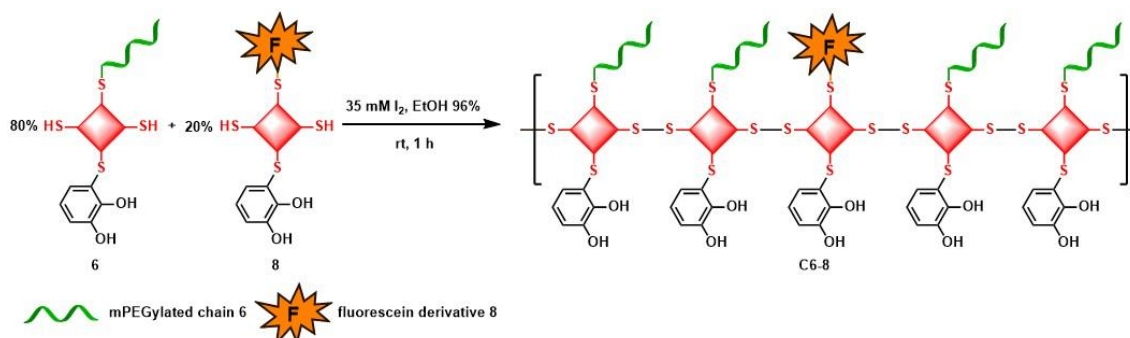


Figure 3.36. Copolymerisation of synthesised building blocks **6** and **8** to obtain a copolymer **C6-8** being biocompatible, hydrophilic and fluorescent, suitable for biomedical applications.

By ^1H NMR it was checked the presence of both functionalities in the resulting product **C6-8** obtained from this copolymerisation reaction: aromatic signals of fluorescein moiety between 8 ppm and 6.5 ppm, and the characteristic signal at ~ 3.6 ppm of the PEGylated chain (see Annex A1.3 for ^1H NMR spectrum).

With this fluorescein-PEG-functionalised copolymer **C6-8**, MSNPs were coated following the same methodology already described, and characterised by STEM, optical microscopy and DLS. By STEM, it was observed that **C6-8**-treated MSNPs showed a thin lighter layer around their surfaces (Figure 3.37a), meaning that they had been coated with a robust coating made with copolymer **C6-8**. By optical microscopy in fluorescence mode with an Alexa Fluor 488 filter, the fluorescence of these **C6-8**-coated MSNPs was checked (Figure 3.37b).

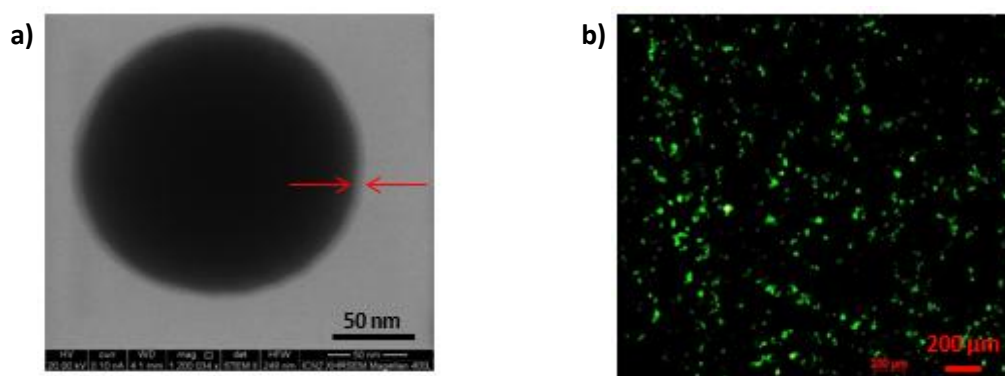


Figure 3.37. a) STEM image of coated MSNPs@**C6-8** showing a lighter outer layer. b) Image taken from inverted optical/fluorescence microscope in fluorescence mode with an Alexa Fluor 488 filter of MSNPs@**C6-8** showing fluorescence.

Finally, with DLS measurements at different pH, it was observed that, as expected, the higher the pH, the more colloiddally stable the MSNPs are, with smaller sizes due to the better electrostatic stabilisation (Figure 3.38). Under acidic conditions, they tended to collapse and form aggregates with sizes around $1\ \mu\text{m}$. In this case, it was also observed that MSNP@C6-8

formed bigger aggregates than non-treated MSNPs between pH 4 and 10. Furthermore, changes on the ζ -potential values of the treated MSNPs vs. the pristine ones at different pH, revealed that MSNPs had been coated with copolymer **C6-8**.

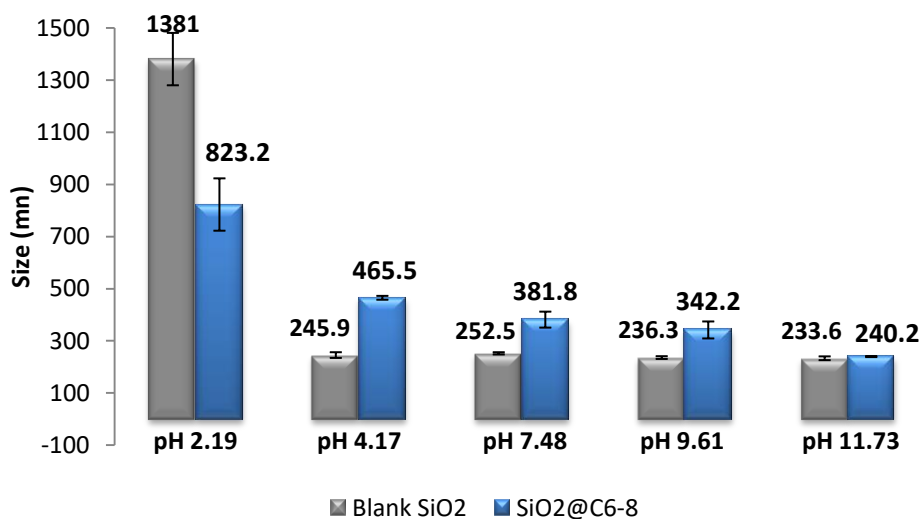


Figure 3.38. Representation of NPs' sizes at different pH taken from DLS analyses. DLS values are the average of three measurements.

From these results, it was concluded that MSNPs could be coated with copolymer **C6-8**. Moreover, since this copolymeric coating would provide biocompatibility and fluorescence to MSNPs, they could have high interest in the biomedical field, such as in bioimaging. Therefore, the cytotoxic effect of the MSNPs@**C6-8** against SH-SY5Y cells was examined.^c These cells were treated for 24 h with MSNPs@**C6-8** at different concentrations, and these coated NPs did not appear to be cytotoxic with respect to control at any concentration used (Figure 3.39a). Hence, an internalisation assay on SH-SY5Y cells was performed too. MSNPs@**C6-8** (200 $\mu\text{g}/\text{ml}$) were added to 6-well plates (10^5 cells per well). At different times (1, 3, 6, 24 h) cells were fixed and stained (Figure 3.39b-f). At 1 h, MSNPs@**C6-8** seemed to be located in cells; at 3 h, located and organised in cells; at 6 h located in the nucleus of the cells; and at 24 h, located and organised in cells. When cells were not treated with the coated MNPs, they did not show any fluorescence.

^c Cytotoxicity analyses were performed in collaboration of Dr. Julia Lorenzo and Paula Alfonso from the *Enginyeria de Proteïnes i Proteòmica* research group at *Institut de Biotecnologia i Biomedicina* (IBB).

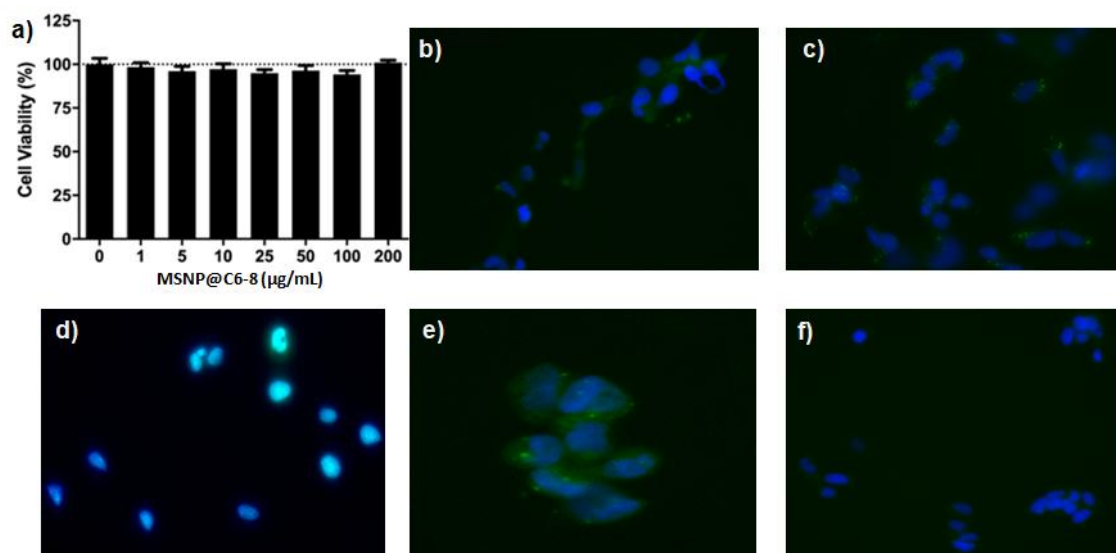
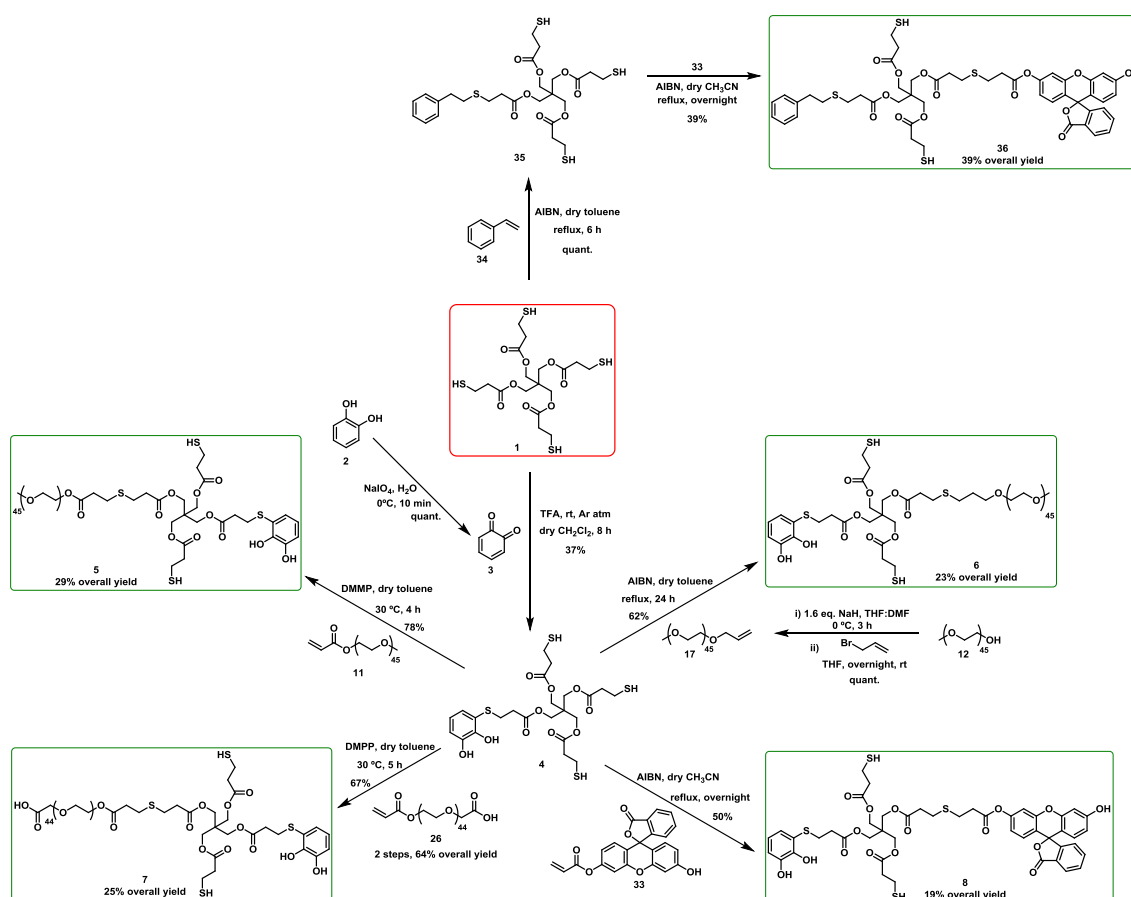


Figure 3.39. a) Effect of MSNPs@C6-8 on the cell viability of SH-SY5Y cells (3000 cells per well). These cells were incubated for 24 h in the presence of indicated concentrations of MSNPs@C6-8. Cell viability is expressed as percentage compared to an untreated control. Values are presented as mean \pm standard error of the mean ($n = 3$). Internalisation assay on SH-SY5Y cells at b) 1 h, c) 3 h, d) 6 h, e) 24 h, and f) 24 h without MSNPs@C6-8. Blue colour shows 4',6-diamidino-2-phenylindole (DAPI) staining of cell nuclei. Green colour shows fluorescein staining of MSNPs@C6-8.

3.5. SUMMARY

Below, the most relevant results are exposed.

All four main building blocks **5**, **6**, **7** and **8** were synthesised following route A from the same S-catechol tris-thiol intermediate **4** in 29%, 23%, 25%, and 19% overall yield, respectively, *via* thia-Michael reactions or radical-catalysed thiol-ene reactions. With regard to the fluorescent styrene-based building block **36**, it was obtained from S-styrene tris-thiol intermediate **35** in 39% overall yield.



Scheme 3.34. All synthetic pathways followed to obtain target building blocks **5**, **6**, **7**, **8** and **36** from the same 4-branched symmetrical molecule **1** framed in red.

Afterwards, **5**, **6**, **7**, **8** and **36** building blocks were polymerised under mild oxidative conditions with the designed strategy affording precipitates in 45%, 28%, 41%, 34%, and 29%, respectively. From ¹H NMR, DOSY NMR experiments and GPC analyses it was checked that product **P6** corresponded to mixtures of short oligomers between 2-5 units. Due to solubility issues, **P5** only could be analysed by ¹H NMR using CDCl₃ and it mainly corresponded to mixtures of dimers and trimers. After a thorough study on the polymerisation of PEGylated building block **7**, it was hypothesised that mixtures of short oligomers, as seen for **P5** and **P6**, were obtained, though **P7** could not be totally chemically characterised using the three aforementioned techniques. Finally, since fluorescein-functionalised products **P8** and **P36** were not soluble in THF, and because their ¹H NMR spectra in (CD₃)₂CO were difficult to be analysed, their polymerisation degrees could not be determined.

Table 3.22. Summary table with yields of polymerisation reaction and polymerisation degrees values of **P5**, **P6**, **P7**, **P8** and **P36**.

35 mM solution of iodine in EtOH					
Product from the polymerisation reaction	P5	P6	P7	P8	P36
Yield (%)	45%	28%	41%	34%	29%
Characterisation technique	¹ H NMR	¹ H NMR, GPC & DOSY experiments	Solubility issues		
Polymerisation degree	2-3 units	2-5 units	-	-	-

With both mPEG-functionalised products **P5** and **P6**, coatings onto MSNPs were performed stabilising them in aqueous environments. These coatings were characterised by STEM and it was observed the presence of a thin lighter layer surrounding the NPs. Moreover, an EDX line scan profile performed on **P6**-coated MSNPs showed the presence of carbon across the whole diameter of coated particles, in contradistinction to the oxygen signal, which appeared circumscribed to their inner sections, *i.e.* to the mineral cores. Finally, **P6**-coated MSNPs were studied at different pH; by DLS it was observed that they were stable between pH 4 and 12 ($\varnothing \sim 240$ nm), and ζ -potentials revealed the presence of a coatings since they values were less negative than the pristine ones (Figure 3.40).

As far as **P7** is concerned, it was used to stabilised MNPs ($\varnothing \sim 8$ nm), previously synthesised in the lab, in aqueous environments. Then, these coated NPs were functionalised with the amino-glucopyranose derivative **43**, as a model targeting molecule, obtained from the commercial 1,2-*O*-isopropylidene- α -D-glucofuranoside **37** in a linear synthesis of 4 steps in 31% overall yield. By ¹H- and ¹³C NMR experiments, it was confirmed the functionalisation of the sugar derivative in the surface of the coating through an amide bond construction. Finally, by DLS it was studied the stability of the MNPs@cat-PEG-sugar in PBS with 10% BSA, and it was observed that they formed aggregates of *ca.* 100 nm, and their ζ -potential values were slightly negative closer to 0 mV (Figure 3.40). Nowadays, *in vitro* and *in vivo* studies with these samples are running by Dr. Julia Lorenzo and Paula Alfonso from IBB.

Finally, taking advantage of the versatility of the designed approach, it was demonstrated that multifunctional coating can be also obtained in a controlled manner. By combining both mPEG- and fluorescein-functionalised building blocks **6** and **8** in a ratio of 4:1, respectively, the copolymer **C6-8**, obtained in 48% yield, was used to coat MSNPs, which were characterised by STEM, optical microscopy, DLS and ζ -potential measurements. Finally, their cytotoxic effects against SH-SY5Y cells were examined and it was found that these coated NPs did not appear to be cytotoxic with respect to control at any concentration used. Furthermore, after an

internalisation assay on SH-SY5Y cells, it was observed that these C6-8-coated MSNPs were located at the nucleus of cells after 6 h (Figure 3.40).

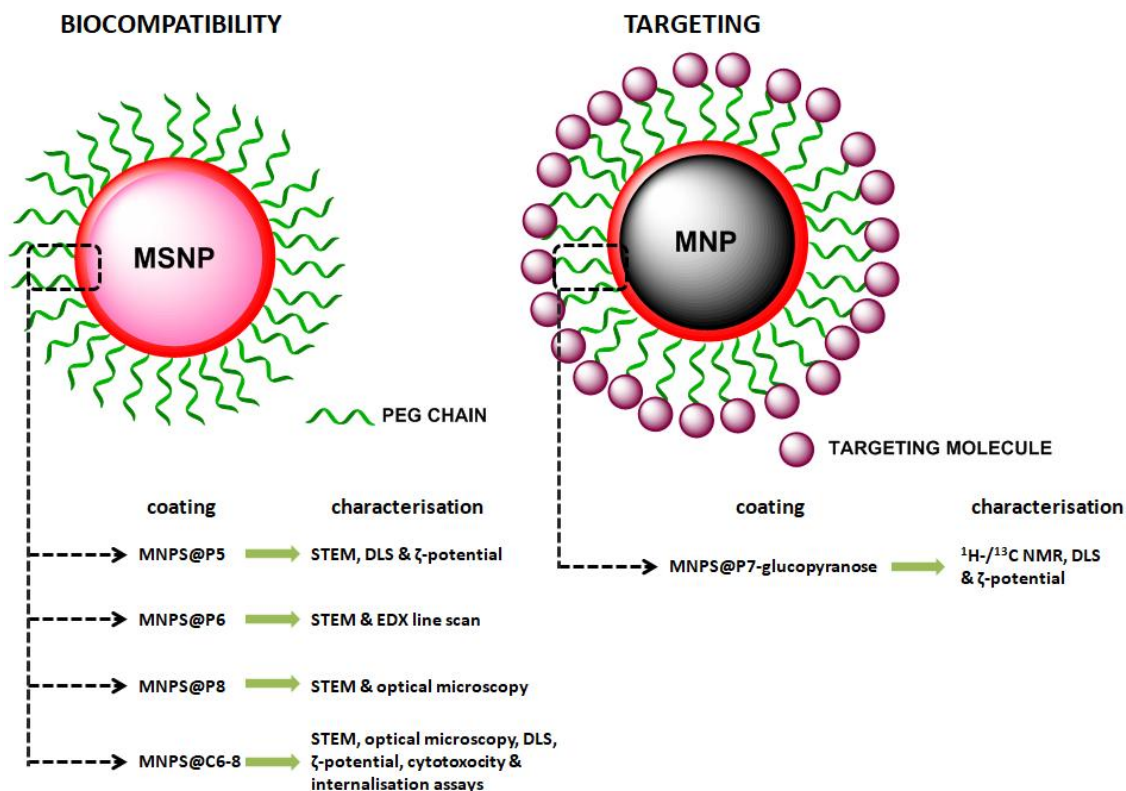


Figure 3.40. Summarised illustration of all the coatings performed and their corresponding characterisations onto MSNPs (left) and MNPs (right).

3.6. REFERENCES

- ¹ Wilke, P.; Helfricht, N.; Mark, A.; Papastavrou, G.; Faivre, D.; Börner, H. *G. J. Am. Chem. Soc.* **2014**, *136*, 12667-12674.
- ² Guo, J.; Wang, W.; Hu J.,; Xie, D.; Gerhard, E.; Nisic, M.; Shan, D.; Qian, G.; Zheng, S.; Yang, J. *Biomaterials* **2016**, *85*, 204-217.
- ³ Jeong, J.-H.; Hong, S. W.; Hong, S. Yook, S.; Jung, Y.; Park J.-B.; Khue, C. D.; Im, B.-H.; Seo, J.; Lee, H. Ahn, C.-H.; Lee, D. Y.; Byun, Y. *Biomaterials* **2011**, *32*, 7961-7970.
- ⁴ Jeong, J.-H.; Yook, S.; Lee, H.; Ahn, C.-H.; Lee, D. Y.; Byun, Y. *Biochem. Bioph. Res. Co.* **2013**, *433*, 513-518.
- ⁵ Haque, M. R.; Jeong, J.-H.; Byun, Y. *Biomaterials* **2016**, *84*, 144-156.
- ⁶ Ji, Y.; Ji, T.; Liang, K.; Zhu, L. *J. Mater. Sci.: Mater. Med.* **2016**, *27*, 1-9.
- ⁷ Barrett, D. G.; Bushnell, G. G.; Messersmith, P. B. *Adv. Healthcare Mater.* **2013**, *2*, 745-755.
- ⁸ Paez, J. I.; Ustahüseyin, O.; Serrano, C.; Ton, X.-A.; Shafiq, Z.; Auernhammer, G. A.; d'Ischia, M.; del Campo, A. *Biomacromolecules* **2015**, *16*, 3811-3818.

-
- ⁹ Murphy, J. L.; Vollenweider, L.; Xu, F.; Lee, B. P. *Biomacromolecules* **2010**, *11*, 2976-2984.
- ¹⁰ Liu, Y.; Meng, H.; Konst, S.; Sarmiento, R.; Rajachar, R.; Lee, B. P. *ACS Appl. Mater. Inter.* **2014**, *6*, 16982-16992.
- ¹¹ Brubaker, C. E.; Messersmith, P. B. *Biomacromolecules* **2011**, *12*, 4326-4334.
- ¹² Brubaker, C. E.; Meng, H.; Konst, S.; Sarmiento, R.; Rajachar, R.; Lee, B. P. *Biomaterials* **2010**, *31*, 420-427.
- ¹³ Haller, C. M.; Buerzle, W.; Brubaker, C. E.; Messersmith, P. B.; Mazza, E.; Ochsenbein-Koelble, N.; Zimmermann, R.; Ehrbar, M. *Prenat. Diagn.* **2011**, *31*, 654-660
- ¹⁴ Ai, Y.; Wei, Y.; Nie, J.; Yang, D. *J. Photochem. Photobiol., B* **2013**, *120*, 183-190.
- ¹⁵ Cristescu, R.; Patz, T.; Narayan, R. J.; Menegazzo, N.; Mizaikoff, B.; Mihaiescu, D. E.; Messersmith, P. B.; Stamatina, I.; Mihailescu, I. N.; Chrisey, D. B. *Appl. Surf. Sci.* **2005**, *247*, 217-224.
- ¹⁶ Ling, D.; Park, W.; Park, Y. I.; Lee, N.; Li, F.; Song, C.; Yang, S.-G.; Choi, S. H.; Na, K.; Hyeon, T. *Angew. Chem. Int. Ed.* **2011**, *50*, 11360-11365.
- ¹⁷ Black, K. C. L.; Liu, Z.; Messersmith, P. B. *Chem. Mater.* **2011**, *23*, 1130-1135.
- ¹⁸ Al-Nahain, A.; Lee, S. Y.; In, I.; Lee, K. D.; Park, S. Y. *Int. J. Pharm.* **2013**, *450*, 208-217.
- ¹⁹ Self-assembled polydopamine nanoparticles improve treatment in Parkinson's disease model mice and suppress dopamine-induced dyskinesia.
- ²⁰ Lee, H.; Lee, K. D.; Pyo, K. B.; Park, S. Y.; Lee, H. *Langmuir* **2010**, *26*, 3790-3793.
- ²¹ Zhang, F.; Liu, S.; Zhang, Y.; Chi, Z.; Xu, J.; We, Y. *J. Mater. Chem.* **2012**, *22*, 17159-17166.
- ²² Wei, Q.; Becherer, T.; Mutihac, R.-C.; Noeske, P.-L. M.; Paulus, F.; Haag, R.; Grunwald, I. *Biomacromolecules* **2014**, *15*, 3061-3071.
- ²³ Wilke, P.; Börner, H. G. *ACS Macro Lett.* **2012**, *1*, 871-875.
- ²⁴ Xu, L. Q.; Pranantyo, D.; Neoh, K.-G.; Kang, E.-T.; Teo, S. L.-M.; Fu, G. D. *Polym. Chem.* **2016**, *7*, 493-501.
- ²⁵ Dang, Y.; Quan, M.; Xing, C.-M.; Wang, Y.-B.; Gong, Y.-K. *J. Mater. Chem. B* **2015**, *3*, 2350-2361.
- ²⁶ Wilke, P.; Börner, H. G. *Eur. Polym. J.* **2015**, *62*, 374-379.
- ²⁷ Dalsin, J. L.; Lin, L.; Tosatti S.; Vörös, J.; Textor, M.; Messersmith, P. B. *Langmuir* **2005**, *21*, 640-646
- ²⁸ Ko, R.; Cadieux, P. A.; Dalsin, J. L.; Lee, B. P.; Elwood, C. N.; Razvi, H. J. *Endourol.* **2008**, *22*, 1153-1160.
- ²⁹ Gillich, T.; Benetti, E. M.; Rakhmatullina, E.; Konradi, R.; Li, W.; Zhang, A.; Schlüter, A. D.; Textor, M. *J. Am. Chem. Soc.* **2011**, *133*, 10940-10950.

- ³⁰ Kim, H. S.; Ham, H. O.; Son, Y. J.; Messersmith, P. B.; Yoo, H. S. *J. Mater. Chem. B* **2013**, *1*, 3940-3949.
- ³¹ Nam, J. A.; Nahain, A.-A.; Kim, S. M.; In, I.; Park, S. y. *Acta Biomater.* **2013**, *9*, 7996-8003.
- ³² Jeong, C. J.; Inb, I.; Park, S. Y. *Surf. Interface Anal.* **2015**, *47*, 253-258.
- ³³ Cheng, L.; Sun, X.; Zhao, X.; Wang, L.; Yu, J.; Pan, G.; Li, B.; Yang, H.; Zhang, Y.; Cui, W. *Biomaterials* **2016**, *83*, 169-181.
- ³⁴ Yin, M.; Yuan, Y.; Liu, C.; Wang, J. *Biomaterials* **2009**, *30*, 2764-2773
- ³⁵ Chen, Y.; Taskin, M. B.; Zhang, Z.; Su, Y.; Han, X.; Chen, M. *Biomater. Sci.* **2019**, *7*, 2165-2173.
- ³⁶ Choi, J. S.; Messersmith, P. B.; Yoo, H. S. *Macromol. Biosci.* **2014**, *14*, 270-279.
- ³⁷ Zeng, G.; Liu, M.; Liu, X.; Huang, Q.; + Xu, D.; Mao, L.; Huang, H.; Deng, F.; Zhang, X.; Wei, Y. *Appl. Surf. Sci.* **2016**, *387*, 399-405.
- ³⁸ Xu, H.; Liu, M.; Lan, M.; Yuan, H.; Yu, W.; Tian, J.; Wan, Q.; Zhang, X.; Wei, Y. *Toxicol. Res.* **2016**, *5*, 1371-1379.
- ³⁹ Zhang, X.; , Zeng, G.; Tian, J.; Wan, Q.; Huang, Q.; Wang, K.; Zhang, Q.; Liu, M.; Deng, F.; Wei, Y. *Appl. Surf. Sci.* **2015**, *351*, 425-432.
- ⁴⁰ Zhou, J.; Wang, C.; Wang, P.; Messersmith, P. B.; Duan, H. *Chem. Mater.* **2015**, *27*, 3071-3076.
- ⁴¹ Xu, L. Q.; Jiang, H.; Neoh, K.-G.; Kang, E.-T.; Fu, G. D. *Polym. Chem.* **2012**, *3*, 920-927.
- ⁴² Xu, L. Q.; Chen, J. C.; Wang, R.; Neoh, K.-G.; Kang, E.-T.; Fu, G. D. *RSC Adv.* **2013**, *3*, 25204-25214.
- ⁴³ Cheng, C.; Li, S.; Zhao, W.; Wei, Q.; Nie, S.; Sun, S.; Zhao, C. *J. Membrane Sci.* **2012**, 228-236.
- ⁴⁴ Mattson, K. M.; Latimer, A. A.; McGrath, A. J.; Lynd, N. A.; Lundberg, P.; Hudson, Z. M.; Hawker, C. J. *J. Polym. Sci. A1* **2015**, *53*, 2685-2692.
- ⁴⁵ Zhang, H.; Zhao, T.; Newland, B.; Duffy, P.; Annaidh, A. N.; O’Cearbhaill, E. D.; Wang, W. *J. Mater. Chem. B* **2015**, *3*, 6420-6428.
- ⁴⁶ Yuan, C.; Chen, J.; Yu, S.; Chang, Y.; Mao, J.; Xu, Y.; Luo, W.; Zeng, B.; Dai, L. *Soft. Matter.* **2015**, *11*, 2243-2250.
- ⁴⁷ Burke, K. A.; Roberts, D. C.; Kaplan, D. L. *Biomacromolecules* **2016**, *17*, 237-245.
- ⁴⁸ Matos-Pérez, C. R.; Wilker, J. J. *Macromolecules* **2012**, *45*, 6634-6639.
- ⁴⁹ Zhang, Q.; Nurumbetov, G.; Simula, A.; Zhu, C.; Li, M.; Wilson, P.; i Kempe, K.; i Yang, B.; Tao, L.; Haddleton, D. M. *Polym. Chem.* **2016**, *7*, 7002-7010.
- ⁵⁰ Stephen, Z. R.; Dayringer, C. J.; Lim, J. J.; Revia, R. A.; Halbert, M. V.; Jeon, M.; Bakthavatsalam, A.; Ellenbogen, R. G.; Zhang, M. *ACS Appl. Mater. Inter.* **2016**, *8*, 6320-6328.
- ⁵¹ Lu, C.; Park, M. K.; Lu, C.; Lee, Y. H.; Chai, K. Y. *J. Mater. Chem. B* **2015**, *3*, 3730-3737.

-
- ⁵² Heng, C.; , Liu, M.; Wang, P.; Wang, K.; Zheng, X.; Fan, D.; Hui, J.; Zhang, X.; Wei, Y. *Chem. Eng. J.* **2016**, *296*, 268-276.
- ⁵³ Marcelo, G.; Kaplan, E.; Tarazona, M. P.; Mendicuti, F. *Colloid. Surface. B.* **2015**, *128*, 237-244.
- ⁵⁴ Chan, J. M. W.; Tan, J. P. K.; Engler, A. C.; Ke, X.; Gao, S.; Yang, C.; Sardon, H.; Yang, Y. Y.; Hedrick, J. L. *Macromolecules* **2016**, *49*, 2013-2021.
- ⁵⁵ Wu, S.; Kuang, H.; Meng, F.; Wu, Y.; Li, X.; Jing, X.; Huang, Y. *J. Mater. Chem.* **2012**, *22*, 15348-15356.
- ⁵⁶ Wu, S.; Qi, R.; Kuang, H.; Wei, Y.; Jing, X.; Meng, F.; Huang, Y. *ChemPlusChem*, **2013**, *78*, 175-184.
- ⁵⁷ Patil, N.; Falentin-Daudré, C.; Jérôme, C.; Detrembleur, C. *Polym. Chem.* **2015**, *6*, 2919-2933.
- ⁵⁸ Na, H. B.; Palui, G.; Rosenberg, J. T.; Ji, X.; Grant, S. C.; Mattouss, H. *ACS Nano* **2012**, *6*, 389-399.
- ⁵⁹ Wang, W.; Ji, X.; Na, H. B.; Safi, M.; Smith, A.; Palui, G.; Perez, J. M.; Mattoussi, H. *Langmuir* **2014**, *30*, 6197-6208.
- ⁶⁰ Wan, Q.; Tian, J.; Liu, M.; Zeng, G.; Li, Z.; Wang, K.; Zhang, Q.; Deng, F.; Zhang, X.; Wei, Y. *RSC Adv.* **2015**, *5*, 25329-25336.
- ⁶¹ Heo, S.; Jeon, Y.-S.; Kim, Y. J.; Kim, S. H.; Kim, J.-H. *J. Coat. Technol. Res.* **2013**, *10*, 811-819.
- ⁶² Xu, L. Q.; Pranantyo, D.; Liu, J. B.; Neoh, K.-G.; Kang, E.-T.; Ng, Y. X.; Teo, S. L.-M.; Fu, G. D. *RSC Adv.* **2014**, *4*, 32335-32344.
- ⁶³ Zhong, J.; Ji, H.; Duan, J.; Tu, H.; Zhang, A. *Colloid. Surface. B.* **2016**, *140*, 254-261.
- ⁶⁴ Statz, A. R.; Meagher, R. J.; Barron, A. E.; Messersmith, P. B. *J. Am. Chem. Soc.* **2005**, *127*, 7972-7973.
- ⁶⁵ Saxer, S.; Portmann, C.; Tosatti, S.; Gademann, K.; Zürcher, S.; Textor, M. *Macromolecules* **2010**, *43*, 1050-1060.
- ⁶⁶ Li, L.; Yan, B.; Zhang, L.; Tian, Y.; Zeng, H. *Chem. Commun.* **2015**, *51*, 15780-15783.
- ⁶⁷ Kang, T.; Banquy, X.; Heo, J.; Lim, C.; Lynd, N. A.; Lundberg, P.; Oh, D. X.; Lee, H.-K.; Hong, Y.-K.; Hwang, D. S.; Waite, J. H.; Israelachvili, J. N.; Hawker, C. J. *ACS Nano* **2016**, *10*, 930-937.
- ⁶⁸ Cheng, W.; Yang, C.; Ding, X.; Engler, A. C.; Hedrick, J. L.; Yang, Y. Y. *Biomacromolecules* **2015**, *16*, 1967-1977.
- ⁶⁹ Lacava, L. M.; Lacava, Z. G.; Da Silva, M. F.; Silva, O.; Chaves, S. B.; Azevedo, R. B.; Pelegrini, F.; Gansau, C.; Buske, N.; Sabolovic, D.; Morais, P. C. *Biophys. J.* **2001**, *80*, 2483-2486.
- ⁷⁰ Strable, E.; Bulte, J. W. M.; Moskowitz, B.; Vivekanandan, K.; Allen, M.; Douglas, T. *Chem. Mater.* **2001**, *13*, 2201-2209.

-
- ⁷¹ Kohler, N.; Sun, C.; Fichtenholtz, A.; Gunn, J.; Fang, C.; Zhang, M. Q. *Small* **2006**, *2*, 785-792.
- ⁷² Smolensky, E. D.; Park, H.-Y. E.; Berquó, T. S.; Pierre, V. C. *Contrast. Media Mol. Imaging* **2011**, *6*, 189-199.
- ⁷³ Park, J. W.; Bae, K. H.; Kim, C.; Park, T. G. *Biomacromolecules* **2011**, *12*, 457-465.
- ⁷⁴ Farokhi, M.; Mottaghitalab, F.; Saeb, M. R.; Thomas, S. J. *Control. Release* **2019**, *303*, 203-219.
- ⁷⁵ Xu, C.; Xu, K.; Gu, H.; Zheng, R.; Liu, H.; Zhang, X.; Guo, Z.; Xu, B. *J. Am. Chem. Soc.* **2004**, *126*, 9938-9939.
- ⁷⁶ Kong, S. D.; Lee, J.; Ramachandran, S.; Eliceiri, B. P.; Shubayev, V. I.; Lal, R.; Jin, S. *J. Control. Release* **2012**, *164*, 49-57.
- ⁷⁷ Yan, F.; Wang, Y.; He, S.; Ku, S.; Gu, W.; Ye, L. *J. Mater. Sci: Mater. Med.* **2013**, *24*, 2371-2379.
- ⁷⁸ Vargas-Osorio, Z.; Da Silva-Candal, A.; Pineiro, Y.; Iglesias-Rey, R.; Sobrino, T.; Campos, F.; Castillo, J.; Rivas, J. *Nanomaterials* **2019**, *9*, 449-470.
- ⁷⁹ D'Elios, M. M.; Aldinucci, A.; Amoriello, R.; Benagiano, M.; Bonechi, E.; Maggi, P.; Flori, A.; Ravagli, C.; Saer, D.; Cappiello, L. *RSC Adv.* **2018**, *8*, 904-913.
- ⁸⁰ Aguilera, G.; Berry, C. C.; West, R. M.; Gonzalez-Monterrubio, E.; Angulo-Molina, A.; Arias-Carrion, O.; Mendez-Rojas, M. A. *Nanoscale Adv.* **2019**, *1*, 671-685.
- ⁸¹ Liu, D.-F.; Qian, C.; An, Y.-L.; Chang, D.; Ju, S.-H.; Teng, G.-J. *Nanoscale* **2014**, *6*, 15161-15167.
- ⁸² Mahou, R.; Wandrey, C. *Polymers* **2012**, *4*, 561-589.
- ⁸³ Mancebo-Aracil, J.; Casagualda, C.; Moreno-Villaécija, M. A.; Nador, F.; García-Pardo, J.; Franconetti-García, A.; Busqué, F.; Alibés, R.; Esplandiú, M. J.; Ruiz-Molina, D.; Sedó-Vegara, *Chem. Eur. J.* **2019**, *25*, 12367-12379.
- ⁸⁴ Font, J.; de March, P.; Busqué, F.; Casas, E.; Benítez, M.; Teruel, L.; García, H. *J. Mater. Chem.* **2007**, *17*, 2336-2343.
- ⁸⁵ Chan, J. W.; Hoyle, C. E.; Lowe, A. B.; Bowman, M. *Macromolecules* **2010**, *43*, 6381-6388.
- ⁸⁶ Zhang, S.; Moussodia, R.-O.; Sun, H.-J.; Leowanawat, P.; Muncan, A.; Nusbaum, C. D.; Chelling, K. M.; Heiney, P. A.; Klein, M. L.; Andre, S. *Angew. Chem. Int. Ed.* **2014**, *53*, 10899-10903.
- ⁸⁷ O'Driscoll, L. J.; Welsh, D. J.; Bailey, S. W. D.; Visontai, D.; Frampton, H.; Bryce, M. R.; Lambert, C. J. *Chem. Eur. J.* **2015**, *21*, 3891-3894.
- ⁸⁸ Hooper, R.; West, R. *Macromolecules* **2001**, *34*, 931-936.
- ⁸⁹ Pohlit, H.; Worm, M.; Langhanki, J.; Berger-Nicoletti, E.; Opatz, T.; Frey, H. *Macromolecules* **2017**, *50*, 9196-9206.
- ⁹⁰ Bouzide, A.; Sauvé, G. *Org. Lett.* **2002**, *4*, 2329-2332.

-
- ⁹¹ Hsu, C. W.; Olabisi, R. M.; Olmsted-Davis, E. A.; Davis, A. R.; West, J. L. *J. Biomed. Mater. Res., Part A* **2011**, *98*, 53-62.
- ⁹² Bouzide, A.; LeBerre, N.; Sauv , G. *Tetrahedron Lett.* **2001**, *42*, 8781-8783.
- ⁹³ Kinbara, K.; Muraoka, T.; Wawro, A. M. *Polym. Chem.* **2016**, *7*, 2389-2394.
- ⁹⁴ Roohnikan, M.; Violeta Toader, V.; Alejandro Rey, A.; Linda Reven, L. *Langmuir* **2016**, *32*, 8442-8450.
- ⁹⁵ Edem, P. E.; Shannon Czorny, S.; Valliant, J. F. *J. Med. Chem.* **2014**, *57*, 9564-9577.
- ⁹⁶ Clave, G.; Boutal, H.; Hoang, A.; Perraut, F.; Volland, H.; Renard, P.-Y.; Romieu, A. *Org. Biomol. Chem.* **2008**, *6*, 3065-3078.
- ⁹⁷ Malisova, B.; Tosatti, S.; Textor, M.; Gademann, K.; Z rcher, S. *Langmuir* **2010**, *26*, 4018-4026.
- ⁹⁸ Z rcher, S.; W ckerlin, D.; Bethuel, Y.; Malisova, B.; Textor, M.; Tossati, S.; Gademann, K. *J. Am. Chem. Soc.* **2006**, *128*, 1064-1065.
- ⁹⁹ Weiss, J.; Laschewsky, A. *Langmuir* **2011**, *27*, 4465-4473.
- ¹⁰⁰ Auvergne, R.; Morel, M.-H.; Menut, P.; Giani, O.; Guilbert, S.; Robin, J.-J. *Biomacromolecules* **2008**, *9*, 664-671.
- ¹⁰¹ Chniti, I.; Sanhoury, M. A. K.; Merlet, D.; Chehidi, I. *J. Fluorine Chem.* **2014**, *168*, 223-229.
- ¹⁰² Wilderspin, A. F.; Green, N. M. *Anal. Biochem.* **1983**, *132*, 449-455.
- ¹⁰³ Liu, K. J.; Liu, Y. *New J. Chem.* **2011**, *35*, 1485-1490.
- ¹⁰⁴ Garanger, E.; Weissleder, R.; Josephson, L. *Bioconjugate Chem.* **2009**, *20*, 170-173.
- ¹⁰⁵ Anraku, Y.; Kuwahara, H.; Fukusato, Y.; Mizoguchi, A.; Ishii, T.; Nitta, T.; Matsumoto, Y.; Toh, K.; Miyara, K.; Uchida, S.; Nishina, K.; Osada, K.; Itaka, K.; Nishiyama, N.; Mizusawa, H.; Yamasoba, T.; Yokota, T.; Kataoka, K. *Nat. Commun.* **2017**, *8*, 1-9.
- ¹⁰⁶ Lal, B.; Pramanik, B. N.; Manhas, M. S.; Bose, A. K. *Tetrahedron Lett.* **1977**, *18*, 1977-1980.
- ¹⁰⁷ Bogdan, N. D.; Matache, M.; Meier, V. M.; Dobrota, C.; Dumitru, I.; Roiban, G. D.; Funeriu, D. *P. Chem. Eur. J.* **2010**, *16*, 2170-2180.
- ¹⁰⁸ Danehy, J. P.; Doherty, B. T.; Egan, C. P. *J. Org. Chem.* **1971**, *36*, 2525-2534.
- ¹⁰⁹ Muro-Cruces, J. Roca, A. G.; L pez-Ortega, A.; Fantechi, E.; del-Pozo-Bueno, D.; Estrade, S.; Peiro, F.; Sepulveda, B.; Pineider, F.; Sangregorio, C. *ACS Nano* **2019**, *13*, 7716-7728.
- ¹¹⁰ Ohta, Y.; Kamijyo, Y.; Yokoyama, A.; Yokozamo, T. *Polymers* **2012**, *4*, 1170-1182.
- ¹¹¹ Han, O.; Liu, H. W. *Tetrahedron Lett.* **1987**, *28*, 1073-1076.
- ¹¹² Dhavale, D. D.; Chaudhari, V. D.; Tilekar, J. N. *Tetrahedron Lett.* **2003**, *44*, 7321-7323.
- ¹¹³ Lee, B. P.; Lin, M.-H.; Narkar, A.; Konst, S.; Wilharm, R. *Sensor. Actuat. B-Chem.* **2015**, *206*, 456-462.

¹¹⁴ Bijlsma, J.; de Bruijn, W. J. C.; Hageman, J. A.; Goos, P.; Velikov, K. P.; Vincken, J.-P. *Sci. Rep* **2020**, *10*, 8288-8298.

¹¹⁵ Borkar, S. R.; Bokolia, N.; Aidhen, I. S.; Khan, I. A. *Tetrahedron: Asymmetr.* **2017**, *28*, 186-195.

¹¹⁶ El Ashry, E.-S. H. *J. Chem. Soc. C.* **1988**, *2*, 139-144.

¹¹⁷ Jones, N. A.; Jenkinson, S. F.; Soengas, R.; Fanefjord, M.; Wormald, M. R.; Dwek, R. A.; Kiran, G. P.; Devendar, R.; Takata, G.; Morimoto, K. *Tetrahedron: Asymmetr.* **2007**, *18*, 774-786.

CHAPTER 4

HYDROPHOBIC AND HYDROPHILIC COATINGS

This chapter includes the synthesis and polymerisation of two building blocks functionalised with long aliphatic and partially fluorinated chains. As a proof-of-concept, the corresponding products from the polymerisation reactions will be used as coatings onto several macroscopic surfaces, and their wettability will be studied. Finally, the versatility of the designed polymerisation approach to systematically fine-tune the wettability of surfaces will be demonstrated.

4.1. INTRODUCTION

Controlling the surface properties of materials is one of the greatest challenges that have been a focus of extensive research throughout history. The biggest challenge is to find solutions to problems such as wettability or corrosion, but also to confer novel properties not seen until now. As a result, platforms can be obtained that effectively exhibit multiple varieties of practical functionalities.¹

A widely pursued example is the formation of hydrophobic coatings which have full application at the industrial level. Nevertheless, its final properties cannot only be achieved through approaches such as the reduction of surface energy, but in most cases, it requires an exquisite design and control of the composition and chemical structure of the coatings.² Application of coatings with aliphatic-/fluorine-based or silicone-based materials such as silanes, wax and polymers is a common and successful strategy for lowering the surface energy of a solid. Macroscopic wettability on a smooth solid surface is commonly evaluated by the WCA (Figure 4.1a).

In the last decade, mussel-inspired surface chemistry, in which catechol derivatives play an important role, has garnered extensive research interest owing to material-independent surface coating capability and easy implementation to a wide range of applications. So, the number of those examples targeted to systematically control and modify the wettability are numbered and summarised next. For this, the classification of the different reports has been done following the three different approaches already presented in previous chapters and represented in Figure 4.1b. First, examples for hydrophobic surfaces will be revised and afterwards hydrophilic.

- **Approach I. Polymerisation through catechol moiety**
 - Post-functionalisation of catechol-based primer coating
 - Polymerisation of functionalised catechol-based molecules
- **Approach II. Catechol grafted to polymeric backbones**
 - Polysaccharide-based coatings
- **Approach III. Building blocks**
 - Copolymerisation

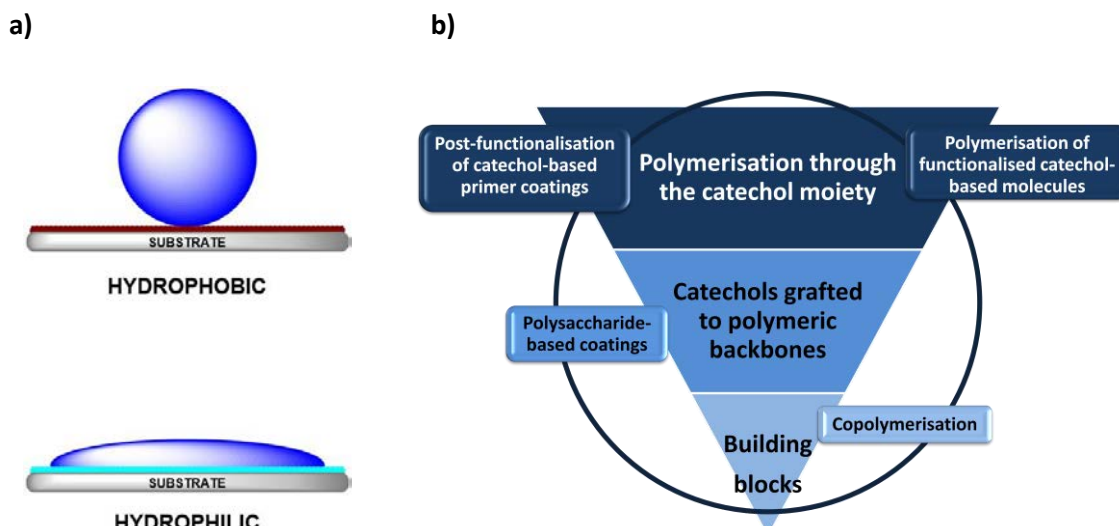


Figure 4.1. a) Schematic representation of a water droplet onto a hydrophobic surface (top) and a hydrophilic one (bottom). b) Scheme that shows the main general three strategies that can be followed to obtain catechol-based coatings.

4.1.1. OLEO-/HYDROPHOBIC COATINGS

4.1.1.1. Post-functionalisation of catechol-based primer coatings



Figure 4.2. Illustration of the functionalisation of a primer catechol-based polymeric coating with a hydrophobe.

In 2014 Ma *et al.* designed a versatile and straightforward strategy to obtain substrate-independent underwater superoleophobic surfaces (OCA up to 163°) through combining the versatile anchoring ability of mussel adhesive proteins and the remarkable oil-repellent ability of fish-skin.³ Catechol-bearing copolymer was synthesised using *N*-(3,4-Dihydroxyphenethyl) methacrylamide and methyl methacrylate and coated to glass, silicon, and aluminium, among others. Subsequently, by layer-by-layer (LBL) a fish-skin inspired top layer was assembled on it. The same year Wei *et al.* developed a rapid and universal approach for multifunctional material coatings based on a mussel-inspired dendritic polyglycerol (MI-dPG).⁴ Due to the high presence of catechol and amine groups, the system was able to establish a heteromultivalent anchoring and cross-linking mechanisms for the formation of functional material. Worth to

mention that after perfluoroalkyl functionalisation, the surface morphology was not changed. However, the WCA increased to about 166.5° (Figure 4.3).

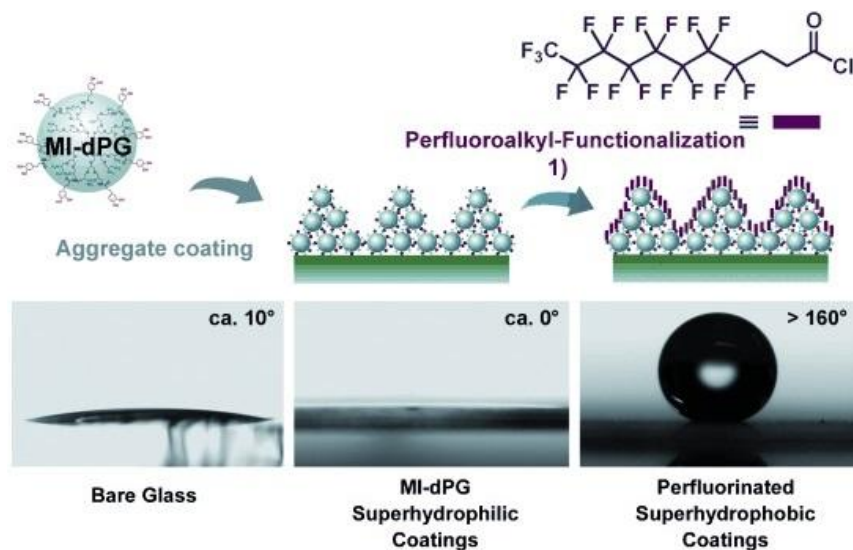


Figure 4.3. Scheme of the MI-dPG constructed superhydrophilic or perfluoroalkyl-functionalised superhydrophobic coatings (top). Left to right, the related static WCA of the bare glass, MI-dPG superhydrophilic coating and perfluorinated superhydrophobic coating, respectively (bottom).⁴

Then, one year later Wang *et al.* prepared for the first time a superhydrophobic fabric by an original and straightforward mussel-inspired strategy with a much lower concentration of dopamine without the use of additional NPs. The approach consisted in a first step where the application of folic acid to the surface induced the formation of rough PDA coatings with hierarchical structures.⁵ Then, after a chemical manipulation with octadecylamine, the resulting fabric exhibited WCA and rolling off angles around 162° and 7° , respectively. In order to show a real application of this coating, the superhydrophobic fabric was used to fabricate a small efficient boat for cleaning up oil spills. Besides, Yu *et al.* also reported the formation of mussel-inspired superhydrophobic surfaces with tuneable water adhesion. In this case, the authors used highly ordered honeycomb porous films which were prepared from a diblock copolymer polystyrene-*block*-poly(*N,N*-dimethylaminoethyl methacrylate) by the breath figure method.⁶ After the removal of the top surface layer of the honeycomb films, they were coated with PDA followed by the reaction with 1*H*, 1*H*, 2*H*, 2*H*-perfluorodecanethiol for fluorination. As a result of the surface modification, both the honeycomb and the pincushion-like surfaces were superhydrophobic with a WCA $> 150^\circ$ (Figure 4.4).

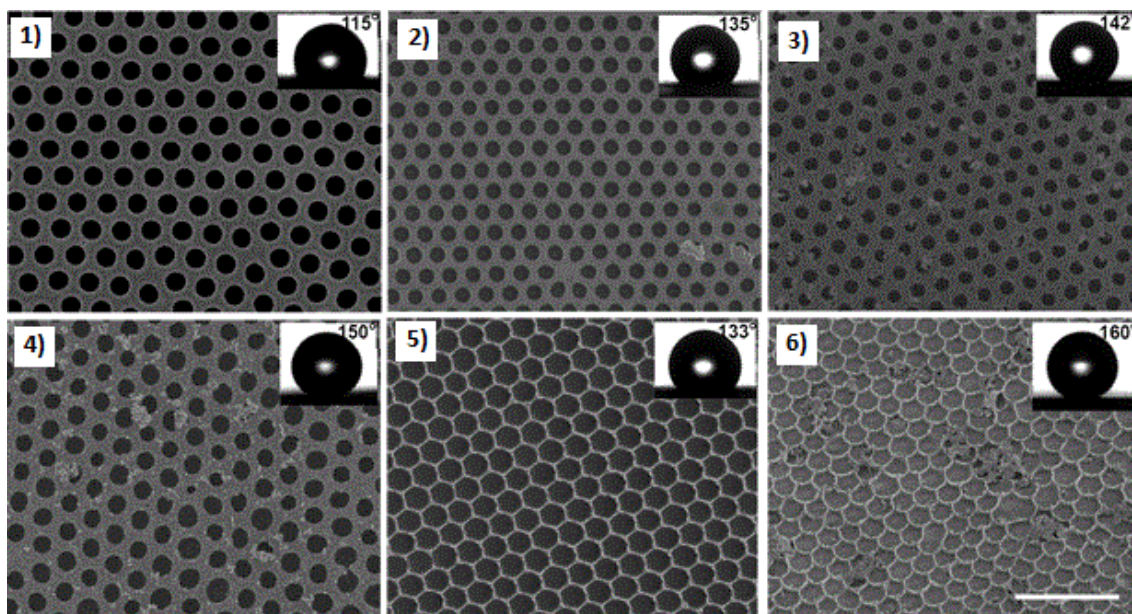


Figure 4.4. Scanning electron microscopy images (SEM) images of honeycomb films with DA deposition time of (1) 0, (2) 6, (3) 18, and (4) 24 h, followed by a 24 h reaction with fluorinated thiol. Pincushion-like surfaces without modification (5) and modified by 24 h DA deposition and 24 h reaction of fluorinated thiol (6). Insets show WCA and the photos. Scale bar: 10 μm .⁶

Furthermore, coatings made by PDA-metal complexes have been also reported. In 2016 Feng *et al.* reported the reaction of DA in the presence of water-swelling HNT.⁷ Interestingly, the authors observed that the interaction between DA and HNT strongly influenced the surface functionality of coated PDA. Additionally, the pH triggered the exposed surface functional groups, resulting in a reduction of the number of secondary/aromatic amine in PDA formed under weakly acidic conditions. Finally, WCA was measured showing variable values depending on the thickness (WCA $\sim 40^\circ$) but always higher when compared with pristine HNT (WCA $\sim 15^\circ$).

Combination of additional applications

With regard to coatings that present antimicrobial activity, Kim *et al.* prepared new platforms that exhibited water-resistant behaviour and long-term antimicrobial activity. On one hand, they conjugated 2-chloro-3',4'-dihydroxyacetophenone (CCDP) to poly(dimethylaminoethyl methacrylate) (PDMA) quaternising the amino groups of this polymer. In order to confer the antimicrobial properties, the polymer CCDP-q-PDMA was further quaternised with 1-bromododecane [CCDP/C12-q-PDMA] taking advantage of known antimicrobial activity of quaternary ammonium compound having long alkyl chains. The coated substrates, such as polyvinyl chloride, polyethylene terephthalate or quartz, were analysed by WCA which ranged from 60° to 80° .⁸ On the other hand, they coated several substrates (noble metals, oxides and

synthetic polymers) with poly(propylene oxide)-*g*-poly(dimethylaminoethyl methacrylate) conjugated with the catechol CCDP. Then, silver NPs (AgNPs) were immobilised to those coated substrates *via* the catechol groups exposed onto the surface, increasing the hydrophobic behaviour (Figure 4.5a).⁹

Regarding the use of hydrophobic coatings for water treatment, in 2013 Cao *et al.* developed an oil/water separation stainless steel mesh with high separation efficiency and intrusion pressure of water.¹⁰ The mesh was immersed afterward in an aqueous basic solution containing DA, forming the PDA coating. Then, through a Michael addition reaction in a second step, the substrate was functionalised with n-dodecyl mercaptan. The resulting mesh showed a high degree of hydrophobicity and superoleophilicity with values of WCA = 144° and OCA = 0°, respectively. Other important water treatments are the processes for the removal of pollutants present in water. In this sense, in 2014 Li *et al.* reported the fabrication of durable superhydrophobic and superoleophilic PU sponges capable of capture some organic pollutants present in the water in a selectively way (Figure 4.5b).¹¹ The developed systems were inspired in both mussel chemistry and lotus leaf. They were prepared by the coating of PU sponges with PDA, along with further functionalisation with dodecyl mercaptan and the immobilisation of AgNPs. The resulting PU sponges showed significant superhydrophobic/superoleophilic properties with WCA of about 155°, and OCA around 0°, respectively. One year later, Wang *et al.* immobilised silica NPs on the cotton surface to form superhydrophobic (WCA = 153°) and superoleophilic coating.¹² The coated fabric was highly efficient for separating mixtures of different organic solvents. And in 2016, Shang *et al.* developed a bioinspired general way to confer superhydrophobicity and modify the wettability of several commercial materials.¹³ The main objective was to provide the materials with the capacity to efficiently remove oils and organic solvents from water using a combination of both bioinspired mussel adhesion properties (PDA) and the well-known superhydrophobicity of lotus leaf resulting in the formation of a hierarchical structure. The procedure consisted in the formation of a thin layer of PDA on the commercial materials (*e.g.* nylon, cotton, melamine sponge and stainless steel mesh). Then, the coated materials were functionalised by anchoring 1*H*, 1*H*, 2*H*, 2*H*-perfluorodecanethiol (PFDT) moieties conferring the final superhydrophobic (WCA = 154°) and superoleophilic properties.

Finally, in 2016 Wu *et al.* developed a bioinspired mussel approach to produce coatings against corrosion on copper substrates effectively.¹⁴ The low-cost methodology was based on the spontaneous polymerisation between pyrocatechol and a polyamine (PA) resulting in an adhesive anti-corrosion coating of P(cat/PA) and then grafted by 1-dodecanethiol (DCT) showing final WCA of ~ 125° (Figure 4.5c).

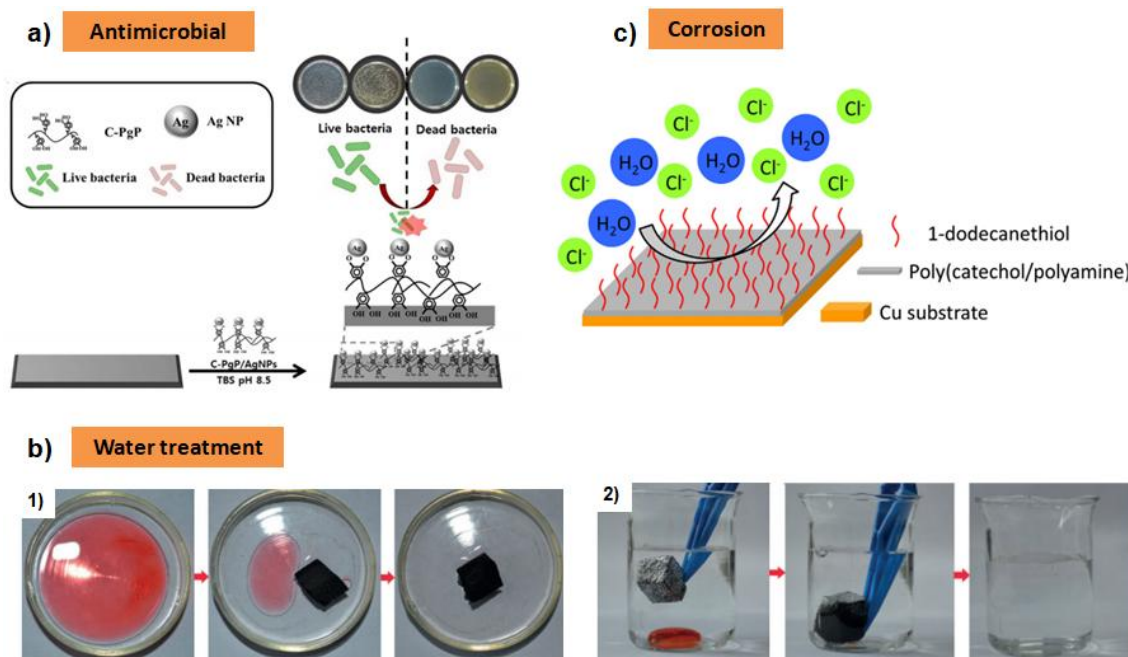


Figure 4.5. a) Illustration of preparation of surface-coated substrates with C-PgP/AgNP.⁹ b) Optical images for the removal of (1) oil on the surface of water and (2) chloroform under water by the PU@PDA@Ag@dodecyl mercaptan sponges.¹¹ c) Illustration of mussel-inspired anti-corrosion coating onto copper slides.¹⁴

4.1.1.2. Polymerisation of functionalised catechol-based molecules

One alternative to overcome limitations of the post-functionalisation is the polymerisation of catechol-based molecules that are previously functionalised with long aliphatic or fluorinated chains. The polymerisation takes place under alkaline media and finally is used to coat macroscopic surfaces via *ex situ* treatments by dipping the substrate into a solution containing the polymer.

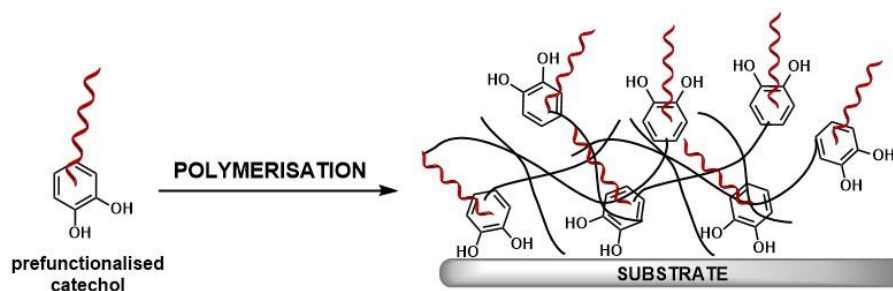


Figure 4.6. Illustration of the polymerisation of functionalised catechols.

Our research group was pioneer using this approach back in 2013,¹⁵ in the development of a new simple strategy to polymerise previously-substituted catechol moieties with appropriate functional chains (alkyl chain and fluorinated chain). The polymerisation process was carried out with ammonia, which was supposed to act as a nucleophile on the reactive *o*-quinones thus formed under basic aqueous media. This novel strategy opened the door to the possibility

of polymer deposition through *ex situ* treatments. Following this simple strategy, both polyester fibres and glass slides were successfully coated with aliphatic- and partially fluorinated-based polymers by immersing the substrates into a solution containing the polymer in non-polar organic solvent without additional washing. After measuring the WCA and the oil contact angle (OCA), results showed that the coated substrates were hydrophobic and oleophobic, with CA of 115°-150° and 150°, respectively (Figure 4.7a). In subsequent work, the ability of these coating for the efficient removal of oil from oil/water mixtures was tested.¹⁶ These novel coatings were highly hydrophobic with the capability to provide enough robust and efficient water repellency on weaved textiles useful for water treatment purposes. This approach demonstrated a new facile strategy to obtain catechol-based polymers already functionalised, unlike PDA. In order to explore the versatility of this methodology, few catechol-based molecules bearing different number and lengths of linear alkyl chain substituents were synthesised and polymerised by using ammonia in the presence of air.¹⁵ The resulting polymers were soluble in a few common organic solvents, thus allowing for the formation of the coatings by *ex situ* treatments. Working in this way, it is possible to fine-tune and optimise the conditions, providing better control and ultrathin coatings onto polyester, cotton weaves and filter paper (Figure 4.7b).

Finally, in 2016 Watanabe *et al.* studied the mechanical robustness of coated thin films made of urushiol and hydrogenated urushiol (h-urushiol) with Fe²⁺ onto glass, silicon and gold substrates.¹⁷ The WCA measurements showed that the values progressively increased with the amount of h-urushiol (the highest value was 90°).

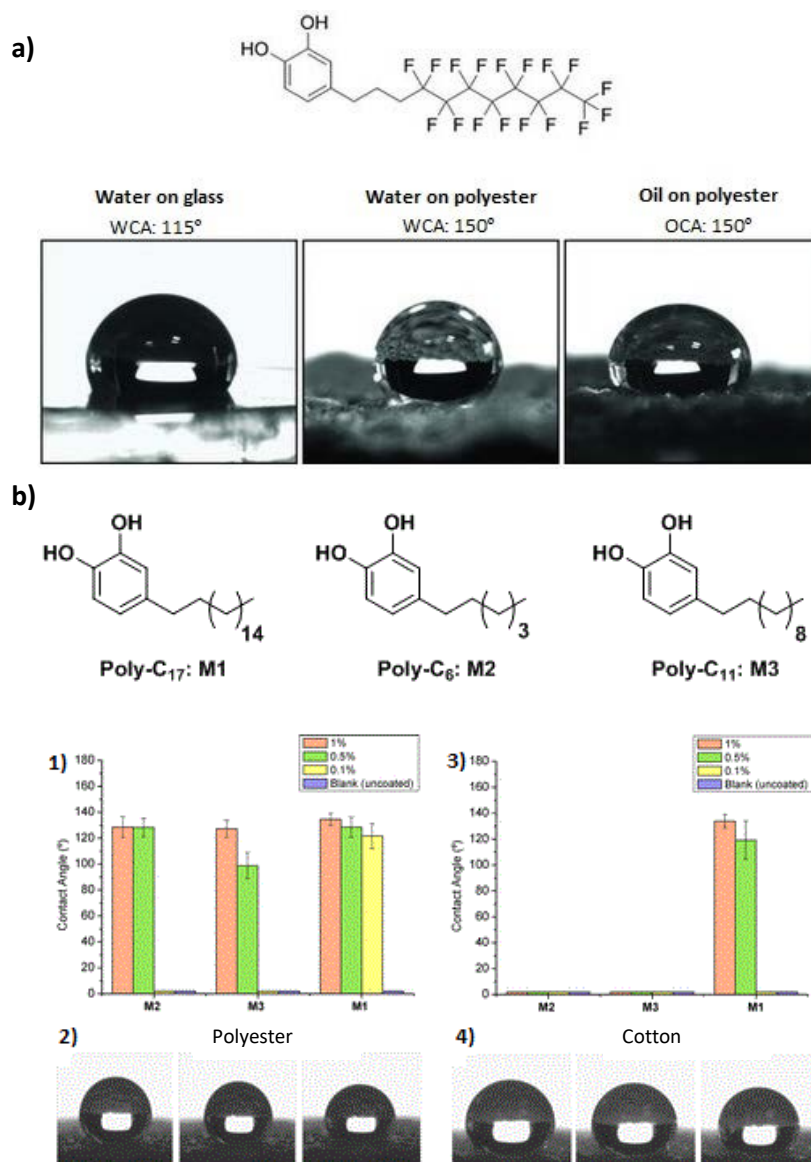


Figure 4.7. a) Molecular structure of a catechol molecule bearing a partially fluorinated alkyl chain (top). CAs obtained with different liquid on different substrates coated with the polymerisation product of partially-based fluorinated catecholic compound (bottom).¹⁵ b) Molecular structure of different aliphatic-functionalised catechol molecules. Effect of the solution concentration used for dip-coating on the efficacy of coating materials **M2–M1** on polyester (1) and cotton (3). Zero values for the CA indicate fast collapse (< 10 s) of the water droplet due to absorption in the textile. Robustness of **M1** coatings on polyester (2) and cotton (4) prepared from 1% w/v chloroform solutions: evolution of the water droplets after 1, 5, and 10 min (left to right).¹⁶

4.1.1.3. Polysaccharide-based coatings and copolymerisation

As already explained in the *General Introduction of Chapter 1*, approach II based on catechols grafted to polymeric backbones is extensively used to obtain bio-inspired adhesive, but not for coatings. However, it can be found an example where polysaccharide materials in combination with catechol derivatives are used for the formation of functional films and membranes. In 2014 Neto *et al.* described the preparation of thin and surface-adherent films and dopamine-

modified HA (HA-DA).¹⁸ The use of layer-by-layer methodology allowed for the formation of multilayer films based on CHT and HA-DA to form polymeric coatings onto glass substrates exhibiting WCA $\sim 77^\circ$. *In vitro* tests showed a remarkable cell adhesion and viability for the corresponding films. Authors claimed that these films could present potential applications as adhesive coatings for biomedical implants.

Finally, approach III is quite a new strategy and only few examples can be found in the literature where building blocks are used to prepare copolymers as hydrophobic coatings. For instance, in 2011 Han *et al.* designed a novel approach for the preparation of antimicrobial glass surfaces by a single dip-coating procedure.¹⁹ The strategy consisted in the free-radical polymerisation synthesis of amphiphilic polycations including different ratios of monomers containing dodecyl quaternary ammonium side chains, methoxyethyl side chains and catechol groups. Interestingly, all the polymeric coatings showed WCA values of two-fold more than pristine glass (WCA $> 80^\circ$). And in 2015 Payra *et al.* prepared several catechol-containing poly(alkyl methacrylates) by free-radical polymerisation for anticorrosion purposes.²⁰ The synthesised copolymers were deposited by spin-coating into several easily corrosive metal-alloy materials containing Mg, Al, Cu and Fe (Figure 4.8). Interestingly, the WCA measurements highlighted the drastic increase of hydrophobic features by tuning the length of the alkyl chains, achieving WCA values ranging from 70° to 110° .

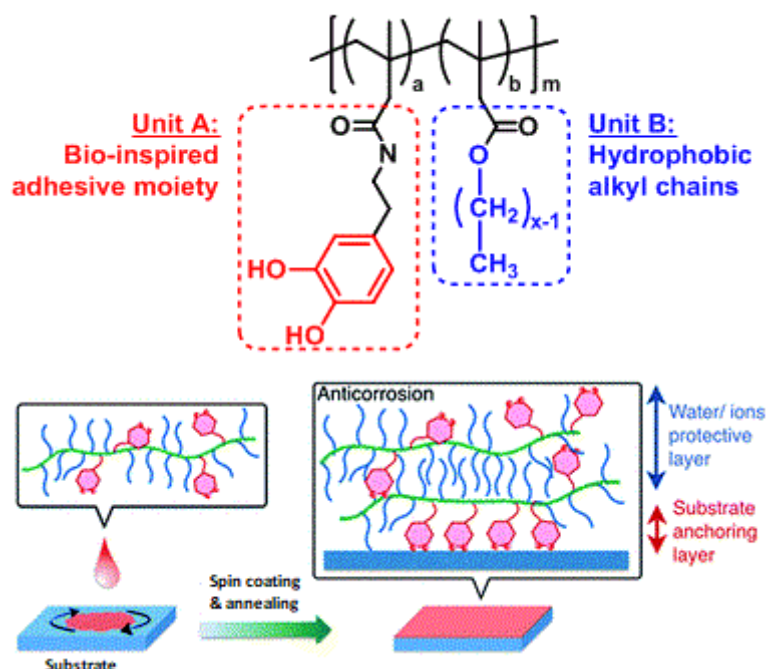


Figure 4.8. On top, chemical structure of poly(dopamine methacrylamide-co-alkyl methacrylate), poly(DOMA-co-AMA). On bottom, schematic illustration of preparing ultrathin polymer coating and possible pathway of forming stable protecting layer on metal/alloy substrates.²⁰

4.1.2. HYDROPHILIC COATINGS

Until now, mainly catechol-based polymers that provided hydrophobicity have been presented and discussed. However, not only is hydrophobicity of functional interest, but its opposite hydrophilicity may be of great importance at the industrial or biological level. This can be achieved by introducing molecules that contribute to the hydrophilicity, mainly with moieties that are charged (carboxylates or quaternary amines), amines or hydroxyl groups. Less examples have been reported for obtaining hydrophilic coatings than hydrophobic ones, and in this section, a selection of relevant examples reported on the use of hydrophilic coatings will be discussed following approach I based on the polymerisation through the catechol moiety. Until 2016 there were hardly any example reported on the use of catechol grafted to polymeric backbones or building blocks, approach II and III respectively, for obtaining hydrophilic coatings. Only one example with regard to catechol-based polysaccharides were reported in 2016, where Rodrigues *et al.* produced nacre-like layered free-standing membranes using LBL deposition methodology combining CHT, HA, previously modified with catechol groups, and bioactive glass NPs for guided tissue regeneration.²¹ Following approach I, the self-polymerisation of DA or norepinephrine (NE) under alkaline conditions without further functionalisation is widely used (Figure 4.9).

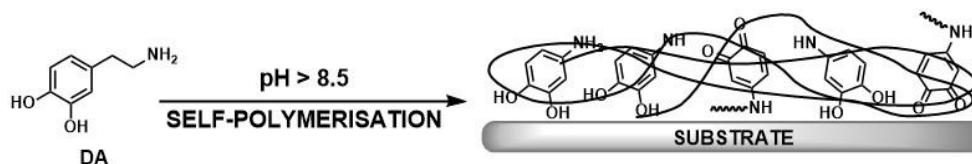


Figure 4.9. Illustration of the self-polymerisation of DA, and the coating of a substrate via *ex situ* treatments.

For example, in 2014 Tsai *et al.* described a procedure based on the deposition of PDA onto biodegradable polymer films such as polycaprolactone, poly(L-lactide) and poly(lactic-co-glycolic acid) for promoting cell adhesion with huge interest for its application in bone tissue regeneration.²² The same year Park *et al.* reported a methodology to obtain bioinspired functional interfaces with improved adherence of human neural cell (hNSC).²³ This novel biointerface was synthesised through the oxidative polymerisation of NE forming a polymeric nanofunctional hNSC-biocompatible thin layer (PNE). Interestingly, independently of the substrate employed, the biocompatible PNE coating drastically reduced the WCA, showing values ranging from 22.76° to 39.86° (Figure 4.10).

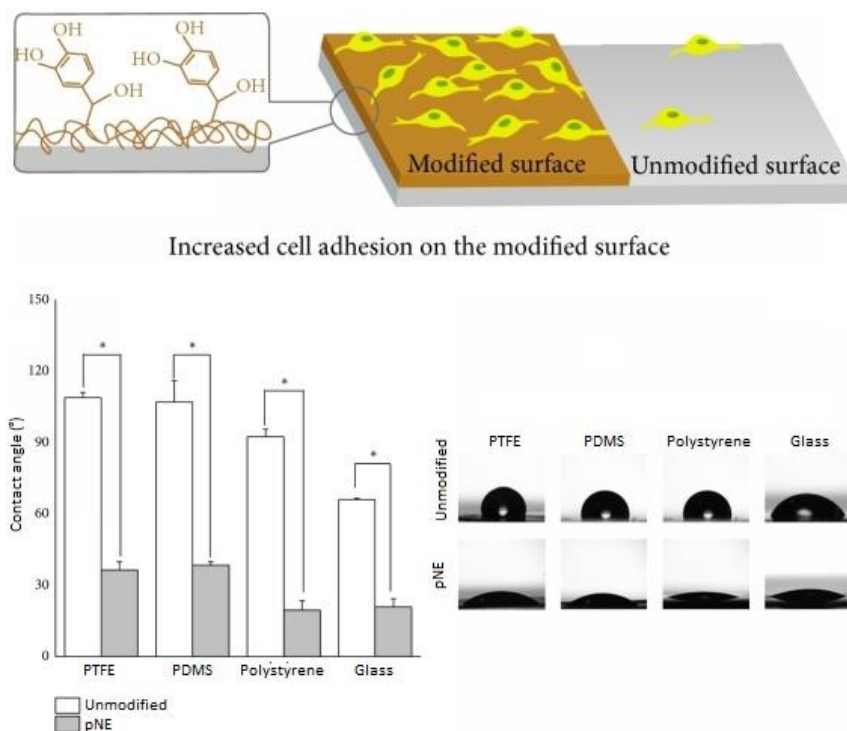


Figure 4.10. Schematic illustration of the PNE-coated biointerfaces onto which hNSCs are adhered (top). WCA values and images onto different substrates (bottom).²³

Furthermore, the use of the self-polymerisation of NE under alkaline conditions and its tendency to form biofilm was used in 2016 by Chen *et al.* for fabricating a facile and eco-friendly strategy to modify a poly(dimethylsiloxane) (PDMS) channel capable of selective enantioseparation of chiral molecules (*e.g.* amino acid enantiomers, drug enantiomers and peptide enantiomers).²⁴ Thanks to abundant catechol and amine functional groups present in the PNE biofilm, the PNE-coated PDMS microchip showed enhanced wettability and lower non-specific adsorption. The WCA of the pristine PDMS was 108°, consistent with its inherent hydrophobicity. After coating the PDMS by the *in situ* self-polymerisation strategy, the WCA of PNE-PDMS abruptly decreased to 13° due to the plentiful active hydroxyl groups in PNE, which was consistent with the results reported previously.²³

Finally, one can also find few reported examples based on the post-functionalisation of catechol-based primer coatings to obtain hydrophilic coatings with antimicrobial activity. In 2014 Liu *et al.* reported a strategy for the formation of versatile self-cross-linked polymer nanolayers for their use in biointerfaces.²⁵ This strategy allowed constructing self-cross-linked nanolayers on PES substrates *via* the pH-induced catechol cross-linking and further immobilisation on the substrate. The resulting coated-PES showed increased roughness and enhanced hydrophilicity ranging from 60° to 50° (WCA of pristine PES was 75°). Two years later, in 2016 Wang *et al.* described a new route to obtain highly stable and durable anti-

adhesion surfaces by combining the outstanding anti-adhesion performance of zwitterionic betaine macromolecules, which have strong hydration capacity, and the robust adhesion of DA and its derivatives, such as dopamine methacrylamide (DMA).²⁶ First of all, some substrates were coated with DMA copolymers and further functionalised with betaine macromolecules. After the modification of the substrates, the hydrophilicity was enhanced, showing WCA values ranging from 10° to 12° and higher superoleophobic character (OCA: 150° - 160°) compared with pristine surfaces (Figure 4.11).

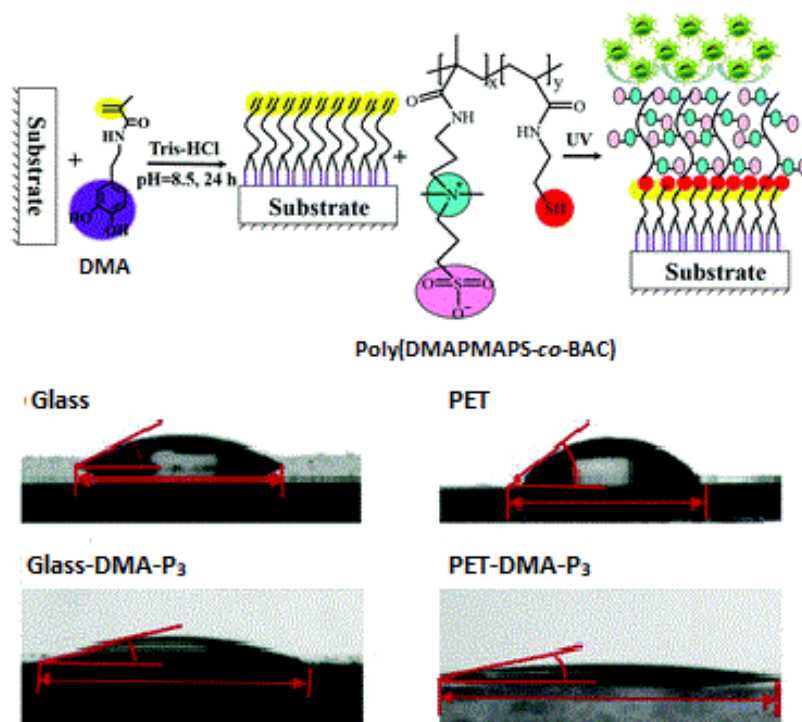


Figure 4.11. Schematic representation for construction process of anti-adhesion surfaces (top). Images of water droplets on the modified surfaces and the corresponding unmodified substrate surfaces (bottom).²⁶

4.1.3. WORK PROGRAMME

Until now, it has been seen that there are many examples reported in the literature based on catechol coatings to change the wettability of the treated surfaces. However, there are no examples where the wettability of these surfaces can be systematically fine-tuned at will over a broad range of WCA. Another important fact to mention is that most of the examples so far reported in the literature involve in more or less degree the coloration of the substrate, which is not desired in most of the cases. So the development of novel approaches, like is our case, which do not involve such coloration are strongly required.

According with the previous considerations, especially, the catecholic systems used here are the ones represented in the next Figure.

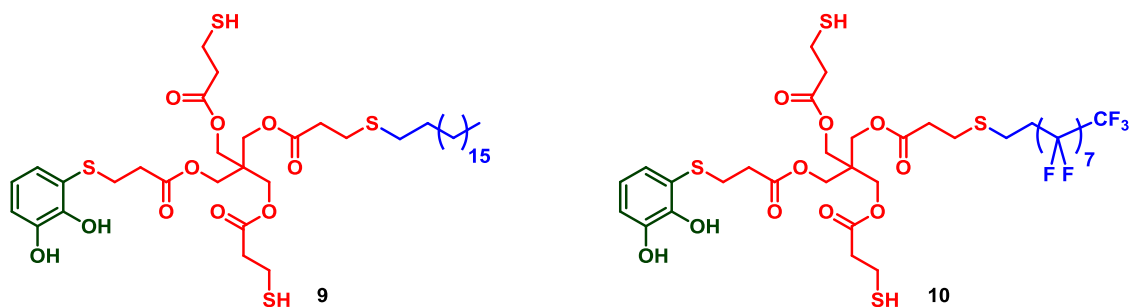


Figure 4.12. Molecular structures of the two target molecules functionalised with a C_{18} aliphatic chain (**9**) (left) and a partially fluorinated chain (**10**) (right).

The length of the chains was selected based on previous results of our group with related hydrophobic catechol-based coatings obtained following approach I.^{15,16}

Once these monomers have been obtained, the next step will be to control their polymerisation under mild oxidative conditions as already seen in the previous *Chapter 3*.

Afterwards, the last step will be the coating of macroscopic surfaces. As a proof-of-concept, different substrates would be coated with the materials obtained from the polymerisation reactions. In particular, glass, aluminium, copper and stainless steel slides will be coated *via ex situ* treatments. Afterwards, following the same methodology, textile waves will be coated with C_{18} -functionalised **P9** material in order to fabricate hydrophobic textiles capable to absorb oils, such as commercial olive oil or tetradecane (TDC).

Finally, in order to demonstrate that this new designed polymerisation strategy is quite versatile controlling the wettability of the surface, aliphatic- and fluorescein-functionalised building blocks will be combined together with controlled ratios, and the resulting polymers used to coat glass slides and cotton fibres. In this case, fluorescein-functionalised building block **8**, already described in *Chapter 3*, was chosen because it would provide fluorescence and it is much less hydrophobic than C_{18} aliphatic chain, so it would provide some hydrophilicity to the treated surface.

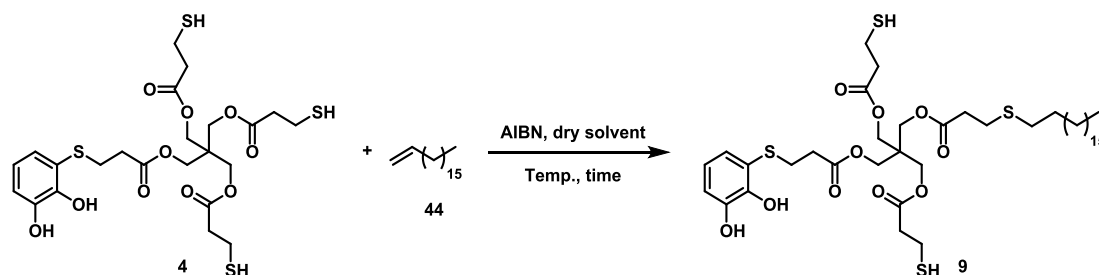
On top of that, and for comparison reasons, a C_{18} -functionalised building block containing a styrene moiety would be also synthesised and tested as coating to demonstrate the role of catechol in the adhesion properties.

4.2. SYNTHESIS OF THE BUILDING BLOCKS

The different target molecules were characterised by ^1H -/ ^{13}C NMR experiments and IR.

4.2.1. SYNTHESIS OF C₁₈-FUNCTIONALISED BUILDING BLOCK 9

As already seen for the preparation of PEGylated and fluorescent building blocks (see *Chapter 3*, section 3.2. *Synthesis of the building blocks and a targeting molecule*), the synthesis of aliphatic derivative **9** was first attempted *via* the functionalisation of monosubstituted S-catechol tris-thiol **4** with commercial 1-octadecene **44**, since the synthesis of the intermediate **4** was already optimised (Scheme 4.1).



Scheme 4.1. Synthesis of aliphatic building block **9** from catechol intermediate **4** *via* the radical-catalysed thiol-ene reaction.

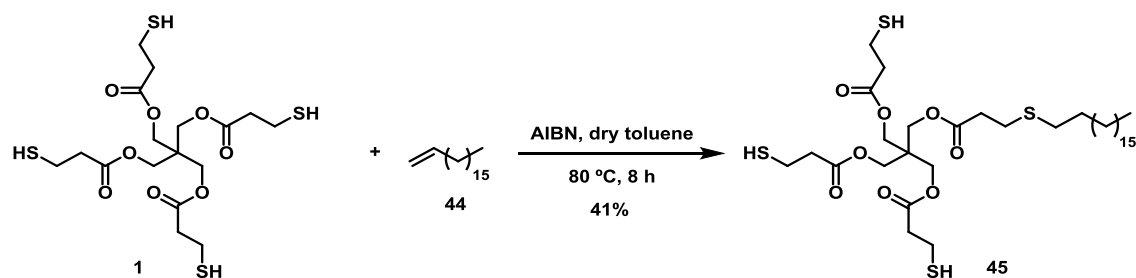
This reaction was attempted several times working with 0.2 equiv. of AIBN, different solvents, different equivalents of 1-octadecene and different reaction times. All the results obtained are summarised in the next Table.

Table 4.1. Reaction conditions used to afford the final aliphatic derivative **9**.

Entry	1-octadecene 44	Solvent	Time	Temperature (°C)	Yield
1	1.5 equiv.	dry CH ₃ CN	24 h	reflux	-
2	1 equiv.	dry toluene	6 h	80 °C	-
3	1 equiv.	dry toluene	24 h	reflux	8%
4	0.9 equiv.	dry toluene	24 h	reflux	11%

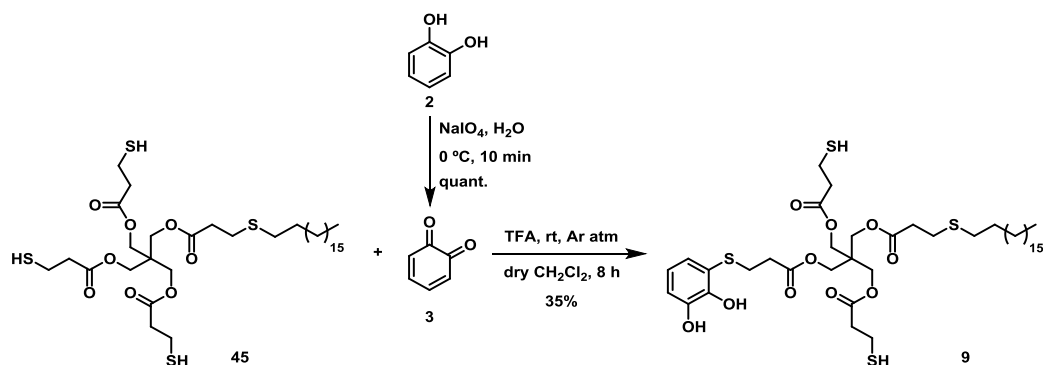
This reaction was monitored by ¹H NMR observing the disappearance of protons coming from the double bond of **44**. The reaction was stopped after a total conversion to the desired product. When the reaction was carried out in dry CH₃CN and with 1.5 equiv. of 1-octadecene **44** (Table 4.1, entry 1), multi-addition of the aliphatic chain was obtained. Hence, it was worked with less than 1 equiv. of molecule **44** in order to avoid the addition of more than one aliphatic chain in the catechol-based molecule **4**, and dry toluene was used to work with higher temperatures (entries 2-4). Finally, working with 0.9 equiv. of **44** for 24 h afforded the highest yield (11%) of compound **9** as a colourless oil (entry 4). The low yield of this reaction was due to the formation of complex reaction mixtures, in which several by-products were formed from multiple-addition and /or coupling reactions between aliphatic chains.

Since following route A only 4% overall yield of compound **9** was obtained, this molecules was attempted to be obtained following route B (see *Chapter 1*, Figure 1.18) in order to improve the yield. Therefore, the starting material **1** was first functionalised with the commercial 1-octadecene **44** via the radical-catalysed thiol-ene reaction (Scheme 4.2) in the same reaction conditions already used to obtain previous building blocks (see *Chapter 3*).



Scheme 4.2. Functionalisation of pentaerythritol tetrakis(3-mercaptopropionate) **1** with the long C₁₈ chain **44** via the radical thiol-ene reaction.

As usual, this thiol-ene reaction was followed by ¹H NMR. After the total disappearance of olefin's protons the reaction was stopped and the crude reaction was purified by a flash column chromatography to afford **45** in 41% yield as a colourless oil. Afterwards, the introduction of the catechol fragment was achieved through the 1,6-conjugated addition between intermediate **45** and *o*-quinone **3** following the same procedure already described. The final aliphatic compound **9** was achieved in 35% yield (Scheme 4.3).

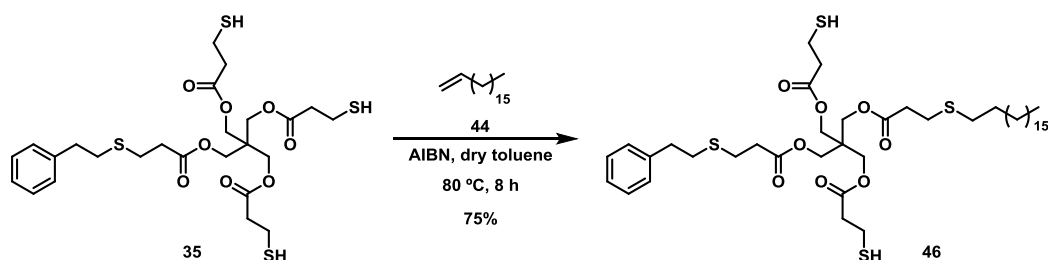


Scheme 4.3. Conjugated addition of molecule **45** to *o*-benzoquinone to afford the building block **9**.

Following route B, the overall yield for this C₁₈-functionalised building block **9** was 14%, whereas following route A, the overall yield of building block **9** was only the 4%. As already mentioned, the low yields could be attributed to the formation of complex reaction mixtures, and solubility and manipulation issues.

4.2.2. SYNTHESIS OF C₁₈-FUNCTIONALISED STYRENIC DERIVATIVE 46

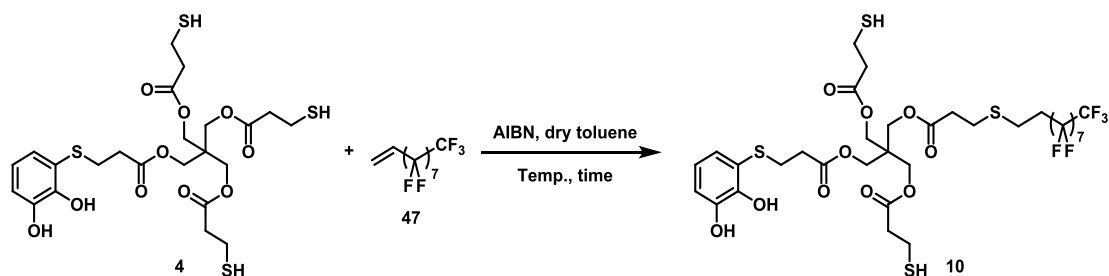
As already seen for the fluorescein-functionalised building block **8**, it was also synthesised an C₁₈-functionalised styrenic one. The target compound **46** was prepared from intermediate **35** (see Chapter 3, section 3.2.6. Synthesis of fluorescein-functionalised styrenic derivative **36**) in 75% yield after purification by column chromatography.



Scheme 4.4. Synthesis of styrenic derivative containing a long aliphatic chain C₁₈ **46**.

4.2.3. SYNTHESIS OF FLUORINE-FUNCTIONALISED BUILDING BLOCK 10

As in the case of aliphatic derivative **9**, firstly it was attempted the synthesis of the fluorinated monomer **10** *via* route A, involving the functionalisation of S-catechol tris-thiol **4** with the commercial fluorinated 1*H*, 1*H*, 2*H*-perfluoro-1-decene chain **47** through the radical-catalysed thiol-ene reaction (Scheme 4.5).



Scheme 4.5. Synthesis of fluorine-functionalised molecule **10** from catecholic intermediate **4** *via* the radical thiol-ene reaction.

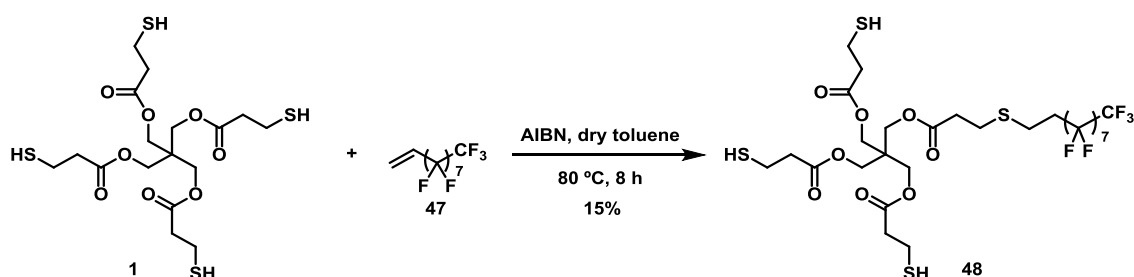
This reaction was attempted several times working with 0.2 equiv. of AIBN in dry toluene and with different equivalents of the fluorinated chain **47** and temperatures (Table 4.2).

Table 4.2. Reaction conditions to afford molecule **10** from S-catechol tris-thiol **4**.

Entry	Fluorinated chain 47	Time	Temperature (°C)	Yield
1	1 equiv.	24 h	reflux	-
2	1.4 equiv.	10 h	80 °C	2%
3	1.4 equiv.	20 h	75 °C	4%

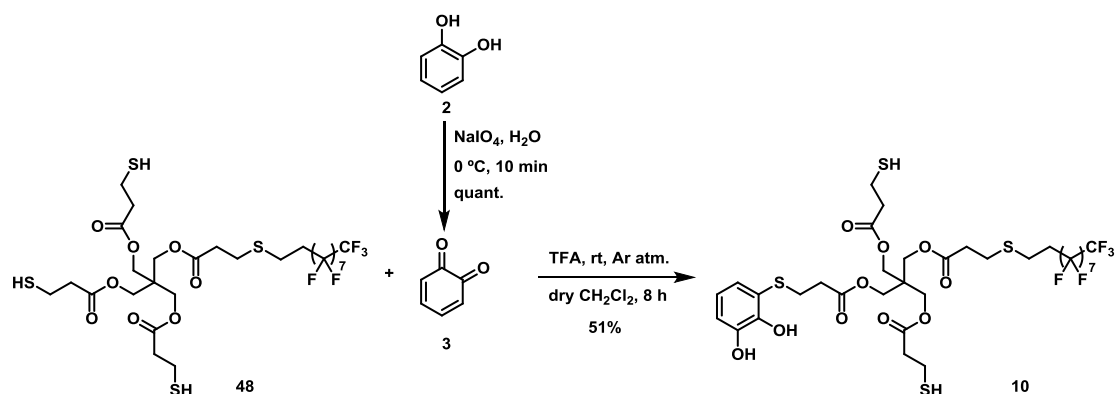
It was observed that more than 1 equiv. of the commercial fluorinated chain **47** (Table 4.2, entries 2 and 3) were needed to obtain the desired product **10**. With less equivalents of **47**, the expected product was not formed, since intermediate **4** was mainly obtained (entry 1). Nonetheless, adding more equivalents led to the addition of more than one chain, resulting in more by-products and in consequence in a difficult purification of compound **10** through several flash column chromatographies.

Therefore, in order to synthesise the fluorinated compound **10**, it was followed route B. The conjugation of the 1*H*, 1*H*, 2*H*-perfluoro-1-decene **47** to the core **1** (Scheme 4.6) was carried out through a radical-catalysed thiol-ene reaction using the same reaction conditions used for the synthesis of intermediate **48**.



Scheme 4.6. Functionalisation of pentaerythritol tetrakis(3-mercaptopropionate) **1** with 1*H*, 1*H*, 2*H*-perfluoro-1-decene chain **47** via the radical thiol-ene reaction.

Intermediate **48** was obtained in 15% yield, and this low yield could be attributed to the formation of complex reaction mixtures and solubility issues. Then, compound **48** was submitted to a conjugated addition with *o*-quinone **3** to deliver product **10** in 51% yield (Scheme 4.7).



Scheme 4.7. 1,6-Conjugated addition of intermediate **48** to *o*-benzoquinone **3** to afford the building block **10**.

4.3. SULPHUR-BASED POLYMERISATION REACTION

Once the three building blocks **9**, **10** and **46** were synthesised and characterised, they were polymerised following the same strategy based on the formation of disulphide bonds already explained in the previous chapter (Figure 4.13).

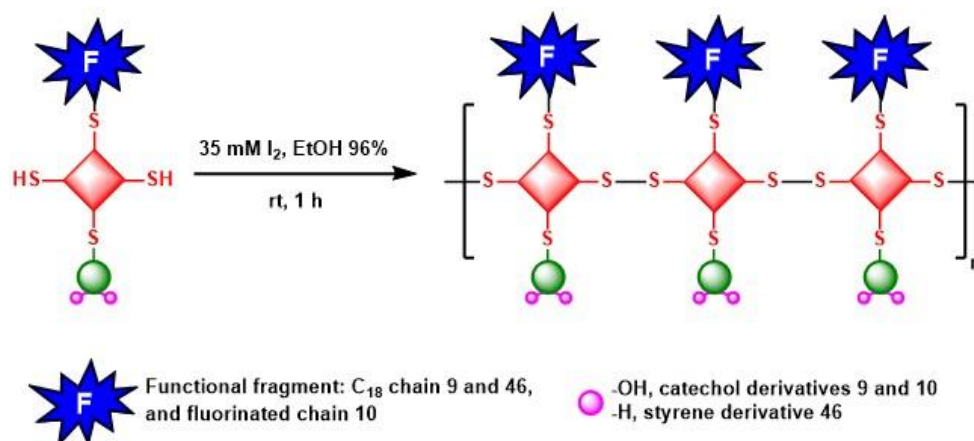


Figure 4.13. Mild oxidative polymerisation of synthesised building blocks using a solution of iodine in EtOH 96%.

Following the same general procedure, 35 mM solution of resublimed iodine (1 equiv.) was added dropwise into a solution containing the corresponding monomer in EtOH 96%, except for the fluorinated derivative **10** in which the polymerisation was performed in CH₂Cl₂. After 1 h, the precipitates formed were isolated and washed with fresh solvent (Table 4.3). (Note: these polymerisations were carried out with the presence of 3-5% of tris-thiol **4**).

Table 4.3. Yields of polymerisation reactions based on the amount of the solid precipitate for each monomer **9**, **10** and **46**.

Product from the polymerisation reaction	Yield (%)
P9 (C ₁₈ -functionalised catecholic derivative)	39%
P10 (fluorine-functionalised catecholic derivative)	48%
P46 (C ₁₈ -functionalised styrenic derivative)	60%

These polymers were characterised by ¹H NMR, DOSY NMR experiments and GPC (see Annex A2.3-6 for GPC spectra).^a Due to solubility issues, only the C₁₈-functionalised derivatives **P9** and **P46** could be characterised by these three techniques since fluorinated derivatives were not soluble in THF. After their characterisation, it was concluded that using those oxidative

^a GPC analyses were performed in collaboration of Dr. Haritz Sardon from the Innovative Polymers Group led by Dr. David Mecerreyes at POLYMAT (Basque Center for Macromolecular Design and Engineering).

conditions, mixtures of short oligomers between 2 and 10 units were obtained for both **P9** and **P46** (Table 4.4).

Table 4.4. Polymerisation's degree results of **P9** and **P46** obtained by ^1H NMR, DOSY NMR experiments and GPC.

Derivative	^1H NMR	DOSY	GPC			
			IR		UV	
P9	2-4 units	6/7 units	Mn	Mw	Mn	Mw
			4017 Da 4/5 units	6013 Da 7 units	-	-
P46	dimer-trimer	< 10 units	IR		UV	
			Mn	Mw	Mn	Mw
3167 Da tetramer	3651 Da tetramer	3637 Da tetramer	4144 5 units			

On the attempt to improve these polymerisation degree values for the polymerisation of catechol-based building block **9**, NaHCO_3 was used in order to neutralise the formation of HI during the polymerisation process. However, the same degree of polymerisation values were obtained by GPC, thus not further studies were performed.

4.4. MACROSCOPIC SUBSTRATE COATINGS

4.4.1. COATINGS WITH C_{18} -FUNCTIONALISED BUILDING BLOCKS **9** AND **46**, AND THEIR CORRESPONDING PRODUCTS **P9** AND **P46** FROM THE POLYMERISATION

4.4.1.1. Hydrophobic surfaces

I. From ex situ polymerised material

First experiments with C_{18} -functionalised derivative **P9** were directed to confer hydrophobicity to glass slides. As a general procedure, $1.5 \times 1.5 \text{ cm}^2$ slides of this material were cleaned by using a plasma cleaner machine (400 W, 5 min), and they were submerged into a $\sim 7 \text{ mM}$ HPLC grade CH_2Cl_2 solution of **P9** overnight, without stirring (Figure 4.14).



Figure 4.14. Schematic representation of coating procedure. The glass slide is submerged into the solution for at least 4 h, washed and dried before measuring WCAs.

After the coating treatment, surfaces were washed with fresh CH₂Cl₂ three times (even in the presence of ultrasounds) and dried in a gentle flux of argon. This treatment, which ensures a proper cleaning of the substrate, is not commonly used as it represents a real challenge test for the robustness of the coating as the coated substrate is washed three times not with water, but with the solvent where the coating is soluble. Finally, WCA of Milli-Q water droplets (*ca.* 5 μ L) on coated substrates were used to evaluate the hydrophobicity and wettability of the coated samples at rt by means of the sessile-drop technique. Reported values arise from averaging CA measurements on three different spots of each sample.

When surfaces were not washed after being coated, they showed a WCA of 95° (5° for the pristine glass). After the cleaning process such value decreased down to 77° (Figure 4.17, *vide infra* pag. 127), showing the influence of this parameter. So the robustness of our approach can clearly be demonstrated as the substrate still retains, though in less degree, the hydrophobic character. For comparison purposes, it was also studied the coating of a glass slide with the corresponding monomer **9** following the same procedure. Initially, the WCA value found was 84° though it experimented a substantial decrease after the whole washing process down to 55°. To conclude, coatings made with monomers were less robust than the ones made with the oligomers, thus the water droplet onto the treated surface was spread out faster (Figure 4.15).

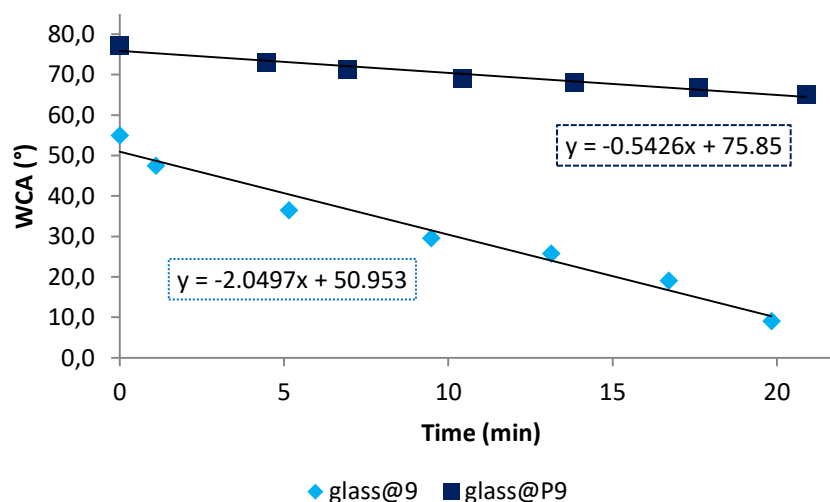


Figure 4.15. WCA values vs. time of **9**-coated glass slide (light blue) and **P9**-coated glass slide (dark blue).

From the Figure above, it was observed that the slope of glass@**9** was more negative than the one from glass@**P9**, meaning that the water droplet was introduced more easily into the coating. As expected, the product from the polymerisation reaction had a larger tendency to attach to surfaces than the monomer thanks to the synergism of the different catechol units, reason why the last one was excluded for further studies.

Moreover, some studies on the influence of the time of the absorption process were also performed. Four cleaned glass slides were submerged into a HPLC grade CH_2Cl_2 solution of **P9** for 1, 4, 8 h and overnight, respectively. Afterwards, they were washed three times with fresh CH_2Cl_2 and dried in a gentle flux of argon. Then WCA measurements were performed on each surface. It was seen that after 4 h, the final coating obtained was comparable with the one obtained after 8 h, or, overnight (WCA values raised between 71° and 76°), indicating the success of the coating after a few hours.

In addition, it was also checked whether the position of the substrate into the solution of **P9** (horizontal vs. vertical) had an important role on the final deposited coating and thus to the hydrophobicity of the resultant surface. Hence, two clean glass slides were submerged into a ~ 7 mM solution of **P9** in HPLC grade CH_2Cl_2 ; one lying down onto the bottom of the vial and the second one resting onto the wall, overnight. Afterwards, they were washed with fresh CH_2Cl_2 , dried with a flux of argon, and WCA values were measured. Both coated surfaces presented comparable hydrophobic values (73° vs. 76° , respectively), so it was concluded that the position of the substrate into the **P9** solution did not influence on the resulting coating.

Beyond glass, three additional surfaces, aluminium, copper and stainless steel with different initial hydrophobic character, were also studied for comparison purposes. As a general procedure, $1.5 \times 1.5 \text{ cm}^2$ slides of such materials were cleaned by sonicating in acetone, EtOH

96% and Milli-Q water for 10 min each and dried in a gentle flux of argon. The coating procedure with **P9** was performed in the same way as explained for glass surfaces and WCAs were measured before and after washing the treated surfaces. Previous to wash, the WCA values were a little bit higher than the ones measured after rinsing the surfaces, but the differences between them were not significant (Figure 4.17, *vide infra* pag. 127). In this case, it was demonstrated the robustness of these coatings against washes.

Images from water droplets onto these treated surfaces were taken, observing how their hydrophobicity increased despite washes when they were coated with catecholic derivative **P9** (Figure 4.16).

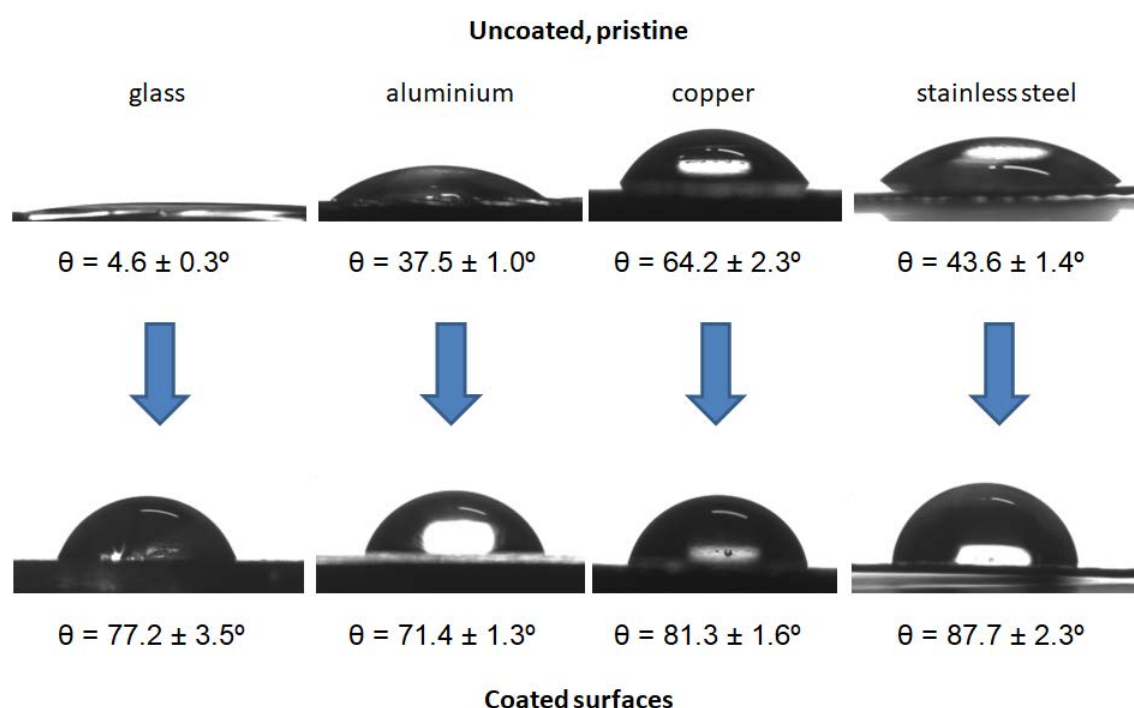


Figure 4.16. Images from water droplets onto pristine surfaces (top) and surface@**P9** after being rinsed (bottom).

Additionally, the four substrates (glass, aluminium, copper and stainless steel) were also coated with styrenic derivative **P46** to study the role of the catechol moiety. Particularly, in the cases of glass, aluminium and stainless steel, the same trend regarding the hydrophobic behaviour of the resulting surfaces was noted. It was observed that when the substrates were treated with product **P46** (Figure 4.17), less hydrophobic surfaces, with WCA values around 55° or below, were obtained than when they were treated with catechol-based derivative **P9**. These results demonstrate that the robustness of the coating in front of the different washes is less for the styrene-based ones, as expected as the role of the catechol moiety is lost. However, the presence still of non-specific interactions allows for some adhesion. In catechol moiety, the presence of the two vicinal alcohols allows forming several kinds of interactions;

hydrogen-bonding with hydroxyl groups exposed onto the glass surface, or, coordination bonds with metals, such as aluminium and iron (stainless steel), among others. In contrast, in the example with copper it was observed that the difference of the WCA between working with **P9** or **P46** was much smaller, only 7° (Figure 4.17). The most plausible explanation would be that sulphur has a high affinity towards copper,^{27,28} this being the interaction that prevails over the interactions that can occur with aromatic rings, and in less degree with the other metallic surfaces. In fact, with glass, as there is no such interaction, the WCA is less. After performing all these experiments, regardless of the surface or the efficiency of the coating, no surface treated with these materials changed its colour, or, appearance.

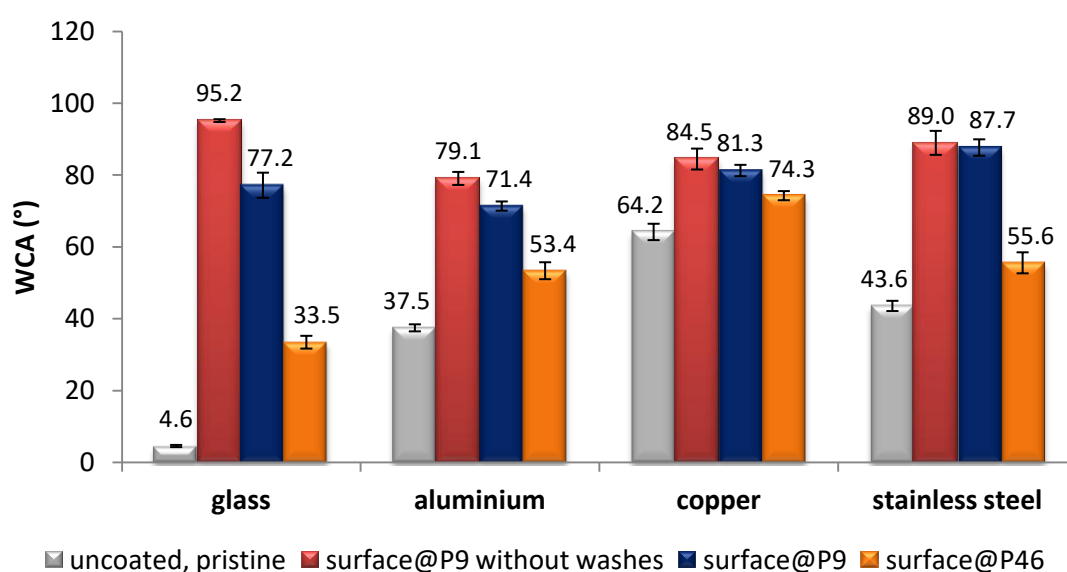


Figure 4.17. WCA values onto four different substrates (glass, aluminium, copper and stainless steel) coated with C₁₈-functionalised derivatives **P9** (blue) and **P46** (orange) after being rinsed, and previously to the washes (red).

Furthermore, surface topography imaging of **P9** coating onto glass was carried out in ambient air in tapping mode using beam shaped silicon cantilevers AFM/SPM microscope. The measurements revealed an average thickness of 1.5 µm (Figure 4.18) and a roughness of 435 ± 32 nm.

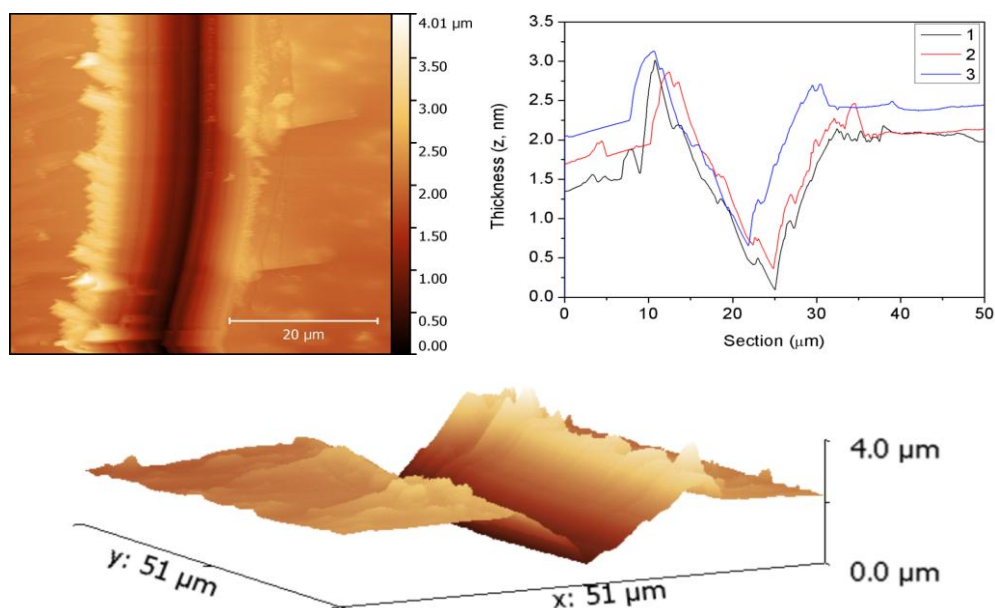


Figure 4.18. AFM image of topography along with the profile graphics and 3D representation.

Finally, **P9**-coated stainless steel, copper and aluminium were also characterised by EDX in order to study the composition of their surfaces (glass ones were not able to be characterised by this technique because it is a non-conductive material and should be previously metallised, altering the future results). The objective was to observe the presence of sulphur atoms, since it was the unique element that could come from our material. In all the cases, it was checked the presence of it at 2.3 KeV²⁹ when the surfaces had been treated. Furthermore, carbon and oxygen were also identified, and the measured percentages of them were around the expected ones ($\pm 10\%$) for the resulting coating (see *Annex A3.1* for EDX spectra).

II. From in situ polymerisation

The concept was, firstly to repeat the coating of substrates with the aliphatic monomer **9** and then placed them onto vials that contained inside sublimated iodine; the hypothesis was that iodine would sublime and polymerise the monomers onto the surfaces *in situ* without solvent as represented in the Figure 4.19a. Hence, four different surfaces (glass, aluminium, copper and stainless steel), previously cleaned with their corresponding method (plasma cleaning for glass and solvent washes for metals), were coated with aliphatic monomer **9** by submerging them into a ~ 7 mM solution of **9** in HPLC grade CH_2Cl_2 . Afterwards, without washing and only dried in a gentle flux of argon, these four surfaces were placed onto vials containing sublimated iodine, overnight. After that time, surfaces were washed three times with fresh EtOH 96% to remove the excess of iodine and dried in a gentle flux of argon. At first sight, it was seen that the area which had been in contact with iodine turned lighter, pointing out to the bases of a polymer reaction.

To evaluate the hydrophobicity of the resulting surfaces, the corresponding WCA were measured (Figure 4.19b). Blanks were the surfaces that had not been coated with monomer **9**, but they had been subjected to the same action of iodine as the treated ones. Comparing the results obtained from both polymerisation approaches (*ex situ* polymerisation in solution and *in situ* one), it was observed that in the cases of glass and copper surfaces, the WCAs achieved from *in situ* polymerisation were comparable, even higher, than the ones obtained when the coatings were performed in solution, 84° vs. 77°, and 89° vs. 81°, respectively (Figure 4.19b). However, with regard to aluminium and stainless steel surfaces, although there was a considerable increasing of WCA values of treated substrates compared to the corresponding blanks, the values obtained were lower than the ones obtained *via* the polymerisation in solution, particularly in the case of stainless steel. It is worthy to mention that when a pristine stainless steel slide was put in contact with iodine the surface became more hydrophilic than the initial one (12° vs. 44°). That could explain the difference in the coating hydrophobicity when polymerisation took place in solution (WCA ~ 88°) or through the iodine sublimation procedure (WCA ~ 44°).

Moreover, EDX analyses were also performed onto the metallic substrates coated with **P9** *via* this methodology before measuring WCAs (see Annex A3.2 for EDX spectra). In the three cases, it was checked the presence of sulphur at 2.3 KeV, carbon at 0.27 KeV, and oxygen at 0.52 KeV.²⁹ With this technique it was seen that coatings formed were not homogenous; although carbon and oxygen were always detected, in some analysed parts of the surfaces the minor element sulphur was not present. It was also seen remaining iodine in some regions, coming from the polymerisation process and a possible reason why the WCA values onto aluminium and stainless steel surfaces were lower than the ones obtained from the *ex situ* polymerisation in solution.

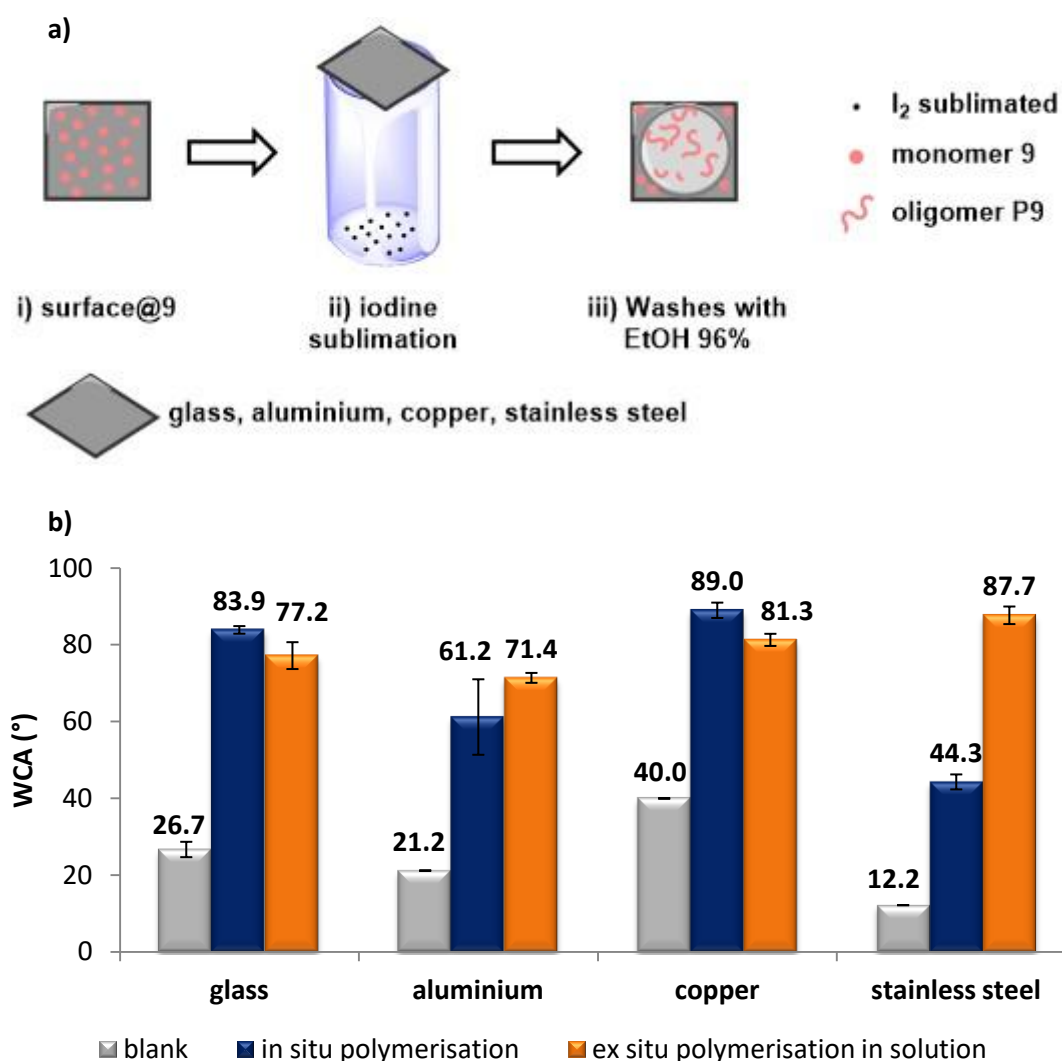


Figure 4.19. a) Representation of the *in situ* polymerisation. (i) Firstly, surfaces were coated with monomer 9, and (ii) then placed overnight onto vials containing iodine sublimated. Afterwards, (iii) substrates were washed with fresh EtOH 96% and dried. b) Reported values arise from averaging WCA measurements on three different spots of each sample. Blanks (pale pink) correspond to non-treated surfaces subjected to the same action of iodine as the treated ones (dark blue). The WCA values of surfaces@P9 via *ex situ* polymerisation in solution are represented in light blue.

4.4.1.2. Hydrophobic textiles

I. Coating and WCA

The next objective was to test the application of this methodology to coat pieces of textiles and conferring them hydrophobic features. As a general procedure, pieces of *ca.* 1.5 x 1.5 cm² of cotton, or, polyester cloths ($\sigma = 25 \text{ mg/cm}^2$), without previous treatment, were submerged into a $\sim 7 \text{ mM}$ solution of the corresponding C₁₈-functionalised material in HPLC grade CH₂Cl₂ and left overnight without stirring. Coated textiles were then washed with 3 x 2 mL of fresh CH₂Cl₂ and dried in a gentle flux of argon. The resulting coated textile pieces had the same

colour and appearance than the pristine ones, concluding that the coatings did not colour the fibres. They were characterised by SEM, and like hydrophobic flat surfaces, the hydrophobicity and wettability of the coated textiles were evaluated by measuring WCA of Milli-Q water droplets at rt by means of the sessile-drop technique.

Previous to measure WCAs, SEM images were taken from **P9**-coated fibres. In Figure 4.20a, it can be appreciated that the fibres of the material are mainly individually coated, along with occasional polymeric material within them. This aspect is relevant to ensure that the flexibility and breathability of the textiles are preserved upon deposition of the coating.

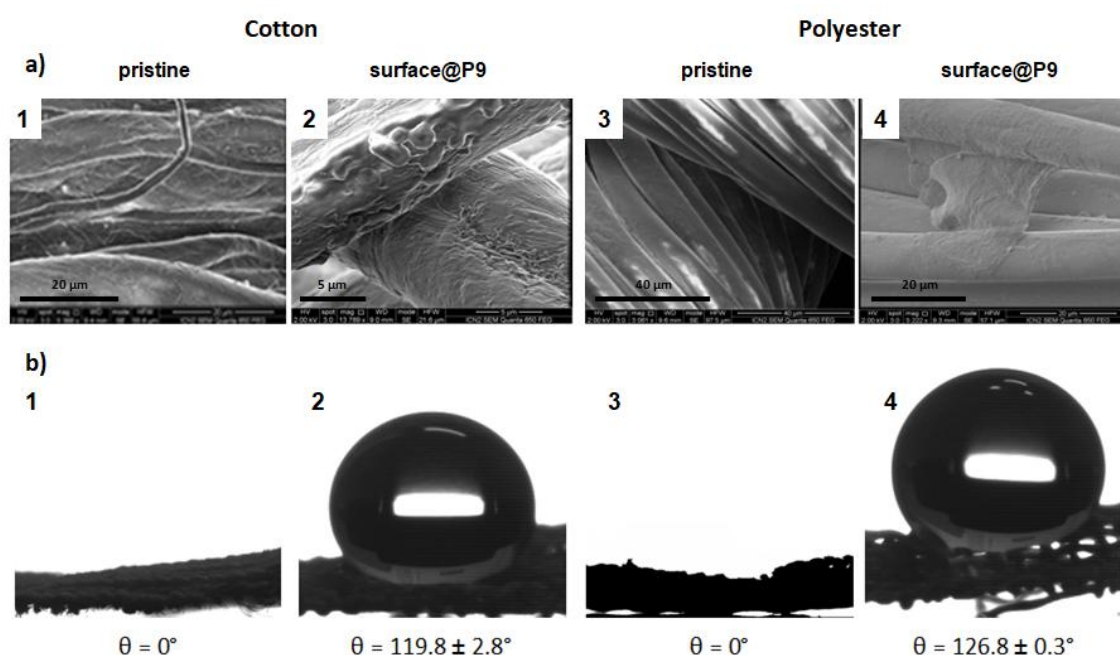


Figure 4.20. a) SEM images of pristine fibres (1 and 3), and **P9**-coated textiles (2 and 4). b) Images from water droplets onto pristine fibres (1 and 3) and **P9**-coated textiles (2 and 4).

For comparison reasons, cotton weaves were coated with both catecholic materials **9** and **P9** and the styrenic ones **46** and **P46**, whereas polyester fibres were only coated with **9** and **P9** (Table 4.5). Initially, both cotton and polyester, without any pre-treatment, showed hydrophilic surfaces (WCA of 0°) and after being submerged into all C_{18} -derivatives solutions they presented high hydrophobic surfaces (WCA $> 130^\circ$). However, after being rinsed, only textile fibres that had been coated with catechol-based oligomers **P9** still showed hydrophobic WCA values; 120° for cotton@**P9** and 127° for polyester@**P9**. In Figure 4.20b, visually it can be seen how the hydrophobicity of those coated textiles was kept after rinsing the substrates once they had been coated with **P9**, since water droplets stand onto the surfaces for a long period of time (< 10 min) with high WCA values. With regard coatings with monomer **9** and styrene derivatives **46** and **P46** onto cotton fibres, they were completely rid off with washes, showing final WCAs of 0° . Remarkably, onto polyester fibres, catechol-based monomer **9** was

able to produce a quite robust coating after washings, showing a significant value of WCA of 111°.

Table 4.5. WCA values onto pristine textiles, and coated fibres with both catecholic and styrenic derivatives, and both monomers and oligomers.

		WCA (°)				
		oligomers			monomers	
Substrate	pristine	no washes	P9	P46	9	46
Cotton	0°	136.7 ± 0.3°	119.8 ± 2.8°	0°	0°	0°
Polyester	0°	162.9 ± 1.0°	126.8 ± 0.3°	-	111.2 ± 0.3°	-

If not indicated, the WCA are measured after the rinse.

II. Oil absorption and phase separation tests

Because of its remarkable water-repellency performance, **P9** was used as the coating material for the assessment of oil-absorbance tests, as well as a simple oil/ water separation experiment simulating the removal of oily pollutants from aqueous phases.

Two oily phases, TDC and olive oil, were used as non-volatile model pollutants. They were coloured with Disperse red 13 and added into 15 mL of distilled water as shown in the Figure 4.21a-1. Afterwards, **P9**-coated cotton fibres of known dry weight were soaked in the oil phase for 15 seconds, taken out, allowed to drain for 3 h, and reweighted (Figure 4.21a-2-5). The same experiment was carried out with uncoated pieces of cotton as blanks. Some SEM images of cotton fibres were taken before and after absorbing the model pollutants (Figure 4.21b). It was seen that the fibres were individually coated with polymer **P9** (Figure 4.21b-2), and after absorbing TDC and olive oil they turned out more smeared.

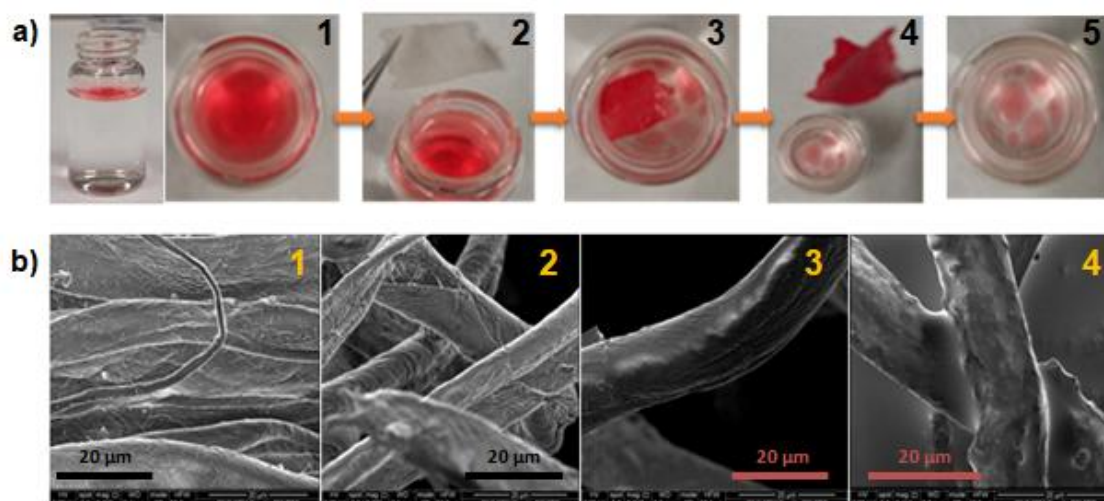


Figure 4.21. a) Selective oil removal: (1) olive oil/water separately phases; (2–5) soaking of a P9-coated cotton sample. b) From left to right, SEM images of pristine cotton weaves (1), cotton@P9 (2), and after absorption of TDC (3) and olive oil (4).

Coated fibres were able to absorb TDC around 127% of its initial weight, whereas uncoated cotton only 25%. When the test was performed within olive oil, treated samples absorbed around 172%, whereas blanks 94% (Table 4.6).

Table 4.6. Percentual weight absorption capacities (%) of cotton@P9, and uncoated cotton for liquid tests.

	Oil phase			
	TDC		Olive oil	
	Coated	Uncoated	Coated	Uncoated
Initial weight	21.6 mg	17.3 mg	16.4 mg	14.7 mg
Final weight	49.0 mg	21.6 mg	44.6 mg	28.6 mg
Absorption capacity*	127%	25%	172%	94%

* It is calculated in percentage (%) and it is the weight gain after absorption (final weight) vs. the initial one (before absorption).

It is well known that absorption capacities rely on porosity, surface area, and regularity of the microstructures of the absorbents,³⁰ as well as the viscosity/smearing ability of the oil test liquids. Cotton@P9 showed more affinity towards olive oil (172%) than TDC (127%). Interestingly, untreated cotton showed a superior olive oil absorbent capacity than the TDC one (94% vs. 25%). This was quite remarkable because TDC had a low viscosity (2-3 cP), comparable to that of water (1 cP), and did not appreciably smear treated substrates, in contrast to olive oil (viscosity *ca.* 80 cP).

Then, P9-coated cotton weaves were used for phase separation by filtration of a water/oil mixture as a water repellent system. A mixture of distilled water and coloured Miglyol® 840

with red Disperse 13 (1:1) was prepared by manual agitation and sonicating. A piece of treated cotton $1 \times 2 \text{ cm}^2$ was placed on top of a 20 mL vial, and with a syringe, the mixture of water and coloured oil was dropped onto the treated surface (Figure 4.22a). Because of the lipophilic and absorbent nature of treated surfaces, oil quickly soaked them and, after oil saturation, permeated though, while water was retained on the top (Figure 4.22b).

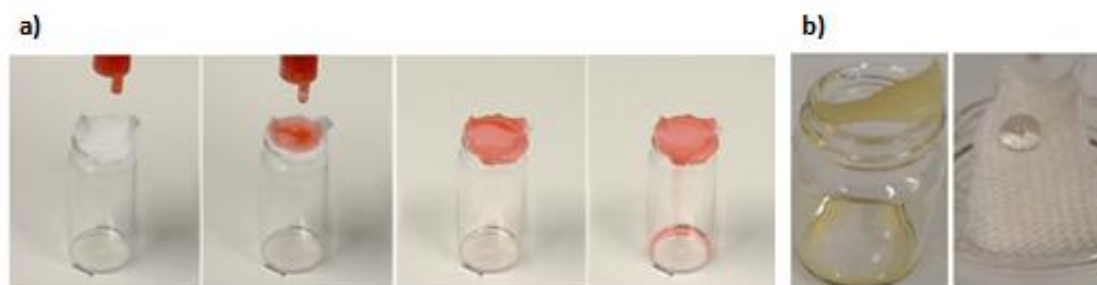


Figure 4.22. a) Sequence of an oil/water phase separation by filtration over a hydrophobic **P9**-coated piece of cotton. It is observed that water phase is retained on the top, whereas oil phase (in red) passes through our household filter into the vial. b) Oil phase saturation onto coated cotton weaves (left), and water repellence character (right).

Thanks to the success of previous experiments, it was decided to go a step further trying to break emulsions with **P9**-coated cotton weaves. Therefore, an emulsion with micro-size around $20 \mu\text{m}$ was prepared by mixing dodecyl sulphate (SDS) dissolved in distilled water with Miglyol® 840 coloured with Disperse red 13. Afterwards, a piece of $1 \times 1 \text{ cm}^2$ of cotton cloth ($\sigma = 25 \text{ mg/cm}^2$, either pristine or coated with aliphatic polymer **P9**) was submerged in a 10 x diluted aliquot of the stock emulsion and gently stirred by hand for 5 min, and subsequently taken out of the treated emulsion and left to dry in air (Figure 4.23, left). By this procedure, it was seen that coated cotton was able to absorb 97% of its own weight, whereas uncoated cotton only 8%. Visually, it was observed that the piece of cotton after being coated with **P9** was still white. However, after the absorption experiments, only **P9**-coated cotton turned red, meaning that it had absorbed the coloured oil. The untreated cotton did not absorb oil as it was seen in both its final weight (almost the same as the initial one) and its appearance (it remains almost white) (Figure 4.23, right).

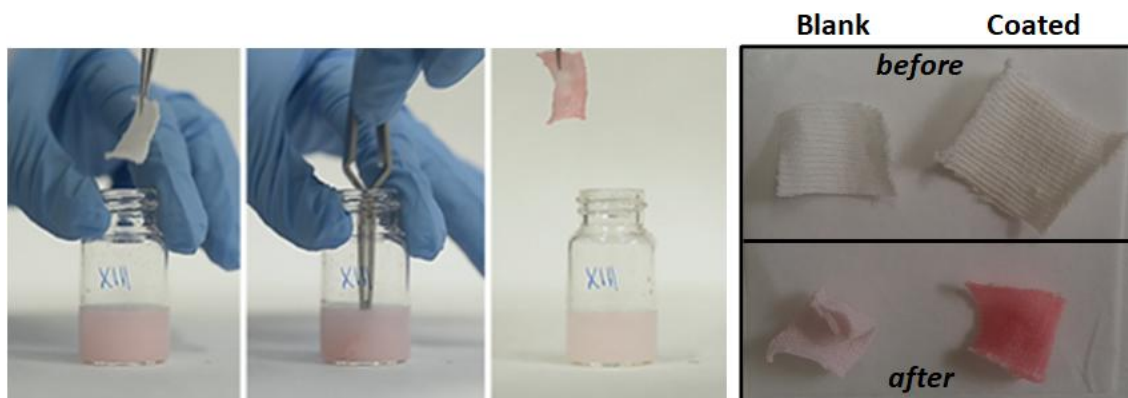


Figure 4.23. Sequence of the emulsion breaking test (left). Pieces of cotton at different points of the experiment (right).

To sum up, these coatings showed effectiveness in the transformation of water-absorbent polyester and cotton weaves, into water-repellent and oil-absorbent substrates capable of retaining roughly twice their weight of model hydrophobic compounds (TDC and olive oil), as well as of separating water/ oil mixtures from an emulsion, or, by simple filtration.

4.4.2. COATINGS WITH FLUORINE-FUNCTIONALISED BUILDING BLOCK 10 AND ITS CORRESPONDING PRODUCT P10 FROM THE POLYMERISATION

4.4.2.1. Oleo-/hydrophobic surfaces

Following the same coating methodology for aliphatic derivatives **9** and **P9**, glass slides were coated with **10** and **P10**. The hydrophobicity and oleophobicity of coated surfaces were evaluated by measuring WCA of Milli-Q water droplets and OCA of olive oil droplets, respectively, by means of the sessile-drop technique.

First results revealed that there were not significant differences between coat the surfaces with monomer **10** towards with oligomers **P10** since the WCA values obtained were very similar (74° for **5** vs. 70° for **10**). Even though the hydrophobicity of glass surfaces increased when they were coated with fluorine-functionalised materials, the WCAs obtained were far away from those expected,¹⁶ since having fluorinated chains, one would expect to have superhydrophobic surfaces ($\theta < 150^\circ$). As conclusion, working with these conditions, superhydrophobic coatings were not obtained, probably due to the low solubility of **10** and **P10** in CH_2Cl_2 ; 0.8 - 0.9 mg/mL for **10** and 0.6 - 0.7 mg/mL for **P10**. As already discussed in the synthesis of these fluorinated derivatives, the same solubility issues were present during the performance of the coatings. In order to solve this main challenge, the coatings were attempted in four more different HPLC grade solvents; DMF, THF, toluene and decafluoropentane (Figure 4.24). It was observed that coatings with **P10** performed with DMF,

THF and decafluoropentane were unsuccessful due to solubility issues, since WCAs only increased to 21.3°, 30.9° and 36.3°, respectively. Afterwards, using toluene the WCA obtained was more or less the same than using CH₂Cl₂ (WCA ~ 73°). Nevertheless, after rinsing a pristine glass slide with the solvent toluene, almost the same contact angle (WCA ~ 70°) was obtained. Therefore, it could not be ensured whether this 73° WCA value was due to the presence of a fluorinated coating, or, because the solvent used for this coating. It is worthy to mention that toluene has some stabilisers with organic nature, such as butylated hydroxytoluene (BHT), thus a surface treated with it could also show high values of WCA.

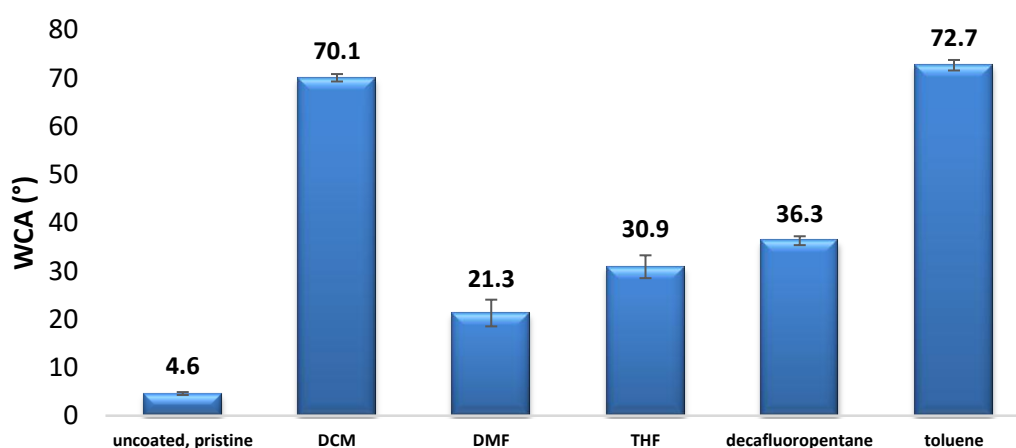


Figure 4.24. WCA values of coated surfaces with fluorine-functionalised oligomers **P10** carried out in five different solvents (CH₂Cl₂, DMF, THF, decafluoropentane and toluene).

As from these WCA values it could not be ensured that glass slides were coated successfully by the fluorinated derivatives, we also studied the morphology of such surfaces were also studied by SEM. It was observed that monomer **10** tended to form non-structured aggregates as seen in Figure 4.25a, whereas **P10** material was rearranged forming a kind of amorphous NPs ($\varnothing \sim 10$ nm) onto the glass surface (Figure 4.25b). Those irregularities and aggregates onto surfaces might be a cause of the no achievement of superhydrophobic WCA values. Hence, in order to avoid solubility issues and being aware of the existence of those aggregates onto the surfaces, both monomer **10** and its derivative **P10** in CH₂Cl₂ were sonicated for 10 min, centrifuged, filtered and the coatings with the soluble fractions were repeated. SEM images revealed that the glass surface **P10**-treated with the filtered solution presented much less aggregates (Figure 4.25c) than the one treated with the initial non-filtered solution (Figure 4.25d). However, no improvements were seen about the hydrophobicity since the WCAs obtained remained more or less the same after removing the insoluble part (WCA ~ 70°).

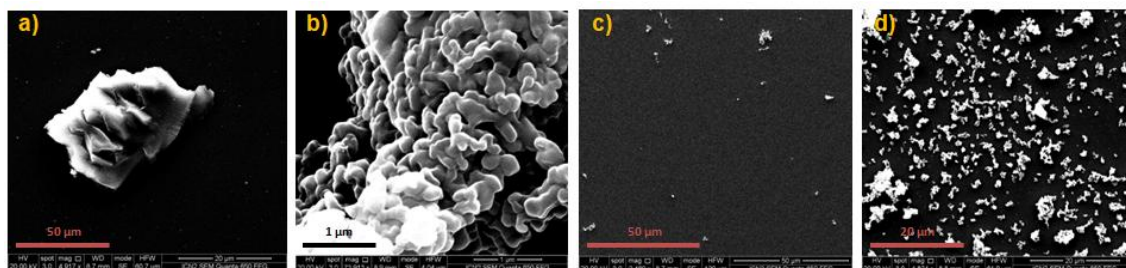


Figure 4.25. SEM images of a) glass@**10**, b) glass@**P10**, and c) **P10**-coated glass treated with the filtered solution and d) with the non-filtered one.

4.4.2.2. Oleo-/hydrophobic textiles

Following the same procedure, pieces of *ca.* 1.5 x 1.5 cm² of cotton and polyester cloths ($\sigma = 25 \text{ mg/cm}^2$) were coated with both fluorine-functionalised derivatives **10** and **P10**. The hydrophobicity and oleophobicity of coated textiles were evaluated by measuring WCA of Milli-Q water droplets and OCA of olive oil droplets, respectively, by means of the sessile-drop technique.

In the case of cotton, the same results for **9**-coated cotton were obtained. It was started from a hydrophilic surface, and when it was treated with a solution of fluorinated monomer **10** it was ended up with a hydrophobic surface that presented a WCA value of *ca.* 115°. However, unlike the C₁₈-functionalised derivative **P9**, working with the fluorinated **P10** one a hydrophobic surface was not obtained (WCA tended to 0°) (Figure 4.26). One possible cause could be the low solubility of this polymer in CH₂Cl₂ and consequently the lack of coating.

Regarding coatings onto polyester fibres, it was seen that working with monomer **10** it was obtained a superhydrophobic surface, since the WCA value recorded was higher than 150°, whereas the corresponding derivative **P10** only provided a high hydrophobic surface (WCA ~ 137°) (Figure 4.26).

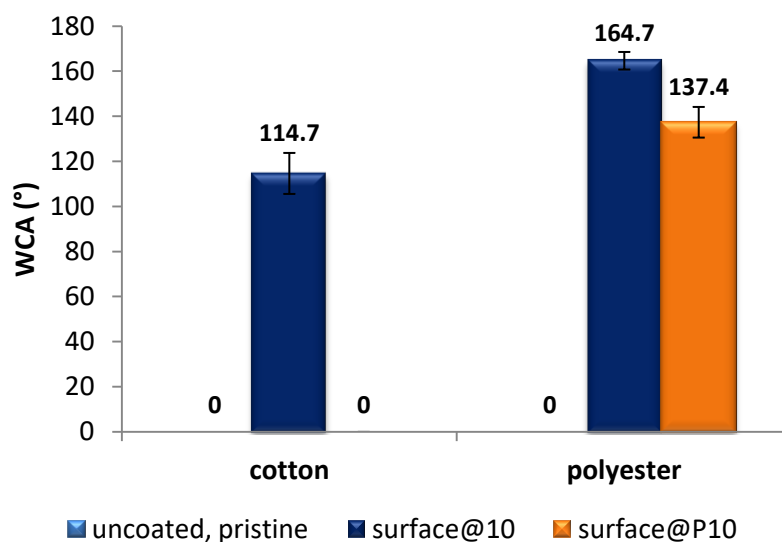


Figure 4.26. WCA of treated fibres with fluorine-based materials.

Moreover, some SEM images of cotton and polyester fibres were taken and it was observed that some material remained onto fibres after being treated with fluorinated derivatives (Figure 4.27). Nonetheless, there were not homogenous coatings.

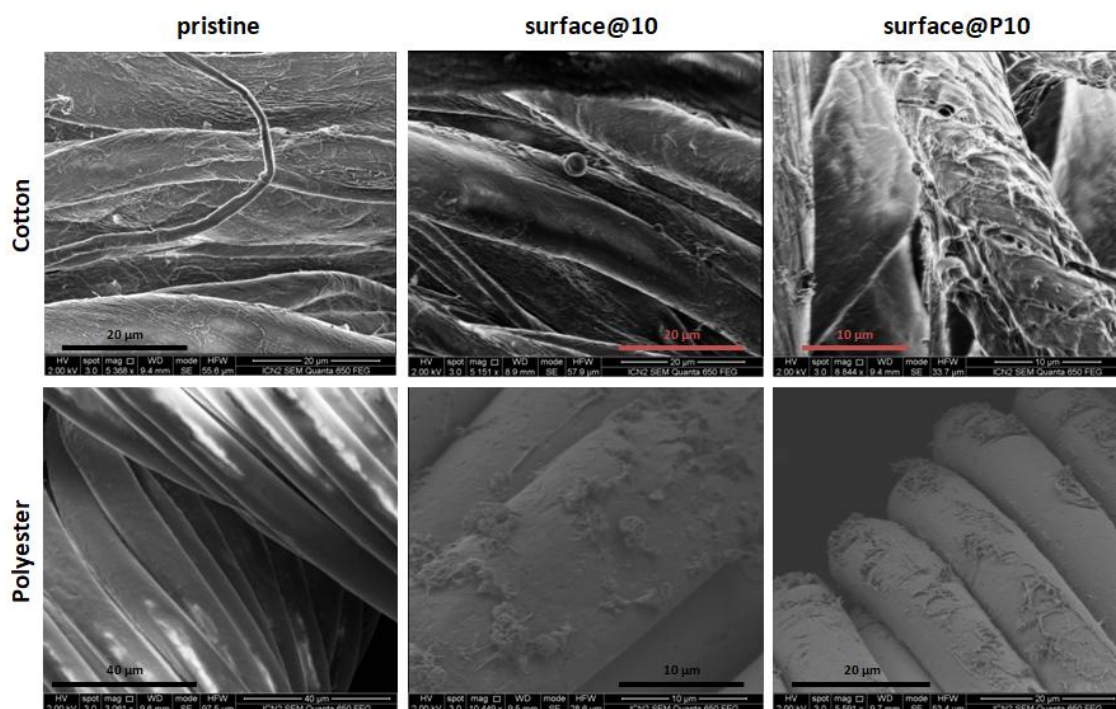


Figure 4.27. SEM images of cotton (top) and polyester (bottom) weaves coated with fluorine-based monomer **10** and its corresponding polymer **P10**.

Finally, beyond studying the hydrophobicity of the fluorinated coated surfaces, their oleophobicity was also evaluated. It was observed that glass surfaces coated with monomer **10** and its derivative **P10** did not present high oleophobicities; their OCA values (Figure 4.28) were lower than their WCA ones in most of the cases. It was also observed that there were not

significant differences with regard to oleophobicity between coatings made by monomer **10** and its derivative **P10**. Regarding the oleophobicity of cotton and polyester treated weaves, surprisingly it was seen that none of these treated surfaces were oleophobic at all, neither with monomer **10**, nor with the oligomers **P10**, although some of them were hydrophobic (Figure 4.28). What happened was that olive oil droplets spread out faster than water droplets.

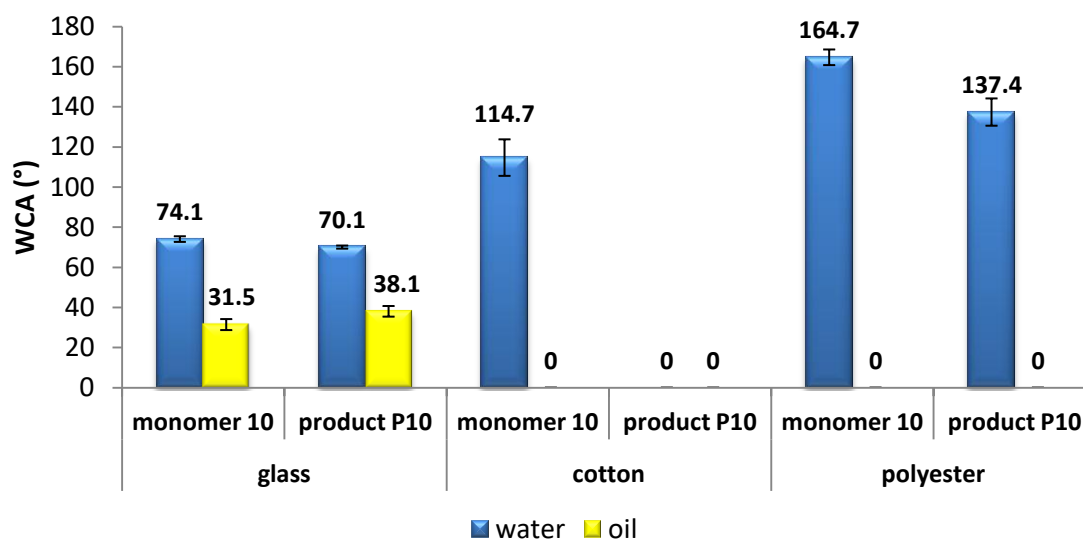


Figure 4.28. WCAs (in blue) and OCAs (in yellow) of coated glass surfaces, and cotton and polyester fibres with fluorinated materials **10** and **P10**.

4.4.3. COATINGS WITH mPEG-FUNCTIONALISED BUILDING BLOCK 6 AND ITS CORRESPONDING PRODUCT P6 FROM THE POLYMERISATION

With the mPEG-functionalised derivatives **6** and **P6** described in *Chapter 3*, beyond NPs, macroscopic surfaces (glass and metals) were also coated following both the *ex situ* polymerisation in solution and the *in situ* one strategies, as already seen for coatings with aliphatic derivatives **9** and **P9**.

I. From *ex situ* polymerised material

After coating glass, aluminium, copper and stainless steel surfaces with **6** and **P6**, the WCA values obtained (Figure 4.29) were comparable to the ones already reported in the literature (from 40° to 64°).^{31,32} In general, in the four cases, **6**-coated surfaces showed lower WCAs than the ones obtained from **P6**-coated ones. Except for the copper example, the values obtained for **6**-coated surfaces were near to the pristine ones, pointing out that the coatings with monomer **6** were not as robust as with oligomers **P6** against washes. Furthermore, in the cases of glass, aluminium and stainless steel, the hydrophobicity character of the surface increased

when the substrates were coated with **P6** as the pristine ones could be considered more hydrophilic. In contrast, since copper was the most hydrophobic pristine surface, in this example it was clearly seen that its hydrophilic character was increased by coating it with mPEGylated derivatives.

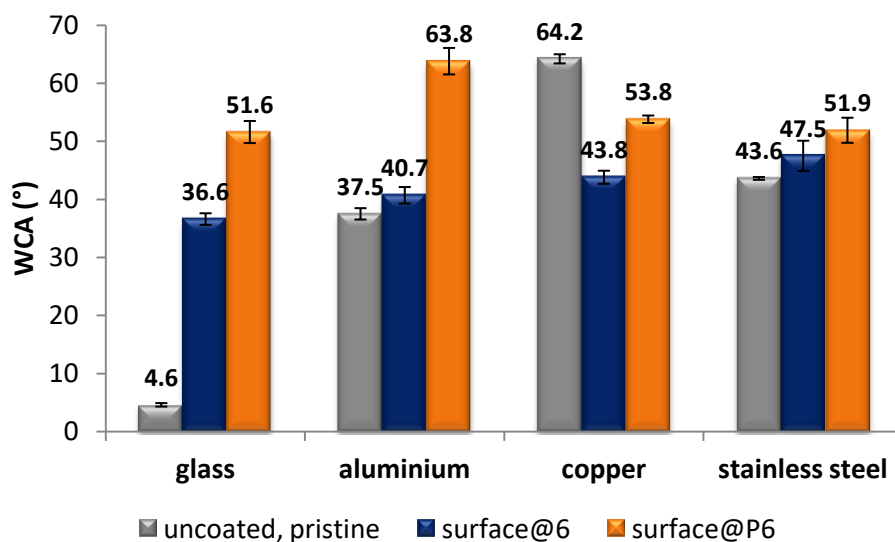


Figure 4.29. b) WCA values of mPEGylated coated surfaces after being rinsed.

II. From in situ polymerisation

From the WCAs (Figure 4.30), it was seen that in all four substrates there was an increasing of the hydrophobicity when they were treated with mPEGylated derivative **6** (Figure 4.30, dark blue) due to the high hydrophilic character of these pristine surfaces after being subjected to the same action of iodine. Comparing the results obtained from both coating strategies (*ex situ* polymerisation in solution (Figure 4.29) and the *in situ* one), it was observed that surfaces coated with derivative **P6** *via in situ* polymerisation presented lower WCA (between 10° and 20° below) than the ones obtained *via ex situ* polymerisation in solution (Figure 4.30, orange), except for copper one which presented an opposite trend. As already discussed, this decrease on WCAs could be attributed to the presence of embedded iodine crystals on the coating, making the final surfaces more hydrophilic.

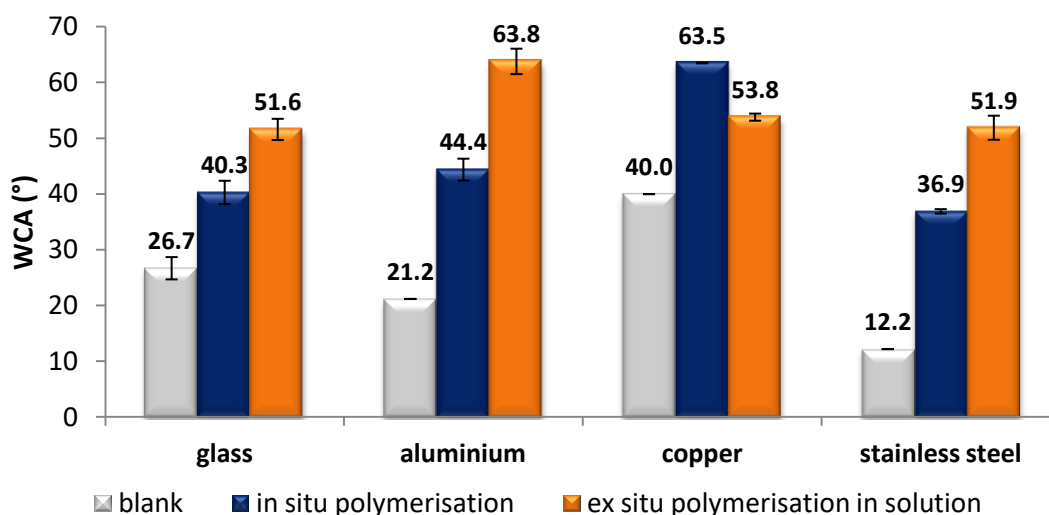


Figure 4.30. Reported values arise from averaging WCA measurements on three different spots of each sample. Blanks (pale pink) correspond to non-treated surfaces subjected to the same action of iodine as the treated ones (dark blue). The WCA values of surfaces@P6 via *ex situ* polymerisation in solution are represented in light blue.

Furthermore, EDX analyses were also performed onto the metal substrates coated with P6 via both *ex situ* polymerisation in solution and *in situ* methodology (see Annexes A3.3 and A3.4 for EDX spectra). In all the cases, the presence of sulphur, carbon and oxygen was checked, and in the case of coating via *in situ* methodology, some remaining iodine was also seen.

4.4.4. MULTIFUNCTIONAL COATINGS

So far, it has been demonstrated that this strategy turns out very efficient to coat different types of substrates, from glass to metals or textiles, while conferring hydrophobicity. It has also been confirmed another of the expected advantages such is the colour inertness of our coatings, *i.e.* do not modify the initial colour of the pristine substrate. Finally, herein it is aimed to demonstrate that on top of all the previous advantages, and thanks to the modular chemistry of our approach, it can systematically be modified the wettability of a given surface by simple reacting different ratios of **8** and **9**. So the first step will be to test the coating capabilities of **P8** (synthesised as described in Chapter 3) with macroscopic substrates, hopefully yielding WCA much lower than those found with **P9** thanks to its higher hydrophobic character. Afterwards, several different polymers with different **8/9** ratios will be synthesised to finally use them to coat glass slides and cotton fibres. This will allow fine-tuning the WCA.

As just already explained, glass slides were coated with fluorescein derivatives **8**, **P8**, **36** and **P36** following the same experimental procedure described for coating glass slides. (*Note:* in this case the solvent used was acetone instead of CH_2Cl_2). Using an inverted optical/fluorescence microscope in fluorescence mode with an Alexa Fluor 488 filter, it was

observed that after rinsing the treated slides, only the **P8**-coated glass showed continuous intense fluorescence in the whole surface (Figure 4.31a). The **8**-coated glass slide showed low fluorescent intensity concentrated in some aggregates (Figure 4.31b), and when styrenic derivatives were used, the coatings were completely rid off with acetone washes, since the final treated surfaces did not show fluorescence (Figure 4.31c).

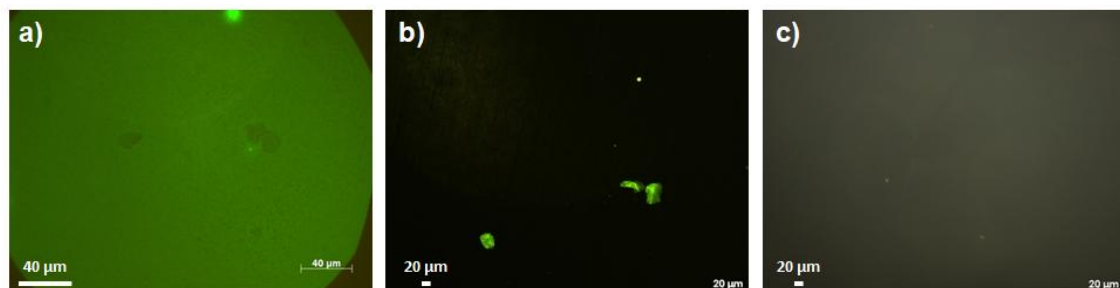


Figure 4.31. Image taken from optical/fluorescence microscope in fluorescence mode of glass slides coated with a) catecholic derivative **P8**, b) catecholic monomer **8**, and c) styrenic derivative **P36**.

As already demonstrated, catechol moieties are very important to make efficient and robust coatings, and the product **P8** from the polymerisation reaction had a larger tendency to attach to surfaces than the monomer **8** thanks to the synergism of the different catechol units.

Once it was checked that fluorescein derivatives could coat glass slides, it was proceeded to fabricate different polymers with different **8/9** ratios (Table 4.7).

Table 4.7. Different copolymers made of fluorescent and hydrophobic building blocks **8** and **9**, respectively.

Copolymer	Aliphatic monomer, X%	Fluorescein monomer, Y%	Yield (%)
C8-9a	80%	20%	64%
C8-9b	60%	40%	64%
C8-9c	40%	60%	64%
C8-9d	30%	70%	65%

Yields were calculated based on the final amount obtained of the resulting copolymer vs. the initial ones used from both starting monomers.

Both monomers were dissolved in EtOH 96%, and a 35 mM solution of iodine (1 equiv.) in EtOH 96% was added dropwise. After 1 h of stirring at rt, the precipitated derivatives were isolated, washed several times with fresh EtOH 96% and dried with a gentle flux of nitrogen (Figure 4.32).

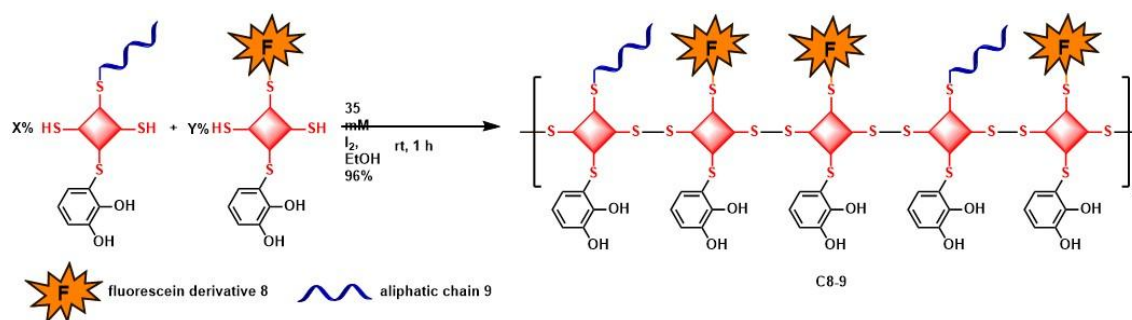


Figure 4.32. Polymerisation with the synthesised monomers **8** and **9** to obtain final copolymers **C8-9** having two main properties; fluorescence and hydrophobicity.

From the ^1H NMR spectra of these polymers it was checked the presence of both functionalities: between 8 ppm and 6.5 ppm the aromatic peaks of the fluorescein moiety, and at ~ 1.3 ppm and ~ 0.9 ppm the characteristic signals of the C_{18} chain.

CC3_51/1 — ^1H NMR 360 MHz

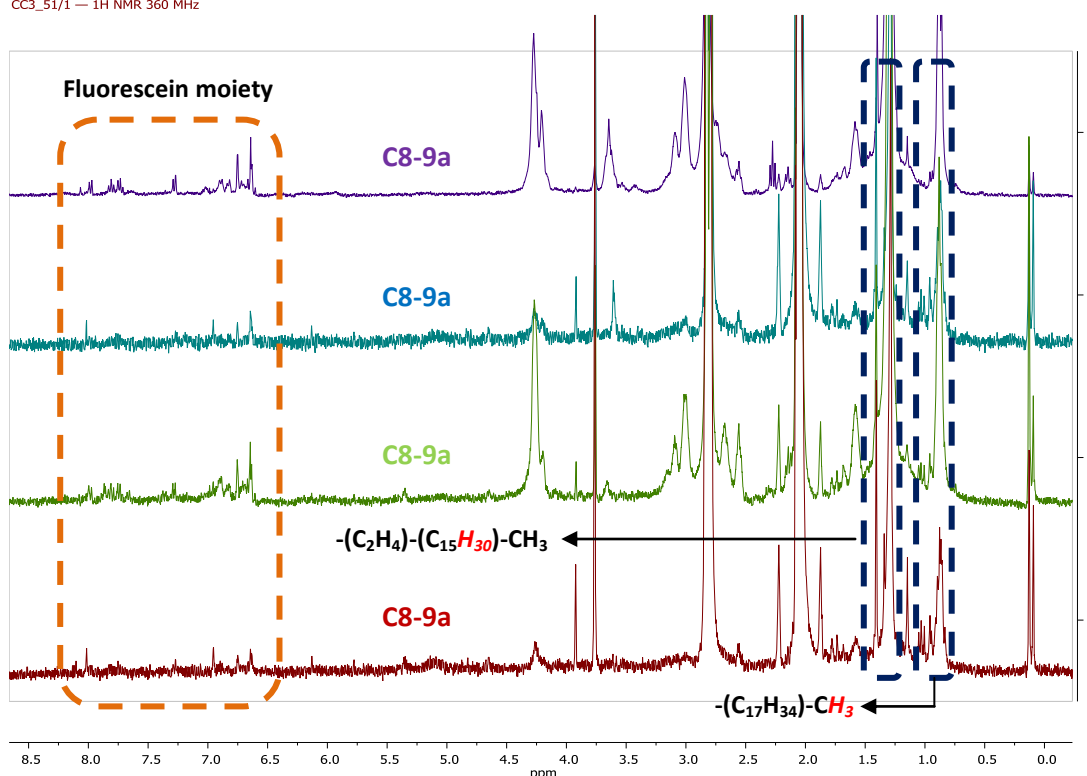


Figure 4.33. ^1H NMR spectra of copolymers **C8-9a-d** where aromatic peaks of fluorescein (framed in orange) and characteristic peaks of C_{18} chain in the aliphatic region (framed in blue) are seen.

Afterwards, it was proceed to perform coatings onto glass slides and cotton fibres with these products **C8-9** following the same described procedures to coat both surfaces. In this case, both substrates were submerged into ~ 7 mM solutions of different copolymers **C8-9** in HPLC grade CH_2Cl_2 for 4 h. Finally, they were washed three times with fresh CH_2Cl_2 and dried in a gentle flux of argon.

The wettability of such surfaces were evaluated from measurements of WCA of Milli-Q water droplets (*ca.* 5 μL) by means of the sessile-drop technique, and fluorescence was checked in an optical/fluorescence microscope.

First results revealed that by changing the initial amount of both starting building blocks **8** and **9**, the final properties present in the resulting copolymers **C8-9** could be tuned, thus the coatings performed with them could modulate the wettability of the treated surfaces, making them more hydrophobic and less fluorescent or *vice versa* (Figure 4.34). As expected, by increasing the amount of aliphatic derivative **9**, the hydrophobicity of both coated glass slides and cotton weaves increased, whereas by increasing the amount of fluorescent monomer **8**, such hydrophobicity proportionally decreased (Figure 4.34a and c). With regard to the fluorescence, it was seen that substrates coated with copolymers with higher amount of fluorescent monomer **8**, or, directly coated with 100% fluorescent **P8** showed high fluorescent intensities (Figure 4.34b and d, right), whereas those coated with **C8-9** with low ratios of monomers **8:9** showed little or none fluorescence (Figure 4.34b and d, left).

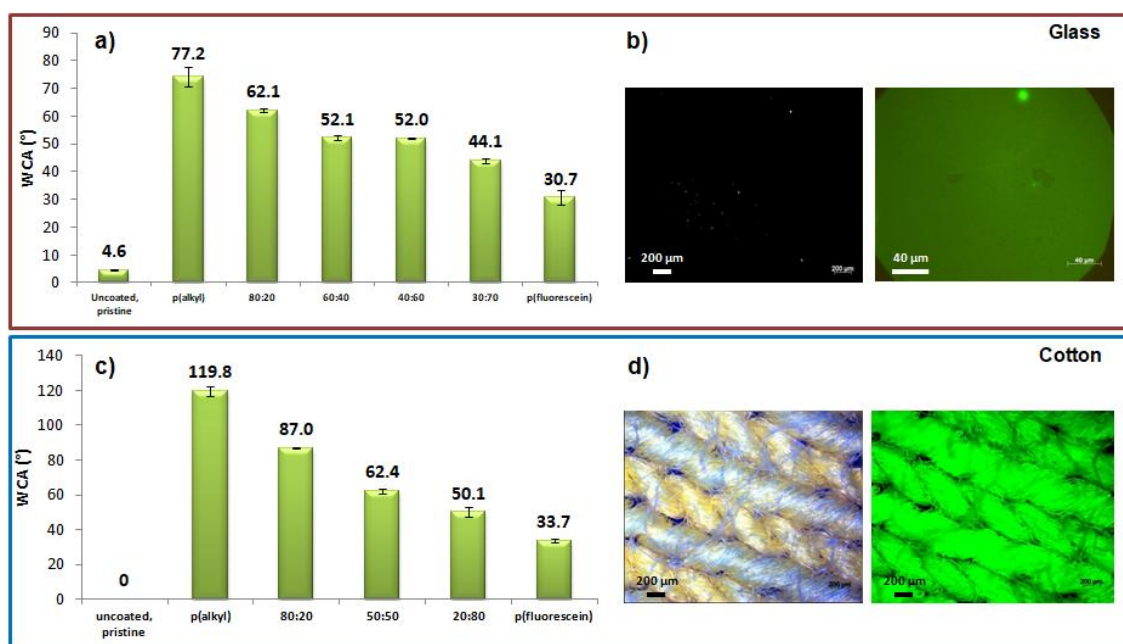


Figure 4.34. In red, coatings onto glass slides. In blue, coatings onto cotton fibres. a) WCA values onto treated glass surfaces with several copolymers **C8-9**. b) Images from an optical/fluorescence microscope of glass slide coated with copolymer 80:20 (monomer **9**: monomer **8**) (left), and homopolymer **P8** (right). c) WCA values onto coated cotton weaves with some copolymers **C8-9**. d) Images from an optical/fluorescence microscope of cotton fibres coated with copolymer 80:20 (monomer **9**: monomer **8**) (left), and homopolymer **P8** (right).

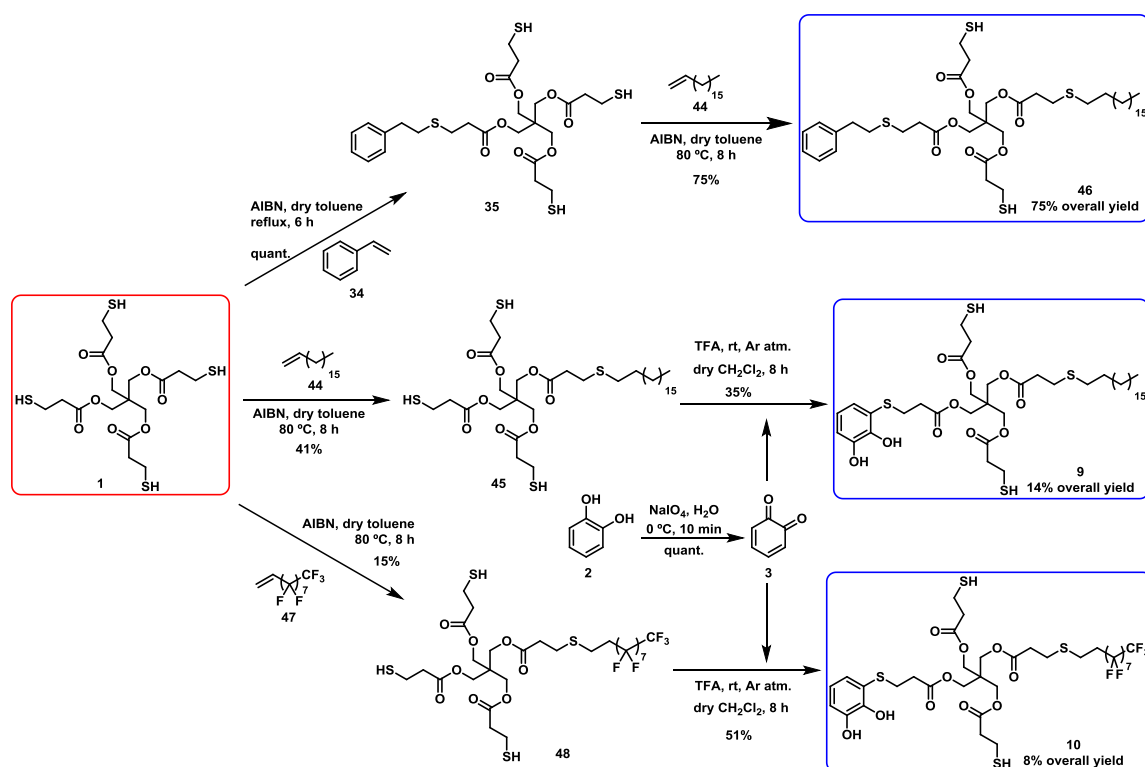
Therefore, herein it has been shown that this designed strategy allows combining building blocks with different functionalities in order to obtain new derivatives bearing at least two properties. In this case, fluorescent and hydrophobic copolymers **C8-9** have been used to coat macroscopic surfaces and it has been proven that these coatings can control the wettability of

the treated surfaces, thus modulating their hydrophobicity and fluorescence by tuning the initial proportions of both fluorescent and aliphatic molecules **8** and **9**, respectively.

4.5. SUMMARY

Below, the most relevant results are exposed.

All three building blocks **9**, **10** and **46** were synthesised in 14%, 8%, and 75% overall yields, respectively, through linear syntheses of two steps that included a radical-catalysed thiol-ene reaction and a 1,6-conjugated Michael reaction for molecules **9** and **10**, and two tandem radical-catalysed thiol-ene reactions for molecule **46** (Scheme 4.8). The low yields for both aliphatic-/fluorinated-functionalised building blocks **9** and **10** could be attributed to the difficulty of its manipulation, the formation of several by-products when the functionalities were introduced to the core **1** and, particularly, in the case of the fluorinated compound due to its low solubility in common organic solvents.



Scheme 4.8. All synthetic pathways followed to obtain target building blocks **9**, **10** and **46** from the same 4-branched symmetrical molecule **1** framed in red.

C₁₈-functionalised building blocks **9** and **46** were polymerised using a solution of iodine in EtOH in 39% and 60% yield, respectively, and fluorinated compound **10** was polymerised using CH₂Cl₂ as solvent in 48% yield. From ¹H NMR, DOSY NMR experiments and GPC analyses it was checked that products **P9** and **P46** corresponded to mixtures of short oligomers between 2-7

units, and 2-10 units, respectively. As far as product **P10** is concerned, since it was even more insoluble than the starting monomer **10** in common organic solvents, such as THF or CHCl_3 , it was impossible to characterise it by GPC or other techniques.

Table 4.8. Summary table with yields of polymerisation reaction and polymerisation degrees values of **P9**, **P10** and **P46**.

35 mM solution of iodine			
Solvent's reaction	EtOH		CH_2Cl_2
Product from the polymerisation reaction	P9	P46	P10
Yield (%)	39%	60%	48%
Polymerisation degree	2-7 units	2-10 units	-

With C_{18} -functionalised materials, coatings onto glass, aluminium, copper, and stainless steel surfaces were performed *via* (i) *ex situ* polymerisation in solution and (ii) *in situ* polymerisation. All these coatings made the treated surfaces hydrophobic, observing a notable increasing of their WCAs ($\text{WCA} > 70^\circ$ in all the cases). Furthermore, this kind of materials was also used to coat textiles, such as cotton and polyester, turned them very hydrophobic surfaces with WCA of 119.8° and 126.8° , respectively. In particular, **P9**-coated cotton weaves, with absorption capacities of 127% for TDC and 172% for olive oil, were used as a household filter for separating water/oil mixtures.

Regarding the coatings performed with the fluorinated materials **P10**, the same solubility issues were suffered as in their syntheses, thus their coatings were not reproducible; by SEM it was observed that the fluorinate derivatives tended to form a kind of non-structured aggregates, or, NPs onto glass surfaces. Although these treated surfaces showed $\text{WCA} > 70^\circ$, those values were far away from the superhydrophobic ones expected. Nonetheless, textiles treated with compound **10** showed WCA values of 114.7° and 164.7° for **10**-coated cotton and polyester, respectively. Finally, it was observed that none of treated substrates showed an oleophobic character (OCAs were between 0° and 40°).

In addition, coatings onto glass, aluminium, copper, and stainless steel surfaces were also performed with mPEG-functionalised **P6**, in that case to provide hydrophilia. In all the cases, the treated surfaces showed WCAs in a range of 40 - 65° , which matched with already reported data.^{31,32}

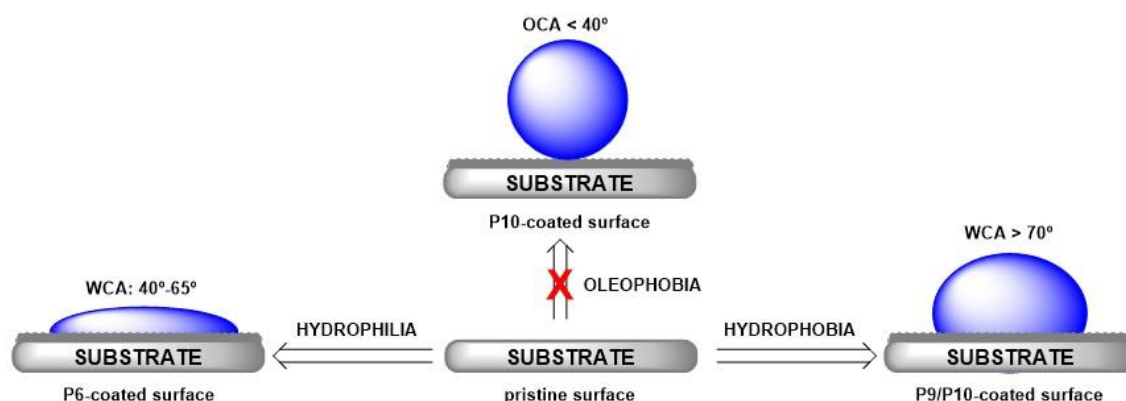


Figure 4.35. Representation of coating a pristine surface with colourless materials that provide hydrophilicity (mPEG-**P6**) and hydrophobicity (C_{18} -**P9** and fluorinated-**P10**). Oleophobic surfaces could not be obtained from **P10** materials.

To finish with, highlight that with the designed polymerisation strategy, the wettability of glass slides and cotton fibres could systematically be modified in over a wide range of WCA by simple reacting different ratios of **8** and **9** in a controlled way (Figure 4.36).

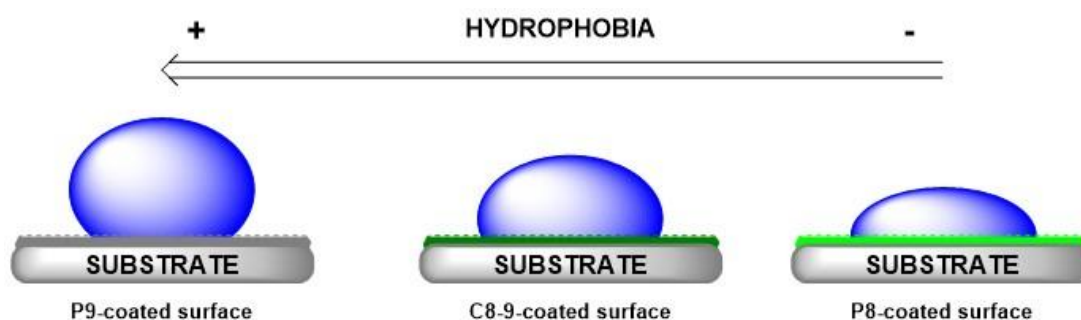


Figure 4.36. Representation of controlling the wettability of treated surface.

4.6. REFERENCES

- ¹ Archer, R. J.; Becher-Nienhaus, B.; Dunderdale, G. L.; Hozumi, A. *Adv. Funct. Mater.* **2020**, *30*, 1907772-1907801.
- ² Nakajima, A. *J. Ceram. Soc. JPN.* **2004**, *112*, 533-540.
- ³ Ma, W.; Xu, H.; Takahara, A. *Adv. Mater. Inter.* **2014**, *1*, 1300092-1300096.
- ⁴ Wei, Q.; Achazi, K.; Liebe, H.; Schulz, A.; Noeske, P.-L. M.; Grunwald, I.; Haag, R. *Angew. Chem. Int. Ed.* **2014**, *53*, 11650-11655.
- ⁵ Wang, Z.; Xu, Y.; Liu, Y.; Shao, L. *J. Mater. Chem. A* **2015**, *3*, 12171-12178.
- ⁶ Yu, X.; Zhong, Q.-Z.; Yang, H.-C.; Wan, L.-S.; Xu, Z.-K. *J. Phys. Chem. C* **2015**, *119*, 3667-3673.
- ⁷ Feng, J.; Fan, H.; Zha, D.; Wang, L.; Jin, Z. *Langmuir* **2016**, *32*, 10377-10386.
- ⁸ Kim, S.; Nam, J. A.; Lee, S.; In, I.; Park, S. Y. *J. Appl. Polym. Sci.* **2014**, 40708-40714.
- ⁹ Kim, S. H.; Lee, S.; Ina, I.; Park, S. Y. *Surf. Interface Anal.* **2016**, *48*, 995-1001.

-
- ¹⁰ Cao, Y.; Zhang, X.; Tao, L.; Li, K.; Xue, Z.; Feng, L.; Wei, Y. *ACS Appl. Mater. Inter.* **2013**, *5*, 4438-4442.
- ¹¹ Li, B.; Li, L.; Wu, L.; Zhang, J.; Wang, A. *Chem. Plus. Chem.* **2014**, *79* (6), 850-856.
- ¹² Wang, J.; Chen, Y. *J. Appl. Polym. Sci.* **2015**, *132*, 42614-42619.
- ¹³ Shang, B.; Wang, Y.; Peng, B.; Deng, Z. *J. Colloid Interfac. Sci.* **2016**, *482*, 240-251.
- ¹⁴ Wu, J.; Cai, C.; Zhou, Z.; Qian, H.; Zha, F.; Guo, J.; Feng, B.; He, T.; Zhao, N.; Xu, J. *J. Colloid Interfac. Sci.* **2016**, *463*, 214-221.
- ¹⁵ Saiz-Poseu, J.; Sedó, J.; García, B.; Benaiges, C.; Parella, T.; Alibés, R.; Hernando, J.; Busqué, F.; Ruiz-Molina, D. *Adv. Mater.* **2013**, *25*, 2066-2070.
- ¹⁶ García, B.; Saiz-Poseu, J.; Gras-Charles, R.; Hernando, J.; Alibés, R.; Novio, F.; Sedó, J.; Busqué, F.; Ruiz-Molina, D. *ACS Appl. Mater. Inter.* **2014**, *6*, 17616-17625.
- ¹⁷ Watanabe, H.; Fujimoto, A.; Nishida, J.; Ohishi, T.; Takahara, A. *Langmuir* **2016**, *32*, 4619-4623.
- ¹⁸ Neto, A. I.; Cibrão, A. C.; Correia, C. R.; Carvalho, R. R.; Luz, G. M.; Ferrer, G. G.; Botelho, G.; Picart, C.; Alves, N. M.; Mano, J. F. *Small* **2014**, *10*, 2459-2469.
- ¹⁹ Han, H.; Wu, J.; Avery, C. W.; Mizutani, M.; Jiang, X.; Kamigaito, M.; Chen, Z.; Xi, C.; Kuroda, K. *Langmuir* **2011**, *27*, 4010-4019.
- ²⁰ Payra, D.; Naito, M.; Fujii, Y.; Yamada, N. L.; Hiromotoe, S.; Singh, A. *RSC Adv.* **2015**, *5* (21), 15977-15984.
- ²¹ Rodrigues, J. R. Alves, N. M.; Mano, J. F. *Rsc Adv.* **2016**, *6*, 75988-75999.
- ²² Tsai, W.-B.; Chen, W.-T.; Chien, H.-W.; Kuo, W.-H.; Wang, M.-J. *J. Biomater. Appl.* **2014**, *28*, 837-848.
- ²³ Park, M.; Shin, M.; Kim, E.; Lee, S.; Park, K. I.; Lee, H.; Jang, J. H. *J. Nanomater.* **2014**, *2014*, 1-10.
- ²⁴ Chen, J.; Liang, R.-P.; Wu, L.-L.; Qiu, J.-D. *Electrophoresis* **2016**, *37*, 1676-1684.
- ²⁵ Liu, X.; Deng, J.; Ma, L.; Cheng, C.; Nie, C.; He, C.; Zhao, C. *Langmuir* **2014**, *30*, 14905-14915.
- ²⁶ Wang, L.; Li, G.; Lin, Y.; Zhang, Z.; Chen, Z.; Wu, S. *Polym. Chem.* **2016**, *7*, 4964-4974.
- ²⁷ Laibinis, P. E.; Whitesides, G. M.; Allara, D. L.; Tao, Y. T.; Parikh, At. N.; Nuzzo, R. G. *J. Am. Chem. Soc.* **1991**, *113*, 7152-7167.
- ²⁸ Laibinis, P. E.; Whitesides, G. M. *J. Am. Chem. Soc.* **1992**, *114*, 9022-9028.
- ²⁹ Microsoft PowerPoint - Periodic_EN_RC4.ppt (unamur.be) (acceded, 11/01/2021).
- ³⁰ Buchholz, F. L.; Peppas, N. A. *Superabsorbent Polymers; ACS Symposium Series 573; American Chemical Society: Washington, DC, 1994.*

³¹ Buxadera-Palomero, J.; Calvo, C.; Torrent-Camarero, S.; Gil, F. J.; Mas-Moruno, C.; Canal, C.; Rodríguez, D. *Colloid. Surface. B.* **2017**, *152*, 367-375.

³² Wei, Q.; Becherer, T.; Noeske, P.-L. M.; Grunwald, I.; Haag, R. *Adv. Mater.* **2014**, *26*, 2688-2693.

CHAPTER 5

SUMMARY AND CONCLUSIONS

After all this work done, it has been validate with a remarkable degree of satisfaction the designed strategy for polymerising catechol derivatives based on approach III through building blocks. Below, a summary of the main results and conclusions are exposed.

I. Synthesis of the functionalised building blocks

The synthesis of eight different building blocks from the same core pentaerythritol tetrakis(3-mercaptopropionate) **1** have been achieved (Figure 5.1) from two-steps syntheses that included two main thiol-ene reactions: (i) a radical one and (ii) a thia-Michael reaction. Hence, a new family of catechol-based molecules diversely functionalised has been obtained through a straightforward unified cheap methodology.

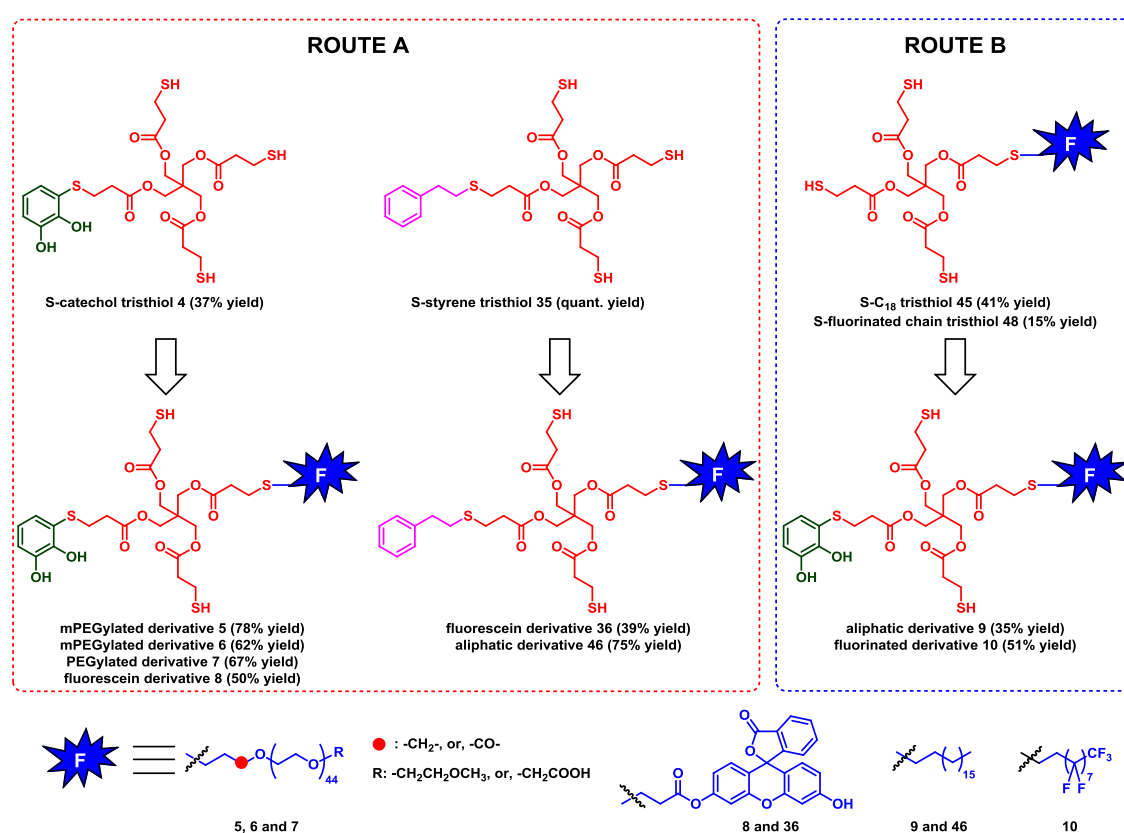


Figure 5.1. The final eight molecules (bottom) synthesised from the corresponding intermediates (top) through thia-Michael reactions and radical thiol-ene reactions following routes A or B.

II. Polymerisation of the building blocks

Their polymerisations have been carried out under mild oxidative conditions using a solution of iodine in EtOH in most of the cases. These reactions take place through the two remaining thiols of the polymerisation unit keeping the catechol moiety unaltered and without the need to be protected. The characterisation of the resultant colourless products (from **P5** to **P10** including styrenic derivatives **P36** and **P46**) has not been easy due to their poor solubility in

THF in most of the cases. Nonetheless, it can be concluded that by using this new strategy, mixtures of short oligomers between 2 and 10 units can be obtained, and these results have been corroborated by three different techniques: ^1H NMR, DOSY NMR experiments and GPC analyses. The small degree of polymerisation, specifically in the case of PEGylated derivatives, could be due to the presence of large functionalities that wrap the polymerisation unit and because of high steric hindrances the linear polymerisation does not seem to prevail. Furthermore, it has also been determined that the presence of a small percentage (3-5%) of a S-catechol derivative favours the formation of polymers and avoids the intramolecular S-S bond formation, fact observed and studied in PEGylated derivative **P7**.

Table 5.1. Summary table with polymerisation conditions for the different building blocks with the corresponding yields and polymerisation degrees.

35 mM solution of iodine	EtOH						CH ₂ Cl ₂	
Product from the polymerisation reaction	P5	P6	P7	P8	P36	P9	P46	P10
Yield (%)	45%	28%	41%	34%	29%	39%	60%	48%
Polymerisation degree (units)	2-3	2-5	-	-	-	2-7	2-10	-

The polymerisation degree of **P7**, **P8**, **P36** and **P10**, could not be determined by none of the three techniques aforementioned.

III. Coatings

With all these oligomeric materials several (multi)functional coatings have been performed onto different substrates ranging from nanostructures (*Chapter 3*), such as MSNPs or MNPs, to macroscopic surfaces (*Chapter 4*), such as glass, metals and fabrics. The resulting treated surfaces have been characterised by different techniques depending on the properties shown. DLS and electron microscopy has been used to characterise the coatings performed onto NPs with PEGylated and fluorescein-functionalised derivatives (**P5**, **P6**, **P7** and **P8**) (Figure 5.2a). Optical microscopy has been used to check the fluorescence of substrate treated with fluorescein-functionalised derivatives **P8** (Figure 5.2b), and WCA measurements have been suitable to determine the wettability of surface treated with aliphatic **P9**, fluorinated **P10** and PEGylated **P6** derivatives onto flat substrates (Figure 5.2c).

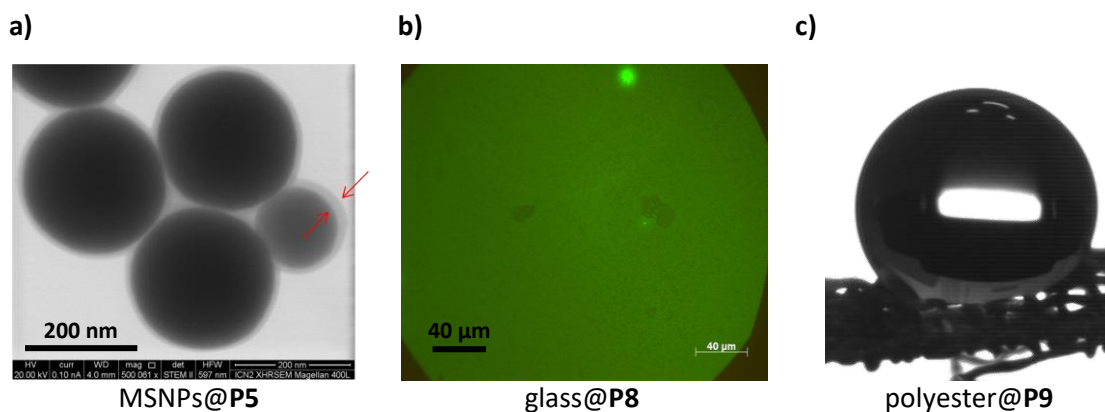


Figure 5.2. Different coatings made by different derivatives. a) STEM image of MSNPs@P5 in which it is identified the coating surrounding the surface of the NPs. b) Glass slide coated with fluorescein-functionalised product **P8** observed within an optical microscope. c) Image of a water droplet onto **P9**-coated polyester fibres with WCA > 125°.

After performing many coatings onto different substrates with different derivatives the most common outstanding conclusions that have been drawn are:

- ❖ All the coatings performed were colourless, thus the appearance of the treated substrates were unaltered.
- ❖ In general, the mixtures of oligomers provide more efficient and more robust coatings against washing than the corresponding monomers. That is due to the synergism of the catechol units when the material is polymerised.
- ❖ Catechol moieties are essential to perform good coatings, since they are the anchors that favour the absorption onto the surfaces by forming different kind of interactions (*e.g.* hydrogen-bonding, coordination and covalent bonds, among others). When coatings were performed with some styrenic analogues, they were rid off easily with washes.
- ❖ All the coatings performed with the different derivatives showed the desired properties; stability in aqueous media when NPs were coated with PEGylated derivatives (**P5**, **P6** and **P7**), fluorescence for substrates treated with fluorescein derivative **P8**, and hydrophobicity for materials coated with C₁₈-functionalised derivatives **P9**. However, coatings made with fluorinated derivatives **P10** were not reproducible due to the lack of solubility of the products in most of the solvents, so neither superhydrophobic, nor oleophobic surfaces were able to be obtained, except for **10-/P10**-coated polyester weaves, which did show very high WCA values (> 110°).

More in detail, regarding the use of the catechol-based toolkit for NP coating, the most highlighted results are exposed below:

1. The synthetic feasibility of our approach has allowed obtaining PEG-based coatings over different families of NPs, *i.e.* MSNPs and MNPs.
2. These PEG-based coatings have shown to be effective to stabilise in aqueous environments both types of NPs making them biocompatible.
3. Particularly, MNPs have been successfully coated with the cat-PEG derivative **P7** and post-functionalised with the amino-glucopyranose derivative **43** as a model targeting molecule (Figure 5.3). It has been checked that these NPs in a simulated physiological medium (PBS + 10% BSA) form aggregates of *ca.* 100 nm.

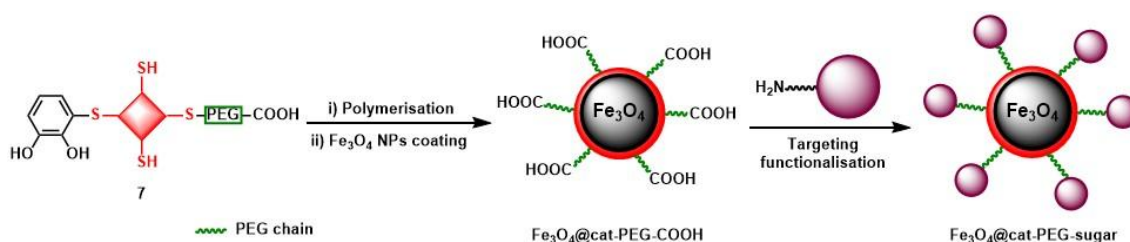


Figure 5.3. Sequence of the construction of a model nanocarrier. Firstly, the polymerisation of building block **7** takes place using the designed disulphide bond formation-based strategy. Afterwards, model MNPs are coated with the resulting **P7** by a ligand exchange procedure. Finally, this coating is functionalised with a targeting molecule through residual carboxylic acids exposed onto the surface *via* amide bond construction.

As far as hydrophobic and hydrophilic coatings onto macroscopic surfaces are concerned, the three great achievements have been the following ones:

1. The validation that our versatile designed strategy allows obtaining functional materials capable to coat different kind of substrates (glass, metals, or, fabrics).
2. The effective transformation of water-absorbent cotton weaves into water-repellent and oil-absorbent substrates by coating them with C₁₈-functionalised derivative **P9**. These coatings have been able to absorb oil from o/w emulsion up to 97% in efficiency, and to separate oil from water from an o/w emulsion by filtration.
3. The development of a new *in situ* polymerisation methodology. By following this one, the resulting C₁₈-/PEG-coated surfaces have shown similar wettabilities than the ones obtained from the *ex situ* polymerisation in solution. However, due to the remaining iodine crystals onto the surfaces, the WCA values obtained have been lower in all the cases, thus pointing out a less wide range of application than the

ex situ methodology. Nonetheless, this strategy could be even more studied and exploited, since it opens a novel way to polymerise catecholic derivatives.

IV. Multifunctional coatings

So far, it has been demonstrated the flexibility and the modular chemistry of our approach by polymerising different building blocks to systematically fine-tune the properties of the treated surfaces.

1. Firstly, fluorescent PEGylated MSNPs@**C6-8** have shown to be stable in a range of pH between 4 and 12, non-cytotoxic against SH-SY5Y cells at any concentrations tested (0-200 $\mu\text{g}/\text{mL}$), and capable to internalise within this type of cells.
2. Secondly, by polymerising building blocks **8** and **9**, it has been able to systematically fine-tune the wettability of glass slides and cotton fibres at will over a broad range of WCA (Figure 5.4).

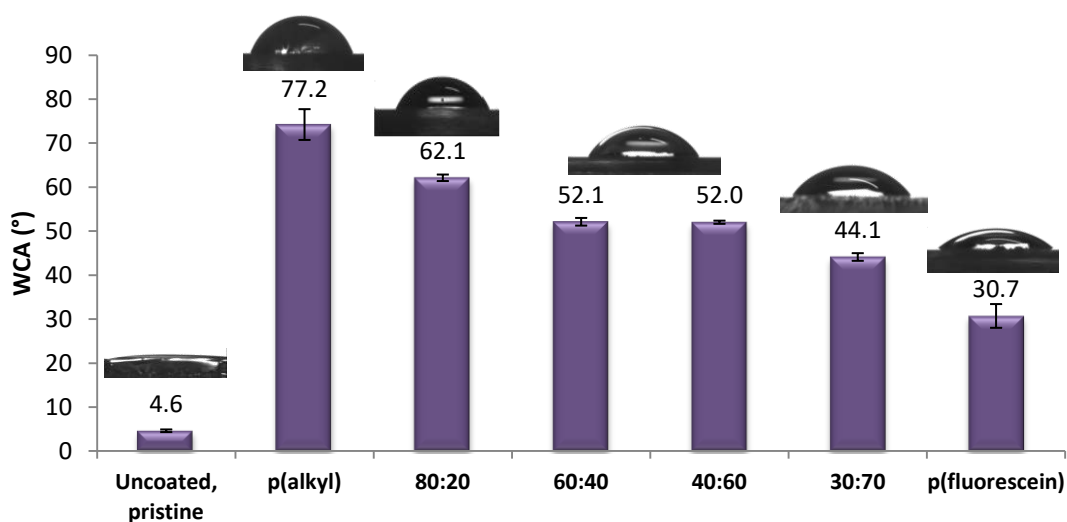


Figure 5.4. WCA values onto treated glass surfaces with different fluorescein-/C₁₈-functionalised copolymers **C8-9**.

To sum up, the main five objectives set at the beginning of this Doctoral Thesis has been achieved:

1. The synthesis of a new family of catechol-based compounds through a straightforward unified cheap methodology.
2. The development of a new polymerisation strategy based on the formation of disulphide bonds with the following characteristics:
 - ❖ Mild oxidative conditions that allow keeping the catechol moieties unchanged.

- ❖ High degree of functionalisation and high synthetic control on the final structure of oligomers.
 - ❖ Colourless oligomers, thus colourless coatings.
 - ❖ The resulting oligomers should be biodegradable due to the presence of disulphide bonds. That should be further studied.
 - ❖ Modular strategy that allows controlling the functionality of treated surfaces in an easy way.
3. The successful preparation of a new catechol-based toolkit for NP coating.
 4. Robust and effective hydrophobic/hydrophilic coatings onto flat surfaces.
 5. The demonstration that our proposed strategy is versatile, flexible and chemically modular, and allows fine-tuning the properties of the coatings.

CHAPTER 6

EXPERIMENTAL SECTION

6.1. GENERAL PROCEDURES

6.1.1. SPECTROSCOPY

Nuclear magnetic resonance spectra (NMR) were registered at the *Servei de Ressonància Magnètica Nuclear* of the *Universitat Autònoma de Barcelona*. ^1H NMR, ^{13}C NMR and ^{19}F NMR spectra were recorded at 250, 360, 400, or, 500 MHz, 90.5, 100.6, or, 125.8 MHz, and 235 MHz, respectively. Proton chemical shifts are reported in ppm (δ) (CDCl_3 , 7.26 ppm; CD_3OD , 3.31 ppm; and acetone- d_6 , 2.06 ppm). Carbon chemical shifts are reported in ppm (CDCl_3 , 77.2 ppm; CD_3OD , 49.0 ppm; and acetone- d_6 , 206.7 ppm and 29.9 ppm). All spectra were measured at 298 K. The abbreviations used to describe signal multiplicities are: s (singlet), bs (broad signal), d (doublet), t (triplet), dd (double doublet), dt (double triplet), td (triple doublet), m (multiplet) and J (coupling constant).

Infrared spectra (IR) were recorded on a Bruker Tensor 27 Spectrophotometer equipped with a Golden Gate Single Refraction Diamond ATR (Attenuated Total Reflectance) accessory at *Servei d'Anàlisi Química* of the *Universitat Autònoma de Barcelona*. Peaks are reported in cm^{-1} .

Electronic absorption spectra (UV-vis) were recorded on a HP 8453 Spectrophotometer. HPLC or spectroscopy quality solvents were used.

Energy dispersive X-ray (EDX) line-scan profiles were obtained at rt and 200 kV on a FEI Tecnai G2 F20 coupled to an EDAX detector.

Size distribution and surface charge of nanoparticles were measured by **dynamic light scattering** (DLS) using a ZetasizerNano 3600 instrument (Malvern Instruments, UK), the size range limit of which is 0.6 nm to 6 μm . Note: the diameter measured by DLS is the hydrodynamic diameter. The samples are comprised of aqueous dispersions of the nanoparticles in distilled water, or, in buffer. All samples are diluted to obtain an adequate nanoparticle concentration (0.5 – 1 mg/mL).

6.1.2. MASS SPECTROMETRY

High resolution mass spectra (HRMS) were recorded at the *Centro de I+D+I* of the *Parque Científico Tecnológico* of the Burgos University in an Argilent 6454 Q-TP spectrometer with an Argilent Jetstream Technology (AJT) source.

6.1.3. CHROMATOGRAPHY

All reactions were monitored by analytical **thin-layer chromatography** (TLC) using silica gel 60 F254 pre-coated aluminium plates (0.25 mm thickness). Development was made using an UV lamp at 254 nm and/or using a KMnO_4/KOH aqueous solution. Flash **column chromatography** was performed using silica gel (230-400 mesh).

The molecular weight distribution of all polymers was determined by **gel permeation chromatography** (GPC) using an Agilent Technologies 1260 Infinity chromatograph and THF as a solvent. The instrument is equipped with three gel columns: PLgel 5 μm Guard/ $50 \times 7.5 \text{ mm}^2$, PLgel 5 μm 10000 Å MW 4 K-400 K, and PL Mixed gel C 5 μm MW 200-3M. Calibration was made by using polystyrene standards. In each experiment, the freshly prepared polymer sample of interest was dissolved in THF (1-2 mg/mL), and immediately analysed by GPC (1 mL/min flow; 30 °C column temperature). The values obtained for M_n are an approximation.

6.1.4. MICROSCOPY

Optical and fluorescence images were recorded on a Zeiss Axio Observer Z-1 inverted optical/fluorescence microscope, equipped with five different magnification lenses (5 \times , 10 \times , 20 \times , 50 \times and 100 \times), a motorised XY stage, Hg-lamp excitation source (HBO 103/2, 100 W), AxioCam HRc digital camera, and standard filters and in fluorescence mode with an Alexa Fluor 488 filter.

Scanning electron microscopy (SEM) measurements were carried out on a Quanta FEI 200 FEG-ESEM microscope operating at 20 kV. All samples were fixed on SEM holders. Prior to observation with SEM, all samples were metalised with a thin 15 nm layer of platinum by sputter coater (Leica).

Transmission electron microscopy (TEM) analyses were performed at the *Servei de Microscòpia* of the *Universitat Autònoma de Barcelona*, with a JEOL JEM-1400 transmission microscope operating at 120 kV. TEM samples were prepared by dipping a carbon copper grid into a dilute suspension of the particles in hexane freshly sonicated. The average particle size and its standard deviation were estimated by measuring the edge length of at least 200 particles using the software ImageJ (Fiji). Data were fitted to a log-normal function and the polydispersity index (PDI) was calculated.

Scanning transmission electron microscopy (STEM) images were acquired on a FEI Magellan 400L in extreme resolution mode (XHR) at 20 kV, using a carbon coated copper grid as support.

Surface topography imaging of the different samples was carried out in ambient air in tapping mode using beam shaped silicon cantilevers (Nanosensors, nominal force constant: $5 \text{ N}\cdot\text{m}^{-1}$, tip radius: $\sim 7 \text{ nm}$) on an Agilent 5500 **AFM/SPM** microscope (Keysight Technologies, Santa Clara, CA, USA) combined with PicoScan5 version 1.20 (Keysight Technologies) software. An external X-Y positioning system (closed loop, NPXY100E from nPoint, USA) was used. Image processing was done using open source software: WSxM version 3.1 (Nanotec Electronica, Madrid, Spain) and Gwyddion version 2.46 (CMI, Brno, Czech Republic).

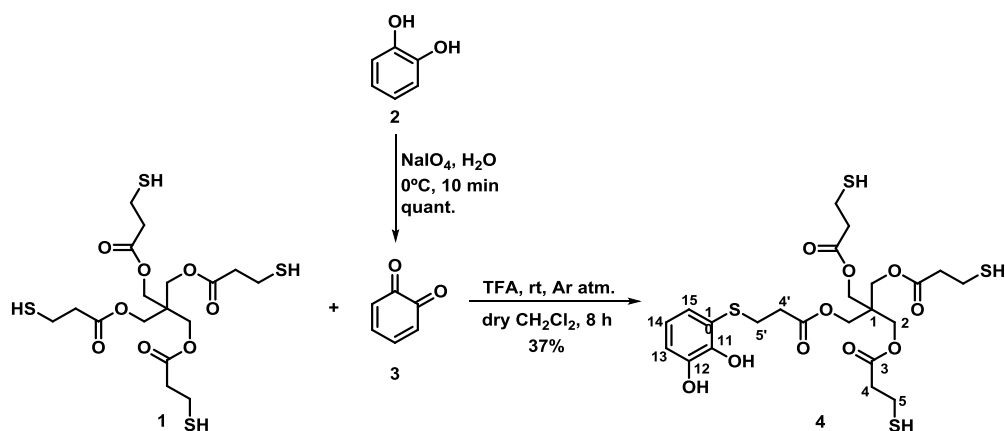
6.1.5. OTHER TECHNIQUES

The **contact angle** of Milli-Q water droplets (ca. $5 \mu\text{L}$) on coated substrates was used to evaluate the hydrophobicity of coated samples at rt by the sessile-drop technique. An Easy Drop Standard analyser and the Drop Shape Analysis DSA 10 software (KRÜSS GmbH, Hamburg, Germany) were used throughout. The reported values arise from averaging CA measurements on three different spots of each sample.

6.2. EXPERIMENTAL DESCRIPTION

All commercially available reagents were used as received. Synthesis-grade solvents were purchased from Scharlab, S. L. and used without further purification. Solvents were dried by distillation over the appropriate drying agents: CH_2Cl_2 (CaH_2), CH_3CN (CaH_2), and THF (Na^0). When needed, reactions were performed avoiding moisture by standard procedures and under N_2 or Ar atmosphere. Furthermore, molecular sieves of 4 \AA (beads, 8-12 mesh) were used to remove moisture from PEG derivatives when the reactions required.

6.2.1. SYNTHESIS OF FUNCTIONAL BUILDING BLOCKS

Synthesis of S-catechol tris-thiol **4**¹

A solution of pyrocatechol **2** (571 mg, 5.2 mmol) in the minimum volume of Et₂O was added into a solution of NaIO₄ (1.393 g, 6.5 mmol) in H₂O (170 mL) cooled down to 0 °C. The final mixture was stirred for 10 min. The resulting quinone **3** was extracted with CH₂Cl₂ (3 x 170 mL) in a quantitative manner. The organic extracts were dried with Na₂SO₄ anhydrous and filtered. In the meantime, a solution of pentaerythritol tetrakis(3-mercaptopropionate) **1** (2.715 g, 5.6 mmol) in CH₂Cl₂ (8 mL) with TFA (1 mL, 13.3 mmol) was prepared under an inert atmosphere. Finally, the solution containing quinone was added into the solution containing pentaerythritol tetrakis(3-mercaptopropionate). The resulting mixture was stirred at rt under argon atmosphere for 8 h in the dark. After this time, the solvent and TFA were removed under vacuum. The resulting oil was purified by column chromatography using hexane:EtOAc 7:3 affording S-catechol tris-thiol **4** (1.148 g, 1.9 mmol, 37% yield).

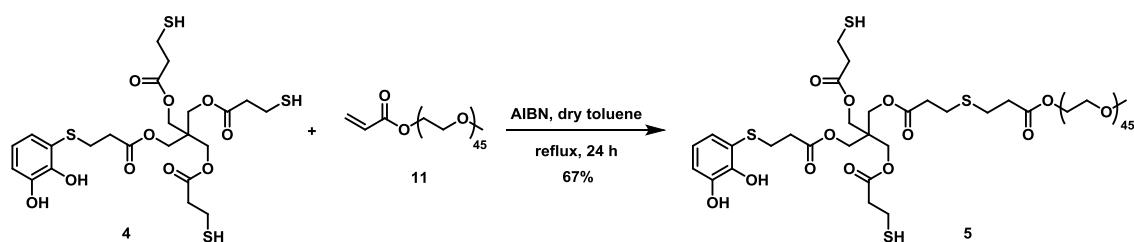
¹H NMR (400 MHz, CDCl₃) δ 6.92 (dd, *J* = 7.7, 1.6 Hz, 1H, H-15), 6.87 (dd, *J* = 7.7, 1.6 Hz, 1H, H-13), 6.73 (t, *J* = 7.7 Hz, 1H, H-14), 4.16 (s, 8H, H-2), 2.93 (t, *J* = 7.1 Hz, 2H, H-5'), 2.72 (m, 6H, H-5), 2.64 (m, 6H, H-4), 2.51 (t, *J* = 7.1 Hz, 2H, H-4'), 1.60 (t, *J* = 8.2 Hz, 3H, -SH).

¹³C NMR (100.6 MHz, CDCl₃) δ 171.6 (C-3), 171.5 (C-3), 171.2 (2 C-3), 144.7 (C-11), 144.2 (C-12), 126.4 (C-14), 120.8 (C-15), 117.7 (C-10), 116.8 (C-13), 62.0 (C-2), 41.9 (C-1), 38.1 (C-4), 33.6 (C-4'), 30.8 (C-5'), 19.5 (C-5).

HRMS (HR-El) calcd. for [C₂₃H₃₂O₁₀S₄Na]⁺: 619.0777; found: 619.0776.

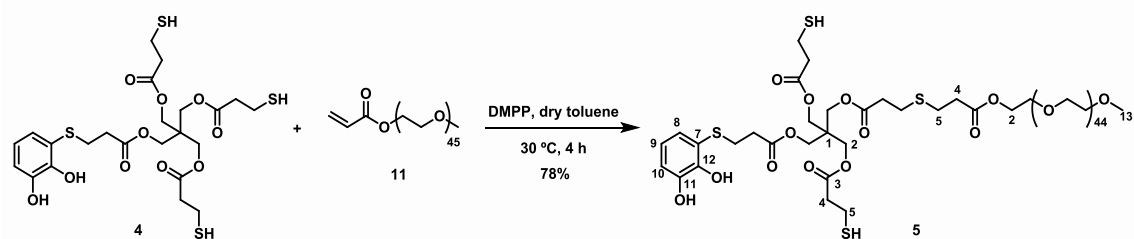
Synthesis of mPEG-functionalised building block **5**

I. Radical-catalysed thiol-ene reaction²



To a solution of MeOPEG2k acrylate **11** (80 mg, 0.04 mmol) in dry toluene (0.5 mL), AIBN (1.3 mg, 0.008 mmol) was added under nitrogen atmosphere. The mixture was heated, and a solution of S-catechol tris-thiol **4** (48 mg, 0.08 mmol) in dry toluene (0.6 mL) was added dropwise. The reaction mixture was heated at reflux temperature for 24 h. The cooled reaction was concentrated under reduced pressure to afford an oil. It was dissolved in the minimum volume of CH_2Cl_2 , and Et_2O was added until cloudiness appeared. The solution was stored in the fridge overnight and the resulting precipitate filtered, washed five times with cold Et_2O and dried at high vacuum to furnish the final mPEG derivative **5** (69 mg, 0.027 mmol, 67% yield).

II. Thia-Michael reaction³



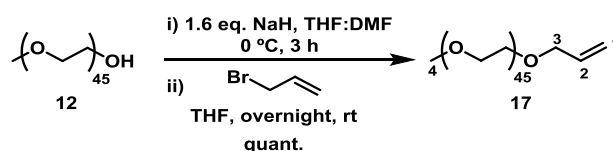
To a solution of catechol-thiol derivative **4** (73 mg, 0.12 mmol) in dry toluene (1 mL) and under inert atmosphere, a solution of dimethylphenylphosphine (DMPP) in toluene (11 μL , 0.007 mmol) was added. To this solution, the commercial MeOPEG2k acrylate **11** (102 mg, 0.051 mmol) was added and the mixture quickly agitated at 30 °C for 4 h. The solvent was removed under vacuum. The oil obtained was dissolved in the minimum volume of CH_2Cl_2 , and Et_2O was added until cloudiness appeared. The suspension was stored in the fridge overnight and the resulting precipitate filtered, washed five times with cold Et_2O and dried at high vacuum to furnish the final PEG derivative **5** (103 mg, 0.040 mmol, 78% yield).

¹H NMR (500 MHz, CDCl_3) δ 6.92 (d, $J = 7.7$ Hz, 1H, H-10), 6.90 (d, $J = 7.7$ Hz, 1H, H-8), 6.75 (t, $J = 7.8$ Hz, 1H, H-9), 4.18 (s, 10H, H-2), 3.79-3.55 (bs, 180H, $-(\text{CH}_2\text{CH}_2\text{O})_n-$), 3.37 (s, 3H, H-13), 2.97-2.54 (m, 20H, H-4, H-5), 1.66 (t, $J = 8.2$ Hz, 2H, -SH).

^{13}C NMR (125.8 MHz, CDCl_3) δ 171.8 (C-3), 171.5 (C-3), 171.4 (C-3), 171.3 (C-3), 171.1 (C-3), 145.1 (C-12), 144.7 (C-11), 125.8 (C-9), 120.7 (C-8), 118.3 (C-7), 116.7 (C-10), 70.6 ($-(\text{CH}_2\text{CH}_2\text{O})_n-$), 62.2 (C-2), 59.0 (C-13), 41.7 (C-1), 38.2 (C-4'), 34.6 (C-4), 26.9 (C-5), 19.6 (C-5').

Synthesis of mPEG-functionalised building block 6

Synthesis of allyl-functionalised mPEG derivative 17⁴

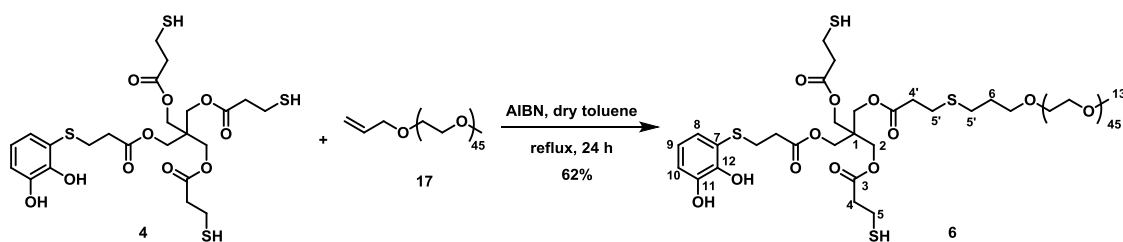


To a suspension of NaH (16 mg, 0.4 mmol) in dry THF (1 mL) cooled into an ice bath, a solution of commercial MeOPEG2kOH **12** (500 mg, 0.25 mmol) in anhydrous DMF (10 mL) was added drop-wise. The reaction mixture was stirred for 3 h at 0 °C. Afterwards, a solution of allyl bromide (100 μL , 0.5 mmol) in dry THF (1.25 mL) was added drop-wise. The mixture was allowed to react overnight at rt to complete the reaction and then filtered to remove unreacted NaH. The solvent was removed under vacuum. The crude was dissolved in the minimum volume of CH_2Cl_2 , and Et_2O was added until cloudiness appeared. The solution was stored in the fridge overnight and the resulting precipitate filtered, washed five times with cold Et_2O and dried at high vacuum to furnish the final allyl-functionalised mPEG derivative **17** (503 mg, 0.25 mmol, quant.).

^1H NMR (360 MHz, CDCl_3) δ 5.98 (q, $J = 9.6$ Hz, 1H, H-2), 5.85 (d, $J = 16.6$ Hz, 1H, H-1 *trans*), 5.76 (d, $J = 9.6$ Hz, 1H, H-1 *cis*), 4.34 (d, $J = 6.8$ Hz, 2H, H-3), 4.00-3.39 (bs, 180H, $-(\text{CH}_2\text{CH}_2\text{O})_n-$), 3.31 (s, 3H, H-4).

^{13}C NMR (90.5 MHz, CDCl_3) δ 130.4 (C-2), 124.2 (C-1), 72.0 (C-3), 70.4 ($-(\text{CH}_2\text{CH}_2\text{O})_n-$), 59.1 (C-4).
HRMS (HR-EI) calcd $[\text{C}_{94}\text{H}_{189}\text{O}_{46}]^{3+}$; 2000; found: 1881.3335.

Synthesis of mPEG-functionalised building block 6²



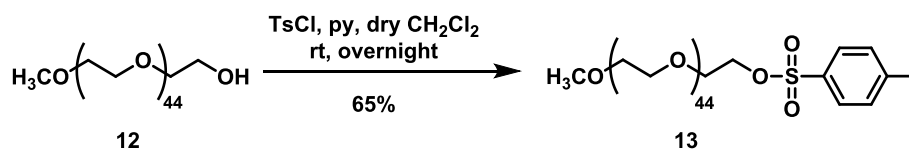
Into a solution of allyl-functionalised mPEG **17** (102 mg, 0.13 mmol) in dry toluene (6 mL), AIBN (8 mg, 0.05 mmol) was added under nitrogen atmosphere. The mixture was heated at reflux temperature and a solution of S-catechol tris-thiol **4** (96 mg, 0.16 mmol) in dry toluene (9 mL) was added drop-wise. The reaction mixture was heated at reflux temperature for 24 h. The cooled reaction was concentrated under reduced pressure to afford an oil. It was dissolved in the minimum quantity of CH₂Cl₂, and Et₂O was added until cloudiness appeared. The solution was stored in the fridge overnight and the resulting precipitate filtered, washed five times with cold Et₂O and dried at high vacuum to give a white powder as a product **6** (209 mg, 0.080 mmol, 62% yield).

¹H NMR (360 MHz, CDCl₃) δ 7.13-6.68 (m, 3H, H-8, H-9, H-10), 4.17 (s, 8H, H-2), 3.70-3.52 (bs, 200H, -(CH₂CH₂O)_n-), 3.37 (s, 3H, H-13), 3.11-2.50 (m, 18H, H-4, H-5, H-4', H-5'), 1.61 (t, *J* = 8.2 Hz, 2H, -SH), 1.31 (q, *J* = 7.2 Hz, 2H, H-6).

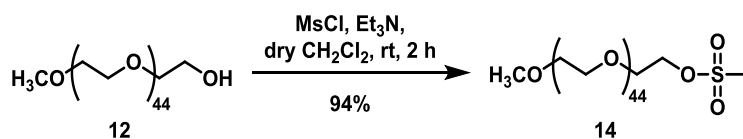
¹³C NMR (125.8 MHz, CDCl₃) δ 171.1 (C-3), 162.5 (C-11), 144.6 (C-12), 122.3 (C9), 119.7 (C-8), 114.1 (C-7), 109.2 (C-10), 70.4 (-(CH₂CH₂O)_n-), 61.6 (C-2), 59.1 (C-13), 41.8 (C-1), 38.3 (C-4'), 36.5 (C-4), 31.5 (C-5), 27.9 (C-6), 19.6 (C-5').

Trial to synthesise mPEG-functionalised building block 6

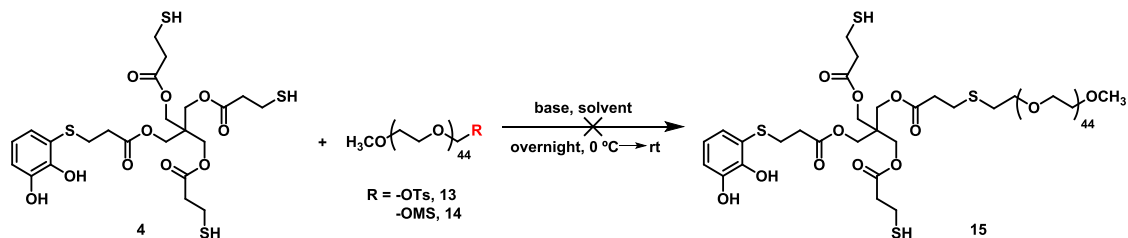
Synthesis of mPEG-OTs 13⁵



Into a solution of *p*-toluenesulfonyl chloride (297 mg, 1.6 mmol) in anhydrous pyridine (1 mL) and dry CH₂Cl₂ (2.5 mL), a solution of commercial mPEG **12** (1.053 g, 0.52 mmol) in dry CH₂Cl₂ (2 mL) was added. The final mixture was let stir overnight at rt under argon atmosphere. The reaction was followed by TLC (hexanes:EtOAc 2:1). When reaction finished, distilled water (10 mL) were added and the mixture was stirred 4 h more. After that time, the product was extracted in CH₂Cl₂ (3 x 10 mL). The organic extracts were dried with anhydrous Na₂SO₄, filtered, and concentrated under vacuum. Afterwards, the oil obtained was dissolved in the minimum volume of CH₂Cl₂, and Et₂O was added until cloudiness appears. The final suspension was stored in the freeze overnight. The white precipitate was filtered and washed several times with cold Et₂O to furnish mPEG-OTs **13** (724 mg, 0.34 mmol, 65% yield).

Synthesis of mPEG-OMs 14⁶

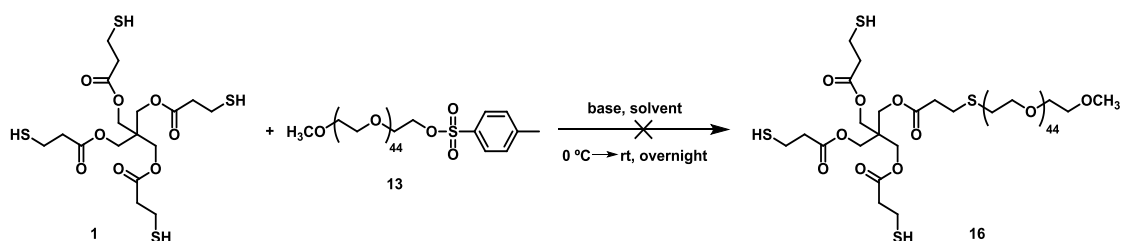
In a Schlenk equipped with a magnetic stirring bar and nitrogen atmosphere, mPEG **12** (1.011 g, 0.5 mmol) was dissolved in dry CH₂Cl₂ (2.5 mL). After cooling to 0 °C in an ice bath, anhydrous Et₃N (105 μL, 0.75 mmol) was added, followed by methanesulfonyl chloride (50 μL, 0.65 mmol). The mixture was stirred for 30 min at 0 °C, and then at rt for 2 h. Afterwards, the reaction mixture was diluted with CH₂Cl₂ (2.5 mL) and NaHCO₃ aqueous saturated solution (4 mL). The aqueous phase was extracted with CH₂Cl₂ (3 x 4 mL), and the combined organic extracts were dried over anhydrous Na₂SO₄, filtered and concentrated under vacuum. The crude was dissolved in the minimum volume of CH₂Cl₂, and Et₂O was added until the solution became turbid. The final suspension was stored in the fridge overnight. The precipitate was filtered, washed several times with cold Et₂O and dried under vacuum to furnish a white solid (988 mg, 0.47 mmol, 94% yield).

Synthesis of mPEG 15

From mPEG-OTs **13**. 1-3 equiv. of a base were added into a 0.04 M solution of S-catechol tris-thiol **4** in a dry solvent (THF, CH₂Cl₂, or, DMF) cooled down into an ice bath. In less than 10 min, a 0.02 M solution of mPEG-OTs **13** (1 equiv.) was added to the solution containing the catecholic derivative. The final mixture was allowed to proceed overnight at rt under argon atmosphere. Afterwards, water was added to the mixture for quenching, and it was let stir 30 min. The resulting aqueous layer was extracted three times with EtOAc. The organic extracts were dried with anhydrous Na₂SO₄, filtered and the solvent evaporated under vacuum. Then, the oil obtained was dissolved in the minimum volume of CH₂Cl₂, and Et₂O was added until cloudiness appeared. The final suspension was stored in the freeze overnight. The white precipitate was filtered and washed several times with cold Et₂O.

From *m*PEG-OMs **14**. A solution of BuLi in hexane (2.5 M, 134 μ L, 0.33 mmol) was added into a solution of S-catechol tris-thiol **4** (67 mg, 0.11 mmol) in dry CH₂Cl₂ (4 mL) cooled down into an ice bath. In less than 10 min, a solution of PEG-OMs **14** (239 mg, 0.11 mmol) in dry CH₂Cl₂ (6 mL) was added to the solution containing the catechol derivative. Then, the final mixture was allowed to proceed overnight at rt under argon atmosphere. The reaction mixture was quenched by adding CH₂Cl₂ (10 mL) and NaHCO₃ saturated solution (15 mL). The product was extracted with CH₂Cl₂ (3 x 15 mL) and the organic phase was dried over anhydrous Na₂SO₄, filtered and concentrated under vacuum. The resulting oil was dissolved in the minimum volume of CH₂Cl₂, and Et₂O was added until the solution became turbid. The solution was stored in the fridge overnight. The white solid precipitate was filtered and washed several times with cold Et₂O.

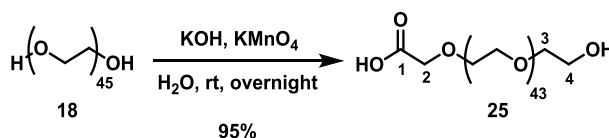
Synthesis of *m*PEG **16**



1.1-1.3 equiv. of BuLi 2.5 M in hexane were added into a 0.04 M solution of starting molecule **1** in a dry solvent (THF, CH₂Cl₂, or, DMF) cooled down into an ice bath. In less than 10 min, a 0.02 M solution of *m*PEG-OTs **13** (0.5-1 equiv.) was added into the solution containing core **1**. Then, the final mixture was allowed to proceed overnight at rt under argon atmosphere. Afterwards, water was added to the mixture for quenching and it was let stir 30 min. The resulting aqueous layer was extracted three times with EtOAc. The organic extracts were dried with anhydrous Na₂SO₄, filtered and the solvent evaporated under vacuum. The oil obtained was dissolved in the minimum volume of CH₂Cl₂, and Et₂O was added until cloudiness appeared. The final suspension was stored in the freeze overnight. The white solid precipitate was filtered and washed several times with cold Et₂O.

Synthesis of PEG-functionalised building block 7

Synthesis of HOOC-PEG-OH **25**^{7,8}

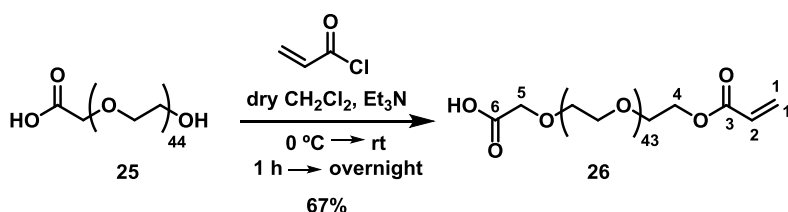


Commercial PEG-2000 **18** (4.099 g, 2 mmol) and KOH (2.088 g, 31.6 mmol) were dissolved in water (60 mL). KMnO_4 (625 mg, 3.84 mmol) was added and the reaction mixture was stirred overnight at rt. The resulting brown suspension (MnO_2) was filtered over Celite® and concentrated HCl 37% was added to the filtrate until acidic pH. The product was extracted into CH_2Cl_2 followed by drying with anhydrous Na_2SO_4 . After reducing the volume by evaporation, Et_2O was added until the solution became turbid. The solution was stored in the freezer overnight and the white precipitate was filtered, washed with cold Et_2O and dried under high vacuum to furnish the desired PEG derivative **25** (3.913 g, 1.9 mmol, 95% yield).

¹H NMR (400 MHz, CDCl_3) δ 4.17 (s, 2H, H-2), 3.82-3.56 (bs, 180H, $-(\text{CH}_2\text{CH}_2\text{O})_n-$, H-3, H-4).

¹³C NMR (100.6 MHz, CDCl_3) δ 171.9 (C-1), 72.7 (C-3), 70.7 ($-(\text{CH}_2\text{CH}_2\text{O})_n-$), 69.3 (C-2), 61.8 (C-4).

Synthesis of heterobifunctional PEG **26**^{9,10}



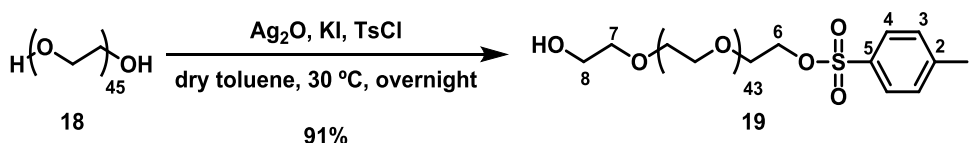
HOOC-PEG-OH **25** (2.002 g, 1 mmol) and anhydrous Et_3N (188 μL , 1.369 mmol) were dissolved in dry CH_2Cl_2 (21 mL) at 0 °C with molecular sieves (3.2 g). Then, acryloyl chloride (239 μL , 2.876 mmol) in dry CH_2Cl_2 (13 mL) was added drop-wise. The reaction was stirred at 0 °C for 1 h, allowed to reach rt and stirred overnight. Molecular sieves were removed and the reaction mixture was washed six times with a saturated solution of NaHCO_3 (6 x 30 mL). The organic phases were dried with anhydrous Na_2SO_4 , filtered and the solvent was removed under vacuum. The crude was re-dissolved in the minimum volume of CH_2Cl_2 and Et_2O was added until the solution became turbid. The solution was stored in the freezer overweekend and the white precipitate was filtered, washed with cold Et_2O and dried under high vacuum to afford the final PEG-acrylate derivative **26** (1.377 g, 0.67 mmol, 67% yield).

$^1\text{H NMR}$ (400 MHz, CDCl_3) δ 6.44 (d, $J = 17.1$ Hz, 1H, H-1), 6.17 (dd, $J = 17.1, 10.8$ Hz, 1H, H-2), 5.85 (d, $J = 10.8$, 1H, H-1'), 4.30 (t, $J = 4.7$ Hz, 2H, H-4), 4.12 (s, 2H, H-5), 3.71-3.51 (bs, 180H, $-(\text{CH}_2\text{CH}_2\text{O})_n-$).

$^{13}\text{C NMR}$ (100.6 MHz, CDCl_3) δ 172.3 (C-6), 166.5 (C-3), 131.3 (C-1), 128.6 (C-2), 70.8 ($-(\text{CH}_2\text{CH}_2\text{O})_n-$), 69.4 (C-5), 63.9 (C-4).

Trial to synthesise heterobifunctional PEG 26

Synthesis of HO-PEG-OTs 19¹¹

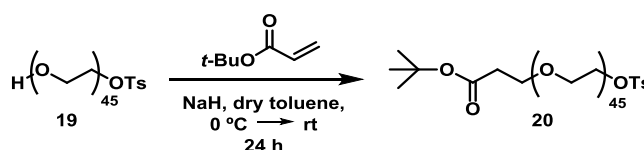


Commercial PEG-2000 **18** (2.056 g, 1 mmol) in dry toluene (18 mL) with the addition of molecular sieves (3.7 g) was stirred for 4 h at 30 °C to remove residual water. Then, Ag_2O (343 mg, 1.48 mmol) and KI (82 mg, 0.49 mmol) were added. Following, to this rapidly stirred solution TsCl (203 mg, 1.06 mmol) was added in one portion. The reaction mixture was left at 30 °C with constant stirring overnight before filtration over Celite® and solvent removal by rotary evaporation. The crude was dissolved in the minimum volume of CH_2Cl_2 and Et_2O was added until cloudiness appeared. The cloudy solution was stored into the freezer overnight. The resulting white precipitate was filtered and dried under high vacuum to furnish the desired product **19** (1.961 g, 0.91 mmol, 91% yield).

$^1\text{H NMR}$ (400 MHz, CD_3OD) δ 7.80 (d, $J = 8.01$ Hz, 2H, H-4), 7.35 (d, $J = 8.01$, 2H, H-3), 4.16 (s, 2H, H-6), 3.79-3.55 (bs, 180H, $-(\text{CH}_2\text{CH}_2\text{O})_n-$, H-7, H-8), 2.46 (s, 3H, H-1).

$^{13}\text{C NMR}$ (100.6 MHz, CDCl_3) δ 144.7 (C-5), 132.9 (C-2), 129.8 (C-4), 128.0 (C-3), 72.6 (C-7), 70.4 ($-(\text{CH}_2\text{CH}_2\text{O})_n-$), 68.5 (C-6), 61.7 (C-8), 21.8 (C-1).

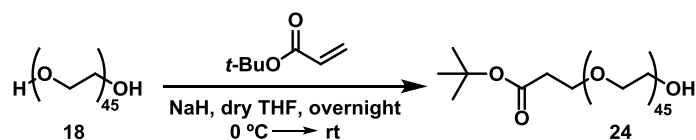
Synthesis of tert-BuO-PEG-OTs 20¹²



HO-PEG-OTs **19** (254 mg, 0.125 mmol) in dry THF (3.6 mL) with the addition of molecular sieves (0.3 g) was stirred for 2 h at rt to remove residual water. Afterwards, the solution was cooled

down to 0 °C into an ice bath, NaH (2 mg, 0.05 mmol) was added, and the mixture was left for 2 h at 0 °C to rt. This was followed by the addition of *tert*-butyl acrylate (171 μL, 1.11 mmol) in three portions over 20 h. The resulting solution was diluted with cold water (5 mL), extracted with CH₂Cl₂ (3 x 5 mL) and the organic layers combined. The resulting organic phase was washed with brine (3 x 20 mL), dried over anhydrous Na₂SO₄, filtered and concentrated under vacuum. The resulting crude was dissolved in the minimum volume of CH₂Cl₂ and Et₂O was added drop-wise until a white precipitate was observed. The white suspension was storage into the freezer overnight. The resulting precipitate was filtered, washed with cold Et₂O and dried under high vacuum to furnish the desired product in 78% of conversion.

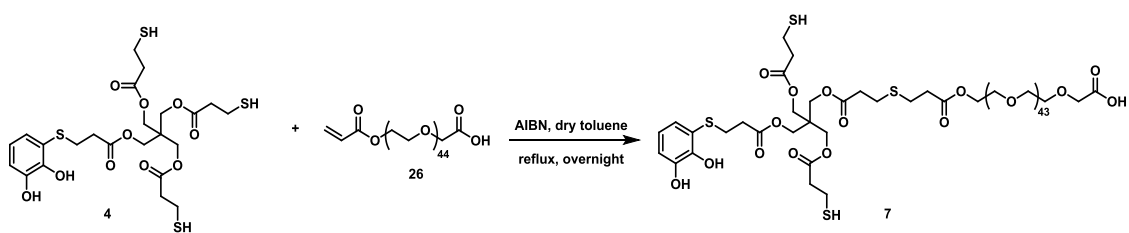
Synthesis of *tert*-BuO-PEG-OH **24**³



Commercial PEG-2000 **18** (102 mg, 0.05 mmol) in dry THF (1.4 mL) with the addition of molecular sieves (0.1 g) was stirred for 3 h at rt to remove residual water. Afterwards, the solution was cooled down to 0 °C into an ice bath, NaH (1mg, 0.025 mmol) was added, and the mixture was left for 2 h at 0 °C to rt. This was followed by the addition of *tert*-butyl acrylate (7.6 μL, 0.04 mmol) and the reaction mixture was stirred at rt overnight. Afterwards, the resulting solution was diluted with cold water (2 mL), extracted with CH₂Cl₂ (3 x 2 mL), and the organic layers combined. The resulting organic phase was washed with brine (3 X 3 mL), dried over anhydrous Na₂SO₄, filtered and concentrated under vacuum. The resulting crude was dissolved in the minimum volume of CH₂Cl₂ and Et₂O was added drop-wise until a white precipitate was observed. The white suspension was storage into the freezer overnight. The resulting white precipitate was filtered and dried under high vacuum to furnish the final product **24** in 50% of conversion.

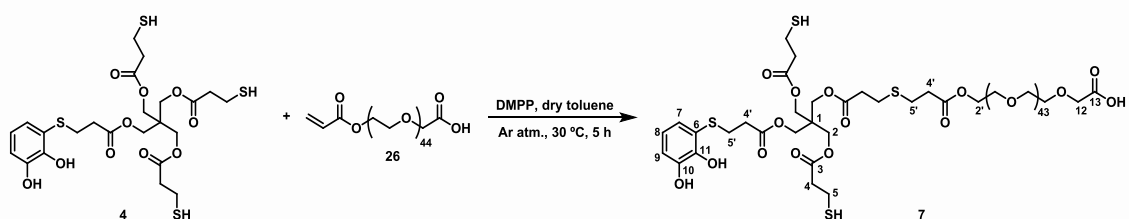
Synthesis of PEG-functionalised building block **7**

I. Radical-catalysed thiol-ene reaction²



To a solution of PEG derivative **26** (25 mg, 0.01 mmol) in dry toluene (1.5 mL), AIBN (4 mg, 0.02 mmol) was added under nitrogen atmosphere. The mixture was heated below reflux temperature and a solution of the S-catechol tris-thiol **4** (32 mg, 0.05 mmol) in dry toluene (2.5 mL) was added drop-wise. The reaction mixture was heated at reflux temperature overnight. The cooled reaction was concentrated under reduced pressure to afford an oil. It was dissolved in the minimum volume of CH_2Cl_2 , and Et_2O was added until a cloudiness appeared. The solution was stored in the fridge overnight and the resulting precipitate filtered and dried at high vacuum to furnish the desired catechol-PEG derivative **7** in 50% of conversion.

II. Thia-Michael reaction³

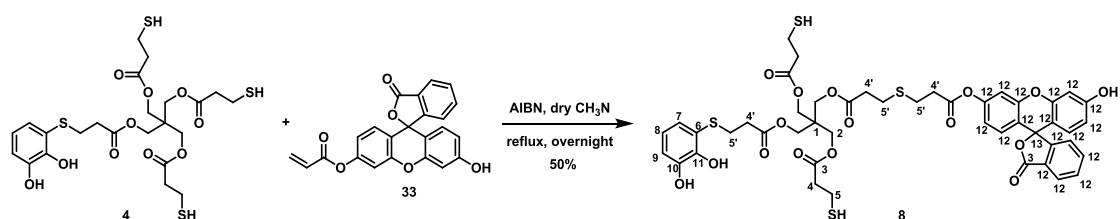


To a solution of the S-catechol tris-thiol **4** (343 mg, 0.57 mmol) in dry toluene (14 mL) with DMPP (61 μL , 0.04 mmol), heterobifunctional PEG derivative **26** (204 mg, 0.1 mmol) was added, and the mixture quickly agitated at 30 °C for 5 h. The solvent was removed under vacuum, the crude re-dissolved in the minimum volume of CH_2Cl_2 , and Et_2O was added until the solution became turbid. The solution was stored in the freezer overnight and the white precipitate was filtered, washed with cold Et_2O and dried under high vacuum to furnish the final catechol-PEG derivative **7** (176 mg, 0.067 mmol, 67% yield).

¹H NMR (360 MHz, CDCl_3) δ 6.97-6.88 (m, 2H, H-7, H-9), 6.75 (t, $J = 7.9$ Hz, 1H, H-8), 4.19 (m, 10H, H-2, H-2'), 4.09 (s, 2H, H-12), 3.74-3.50 (bs, 180H, $-(\text{CH}_2\text{CH}_2\text{O})_n-$), 3.08-2.51 (m, 20H, H-4, H-5, H-4', H-5'), 1.63 (t, $J = 8.3$ Hz, 2H, -SH).

¹³C NMR (90.5 MHz, CDCl_3) δ 171.2 (C-3, C-13), 151.9 (C-10), 139.5 (C-11), 130.3 (C-7), 126.0 (C-6), 120.8 (C-8), 117.0 (C-9), 70.8 ($-(\text{CH}_2\text{CH}_2\text{O})_n-$), 62.1 (C-2), 38.2 (C-1), 31.0 (C-4, C-4'), 19.6 (C-5, C-5').

Synthesis of fluorescein-functionalised building block **8**²



Into a solution of fluorescein *O*-acrylate **33** (150 mg, 0.39 mmol) in dry CH₃CN (12 mL), AIBN (36 mg, 0.22 mmol) was added under nitrogen atmosphere. The mixture was heated at reflux temperature and a solution of *S*-catechol-based tris-thiol **4** (450 mg, 0.75 mmol) dry CH₃CN (5 mL) was added drop-wise for 1 h. The reaction mixture was heated at reflux temperature overnight. The cooled reaction was concentrated under reduced pressure to afford an oil. This oil was purified by column chromatography through silica gel using a gradient of hexane:EtOAc. The fraction of interest was crystallised with Et₂O to afford the final pure compound as an orange powder (192 mg, 0.19 mmol, 50% yield).

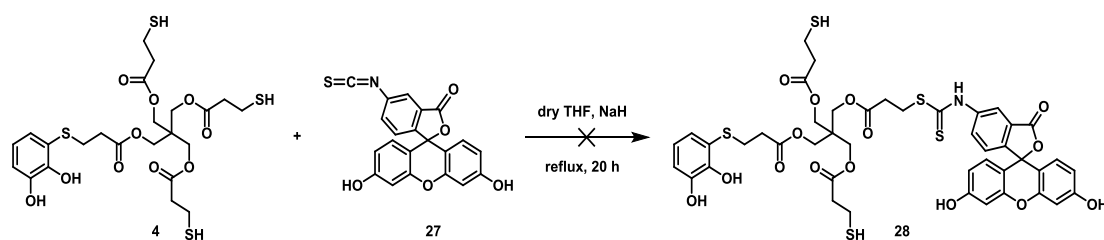
¹H NMR (400 MHz, (CD₃)₂CO) δ 8.01 (m, 1H, H-12), 7.79 (m, 1H, H-12), 7.72 (m, 1H, H-12), 7.32-7.17 (bs, 3H, H-7, H-8, H-9), 6.95-6.87 (bs, 3H, H-12), 6.79 (bs, 1H, H-12), 6.74 (s, 1H, H-12), 6.66 (s, 1H, H-12), 6.63 (bs, 1H, H-12), 4.26 (s, 8H, H-2), 3.17-2.61 (bs, 20 H, H-4, H-5, H-4', H-5'), 1.61 (t, *J* = 8.0 Hz, 2H, SH).

¹³C NMR (100.6 MHz, (CD₃)₂CO) δ 170.8 (C-3), 171.5 (C-3), 171.3 (C-3), 171.1 (C-3), 170.8 (C-3), 168.8 (C-12), 159.9 (C-12), 159.5 (C-12), 153.1 (C-12), 152.9 (C-12), 152.4 (C-12), 152.3 (C-12), 152.1 (C-12), 151.7 (C-11), 135.4 (C-10), 135.1 (C-12), 130.1 (C-12), 129.2 (C-12), 129.1 (C-12), 126.6 (C-8), 124.7 (C-6), 124.4 (C-12), 124.1 (C-7), 117.8 (C-9), 112.8 (C-12), 112.3 (C-12), 110.7 (C-12), 110.3 (C-12), 102.5 (C-12), 69.1 (C-13), 62.3 (C-2), 43.4 (C-1), 33.7 (C-4'), 27.6 (C-4), 25.7 (C-5'), 14.7 (C-5).

HRMS (HR-EI) calcd. for [C₄₆H₄₇O₁₆S₄]⁺: 983.1742; found: 983.1747.

Trial to synthesise fluorescein-functionalised building block 8

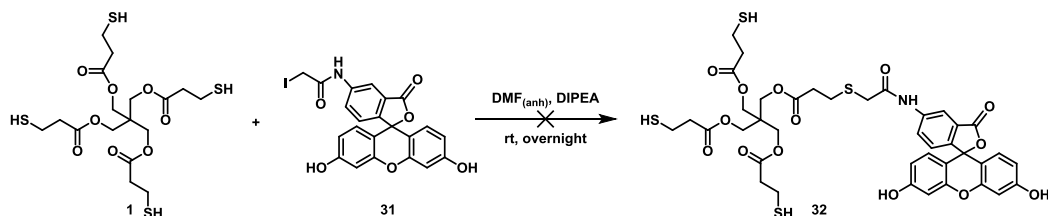
I. Thiourea construction reaction, from fluorescein 5(6)-isothiocyanate 27¹³



A solution of *S*-catechol-tris-thiol **4** (30 mg, 0.05 mmol) in dry THF (2 mL) was added drop-wise into a suspension of NaH (6.9 mg, 0.17 mmol) in dry THF (1 mL) cooled down to 0 °C. After 20 min, a solution of fluorescein 5-(6)-isothiocyanate **27** (20.9 mg, 0.05 mmol) in dry THF (1.5 mL) was added into the previous solution. The reaction mixture was refluxed for 20 h. After this

time, the reaction was quenched by ice water (6 mL) and extracted with EtOAc. The organic phases were combined, dried with anhydrous Na_2SO_4 , filtered and reduced in the rotavapour.

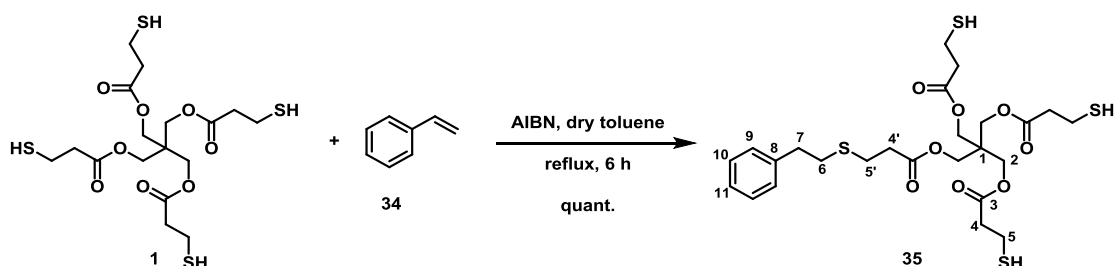
II. $\text{S}_{\text{N}}2$, from 5-(iodoacetamido)fluorescein **31**¹⁴



Into a solution of 5-(iodoacetamido)fluorescein **31** (8 mg, 0.019 mmol) in anhydrous DMF (0.2 mL) and DIPEA (7 μL , 0.040 mmol), a solution of pentaerythritol tetrakis(3-mercaptopropionate) **1** (16 mg, 0.032 mmol) in anhydrous DMF (0.6 mL) was added under inert atmosphere. The mixture was stirred overnight at rt. The solvent was removed under vacuum and the crude was purified by column chromatography.

Synthesis of fluorescein-functionalised styrenic building block **36**

Synthesis of *S*-styrene tris-thiol **35**²



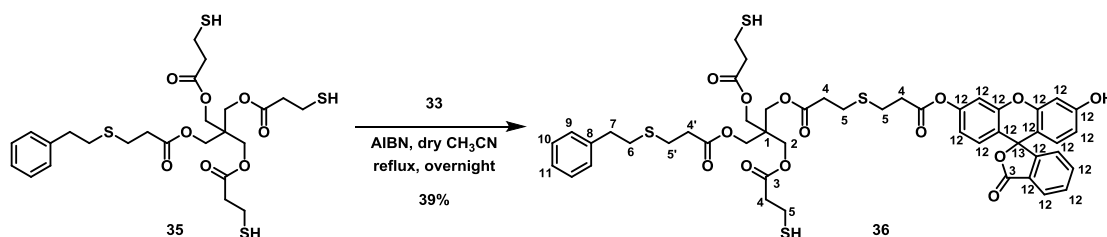
A solution of pentaerythritol tetrakis(3-mercaptopropionate) **1** (436 mg, 0.89 mmol) in dry toluene (5 mL) was added into a Schlenk containing AIBN (31 mg, 0.19 mmol). Afterwards, styrene **34** (100 μL , 0.87 mmol) was added into the reaction mixture. The mixture was heated at reflux temperature under argon atmosphere. After 6 h, the cooled reaction was concentrated under reduced pressure to afford a colourless oil (513 mg, 0.87 mmol, quant.).

¹H NMR (360 MHz, CD_2Cl_2) δ 7.30-7.16 (m, 5H, H-9, H-10, H-11), 4.16 (s, 8H, H-2), 2.86 (t, J = 7.2 Hz, 6H, H-5', H-6, H-7), 2.74 (m, 6H, H-5), 2.64 (m, 8H, H-4, H-4'), 1.66 (t, J = 8.2 Hz, 3H, -SH).

^{13}C NMR (90.5 MHz, CD_2Cl_2) δ 171.8 (C-3), 171.5 (C-3), 171.3 (2 C-3), 171.0 (C-3), 140.8 (C-8), 128.5 (C-10), 128.4 (C-9), 126.3 (C-11), 62.6 (C-2), 41.9 (C-1), 38.3 (C-4), 36.0 (C-4'), 34.8 (C-6), 33.6 (C-7), 26.9 (C-5'), 19.6 (C-5).

HRMS (HR-EI) calcd. $[\text{C}_{25}\text{H}_{38}\text{O}_9\text{S}_4]^+$: 610.1335; found: 610.1399.

Synthesis of fluorescein-functionalised styrenic building block **36**²



A solution of S-styrene tris-thiol **35** (152 mg, 0.26 mmol) in dry CH_3CN (1 mL) was added into a Schlenk containing AIBN (10 mg, 0.06 mmol), followed by the addition of a solution of fluorescein *O*-acrylate (100 mg, 0.26 mmol) **33** in dry CH_3CN (2 mL). The mixture was heated at reflux temperature under argon atmosphere overnight. The cooled reaction was concentrated under reduced pressure to afford a yellow oil which was purified by column chromatography performed using silica gel with a gradient of hexane:EtOAc (99 mg, 0.101 mmol, 39% yield).

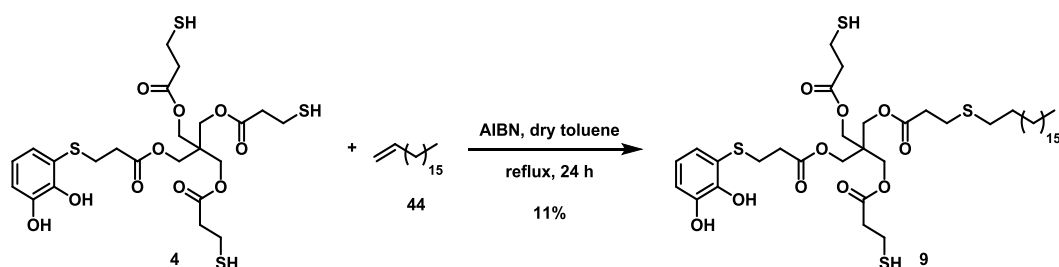
^1H NMR (360 MHz, $(\text{CD}_3)_2\text{CO}$) δ 8.01 (m, 2H, H-12), 7.86-7.67 (bs, 3H, H-12), 7.38-7.12 (bs, 5H, H-9, H-10, H-11), 6.96-6.82 (bs, 2H, H-12), 6.80 (s, 1H, H-12), 6.74-6.62 (bs, 2H, H-12), 4.25 (s, 8H, H-2), 3.17-2.65 (bs, 24H, H-4, H-5, H-4', H-5', H-6, H-7), 1.67 (t, $J = 8.0$ Hz, 2H, -SH).

^{13}C NMR (90.5 MHz, $(\text{CD}_3)_2\text{CO}$) δ 172.0 (C-3), 171.5 (C-3), 171.3 (C-3), 171.1 (C-3), 170.8 (C-3), 168.8 (C-12), 159.6 (C-12), 153.1 (C-12), 152.9 (C-12), 152.5 (C-12), 152.3 (C-12), 152.2 (C-12), 141.4 (C-8), 135.2 (C-10), 130.7 (C-12), 130.1 (C-12), 129.8 (C-9), 129.3 (C-12), 129.1 (C-12), 128.8 (C-11), 124.7 (C-12), 112.8 (C-12), 112.4 (C-12), 110.8 (C-12), 110.3 (C-12), 102.5 (C-12), 102.4 (C-12), 82.4 (C-13), 62.9 (C-2), 42.6 (C-1), 38.5 (C-4'), 36.5 (C-4), 33.9 (C-6), 33.6 (C-7), 24.8 (C-5), 19.7 (C-5').

HRMS (HR-EI) calcd $[\text{C}_{48}\text{H}_{51}\text{O}_{14}\text{S}_4]^+$: 979.2141; found: 979.2161.

Synthesis of C₁₈-functionalised building block 9

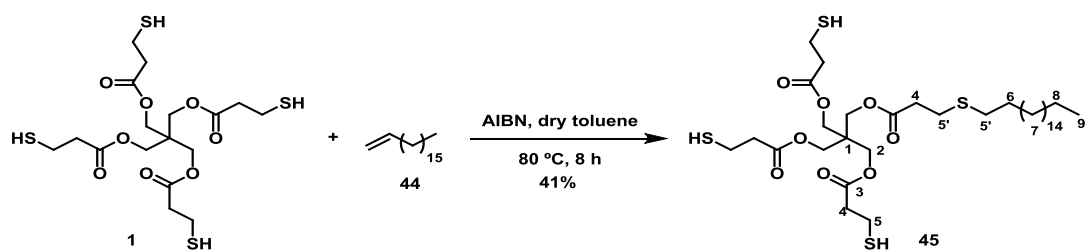
I. Route A²



AIBN (31 mg, 0.2 mmol) and S-catechol tris-thiol **4** (535 mg, 0.9 mmol) were dissolved in dry toluene (10 mL), and 1-octadecene **44** (291 μ L, 0.8 mmol) were added. The mixture was heated at reflux temperature under argon atmosphere for 24 h. The cooled reaction was concentrated under reduced pressure to afford a yellow oil which was purified by column chromatography performed using silica gel using a gradient of hexane:EtOAc. The final compound was obtained as a colourless oil (75 mg, 0.088 mmol, 11% yield).

II. Route B

Synthesis of S-C₁₈-functionalised tris-thiol 45²



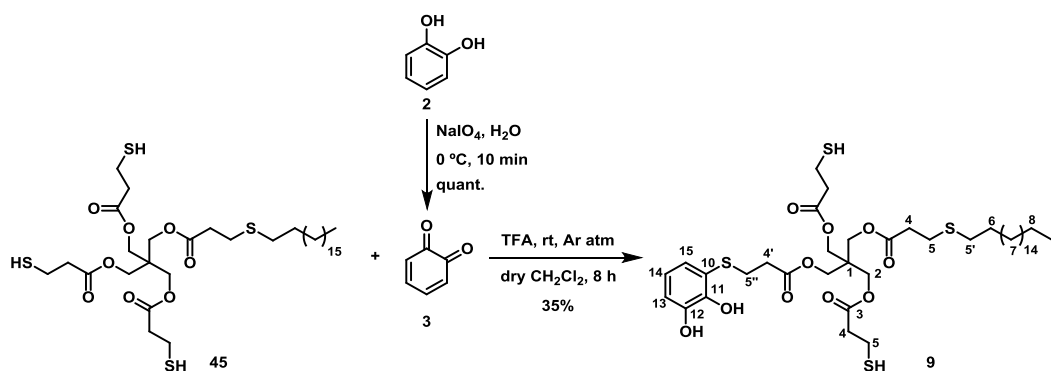
AIBN (180 mg, 1.1 mmol) was dissolved in the minimum volume of dry toluene. Pentaerythritol tetrakis(3-mercaptopropionate) **1** (2.541 g, 5.2 mmol) was dissolved in dry toluene (30 mL). AIBN solution and 1-octadecene **44** (1.8 mL, 5.0 mmol) were added into the pentaerythritol tetrakis(3-mercaptopropionate) solution. The mixture was heated at 80 °C under argon atmosphere for 8 h. The cooled reaction was concentrated under reduced pressure to afford a yellow oil. The mixture was purified by column chromatography through silica gel using a gradient of hexane:EtOAc as eluent to obtain title compound **45** as a colourless oil (1.519 g, 2.0 mmol, 41% yield).

$^1\text{H NMR}$ (400 MHz, CDCl_3) δ 4.16 (s, 8H, H-2), 2.73 (m, 6H, H-5), 2.64 (m, 8H, H-4), 2.48 (t, $J = 7.1$ Hz, 4H, H-5'), 1.60 (t, $J = 7.8$ Hz, 3H, -SH), 1.53 (q, $J = 7.2$ Hz, 2H, H-6), 1.42-1.08 (bs, 30H, H-7, H-8), 0.84 (t, $J = 7.1$ Hz, 3H, H-9).

$^{13}\text{C NMR}$ (100.6 MHz, CDCl_3) δ 171.9 (C-3), 171.5 (C-3), 171.4 (C-3), 171.0 (C-3), 62.1 (C-2), 38.3 (C-4), 34.6 (C-1), 31.9 (C-4'), 29.7 (C-6, C-7), 26.9 (C-5'), 22.7 (C-8), 19.7 (C-5), 14.1 (C-9).

HRMS (HR-EI) calcd. $[\text{C}_{35}\text{H}_{64}\text{O}_8\text{S}_4\text{Na}]^+$: 763.3379; found: 763.3382.

Synthesis of C_{18} -functionalised building block **9**¹



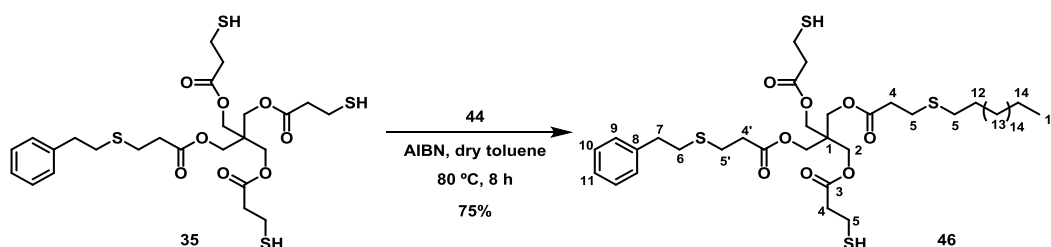
A solution of pyrocatechol **2** (110 mg, 1 mmol) in the minimum value of Et_2O was added into a solution of NaIO_4 (265 mg, 2.9 mmol) in H_2O (34 mL) cooled down to 0°C . The final mixture was stirred for 10 min. The resulting quinone **3** was extracted with dry CH_2Cl_2 (3 x 34 mL) in a quantitative manner. The organic extracts were dried with Na_2SO_4 anhydrous and filtered. In the meantime, a solution of aliphatic chain precursor S-C_{18} -functionalised tris-thiol **45** (693 mg, 0.9 mmol) in dry CH_2Cl_2 (2.5 mL) with TFA (0.22 mL, 2.9 mmol) was prepared under an inert atmosphere. Then, the solution containing the quinone was added into the solution containing S-C_{18} -functionalised tris-thiol **45**. The resulting mixture was stirred at rt under inert atmosphere for 8 h in the dark. After this time, the solvent and TFA were removed under vacuum. The resulting oil was purified by column chromatography through silica gel using a gradient of hexane:EtOAc affording $\text{S,S}'$ -catechol- C_{18} -bis-thiol **9** (268 mg, 0.323 mmol, 35% yield).

$^1\text{H NMR}$ (400 MHz, CDCl_3) δ 7.00 (dd, $J = 8.0$, 1.6 Hz, 1H, H-15), 6.95 (dd, $J = 8.0$, 1.6 Hz, 1H, H-13), 6.81 (td, $J = 8.0$, 2.5 Hz, 1H, H-14), 4.20 (s, 8H, H-2), 3.03 (t, $J = 7.1$ Hz, 2H, H-5'), 2.73 (m, 6H, H-5), 2.64 (m, 6H, H-4), 2.56 (t, $J = 7.1$ Hz, 4H, H-4', H-5''), 1.66 (t, $J = 8.3$ Hz, 2H, -SH), 1.60 (q, $J = 7.2$ Hz, 2H, H-6), 1.43-1.18 (bs, 30H, H-7, H-8), 0.90 (t, $J = 7.2$ Hz, 3H, H-9).

^{13}C NMR (100.6 MHz, CDCl_3) δ 172.0 (C-3), 171.6 (C-3), 171.1 (C-3), 170.8 (C-3), 145.1 (C-11), 144.2 (C-12), 127.0 (C-14), 126.0 (C-10), 121.2 (C-15), 117.2 (C-13), 62.6 (C-2), 42.5 (C-1), 38.5 (C-4'), 31.9 (C-4), 29.7 (C-6, C-7), 26.9 (C-5', C-5''), 22.7 (C-5), 19.6 (C-8), 14.1 (C-9).

HRMS (HR-EI) calcd. $[\text{C}_{41}\text{H}_{68}\text{O}_{10}\text{S}_4\text{Na}]^+$: 872.3604; found: 872.3593.

Synthesis of C_{18} -functionalised styrenic building block **46**²



A solution of AIBN (48 mg, 0.29 mmol) in dry toluene (8 mL), and 1-octadecene **44** (0.4 mL, 1.1 mmol) were added into a solution of *S*-styrene tris-thiol **35** (740 mg, 1.2 mmol) in dry toluene (5 mL). The reaction mixture was heated at 80 °C under argon atmosphere for 8 h. The cooled reaction was concentrated by reduced pressure to afford a yellowish oil which was purified by column chromatography performed using silica gel with a gradient of hexane:EtOAc (696 mg, 0.823 mmol, 75% yield).

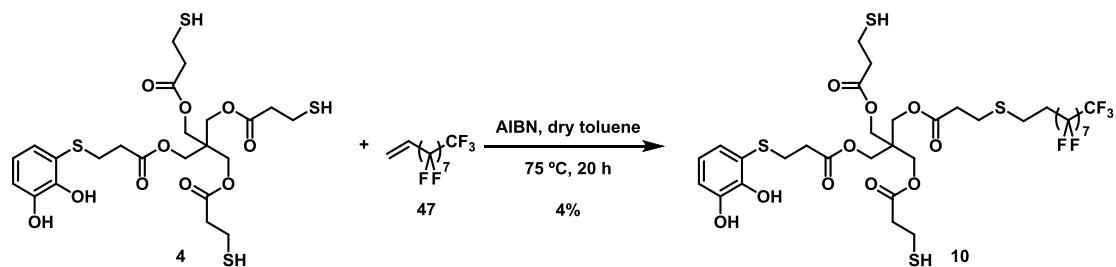
^1H NMR (400 MHz, CD_2Cl_2) δ 7.31-7.16 (m, 5H, H-9, H-10, H-11), 4.15 (s, 8H, H-2), 2.87 (t, $J = 7.2$ Hz, 6H, H-5', H-6, H-7), 2.75 (m, 8H, H-5, H-12), 2.62 (m, 6H, H-4), 2.50 (t, $J = 7.2$ Hz, 2H, H-4'), 1.65 (t, $J = 8.3$ Hz, 2H, -SH), 1.56 (q, $J = 7.0$ Hz, 2H, H-13), 1.30-1.17 (bs, 30H, H-14, H-15), 0.87 (t, $J = 7.0$ Hz, 3H, H-16).

^{13}C NMR (100.6 MHz, CDCl_3) δ 171.9 (C-3), 171.4 (C-3), 171.3 (2 C-3), 171.1 (C-3), 140.4 (C-8), 128.6 (C-10), 128.4 (C-9), 126.6 (C-11), 62.6 (C-2), 42.0 (C-1), 38.5 (C-4'), 36.5 (C-4), 33.9 (C-6), 33.1 (C-7), 32.0 (C-12), 29.9 (C-13, C-14), 27.0 (C-5'), 22.9 (C-5), 20.0 (C-15), 14.5 (C-16).

HRMS (HR-EI) calcd $[\text{C}_{43}\text{H}_{72}\text{O}_8\text{S}_4]^+$; 844.2897; found: 844.4110.

Synthesis of fluorine-functionalised building block 10

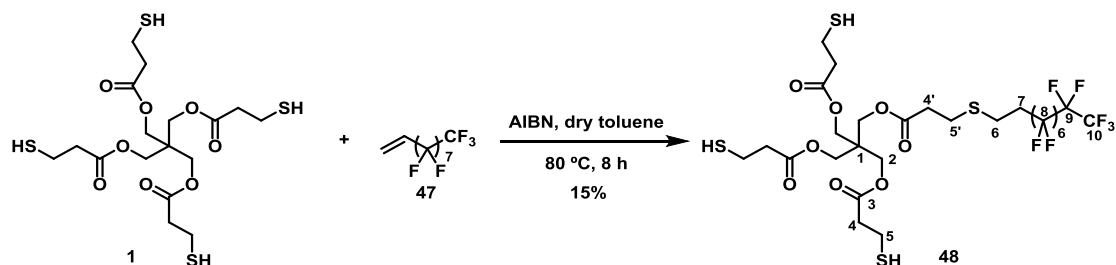
I. Route A²



A solution of 1*H*, 1*H*, 2*H*-perfluoro-1-decene **47** (183 μ L, 0.36 mmol) in dry toluene (6 mL) was added into a Schlenk containing AIBN (22 mg, 0.13 mmol) and S-catechol tris-thiol **4** (307 mg, 0.5 mmol). The mixture was heated at 75 °C for 20 h. under argon atmosphere. The cooled reaction was concentrated under reduced pressure to afford a yellowish oil which was purified by column chromatography performed using silica gel using a gradient of hexane:EtOAc. The final compound was obtained as a colourless oil (15 mg, 0.014 mmol, 4% yield).

II. Route B

Synthesis of *S*-fluorine-functionalised tris-thiol **48**²



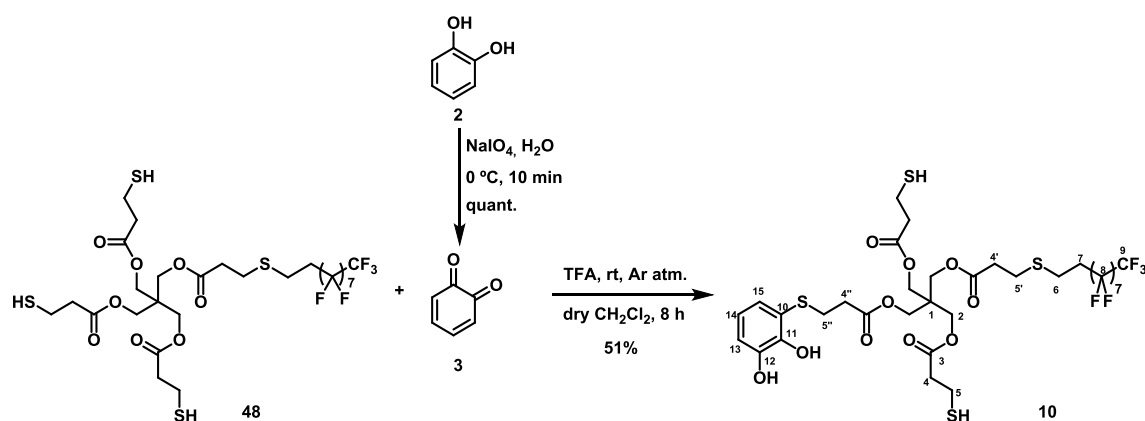
AIBN (120 mg, 0.73 mmol) solution in dry toluene (4 mL), and 1*H*, 1*H*, 2*H*-perfluoro-1-decene **47** (0.7 mL, 2.6 mmol) were added into a solution of pentaerythritol tetrakis(3-mercaptopropionate) **1** (2.083 g, 4.3 mmol) in dry toluene (20 mL). The mixture was heated at 80 °C under argon atmosphere and 3 h later 1*H*, 1*H*, 2*H*-perfluoro-1-decene **47** (0.3 mL, 1.1 mmol) were added, and the reaction mixture was left at 80 °C 5 h more. The cooled reaction was concentrated under reduced pressure to afford a yellow oil. The mixture was purified by column chromatography through silica gel using a gradient of hexane:EtOAc as eluent to obtain title compound **48** as a non-coloured oil (511 g, 0.547 mmol, 15% yield).

¹H NMR (360 MHz, CDCl₃) δ 4.18 (s, 8H, H-2), 2.91 (t, J = 6.31 Hz, 4H, H-5', H-6), 2.83-2.73 (m, 8H, H-4, H-4'), 2.72-2.64 (m, 6H, H-5), 1.64 (t, J = 7.8 Hz, 3H, -SH), 1.29 (m, 2H, H-7).

^{19}F NMR (235 MHz, CDCl_3) δ -114.64 (F-10), -122.30 (F-8), -123.07 (F-8), -123.72 (F-8), -126.50 (F-9).

^{13}C NMR (90.5 MHz, CDCl_3) δ 171.7 (C-3), 171.2 (C-3), 62.5 (C-2), 42.2 (C-1), 38.4 (C-4), 33.9 (C-4'), 32.9 (C-5'), 31.1 (C-7), 29.9 (C-6), 19.7 (C-5).

Synthesis of fluorine-functionalised building block **10**¹



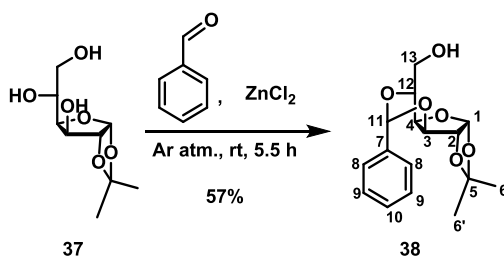
A solution of pyrocatechol **2** (85 mg, 0.77 mmol) in the minimum volume of Et_2O was added into a solution of NaIO_4 (186 mg, 0.87 mmol) in H_2O (30 mL) cooled down to $0\text{ }^\circ\text{C}$. The final mixture was stirred for 10 min. The resulting quinone **3** was extracted with dry CH_2Cl_2 (3 x 30 mL) in a quantitative manner. The organic extracts were dried with Na_2SO_4 anhydrous and filtered. In the meantime, a solution of fluorinated intermediate **48** (511 mg, 0.55 mmol) in dry CH_2Cl_2 (12 mL) with TFA (142 μL , 1.71 mmol) was prepared under an inert atmosphere. Then, the solution containing quinone was added into the solution containing S-fluorine-functionalised tris-thiol **48**. The resulting mixture was stirred at rt under inert atmosphere for 8 h in the dark. After this time, the solvent and TFA were removed under vacuum. The resulting oil was purified by column chromatography performed using silica gel with a gradient of hexane:EtOAc affording S,S'-catechol-fluorinated chain bis-thiol **10** (294 mg, 0.28 mmol 51% yield).

^1H NMR (360 MHz, CDCl_3) δ 7.02-6.88 (m, 2H, H-13, H-15), 6.79 (m, 1H, H-14), 4.19 (s, 8H, H-2), 3.22-2.40 (m, 16H, H-4, H-4', H-5, H-5'), 1.77 - 1.55 (m, 6H, -SH, H-6, H-7).

^{19}F NMR (235 MHz, CDCl_3) δ -114.74 (F-10), -122.14 (F-8), -123.21 (F-8), -123.79 (F-8), -126.56 (F-9).

^{13}C NMR (90.5 MHz, CDCl_3) δ 173.6 (C-3), 171.3 (C-3), 145.2 (C-12), 135.3 (C-11), 127.0 (C-14), 125.1 (C-10), 121.2 (C-15), 117.2 (C-13), 66.9 (C-2), 42.2 (C-1), 38.1 (C-4), 34.1 (C-7), 32.1 (C-4''), 29.8 (C-5''), 27.2 (C-4'), 24.6 (C-5'), 22.8 (C-6), 19.8 (C-5).

6.2.2. SYNTHESIS OF GLUCOSE DERIVATIVES

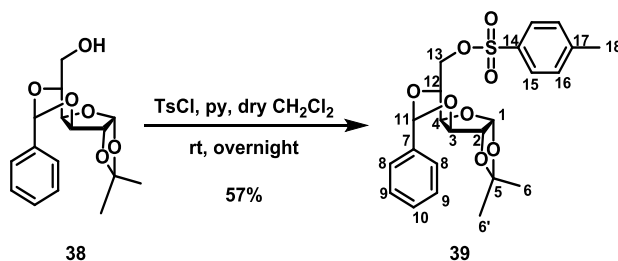
Synthesis of protected glucofuranose derivative **38**¹⁵

1,2-*O*-isopropylidene- α -D-glucofuranoside **37** (1.012 g, 4.6 mmol) and ZnCl_2 (1.325 g, 9.4 mmol) were mixed in benzaldehyde (4.5 mL, 44 mmol) at rt. The mixture was stirred for 5.5 h under argon atmosphere, and then diluted with EtOAc (7 mL). The resulting solution was washed with brine (4 x 10 mL), dried over anhydrous Na_2SO_4 , filtered, evaporated at 35 °C, and finally recrystallised from hexane at 4 °C to afford the final protected glucofuranose derivative **38** (808 mg, 2.6 mmol, 57% yield).

$^1\text{H NMR}$ (360 MHz, CD_3OD) δ 7.49-7.41 (m, 2H, H-8), 7.40-7.29 (m, 3H, H-9, H-10), 5.99 (d, J = 3.72 Hz, 1H, H-1), 5.93 (s, 1H, H-11), 4.64 (d, J = 3.72 Hz, 1H, H-2), 4.54 (d, J = 2.24 Hz, 1H, H-4), 4.18 (m, 2H, H-3, H-12), 3.98 (m, 2H, H-13), 1.48 (s, 3H, H-6), 1.33 (s, 3H, H-6').

$^{13}\text{C NMR}$ (90.5 MHz, CD_3OD) δ 139.8 (C-7), 130.0 (C-10), 129.2 (C-9), 127.6 (C-8), 113.2 (C-5), 106.5 (C-1), 95.8 (C-11), 85.4 (C-3), 79.2 (C-2), 75.2 (C-4), 74.5 (C-12), 62.8 (C-13), 27.0 (C-6), 26.3 (C-6').

HRMS (HR-EI) calcd. for $[\text{C}_{16}\text{H}_{20}\text{O}_6\text{Na}]^+$: 331.1151; found: 331.1158.

Synthesis of tosyl-functionalised glucofuranose derivative **39**¹¹

To a stirred solution of *p*-toluenesulfonyl chloride (0.8996 g, 4.7 mmol) in dry CH_2Cl_2 (7 mL) and anhydrous pyridine (2 mL, 24.7 mmol), a solution of protected glucofuranose derivative **38** (0.4832 g, 1.6 mmol) in dry CH_2Cl_2 (6 mL) was added at rt. The reaction mixture was stirred overnight under inert atmosphere. When the reaction was finished, distilled water (25 mL)

was added and the mixture was stirred for 4 h more. After that time, the organic phase was washed with brine (4 x 15 mL), dried with anhydrous Na₂SO₄, filtered, and concentrated under vacuum. The final product was recrystallised with hexane to afford a white powder, corresponding to the tosyl-functionalised glucofuranose derivative **39** (414 mg, 0.89 mmol, 57% yield).

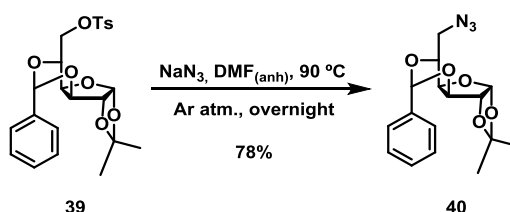
¹H NMR (360 MHz, CD₃OD) δ 7.83 (d, *J* = 8.17 Hz, 2H, H-15), 7.40 (d, *J* = 8.17 Hz, 2H, H-16), 7.33 (bs, 5H, H-8, H-9, H-10), 5.94 (d, *J* = 3.70 Hz, 1H, H-1), 5.67 (s, 1H, H-11), 4.65 – 4.50 (m, 2H, H-2, H-13), 4.48 – 4.27 (m, 3H, H-3, H-4, H-12), 3.99 (m, 1H, H-13'), 2.42 (s, 3H, H-18), 1.45 (s, 3H, H-6), 1.31 (s, 3H, H-6').

¹³C NMR (90.5 MHz, CD₃OD) δ 139.2 (C-17), 134.1 (C-14), 131.3 (C-7), 130.0 (C-10), 129.1 (C-15, C-16), 129.0 (C-9), 127.3 (C-8), 113.2 (C-5), 106.4 (C-1), 95.5 (C-11), 85.4 (C-2, C-3), 79.1 (C-4), 73.0 (C-12), 70.2 (C-13), 27.0 (C-6), 26.4 (C-6'), 21.7 (C-18).

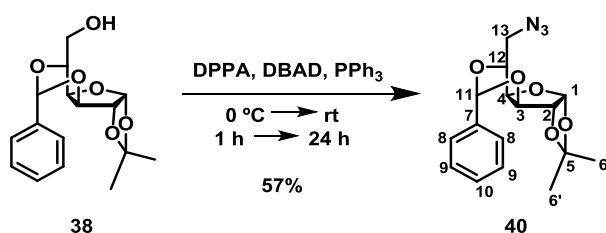
HRMS (HR-EI) calcd. for [C₂₃H₂₆O₈SNa]⁺: 485.1236; found: 485.1246.

Synthesis of azide-functionalised glucofuranose derivative **40**

I. From tosyl-functionalised glucofuranose derivative **39**¹¹



To a solution of tosyl-functionalised glucofuranose derivative **39** (297 mg, 0.64 mmol) in anhydrous DMF (18 mL), sodium azide (0.316 mg, 4.805 mmol) was added, and the mixture was stirred overnight at 90 °C under argon atmosphere. After cooling down to rt and filtration, DMF was removed under vacuum. The crude product was dissolved in CH₂Cl₂ (20 mL) and washed with brine (4 x 20 mL). The organic layer was dried over anhydrous Na₂SO₄, filtered and the solvent removed under vacuum. The final product was purified by column chromatography performed using silica gel with a mixture of hexane:EtOAc (20:1) to afford the product as a yellow oil (167 mg, 0.5 mmol, 78% yield).

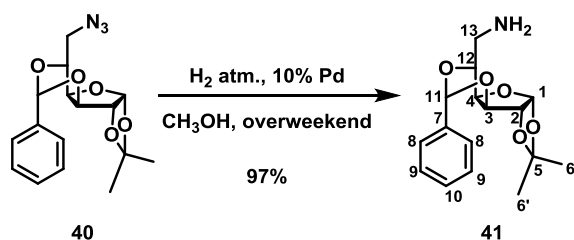
II. Mitsunobu reaction¹⁶

DBAD (559 mg, 2.4 mmol) was added in one portion into a solution of PPh_3 (301 mg, 2.29 mmol) in dry toluene (20 mL) at 0 °C. The mixture was stirred at this temperature for 1 h. Afterwards, DPPA (407 μL , 1.6 mmol) and a solution of the protected glucofuranose derivative **38** (521 mg, 1.7 mmol) in dry toluene (17 mL) were added, and the reaction mixture was left stirring at rt for 24 h. The crude was filtered over Celite[®] and the solvent removed under vacuum. The final product was purified by column chromatography performed using silica gel with a mixture of hexane:EtOAc (20:1) to afford the final product **40** as a yellow oil (304 mg, 0.92 mmol, 57% yield).

¹H NMR (360 MHz, CD_3OD) δ 7.48-7.43 (m, 2H, H-8), 7.36-7.32 (m, 3H, H-9, H-10), 5.98 (d, J = 3.70 Hz, 1H, H-1), 5.87 (s, 1H, H-11), 4.65 (d, J = 3.70 Hz, 1H, H-2), 4.53 (d, J = 1.73 Hz, 1H, H-4), 4.34 (dd, J = 9.06, 4.95 Hz, 1H, H-12), 4.02 (d, J = 9.50, 1H, H-3), 3.99 (d, J = 10.48 Hz, 1H, H-13), 3.50 (dd, J = 13.29, 5.04 Hz, 1H, H-13'), 1.49 (s, 3H, H-6), 1.33 (s, 3H, H-6').

¹³C NMR (90.5 MHz, CD_3OD) δ 139.2 (C-7), 130.0 (C-10), 129.1 (C-9), 127.4 (C-8), 113.2 (C-5), 106.5 (C-1), 94.7 (C-11), 85.2 (C-2, C-3), 78.7 (C-4), 74.6 (C-12), 50.9 (C-13), 27.0 (C-6), 26.4 (C-6').

HRMS (HR-EI) calcd. for $[\text{C}_{16}\text{H}_{19}\text{N}_3\text{O}_5\text{Na}]^+$: 356.1217; found: 356.1222.

Synthesis of amino-glucofuranose derivative **41**¹⁷

Azide-functionalised glucofuranose **40** (297 mg, 0.89 mmol) was dissolved in CH_3OH (59 mL), and 10% in weight of palladium on activated charcoal (30 mg) was added. The reaction mixture was stirred under hydrogen atmosphere at rt overweekend. Afterwards, the solution was

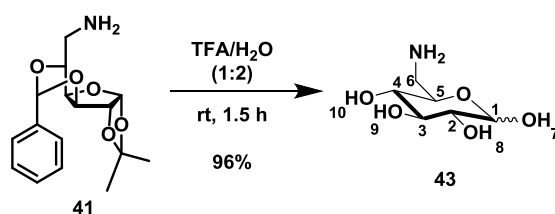
filtered over Celite® and the solvent removed under vacuum to furnish the desired amino-glucofuranose derivative **41** (266 mg, 0.87 mmol, 97% yield).

¹H NMR (400 MHz, CD₃OD) δ 7.48-7.43 (m, 2H, H-8), 7.35-7.30 (m, 3H, H-9, H-10), 5.97 (d, *J* = 3.75 Hz, 1H, H-1), 5.74 (s, 1H, H-11), 4.61 (d, *J* = 3.75 Hz, 1H, H-2), 4.47 (d, *J* = 1.91 Hz, 1H, H-4), 4.17 (dd, *J* = 9.81, 5.11 Hz, 1H, H-12), 4.0 (d, *J* = 1.36, 1H, H-3), 3.24 (d, *J* = 3.66 Hz, 1H, H-13), 2.86 (dd, *J* = 13.61, 5.38 Hz, 1H, H-13'), 1.47 (s, 3H, H-6), 1.30 (s, 3H, H-6').

¹³C NMR (100.6 MHz, CD₃OD) δ 139.6 (C-7), 130.0 (C-10), 129.2 (C-9), 127.6 (C-8), 113.2 (C-5), 106.5 (C-1), 94.1 (C-11), 85.2 (C-3), 78.4 (C-2), 76.5 (C-4), 74.7 (C-12), 41.1 (C-13), 27.1 (C-6), 26.5 (C-6').

HRMS (HR-EI) calcd. for [C₁₆H₂₂NO₅]⁺: 308.1496; found: 308.1496.

Synthesis of amino-glucofuranose derivative **43**¹⁵



To a stirred solution of protected amino-glucofuranose derivative **41** (28.3 mg, 0.092 mmol) in MilliQ H₂O (6 mL), TFA (3 mL, 39.2 mmol) was added. The mixture was stirred at rt for 1.5 h. The reaction mixture was washed with CH₂Cl₂ (3 x 10 mL) and concentrated under vacuum. The deprotected amino-glucofuranose derivative **43** was obtained as an orange oil (27.1 mg, 0.092 mmol, 96% yield).

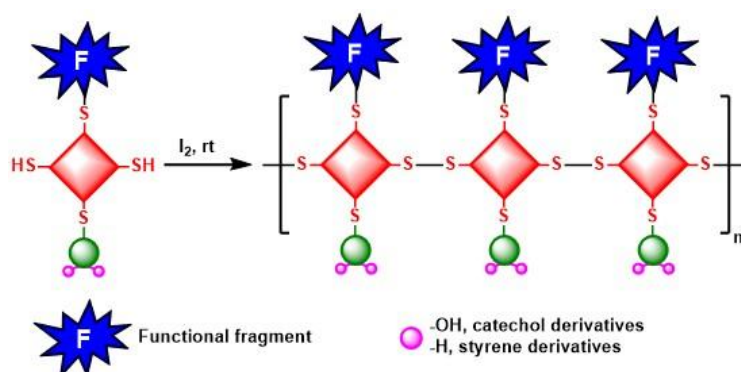
¹H NMR (360 MHz, CD₃OD) δ 5.11 (d, *J* = 3.64 Hz, 1H, H-1), 4.48 (d, *J* = 7.83 Hz, 1H, H-5), 3.93 (td, *J* = 9.16, 3.19 Hz, 1H, H-2), 3.63 (t, *J* = 9.21 Hz, 1H, H-6), 3.45 (td, *J* = 9.22, 3.08 Hz, 1H, H-3), 3.36 (d, *J* = 3.78 Hz, 1H, H-6'), 3.33 (m, 1H, H-4), 3.14 (m, 3H, H-8, H-9, H-10), 2.96 (m, 1H, H-7).

¹³C NMR (90.5 MHz, CD₃OD) δ 98.4 (C-1), 77.6 (C-3), 76.0 (C-2), 74.4 (C-5), 73.5 (C-4), 42.2 (C-6).

HRMS (HR-EI) calcd. for [C₆H₁₄NO₅]⁺: 180.0872; found: 180.0869.

6.3. METHODOLOGIES

Oxidative polymerisation of functional bis-thiol building blocks with iodine



I. *Ex situ* polymerisation in solution¹⁸

As a general procedure, 1.1 equiv. of a solution of 35 mM of resublimed iodine in EtOH 96% was added drop-wise into a ~ 7 mM solution of functional bis-thiol building blocks (**5**, **6**, **7**, **8**, **9**, **10**, **36** and **46**) in EtOH 96%. The reaction mixture was stirred for 1 h at rt, after which a yellowish solid precipitated. The supernatant was decanted, and the solid washed with fresh EtOH 96% three times, and dried under vacuum.

(*Note*: starting building blocks (**5**, **6**, **7**, **8**, **9**, **10**, **36** and **46**) contained roughly 3-5% of a doping catechol-functionalised sulphur-based molecule to favour the formation of polymers and avoid the intramolecular S-S bond formation).

Table 6.1. Polymerisation reactions' yields of building blocks **5**, **6**, **7**, **8**, **9**, **10**, **36** and **46**, and copolymers **C6-8** and **C8-9** based on the amount of the solid precipitated.

Product from the polymerisation reaction	Yield (%)
P5 (mPEG-functionalised catecholic derivative, (-acryl))	45%
P6 (mPEG-functionalised catecholic derivative, (-allyl))	28%
P7 (HOOC-PEG-functionalised catecholic derivative, (-acryl))	41%
P8 (fluorescein-functionalised catecholic derivative)	34%
P9 (C ₁₈ -functionalised catecholic derivative)	39%
P10 (fluorine-functionalised catecholic derivative)	48%
P36 (fluorescein-functionalised catecholic derivative)	29%
P46 (C ₁₈ -functionalised styrenic derivative)	60%

Copolymers	Yield (%)
C6-8	48%
C8-9a	64%
C8-9b	64%
C8-9c	64%
C8-9d	65%

II. *In situ* polymerisation

50 mg of resublimed iodine were placed at the bottom of a 20 mL vial. Test slides coated with the mPEGylated monomer **6**, or, C₁₈-functionalised monomer **9** were placed face-down on top of vials and left standing overnight. Then, slides were washed three times of EtOH 96% (3 x 3 mL) to remove the excess of adsorbed iodine, and dried in a gentle flux of argon.

Static water contact angle measurements

Static contact angle measurements on coated substrates (metals, glass, cotton and polyester) were carried at rt out with Milli-Q water droplets (*ca.* 5 μ L) by means of the sessile-drop technique. Reported values arise from averaging CA measurements on three different spots of each sample.

Coating of solid macroscopic substrates

All substrates were cut into 1.5 x 1.5 cm² square slides. Aluminium, copper and stainless steel slides were cleaned by sonicating successively in HPLC-grade acetone, EtOH 96% and Milli-Q water (10 min each), and dried in a gentle flux of argon. Glass slides were cleaned with a plasma cleaner machine (400 W, 5 min). Clean slides were submerged into a ~ 7 mM solution of the corresponding derivatives in HPLC-grade CH₂Cl₂ (for **P6**, **P9**, **P10** and **P46**), or, HPLC-grade acetone (4 mL) (for **P8** and **P36**), and left overnight without stirring. Finally, slides were washed three times with fresh HPLC-grade solvent (CH₂Cl₂ or acetone), and dried in a gentle flux of argon.

Coating of MSNPs

Into a suspension of MSNPs (10 mg) in HPLC-grade CH₂Cl₂, or, acetone (1 mL) was added a solution of the corresponding derivative (0.007 mmol) in HPLC-grade CH₂Cl₂ (for **P5** and **P6**), or, HPLC-grade acetone (for **P8** and **P36**) (1 mL). The mixture was left stirring at 300 rpm at rt

overnight. After this time, the final dispersion was centrifuged at 14000 rpm for 2 min, and the coated NPs washed with fresh HPLC-grade solvent (3 x 2 mL).

Coating of cotton and polyester cloths

A piece of *ca.* 1.5 x 1.5 cm² of cotton and polyester cloths ($\sigma = 25 \text{ mg/cm}^2$) were submerged into a $\sim 7 \text{ mM}$ solution of the corresponding derivative in HPLC-grade acetone (for **P8**), or, HPLC-grade CH₂Cl₂ (**P9**, **P10** and **P46**) (4 mL) and left overnight without stirring. The coated textiles were then washed with fresh HPLC solvent (CH₂Cl₂ or acetone) (3 x 2 mL), and dried in a gentle flux of argon.

Oil absorption in a o/w mixtures

TDC, or, olive oil (4 g) coloured with Disperse Red 13 (200 ppm) were mixed with distilled water (15 mL). A piece of 1.5 x 1.5 cm² of cotton cloth ($\sigma = 25 \text{ mg/cm}^2$, either pristine or coated with C₁₈-functionalised derivative **P9**) put submerged in the o/w mixture for 15 sec, taken out and left hanging until the excess of liquid drained completely.

Filtration of a o/w mixture

A round piece ($\emptyset \sim 2 \text{ cm}$) of cotton cloth ($\sigma = 25 \text{ mg/cm}^2$), either pristine or coated with C₁₈-functionalised derivative **P9**, was carefully placed on the mouth of a glass vial and slightly folded inwards. A 1:1 (v/v) hand-shaken mixture of distilled water and a solution of Disperse red 13 in Miglyol® 840 was carefully added drop-wise on the textile until liquid started to filter through it.

Preparation of MNPs

Fe(acac)₃ (0.441 g, 1.24 mmol), sodium oleate (0.2133 g, 0.68 mmol), and oleic acid (1.485 g, 5.26 mmol) in a mixture of solvents composed by dibenzyl ether (10 mL), 1-octadecene (10 mL), and 1-tetradecene (3 mL) were heated up to 110 °C and kept at this temperature during 1.5 h under vacuum. During this time, reactive intermediates were formed. The reaction mixture was then heated up to 290 °C with a heating rate of 3 °C/min, kept at this temperature during 1 h under argon flow. In this step, the nucleation and the subsequent growing of the NPs took place. Finally, the reaction mixture was cooled down to 50 °C. To purify the MNPs, isopropanol (40 mL) and acetone (40 mL) were added to the reaction mixture, which was centrifuged (10000 rpm, 12 min) to separate the MNPs from the supernatant. The MNPs were resuspended in a mixture of CHCl₃ (10 mL), acetone (40 mL), and isopropanol (40 mL), and the

same centrifugation conditions were applied. Finally, the MNPs were redispersed in CHCl_3 (~6.5 mg/mL).

Coating of MNPs

Into a suspension of MNPs (6.5 mg/mL, 2.6 mL, 17 mg), a solution of the corresponding cat-PEG derivative **P7** (10 mg, 0.0038 mmol) in HPLC-grade CHCl_3 (1.1 mL) was added. The reaction mixture was left stirring at rt for 3-4 days. The final MNPs were transferred to the aqueous phase, washed with CHCl_3 once, and the solvent removed under vacuum.

Coupling reaction in a heterogeneous phase

As a general procedure, into a suspension of MNPs@**P7** (12 mg, 0.0046 mmol) cooled down to 0 °C, amino-glucofuranose derivative **41** (15.4 mg, 0.05 mmol) and DMAP (3.4 mg, 0.028 mmol) were added. After 10 min stirring at 0 °C, EDCI (20.8 μL , 0.115 mmol) was added and the reaction mixture was stirred at rt for 3-4 days under argon atmosphere. The final MNPs were transferred to the aqueous phase, washed with CHCl_3 once, and the solvent removed under vacuum. The resulting nanoparticles were treated with DCI 35% w/w in H_2O to be analysed by ^1H NMR technique.

In the case of working with deprotected amino-glucofuranose derivative **43**, the procedure followed was the same, but sugar derivative **43** was first dissolved in the minimum volume of CH_3OH with 18 equiv. of DIPEA, and then added into MNPs@**P7** suspension.

Deprotection reaction in a heterogeneous phase

As a general procedure, to a ~ 1.5 mg/mL suspension of MNP@cat-PEG-glucofuranose a mixture of $\text{AcOH}/\text{H}_2\text{O}$ with the corresponding ratio was added, and the reaction mixture stirred. Afterwards, the aqueous phase was washed with CHCl_3 (x 3) to remove non-polar impurities and evaporated under vacuum. The resulting NPs were treated with DCI 35% w/w in H_2O to be analysed by ^1H NMR technique.

Cytotoxicity assay of C6-8-coated MSNPs

Human SH-SY5Y cells were cultured in DMEM/F-12 culture medium supplemented with 10% FBS and 1% antibiotic-antimycotic solution (Gibco-BRL), and incubated at 37 °C in a humidified atmosphere with 5% CO_2 . Cells were seeded into a 96-well plate at a cell density of 3.0×10^3 cells per well and then incubated for 24 h. **C6-8**-coated MSNPs were resuspended in the

medium discussed above to achieve the different concentrations used in this assay: 0, 1, 5, 10, 25, 50, 100 and 200 $\mu\text{g}/\text{mL}$. Then, the cells were incubated at 37 °C, in a humidified atmosphere with 5% CO₂ and 98% humidity for 24 h. The cytotoxicity effect was measured after 24 h treatment employing the PrestoBlue cell viability reagent (ThermoFisher). PrestoBlue (10 μL ; resazurin-based solution) was added to each well. After a two-hour incubation period (37 °C, 5% CO₂, 98% humidity), the fluorescence was quantified using a fluorescent multilabel plate reader (Victor3, PerkinElmer) with excitation at $\lambda = 531 \text{ nm}$ and recorded at $\lambda = 572 \text{ nm}$. Cell cytotoxicity was evaluated in terms of cell viability and expressed as a percentage of the control conditions. Each experiment was repeated at least three times and each concentration was tested in at least three replicates.

Internalisation assay of C6-8-coated MSNPs

Human SH-SY5Y cells were cultured in DMEM/F-12 culture medium supplemented with 10% FBS and 1% antibiotic-antimycotic solution (Gibco-BRL), and incubated at 37 °C in a humidified atmosphere with 5% CO₂. Cells were seeded into a 6-well plate with coverslips at a cell density of 1.0×10^4 cells per well and then incubated (37 °C, 5% CO₂, 98% humidity) for 24 h. C6-8-coated MSNPs (200 $\mu\text{g}/\text{mL}$) was then added to 4 of the 6 wells (the other two were used as a negative control). One of the wells with C6-8-coated MSNPs was washed with 1% PBS and its cells were fixed with 4% paraformaldehyde (PFA) for 15 min at rt. The PFA was then removed and PBS 1% was added to the well. This procedure was repeated at 3, 6 and 24 h with one of the wells with C6-8-coated MSNPs. At 6 and 24 h, it was also done with one of the wells without C6-8-coated MSNPs. Afterwards, the samples were blocked by adding a blocking buffer (5% Bovine serum albumin solution in PBS buffer supplemented with 0.1% Triton X-100) (1 mL) and incubating for 1 h at rt. The blocking buffer was then removed and the samples were washed with PBS for 5 min in agitation. Then, the samples were incubated with 4',6-diamidino-2-phenylindole (DAPI; 1/500) for 10 min at rt. After removing DAPI and washing the samples in PBS for 5 min in darkness, the samples were mounted on a drop of ProLong Gold mounting medium (Life Technologies). Finally, immunofluorescence images were collected on an inverted confocal microscope (LEICA SP5). Images were analysed using LAF AS Lite 1.8.1 (Leica) and composed in illustrator 15.0.2.

6.4. REFERENCES

- ¹ Mancebo-Aracil, J.; Casagualda, C.; Moreno-Villaécija, M. A.; Nador, F.; García-Pardo, J.; Franconetti-García, A.; Busqué, F.; Alibés, R.; Esplandiu, M. J.; Ruiz-Molina, D.; Sedó-Vegara, J. *Chem. Eur. J.* **2019**, *25*, 12367-12379.
- ² Font, J.; de March, P.; Busqué, F.; Casas, E.; Benítez, M.; Teruel, L.; García, H. *J. Mater. Chem.* **2007**, *17*, 2336-2343.
- ³ Chan, J. W.; Hoyle, C. E.; Lowe, A. B.; Bowman, M. *Macromolecules*, **2010**, *43*, 6381-6388.
- ⁴ Hooper, R.; West, R. *Macromolecules* **2001**, *34*, 931-936
- ⁵ Zhang, S.; Moussodia, R.-O.; Sun, H.-J.; Leowanawat, P.; Muncan, A.; Nusbaum, C. D.; Chelling, K. M.; Heiney, P. A.; Klein, M. L.; Andre, S. *Angew. Chem. Int. Ed.* **2014**, *53*, 10899-10903.
- ⁶ O'Driscoll, L. J.; Welsh, D. J.; Bailey, S. W. D.; Visontai, D.; Frampton, H.; Bryce, M. R.; Lambert, C. J. *Chem. Eur. J.* **2015**, *21*, 3891-3894.
- ⁷ Zürcher, S.; Wäckerlin, D.; Bethuel, Y.; Malisova, B.; Textor, M.; Tossati, S.; Gademann, K. *J. Am. Chem. Soc.* **2006**, *128*, 1064-1065.
- ⁸ Malisova, B.; Tosatti, S.; Textor, M.; Gademann, K.; Zürcher, S. *Langmuir* **2010**, *26*, 4018-4026.
- ⁹ Auvergne, R.; Morel, M.-H.; Menut, P.; Giani, O.; Guilbert, S.; Robin, J.-J. *Biomacromolecules* **2008**, *9*, 664-671.
- ¹⁰ Weiss, J.; Laschewsky, A. *Langmuir* **2011**, *27*, 4465-4473.
- ¹¹ Mahou, R.; Wandrey, C. *Polymers* **2012**, *4*, 561-589.
- ¹² Kinbara, K.; Muraoka, T.; Wawro, A. M. *Polym. Chem.* **2016**, *7*, 2389-2394.
- ¹³ Chniti, I.; Sanhoury, M. A. K.; Merlet, D.; Chehidi, I. *J. Fluorine Chem.* **2014**, *168*, 223-229.
- ¹⁴ Liu, K. J.; Liu, Y. *New J. Chem.* **2011**, *35*, 1485-1490.
- ¹⁵ Anraku, Y.; Kuwahara, H.; Fukusato, Y.; Mizoguchi, A.; Ishii, T.; Nitta, T.; Matsumoto, Y.; Toh, K.; Miyara, K.; Uchida, S.; Nishina, K.; Osada, K.; Itaka, K.; Nishiyama, N.; Mizusawa, H.; Yamasoba, T.; Yokota, T.; Kataoka, K. *Nat. Commun.* **2017**, *8*, 1-9.
- ¹⁶ Lal, B.; Pramanik, B. N.; Manhas, M. S.; Bose, A. K. *Tetrahedron Lett.* **1977**, *18*, 1977-1980.
- ¹⁷ Bogdan, N. D.; Matache, M.; Meier, V. M.; Dobrota, C.; Dumitru, I.; Roiban, G. D.; Funeriu, D. *P. Chem. Eur. J.* **2010**, *16*, 2170-2180.
- ¹⁸ Danehy, J. P.; Doherty, B. T.; Egan, C. P. *J. Org. Chem.* **1971**, *36*, 2525-2534.

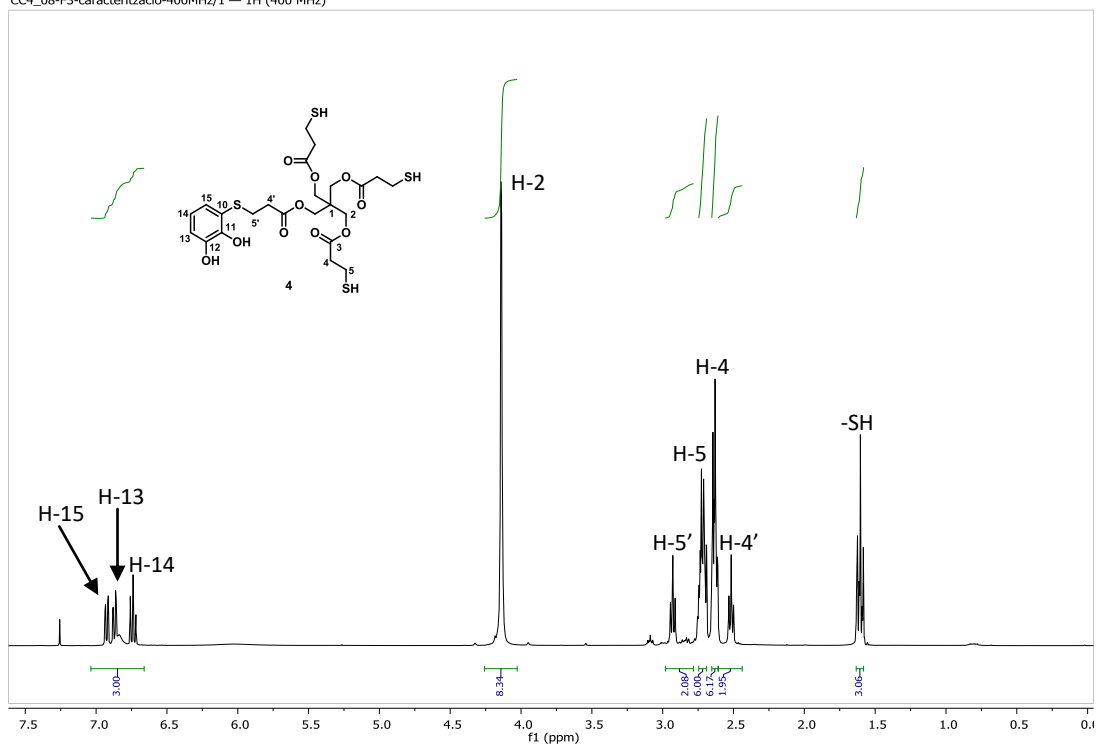
ANNEX

SPECTRA OF SELECTED COMPOUNDS

A1. NMR AND IR SPECTRA

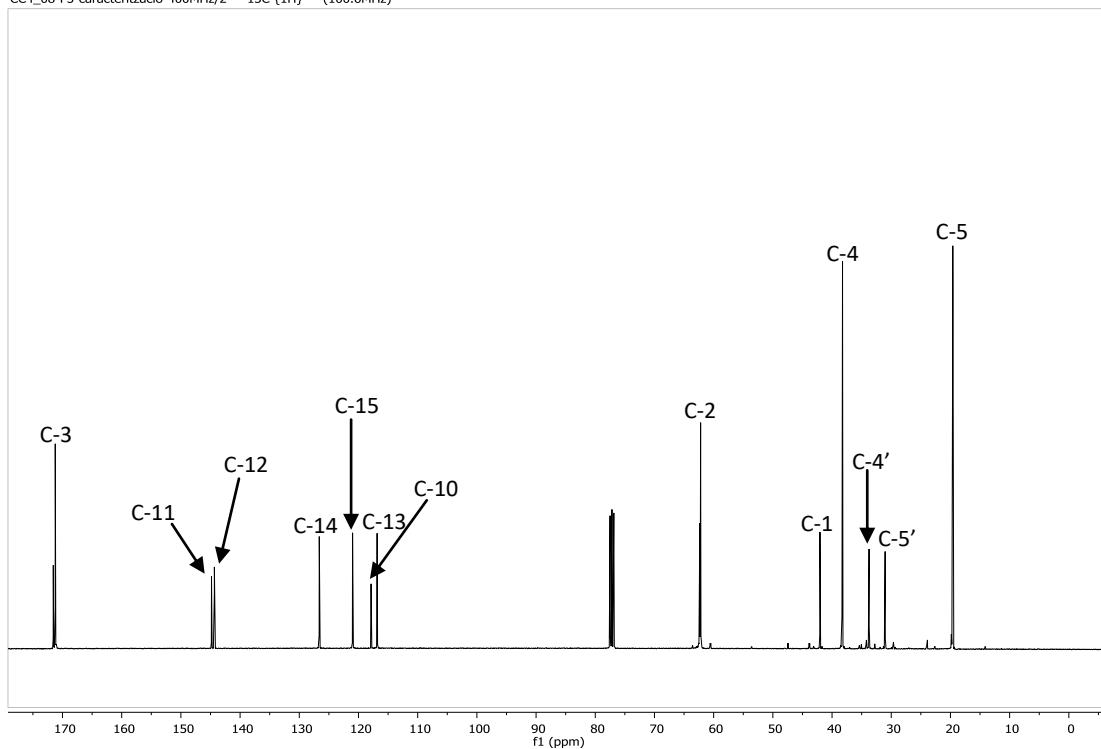
A1.1. Building blocks

CC4_08-F3-caracteritzacio-400MHz/1 — 1H (400 MHz)

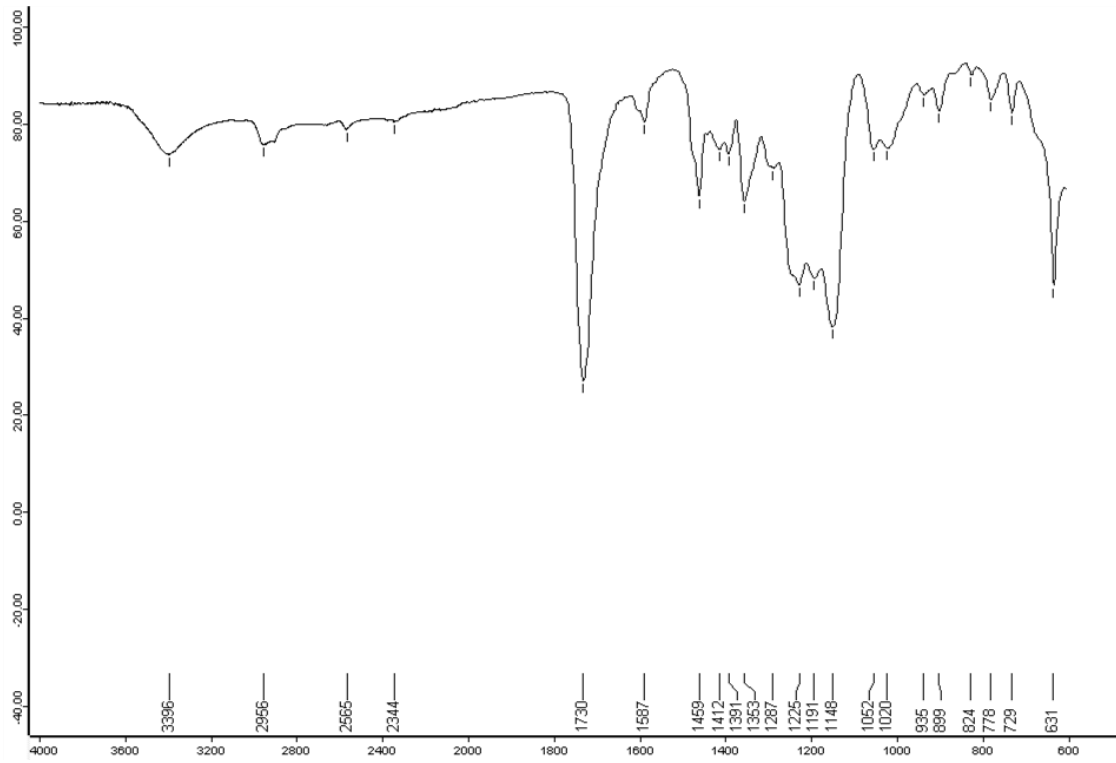


¹H NMR (400 MHz, CDCl₃)

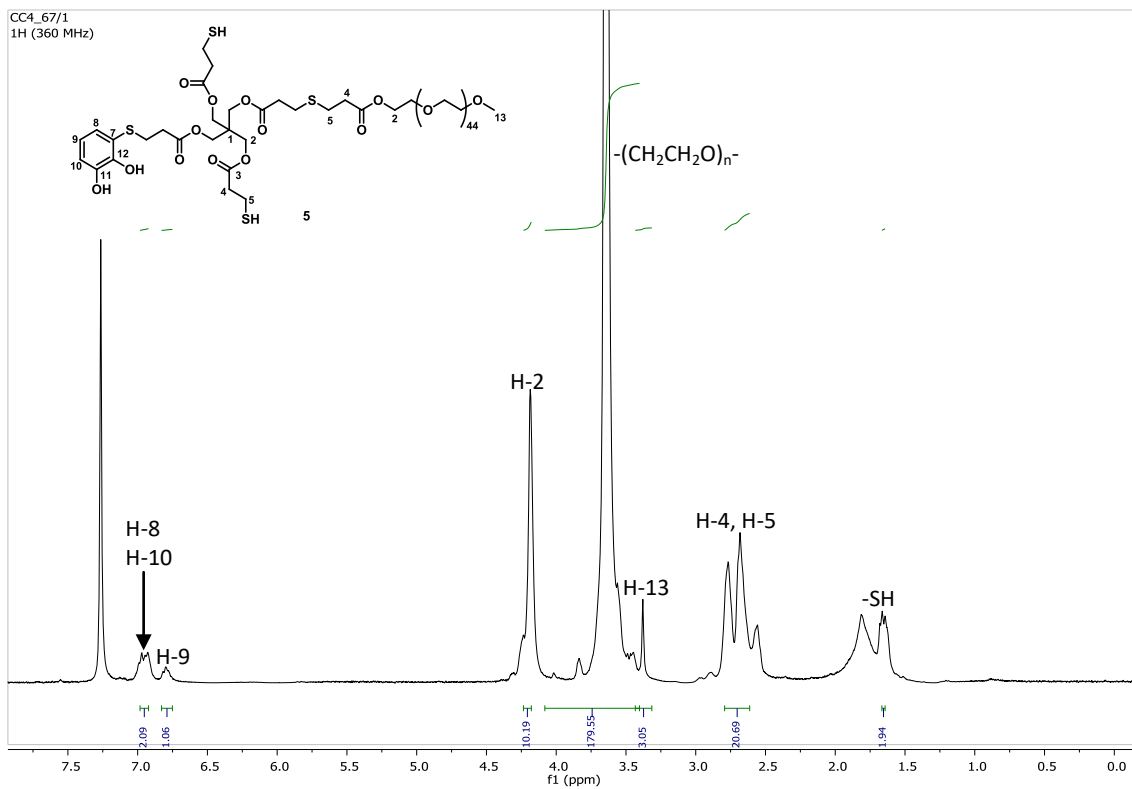
CC4_08-F3-caracteritzacio-400MHz/2 — 13C {1H} — (100.6MHz)

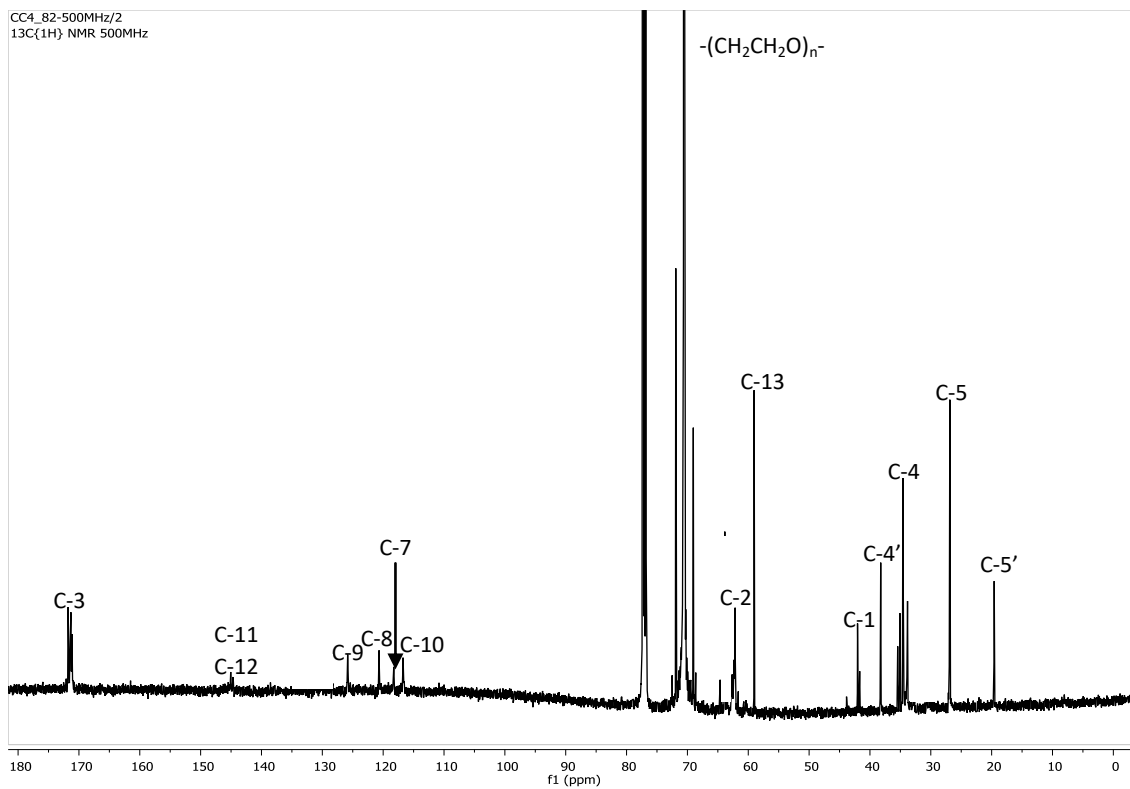


¹³C NMR (100.6 MHz, CDCl₃)

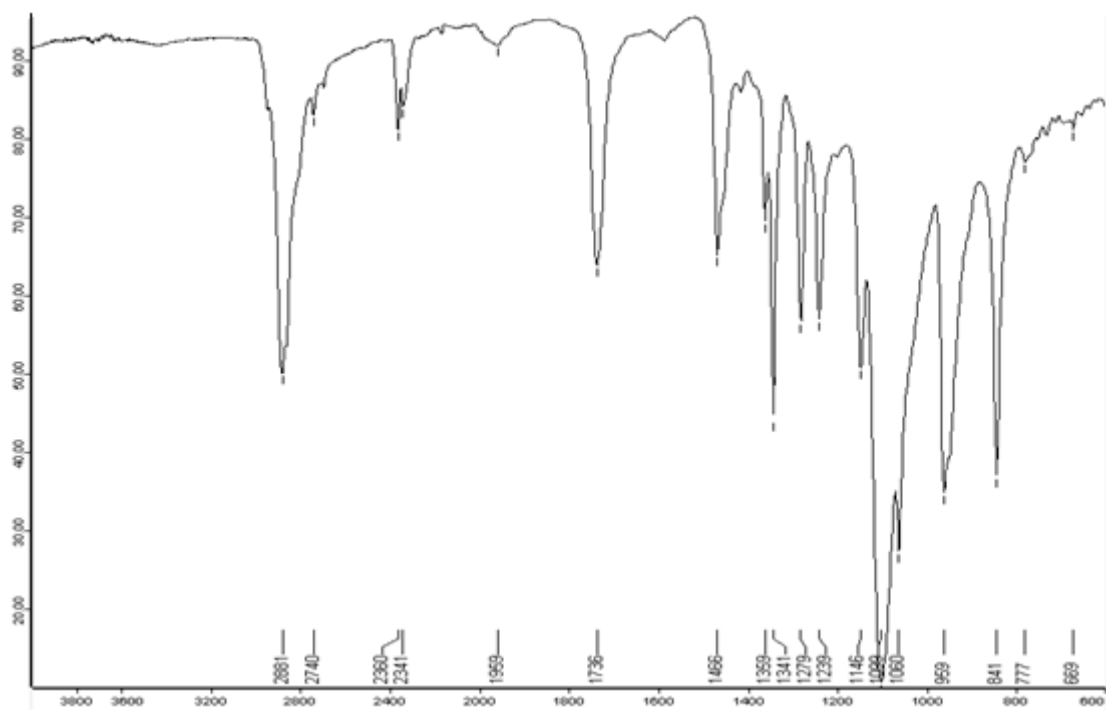


IR (ATR)

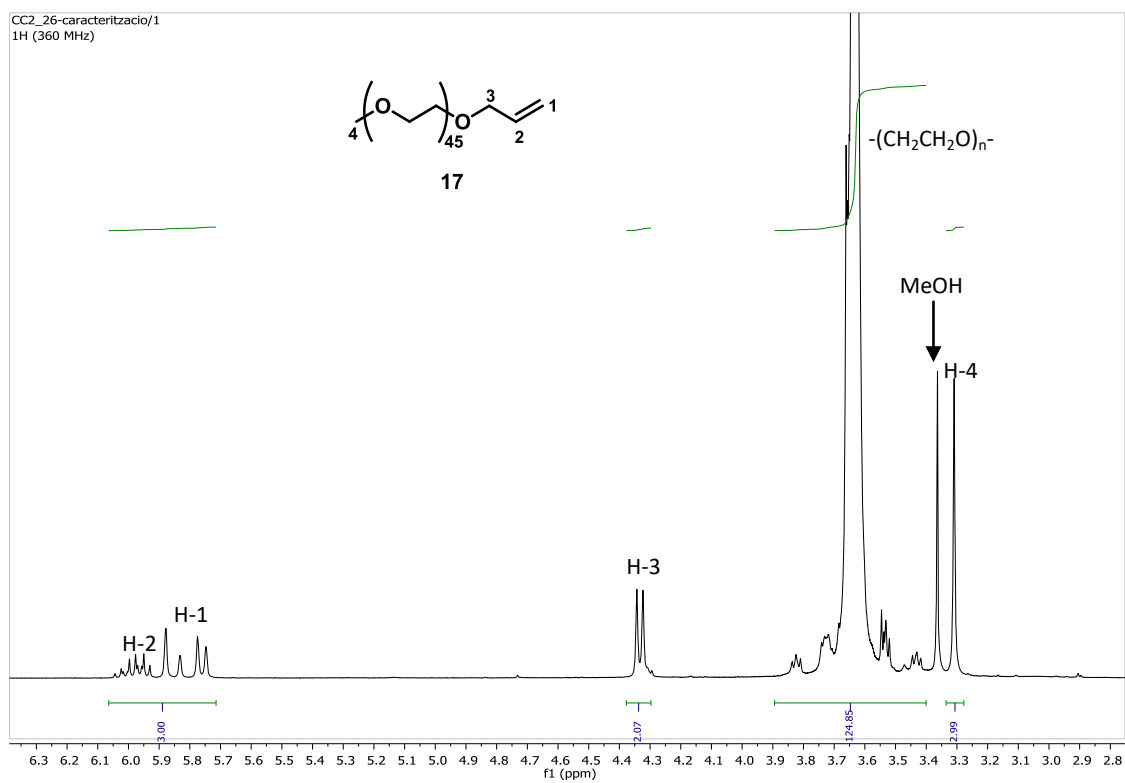
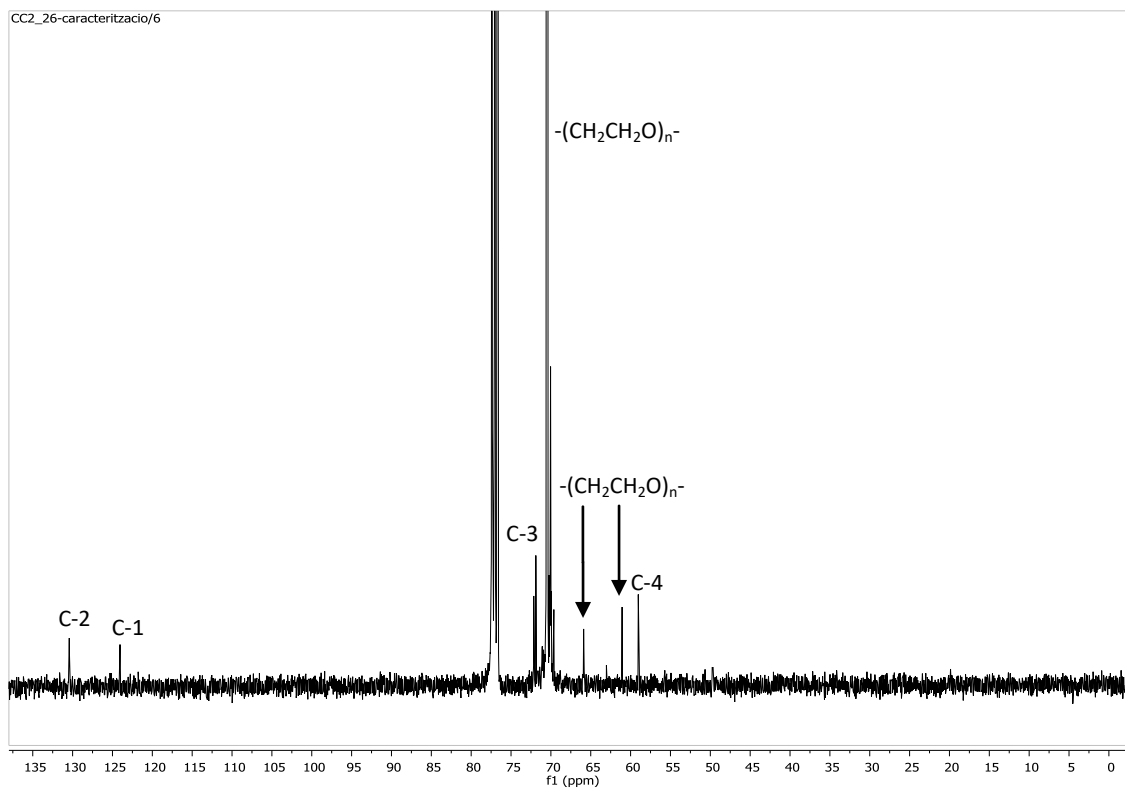
¹H NMR (500 MHz, CDCl₃)

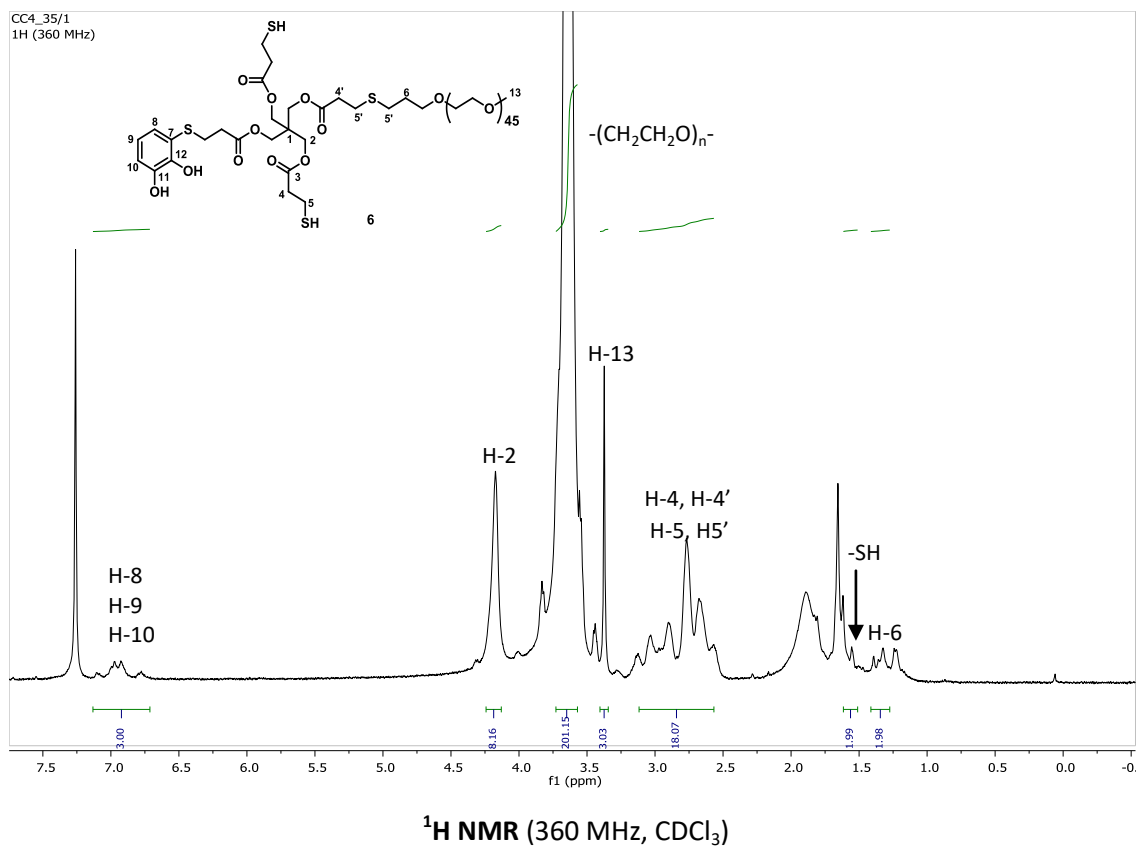
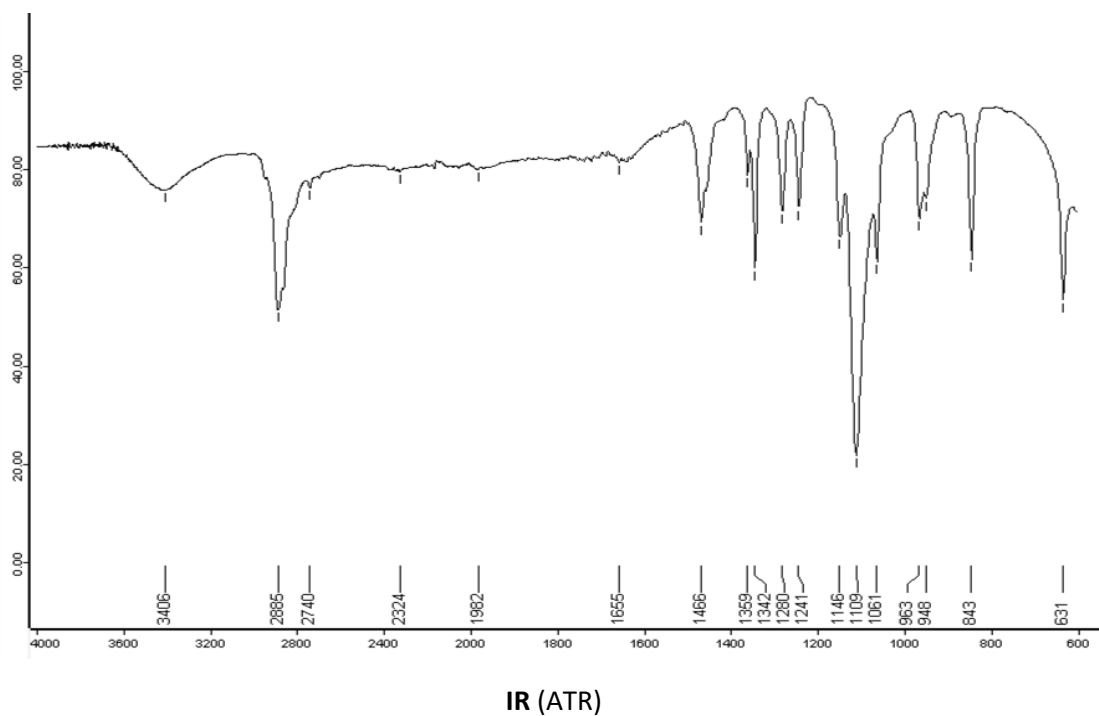


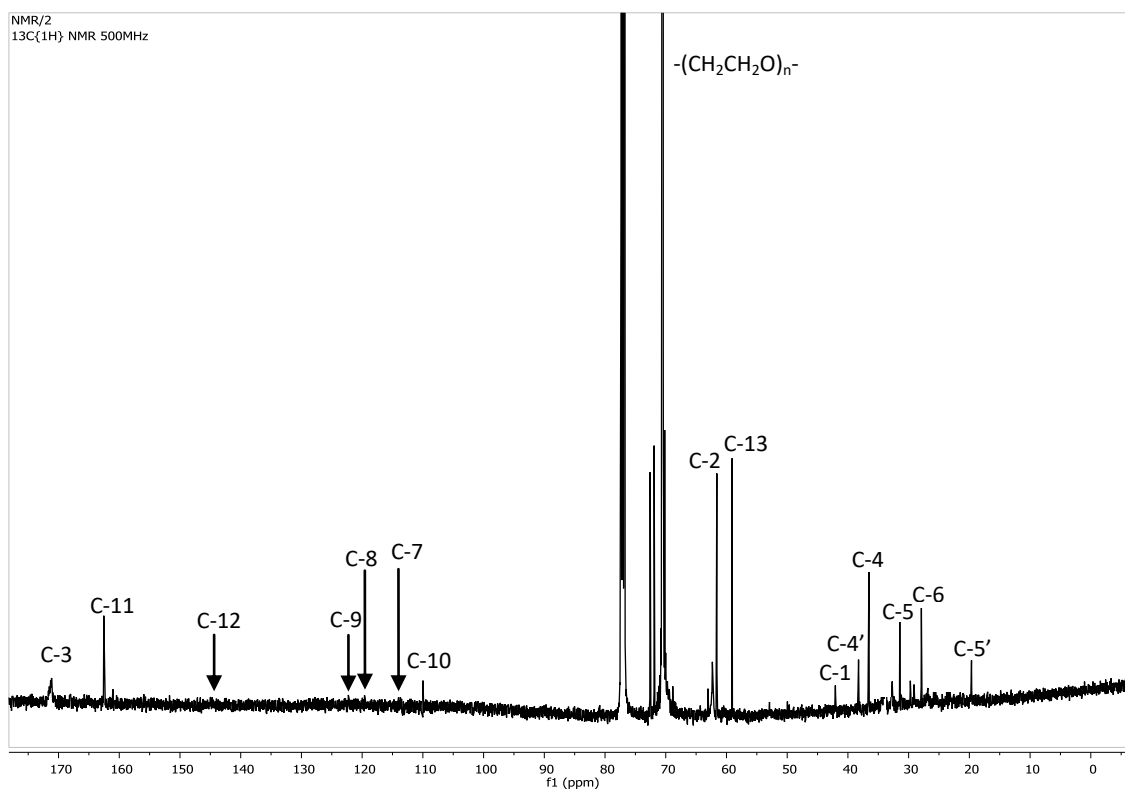
¹³C NMR (125.8 MHz, CDCl₃)



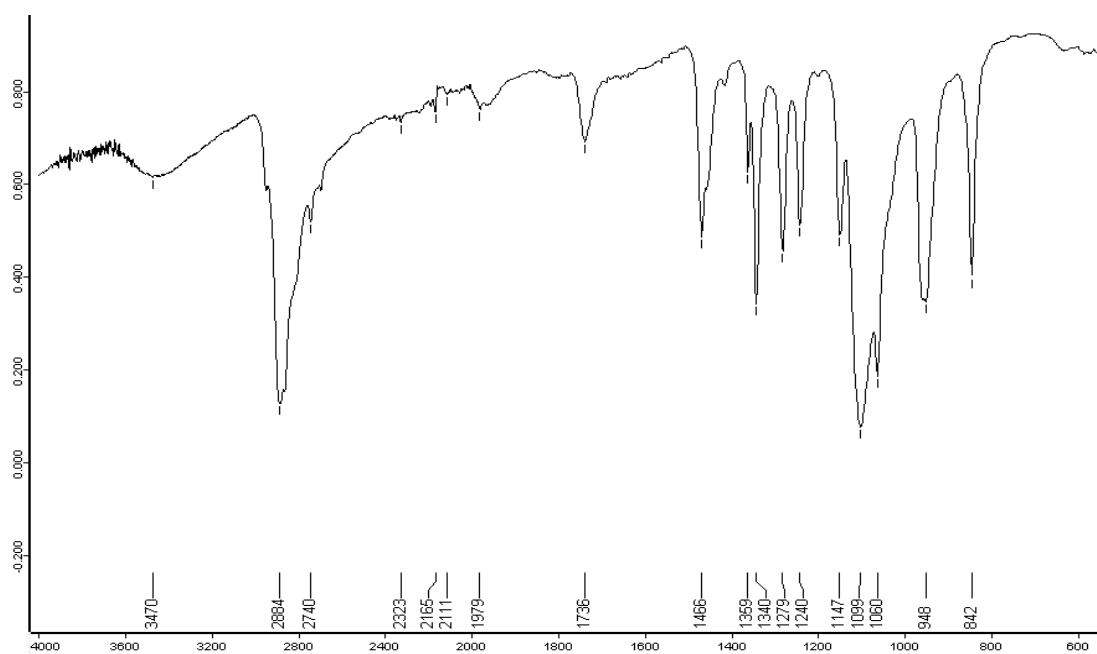
IR (ATR)

 ^1H NMR (360 MHz, CDCl_3) ^{13}C NMR (90.5 MHz, CDCl_3)

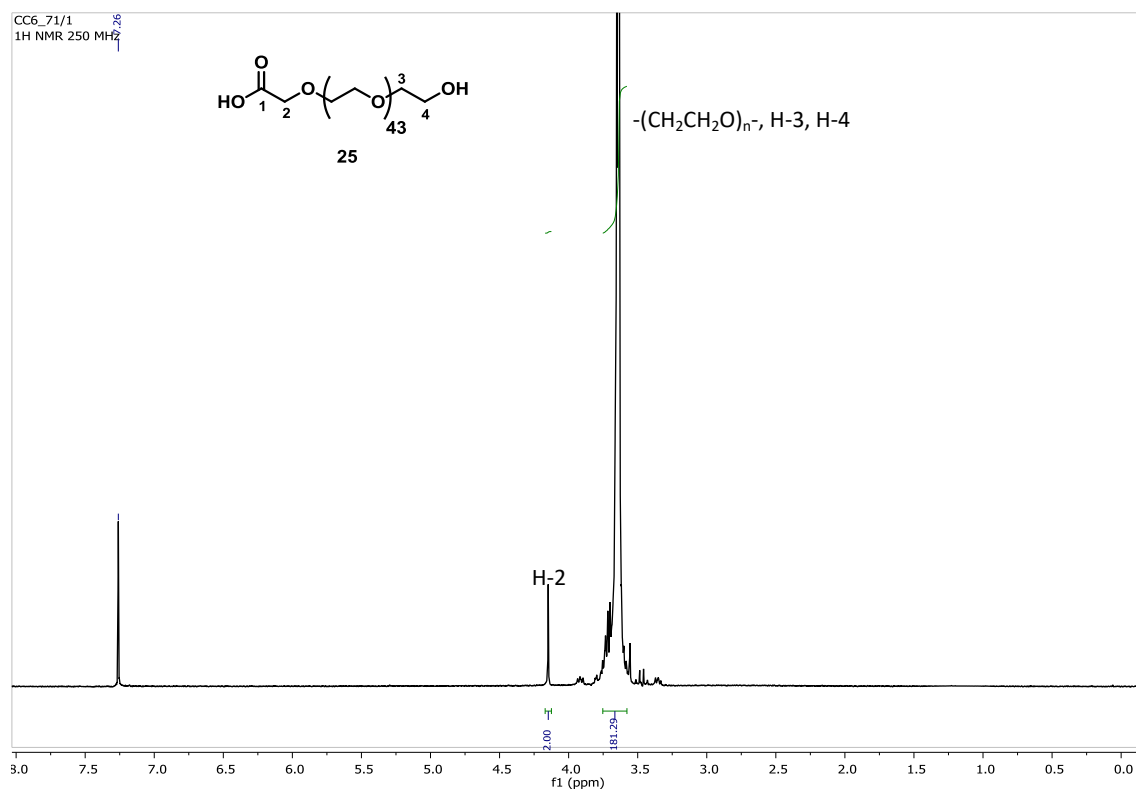
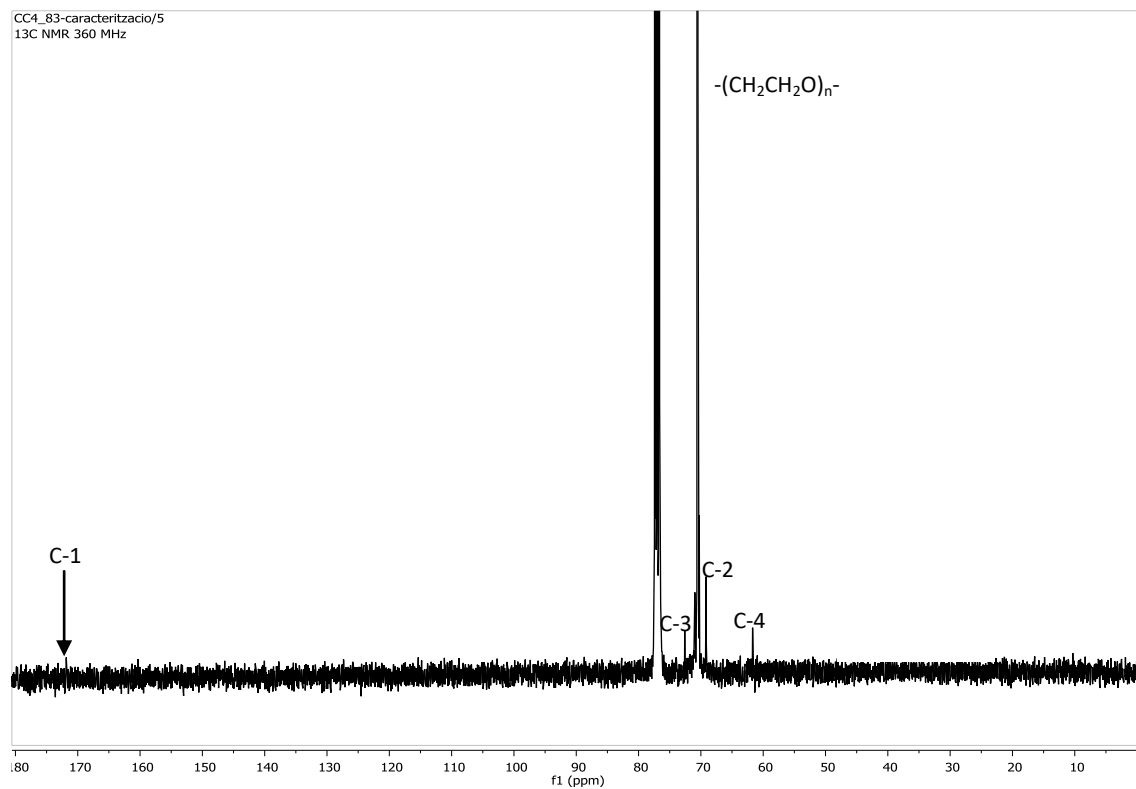


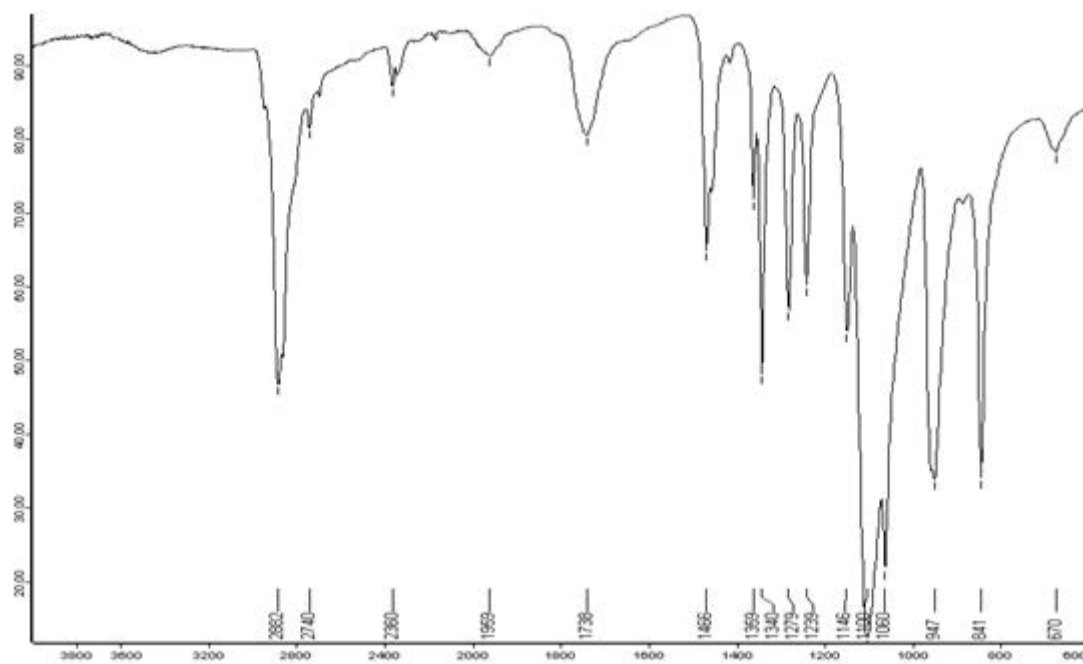


¹³C NMR (125.8 MHz, CDCl₃)

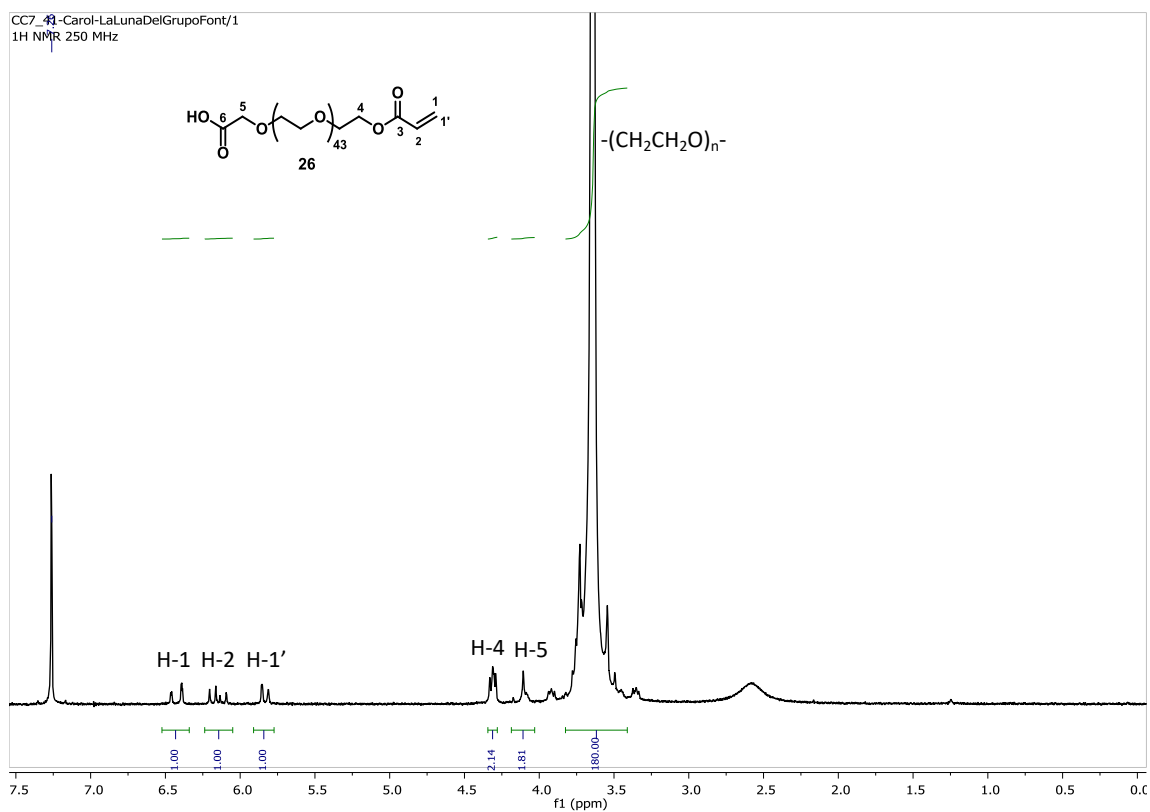


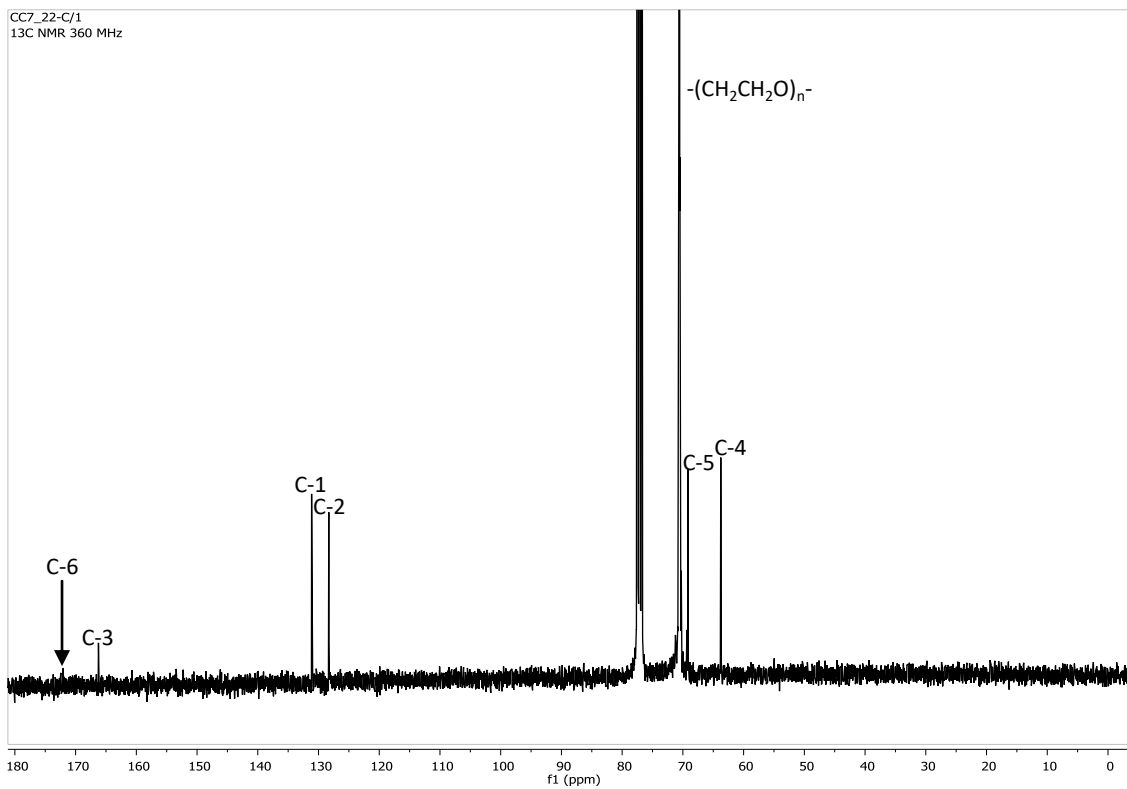
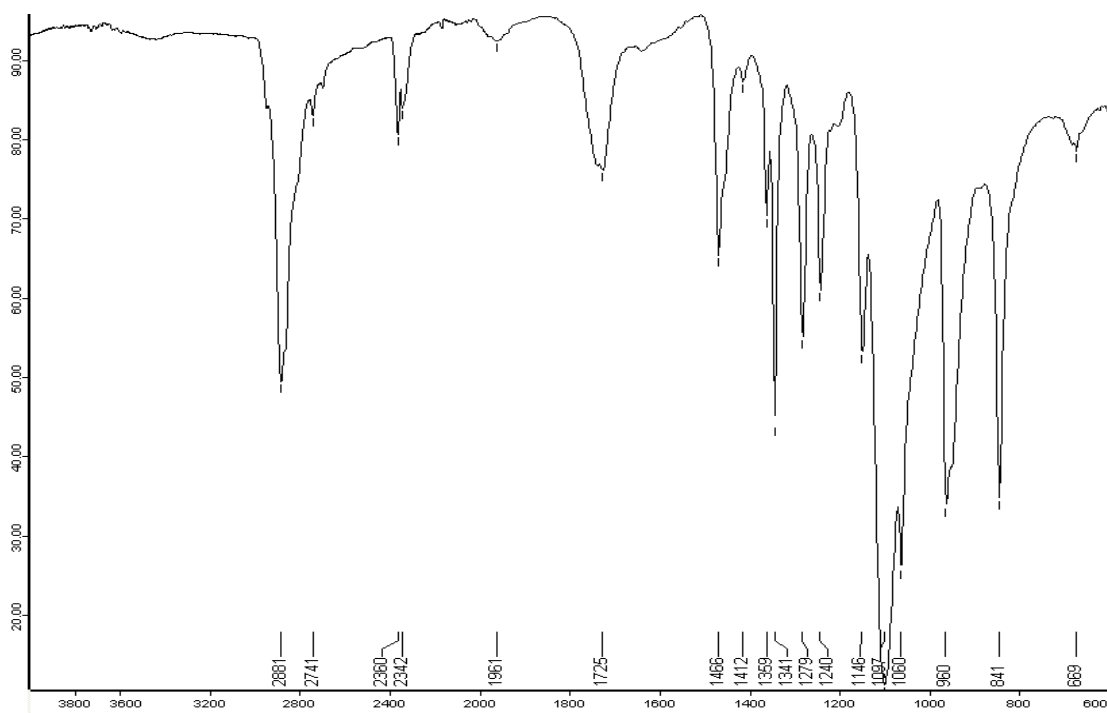
IR (ATR)

 ^1H NMR (400 MHz, CDCl_3) ^{13}C NMR (100.6 MHz, CDCl_3)

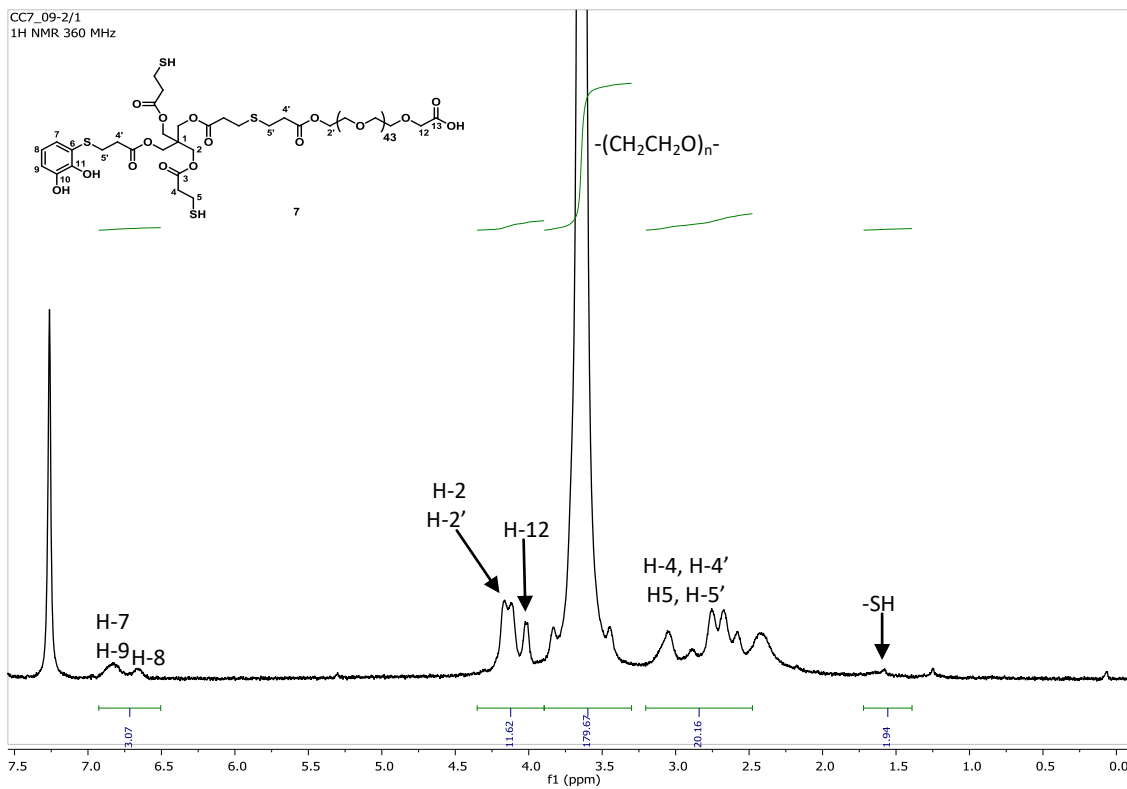
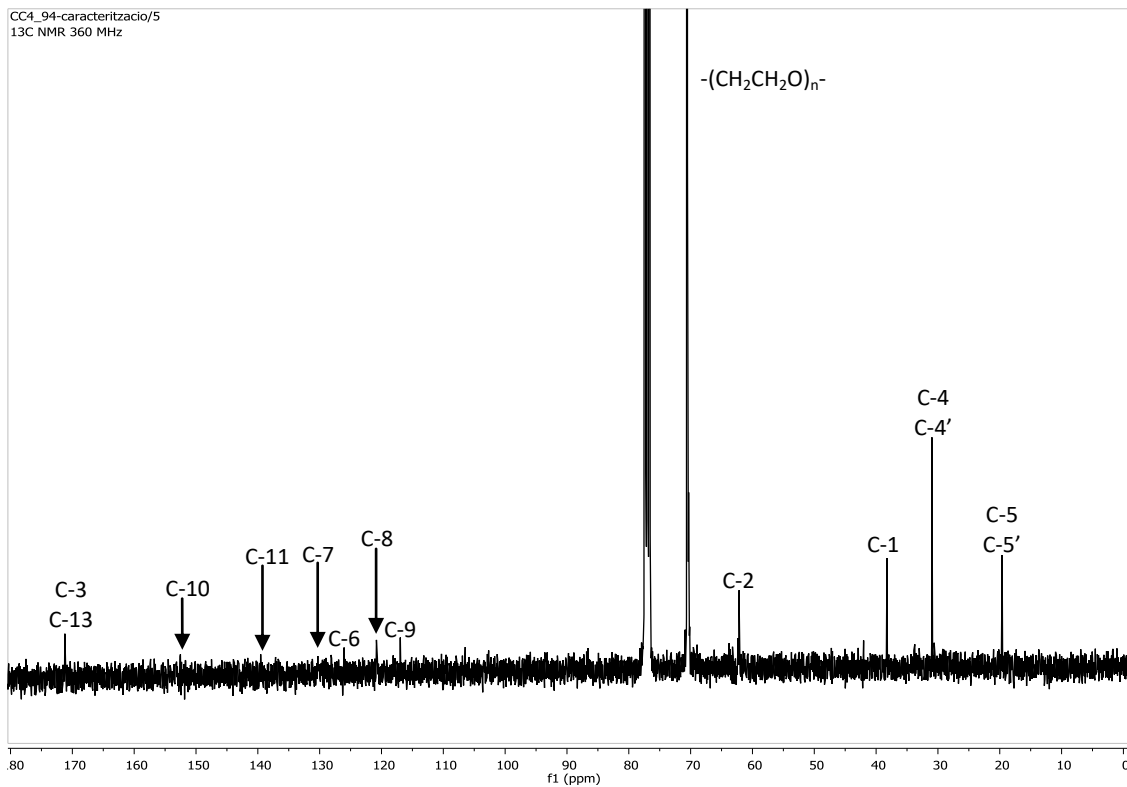


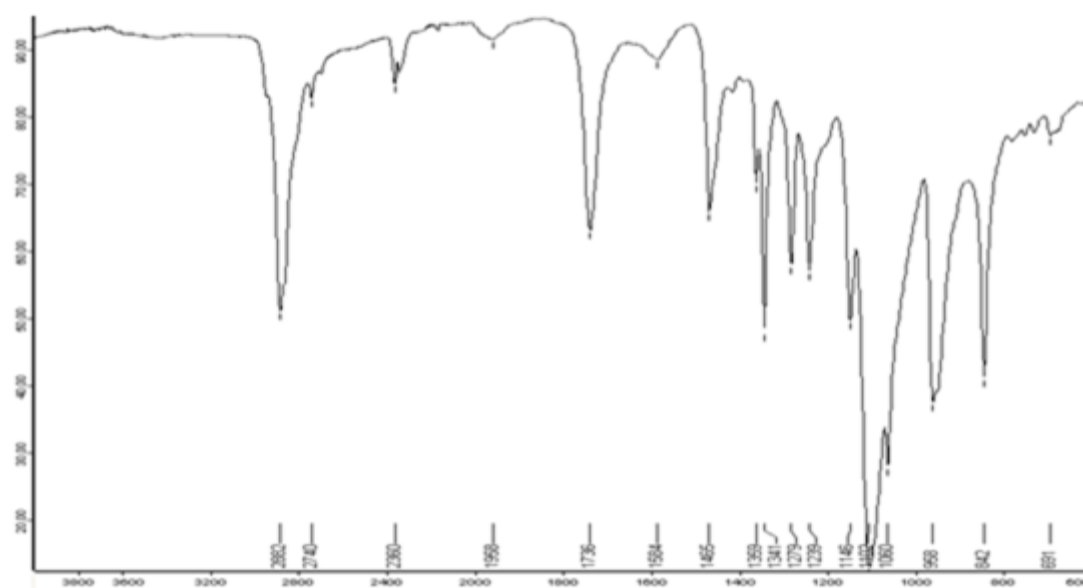
IR (ATR)

CC7_43-Carol-LaLunaDelGrupoFont/1
1H NMR 250 MHz ^1H NMR (400 MHz, CDCl_3)

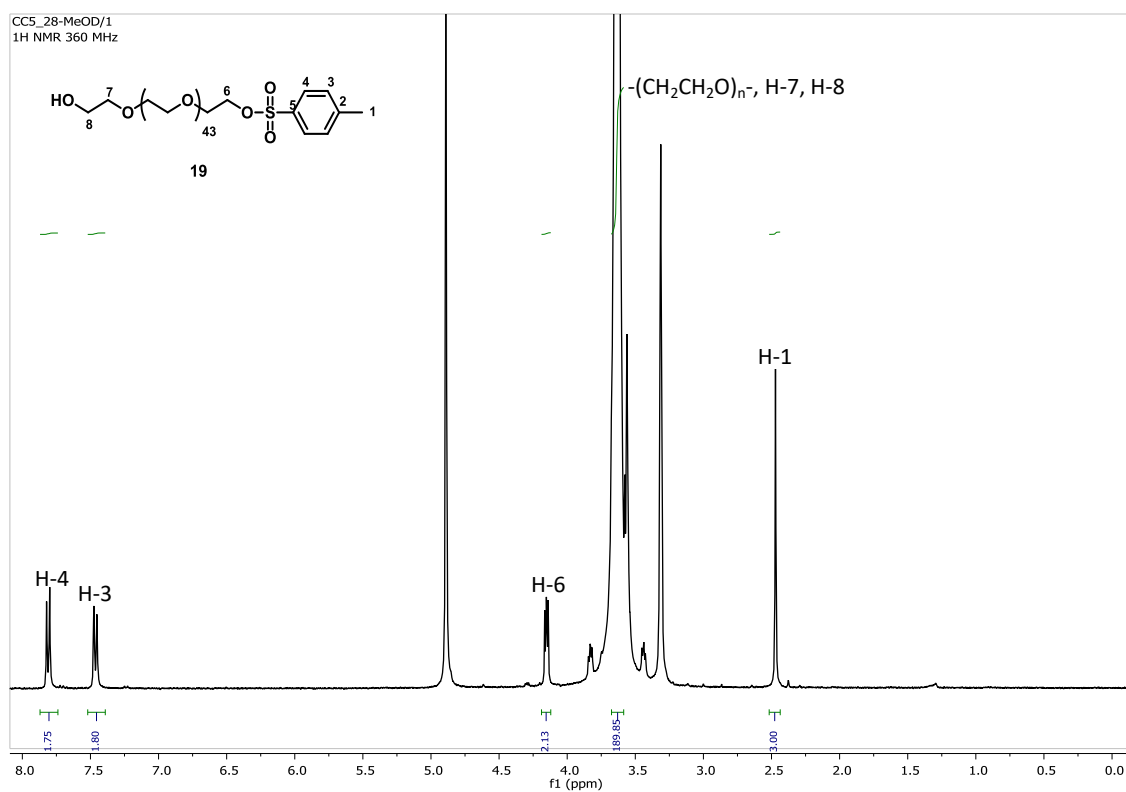
 ^{13}C NMR (100.6 MHz, CDCl_3)

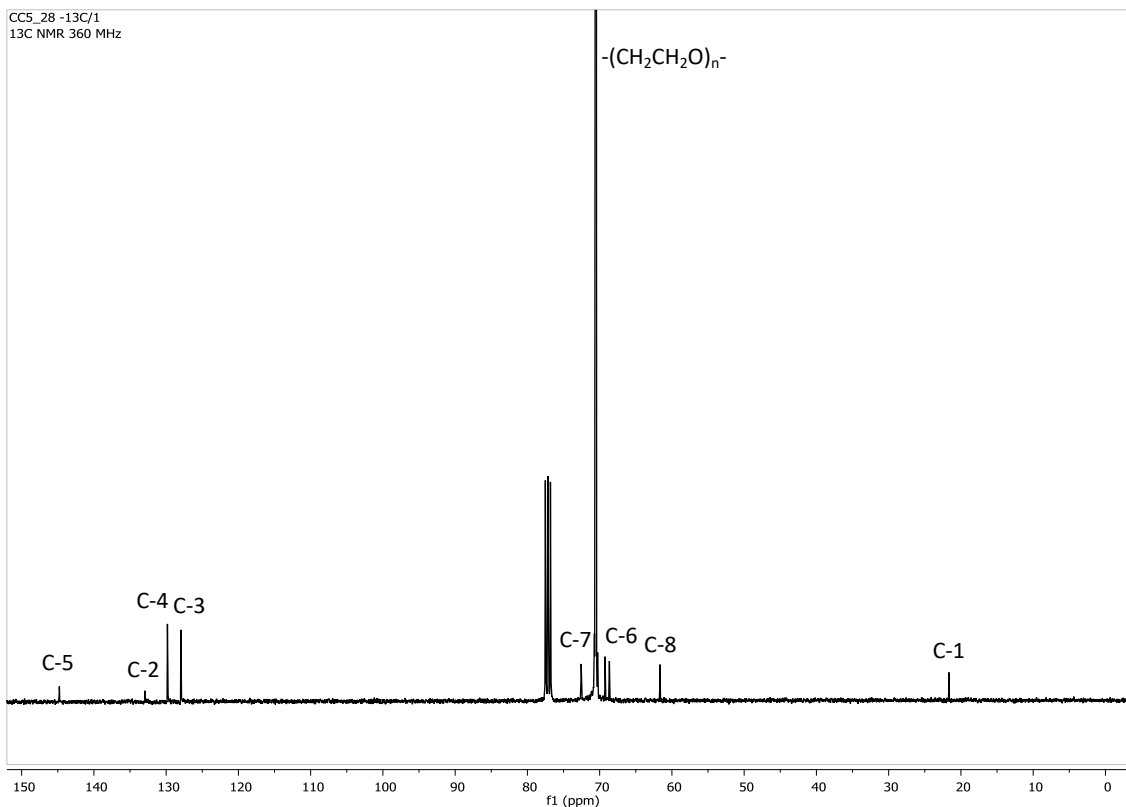
IR (ATR)

 ^1H NMR (360 MHz, CDCl_3) ^{13}C NMR (90.5 MHz, CDCl_3)

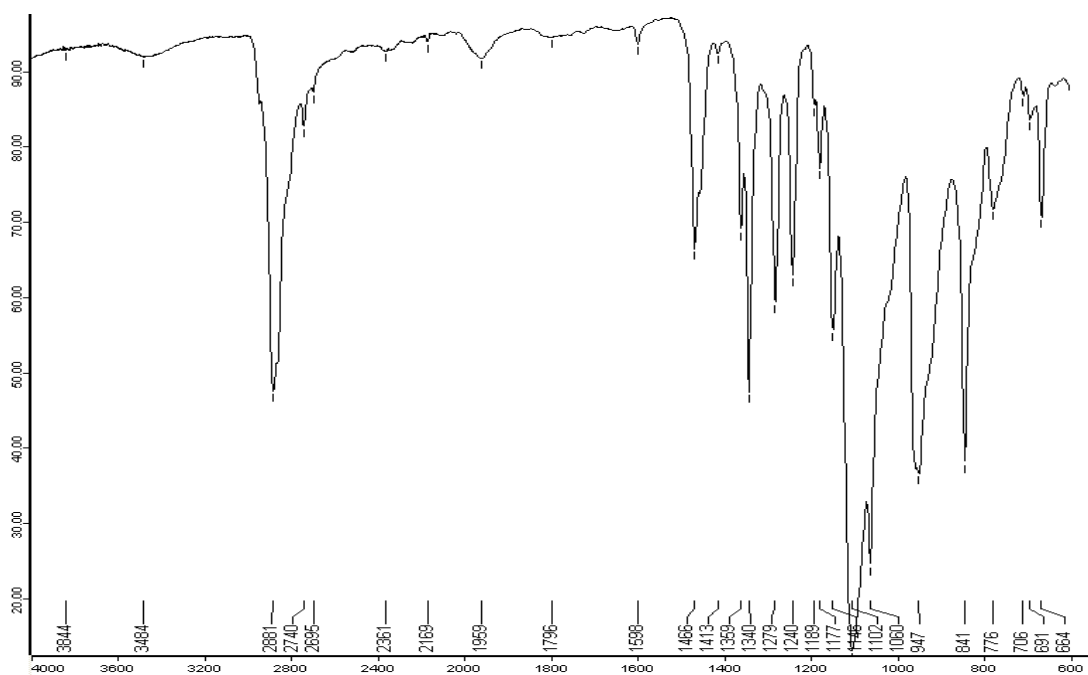


IR (ATR)

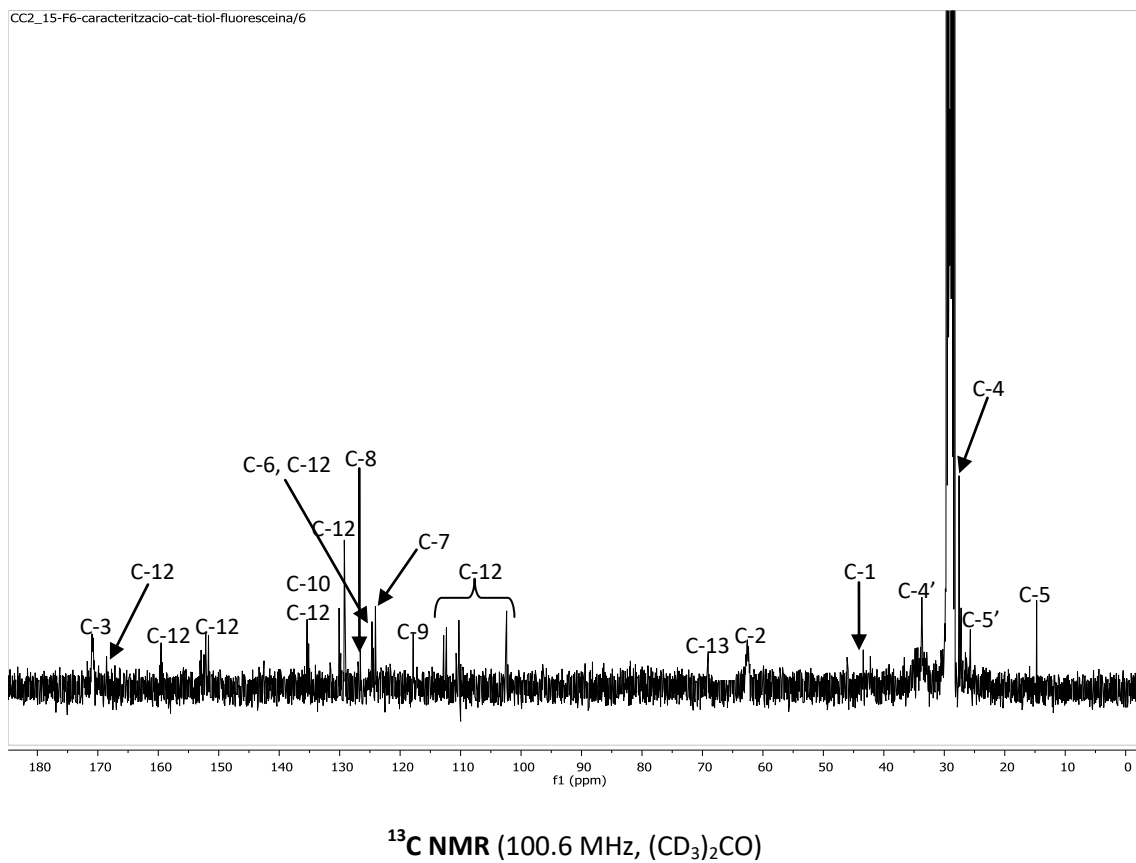
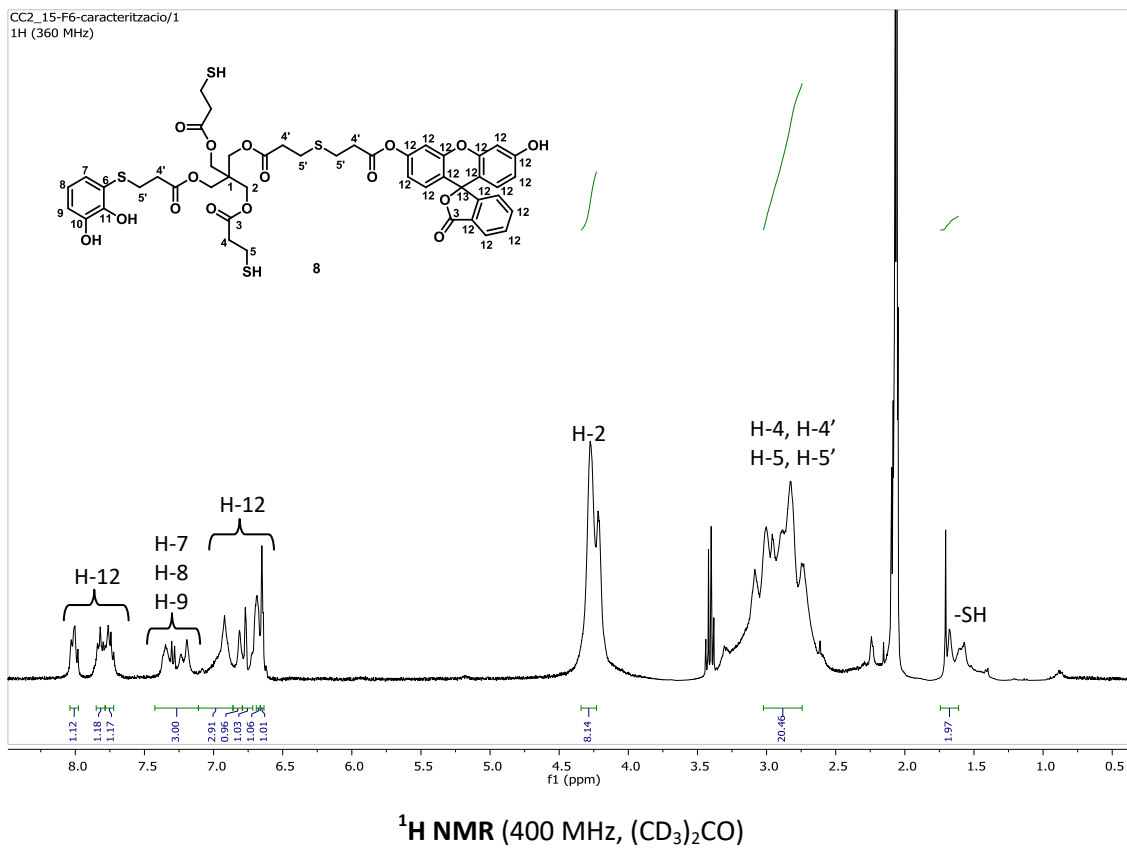
¹H NMR (400 MHz, CD₃OD)

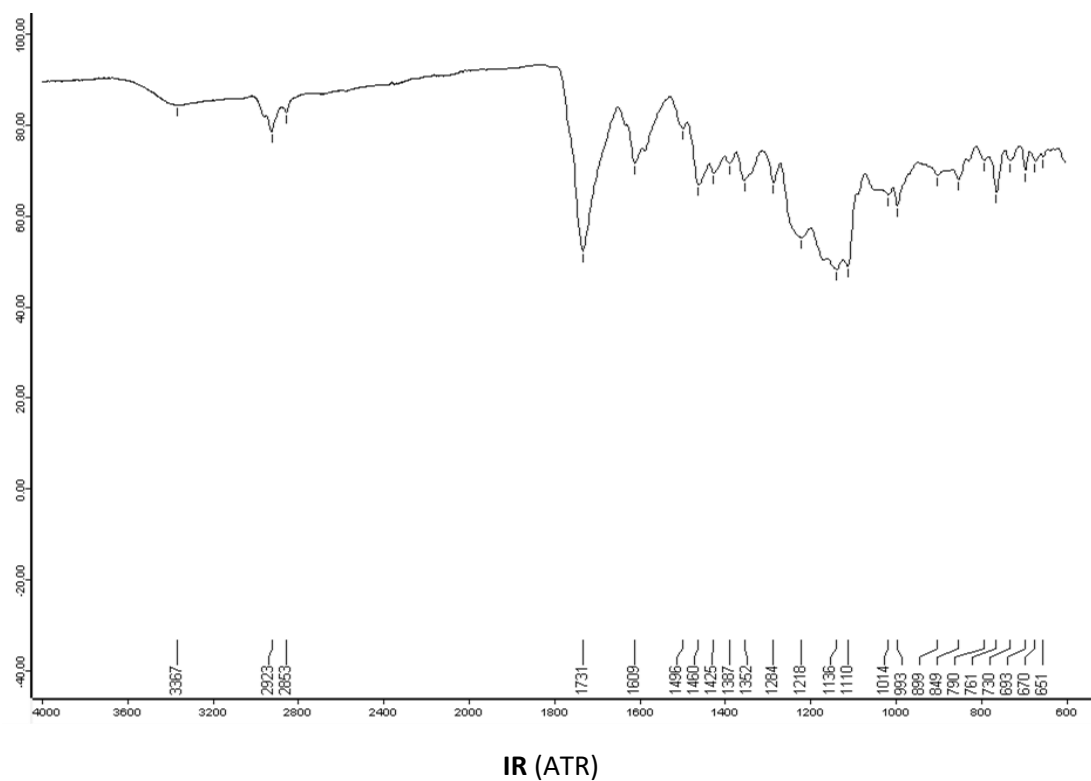


¹³C NMR (100.6 MHz, CDCl₃)

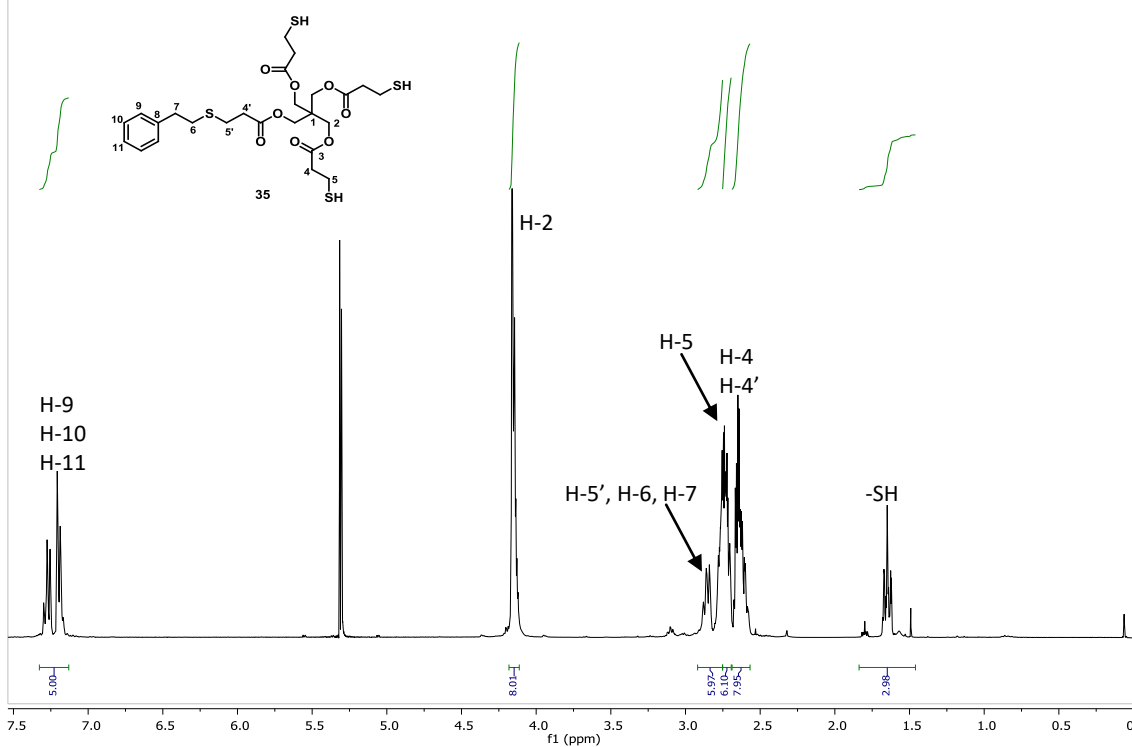


IR (ATR)



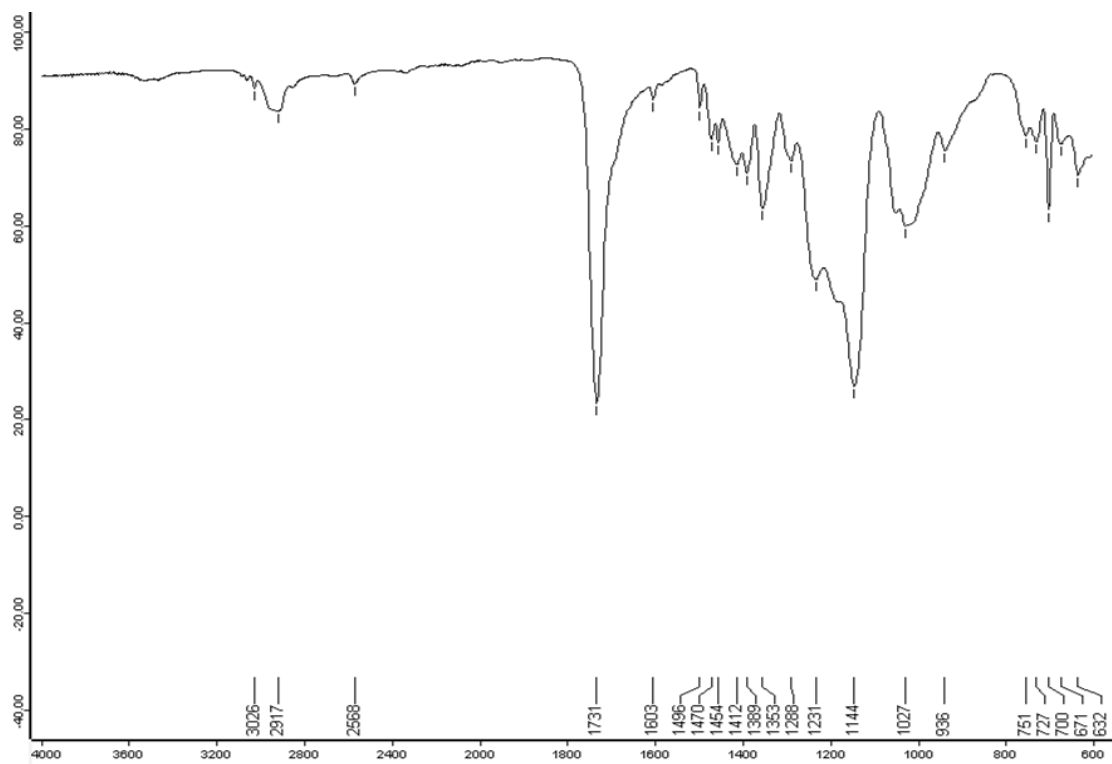
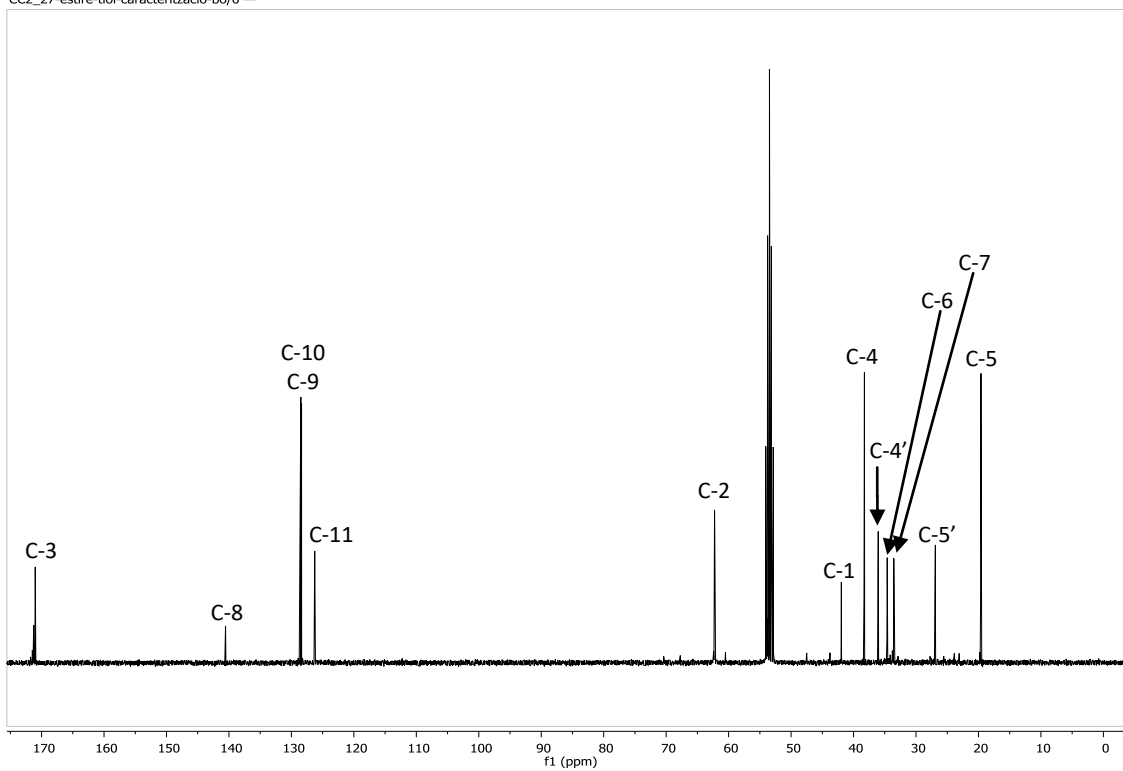


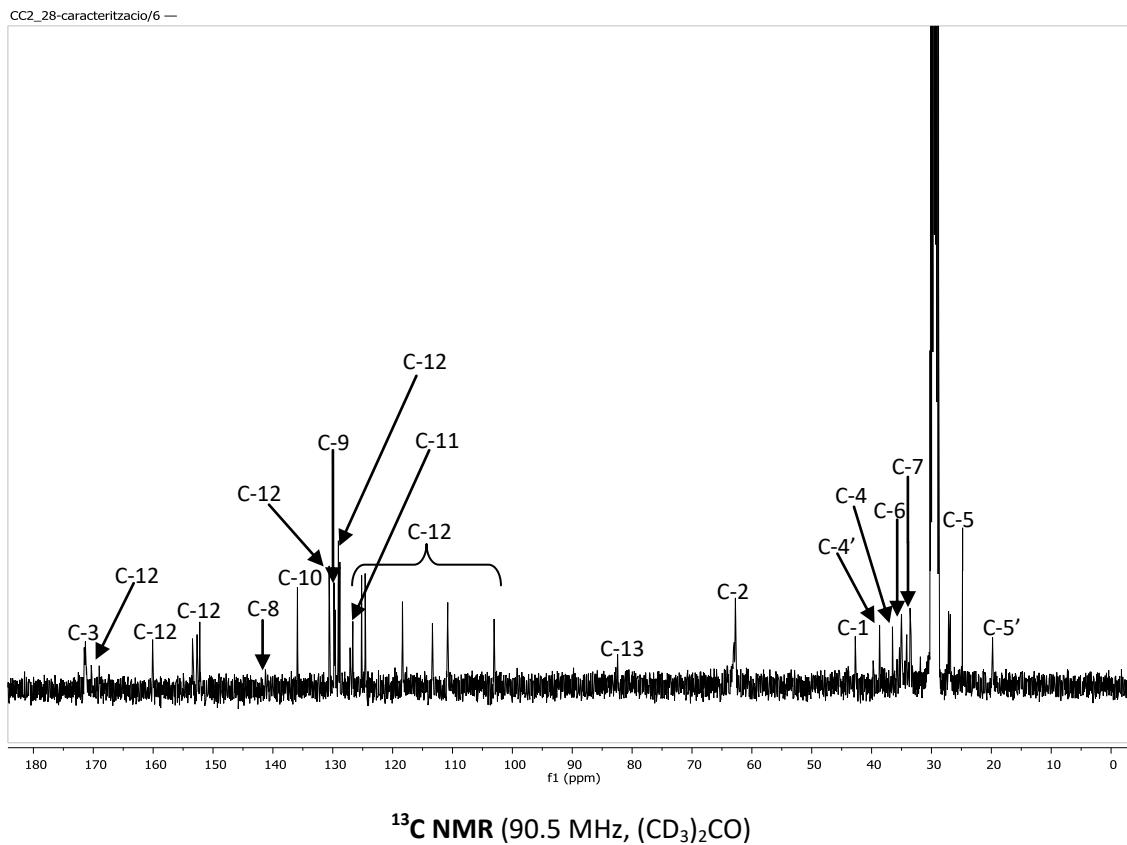
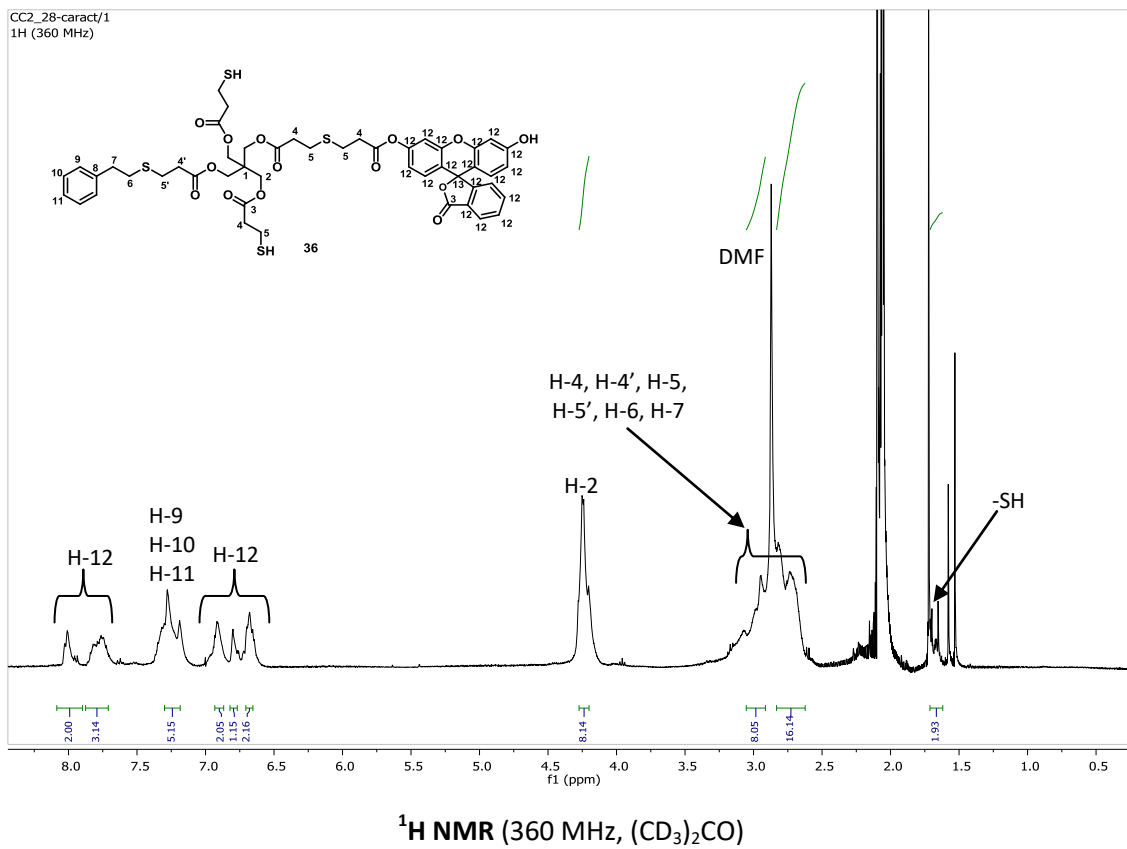
CC2_27-estire-tiol-caracterizacio-bo/1
1H (360 MHz)

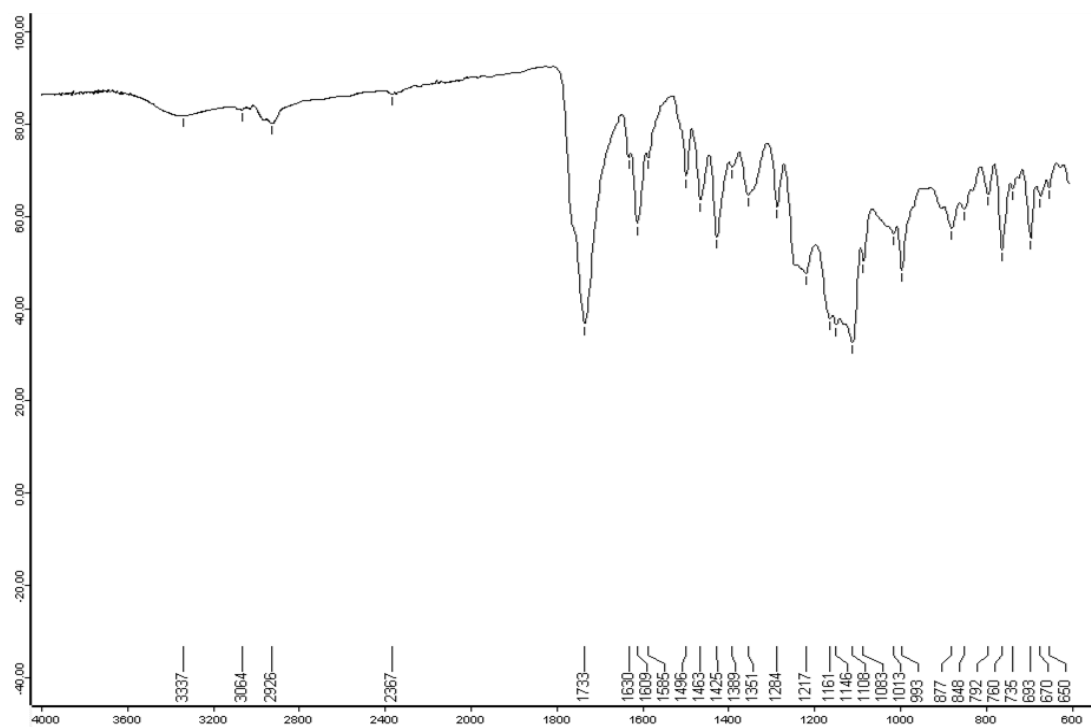


^1H NMR (360 MHz, CD_2Cl_2)

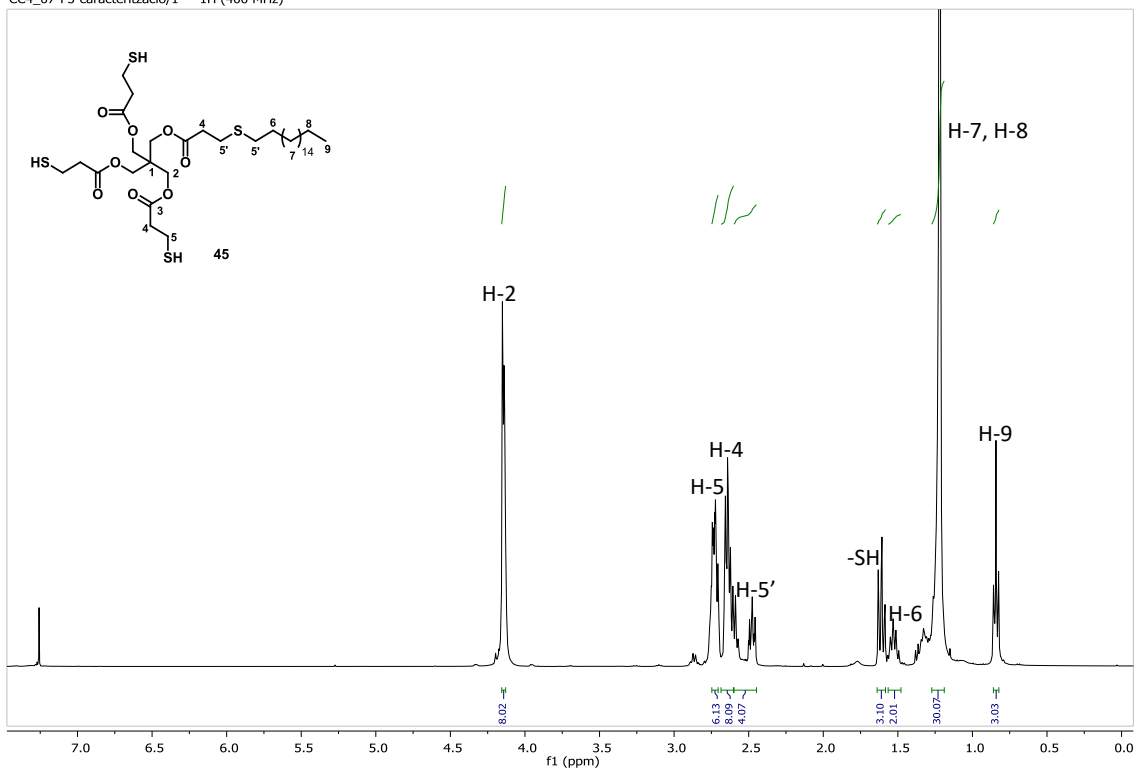
CC2_27-estire-tiol-caracterizacio-bo/6 —



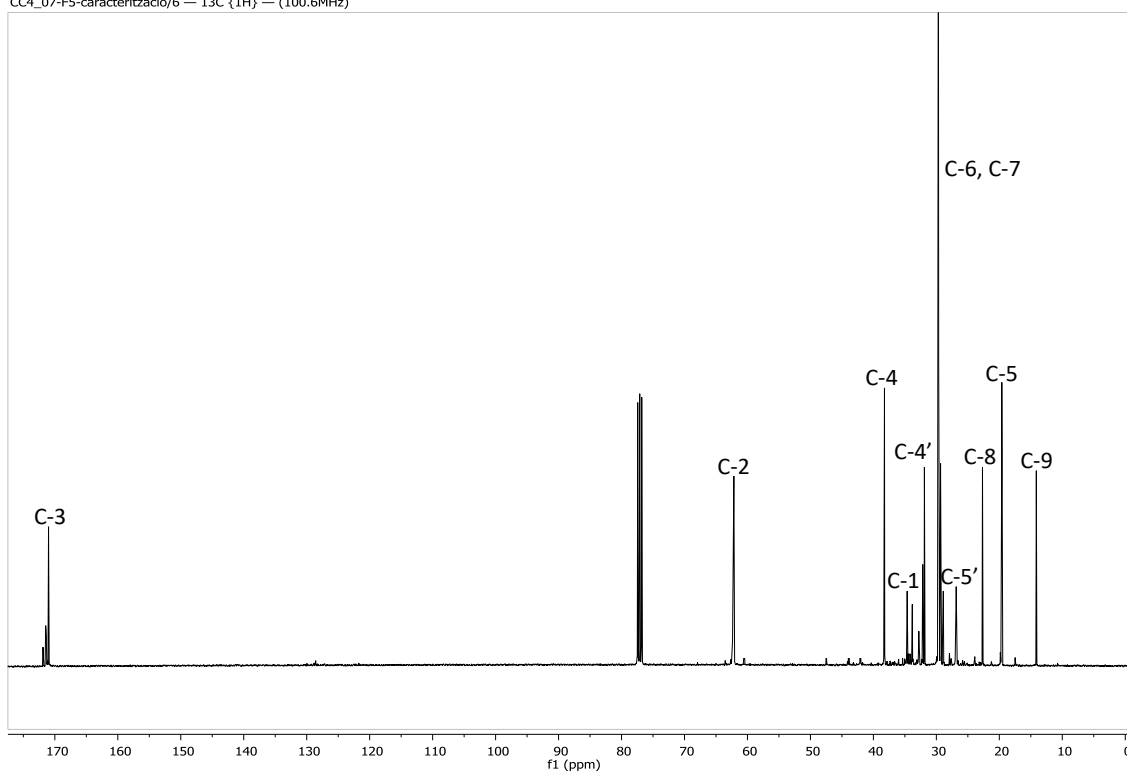
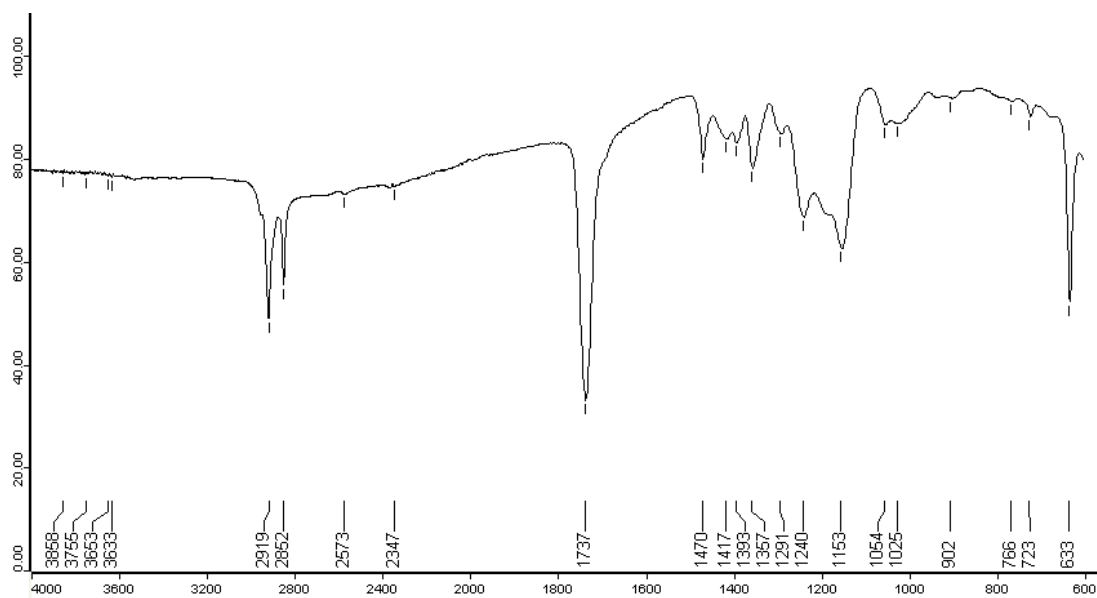




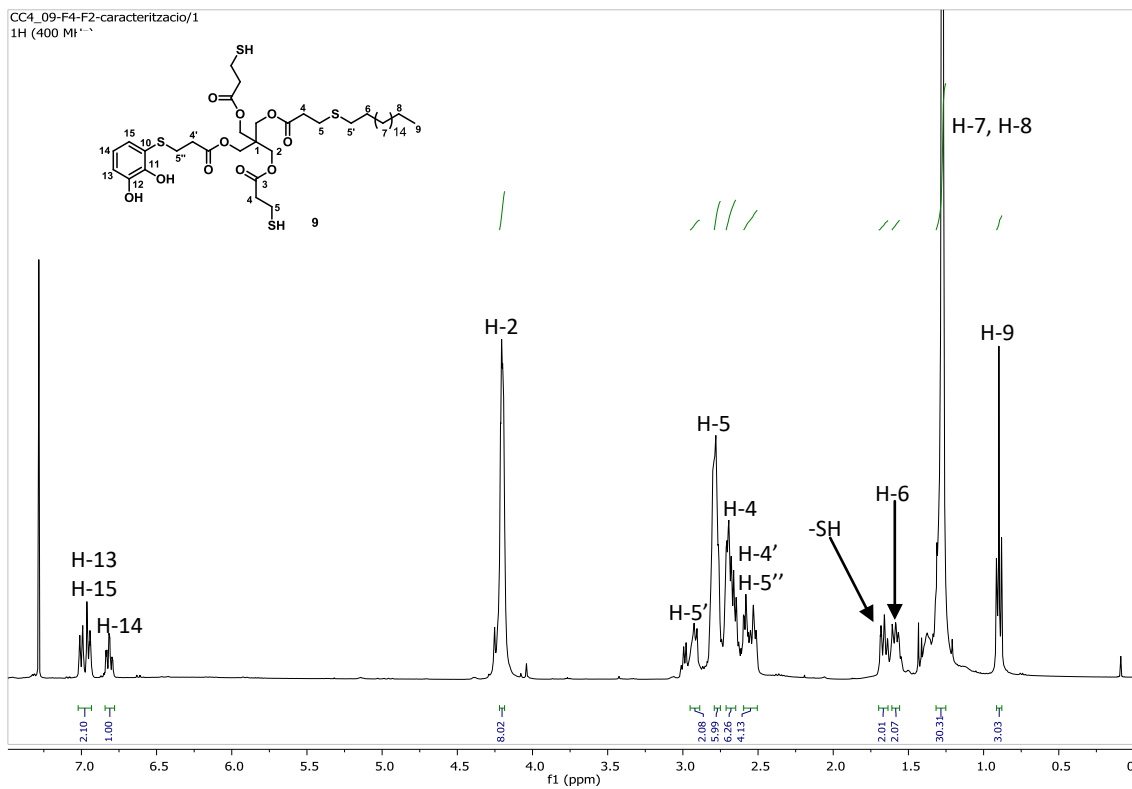
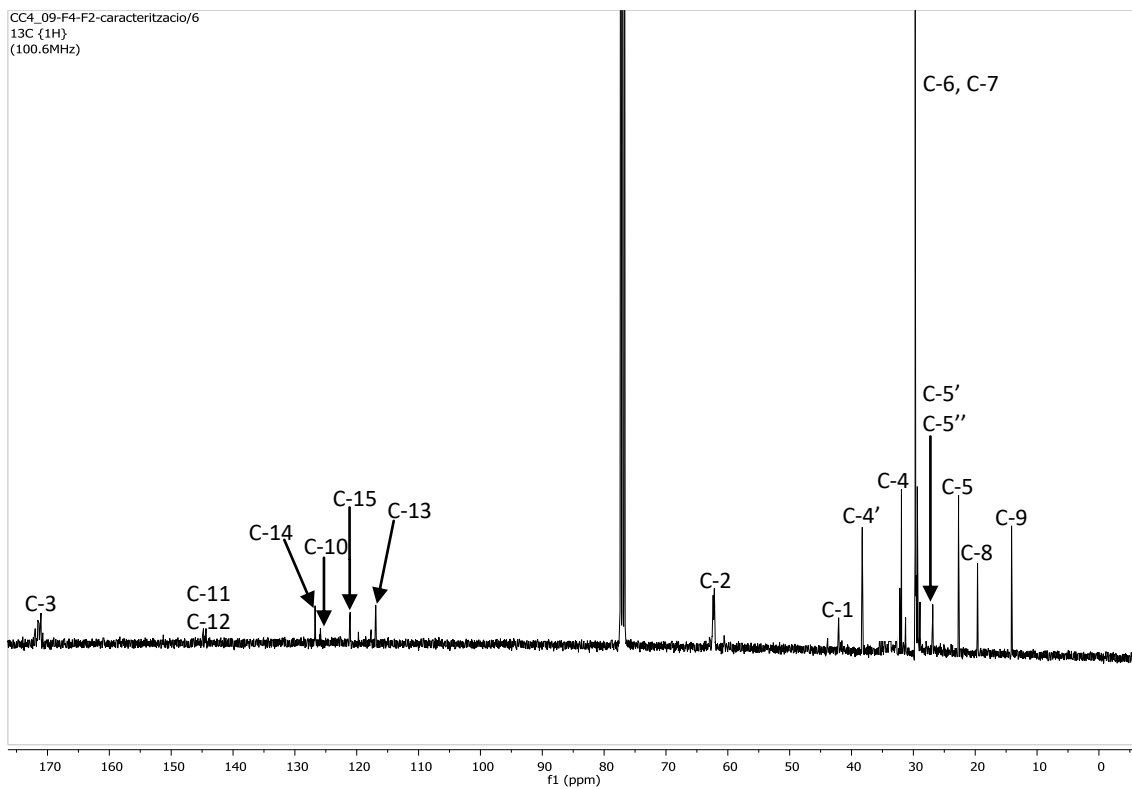
CC4_07-F5-caracterizacio/1 — 1H (400 MHz)

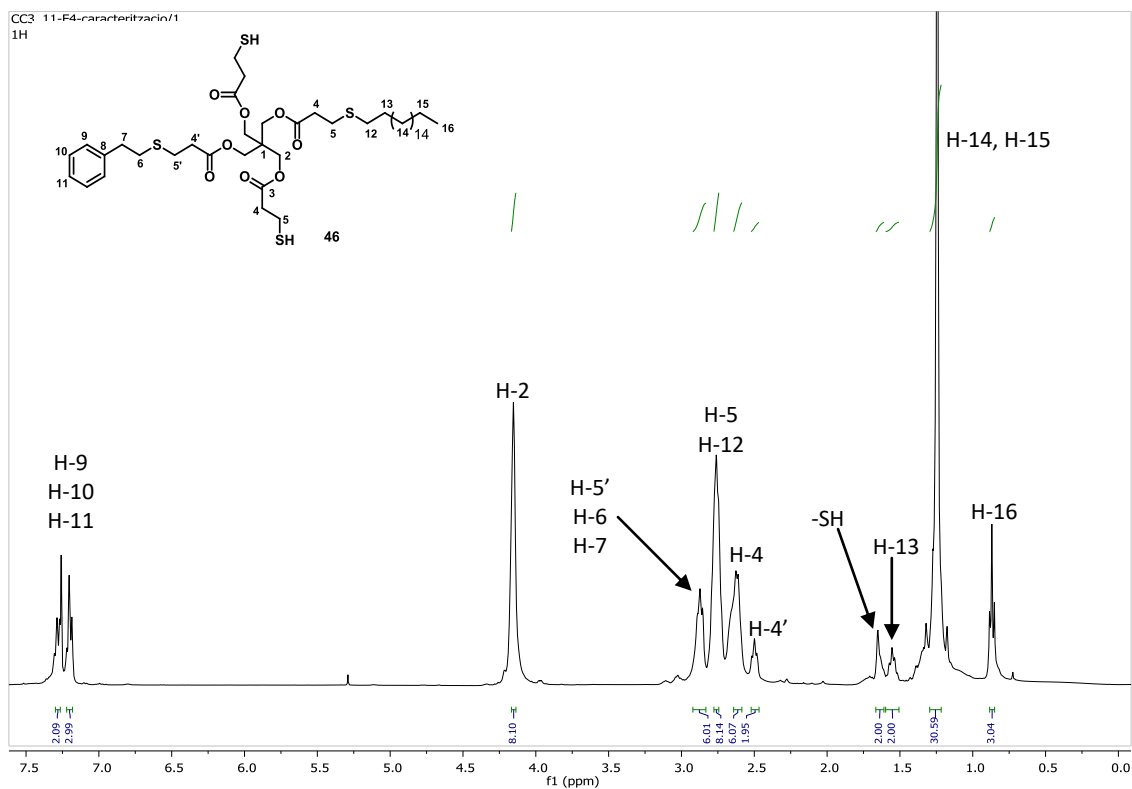
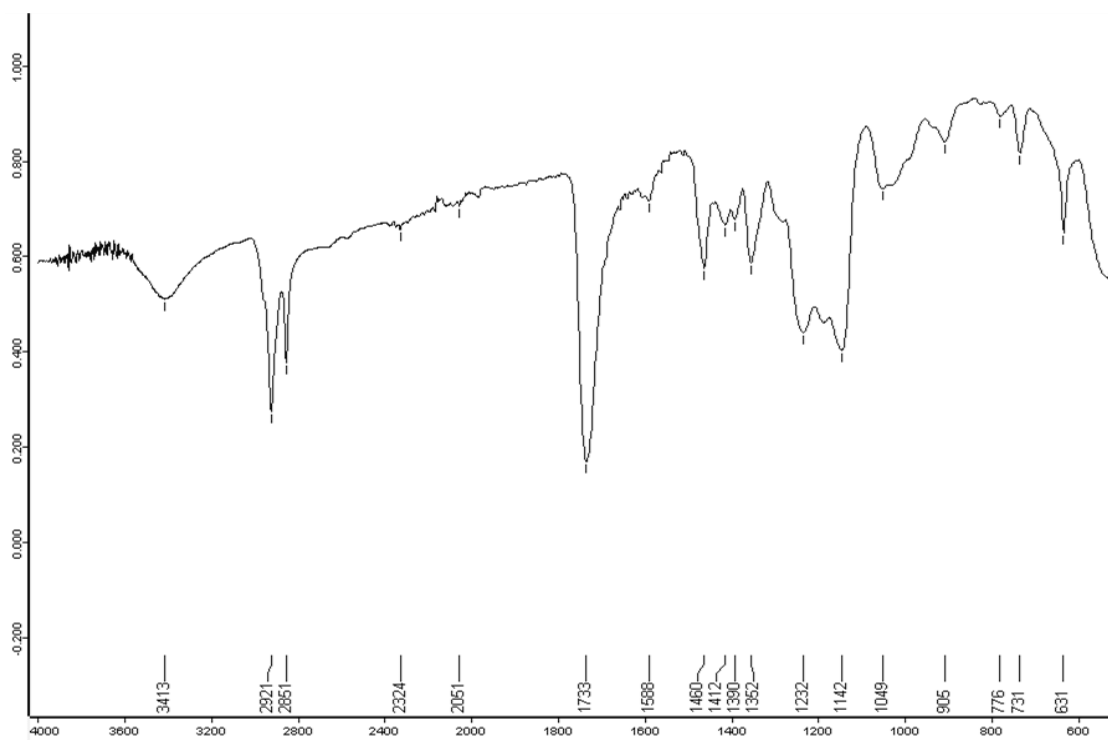


CC4_07-F5-caracteritzacio/6 -- 13C {1H} -- (100.6MHz)

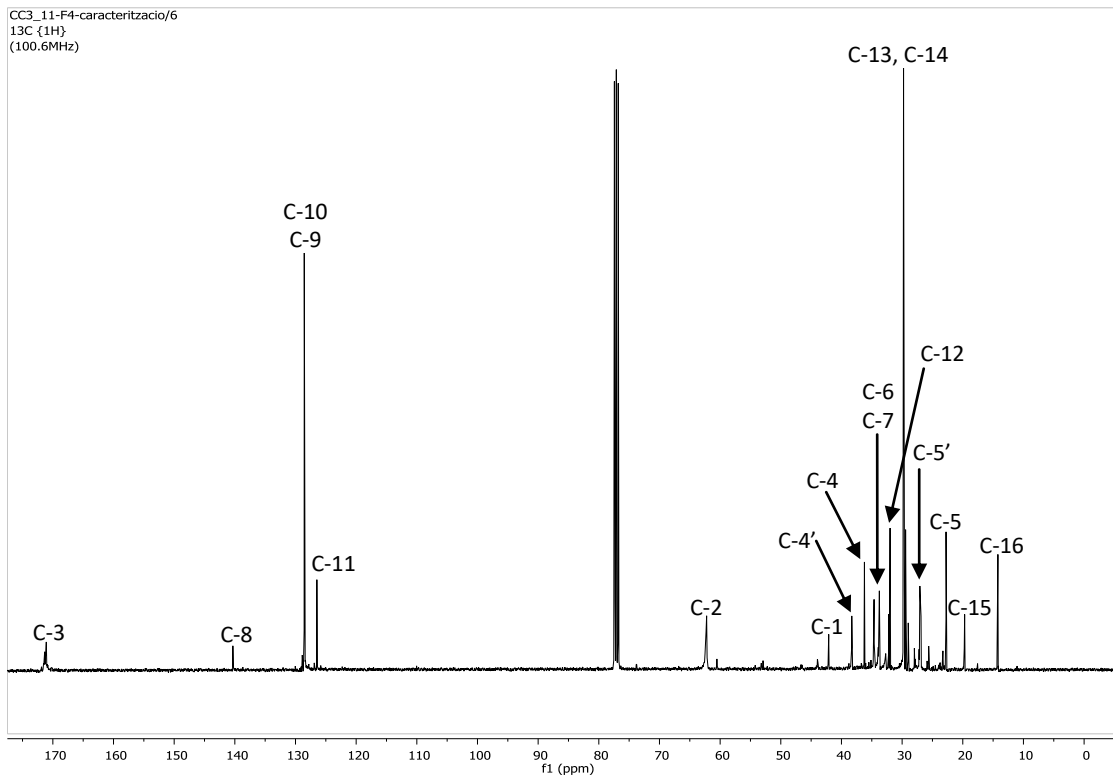
 ^{13}C NMR (100.6 MHz, CDCl_3)

IR (ATR)

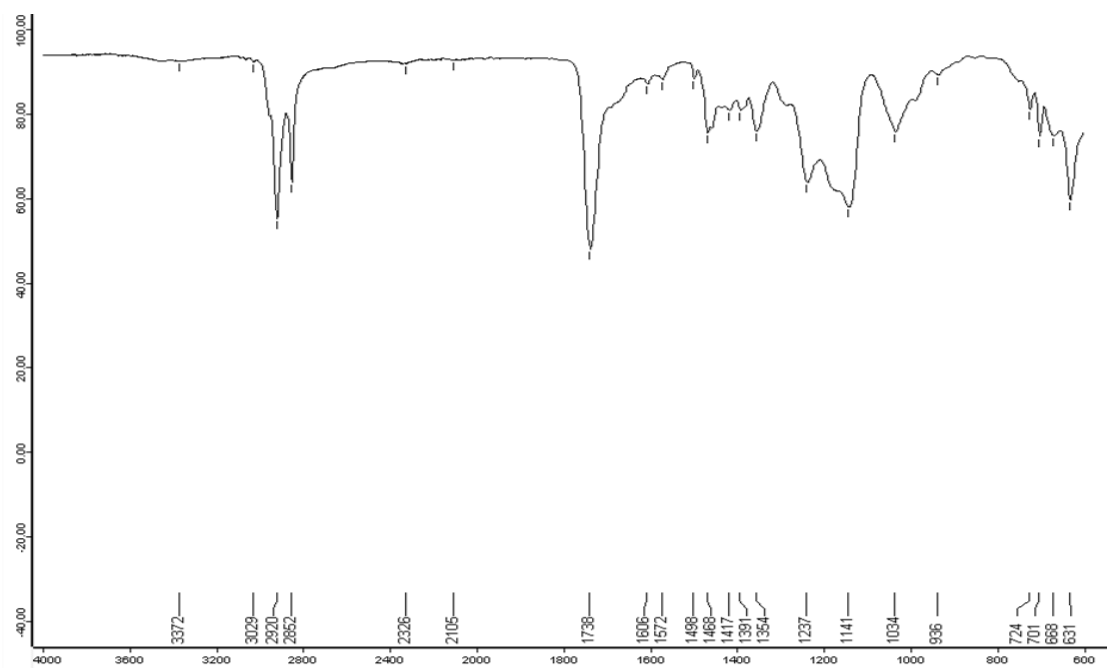
 ^1H NMR (400 MHz, CDCl_3) ^{13}C NMR (100.6 MHz, CDCl_3)



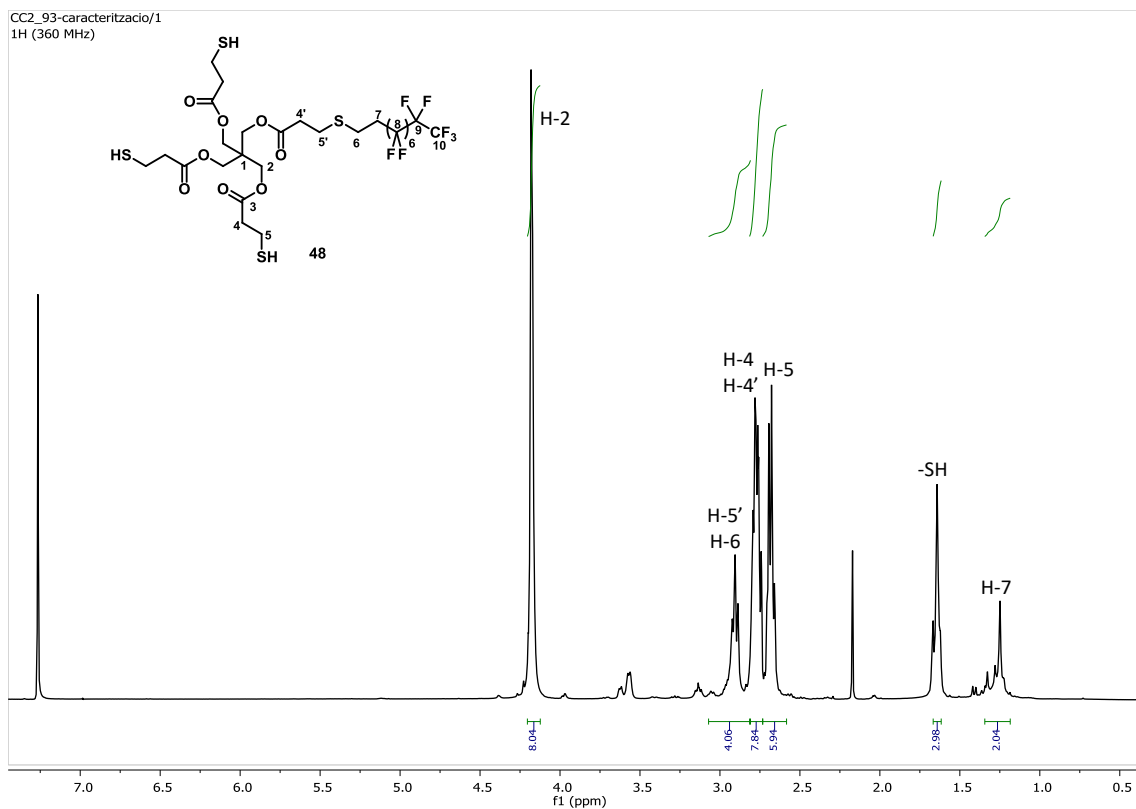
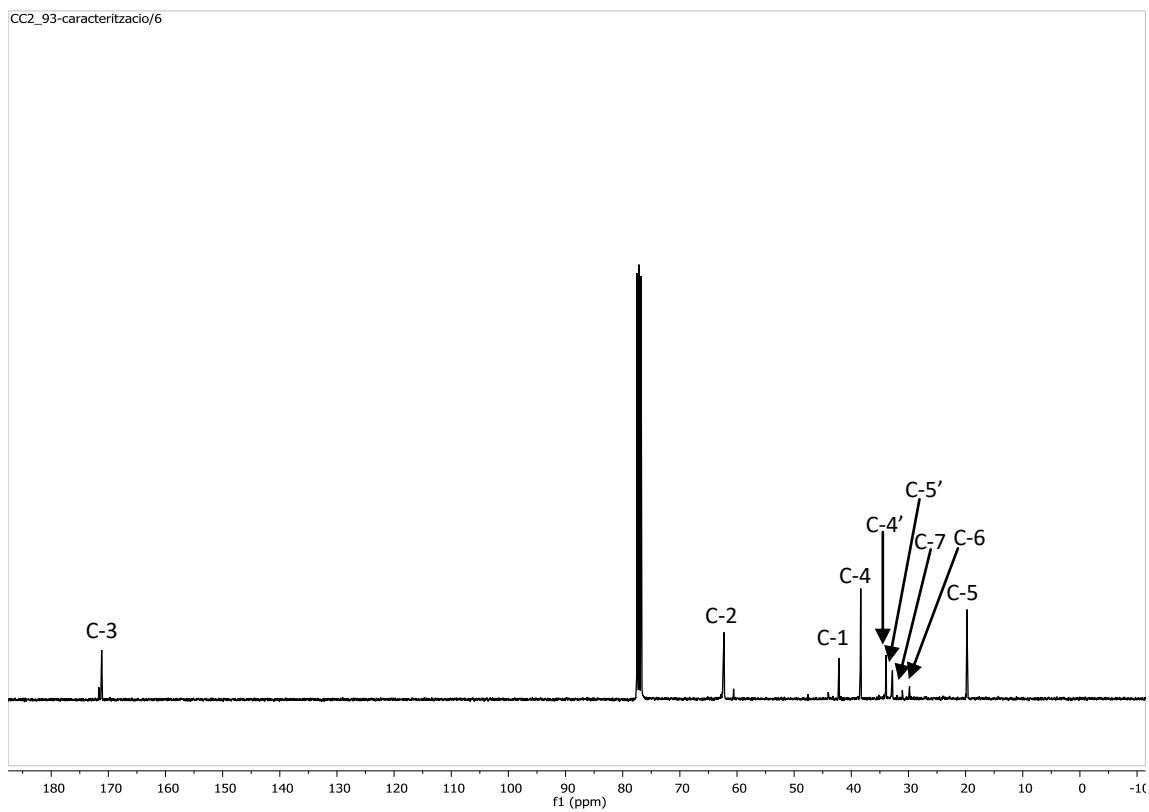
¹H NMR (400 MHz, CD₂Cl₂)

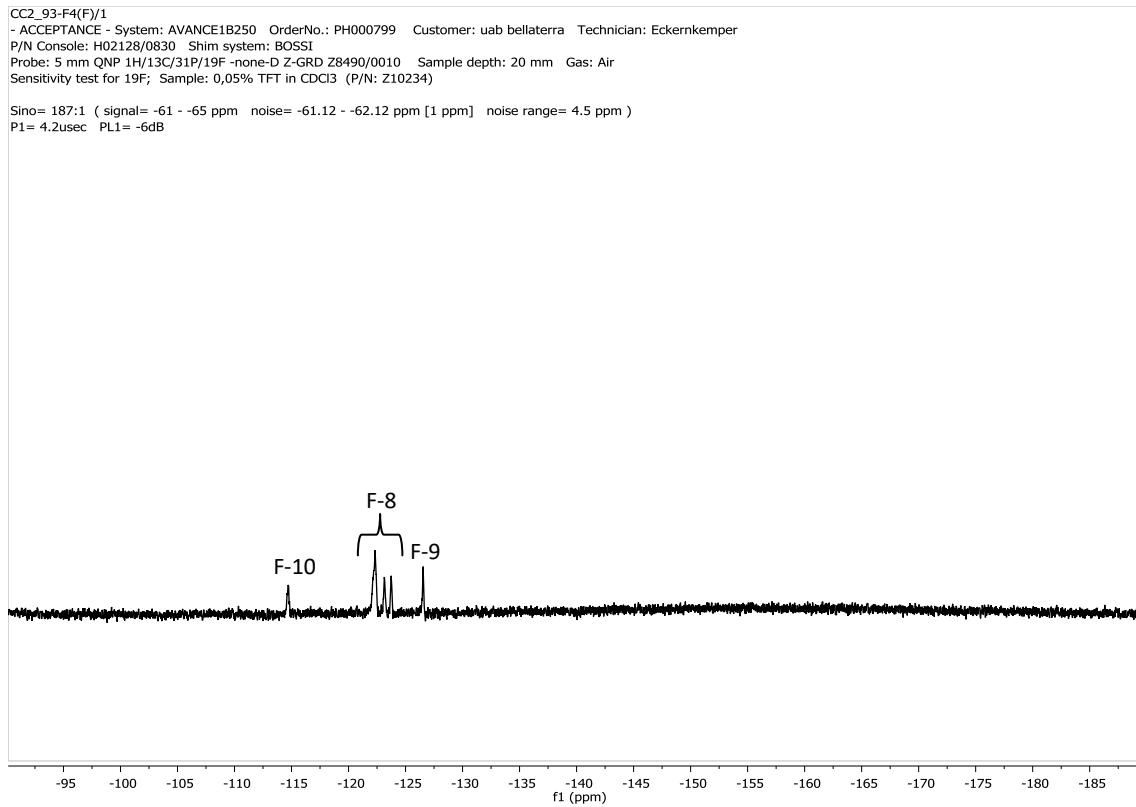
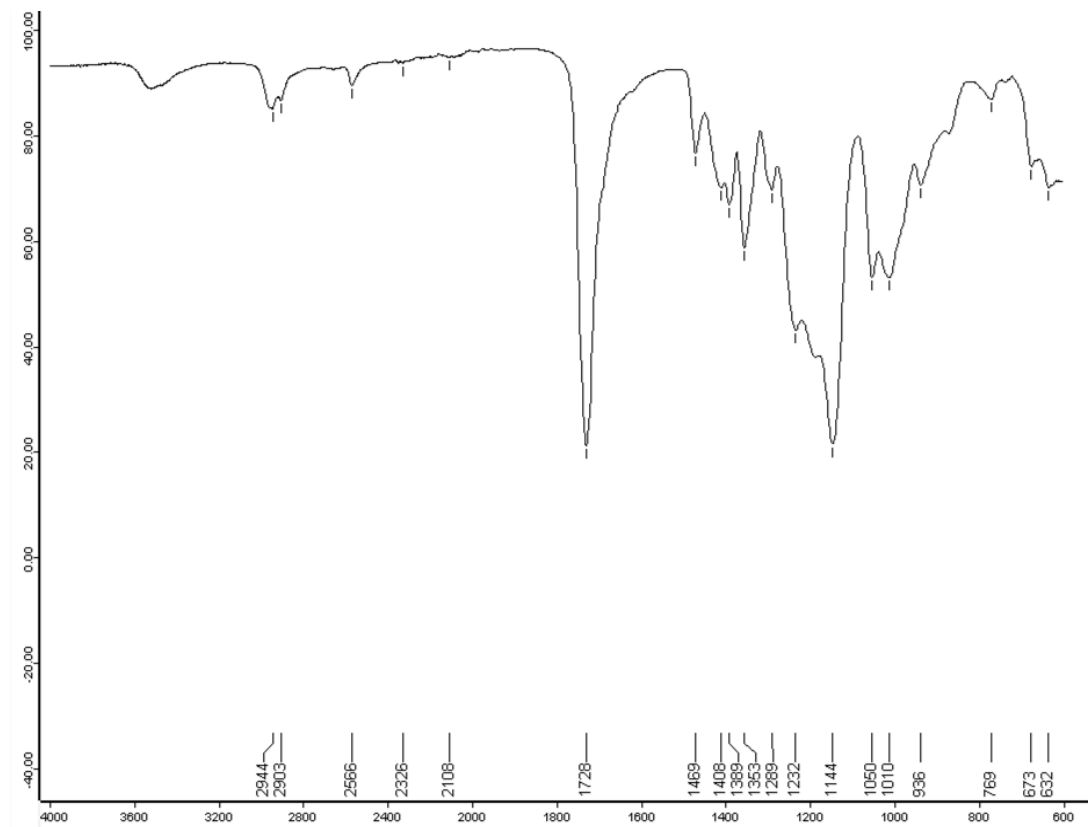


¹³C NMR (100.6 MHz, CDCl₃)

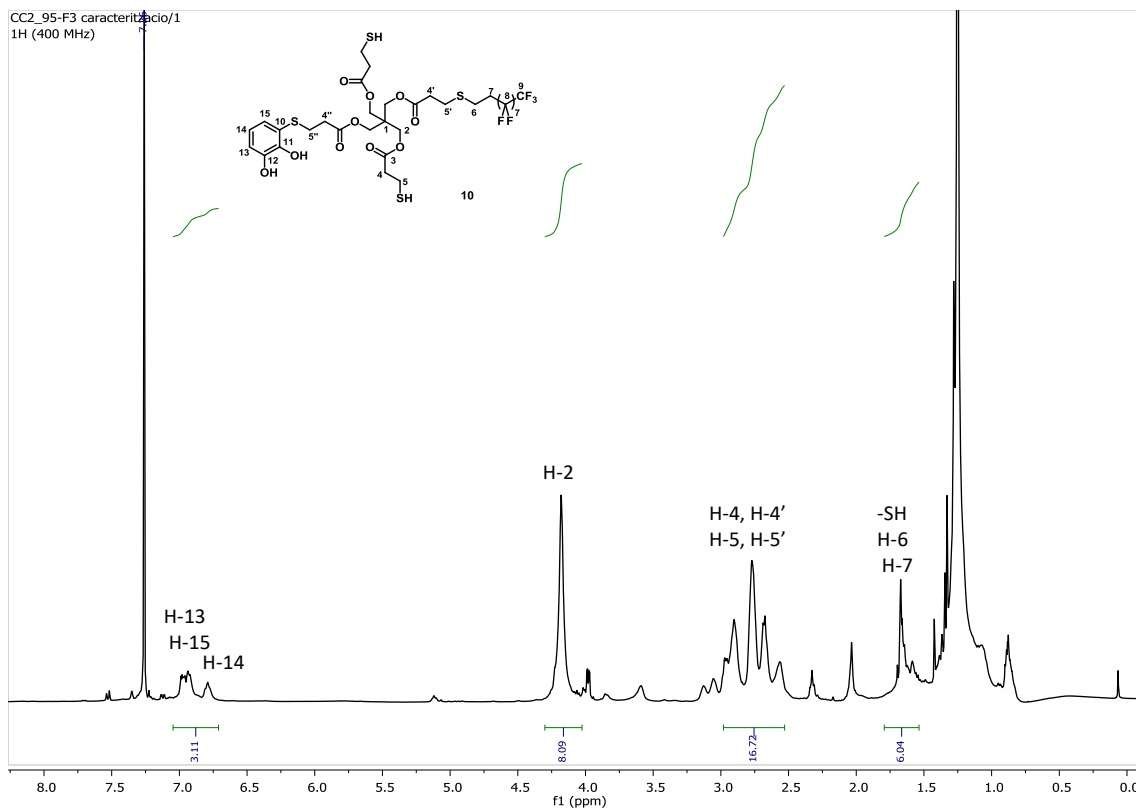
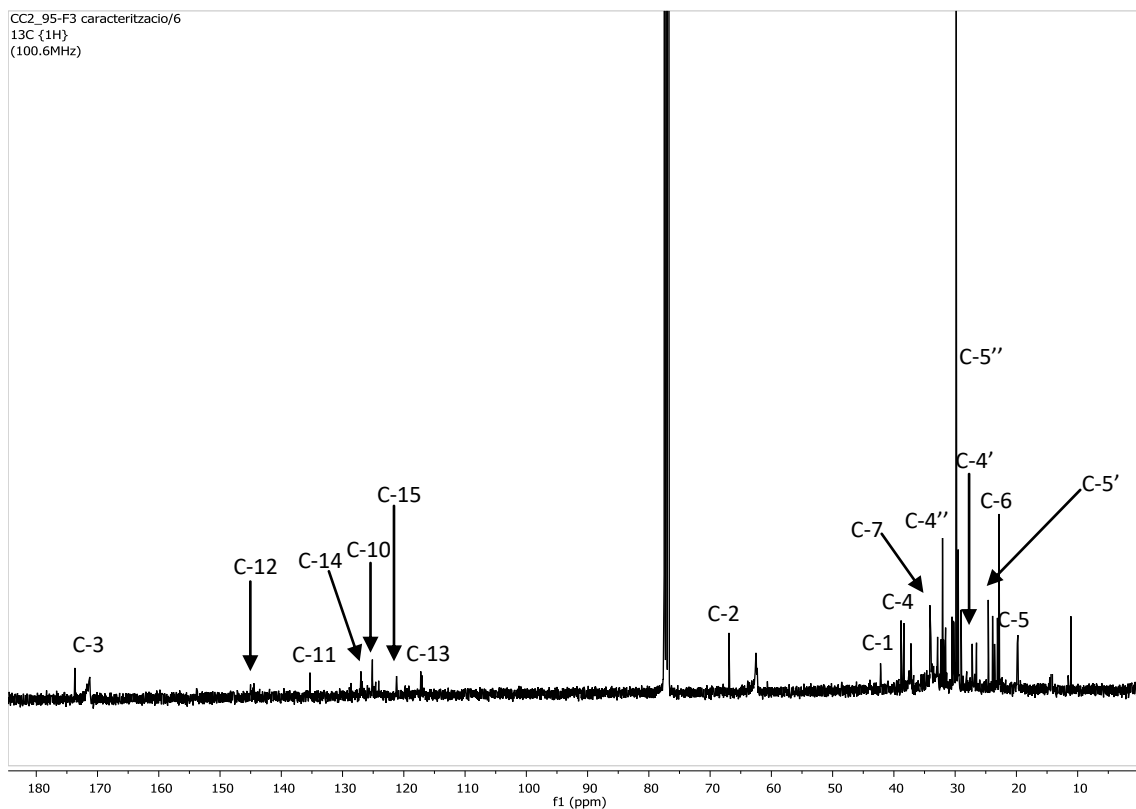


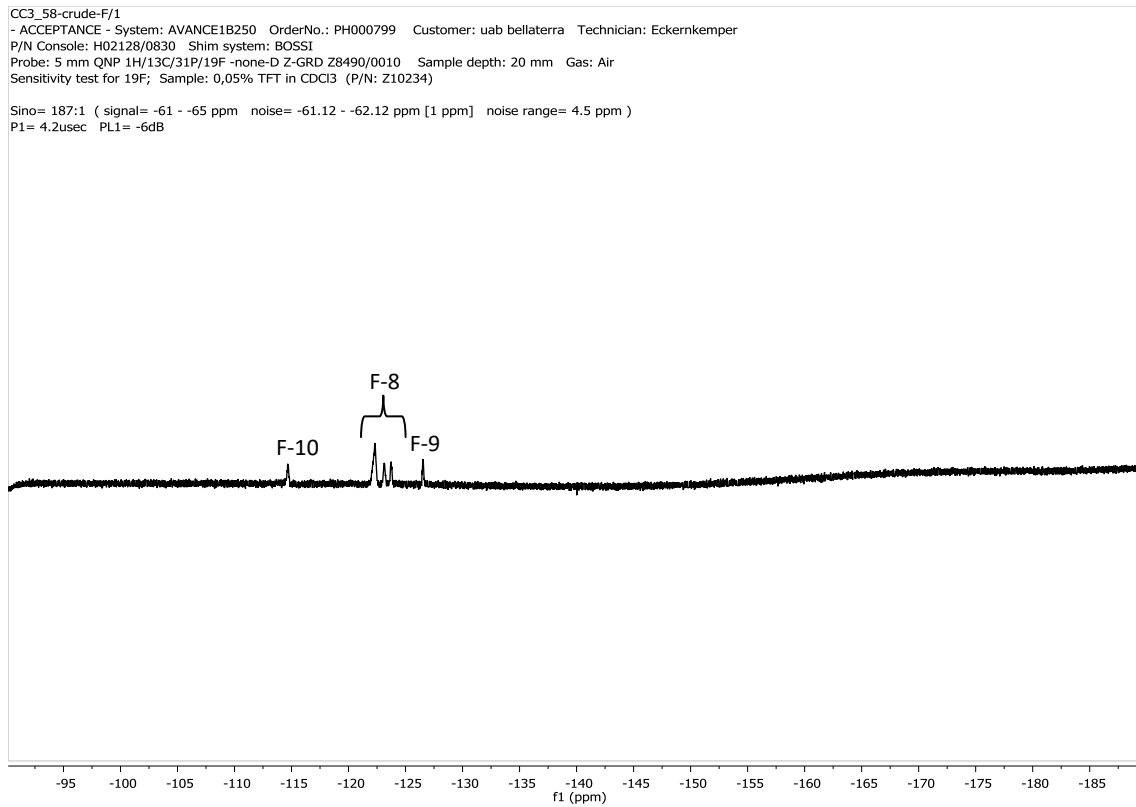
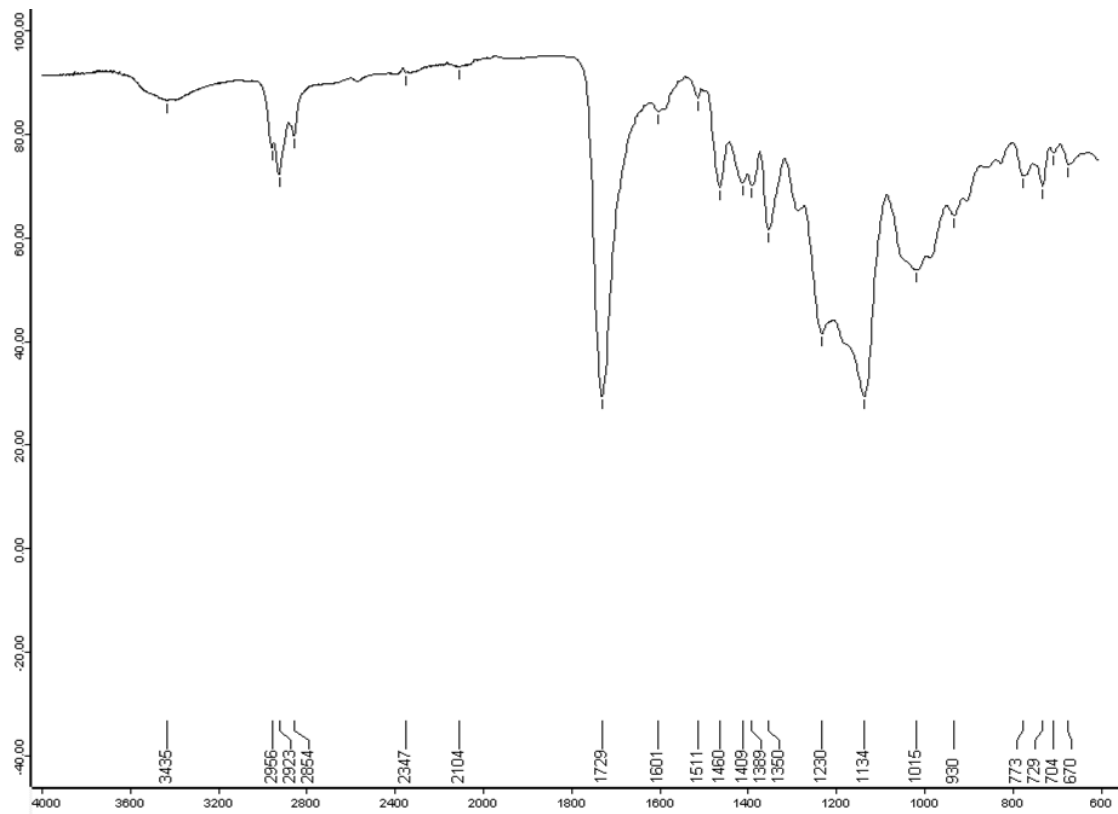
IR (ATR)

 ^1H NMR (360 MHz, CDCl_3) ^{13}C NMR (90.5 MHz, CDCl_3)

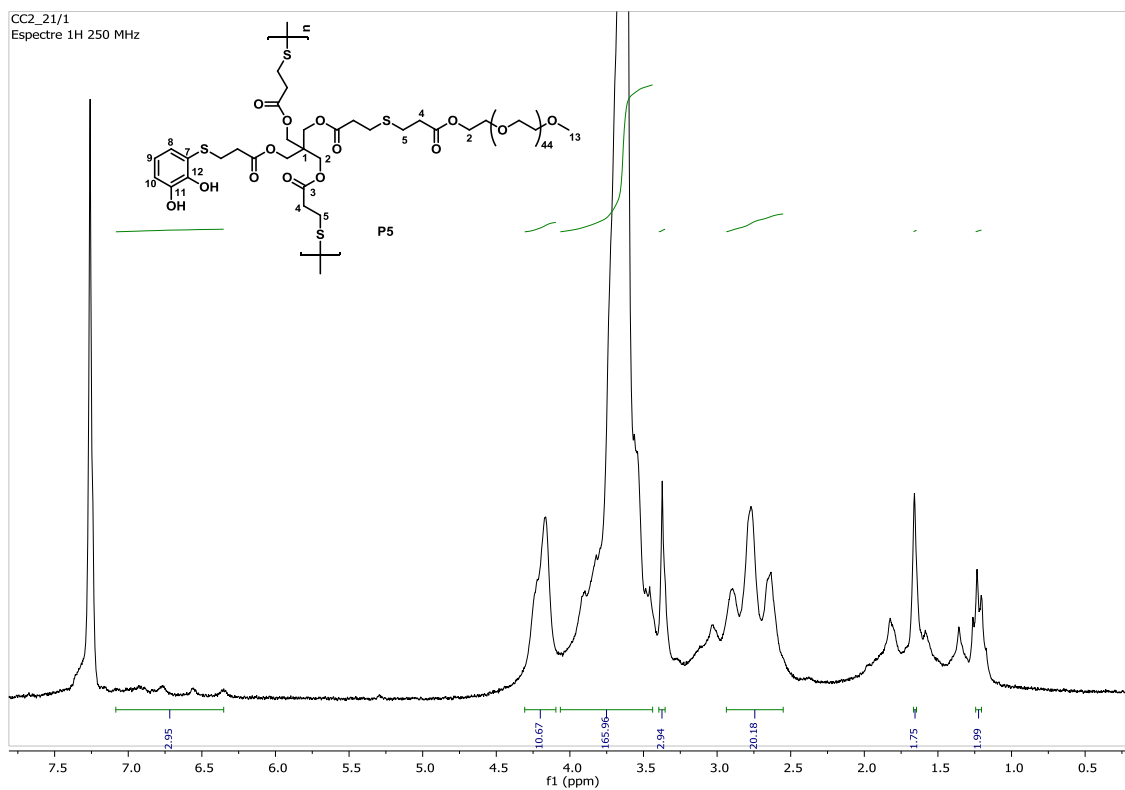
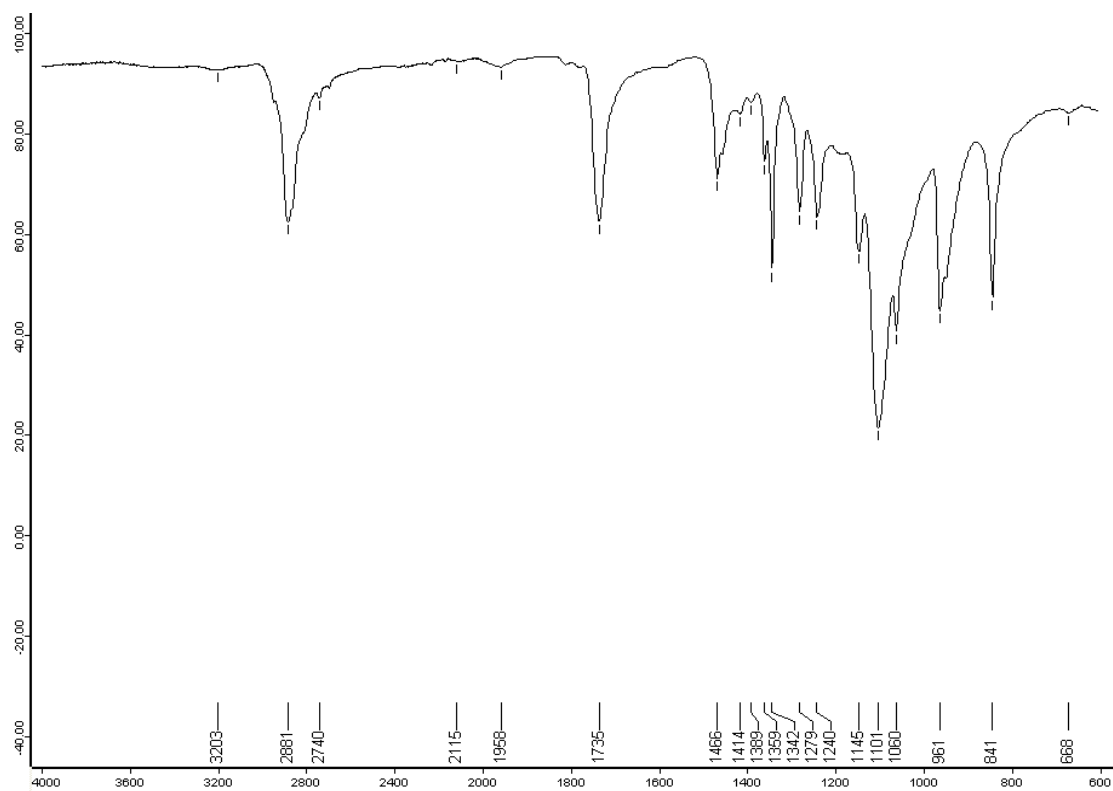
 ^{19}F NMR (235 MHz, CDCl_3)

IR (ATR)

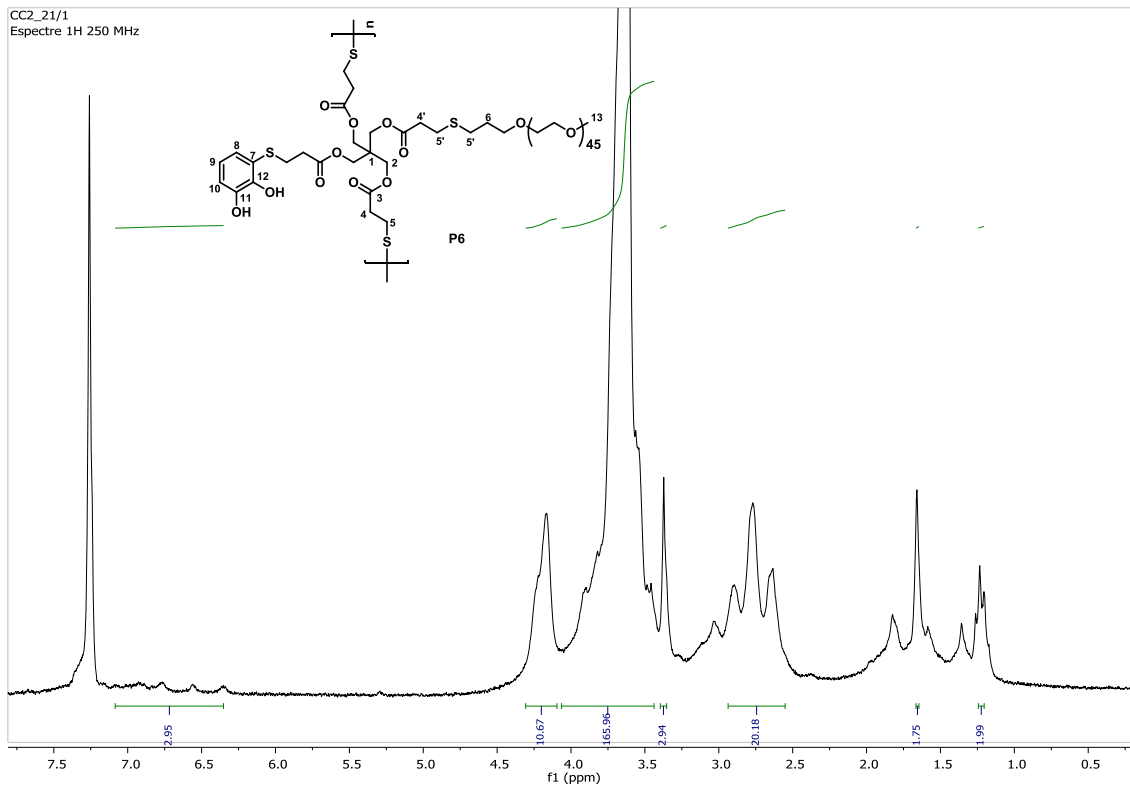
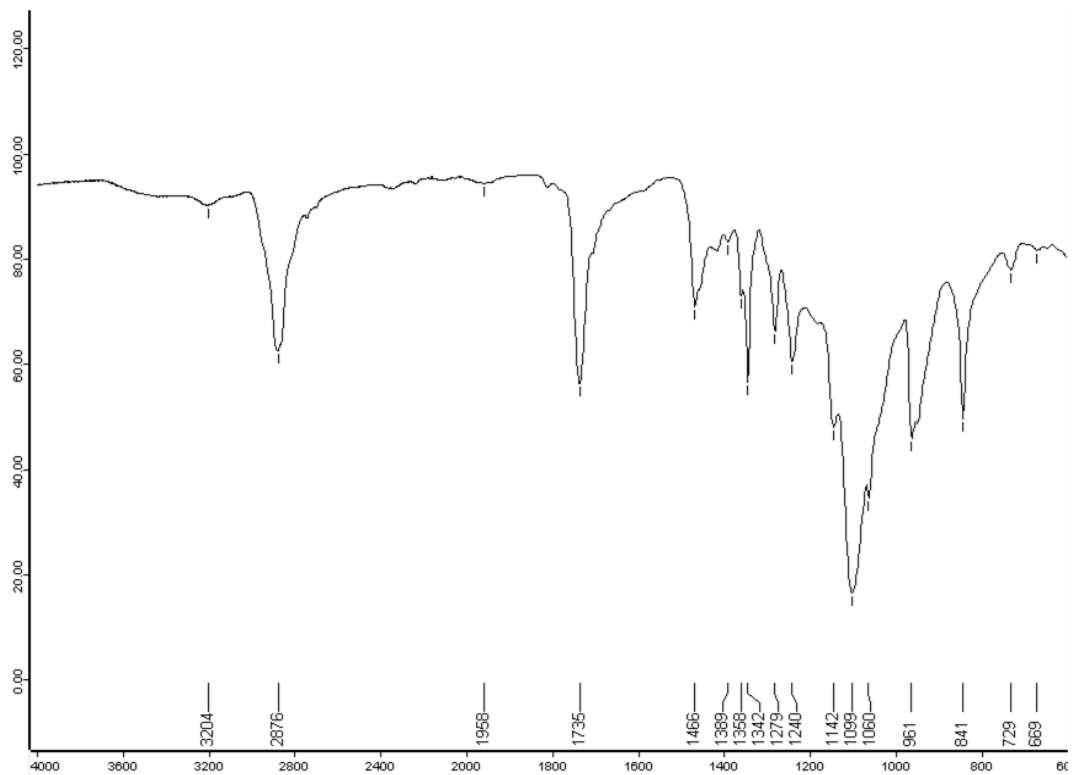
 ^1H NMR (360 MHz, CDCl_3) ^{13}C NMR (90.5 MHz, CDCl_3)

**¹⁹F NMR (235 MHz, CDCl₃)****IR (ATR)**

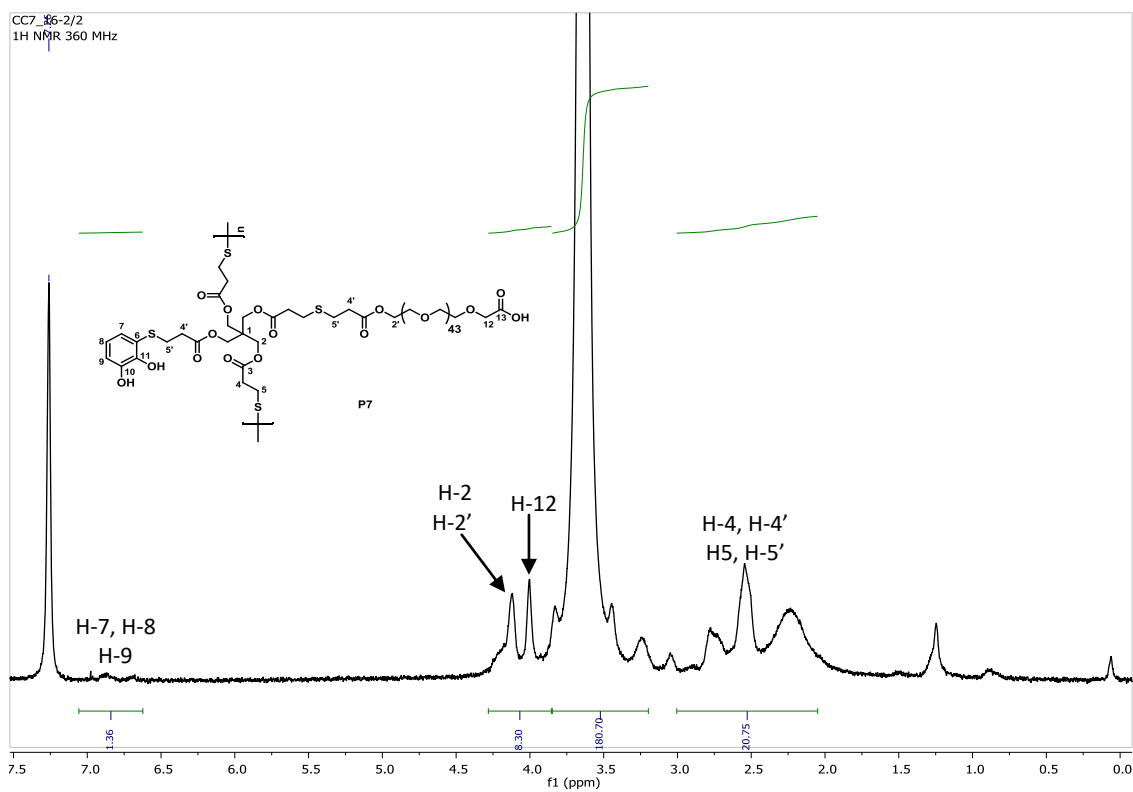
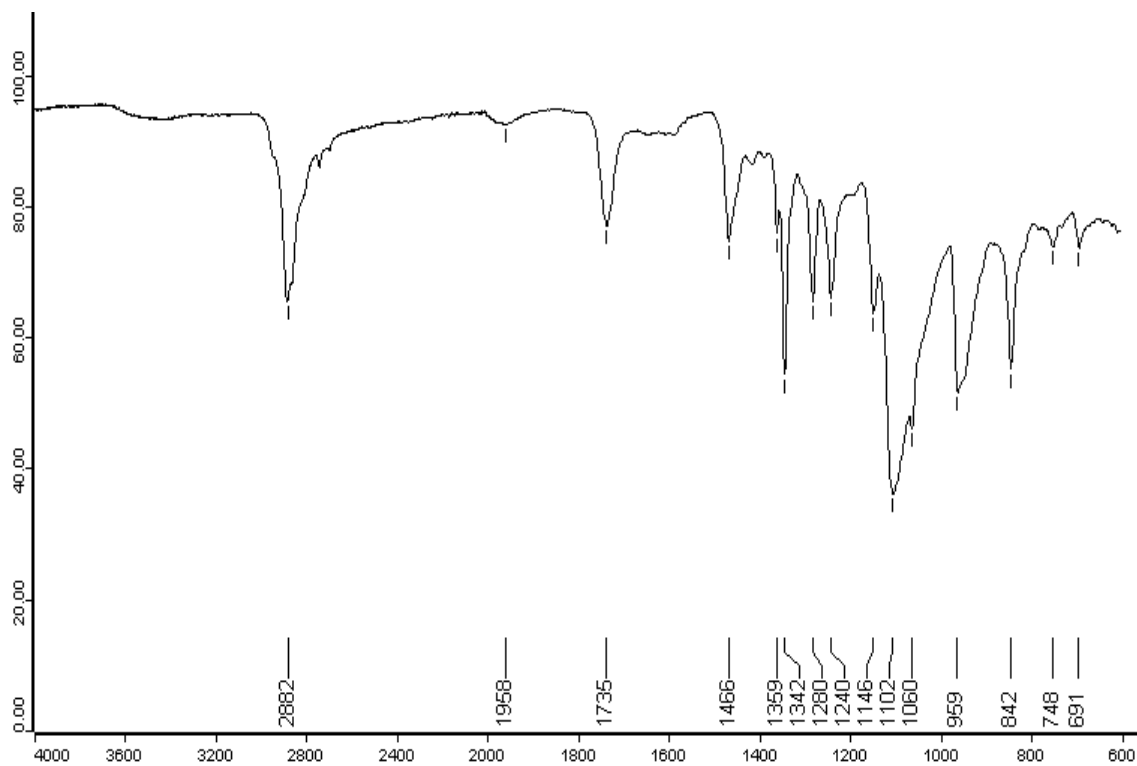
A1.2. Products from polymerisation reactions

 ^1H NMR (400 MHz, CDCl_3)

IR (ATR)

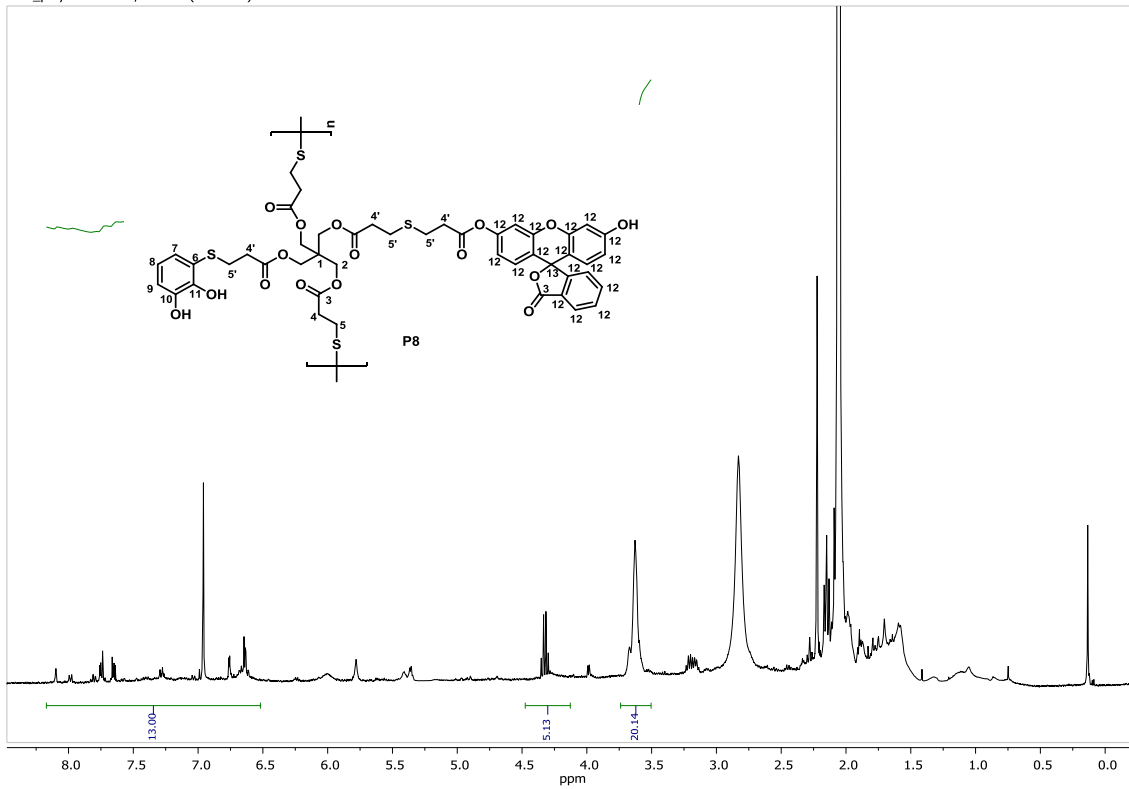
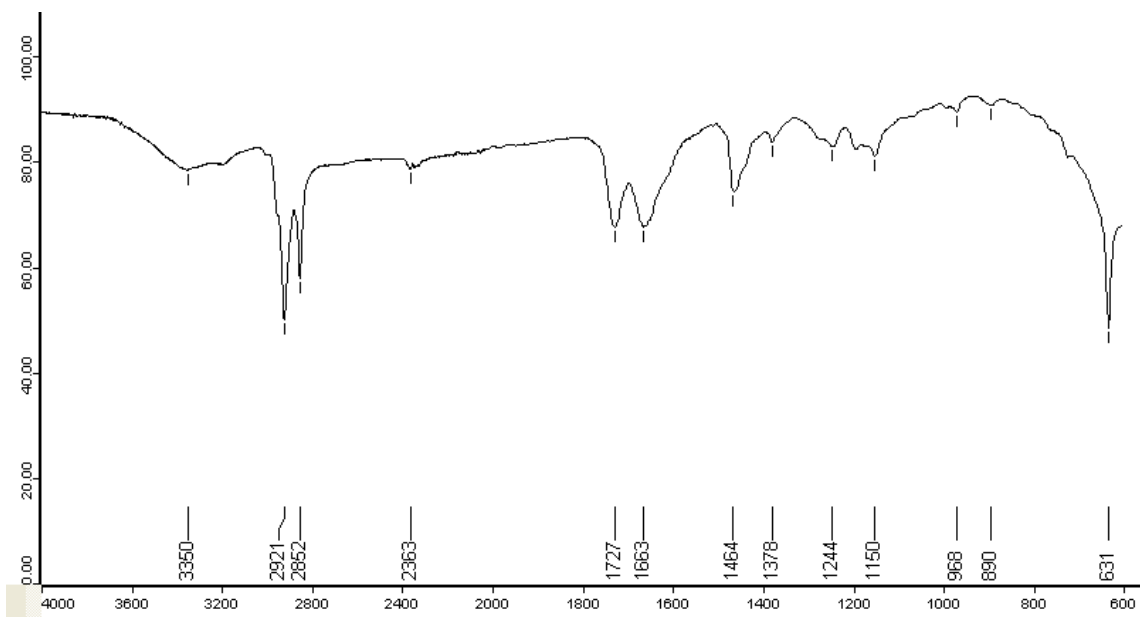
 ^1H NMR (360 MHz, CDCl_3)

IR (ATR)

 ^1H NMR (360 MHz, CDCl_3)

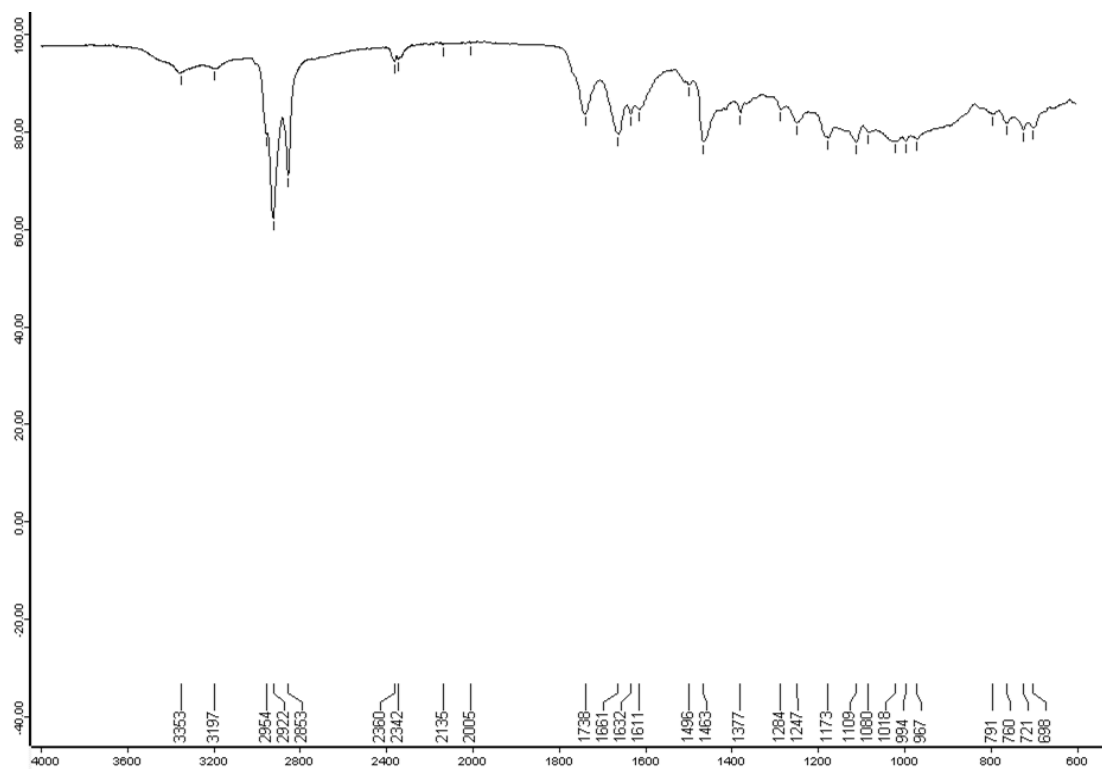
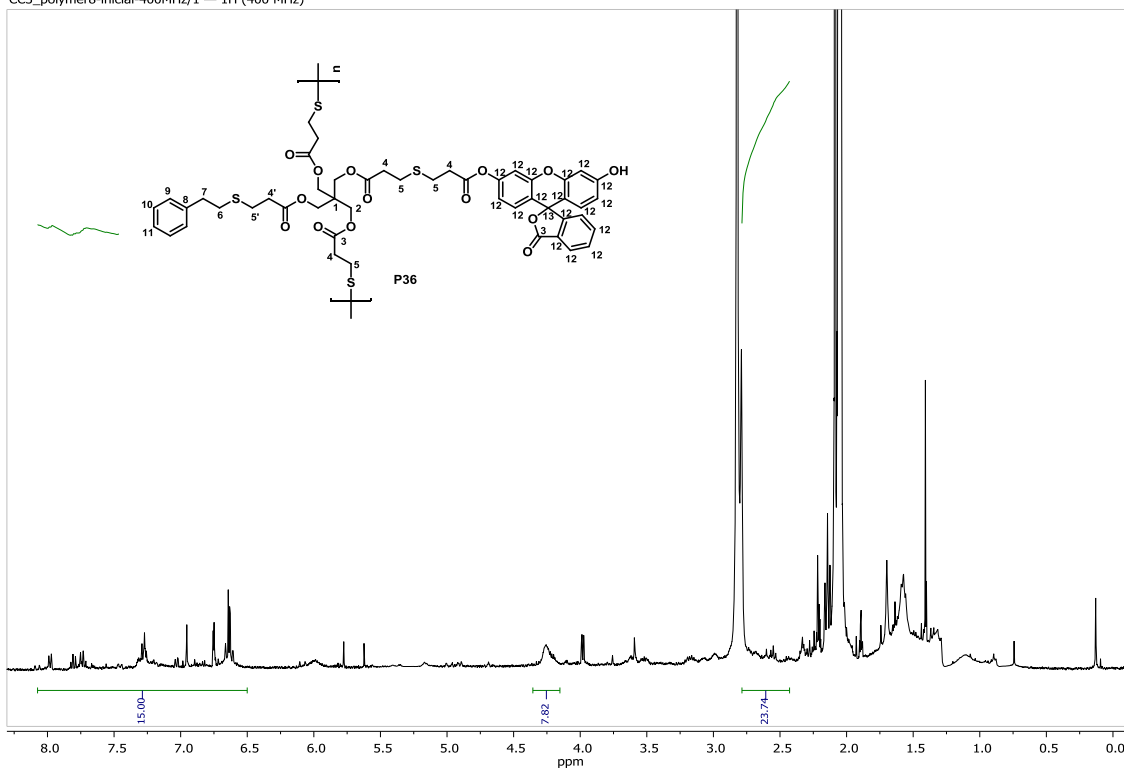
IR (ATR)

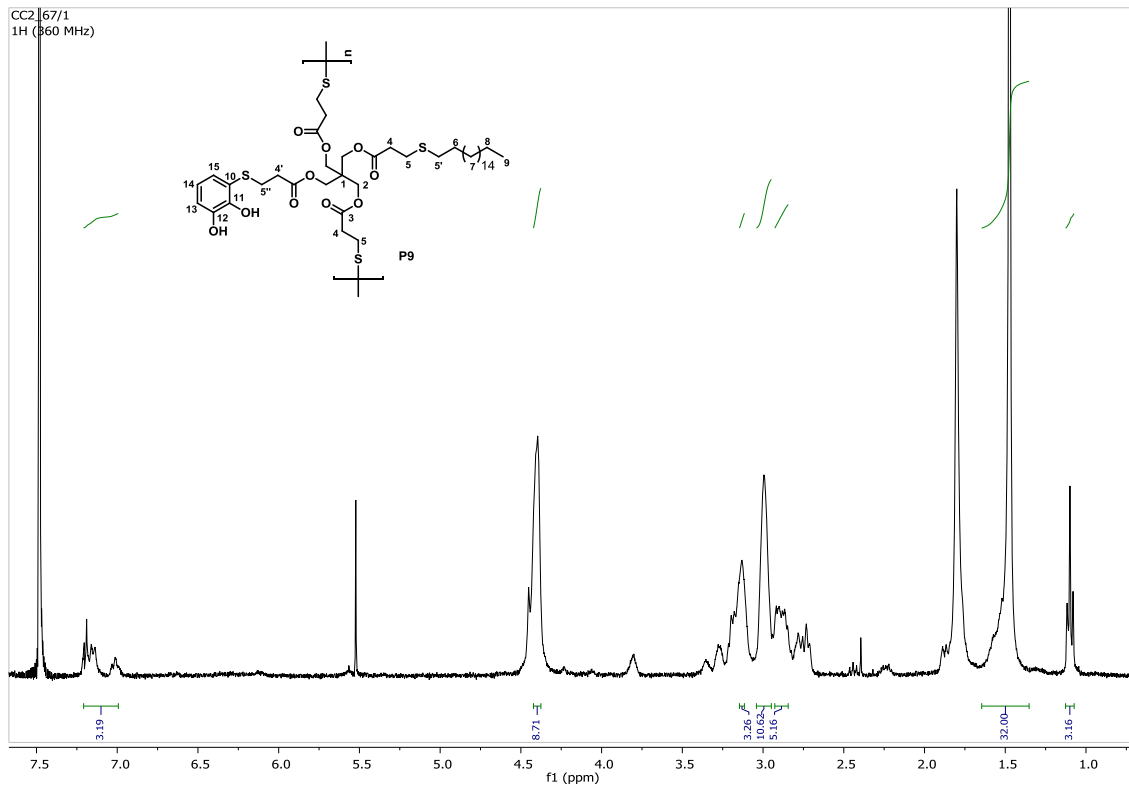
CC3_polymer7-inicial/4 — 1H (400 MHz)

¹H NMR (400 MHz, CDCl₃)

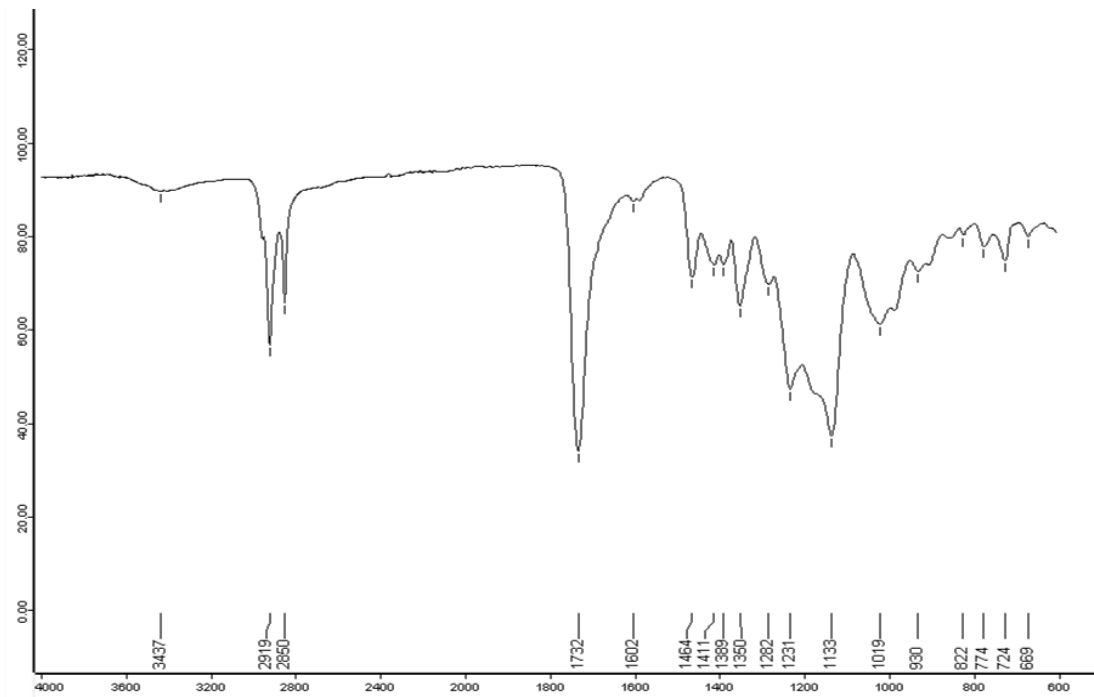
IR (ATR)

CC3_polymer8-inicial-400MHz/1 — 1H (400 MHz)

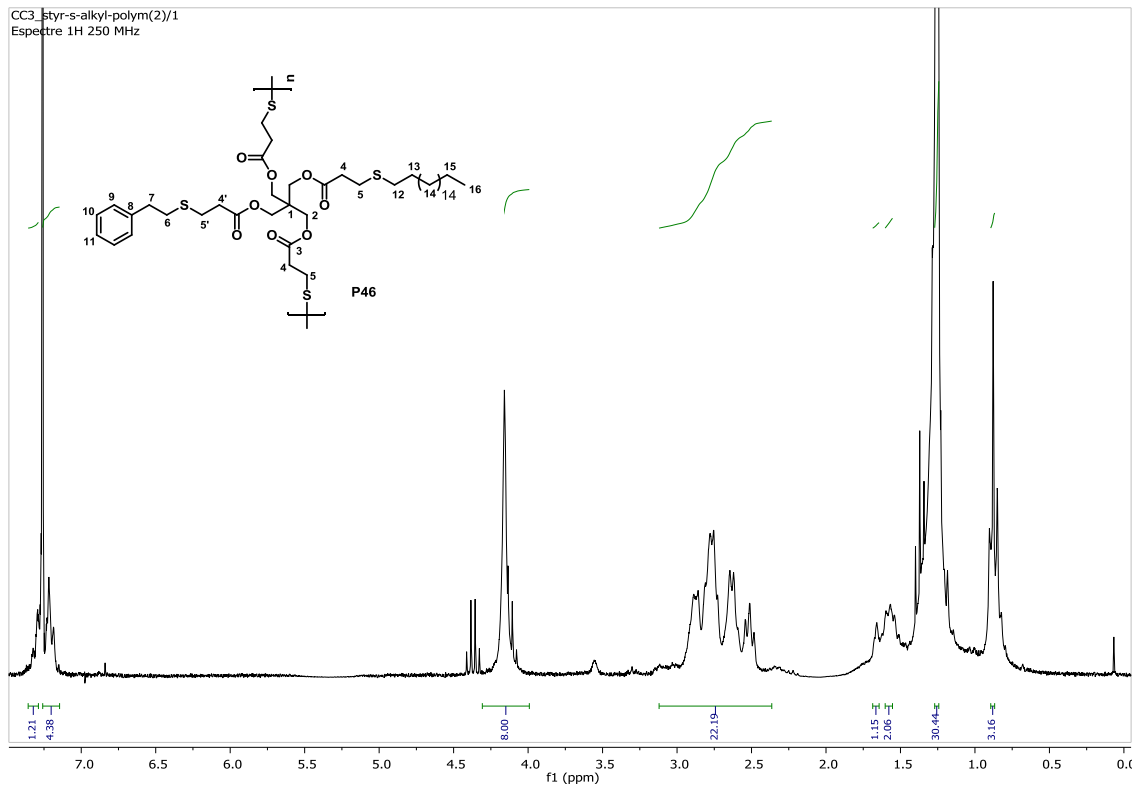
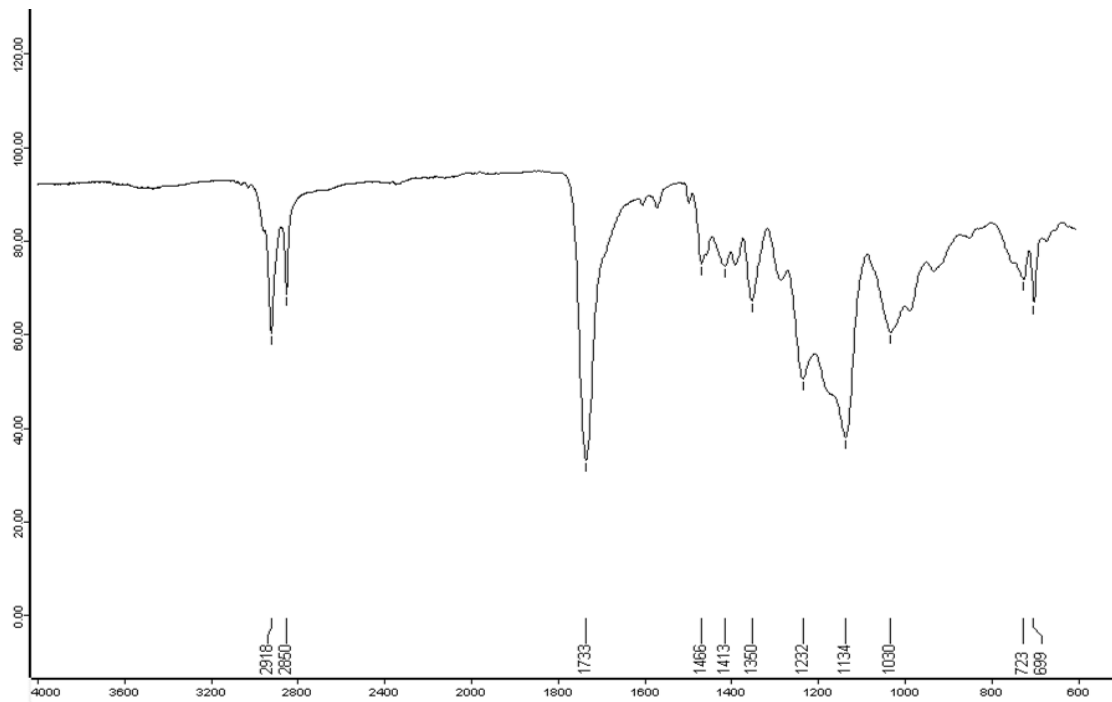




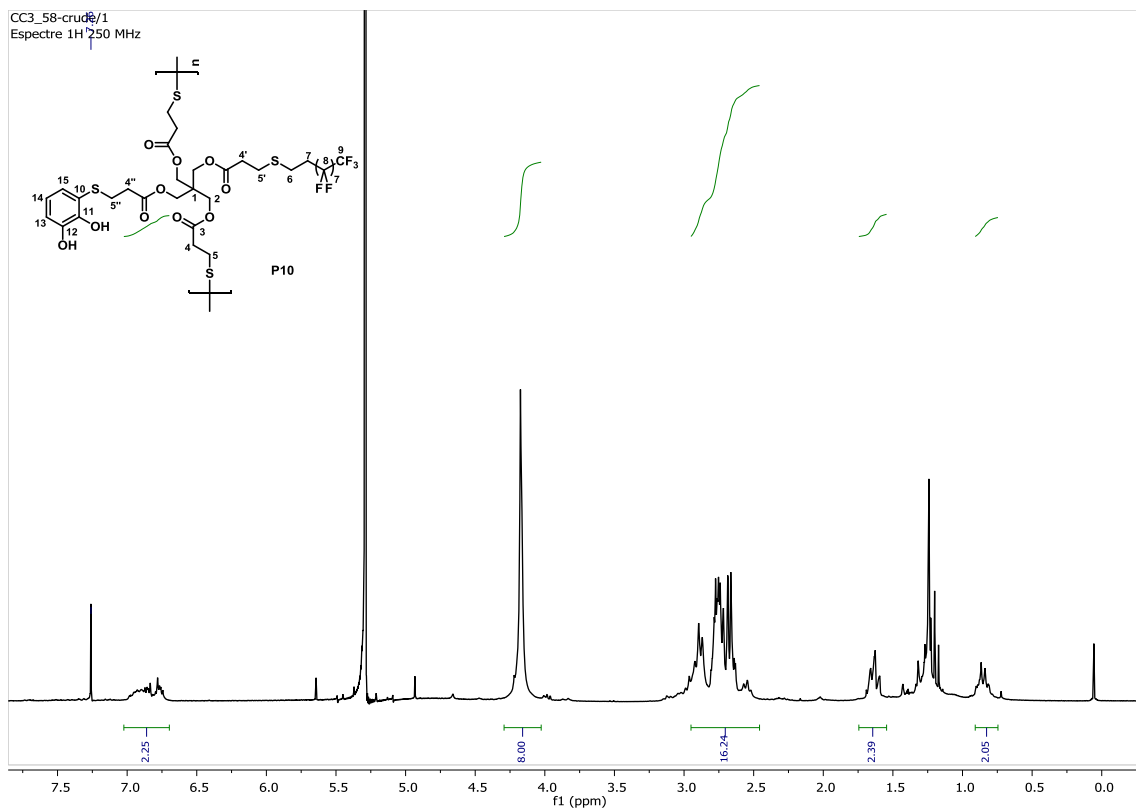
¹H NMR (400 MHz, CDCl₃)



IR (ATR)

 ^1H NMR (400 MHz, CDCl_3)

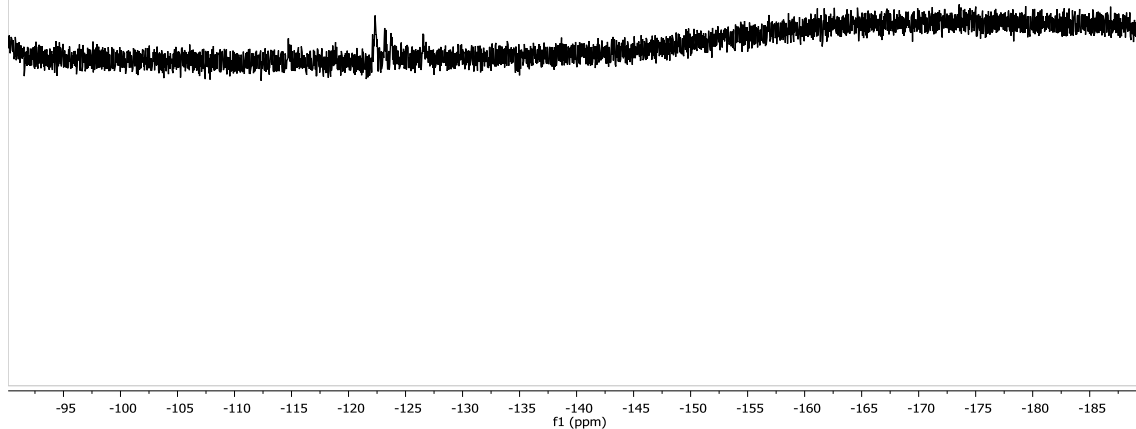
IR (ATR)



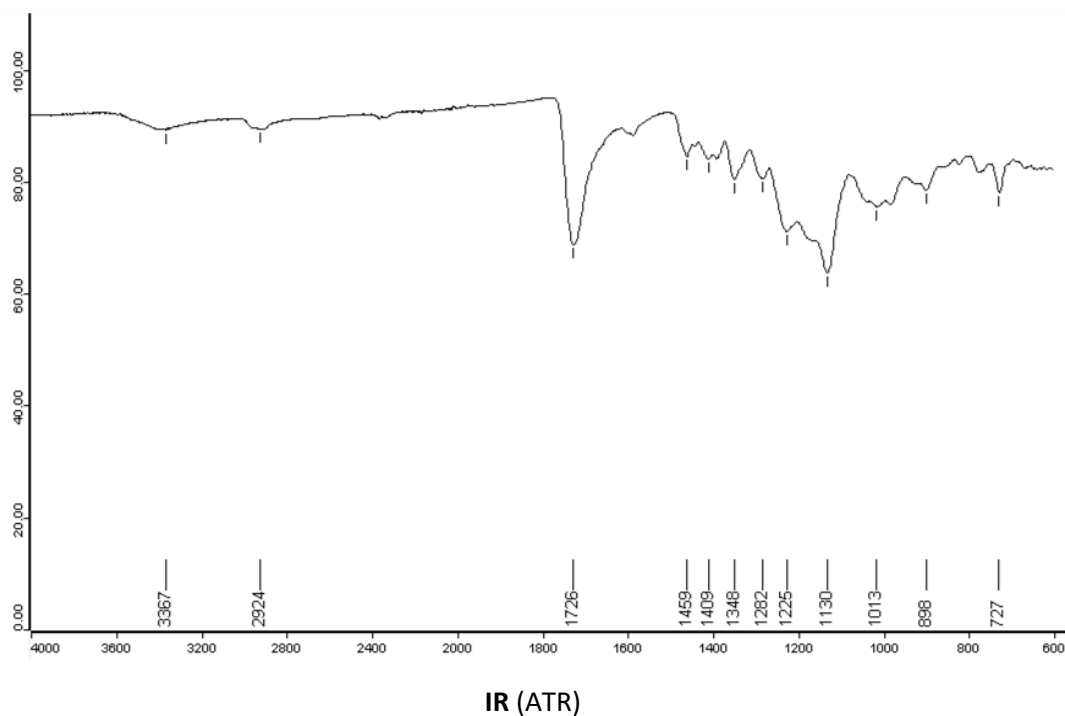
¹H NMR (360 MHz, CDCl₃)

CC2_95-F3(F)/1
- ACCEPTANCE - System: AVANCE1B250 OrderNo.: PH000799 Customer: uab bellaterra Technician: Eckernkemper
P/N Console: H02128/0830 Shim system: BOSSI
Probe: 5 mm QNP 1H/13C/31P/19F -none-D Z-GRD Z8490/0010 Sample depth: 20 mm Gas: Air
Sensitivity test for 19F; Sample: 0,05% TFT in CDCl₃ (P/N: Z10234)

Sino= 187:1 (signal= -61 - -65 ppm noise= -61.12 - -62.12 ppm [1 ppm] noise range= 4.5 ppm)
P1= 4.2usec PL1= -6dB



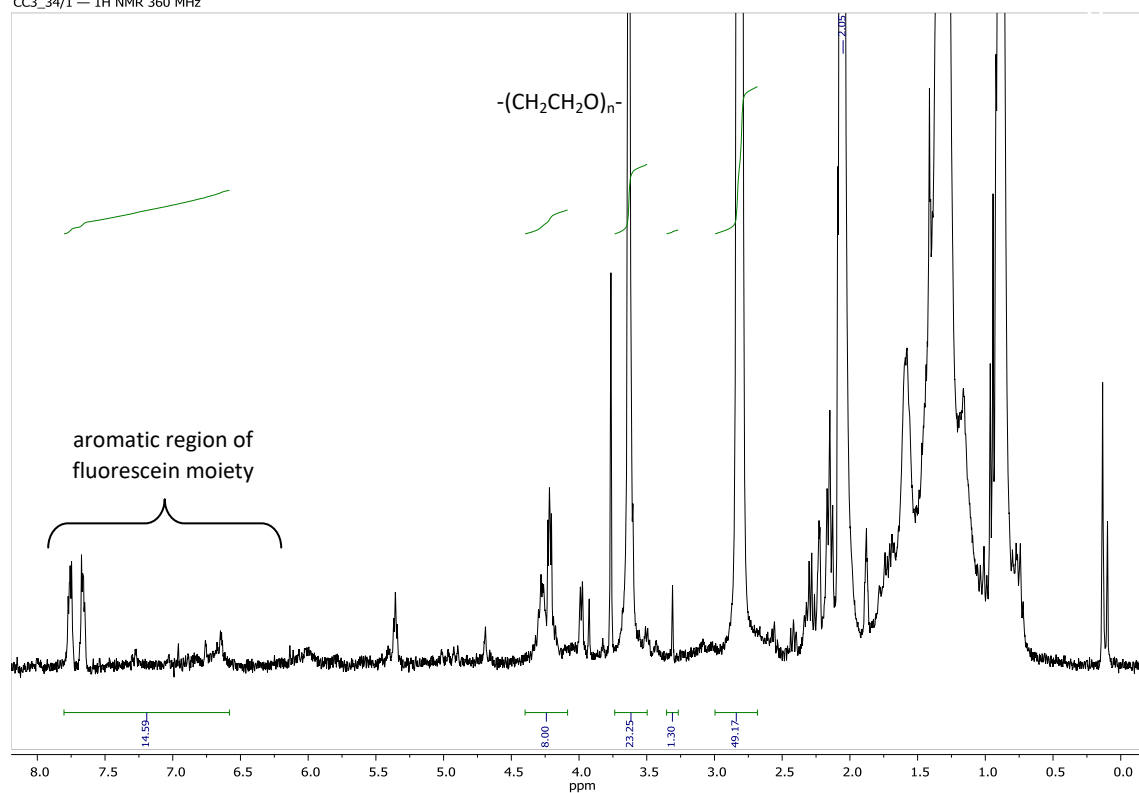
¹⁹F NMR (235 MHz, CDCl₃)



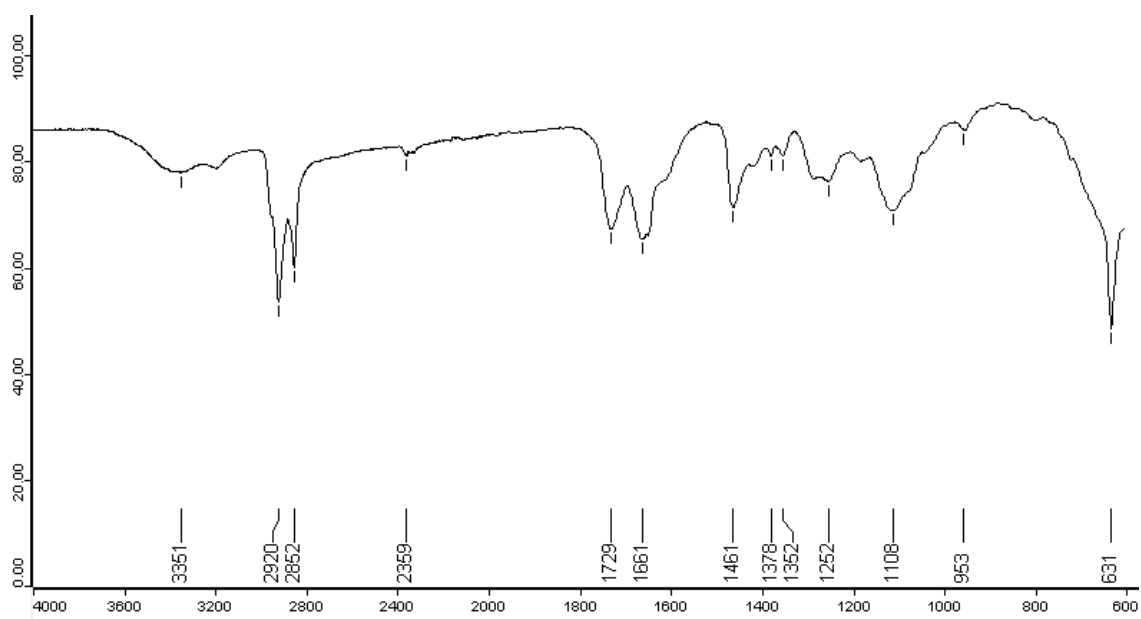
A1.3. Copolymers

Fluorescein-PEG-functionalised copolymer C6-8

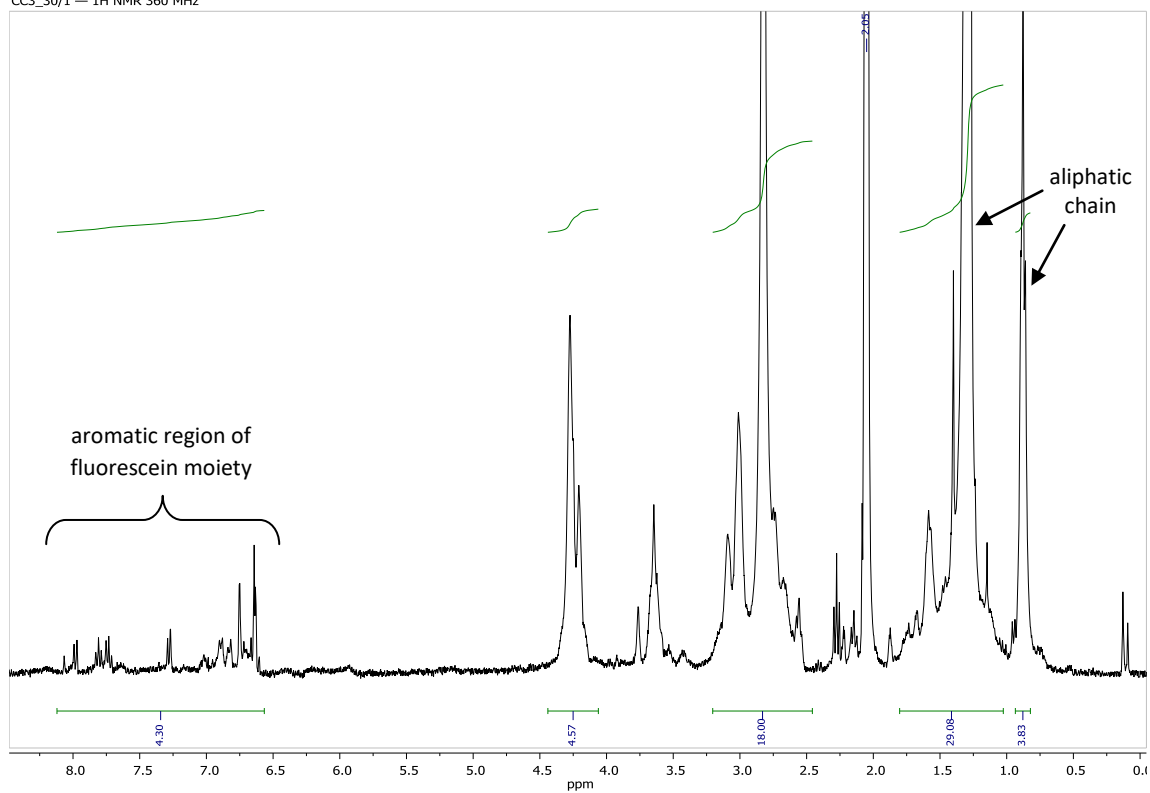
CC3_34/1 — 1H NMR 360 MHz

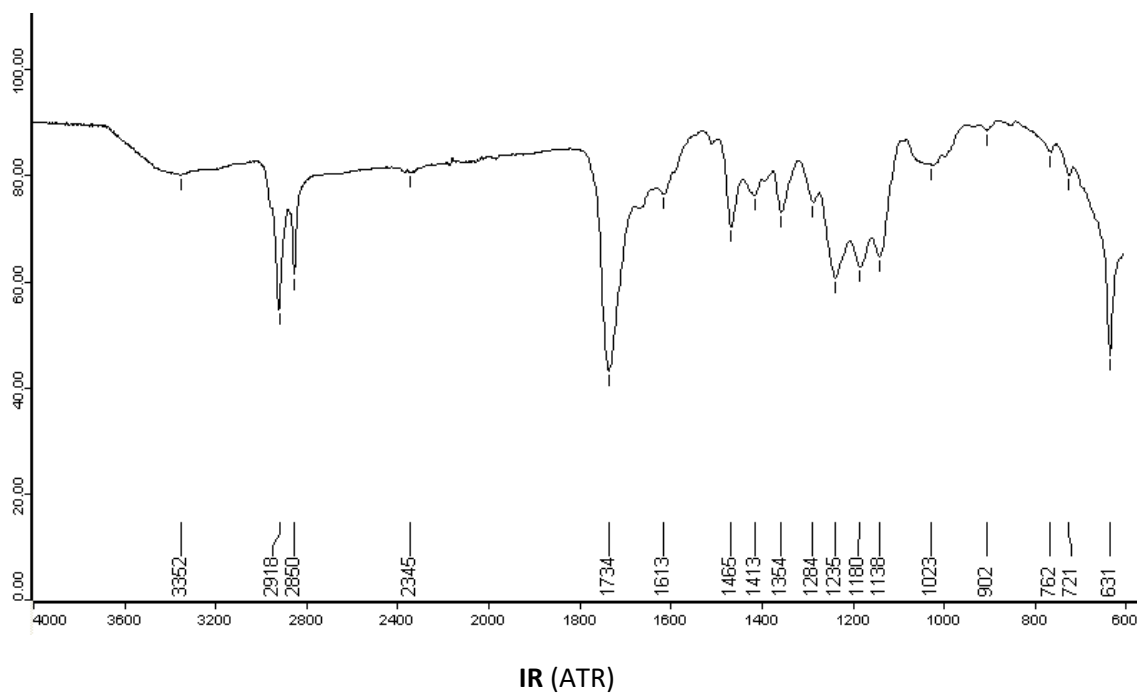
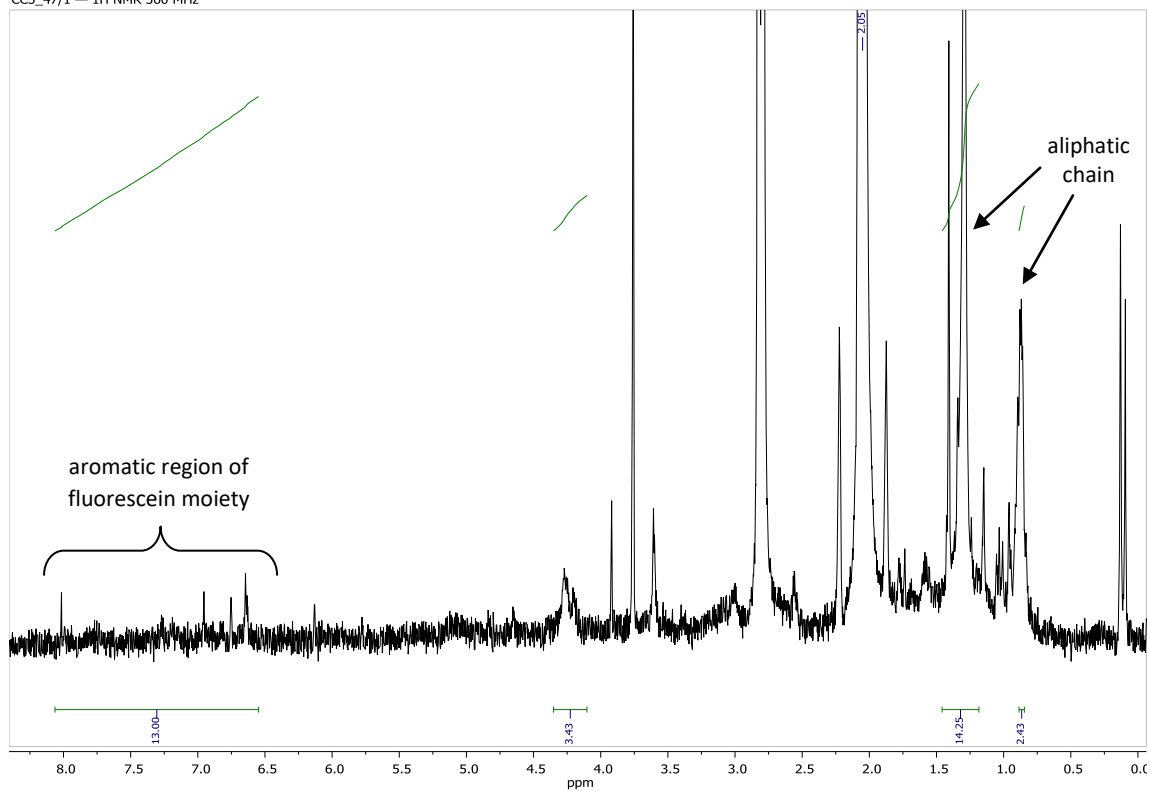


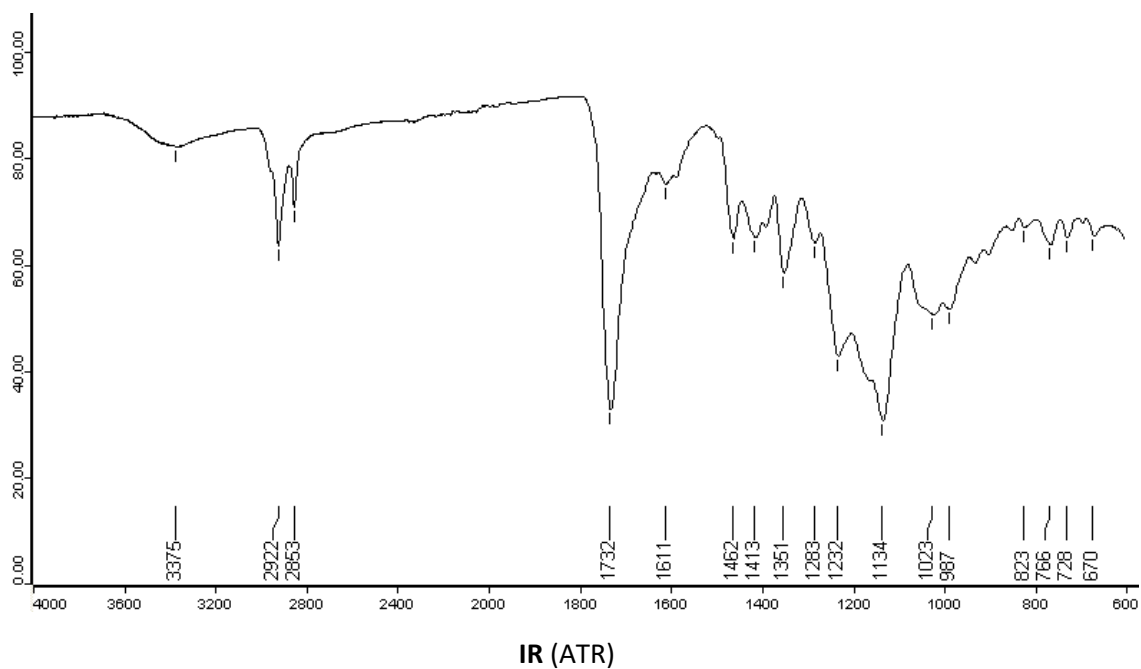
$^1\text{H NMR}$ (360 MHz, $(\text{CD}_3)_2\text{CO}$)



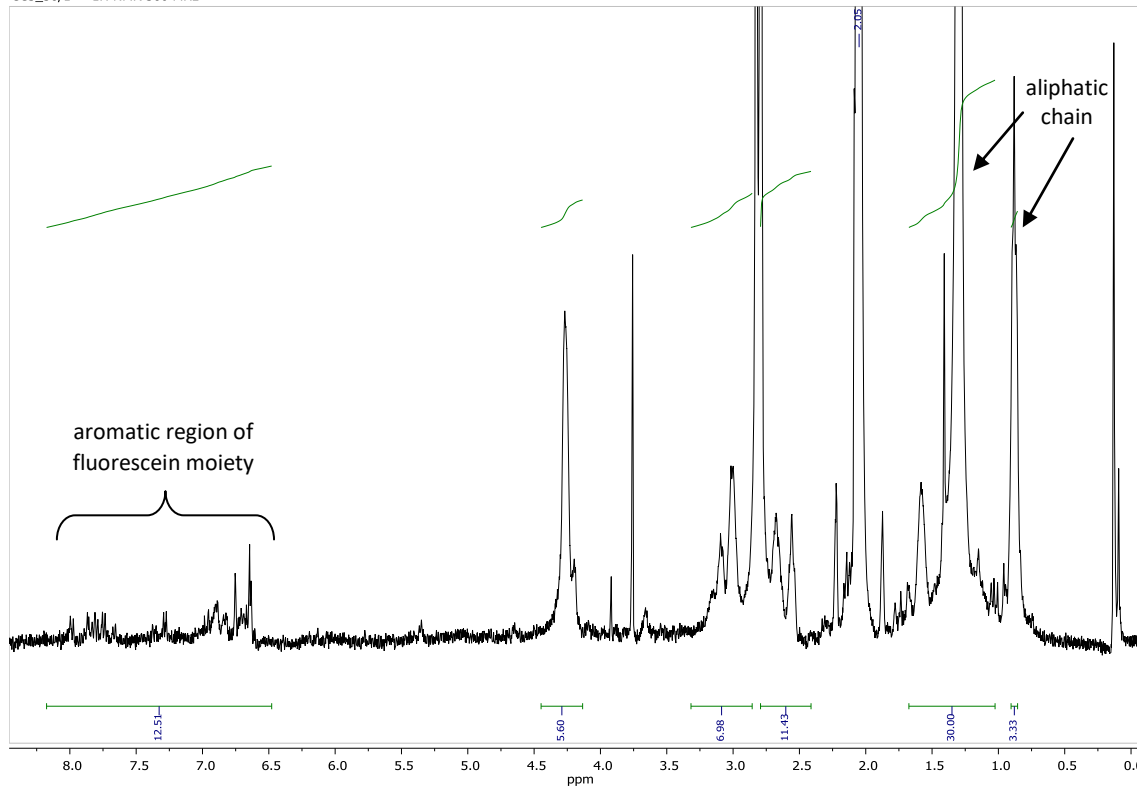
IR (ATR)

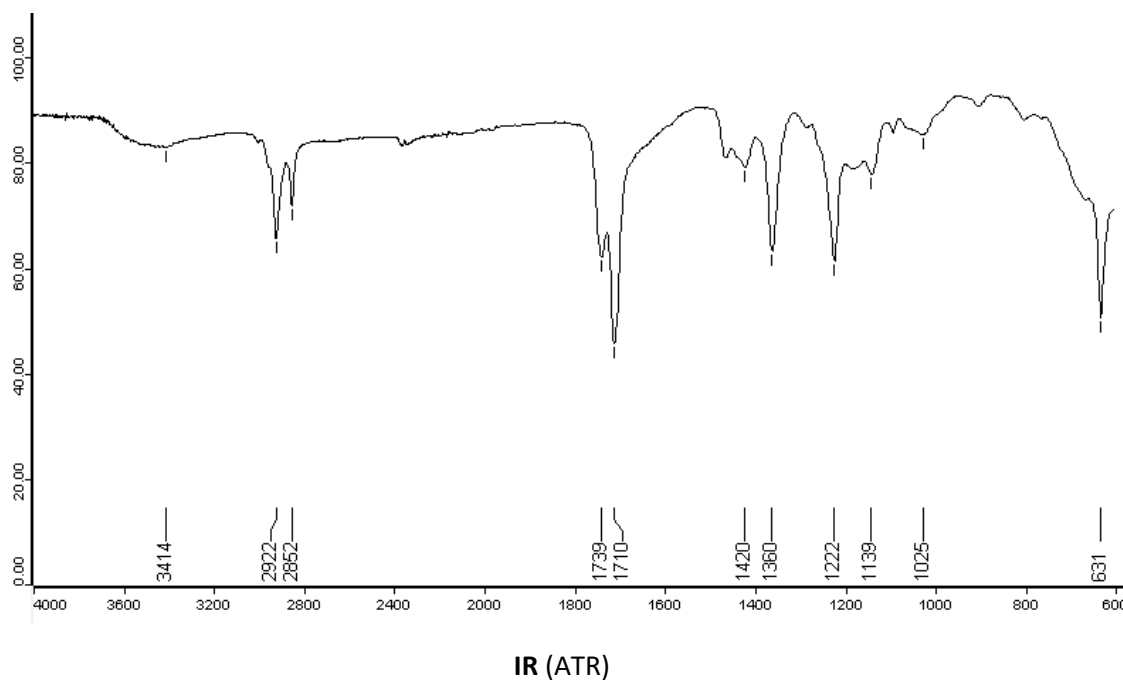
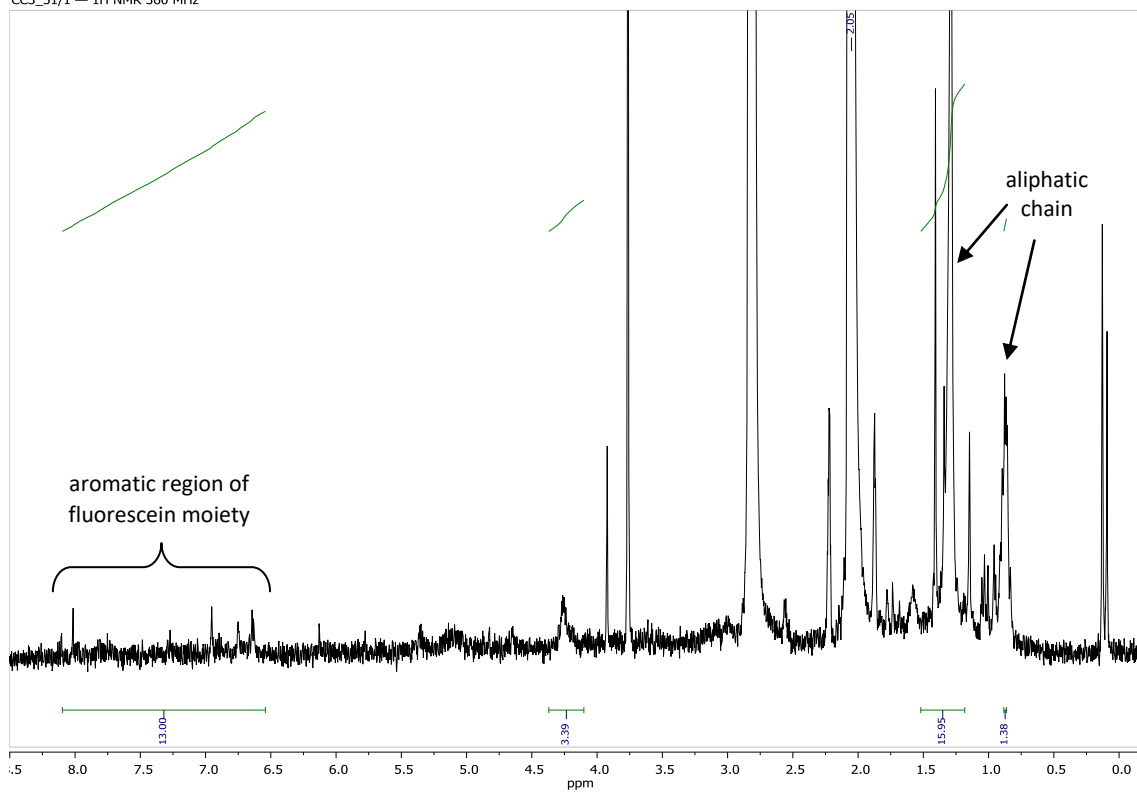
Fluorescein- C_{18} -functionalised copolymer C8-9aCC3_30/1 — ^1H NMR 360 MHz ^1H NMR (360 MHz, $(\text{CD}_3)_2\text{CO}$)

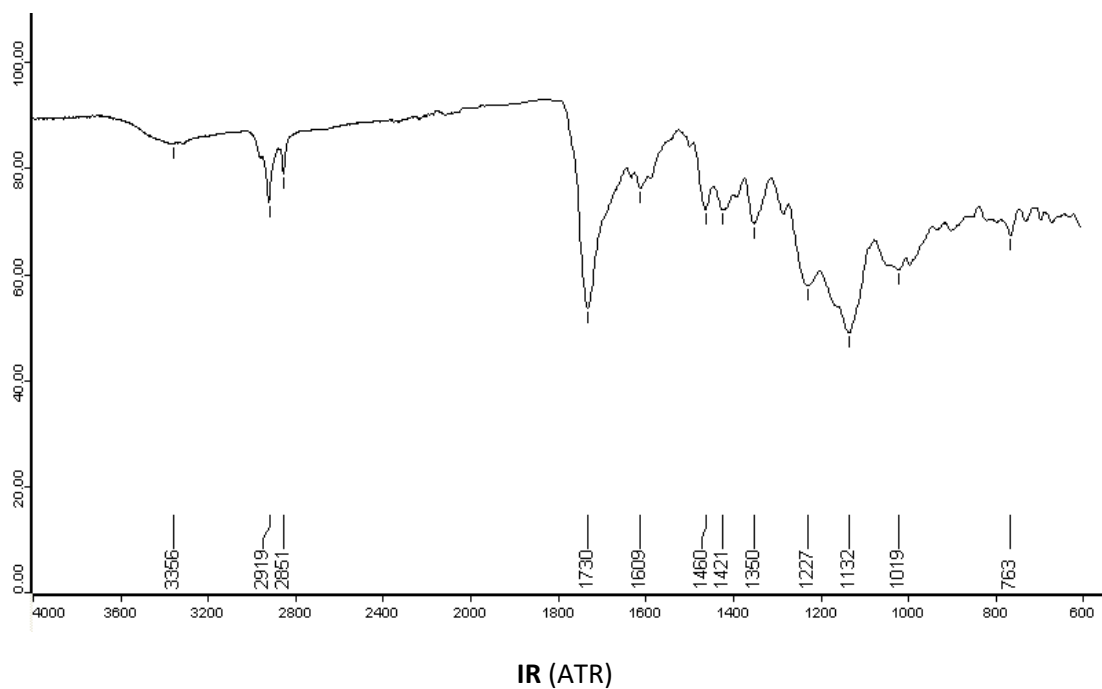
**Fluorescein- C_{18} -functionalised copolymer C8-9b**CC3_47/1 — ^1H NMR 360 MHz ^1H NMR (360 MHz, $(\text{CD}_3)_2\text{CO}$)

**Fluorescein- C_{18} -functionalised copolymer C8-9c**

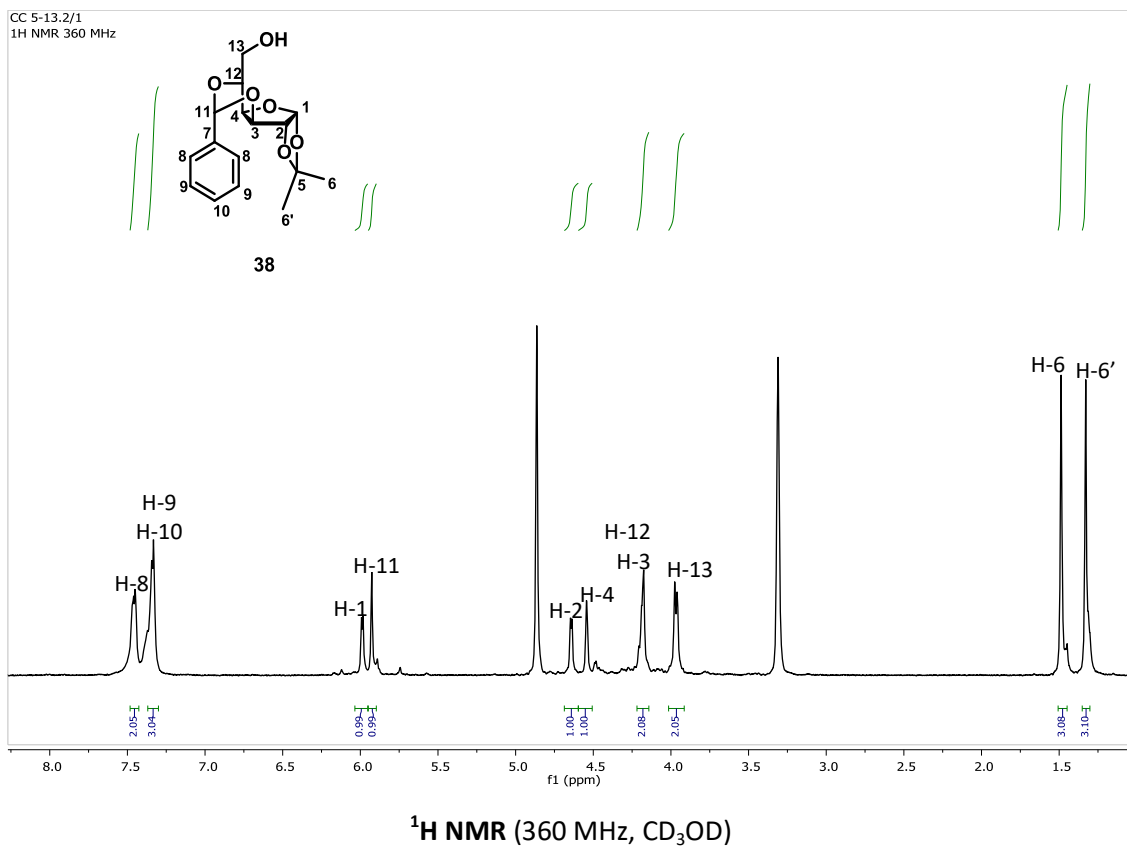
CC3_56/1 — 1H NMR 360 MHz

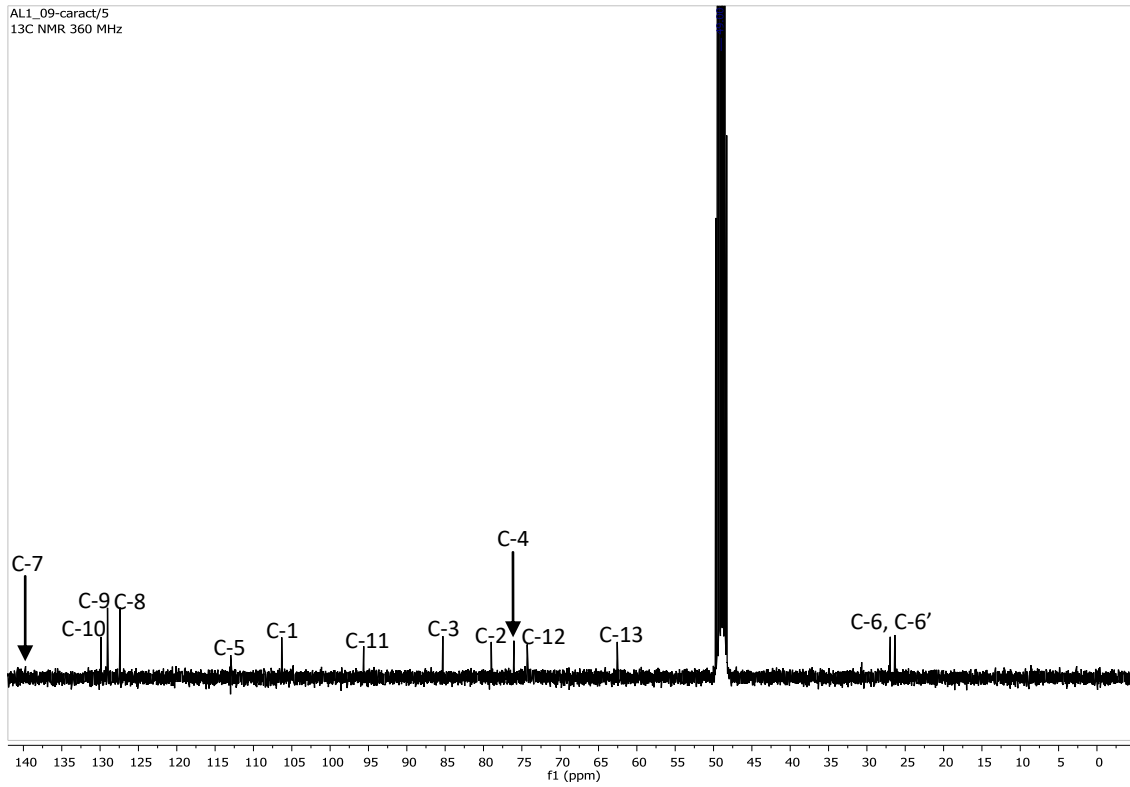
 $^1\text{H NMR}$ (360 MHz, $(\text{CD}_3)_2\text{CO}$)

**Fluorescein- C_{18} -functionalised copolymer C8-9d**CC3_51/1 — ^1H NMR 360 MHz ^1H NMR (360 MHz, $(\text{CD}_3)_2\text{CO}$)

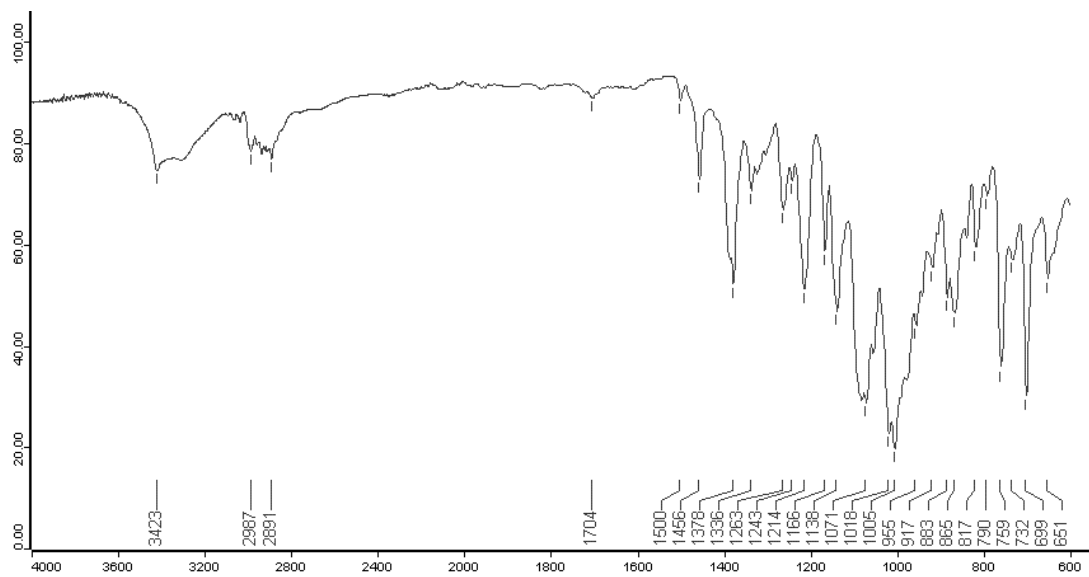


A1.4. Glucose derivatives

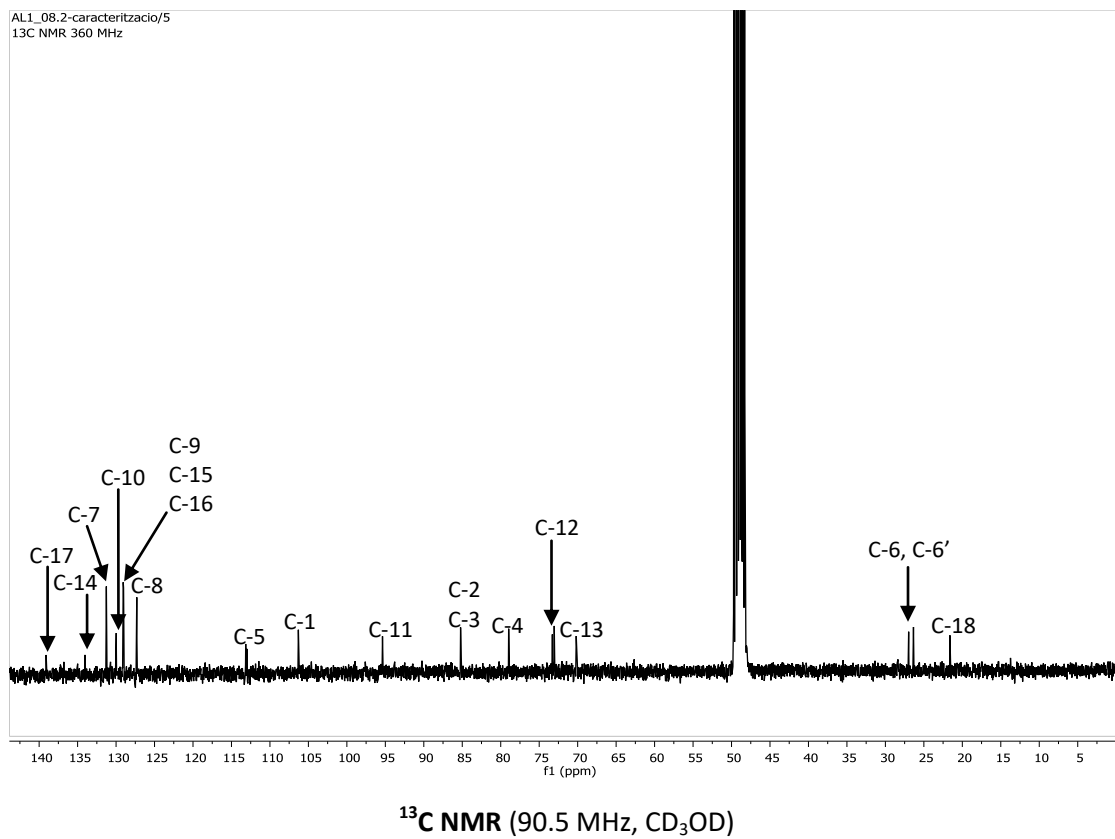
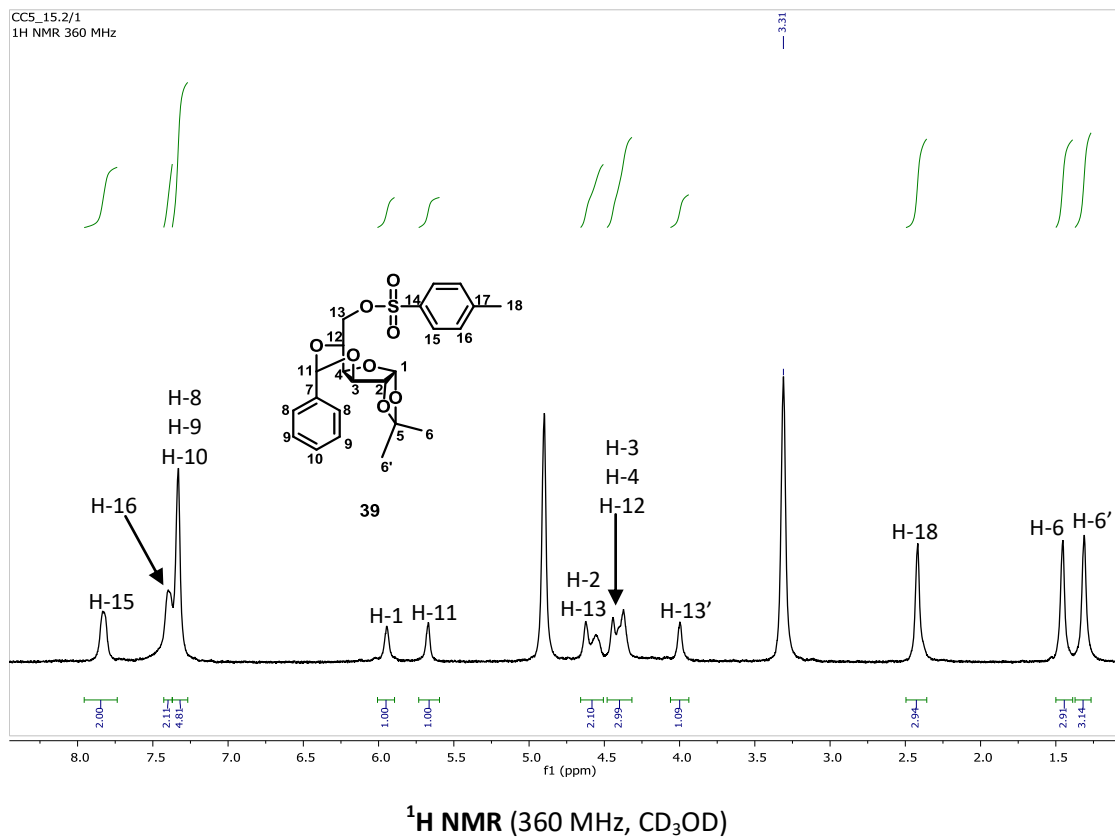


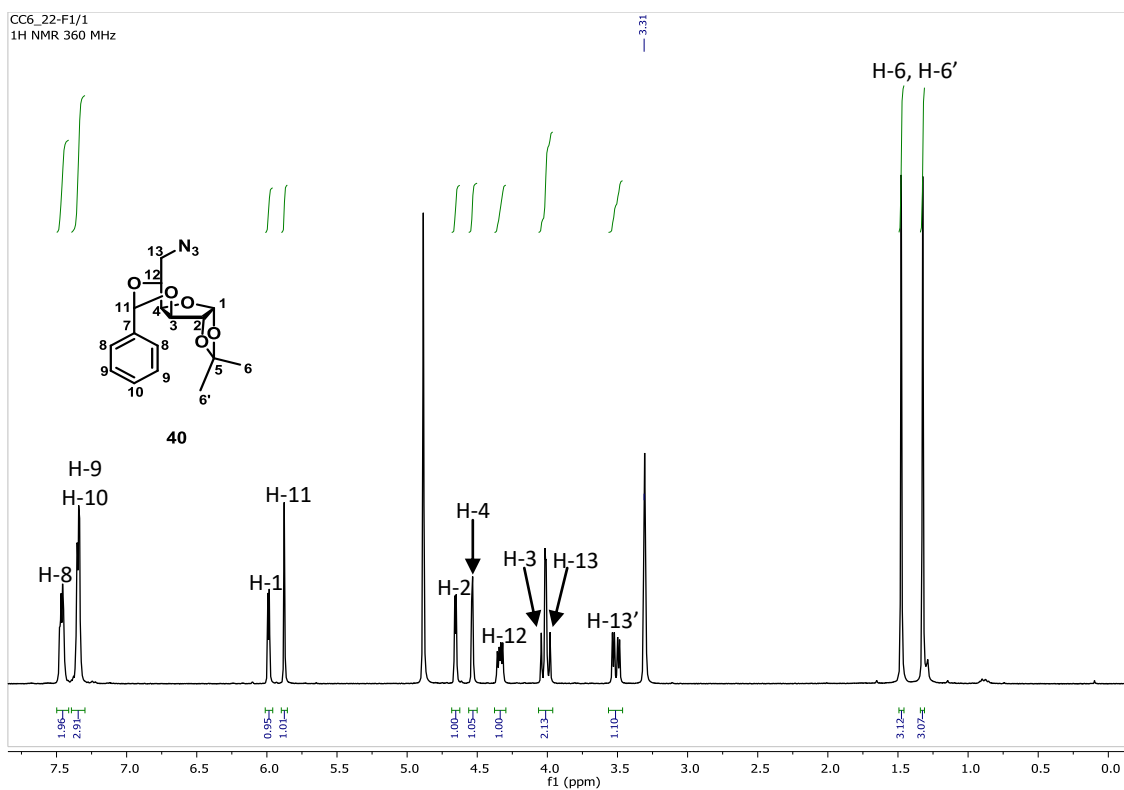
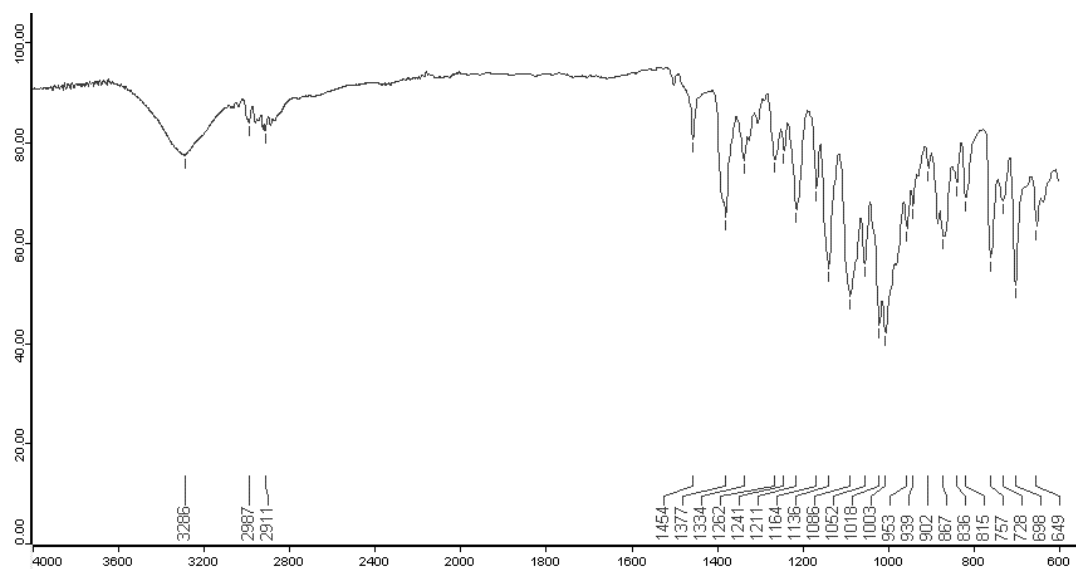


^{13}C NMR (90.5 MHz, CD_3OD)

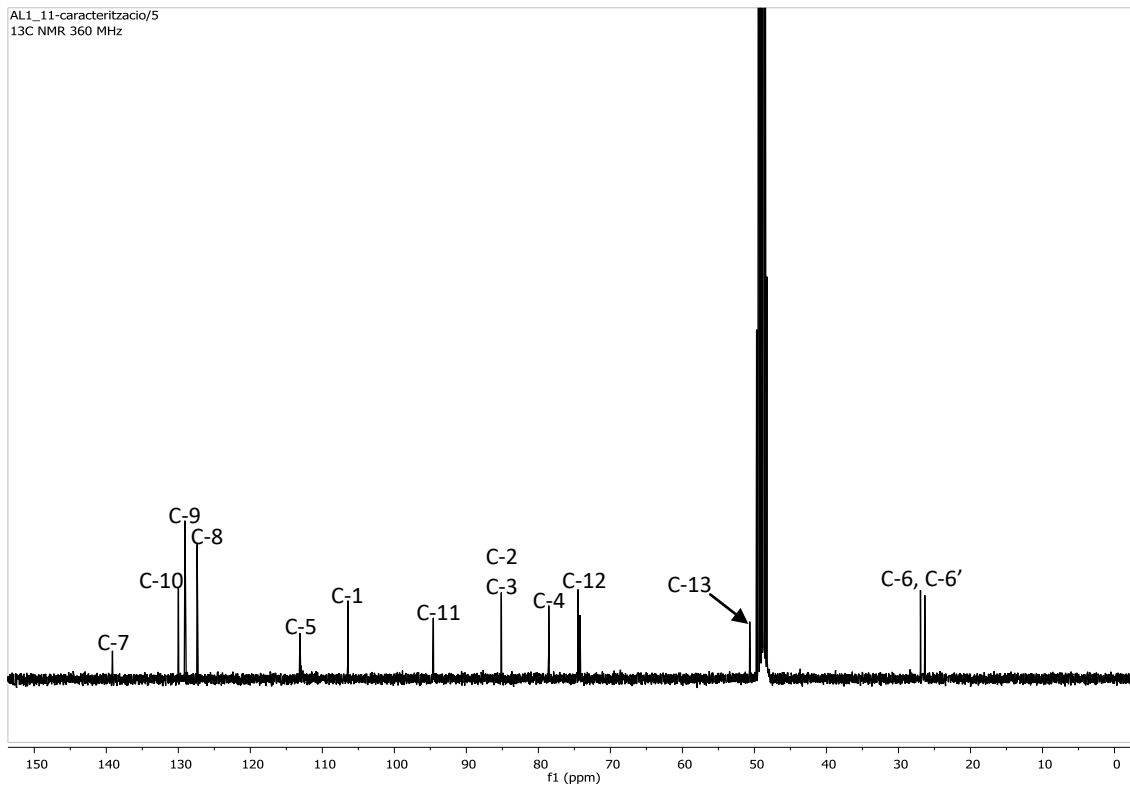


IR (ATR)

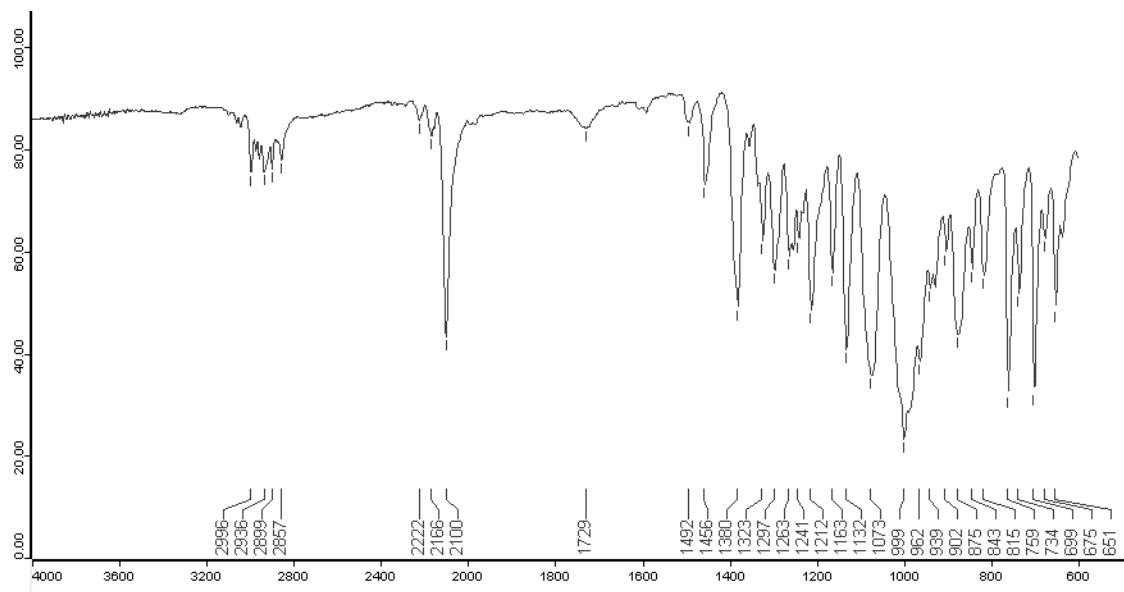




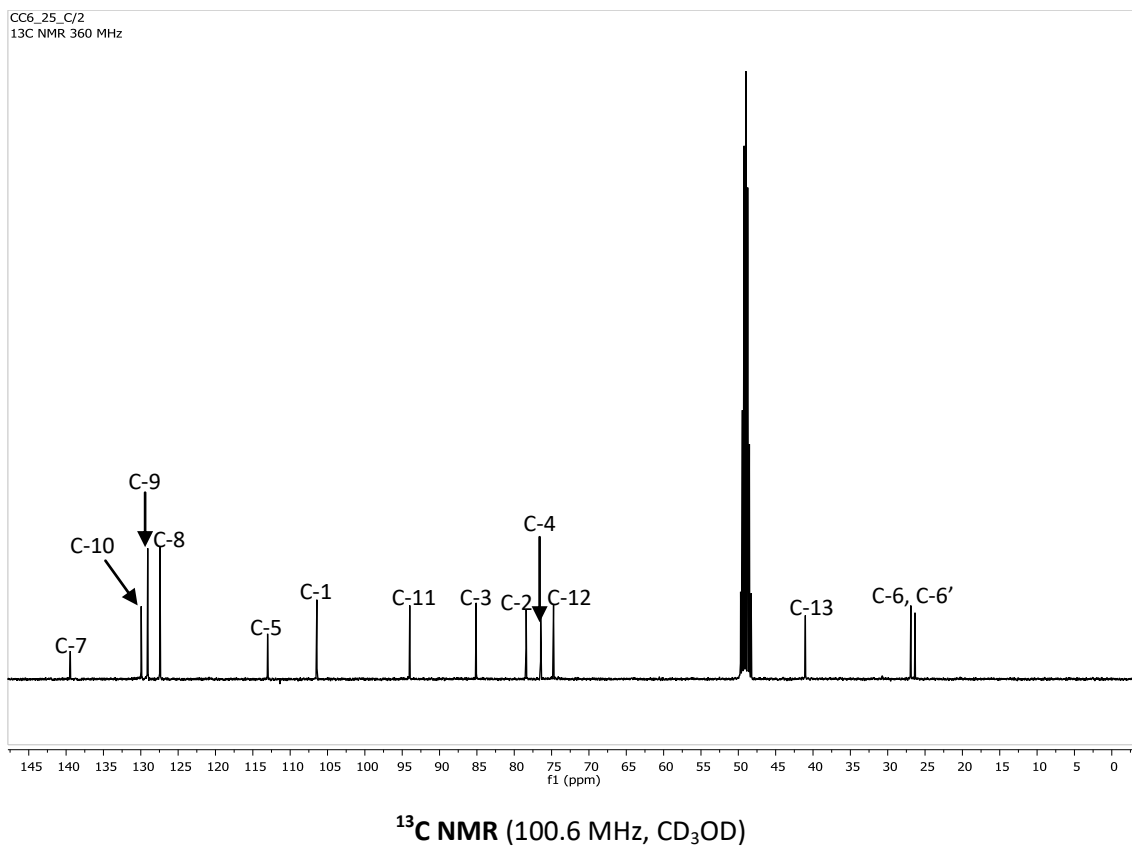
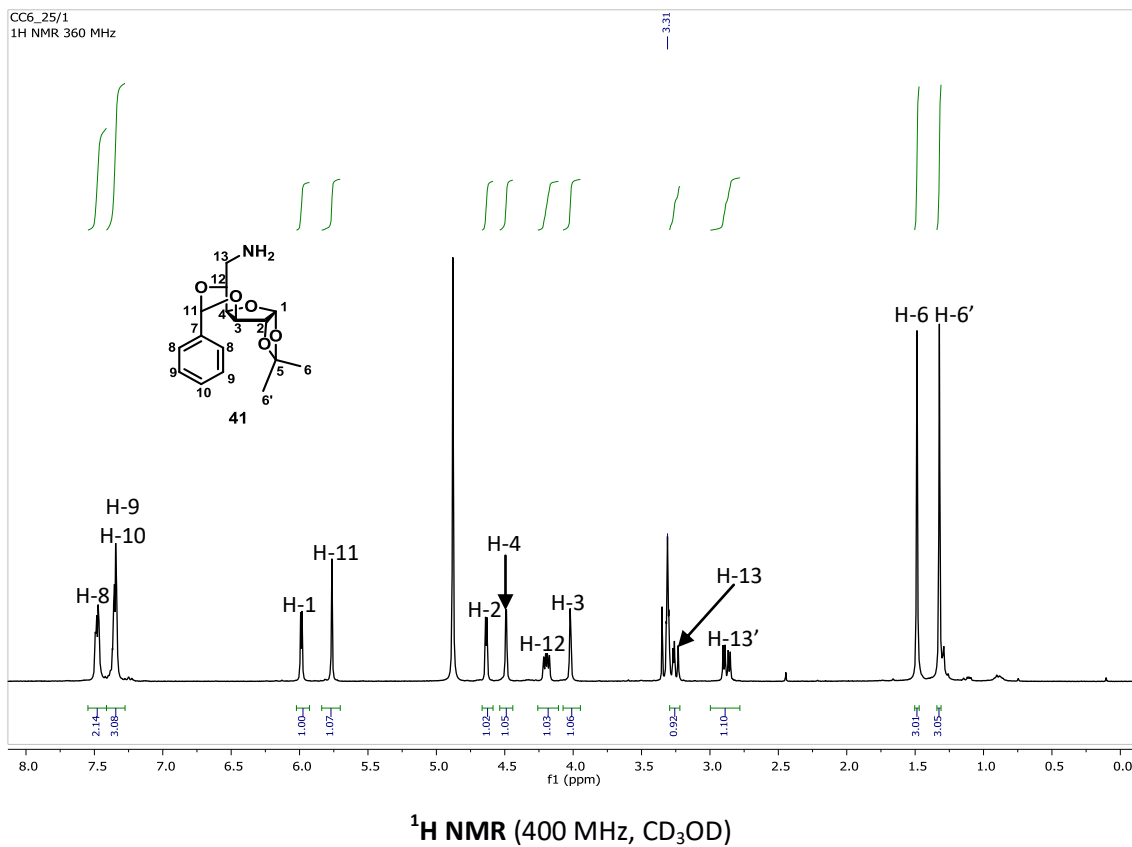
¹H NMR (360 MHz, CD₃OD)

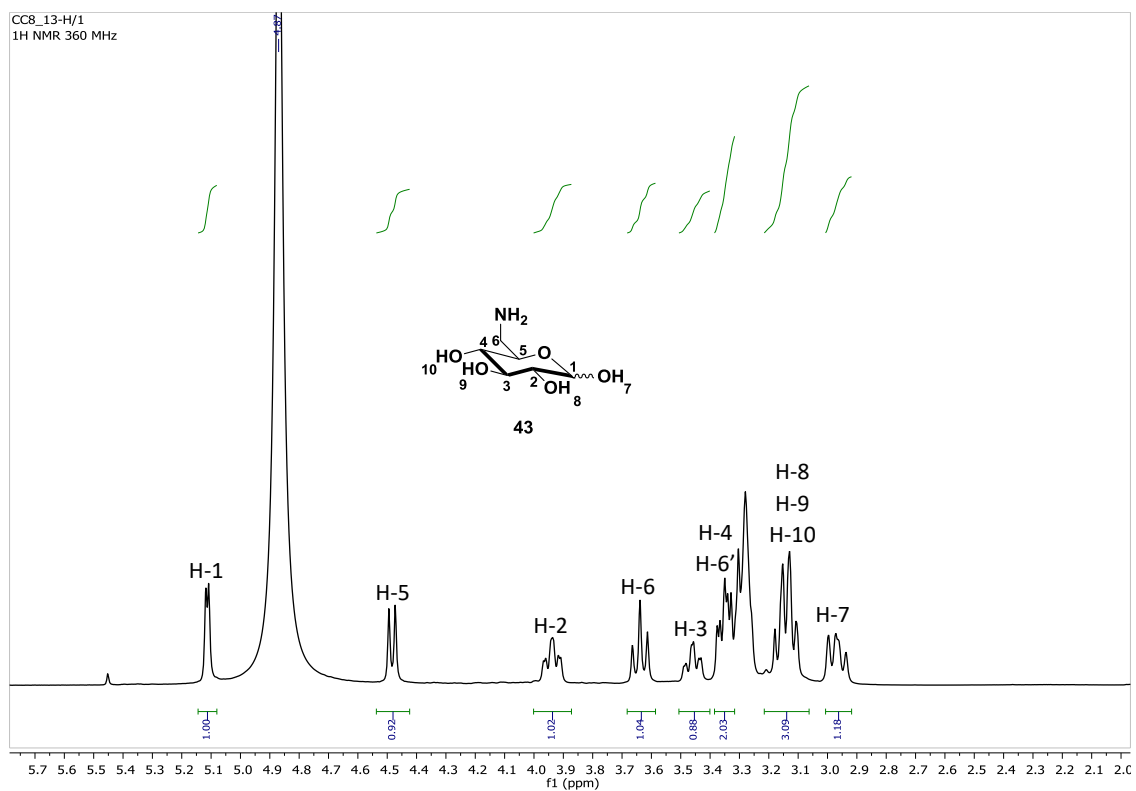
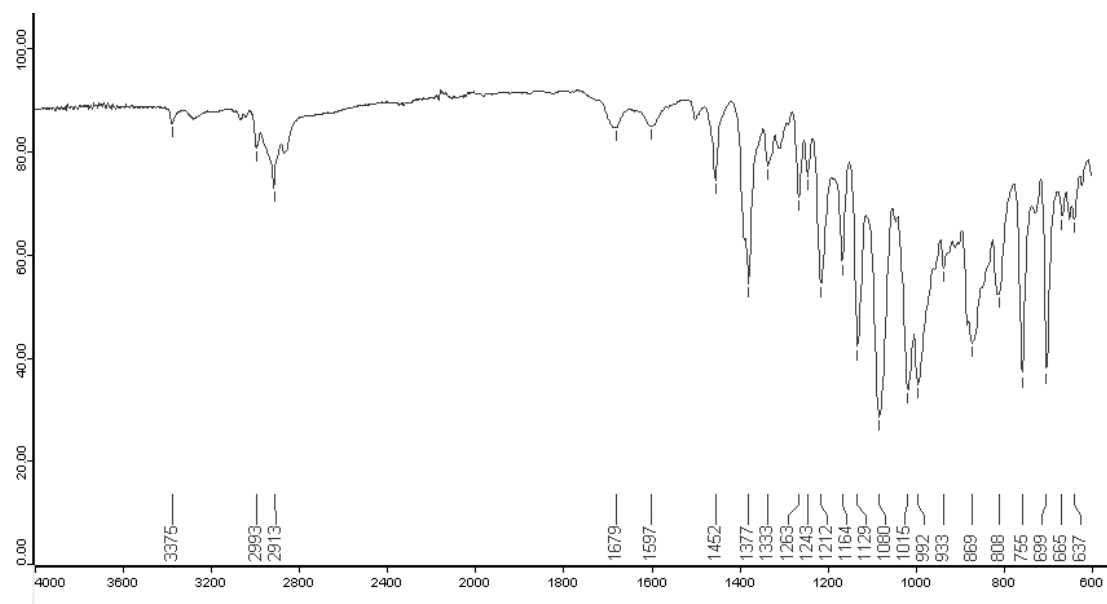


¹³C NMR (90.5 MHz, CD₃OD)

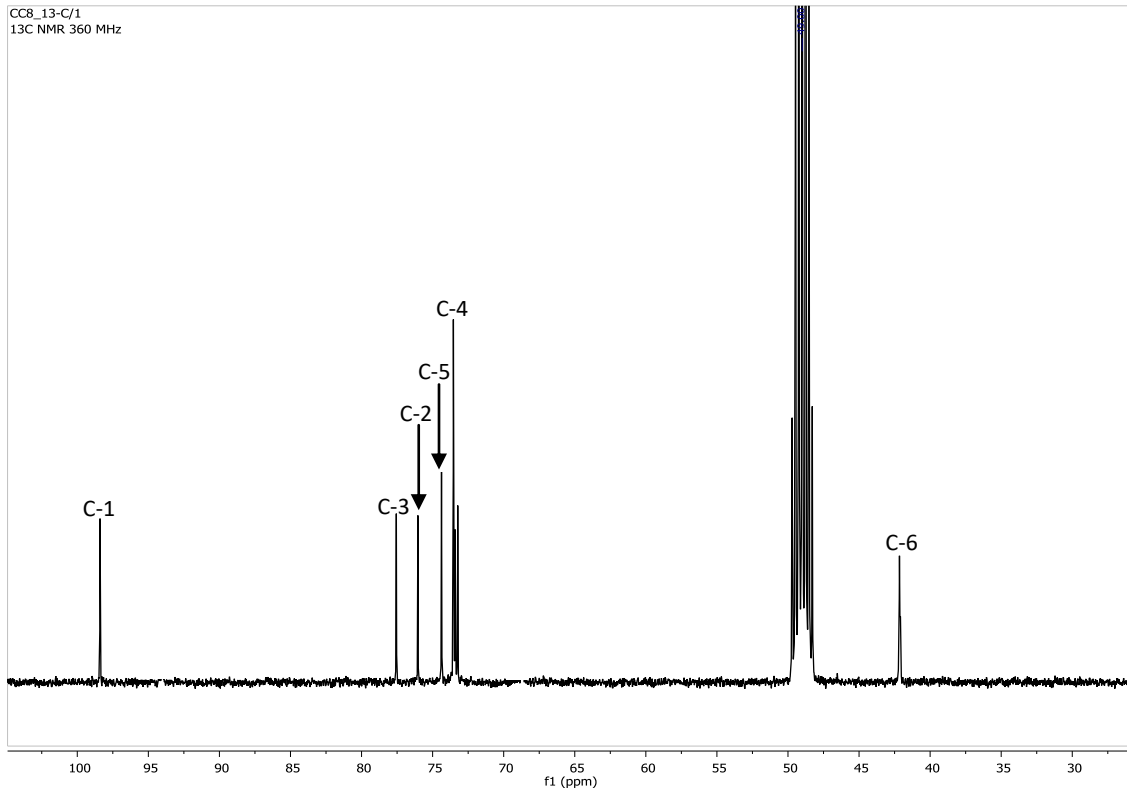
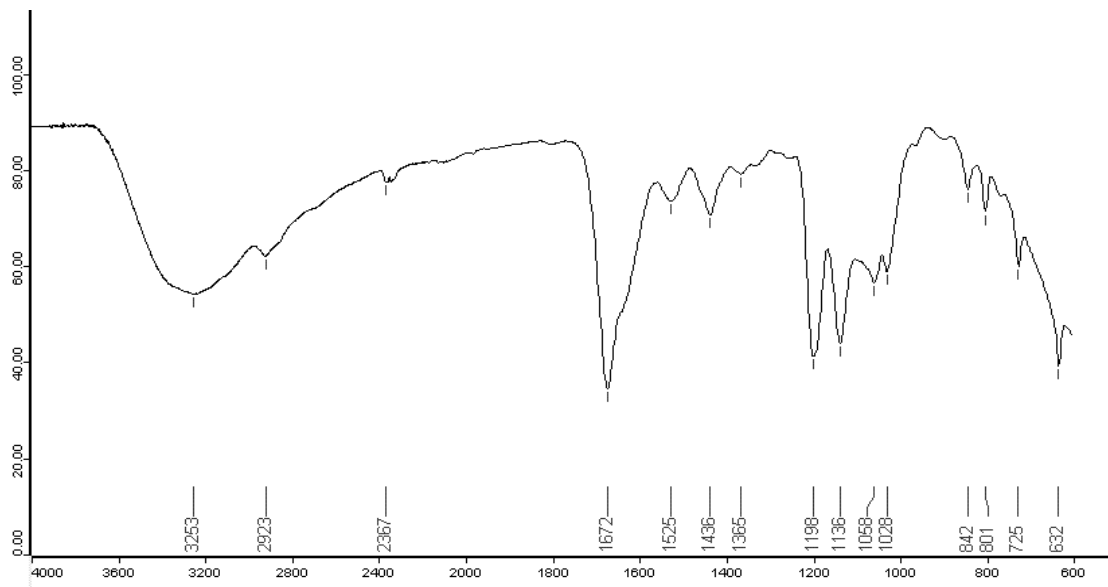


IR (ATR)





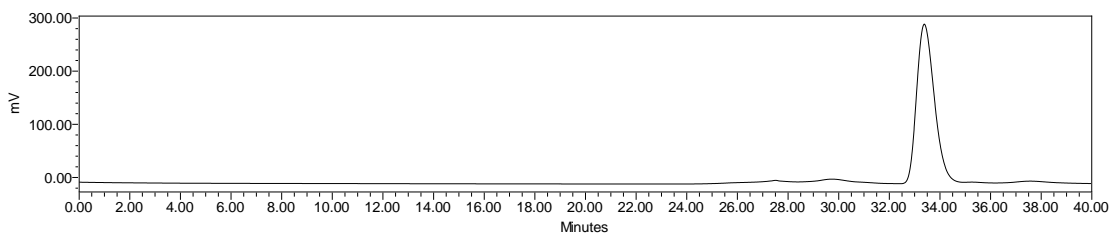
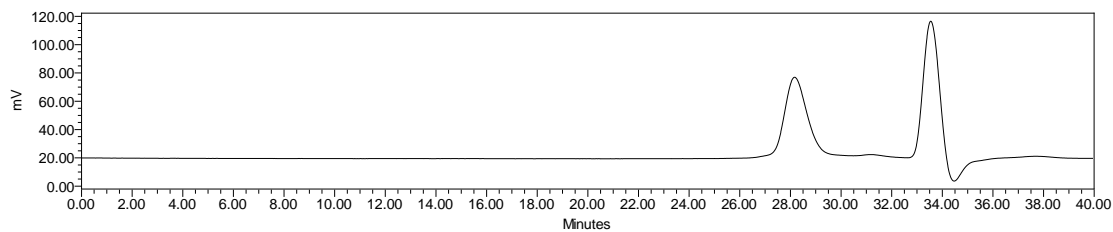
¹H NMR (360 MHz, CD₃OD)

 ^{13}C NMR (90.5 MHz, CD_3OD)

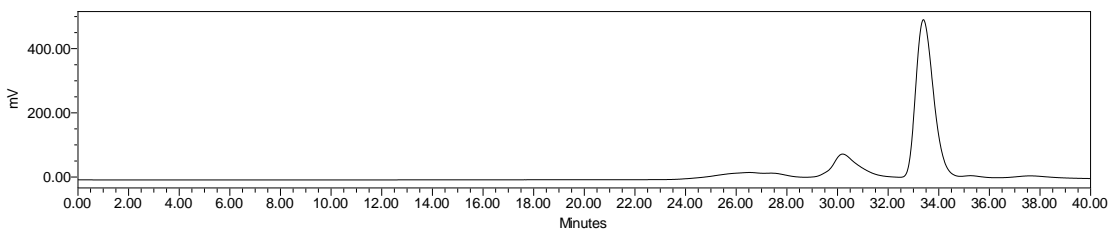
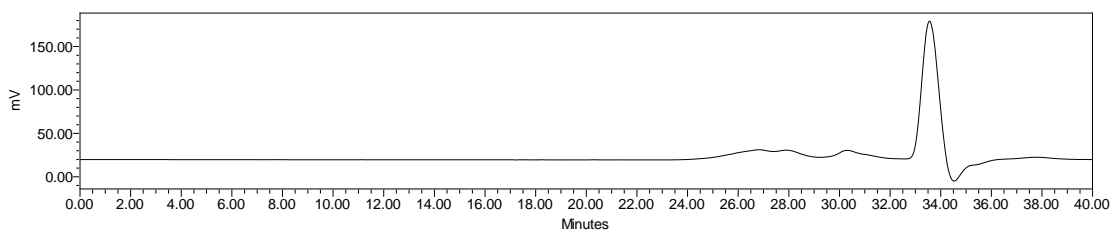
IR (ATR)

A2. GPC SPECTRA

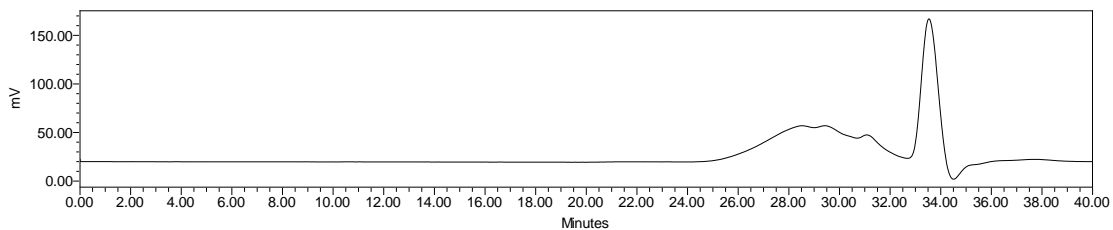
A2.1. GPC spectra with both IR (top) and UV (bottom) detectors of building block 6

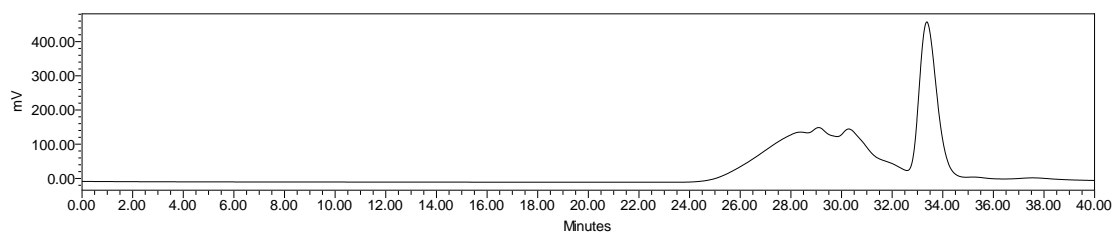


A2.2. GPC spectra with both IR (top) and UV (bottom) detectors of P6

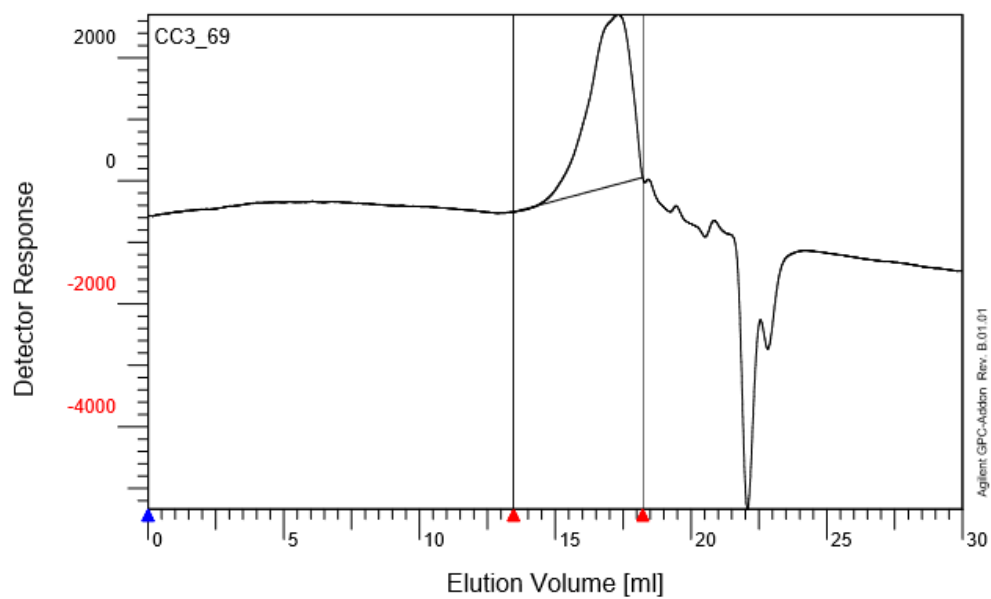


A2.3. GPC spectra with both IR (top) and UV (bottom) detectors of building block 9

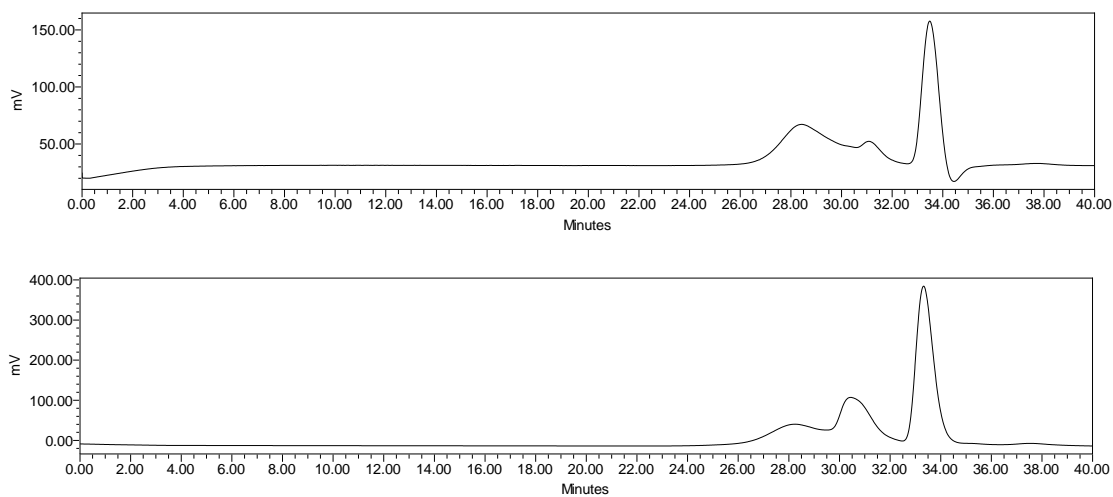


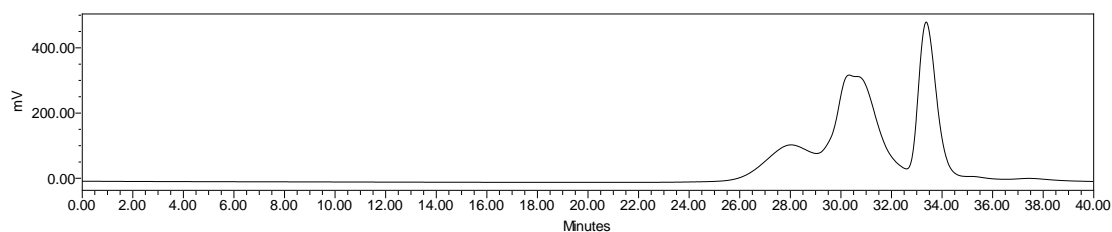
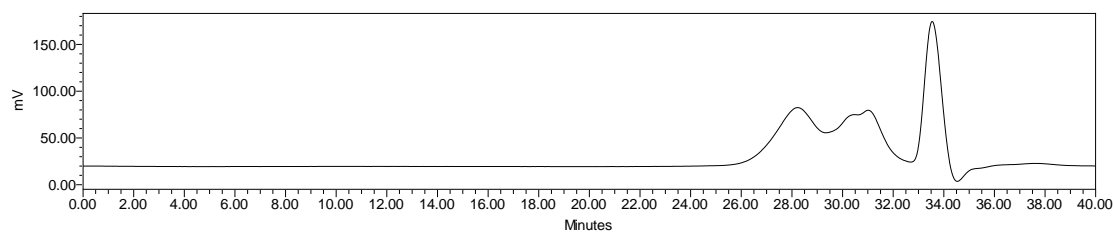
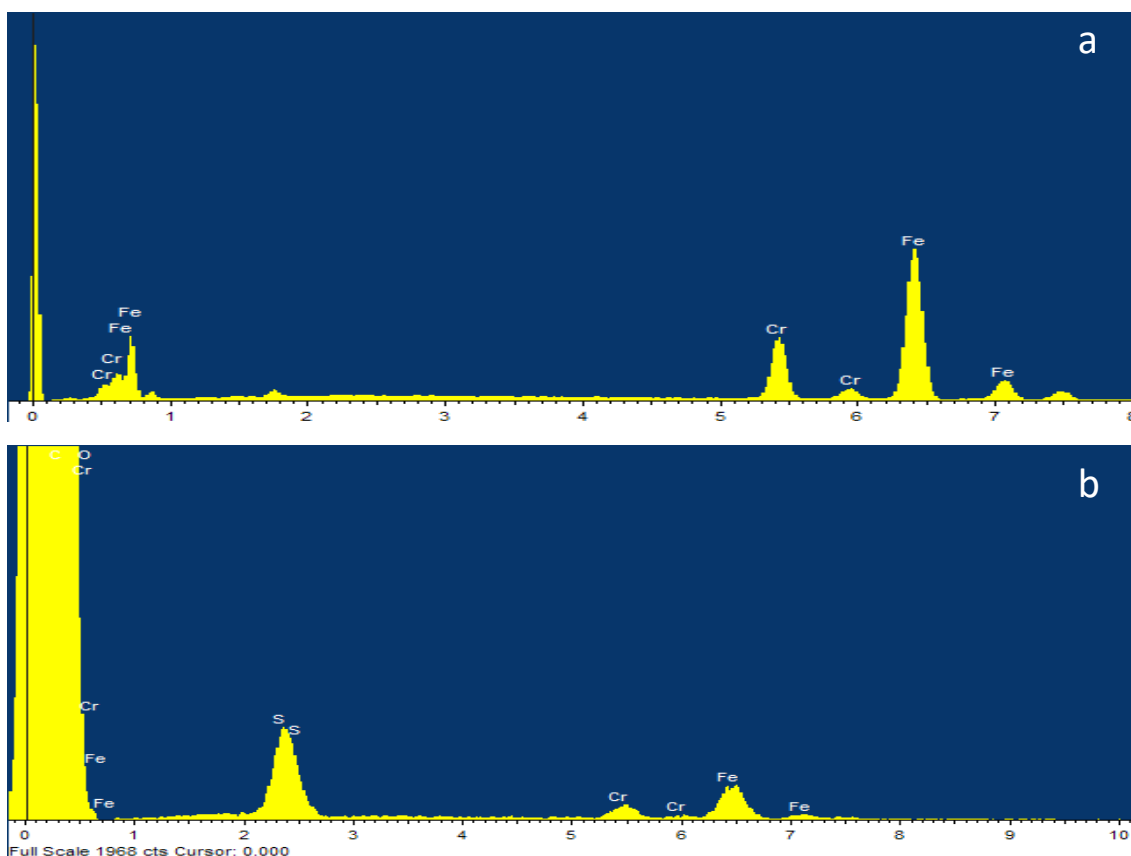


A2.4. GPC spectrum with IR detector of P9



A2.5. GPC spectra with both IR (top) and UV (bottom) detectors of building block 46



A2.6. GPC spectra with both IR (top) and UV (bottom) detectors of P46**A3. EDX SPECTRA****A3.1. Images from EDX experiments of pristine and coated surfaces with P9 *via ex situ* polymerisation in solution**

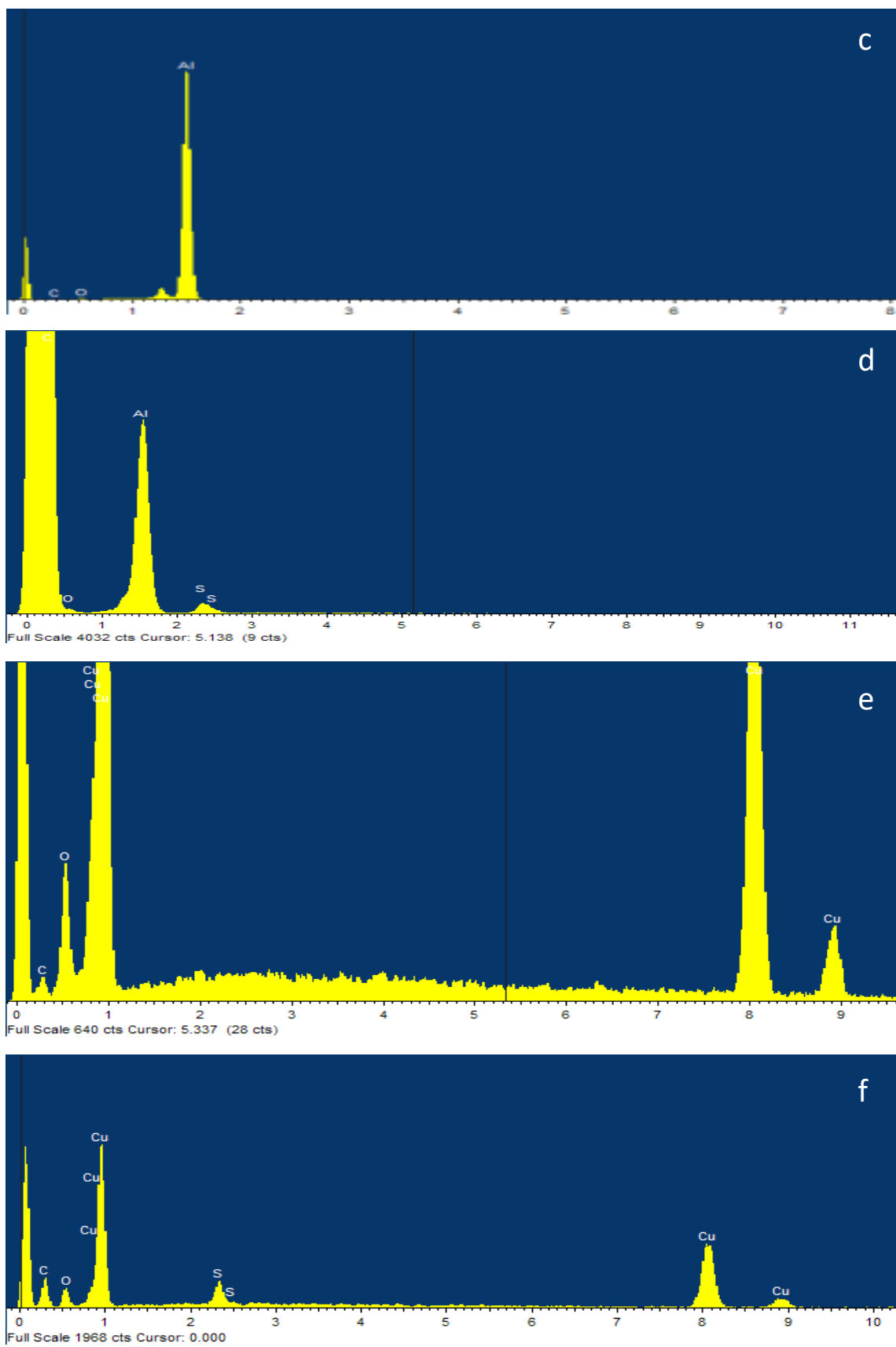


Figure A3.1. EDX experiments onto a) pristine stainless steel (SS), b) SS@P9, c) pristine aluminium, d) Al@P9, e) pristine copper and f) Cu@P9.

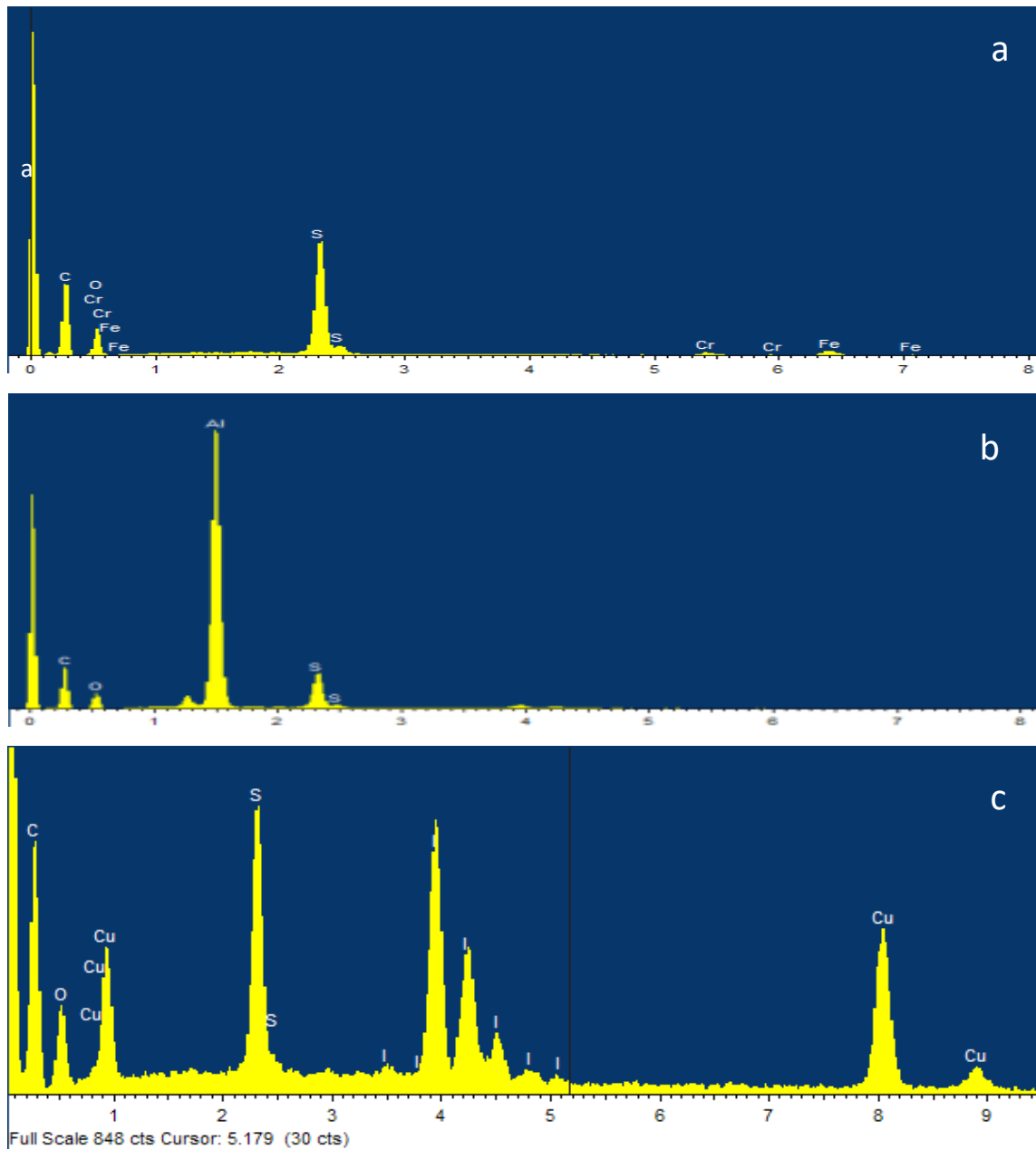
A3.2. Images from EDX experiments of coated surfaces with P9 via *in situ* polymerisation

Figure A3.2. EDX experiments onto a) SS@P9, b) Al@P9 and c) Cu@P9.

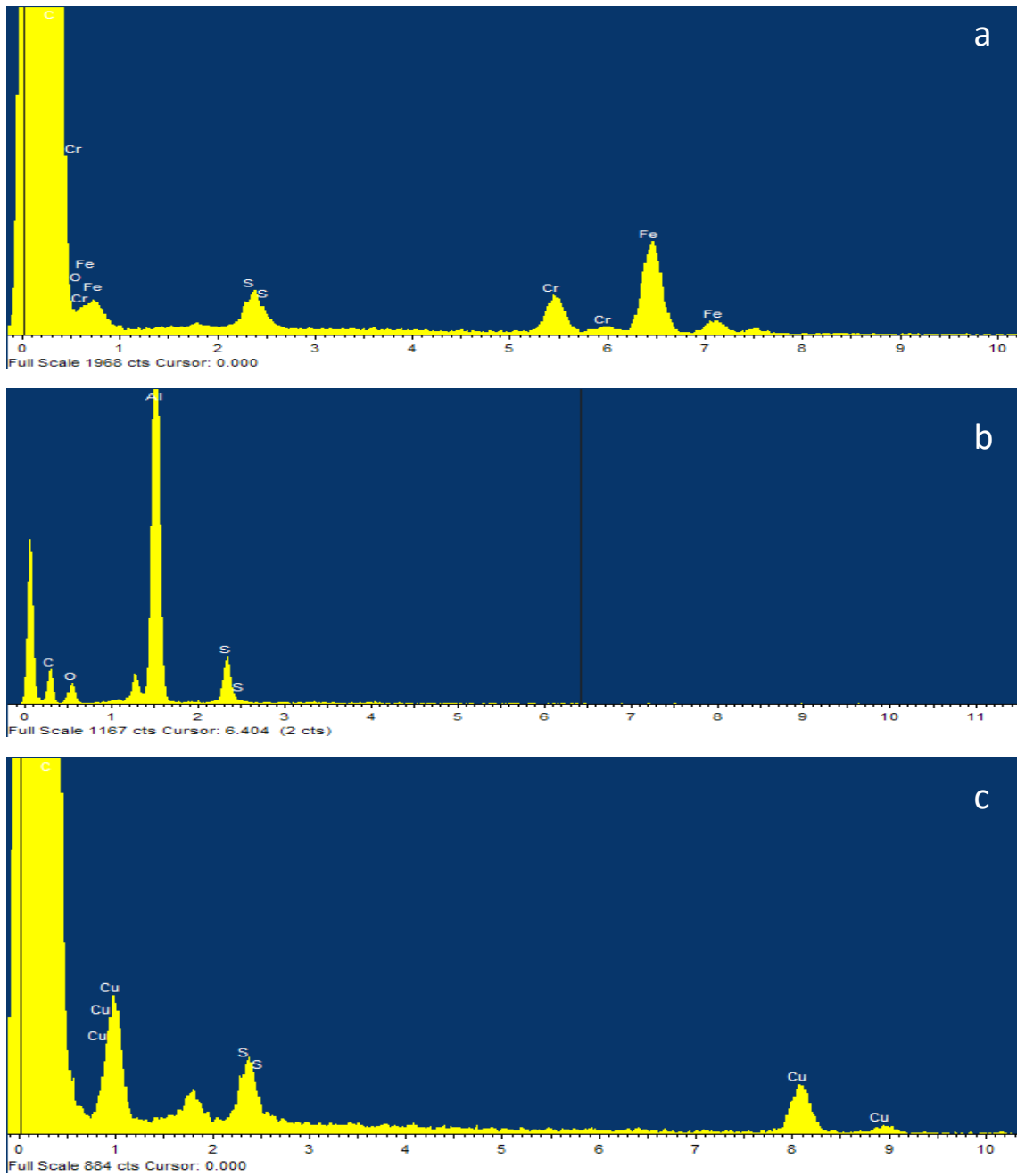
A3.3. Images from EDX experiments of coated surfaces with P6 via *ex situ* polymerisation in solution

Figure A3.3. EDX experiments onto a) SS@P6, b) Al@P6 and c) Cu@P6.

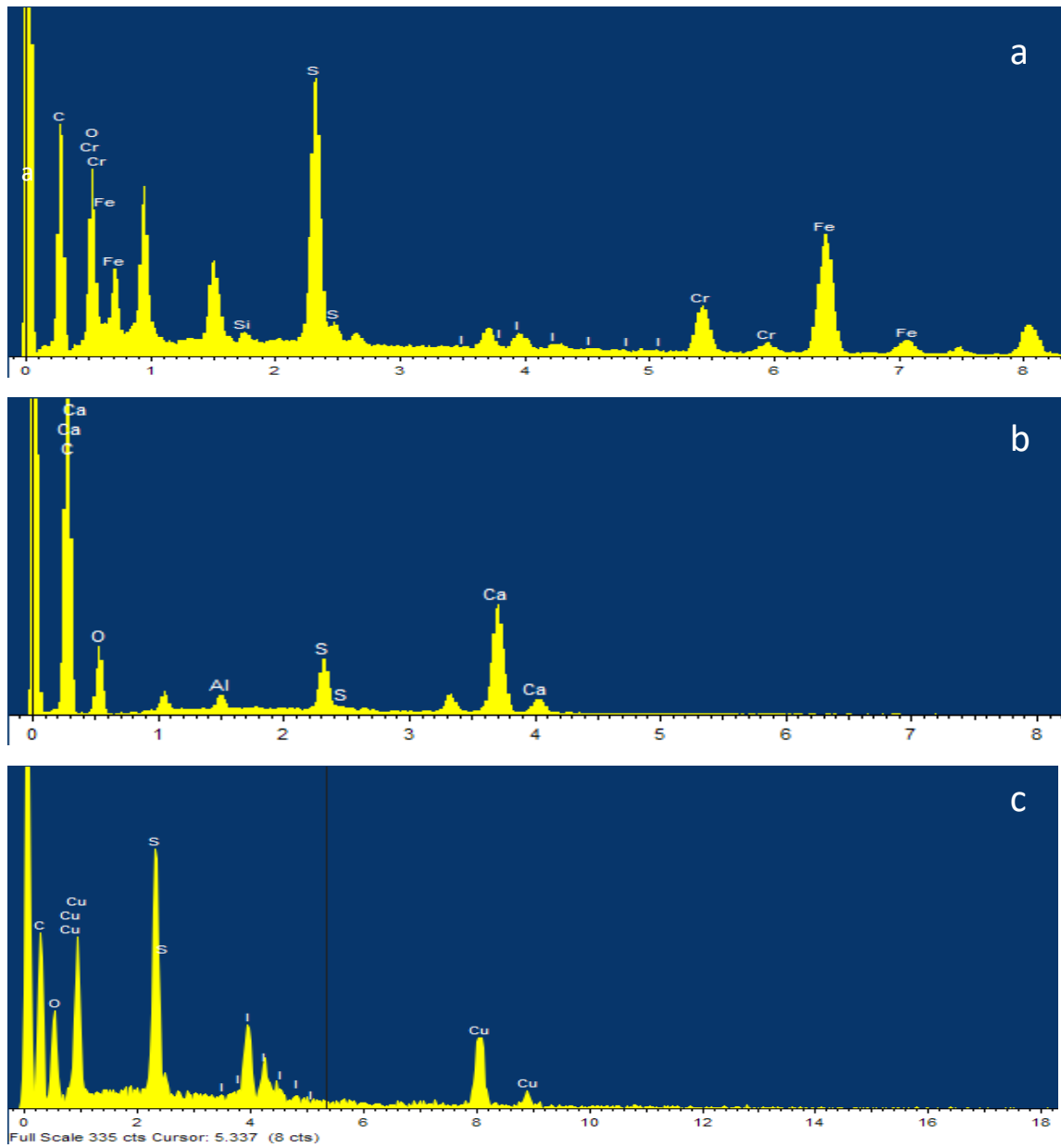
A3.4. Images from EDX experiments of coated surfaces with P6 via *in situ* polymerisation

Figure A3.4. EDX experiments onto a) SS@P6, b) Al@P6 and c) Cu@P6.